

Origin and geochemical evolution of localized, high-ferrous-iron zones in the Upper Castle  
Hayne Aquifer, Beaufort County, North Carolina

By

Mark J. Akland

May, 2017

Director of Thesis: Dr. Terri L. Woods

Major Department: Geological Sciences

The Tertiary Upper Castle Hayne Aquifer (UCHA) is one of the most productive aquifers in North Carolina's Coastal Plain; however, localized zones containing high, dissolved-iron concentrations ( $>0.3$  mg/L) are present near the recharge area. Iron-rich groundwater is an expensive water quality and infrastructure problem affecting water suppliers in eastern North Carolina but the evolution of high-iron zones in the UCHA is poorly understood. This study integrates geochemistry, mineralogy, sedimentology, and geochemical groundwater modeling to identify likely sources and sinks of dissolved iron near Washington, NC.

Two adjacent sediment cores were collected from the Yorktown and surficial aquifers, which overlie the UCHA at the core site in western Beaufort County. Orangish-brown sediments, extracted between 3.7 and 6.1 meters below the land surface (m BLS), have the highest iron concentrations measured in the core sediments (ranging from 2.2 to 9.0 wt. %). Several additional anomalies occur within this depth range including the highest increase in pH (from 4.9 to 8.1), the largest increase in cation-exchange capacity (from 2.3 to 124.6 meq/100 cm<sup>3</sup>), and the highest mud content (87.1 wt. %). X-ray diffraction, optical microscopy, and scanning electron microscopy indicate that amphiboles, ilmenite, glauconite, iron-oxyhydroxides, and pyrite are important iron-bearing minerals in the coastal plain overburden.

Three hydrogeochemical zones, distinguished by variations in sediment composition, depth, and inferred biogeochemical and hydrologic processes, are identified in the sediments overlying the UCHA. The Iron Depletion Zone, extending from the ground surface to approximately 3.8 m BLS, may be characterized by progressive depletion of iron-bearing constituents over time. The Iron Pigmentation Zone (IPZ), extending from the basal portion of the IDZ to approximately 6.4 m BLS, likely transitions from oxidizing conditions to reducing conditions, resulting in iron-oxyhydroxide precipitation in the upper IPZ and the reduction of ferric iron to ferrous iron in the lower IPZ. High-dissolved-iron concentrations in the UCHA are most likely derived from conditions that are similar to those of the lower IPZ, where in the presence of organic matter, microbially catalyzed reduction of abundant iron-oxyhydroxides results in the production of dissolved-ferrous iron. Geochemical groundwater modeling confirms that microbially catalyzed reduction of iron-oxyhydroxides via organic-matter oxidation yields the highest, dissolved-iron concentrations in slightly acidic, surficial-aquifer water. Below 6.4 m BLS, evidence suggests that the dominant electron-accepting process in the Iron Sulfide Zone is microbially catalyzed sulfate reduction, resulting in the attenuation of dissolved-iron concentrations via the formation of iron-sulfide minerals.

Iron-oxyhydroxide reduction, proximal to the upper contact of the UCHA, may be essential to the development of high-iron groundwater along the western edge of the UCHA recharge area. Geochemical modeling indicates that cation-exchange reactions between ferrous iron and glauconite may substantially deplete dissolved iron after groundwater enters the UCHA. Future studies integrating contemporaneous investigation of groundwater geochemistry, sediment composition, and redox-related microorganisms are necessary to better elucidate the formation of high-iron zones in the UCHA.



**Origin and geochemical evolution of localized, high-ferrous-iron zones in the Upper Castle  
Hayne Aquifer, Beaufort County, North Carolina**

A Thesis

Presented to the Faculty of the Department of Geological Sciences

East Carolina University

In Partial Fulfillment of the Requirements for the Degree

Master of Science in Geology

by

Mark J. Akland

May, 2017



© Mark J. Akland, 2017

Origin and geochemical evolution of localized, high-ferrous-iron zones in the Upper Castle Hayne Aquifer, Beaufort County, North Carolina

By

Mark J. Akland

APPROVED BY:

DIRECTOR OF  
THESIS: \_\_\_\_\_

Terri L. Woods, PhD

COMMITTEE MEMBER: \_\_\_\_\_

Richard K. Spruill, PhD

COMMITTEE MEMBER: \_\_\_\_\_

Eduardo Leorri, PhD

COMMITTEE MEMBER: \_\_\_\_\_

Richard L. Mauger, PhD

CHAIR OF THE DEPARTMENT  
OF GEOLOGICAL SCIENCES: \_\_\_\_\_

Stephen J. Culver, PhD

DEAN OF THE  
GRADUATE SCHOOL: \_\_\_\_\_

Paul J. Gemperline, PhD

## **Acknowledgements**

This thesis would not have been possible without the assistance from friends, family, faculty, staff, and a couple of kind strangers. First, I would like to thank my thesis advisor, Dr. Terri Woods for her unwavering support and guidance during this project. I could not have asked for a more helpful and accessible mentor. I am truly grateful to my committee members, Dr. Eduardo Leorri, Dr. Richard Mauger, and Dr. Richard Spruill for their advice and constructive criticism. I would like to extend a special thanks to Mr. Jim Watson and Mr. John Woods for their help with operating the Geoprobe, maintaining field and lab equipment, and for teaching me how to use various pieces of field and lab equipment. I would also like to thank Mr. Tom Fink for all of his SEM/EDX instruction and advice. I am very grateful to Dr. Adriana Heimann, Dr. Eric Horsman, Dr. Alex Manda, and Dr. Donald Neal for all of their advice and assistance with my polished-thin sections. I owe a special thanks to Mr. Jay Holley and Dr. Steve Campbell for providing me with information and guidance concerning the Castle Hayne Aquifer. I would like to take this opportunity to thank Caroline Smith, Nick Zaremba, Mike Barbour, Jared Crenshaw, Joe Perry, Stephen Woods, and Beth Lang for their field assistance. I would like to thank Dr. Seth Tabb for all of the counsel and assistance that he has provided to me over the years. I would also like to thank my wife, Katie Akland and my parents, Ann and Gerry Akland for their support and encouragement while working to fulfill my aspirations.

## Table of Contents

Acknowledgements.....	iv
Table of Contents.....	v
List of Tables.....	xii
List of Figures.....	xiv
List of Common Symbols and Abbreviations.....	xvii
1.0 Introduction.....	1
1.2 Geologic and Hydrogeologic Framework.....	6
1.3 Iron Geochemistry.....	12
1.4 Iron Biogeochemistry.....	14
1.5 Formation and Characteristics of Common Iron-Oxyhydroxides.....	17
1.6 Previous Work.....	21
1.7 Hypothesis and Objectives.....	25
1.7.1 Hypothesis.....	25
1.7.2 Objectives.....	25
2.0 Study Area.....	26
3.0 Procedures.....	29
3.1 Core Acquisition and Processing.....	29
3.2 Grain-Size Analysis and Hydraulic Conductivity.....	34
3.3 X-ray Fluorescence.....	35

3.4 Loss on Ignition .....	38
3.5 Sediment Testing by NCAG .....	39
3.6 Magnetic Separation .....	40
3.7 X-ray Diffraction .....	43
3.8 Polished-Thin Sections .....	43
3.9 Energy Dispersive X-ray Analysis.....	44
3.10 Mineralogical Analysis .....	44
3.11 Geochemical Modeling with PHREEQC.....	45
3.11.1 Input Data in PHREEQC .....	49
3.11.2 Output Data in PHREEQC.....	49
3.11.3 Model Setup .....	50
3.11.3.1 Simple Dissolution Simulations.....	52
3.11.3.2 Pyrite Oxidation Simulations.....	52
3.11.3.3 Goethite Reduction in Surficial Groundwater .....	53
3.11.3.4 Reactive-Transport Modeling of the UCHA.....	53
3.11.4 Calibration of the Reactive-Transport Model .....	58
3.11.5 Conservative-Transport Model .....	58
4.0 Results.....	61
4.1 Sediment Descriptions .....	61
4.2 Mineralogy.....	65

4.3 Magnetic Separation Results.....	73
4.4 Sediment Geochemistry .....	76
4.4.1 Statistical Analysis of XRF Results.....	76
4.4.2 XRF Results .....	81
4.4.3 LOI Results .....	85
4.4.4 NCAG Sediment-Test Results .....	85
4.4.5 Comparison of XRF and NCAG Results .....	90
4.5 SEM/EDX Results .....	92
4.5.1 Statistical Analysis of Mineral Standards .....	92
4.5.2 Chemistry of Fe-Rich Aggregates and Grain Coatings .....	95
4.5.3 Mineral Chemistry .....	100
5.0 Discussion.....	105
5.1 Transformation of Iron in Sediments Overlying the UCHA .....	105
5.1.1 Iron Depletion Zone.....	111
5.1.2 Iron Pigmentation Zone .....	112
5.1.2.1 Iron-Oxyhydroxide Accumulation in the IPZ.....	114
5.1.2.2 Iron-Oxyhydroxide Depletion in the IPZ.....	117
5.1.3 Iron-Sulfide Zone.....	118
5.3 Temporal Hydrologic Considerations.....	125
5.4 Insights from Modeling.....	128

5.4.1 Simple Dissolution.....	128
5.4.2 Pyrite Oxidation.....	131
5.4.3 Goethite Titration with DOC.....	138
5.4.4 Calibrated Transport Models.....	143
5.4.4.1 Conservative-Transport Modeling.....	146
5.4.4.2 Reactive-Transport Modeling.....	148
6.0 Conclusions.....	151
7.0 References.....	157
Appendix A: Core Subsample Data.....	167
Appendix A1: TC14 Data.....	167
Appendix A2: TC14C Data.....	180
Appendix B: Descriptions of Analytical Procedures.....	182
Appendix B1: Grain-Size Analysis of Sediment Samples.....	182
Appendix B2: XRF Pellet Preparation.....	184
Appendix B3: Loss on Ignition Analysis.....	186
Appendix B4: Magnetic Separation Procedure.....	187
Appendix B5: XRD Analysis.....	192
Appendix C: Results of Grain-Size Analyses.....	199
Appendix C1: Grain-Size Data.....	199
Appendix C2: Grain-Size Percentages and Error.....	203

Appendix C3: Grain-Size Statistics and Hydraulic Conductivity.....	206
Appendix D: Results of Magnetic Separations.....	209
Appendix D1: Grain-Size Data Used in Magnetic Separations.....	209
Appendix D2: Magnetic Separation Data.....	210
Appendix E: Polished-Thin-Section Data.....	211
Appendix F: EDX Data.....	218
Appendix F1: Composition and Statistics of Mineral Standards.....	218
Appendix F2: Replicate-EDX-Analysis Data of Reference Standards.....	226
Appendix F3: Eliminated EDX Spectra from Statistical Evaluation of Iron-oxyhydroxide Aggregates and Coatings .....	233
Appendix F4: Elemental Concentrations Measured from Iron-oxyhydroxide Aggregates and Coatings .....	237
Appendix F5: Mineral Chemistry Data.....	247
Appendix F6: Statistics of Evaluated Minerals .....	264
Appendix G: XRF Data .....	276
Appendix G1: Pellet Data and Descriptions of Reference Samples.....	276
Appendix G2: Accepted Values of XRF Reference Samples.....	277
Appendix G3: Sediment and Binder Weights of TC14 Pellet Samples.....	278
Appendix G4: Total Elemental Concentrations of TC14 Pellet Samples.....	280
Appendix G5: Results of Replicate XRF Analyses .....	284



Appendix G6: Statistics of XRF Pellet Samples .....	291
Appendix G7: Linear Regression Plots comparing the Initial 2014 Concentration with the Mean concentration of 2015 Analyses for TC14 Pellet Samples .....	296
Appendix H: LOI Data.....	303
Appendix I: NCAG DATA.....	304
Appendix J: Comparison of XRF and NCAG Results.....	306
Appendix K: Results of Geochemical Modeling and PHREEQC Input Files.....	312
Appendix K1: Simple Dissolution in Pure Water at pH 5 .....	312
Appendix K2: Simple Dissolution in Pure Water at pH 7 .....	313
Appendix K3: Simple Dissolution in Pure Water at pH 9 .....	314
Appendix K4: Simple Dissolution in Surficial Water .....	315
Appendix K5: Pyrite Titration with Oxygen in Pure Water .....	316
Appendix K7: Pyrite Titration with Oxygen in Surficial Water.....	326
Appendix K8: Pyrite Titration with Oxygen and Simultaneous Calcite Dissolution in Surficial Water.....	331
Appendix K9: Goethite Titration in Surficial Water .....	335
Appendix K10: Goethite Titration with DOC and Simultaneous Calcite Dissolution in Surficial Water .....	342
Appendix K11: Percent Glauconite and Simulated Dissolved-Fe Concentrations.....	350
Appendix K12: Conservative Model Results .....	351

Appendix K13: Reactive Transport Model Results .....	352
Appendix L: PHREEQC Input Files.....	353
Appendix L1: Dissolving Individual Fe-Bearing Minerals in Pure Water at pH 5 .....	353
Appendix L2: Dissolving Individual Fe-Bearing Minerals in Pure Water at pH 7 .....	359
Appendix L3: Dissolving Individual Fe-Bearing Minerals in Pure Water at pH 9 .....	365
Appendix L4: Dissolving Individual Fe-Bearing Minerals in Surficial Water [water chemistry from Woods et al. (2000)].....	371
Appendix L5: Titrating 10 moles of Pyrite with 8 mg/L Oxygen in Pure Water .....	382
Appendix L6: Titrating 10 moles of Pyrite with 8 mg/L Oxygen in Pure Water and 10 moles of Calcite.....	383
Appendix L7: Titrating 10 moles of Pyrite with 8 mg/L Oxygen in Surficial Water [(water chemistry from Whitley (2003)] .....	384
Appendix L8: Titrating 10 moles of Pyrite and 10 moles of Calcite with 8 mg/L Oxygen in Surficial Water [(water chemistry from Whitley (2003)] .....	386
Appendix L9: Titrating 10 moles Goethite with 5 mg/L DOC in Surficial Water [(water chemistry from Whitley (2003)] .....	388
Appendix L10: Titrating 10 moles Goethite and 10 moles Calcite with 5 mg/L DOC in Surficial Water [(water chemistry from Whitley (2003)] .....	390
Appendix L11: Conservative-Transport Model.....	392
Appendix L12: Reactive-Transport Model.....	396

## List of Tables

Table 1: Stratigraphic and hydrogeologic subdivisions.....	10
Table 2: Formation and characteristics of common iron-oxyhydroxide minerals.....	20
Table 3: Water quality data for secondary drinking water regulations measured at the Tranters Creek core site.....	24
Table 4: Formulas and equilibrium constants for modeled Fe-bearing minerals .....	47
Table 5: $\Delta G_f^\circ$ values for species involved in the dissolution of almandine. ....	48
Table 6: Solution data used for geochemical modeling in PHREEQC .....	55
Table 7: Solution data used for geochemical modeling in PHREEQC (continued).....	56
Table 8: Geochemical and transmissivity data for seven UCHA wells near Washington, NC ....	60
Table 9: Photographs of representative sediment intervals and sediment descriptions.....	64
Table 10: Generalized mineral formulas of XRD-detected minerals .....	69
Table 11: Origins, sources, and important characteristics of XRD-detected minerals. ....	70
Table 12: Abundances of dominant, non-Fe-bearing minerals estimated in polished-thin sections .....	71
Table 13: Abundances of dominant, Fe-bearing minerals estimated in polished-thin sections....	72
Table 14: Statistics for reference standard MRG-1. ....	78
Table 15: Statistics for reference standard NCS DC 71302. ....	79
Table 16: Average of absolute-percent deviations of elements comprising XRF pellet samples	80
Table 17: A table illustrating potentially problematic XRF data.....	82
Table 18: Generalized mineral formulas of EDX reference samples .....	94
Table 19: EDX statistics of Fe-rich Ags/Cs.....	99
Table 20: Mean chemical compositions of minerals. ....	104

Table 21: Mean abundances of dominant minerals comprising the Iron Depletion Zone, Iron Pigmentation Zone, and the Iron Sulfide Zone. ....	110
Table 22: Results of modeling the dissolution of individual Fe-bearing minerals in “Pure Water” at pH 5, 7, and 9 and the “Surficial Water” at pH 5.3 .....	130
Table 23: Results of the pyrite titration with O <sub>2</sub> in the “Pure Water” and “Surficial Water” simulations .....	137
Table 24: Results of goethite titration with DOC for the “Surficial Water” simulations .....	142

## List of Figures

Figure 1: Regional Fe concentrations in the UCHA and the major physiographic provinces of North Carolina .....	3
Figure 2: Location of the study area in eastern North Carolina.....	4
Figure 3: 1992 observed potentiometric surface map of the UCHA near Washington, NC .....	5
Figure 4: Hydrogeologic cross-section of NCCP .....	11
Figure 5: Illustration of cation exchange in a glauconitic aquifer .....	13
Figure 6: Relative concentrations of redox-related constituents in groundwater with increasing distance from the recharge zone .....	16
Figure 7: Map showing the location of potential recharge boundaries or discharge areas at the Tranters Creek core site .....	28
Figure 8: Illustration of core components used in depth calculations that were applied to account for variations in core recovery .....	33
Figure 9: Cross-section from near Tranters Creek, NC illustrating conceptual design for thesis project .....	51
Figure 10: Illustration of the one-dimensional flow path in PHREEQC .....	57
Figure 11: Variations in grain size and grain-size estimated permeability with depth.....	63
Figure 12: XRD-detected minerals by depth .....	67
Figure 13: Occurrence and relative abundance of minerals that were both detected by XRD and confirmed via microscopy.....	68
Figure 14: Weight percentages of magnetically susceptible grains with depth.....	75
Figure 15: XRF-determined changes in major elemental concentrations with depth in TC14 ....	83
Figure 16: XRF-determined changes in minor elemental concentrations with depth in TC14 ....	84

Figure 17: Changes in % LOI, HM %, W/V, Sediment-water pH, BS %, AC, and CEC with depth.....	87
Figure 18: NCAG-determined changes in major elemental concentrations with depth in TC14C .....	88
Figure 19: NCAG-determined changes in minor elemental concentrations with depth in TC14C .....	89
Figure 20: Comparison of NCAG and XRF results for sodium .....	91
Figure 21: Photomicrographs showing ilmenite and iron-oxyhydroxide-aggregates around quartz grains.....	97
Figure 22: Photomicrographs showing an Fe-rich coating around dolomite and authigenic pyrite on glauconite, ilmenite, and dolomite.....	98
Figure 23: Stratigraphic section, sediment photographs and inferred hydrogeochemical zones at the Tranters Creek core site .....	107
Figure 24: Photographs and bivariate plots showing depth-related variations in Fe, S, pyrite abundance, % LOI, and HM % .....	108
Figure 25: Photographs and bivariate plots showing depth-related variations in mud content, grain-size-estimated permeability, Ca, and CEC .....	109
Figure 26: Geochemical profiles illustrating variations in Fe concentrations and Fe/Al ratios with respect to depth and inferred hydrogeochemical zones .....	122
Figure 27: Eh-pH stability diagram of aqueous Fe species and common Fe-bearing minerals .	123
Figure 28: A conceptual diagram representing the inferred transformation and transfer of Fe species with increasing relative depth in sediments that overlie the UCHA .....	124

Figure 29: Hydrograph showing water-level elevations in the UCHA, surficial aquifer, and Tranters Creek between August 1987 and January 1988.....	127
Figure 30: Simulation of pyrite titrated with oxygen in the “Pure Water” solution.....	133
Figure 31: Simulation involving pyrite titration with oxygen and simultaneous calcite dissolution in the “Pure Water” solution.....	134
Figure 32: Simulation of pyrite titrated with oxygen in the “Surficial” solution .....	135
Figure 33: Simulation involving pyrite titration with oxygen and simultaneous calcite dissolution in the “Surficial Water” solution.....	136
Figure 34: Simulations of goethite titrated with DOC in the “Surficial Water” solution.....	140
Figure 35: Simulations involving goethite titration with DOC and simultaneous calcite dissolution in the “Surficial Water” solution .....	141
Figure 36: Measured and simulated dissolved-Fe concentrations graphed with increasing distance from Well T15 near Washington, NC.....	144
Figure 37: Impact of glauconite-abundance variations on dissolved-Fe concentrations along a simulated flow path in the UCHA .....	145
Figure 38: Results of the conservative-transport simulation. ....	147
Figure 39: Results of the reactive-transport simulation.....	150

## List of Common Symbols and Abbreviations

AAPD: Average of absolute-percent deviations

Ac: Exchangeable acidity

Ags/Cs: Aggregates/coatings

BS %: Percent base saturation

Ca<sub>e</sub>: Extractable calcium

CEC: Cation exchange capacity

CH<sub>2</sub>O: Organic matter

CHAS: Castle Hayne Aquifer System

CO<sub>2</sub>: Carbon Dioxide

Cu<sub>e</sub>: Extractable copper

CV %: Coefficient of variation or relative standard deviation

DOC: Dissolved-organic carbon

EDX: Energy-dispersive X-ray spectroscopy

Fe: Iron

Fe<sup>2+</sup>: Ferrous iron

Fe<sup>3+</sup>: Ferric Iron

ft BLS: Feet below the land surface

H<sub>2</sub>S: Hydrogen Sulfide

HM %: Percent humic matter

IDZ: Iron Depletion Zone

IPZ: Iron Pigmentation Zone

Iron-Oxyhydroxides: Largely refers to ferrihyrite, goethite, hematite, and lepidocrocite.

ISZ: Iron Sulfide Zone

K: Hydraulic conductivity

K<sub>e</sub>: Extractable potassium

LCHA: Lower Castle Hayne Aquifer

log K: Equilibrium constant

LOI: Loss on ignition

m BLS: meters below the land surface

Mg<sub>e</sub>: Extractable magnesium



Mn<sub>e</sub>: Extractable manganese

Na<sub>e</sub>: Extractable sodium

NC: North Carolina

NCAG: Soil Testing Division of the North Carolina Department of Agriculture

NCCP: North Carolina's Coastal Plain

NO<sub>3</sub><sup>-</sup>: Nitrate

O<sub>2</sub>: Oxygen

P<sub>e</sub>: Extractable phosphorous

RCL: Recommended concentration limit

S<sup>2-</sup>: Sulfide

S<sub>e</sub>: Extractable sulfur

SEM: Scanning electron microscopy

SO<sub>4</sub><sup>2-</sup>: Sulfate

*spp.*: Species

UCHA: Upper Castle Hayne Aquifer

Wt. %: Weight percent

W/V: Weight to volume

XRD: X-ray diffraction

XRF: X-ray fluorescence

Zn<sub>e</sub>: Extractable zinc

## 1.0 Introduction

Groundwater withdrawals from coastal plain aquifers have greatly increased over the last 30 years in eastern North Carolina (NC). Population growth, in conjunction with industry and farming, is driving higher demand for groundwater resources. Overpumping of Cretaceous aquifers in North Carolina's Coastal Plain (NCCP) has caused regional water-level decline, aquifer dewatering, and saltwater intrusions (Campbell and Coes, 2010). As a result, municipal water suppliers are becoming more dependent on the higher yielding, Tertiary, Upper Castle Hayne Aquifer to accommodate accelerating groundwater consumption (Fine and Kuniandy, 2014). The Upper Castle Hayne Aquifer is one of the most productive and most extensively developed aquifers in NCCP; however, localized zones containing high, dissolved-iron concentrations are present near the recharge area (Figure 1; Sutton and Woods, 1995; Woods et al., 2000).

Excessive iron (Fe) concentration in coastal plain groundwater is a common and expensive water-quality problem faced by municipal water suppliers. Although Fe in drinking water may not be harmful to human health, Fe concentrations exceeding the secondary drinking-water standard (0.3 mg/L) adversely affect aesthetic properties of drinking water (USEPA, 2012). High-dissolved Fe may stain exposed chattels and fixtures, induce unpleasant tastes and odors, and damage various components in the water distribution system. Additionally, Fe-rich groundwater frequently contains microorganisms that elevate dissolved-Fe concentrations and diminish the specific capacity of wells (Brown et al., 1999; Chapelle, 2001; Houben, 2003).

The evolution of these high-Fe zones in the Upper Castle Hayne Aquifer is poorly understood. This study evaluates likely relationships among mineralogical, chemical, and hydrological components to elucidate multifaceted mechanisms that are involved in the

formation and distribution of high-Fe zones in the Upper Castle Hayne Aquifer. Specifically, this investigation integrates mineral geochemistry, mineralogy, sedimentology, and geochemical groundwater modeling techniques to identify potential sources and sinks of dissolved Fe near Washington, NC (Figures 1 – 3).



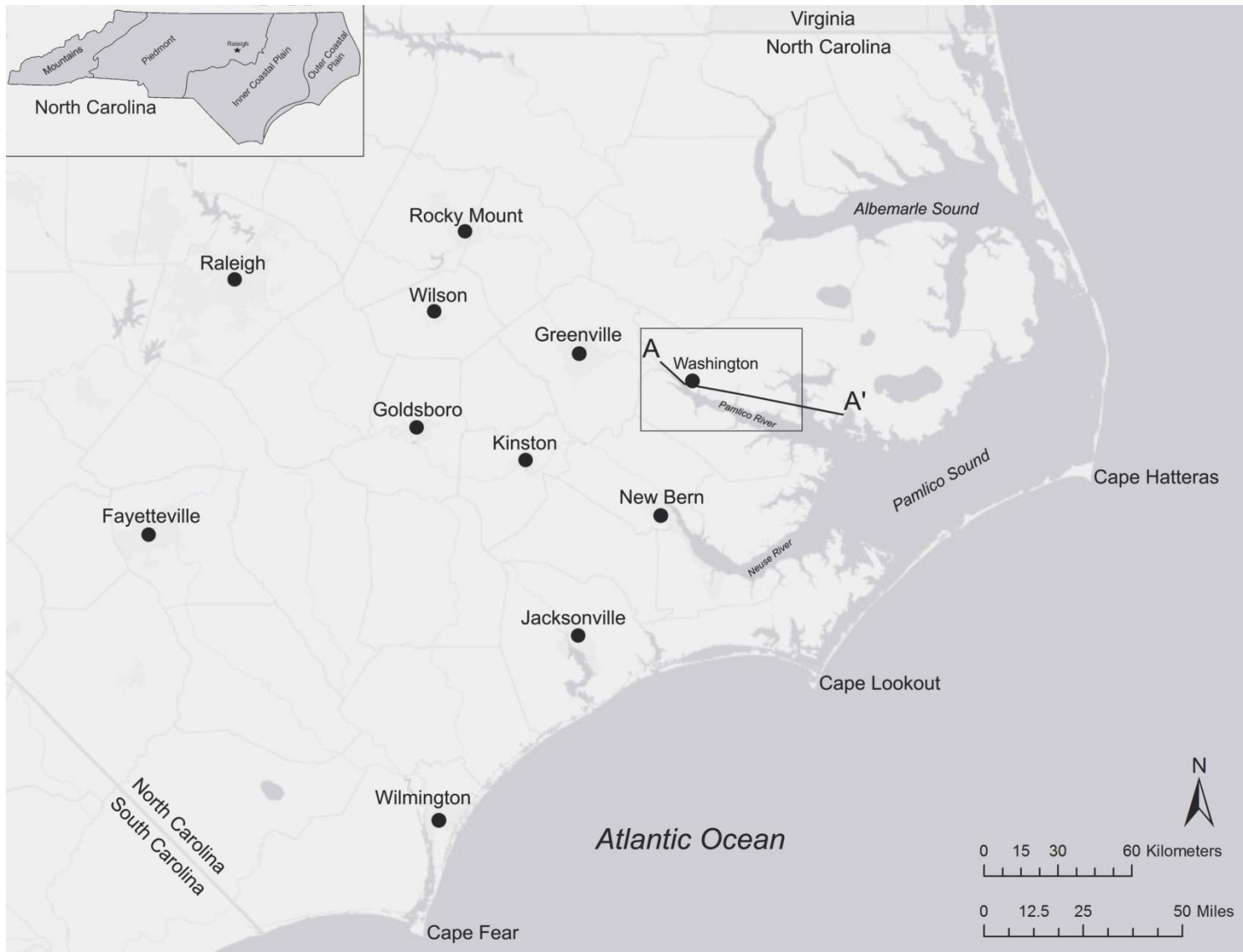


**Figure 2:** Location of the study area in eastern North Carolina. The line of section corresponds to the hydrogeologic cross-section shown in Figure 4.

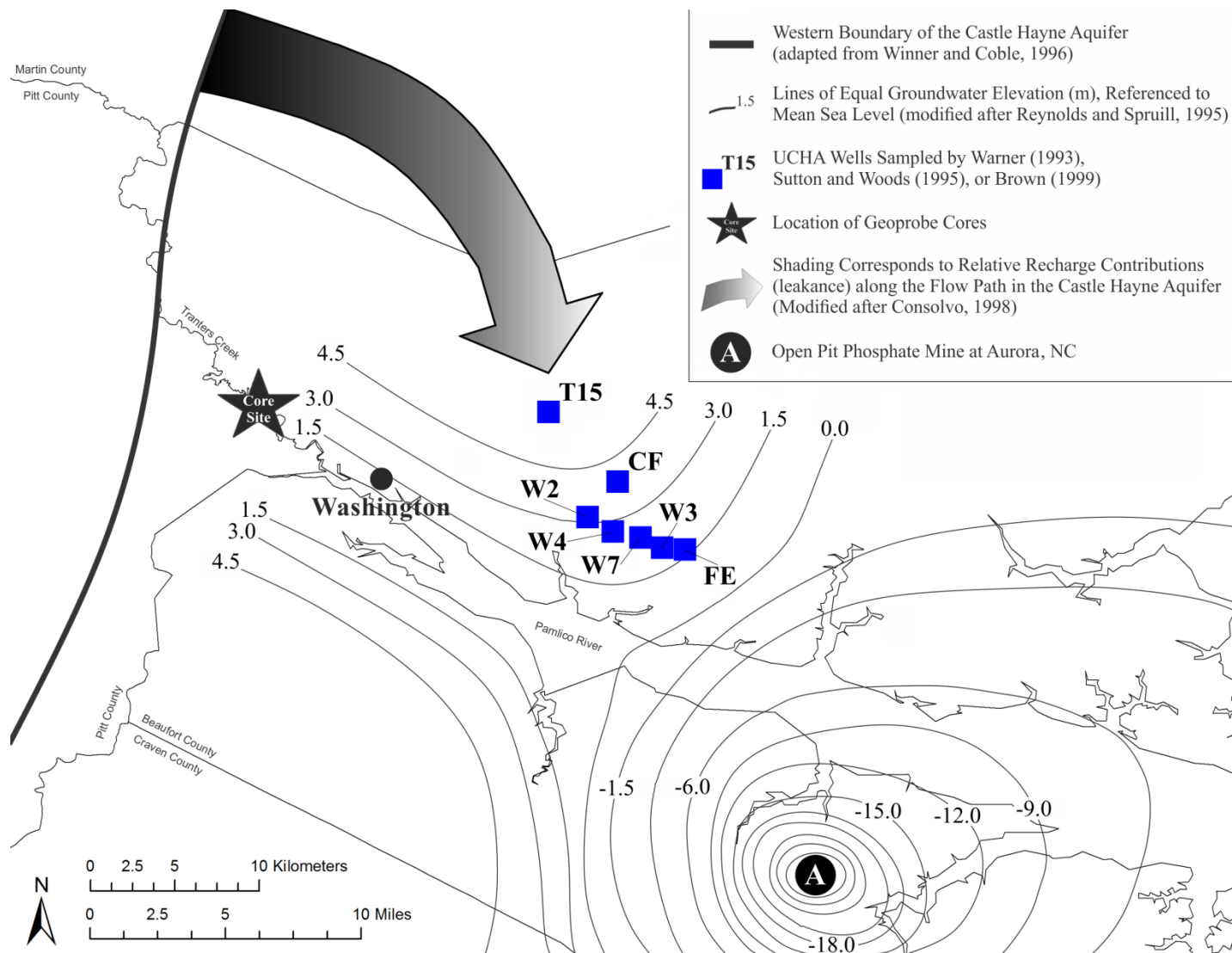


**Figure 3:** 1992 observed potentiometric surface map of the UCHA (modified after Reynolds and Spruill, 1995 and Consolvo, 1998). The core site (black star) and modeled well locations (blue squares) are located near Washington, NC.

## 1.2 Geologic and Hydrogeologic Framework

North Carolina's Coastal Plain covers approximately 65,000 km<sup>2</sup> and extends eastward from the fall line to the Atlantic Ocean (Figures 1 – 2) (Giese et al., 1987). The coastal plain in NC consists of a wedge-shaped sequence of Cretaceous to Quaternary age sediments that dip and thicken toward the southeast. The sediments unconformably overlie Paleozoic basement rocks, which consist of igneous and metamorphic rocks (Lautier, 2009). In western Beaufort County, the sediments are approximately 365 m thick, consisting of locally discontinuous layers and lenses composed of variable proportions of limestone with marine fossils, gravel, sand, silt, and clay (Giese et al., 1987; Lautier, 2009). The sedimentary deposits have been divided into geologic units according to their stratigraphic, lithologic, and fossil characteristics. Listed from oldest to youngest, the principal formations underlying the study area are: the Cretaceous, Beaufort, Lower Castle Hayne, Upper Castle Hayne, Pungo River, Yorktown, and surficial units (Table 1 and Figure 4; Giese et al., 1987; Winner and Coble, 1996; Lautier, 2009). Figure 4 shows the formations underlying the study area along a west-east transect (A – A') through the investigated area (Figure 2). Although a recent analysis of NCCP hydrostratigraphy combines the Pungo River aquifer with the Castle Hayne Aquifer (Campbell and Coes, 2010), these Tertiary aquifers are treated as separate hydrostratigraphic units in Table 1 and Figure 4.

The highest yielding and most productive aquifer in NCCP is the Castle Hayne Aquifer System (CHAS). The CHAS ranges in thickness from 9 m or less in western Beaufort County to over 330 m in the east (Giese et al., 1987; Lautier, 2009), where it extends beneath the Atlantic Ocean. The aquifer underlies the majority of NCCP, extending approximately 320 km from the middle of the southern border of Brunswick County to near the western border of Gates County

at the North Carolina-Virginia boundary. The western extent of the CHAS is located along eastern Pitt County and northwestern Beaufort County.

The CHAS includes the Oligocene Belgrade and River Bend Formations, the Eocene Upper Castle Hayne Limestone, the Eocene to Paleocene Lower Castle Hayne Limestone, and the Paleocene Beaufort Formation (Gamus, 1972; Lloyd and Daniel, 1988; Winner and Coble, 1996; Lautier, 2009). Transmissivity values of the CHAS generally increase toward the east (Trapp and Horn, 1997; Campbell and Coes, 2010). The CHAS is a limestone, consisting mostly of calcite, quartz sand, and glauconite with minor proportions of apatite, dolomite, feldspar, hematite, iron sulfides, and aluminosilicates (e.g. feldspars and zeolites). The dominant clay mineral is glauconite that typically occurs as well-rounded peloids. The abundance of glauconite is highest along the basal portion of the aquifer, and decreases in abundance from southwest to northeast. The average Fe content of glauconite decreases from southwest to northeast (Mehlhop et al., 2005).

Gamus (1972) subdivided the CHAS into three hydrogeologic units; Upper Castle Hayne Aquifer (UCHA), Lower Castle Hayne Aquifer (LCHA), and the Beaufort Aquifer. The Beaufort Aquifer is largely comprised of glauconitic sand and sandy limestone strata (Lautier, 2009). In the northern coastal plain, the UCHA is predominantly composed of moldic carbonates, principally calcite and some dolomite, while the LCHA is composed of calcareous sands interbedded with limestones (Gamus, 1972). Amsbaugh (1996) characterized the UCHA in the central coastal plain as a quartz-rich (40 – 60%), fossiliferous limestone, with minor glauconitic and phosphatic sand, whereas the LCHA is composed of a quartz-rich (20 – 60%), fossiliferous limestone, with minor glauconitic and phosphatic sand and lime mud. In western Beaufort



County, the UCHA consists of alternating layers of glauconite-rich sand and sandy, fossiliferous limestone (Johnson, 1992).

The UCHA, LCHA, and Beaufort subdivisions have hydraulic conductivity values of around 40 – 60, 1.5 – 6, and 0.6 – 2.4 m/d, respectively (Table 1; Reynolds and Spruill, 1995). The CHAS is underlain by the Cretaceous Peedee hydrogeologic unit, which is approximately 210 m thick and consists of fine -to coarse-grained, glauconitic and fossiliferous sands, and dark-gray micaceous clays (Lautier, 2009).

The Pliocene Yorktown and Quaternary hydrogeologic units overlie the CHAS. The Yorktown is largely composed of fine -to medium-grained shelly, clayey, bluish-gray sand with alternating beds of bluish-gray clay (Lautier, 2009). The undifferentiated Quaternary unit is the shallowest hydrogeologic unit and comprises the unconfined or “water table” aquifer. It is the first unit to receive recharge via infiltrating rainwater, which flows through the vadose zone to the water table. This unit is principally composed of Pleistocene -to Recent-age sand, silt, shells, and thin clay layers but it may also contain sands of the Yorktown Formation where the confining unit is situated at a lower position in the stratigraphic section (Lautier, 2009). Henceforth, the undifferentiated unit between the Yorktown and the ground surface is referred to as the surficial unit.

Generally, groundwater from the CHAS flows in a southeasterly direction and discharges into streams and the Atlantic Ocean (Sherwani, 1980; Lyke and Treece, 1988); however, groundwater withdrawals and leaky aquitards “can alter the natural flow direction of ground water, both horizontally and vertically” (Lyke and Treece, 1988, p. 472). For example, a large, phosphate-mining operation directs proximal groundwater flow toward Aurora, NC (Figure 3).

The majority of direct recharge to the CHAS occurs via rainfall in western portions of the study area where the CHAS is exposed or is overlain by highly permeable sandy sediments (Figure 1). Direct recharge largely occurs in swamps (called pocosins) that contain acidic, organic-rich, and nutrient-deficient sandy sediments (Reynolds and Spruill, 1995; Richardson, 2003). In the central coastal plain, average total rainfall is approximately 130 cm/yr and about 2.5 cm/yr or less percolates through the surficial aquifer to recharge the deeper aquifers (Lautier, 2009). DeWiest (1969) estimated that the area of direct recharge encompasses about 750 km<sup>2</sup> and roughly coincides with the subcrop pattern for the CHAS.

The confining units of the CHAS are composed of locally discontinuous clay and silt beds (Lautier, 2009; Campbell and Coes, 2010). As a result, leakance is a substantial component of recharge in certain areas of NCCP; the contribution of recharge derived from leakance generally increases from east to west across the study area (Figure 3; Warner, 1993; Consolvo, 1998; Campbell and Coes, 2010). In certain areas of NCCP, groundwater flows upward from the underlying Beaufort and Cretaceous aquifers to the Lower Castle Hayne Aquifer (Giese et al., 1997; Lautier, 2009). Although the confining units between the UCHA and LCHA are discontinuous, the lower hydraulic conductivity of the LCHA substantially inhibits water leaking upward into the UCHA from the underlying units (Mehlhop et al., 2005; Fine and Kuniatsky, 2014).

**Table 1:** Stratigraphic and hydrogeologic subdivisions (modified from Gamus, 1972; Lloyd and Daniel; 1988; Reynolds and Spruill, 1995; Winner and Coble, 1996; Consolvo, 1998).

System	Series	Stratigraphic Units	Hydrogeologic Units	Description	Hydraulic Conductivity	
Quaternary	Recent and Pleistocene	Undifferentiated Unnamed Unit	Surficial Unit	Sand, silt, shells, and clay	1 - 120 ft/d 0.3 - 36.6 m/d	
Tertiary	Pliocene	Yorktown Formation	Yorktown Unit	Interbedded silt, sand, and clay with some shell beds	1 ft/d 0.3 m/d	
	Miocene	Pungo River Formation	Pungo River Unit	Phosphate and quartz sand, silt, clay, and limestone	33 ft/d 10.1 m/d	
	Oligocene Eocene	Castle Hayne Formation	Castle Hayne Aquifer System	Upper Castle Hayne Unit	Well-indurated moldic limestone containing calcite, quartz, glauconite, and dolomite with interlayered calcareous sands	125 - 200 ft/d 38.1 - 61.0 m/d
				Lower Castle Hayne Unit	Shell limestone interbedded with calcareous sands	5 - 20 ft/d 1.5 - 6.1 m/d
	Paleocene	Beaufort Formation	Beaufort Unit	Fine glauconitic sand, silt, and clay	3 ft/d 0.9 m/d	
Cretaceous	Upper Cretaceous	Peedee Formation	Cretaceous Aquifer System	Peedee Unit	Interbedded clay, fine sand, and silt becoming calcareous in the Peedee	10 - 40 ft/d 3.0 - 12.2 m/d
		Black Creek Formation		Black Creek Unit		
		Cape Fear Formation		Cape Fear Unit		
	Lower Cretaceous	Unnamed Formation		Lower Cretaceous Unit		
Mesozoic-Precambrian Basement Complex						

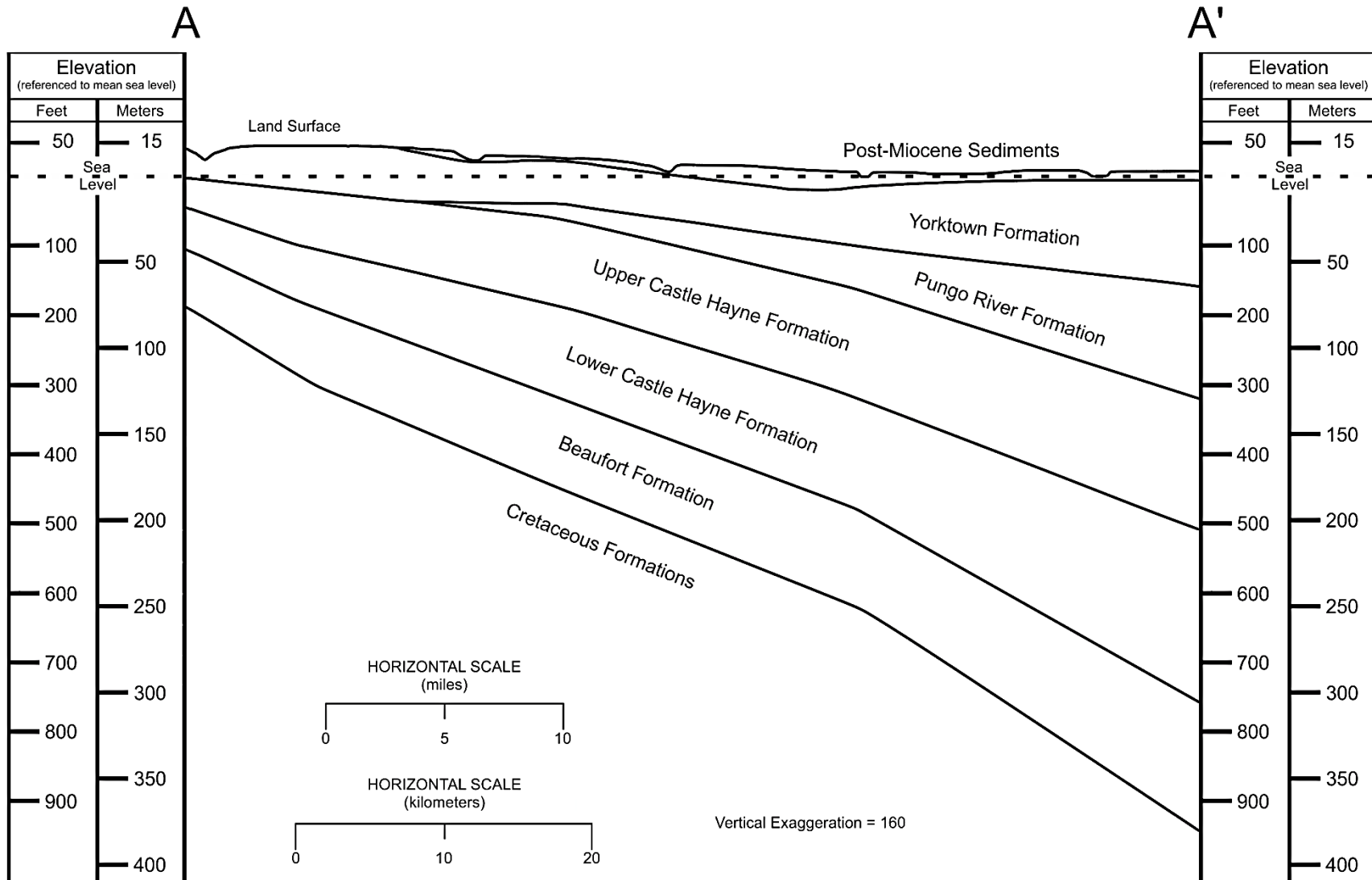


**Figure 4:** Hydrogeologic cross-section of NCCP (modified from Consolvo, 1998).

### 1.3 Iron Geochemistry

Under oxidizing and circumneutral conditions, iron generally exists in the relatively insoluble Fe(III) oxidation state ( $\text{Fe}^{3+}$ ). In coastal plain recharge zones (areas in which head decreases with increasing depth), near-surface sediments commonly contain abundant iron-oxyhydroxide minerals and grain coatings, which are believed to be important sources of high-dissolved iron in groundwater (e.g. Chapelle and Lovley, 1992; Penny et al., 2003; Park et al., 2006). Under circumneutral pH and reducing conditions, Fe typically occurs in the highly mobile Fe(II) oxidation state ( $\text{Fe}^{2+}$ ) (Johnson and Beard, 2006). Ferrous iron is the dominant species in natural groundwater systems that contain little to no dissolved oxygen ( $\text{O}_2$ ). Dissolution, precipitation, and cation-exchange reactions are the principal mechanisms by which Fe-bearing minerals and aqueous Fe species interact in the aquifer (Park et al., 2006; Lin et al., 2012; Stucki et al., 2012).

Basic concepts of cation exchange are illustrated in Figure 5. Cation-exchange reactions generally involve the transfer of cations between solid aquifer materials and the groundwater. These reactions can remove large quantities of Fe from groundwater (Faure, 1998; Park et al., 2006). Grains that have large surface areas (grain size  $<2 \mu\text{m}$ ), such as clays generally have a greater capacity to exchange dissolved Fe than coarser sediments (grain size  $>2 \mu\text{m}$ ). Where the aquifer matrix includes abundant clay and organic matter, the exchange capacity of the aquifer is generally high (Breeuwsma et al., 1986). Therefore, variations in clay content and organic carbon may be important controls on Fe concentrations in the UCHA and in overlying aquifers.

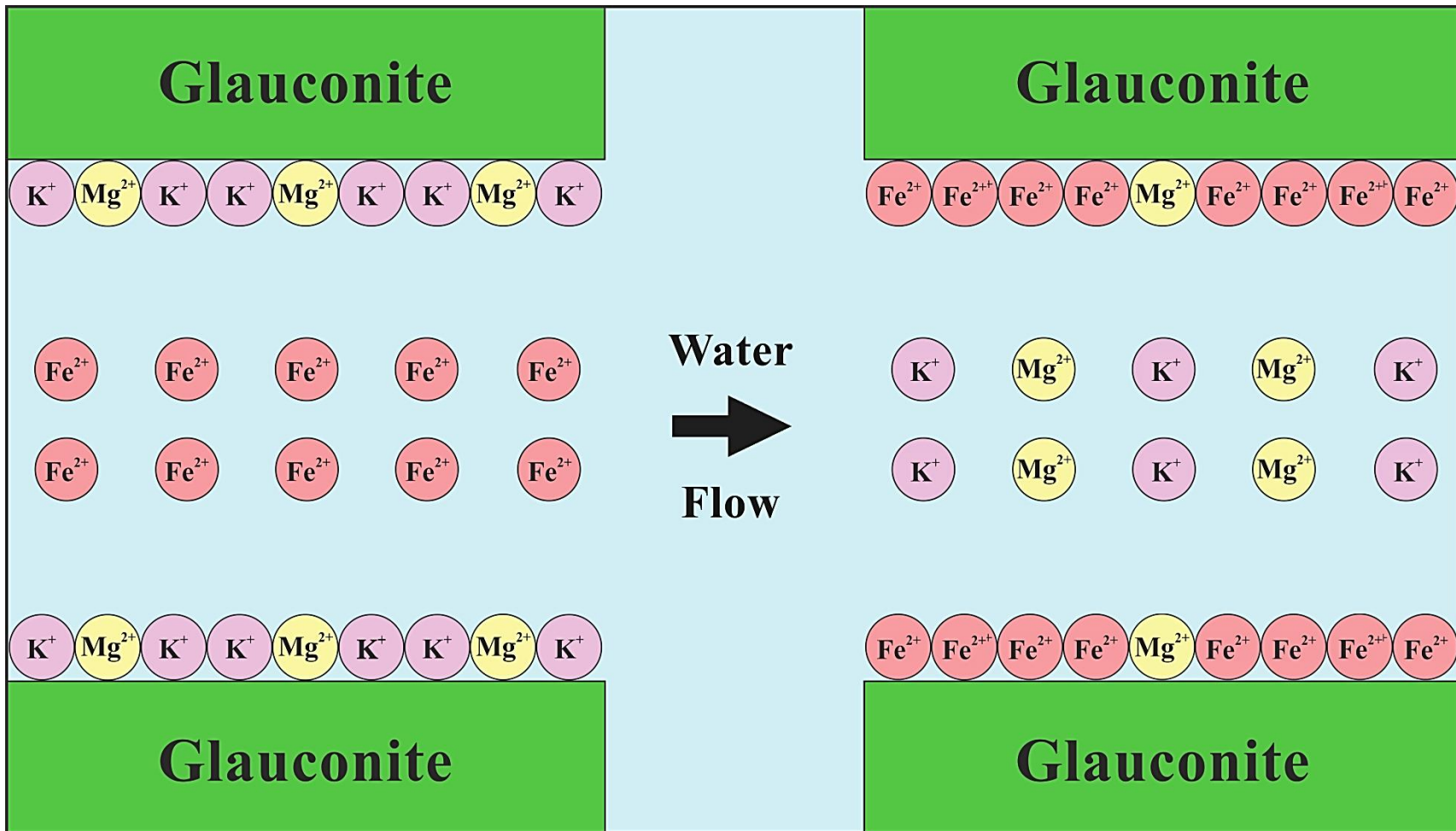


**Figure 5:** Illustration of cation exchange in a glauconitic aquifer. Each  $\text{Fe}^{2+}$  ion in an aqueous solution can exchange with two  $\text{K}^+$  ions or one  $\text{Mg}^{2+}$  ion on a clay-mineral surface (left) such as glauconite, resulting in lower  $\text{Fe}^{2+}$  concentration and increased  $\text{K}^+$  and  $\text{Mg}^{2+}$  concentrations in solution (right).

## 1.4 Iron Biogeochemistry

Both abiotic and microbially mediated reactions can readily oxidize or reduce Fe species in aquifers, depending on physicochemical conditions. Although many redox processes were previously assumed to occur entirely by abiotic reactions (e.g. Zehnder and Stumm, 1988), numerous studies demonstrate that abiotic and microbially mediated reactions involving Fe are inseparable under natural conditions (e.g. Lovely and Goodwin, 1988; Chapelle and Lovely, 1992; Nealson and Saffarini, 1994; Stucki et al., 2012; Ionescu et al., 2015; Melton et al., 2014). Most Fe-related reactions in sediments are mediated or influenced by microorganisms, which are ubiquitous in most aquifers. Some exceptions include Fe<sup>2+</sup> oxidation under highly alkaline conditions, hydrolysis of Fe<sup>3+</sup> during the formation of iron-oxyhydroxides, and Fe reactions involving ion exchange (Stucki et al., 2012).

Diverse microorganisms are known to derive metabolic energy by Fe-redox reactions. Biotic Fe oxidation is carried out by microaerophiles (e.g. *Gallionella spp.*, *Leptothrix spp.*, *Mariprofundus spp.*, and *Sideroxydabs spp.*) and nitrate-reducing bacteria (e.g. *Acidovorax spp.* and *Thiobacillus denitrificans*) that utilize oxygen and nitrate, respectively to oxidize Fe<sup>2+</sup> to Fe<sup>3+</sup> (Melton et al., 2014). Iron-oxidizing microorganisms can be problematic for municipal water suppliers because they produce aggregates of weakly soluble, Fe-oxide compounds (typically ferrihydrite or lepidocrocite) that can clog well systems (Table 2: Houben, 2003; Stucki et al., 2012; Melton et al., 2014). Microbially mediated, Fe reduction involves the oxidation of organic compounds, hydrogen, or ammonium and the simultaneous reduction of Fe<sup>3+</sup>, which releases dissolved Fe<sup>2+</sup> and frequently results in high-Fe groundwater. Common Fe-reducing microbes in aquifer systems include *Geobacter spp.*, *Shewanella spp.*, *Albidoferax ferrireducens*, and *Geothrix spp* (Melton et al., 2014).

Coastal plain aquifers frequently develop a series of localized biogeochemical zones where the reduction of electron acceptors typically proceeds from highest to lowest energy yield along aquifer-flow paths (Figure 6; Chapelle and Lovley, 1992; Stumm and Morgan, 1996; Brown et al., 1999; McMahon and Chapelle, 2008). As water percolates through Fe-rich and organic-rich sediments in the recharge zone, microbial processes such as fermentation and aerobic respiration consume dissolved O<sub>2</sub> as organic matter is broken down to more reactive compounds that can readily transfer electrons to available electron acceptors via redox reactions (Park et al., 2006). Near the surface, the dominant redox processes affecting groundwater chemistry commonly involve abiotic and microbially catalyzed oxidation of organic matter and simultaneous reduction of dissolved O<sub>2</sub>. Subsequently, microbial activity and increasing isolation from the atmosphere deplete dissolved O<sub>2</sub> downgradient from the recharge zone. As the groundwater approaches anoxia, other available electron acceptors oxidize organic matter (Brown et al., 1999). In order of favorability, other naturally occurring oxidizers in groundwater include nitrate (NO<sub>3</sub><sup>-</sup>), manganese(IV) (Mn<sup>4+</sup>), Fe<sup>3+</sup>, sulfate (SO<sub>4</sub><sup>2-</sup>), and carbon dioxide (CO<sub>2</sub>) (McMahon and Chapelle, 2008). Although the rate of abiotic reduction of these species by organic matter is generally very slow, microorganisms can significantly increase the rate of redox reactions, especially those involving the reduction of Fe<sup>3+</sup> (Stucki et al., 2012).



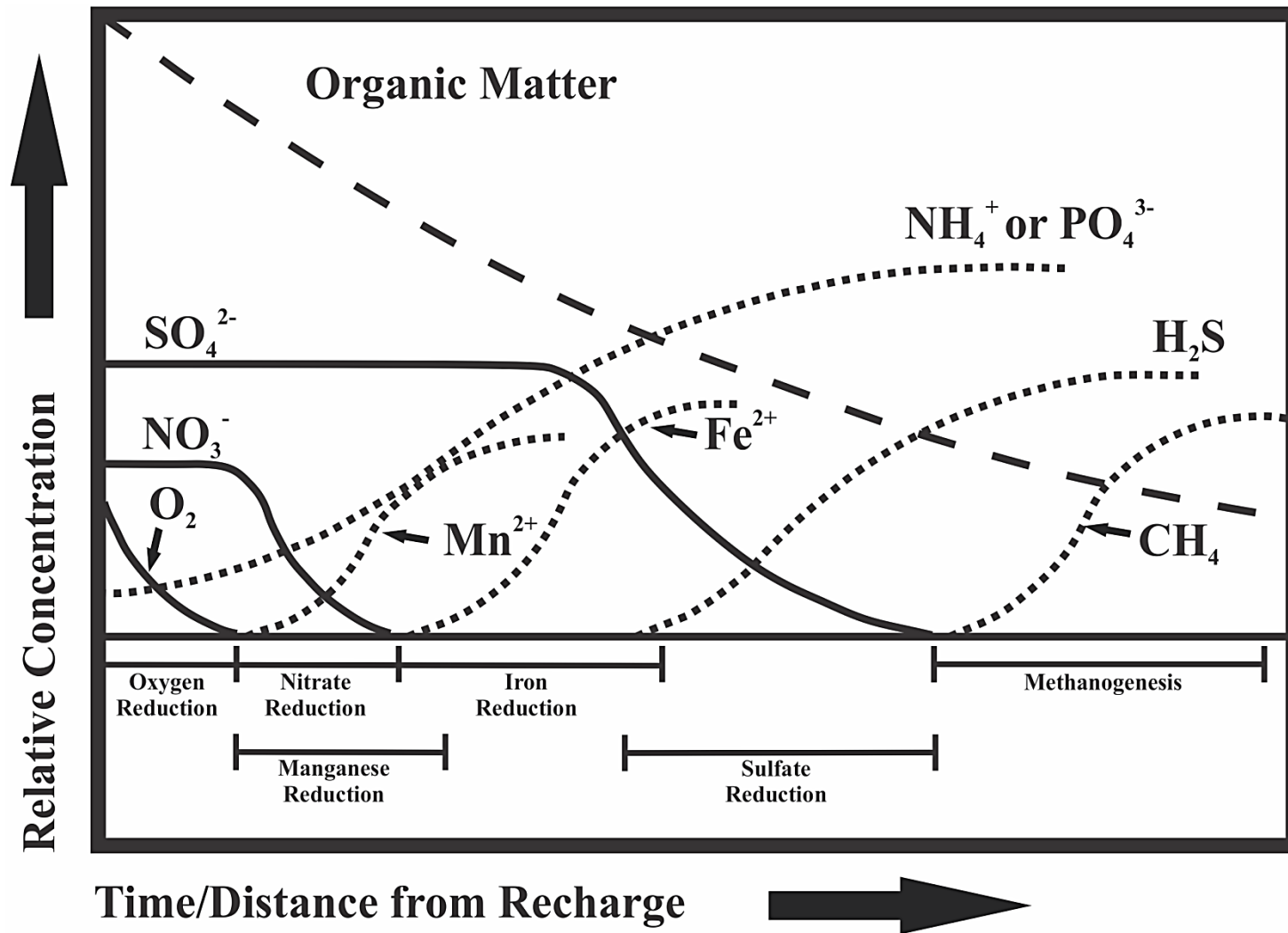
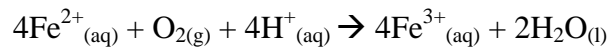


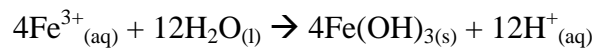
**Figure 6:** Relative concentrations of redox-related constituents in groundwater with increasing distance from the recharge zone (modified from Wiedemeier, 1999). Note that the concentrations are associated with the typical sequence of terminal electron-accepting processes in an aquifer.

## 1.5 Formation and Characteristics of Common Iron-Oxyhydroxides

Typical characteristics and necessary conditions of formation for common iron-oxyhydroxide minerals are summarized in Table 2. The weathering of Fe-bearing minerals releases either Fe<sup>2+</sup> or Fe<sup>3+</sup> from mineral surfaces. In near-surface, oxygenated environments, Fe<sup>2+</sup>-containing minerals such as ilmenite, amphiboles, and pyroxenes are unstable (Curtis, 1976). Dissolved Fe<sup>2+</sup> may migrate elsewhere in the sediment column as a complexed species or remain in its reduced form in an oxygen-deficient environment. In the presence of O<sub>2</sub>, the Fe<sup>2+</sup> may oxidize rapidly to Fe<sup>3+</sup>:



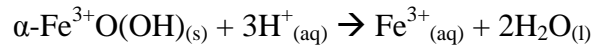
The time required for about 90% of uncomplexed Fe<sup>2+</sup> to oxidize can range from about 30 seconds at pH 8 to several weeks at pH 6 (Vance, 1994). After Fe<sup>3+</sup> is released by mineral dissolution or Fe<sup>2+</sup> oxidation in saturated sediments, most of the dissolved Fe<sup>3+</sup> undergoes hydrolysis and precipitates as an amorphous, iron-oxyhydroxide compound represented by Fe(OH)<sub>3</sub>:



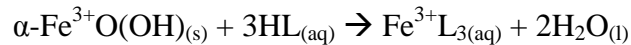
Over time, the atomic arrangement of the iron-oxyhydroxide becomes increasingly ordered, resulting in progressive mineralization. During the mineralization process, the surface area and solubility of ferric hydroxide decrease while the degree of crystallization increases, resulting in the formation of an iron-oxyhydroxide crystallite over time (Vance, 1994). The size of individual iron-oxyhydroxide crystals usually ranges between 10 and 100 nm. As a result of their extremely small size, iron-oxyhydroxides can comprise the majority of a sediment's total surface area, even at proportions of only a few percent (Stucki et al., 2012).

In decreasing order of solubility and increasing order of crystallinity, common iron-oxyhydroxide minerals include ferrihydrite ( $[\text{Fe}^{3+}]_2\text{O}_3 \cdot x\text{H}_2\text{O}$ ), lepidocrocite ( $\gamma\text{-Fe}^{3+}\text{O}[\text{OH}]$ ), hematite ( $\text{Fe}^{3+}_2\text{O}_3$ ), and goethite ( $\alpha\text{-Fe}^{3+}\text{O}[\text{OH}]$ ), which are reddish brown, bright orange, bright red, and yellowish brown to dark-orangish brown, respectively (Vance, 1994; Montes-Hernandez et al., 2011). Under oxic and circumneutral conditions, iron-oxyhydroxide minerals are weakly soluble. For example, the solubility of ferrihydrite is around 0.6  $\mu\text{g/L}$ , which is 3 or 4 orders of magnitude greater than that of goethite, depending on crystallinity variations (Vance, 1994; Stucki et al., 2012).

Once formed, three principal processes can result in the dissolution of iron-oxyhydroxides under natural conditions. In increasing order of effectiveness, these dissolution processes include protonation, complexation, and reduction by organic-matter oxidation. Protonation of goethite, for example, releases soluble  $\text{Fe}^{3+}$  (Stucki et al., 2012):



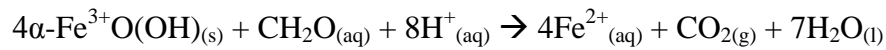
However, this process is not expected to be a significant dissolution process at the study area because protonation is ineffective under slightly acidic conditions. In the presence of organic compounds (e.g. humic acid, fulvic acid, and tannic acid), complexation can dissolve iron-oxyhydroxides to produce soluble  $\text{Fe}^{3+}$ -organic complexes:



where L in the above reaction represents organic ligands (L) (Stucki et al., 2012). Ligands are atoms or molecules that have unshared valence electrons that temporarily bind to a central-metal atom through coordinate-covalent bonding (Faure, 1998). Both  $\text{Fe}^{2+}$  and  $\text{Fe}^{3+}$  can form complexes but the major abiotic process resulting in significant dissolution of  $\text{Fe}^{3+}$  in most circumneutral groundwaters is for it to complex with organic ligands. Iron complexes can

increase the mobility of Fe because they usually react more slowly during redox reactions (Stucki et al., 2012).

Although complexation may enhance the dissolution of iron-oxyhydroxides, microbially mediated  $\text{Fe}^{3+}$  reduction is a much more significant dissolution process in most aquifers. In low-oxygen groundwater, respiring microorganisms catalyze  $\text{Fe}^{3+}$  reduction by organic-matter oxidation (represented by  $\text{CH}_2\text{O}$ ), resulting in the relatively rapid release of soluble  $\text{Fe}^{2+}$  (Stucki et al., 2012):



Goethite is the most frequently occurring iron-oxyhydroxide. It is predominantly formed in temperate regions via precipitation in oxic groundwater or by aging of ferrihydrite over time. Hematite is the second most common iron-oxyhydroxide. Ferrihydrite is a necessary precursor for the formation of hematite which typically occurs in warm climates such as the tropics and subtropics. Hematite development is dependent on the alteration of ferrihydrite where the abundance of organic matter is low or nonexistent. Lepidocrocite is derived from the oxidation of  $\text{Fe}^{2+}$  and is frequently associated with goethite in non-calcareous sediments. Ferrihydrite is a common iron-oxyhydroxide, consisting of a poorly ordered to amorphous structure. It forms in organic-rich sediments where  $\text{Fe}^{2+}$  is rapidly oxidized (Stucki et al., 2012). In well-crystallized samples, common morphologies for iron-oxyhydroxides are needles or lathes for goethite, rhombohedra or hexagonal plates for hematite, needles, lathes, or elongated plates for lepidocrocite, and spheres for ferrihydrite (Cornell and Schwertmann, 2003; Stucki et al., 2012).

**Table 2:** Formation and characteristics of common iron-oxyhydroxide minerals in sediments (Vance, 1994; Montes-Hernandez et al., 2011; Stucki et al., 2012).

<b>Mineral Name</b>	Ferrihydrite	Goethite	Hematite	Lepidocrocite
<b>Formula</b>	$(\text{Fe}^{+3})_2\text{O}_3 \cdot \text{XH}_2\text{O}$	$\alpha\text{-Fe}^{3+}\text{O}(\text{OH})$	$\text{Fe}^{3+}_2\text{O}_3$	$\gamma\text{-Fe}^{3+}\text{O}(\text{OH})$
<b>Crystal System</b>	Hexagonal	Orthorhombic	Trigonal	Orthorhombic
<b>Usual Crystal Shape</b>	Spheres	Needles, Laths	Hexagonal Plates, Rhombohedra	Laths, Needles
<b>Color</b>	Reddish Brown	Yellowish Brown	Bright Red	Bright Orange
<b>Occurrence and Formation</b>	Rapid oxidation in humic environments	Most frequently occurring Fe-oxide in soils and forms wherever weathering takes place	High soil temperature, well-drained soils, high Fe-release rate from rocks	Mostly anaerobic, non-calcareous systems
<b>Soils</b>	Wet soils	All soils with Fe release	Aerobic soils of the tropics and subtropics	Saturated soils under reducing conditions in temperate regions
<b>Additional Characteristics</b>	Typically indicates recent formation or that conditions are not favorable for crystal growth	Most frequently occurring iron-oxyhydroxide in soil	Formation only occurs via ferrihydrite alteration where little organic matter is present	Forms from slow oxidation of $\text{Fe}^{2+}$

## 1.6 Previous Work

The geochemistry of UCHA water is largely controlled by the dissolution of aquifer materials, groundwater leakage from overlying aquifers and surface waters, groundwater mixing along the saltwater/freshwater interface, and exchange with aquifer minerals (Sutton and Woods, 1995; Woods et al., 2000). According to Giese et al. (1997), CHAS water is hard (120 – 180 mg/L) to very hard (>180 mg/L). Hardness is attributed to the release of calcium ( $\text{Ca}^{2+}$ ) and magnesium ( $\text{Mg}^{2+}$ ) ions during the dissolution of limestone and dolomite (Wilder et al., 1978). The hardness is lower near recharge areas and increases with residence time in the aquifer (Giese et al., 1987). In the western portion of NCCP, carbonate dissolution enriches groundwater with  $\text{Ca}^{2+}$  and bicarbonate ( $\text{HCO}_3^-$ ). In the eastern coastal plain, groundwater mixing near heavily pumped regions increases the alkali metal and chloride content in the UCHA (Sutton and Woods, 1995). Ion-exchange reactions are prevalent throughout NCCP but the associated geochemical processes are complex and spatially variable (Woods et al., 2000). CHAS water has a median dissolved-solids concentration of 300 mg/L and a median pH of 7.3 (Lloyd and Daniel, 1988). UCHA pH values near Washington, NC are circumneutral, ranging from 6.9 to 7.3 (Sutton and Woods, 1995; Woods et al., 2000).

Sulfide ( $\text{S}^{2-}$ ) concentrations are typically very low; those in western portions of the UCHA were generally lower than in eastern wells. The mean  $\text{S}^{2-}$  concentration in LCHA waters is generally higher than in the UCHA waters. High  $\text{S}^{2-}$  concentrations can be indicative of bacterial reduction of  $\text{SO}_4^{2-}$ ; however,  $\text{S}^{2-}$  is probably removed rapidly from solution via the reaction with  $\text{Fe}^{2+}$  to produce Fe sulfides (Woods et al., 2000).

High dissolved-Fe concentrations characterize the UCHA. Regionally, Fe concentrations are highest in the east and decrease downgradient (Figure 1). They drop sharply near

Washington, NC but fall more gradually between Jacksonville and New Bern (Woods et al., 2000). Consolvo (1998) indicates that dissolved Fe near Washington decreases downgradient by >6 mg/L in less than 5.2 km. Groundwater from wells in Onslow County has a median Fe concentration of 1.1 mg/L (Amsbaugh, 1996). Fe concentrations frequently exceed the North Carolina Maximum Contaminant Level of 0.3 mg/L (Giese et al., 1987).

Johnson (1992) evaluated water quality parameters for groundwater samples collected from a shallow well 2.7 – 3.7 m below the land surface (m BLS), an intermediate well 5.3 – 6.9 m BLS and two deep wells 15.2 – 24.4 m BLS at the Tranters Creek core site (Table 3 and Figure 3). The shallow well likely tapped the surficial aquifer, the screen at the intermediate well may have traversed both the surficial and the Yorktown aquifers, and the deep wells were screened in the UCHA. The manganese (Mn) concentration in the shallow well was 0.14 mg/L, which exceeded the recommended concentration limit (RCL) of 0.05 mg/L for secondary contaminants. Both the shallow and intermediate wells were acidic with pH values of 5.0 and 6.3, respectively. pH values, measured at the deep wells, were 7.8 and 7.9, which is within the RCL range of 6.5 to 8.5. All of the wells sampled exceeded the RCL for dissolved Fe (Johnson, 1992).

Although few studies have examined dissolved Fe in the UCHA, some ideas have been presented to explain why Fe concentrations peak near the recharge zone and rapidly decrease from west to east. Wilder et al. (1978) believed that Fe concentrations are highest near the recharge zone because Fe entering the aquifer has not had enough time to precipitate. Woods et al. (2000) proposed several additional hypotheses regarding Fe trends in the UCHA:

- 1) high-Fe concentrations along the western portion of the CHAS likely originate from acidic recharge waters reducing iron-oxyhydroxide compounds that are present in surficial sediments where microorganisms reduce  $\text{Fe}^{3+}$  to  $\text{Fe}^{2+}$  in anaerobic environments,
- 2) leaky confining beds may supply oxygen to the groundwater and cause dissolved Fe to precipitate in certain areas of the NCCP,
- 3) cation-exchange reactions may quickly deplete ferrous Fe as other cations (sodium,  $\text{Mg}^{2+}$ , and  $\text{Ca}^{2+}$ ) are released into solution,
- 4) groundwater reactions with aquifer carbonates raise pH and precipitate Fe, and
- 5) the composition and thickness of the overlying units through which recharge waters percolate may control Fe concentrations in groundwater.



**Table 3:** Water quality data for secondary drinking water regulations measured by Johnson (1992) at the Tranters Creek core site.

Constituent <sup>1</sup>	Shallow Well <sup>2</sup>	Intermediate Well <sup>3</sup>	Deep Well 1 <sup>4</sup>	Deep Well 2 <sup>4</sup>	RCL
Total Dissolved Solids	50	94	530	450	500
Chloride	5	2	92	68	250
Sulfate	8	9	20	14	250
Nitrate	0.01	0.01	0.01	<.1	10
Iron	2.3	13	1.2	0.68	0.3
Manganese	<0.025	0.14	<0.025	0.03	0.05
Copper	<0.01	<0.01	<0.01	<0.01	1
Zinc	<0.01	0.039	0.015	<0.01	5
Boron	ND <sup>5</sup>	ND <sup>5</sup>	ND <sup>5</sup>	ND <sup>5</sup>	1
Sulfide	ND <sup>5</sup>	<0.1	<0.1	<0.1	6
pH	5	6.3	7.9	7.8	6.5 – 8.5

1. Water quality data (concentrations are in mg/L) for secondary drinking-water regulations (Johnson, 1992)

2. Depth range is 2.7 – 3.7 m BLS

3. Depth range is 5.3 – 6.7 m BLS

4. Depth range is 15.2 – 24.4 m BLS

5. ND: Not detected

## **1.7 Hypothesis and Objectives**

### **1.7.1 Hypothesis**

Localized, Fe-rich groundwater zones reflect a variety of geochemical and hydrogeologic processes along CHAS flow paths. High-Fe concentrations measured in the UCHA are likely derived from overlying aquifers where the oxidation of dissolved organic carbon and concurrent, microbially catalyzed reduction of iron-oxyhydroxide compounds enriches the UCHA recharge water with dissolved-Fe<sup>2+</sup>. Once the iron-enriched-recharge water enters the UCHA, dissolved Fe likely interacts with glauconite in the UCHA via cation-exchange reactions, resulting in the rapid depletion of dissolved Fe over a relatively short distance along the UCHA flow path.

### **1.7.2 Objectives**

The primary objective of this investigation is to elucidate the origin and geochemical evolution of high-ferrous-iron zones in the UCHA by examining the mineralogical, geochemical, and sedimentological characteristics of sediment cores acquired in western Beaufort County. This objective was addressed through a specific set of subobjectives that included the determination of the:

1. major Fe-bearing minerals in the sediments overlying the UCHA,
2. potential of the identified Fe-containing minerals to yield high dissolved-Fe concentrations,
3. effect of variations in sediment geochemistry and sedimentological composition on the precipitation, retention, and dissolution of iron-oxyhydroxide compounds, and
4. capacity of cation-exchange to explain the rapid, downgradient depletion of dissolved Fe in the UCHA near Washington, NC.

## 2.0 Study Area

Beaufort County is situated in the inner coastal plain of North Carolina and is included within the Central Coastal Plain Capacity Use Area, which includes Beaufort, Carteret, Craven, Duplin, Edgecombe, Green, Jones, Lenoir, Martin, Onslow, Pamlico, Pitt, Washington, Wayne, and Wilson counties. A capacity use area is a region where the use of water resources exceeds, or threatens to surpass, the replenishment rate of the resource in a manner that necessitates water use regulation. Within this area, a state permit is required to withdraw more than 380 m<sup>3</sup>/day from groundwater or surface water resources (NCDENR, 2008).

Two Geoprobe cores were collected at a field area near the western end of the CHAS recharge zone in western Beaufort County (Figures 1 – 3). The field area is located about 1.6 km south of U.S. Highway 264, around 8 km northwest of Washington, NC, and adjacent to Tranters Creek. Tranters Creek encompasses the site to the west (~46 m), to the south (365 m), and to the east (440 m). A small tributary of Tranters Creek is located about 285 m to the north of the core site (Figure 7). Elevations across the field area range from less than 1.5 m above mean sea level along the creek to over 7.6 m northeast of the core site. The location of the study area was selected due to the site's proximity to the western extent of the CHAS recharge boundary where previous investigators have reported the presence of high-dissolved-Fe zones (Wilder et al., 1978; Sutton and Woods, 1995; Brown, 1999; Woods et al., 2000.). In addition, the Tranters Creek field area was chosen because Johnson (1992) provided the following information:

1. the depth of the upper contact of the UCHA is shallow enough to permit the collection of core samples near the UCHA contact using East Carolina University's truck-mounted, Geoprobe-coring equipment;

2. essential hydrologic information such as groundwater-flow patterns and aquifer characteristics;
3. and his investigation included groundwater chemistry data for selected depths in the UCHA and in the overlying aquifers.

According to Johnson (1992)'s one-year investigation, the depth of the free water table surface ranges from about 0.9 to 2.2 m BLS but is generally less than 1.5 m BLS in the area encompassing the core site. Tranters creek and the small tributary north of the core site (Figure 7) are likely recharge boundaries (aquifer boundaries that contribute water to the aquifer) or discharge areas (an area in which hydraulic head increases with increasing depth) for the underlying aquifers. A hydraulic connection exists between the UCHA, surficial aquifer, and Tranters Creek. Under static conditions, groundwater in the aforementioned aquifers discharges into Tranters Creek; however, when the water-level elevation in Tranters Creek is higher than the elevation of the water table in the surficial aquifer, water in Tranters Creek likely recharges the surficial aquifer. The principal direction of groundwater flow in the UCHA and surficial aquifer is to the south and southwest, respectively. Groundwater also travels vertically from the UCHA to the surficial aquifer via a semi-pervious layer, which has a vertical hydraulic conductivity of  $3.6 \times 10^{-3}$  m/day (Johnson, 1992).

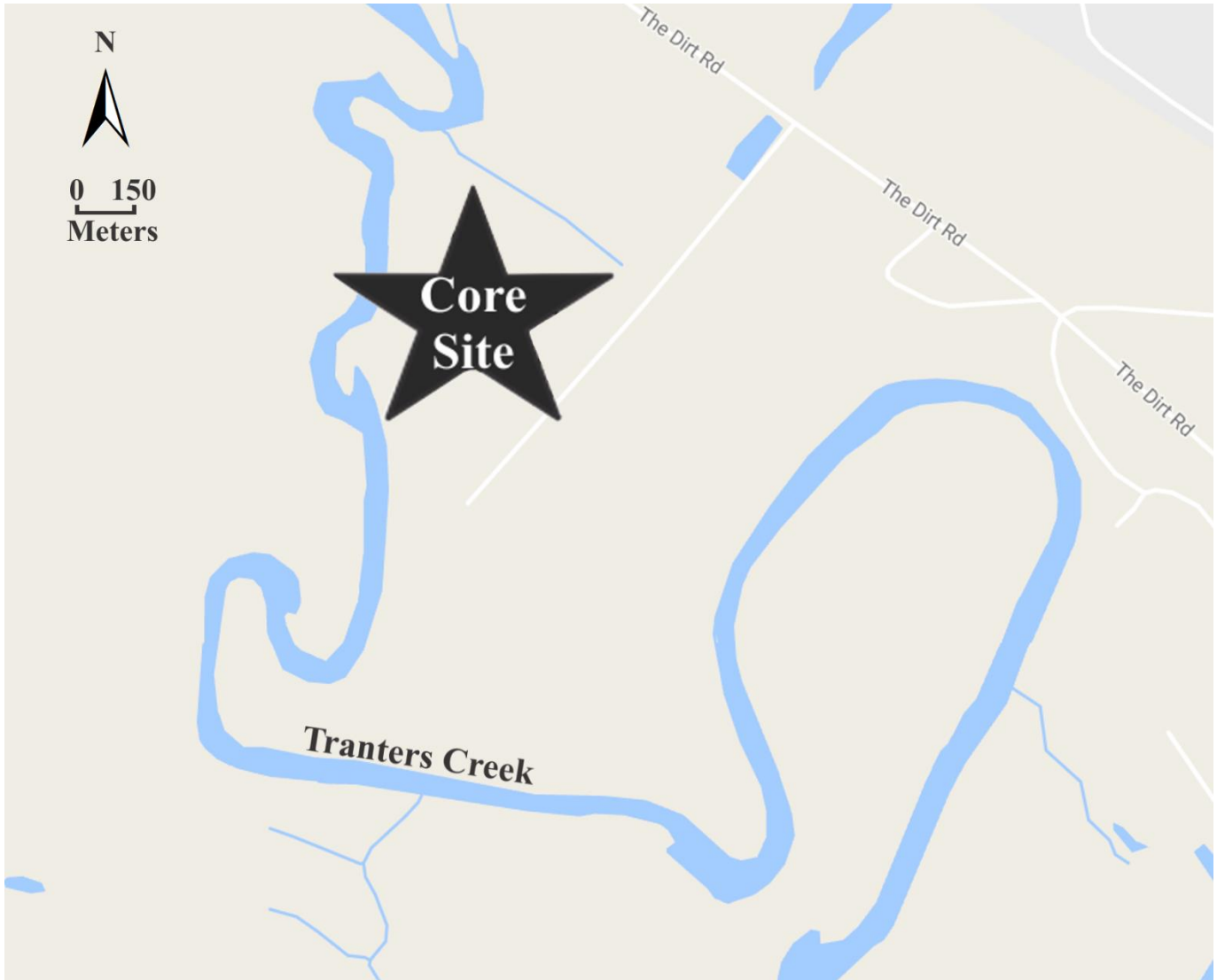


**Figure 7:** Map showing the location of the core site relative to Tranters Creek and the small tributary to the north of the core site, which are potential recharge boundaries or discharge areas to the underlying aquifers (Johnson, 1992).

### **3.0 Procedures**

Two spatially adjacent (a 0.6 m separation between the core locations), sediment cores were collected in the Tranters Creek field area. Subsamples from the first sediment core (TC14) were subjected to grain size, X-ray fluorescence, and loss on ignition analyses. Sediment samples from the second core (TC14C) were sent to the Sediment Testing Division of the North Carolina Department of Agriculture (NCAG) in Raleigh to compare with X-ray fluorescence results for selected nutrients and, to determine changes in sediment-water pH, cation-exchange capacity, exchangeable acidity, base saturation, and humic matter. The remaining portions of TC14C samples were magnetically separated and subsequently evaluated using X-ray diffraction, optical microscopy, and scanning electron microscopy/energy-dispersive X-ray spectroscopy. The analytical results from the sediment cores were used to identify minerals and possible sources of Fe in sediments overlying the UCHA. Finally, a geochemical modeling program (PHREEQC) was used to investigate potential sources of dissolved Fe in sediments overlying the UCHA and to determine if cation exchange is a plausible hypothesis explaining the rapid depletion of dissolved Fe in the UCHA. The methodologies are explained in the following subsections and detailed protocols are included in Appendix B.

#### **3.1 Core Acquisition and Processing**

On May 28 and July 9, 2014, a truck-mounted, direct push, hydraulic-sampling unit (Geoprobe) was used to acquire two sediment cores. Each core consisted of nine 1.2 m sections and included sediments from the ground surface to around 11 m BLS. A plastic cylinder, approximately 5 cm diameter and 1.2 m long, was placed in a 1.2 m-long, steel-core barrel and pneumatically hammered into the subsurface. Following insertion, the core-barrel assembly was extracted from the ground and the plastic tube containing the sediment sample was removed. The

sediment-sample tube was immediately capped with plastic endcaps, sealed with duct tape, and labeled with the core name and depth interval. Deeper samples were collected by attaching 1.2 m-long, outer-steel tubes to the core barrel assembly. Light-weight center rods were installed from the top of the uppermost outer tube to the bottom of the core barrel to prevent sediment from entering the plastic sample tube while hammering through previously cored depth intervals. After reaching the deepest part of the preceding core section, the inner rod was removed, permitting collection of the subjacent depth interval. Sediment cores were acquired at 1.2 m intervals until the drilling apparatus was not able to penetrate further into the ground. After the field work was completed, the Geoprobe cores were placed vertically (shallowest end facing upward) in a walk-in refrigerator until they were processed at the Department of Geological Sciences at East Carolina University.

The plastic sample tube was cut lengthwise for each 1.2 m core section to expose the collected sediment. Subsequently, the core sections were photographed, logged for lithologic variations, and contiguously subsampled from the top of the retained sediment to the bottom of each core section. Stratigraphically adjacent sediment samples from TC14 were cut to thicknesses ranging from 2 – 4 cm (Appendix A). The thicknesses of the TC14 subsamples were determined based on compositional heterogeneity (e.g. grain size, color, moisture content, and lithology). Prior to processing the TC14 core samples, the initial wet weights of grain-size samples were recorded. Subsequently, the TC14 samples were desiccated in a laboratory oven at 40°C for at least 36 hours. After the dry weights of the grain-size samples were measured, moisture-content variations were determined and the remaining TC14 samples were sealed in plastic sample bags until they were processed further for grain-size, X-ray fluorescence, and loss on ignition analyses.

Sediment samples from TC14C were cut to thicknesses ranging from 12.6 – 36.6 cm (Appendix A), placed into sealable plastic containers, stirred with plastic utensils, and partially dried in an oven at 40°C for around 4.5 days. The samples were then gently disaggregated with a ceramic mortar and pestle, stirred with a plastic spoon to improve homogeneity, and a cardboard sample box (provided by NCAG) was filled with individual sediment samples (the volume of each sample was approximately one pint). The sample boxes were subsequently sealed and shipped for analysis by NCAG. The remaining portions of 27 TC14C samples (2 samples did not have leftover sediment) were completely desiccated in a laboratory at 40°C for at least 36 hours, weighed, and stored in sealed plastic containers until they were processed further for magnetic susceptibility, X-ray diffraction, optical microscopy, and scanning electron microscopy/energy-dispersive X-ray spectroscopy analyses.

Appendix A presents subsample data for cores TC14 and TC14C. The subsamples were cut at two specified points within each core section. The lengths, measured downward from the top of the core section to the endpoints of the subsample, are referred to the upper and lower subsample depths. Subsample identifiers in this manuscript include the name of the core, the depth range of each core section in feet and the sample number, which indicates relative depth along the core. For example, TC14: 4 – 8' #5 indicates that the subsample was the fifth shallowest subsample collected from the TC14 core section representing 4 – 8 ft BLS (1.2 – 2.4 m BLS). The sampling resolution was much higher for TC14 than TC14C because NCAG's laboratory required approximately one pint of each sediment sample to conduct their analyses while the amount of material needed for grain-size, X-ray fluorescence, and loss on ignition analyses was much less.



Depth calculations were applied to account for variations in core recovery (Figure 8 and Appendix A). The following calculations operate under the assumption that the recovered samples are representative of the undisturbed sediments that are present at corresponding 1.2 m depth intervals beneath the land surface:

1. Adjusted subsample depth (m) = mean of the upper and lower subsample depths (m) – length void space (m)
2. Conversion factor = 1.219 (m) ÷ length recovered (m)
3. Calculated depth (m) = [conversion factor × adjusted sample depth (m)] + shallowest possible depth BLS for the core section (m).

Bottom

Top

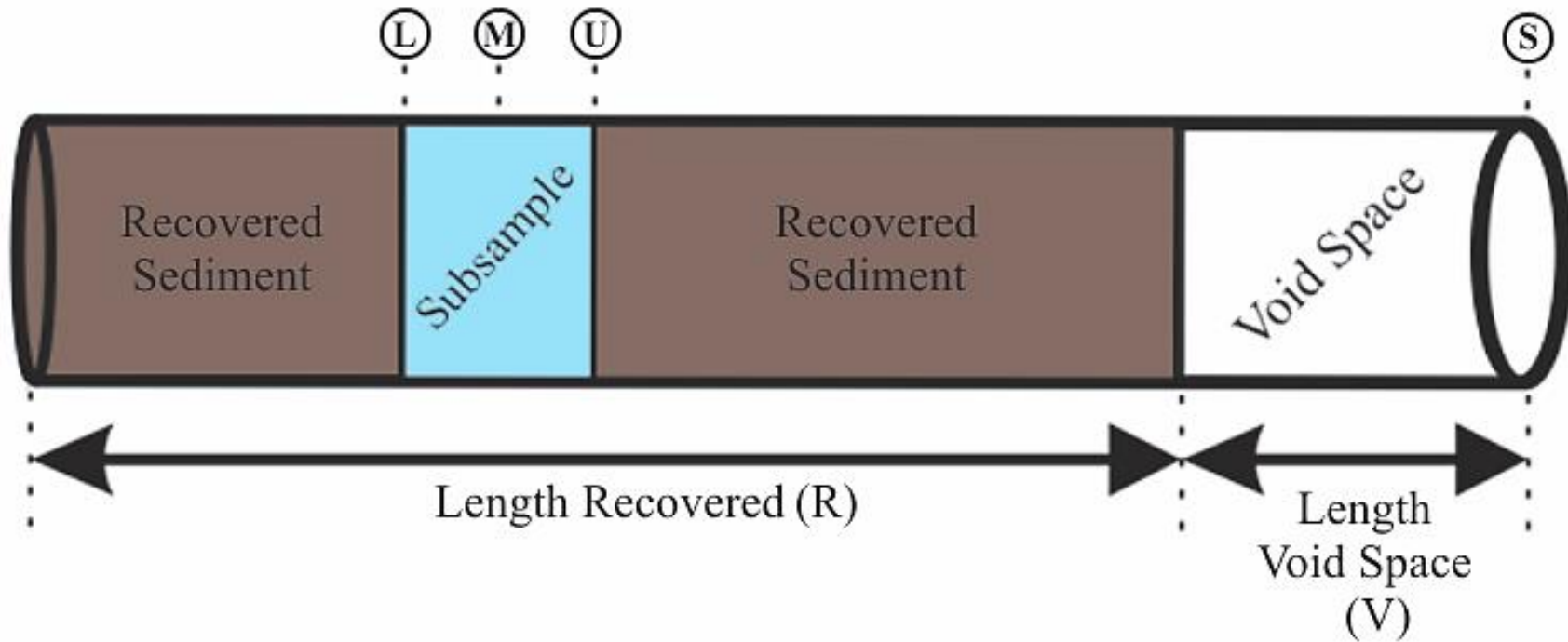


**Figure 8:** Illustration of core components used in depth calculations that were applied to account for variations in core recovery. Subsample depths were measured downward from the top of the core section to each of the subsample's endpoints. Mean subsample depth (M) is the average of the upper subsample depth (U) and the lower subsample depth (L). Adjusted subsample depth =  $M - \text{length void space (V)}$ . The conversion factor =  $(\text{length recovered (R)} + V) \div R$ . Calculated depth BLS =  $[\text{conversion factor} \times \text{adjusted subsample depth (m)}] + \text{shallowest possible depth for the core (S)}$ . The length of the core tube =  $R + V$ .

### 3.2 Grain-Size Analysis and Hydraulic Conductivity

Wet and dry sieving techniques were used to determine grain-size variations. Fifty-eight grain-size samples from TC14 were each soaked overnight in a 300-mL beaker containing ultrapure water and sodium hexametaphosphate ( $\text{NaPO}_3$ )<sub>6</sub> to deflocculate mud particles. The sediment samples were then washed by hand over a 4  $\Phi$  (63  $\mu\text{m}$ ) stainless-steel sieve to remove the mud portion from each sample. The retained sediment was dried in an oven at 40°C for at least 36 hours and weighed to determine the amount of mud that was lost during the wet-sieve procedure. Subsequently, the samples were dry sieved for 15 minutes in a nested column of sieves ( $\frac{1}{2}$   $\Phi$  intervals) using a Ro-Tap sieve shaker to obtain fractions of sediment grains ranging from <4  $\Phi$  to >-2  $\Phi$  (<63  $\mu\text{m}$  to >4000  $\mu\text{m}$ ), representing size fractions ranging from mud to very fine gravel (i.e. granule). After each fraction was weighed, grain-size parameters such as textural group, median grain size, sorting (determined from the standard deviation of the grain-size sample), and grain-size percentages were calculated using the statistical software program, GRADISTAT 4.0 (Blott and Pye, 2001). The grain-size procedure followed is presented in Appendix B.

Hydraulic conductivity (K) is a measure of a fluid's capacity to flow through pore spaces in sediment and varies according to physical properties of the permeating fluid (e.g. viscosity and density) and the physical attributes of the sediment (e.g. particle size, shape, sorting, and porosity) (Heath, 1983). Using grain-size statistics calculated via GRADISTAT 4.0, K was estimated according to the technique proposed by Hazen (1892):

$$K \text{ (cm/s)} = C(D_{10})^2$$

where C is a constant ranging from 0.4 to 1.2 depending on grain size and particle-size distribution of the sediment, typically assumed to be 1.0 and  $D_{10}$  is the grain-size diameter at

which finer material is equal to 10% of the total sediment weight and 90% are coarser, also referred to as the effective size (mm) (Freeze and Cherry, 1979). Although this is one of the most common methods to quickly estimate K from grain-size data, the calculation is based only on one size fraction ( $D_{10}$ ) and is best suited for clean sands ranging from 0.1 to 3.0 mm (Holtz et al., 2011). Hydraulic conductivity estimated from grain-size data commonly results in higher values than those derived from direct measurements; however, general trends in grain-size-estimated K are typically similar to trends in field-measured hydraulic conductivity (Eggleston and Rojstaczer, 2001).

### **3.3 X-ray Fluorescence**

Fifty-four, pressed-powder pellets were prepared for XRF analysis. Following desiccation, sediment samples from Geoprobe core TC14 were ground to approximately 63  $\mu\text{m}$  using a ceramic mortar and pestle. A tungsten-carbide-ball mill was then used to reduce the particle size of the samples to a very fine powder (ten minutes each). For each XRF sample, six grams of sediment, 1.2 grams of binder (PelletBlend Powder – PB100), and 5 acrylic balls were placed inside a plastic mixing chamber (see Appendix G for precise pellet data). The sample was then homogenized using a Spex Mill sample shaker for 10 minutes. The homogenized sediment sample (80%) and binder (20%) were compressed (40 – 45 psi) with a hydraulic press for at least 4 minutes to make pressed-powder pellets (40 mm in diameter), which were stored in a desiccator to remove moisture. A detailed procedure for making XRF pellets is explained in Appendix B.

In August 2014, an Axios (PANalytical) wavelength-dispersive XRF spectrometer was used to determine the total elemental compositions (expressed as either a percentage of dry sediment weight (wt. %) or in parts per million (ppm or mg/kg) of dry sediment weight) of 54

pressed-powdered pellets. Twenty-one reference samples (Govindaraju, 1994; Appendix G) were selected to generate calibration curves for 14 elements including aluminum (Al), sulfur (S), Fe, potassium (K), magnesium (Mg), manganese (Mn), sodium (Na), phosphorous (P), silicon (Si), titanium (Ti), calcium (Ca), fluorine (F), chlorine (Cl), and strontium (Sr). These elements were selected because they comprise common coastal plain minerals including quartz, feldspars, marine fossils, heavy minerals, amphiboles, pyroxenes, and many others. A monitor sample was analyzed on a weekly basis to correct for long-term drift of the instrument.

Precision of the XRF spectrometer was determined by the coefficient of variation (CV %), which can be used to compare the standard deviation and the mean for a set of analyses:

$$\text{CV \%} = (\text{standard deviation} \div \text{mean}) \times 100$$

Percent error (% Error) was calculated to determine accuracy of the XRF spectrometer according to the following equation:

$$\% \text{ Error} = [(\text{experimental mean} - \text{accepted value}) \div \text{accepted value}] \times 100$$

where the experimental mean is the average concentration of an element comprising a reference sample and the accepted value was acquired from 3<sup>rd</sup> party laboratories or publications (e.g. Govindaraju, 1994). Concentration units are expressed either as a weight percentage of dry sediment or in parts per million (ppm or mg/kg) of dry sediment weight. A positive % Error value indicates that the experimental mean is higher than the accepted value. A negative % Error value indicates that the experimental mean is lower than the accepted value.

Some elements could not be evaluated due to detection limits. The sensitivity of East Carolina University's XRF spectrometer is not sufficient for precise and accurate measurements of elements that are lighter than Na because X-ray-induced fluorescence is typically too low for elements with low atomic numbers (<11). During the study period, the gas flow proportional

detector was the only functioning detector. Only elements lighter than Zn were well suited for our XRF analyses because the flow counter largely measures long-wavelength X-rays (>0.15 nm), which are emitted as secondary radiation by lighter elements during fluorescence (Van Loon and Barefoot, 2013).

Approximately one year following the completion of the initial XRF analyses, two standards and five pellet samples were subjected to replicate analyses to determine the accuracy and precision of the instrument and to test the reproducibility of the original XRF data (Appendix G). Microsoft Excel was used to calculate basic statistics (e.g. mean, median, standard deviation,  $R^2$ , and 95% confidence level), construct bivariate plots, and perform linear regression analyses.  $R^2$  values range from 0 to 1 with an  $R^2$  value of zero indicating a total absence of linear correlation between the data and the calculated line of perfect fit and, a  $R^2$  value of one representing a perfectly linear correlation among the data.

Percent deviation (% Deviation) was calculated for the five pellet samples to determine the degree to which the newly acquired replicate data compares to the originally measured concentration. The equation for % Deviation is as follows:

$$\% \text{ Deviation} = ((\text{experimental mean} - \text{original value}) \div \text{original value}) \times 100$$

where the experimental mean is the average elemental concentration determined in 2015 via replicate XRF analyses for five pellet samples and the original value is the XRF-determined concentration that was measured in 2014 (i.e. only one XRF analysis per pellet sample was completed). Concentration units are expressed either as a weight percentage of dry sediment or in ppm (mg/kg) of dry sediment weight. Positive % Deviations indicate that the experimental mean is higher than the original value and negative values denote that the experimental mean is lower than the original value.

The average of absolute-percent deviations (AAPD) was calculated for each element to determine how well the XRF spectrometer was capable of reproducing the initial 2014 concentrations. AAPD was calculated in the following manner:

1. The absolute value of % Deviations was computed for each element.
2. The mean of the resulting absolute-percent deviations for each element was calculated for the five XRF pellet samples.

### **3.4 Loss on Ignition**

Loss on ignition (LOI) is a time-efficient and cost-effective technique to approximate variations in organic-matter content. The approach generally requires that a small quantity of a desiccated-sediment sample be precisely weighed, combusted in a muffle furnace, and precisely weighed again. The assumption is that the weight that is lost during combustion should closely approximate the weight of organic matter that initially comprised the sample (i.e. combustion only removes organic matter). However, the results of LOI analyses performed on lithologically diverse sediments may not be suitable for quantitative estimation of organic matter because, in addition to organic-matter removal, additional combustion-related losses can be derived from structural water from clay minerals and volatile salts, and from CO<sub>2</sub> from carbonates. Nevertheless, studies have shown that LOI is a suitable proxy for the qualitative discernment of general trends in organic-matter content (Ball, 1964; Bengtsson and Enell, 1986; Dankers and Laane, 1983; Sutherland, 1998; Santisteban et al., 2004).

Variations in organic-carbon content were qualitatively assessed by proxy from LOI measurements. Nineteen bulk-sediment samples (2 – 4 cm intervals) were chosen from TC14 for LOI analysis based on lithological contrasts and XRF-determined variations in Fe content. However, the selected sample density is not sufficient for high-resolution LOI characterization

and, because only one trial was conducted for this investigation, the reproducibility of LOI values cannot be evaluated for these data.

Dried sediment (1.2 grams) was weighed, placed into a porcelain crucible, and combusted in a muffle furnace for 4 hours at 550°C. The samples were then cooled to room temperature inside a desiccator and the final weight was determined to calculate percent LOI (% LOI) (Bengtsson and Enell, 1986; Heiri et al., 2001):

$$\% \text{ LOI} = [(\text{initial weight (g)} - \text{final weight (g)}) \div \text{initial weight (g)}] \times 100$$

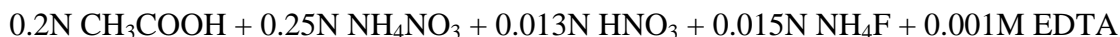
where the initial weight is the dry sediment weight of the sample prior to combustion in the muffle furnace and the final weight is the dry sediment weight of the sample following combustion in the muffle furnace. A procedure detailing the LOI procedure is included in Appendix B.

### **3.5 Sediment Testing by NCAG**

Twenty-nine samples (~1 pint each) from Geoprobe core TC14C were delivered to NCAG to determine the extractable amounts of phosphorus ( $P_e$ ), potassium ( $K_e$ ), calcium ( $Ca_e$ ), magnesium ( $Mg_e$ ), sodium ( $Na_e$ ), manganese ( $Mn_e$ ), sulfur ( $S_e$ ), zinc ( $Zn_e$ ), and copper ( $Cu_e$ ) in desiccated sediment samples and, to evaluate changes in sediment-water pH, cation exchange capacity (CEC), base saturation (BS %), exchangeable acidity (AC), weight per volume (W/V), and percent humic matter (HM %). CEC values are indicative of the nutrient-retention capacity of a sediment and are calculated via the summation of  $Ca_e$ ,  $Mg_e$ ,  $K_e$ , and  $Ac$ . NCAG does not include  $Na_e$  in CEC calculations because sodium concentrations are usually low in NC soils. Base saturation is the percentage of the CEC that is occupied by  $Ca_e$ ,  $Mg_e$ , and  $K_e$ . AC denotes the portion of CEC that contains hydrogen ( $H^+$ ) and aluminum ( $Al^{3+}$ ) ions. Weight to volume ratios can be used for sediment classification. Percent humic matter is a measurement of the



chemically active fractions of organic matter (humic and fulvic acid) in sediment (Hardy et al., 2012). NCAG analyzes on a volumetric basis and uses procedures described in Mehlich (1984a) and Mehlich (1984b) to measure sediment nutrients (via photometry) after applying the following extractant to the sediment samples:



where acetic acid ( $\text{CH}_3\text{COOH}$ ) buffers the solution to pH 2.5 to prevent the precipitation of Ca, ammonium nitrate ( $\text{NH}_4\text{NO}_3$ ) extracts cations such as  $\text{Ca}^{2+}$ ,  $\text{Mg}^{2+}$ ,  $\text{Na}^+$ , and  $\text{K}^+$ , nitric acid ( $\text{HNO}_3$ ) extracts a portion of Ca phosphates, ammonium fluoride ( $\text{NH}_4\text{F}$ ) extracts Fe and Al phosphates, and ethylenediaminetetraacetic acid (EDTA) chelates micronutrients. The Mehlich-Buffer Acidity Procedure (Mehlich and Bowling, 1975) was conducted to measure AC of the sediment solution. This technique relates pH changes of a buffered reagent to corresponding changes in AC. The buffered reagent is composed of sodium glycerophosphate ( $\text{C}_3\text{H}_5(\text{OH})_2\text{PO}_4 \text{Na}_2 \cdot 2.5\text{H}_2\text{O}$ ), ammonium chloride ( $\text{NH}_4\text{Cl}$ ), barium chloride ( $\text{BaCl}_2 \cdot 2\text{H}_2\text{O}$ ), glacial acetic acid ( $\text{CH}_3\text{COOH}$ ), and triethanolamine (TEA), which act as a buffering agent, a displacement reagent of AC, a supplementary displacement agent of AC and a preservative, a buffer within the pH range of 3.8 to 5.2, and a supplementary agent with  $\text{CH}_3\text{COOH}$  to extend the range of the buffer from 3.5 to 5.2, respectively. Finally, NCAG follows a photometric procedure described by Mehlich (1984b) to measure the extractable humic substances in sediment samples and to quantify HM % (Hardy et al., 2012).

### **3.6 Magnetic Separation**

Sediment samples from TC14C were subjected to a series of magnetic separations. These procedures reduced the amount of quartz and calcite grains to facilitate mineral identification via X-ray diffraction, optical microscopy, and scanning electron microscopy/energy-dispersive X-

ray spectroscopy. Prior to processing, a 2 M acetic acid solution ( $\text{CH}_3\text{COOH}$ ) was buffered to a pH of 4 with Na acetate ( $\text{CH}_3\text{COONa}$ ), and a 6.6% Na-hexametaphosphate ( $\text{NaPO}_3$ )<sub>6</sub> solution were filtered through a 1.2  $\mu\text{m}$  Whatman microfiber filter and a 0.2  $\mu\text{m}$  Millipore membrane filter via a vacuum filtration apparatus (Hounslow and Maher, 1999).

A total of 23 sediment samples were split into two groups based on  $\text{Ca}_e$  concentrations from NCAG; 10 samples consisting of less than 8,000  $\text{mg}/\text{dm}^3$  (low carbonates) and 13 samples with greater than 8,000  $\text{mg}/\text{dm}^3$  (high carbonates). High carbonate samples were treated with buffered acetic acid to dissolve the carbonate because it may cement the grains, adversely affect extraction efficiency, and magnetic grains may be attached to the carbonate (Hounslow and Maher, 1999). After the overlying liquid became clear (at least 24 hours), a pipette was used to remove as much of the acetic acid solution as possible without disturbing the sediment at the bottom of the glass beaker.

The subsequent methodologies for the carbonate and non-carbonate samples were identical. Five-hundred mLs of ultrapure water and 20 mL of the ( $\text{NaPO}_3$ )<sub>6</sub> solution were added to the samples inside a beaker, stirred with plastic spoons, and soaked overnight to disaggregate the sediments. Sediment samples were then washed by hand with ultrapure water over a 4  $\Phi$  (63  $\mu\text{m}$ ) sieve placed on top of a beaker, thus separating out the mud-sized grains. Subsequently, the two size fractions of each sample were transferred to labeled weigh boats and dried in an oven at 40°C. To facilitate magnetic separation, sediment samples were dry sieved using 1.25  $\Phi$ , 2.25  $\Phi$ , 3.25  $\Phi$ , and 4  $\Phi$  stainless-steel apertures, therefore fractionating each sediment sample into the following grain-size categories: >425  $\mu\text{m}$ , 0.212  $\mu\text{m}$ , 106  $\mu\text{m}$ , 63 $\mu\text{m}$ , and <63  $\mu\text{m}$ . Grain-size portions that were >425  $\mu\text{m}$  and <63 $\mu\text{m}$  were not used for magnetic separations to avoid clogging the instrument.

A hand magnet and a Frantz Isodynamic Magnetic Separator were used to concentrate the mineral particles in each sample according to their magnetic susceptibilities. In this report, grains are considered to be magnetically susceptible if they were separated from a sediment sample via a hand magnet or by applying an electric current to the magnetic coil of the Frantz separator during the magnetic separation procedure (Appendix B). Prior to using the electromagnetic separator, ferromagnetic minerals such as magnetite and pyrrhotite were removed from the sample with a hand magnet to avoid blocking the chute. The side slope and forward slope of the Frantz were set to 20° and 25°, respectively. After setting the magnetic coil to 0.2 amperes (amps) to induce a magnetic field, sediment retained from the 2.25  $\Phi$ , 3.25  $\Phi$ , and 4  $\Phi$  sieves were successively poured (smallest to largest grain size) into the funnel at the top of the separator. Subsequently, the sediment flowed down a vibrating chute toward the lower end of the chute where the particles bifurcated into two streams: one consisting of grains of higher magnetic susceptibility than that of the corresponding amperage setting of the magnetic coil, and the other consisting of grains of lower susceptibility. After the three grain-size fractions were separated, the minerals that were susceptible at the 0.2 amps setting were combined with those attracted via the hand magnet, weighed, and sealed in a plastic sample bag.

Four additional magnetic separations were then conducted using the remaining non-susceptible portion from the three size fractions (2.25  $\Phi$ , 3.25  $\Phi$ , and 4  $\Phi$  sieves). The magnetic coil was set to 0.4 amps, 0.8 amps, 1.2 amps, and for the maximum amperage setting (~1.8 amps) for each subsequent magnetic separation. After the magnetic separations were completed, minerals that were susceptible below 0.8 amps were combined with those attracted via the hand magnet (collectively comprising the highly susceptible fractions), weighed, and sealed in a plastic sample bag. Grains that were susceptible at amperage settings exceeding 0.8 amps were

combined to form the poorly susceptible fractions. The remaining, non-susceptible portions were stored in separate plastic bags according to grain size.

### **3.7 X-ray Diffraction**

Powder X-ray diffraction (XRD) analyses were conducted on a total of 98 magnetically separated, sediment samples from TC14C to determine the mineralogy of sediments overlying the UCHA. Mineral identification via XRD is tentative because in these sediment samples, peak intensities for the minerals of interest are generally very low compared to the dominant calcite and quartz peaks. Each sample was ground to a fine powder with a ceramic mortar and pestle and subsequently X-rayed from  $3^\circ 2\theta$  to  $73^\circ 2\theta$ . A procedure explaining sample preparation and XRD analysis is provided in Appendix B.

### **3.8 Polished-Thin Sections**

Twenty-one magnetically separated sediment samples were sent to Burnham Petrographics, LLC to prepare seven polished-thin sections. Stratigraphically adjacent samples were combined and mounted atop a 27 x 46 mm glass slide. Loose sediment grains were embedded in epoxy (Petropoxy 154), mounted to one of four assigned quadrants (A, B, C, and D), and polished to thickness of 30  $\mu\text{m}$ . Each quadrant consists of one of the following: mud (<63  $\mu\text{m}$ ), non-susceptible grains (Frantz settings: 0 – 1.75 amps,  $20^\circ$  side slope,  $25^\circ$  forward slope), susceptible grains (Frantz settings: 0 – 1.75 amps,  $20^\circ$  side slope,  $25^\circ$  forward slope), highly susceptible grains (Frantz settings: 0 – 0.8 amps,  $20^\circ$  side slope,  $25^\circ$  forward slope), and poorly susceptible grains (Frantz settings: >0.8 amps,  $20^\circ$  side slope,  $25^\circ$  forward slope). Polished-thin sections were subsequently analyzed via reflected and transmitted light microscopy and via scanning electron microscopy/energy dispersive X-ray spectroscopy to ascertain

mineralogical and semi-quantitative geochemical variations. Quadrant-specific data for the polished-thin sections are presented in Appendix E.

### **3.9 Energy Dispersive X-ray Analysis**

Seven polished-thin sections were analyzed using an Oxford Instruments INCA X-act EDX system installed to a FEI Quanta 200 Mark 1 Environmental SEM to facilitate the identification of minerals and iron-oxyhydroxide aggregates. INCA, a data reduction program (Oxford Instrument's Microanalysis Suite Issue 18d + SP2, INCA Suite version 4.15), was used to determine the elemental compositions of sediment constituents. Quantitative peak optimization was performed at least every two hours using a copper standard to maximize the software's ability to identify peaks and convert peak heights to weight-percents. Each sample was analyzed at 0 – 20 KeV for 50 seconds of Live Time. These parameters are selected because they yielded the best analyses of known standards similar in structure and chemistry to the unknown minerals.

INCA's point identification (Point & ID) and elemental mapping features were used to determine the chemistry of unknown minerals, aggregates, and coatings. Point & ID acquires a spectrum at a specified point on a sample. The elemental-mapping approach involves the concurrent detection of all possible elements for each pixel over a specified area. The software compiled X-ray data over a three-frame period at a 512 resolution to generate qualitative element maps, which show the distribution of elements over an area of interest (Oxford Instruments, 2006).

### **3.10 Mineralogical Analysis**

Multiple techniques were used to estimate mineral-abundance variations. The percent area various minerals occupied was approximated by examining polished-thin sections and loose

sediment grains with an optical microscope and the SEM. Optical properties including birefringence, relief, fracture, cleavage, color, pleochroism, twinning, and diaphaneity (i.e. transparency) were used, in conjunction with XRD and EDX data, to identify the dominant minerals that comprise the cores at various depth intervals. After the dominant minerals were identified, the relative abundance of each mineral was semi-quantitatively determined by visual estimation. More quantitative methods such as point-count analyses were not performed due to time constraints.

### **3.11 Geochemical Modeling with PHREEQC**

The computer program PHREEQC (Version 2, Parkhurst and Appelo, 1999) is one of the most widely utilized programs for modeling chemical reactions and transport processes in low-temperature aqueous systems. The program uses thermodynamic constants to simulate equilibrium reactions including, precipitation and dissolution, oxidation and reduction, speciation, and solution saturation. The thermodynamic constants are derived from numerous field and laboratory investigations and are adjusted to reflect applicable abiotic and biotic processes (David Parkhurst, pers. comm., 2015). The default database chosen for modeling was the Lawrence Livermore National Laboratory database (llnl.dat, Johnson et al., 2000). However, supplementary minerals and associated equilibrium constants ( $\log K$ ) of additional minerals of interest have been added (Table 4).

For minerals of interest not included in llnl.dat, a series of calculations were applied to calculate  $\log K$  values for their dissolution reactions. The calculations use empirically determined values that define the energy content of species that are involved in the reaction. The energy content of each reaction species is called the “Gibbs Free Energy of Formation” ( $\Delta G_f^0$ ) and is determined by measuring the amount of heat energy that is released or consumed during

the formation reaction of the species. An equation describing the change of the Gibbs Free Energy of Reaction ( $\Delta G_R$ ) at a given temperature and 1 atm pressure can be written as follows:

$$\Delta G_R = \Sigma \Delta G_f^O (\text{products}) - \Sigma \Delta G_f^O (\text{reactants})$$

The equilibrium constant of a reaction is related to  $\Delta G_R$  by the following relationship:

$$\Delta G_R = - R \times T \times \ln K_{eq}$$

where R is the gas constant (0.001987 kcal/deg-mol), T is the temperature in degrees kelvin (298.15 at 25°C), and ln K is equal to the product of log K and 2.3025. A simplified equation relating log K to  $\Delta G_R$  at 25°C and 1 atm pressure can be written as follows:

$$\Delta G_R = -1.364 \times \log K$$

where  $\Delta G_R$  is in units of kcal/mol (Faure, 1998).

For example, the following is a reaction describing the dissolution of almandine:

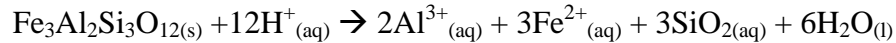


Table 5 presents  $\Delta G_f^O$  values for species that are involved in the dissolution of almandine. Note that a value for  $\text{H}^+_{(aq)}$  is not provided in Table 5 because, by convention,  $\Delta G_f^O$  of  $\text{H}^+_{(aq)}$  is zero.

The sum of reactants and the sum of the products is calculated as follows:

$$\Sigma \Delta G_f^O (\text{reactants}) = (1 \text{ almandine} \times -1187.8) + (1 \text{ H}^+_{(aq)} \times 0) = \underline{-1187.8 \text{ kcal/mol}}$$

$$\Sigma \Delta G_f^O (\text{products}) = (2 \text{ Al}^{3+}_{(aq)} \times -115.609) + (3 \text{ Fe}^{2+}_{(aq)} \times -21.87) + (3 \text{ SiO}_{2(aq)} \times -199.19) + 6 \text{ H}_2\text{O}_{(l)} \times -56.687) = \underline{-1234.52 \text{ kcal/mol}}$$

The difference between the products and reactants is -46.72 kcal/mol, which is equivalent to  $\Delta G_R$  for this reaction. Finally, the value of log K for the dissolution of almandine can be determined by dividing -46.72 kcal/mol by -1.364, resulting in a log K value of 34.25.

**Table 4:** Formulas and equilibrium constants for modeled Fe-bearing minerals. Thermodynamic data were used to calculate log K for minerals that are referenced with multiple sources. Log K values were obtained directly for minerals with only one source.

Mineral	Formula	log K
Actinolite <sup>2,4,5</sup>	$\text{Ca}_2\text{Fe}_5^{2+}\text{Si}_8\text{O}_{22}(\text{OH})_2$	50.22
Almandine <sup>2,4,5,6</sup>	$\text{Fe}_3^{2+}\text{Al}_2\text{Si}_3\text{O}_{12}$	34.25
Epidote <sup>1</sup>	$\text{Ca}_2\text{Fe}^{3+}\text{Al}_2\text{Si}_3\text{O}_{12}\text{OH}$	32.93
Ferrihydrite <sup>1</sup>	$\text{Fe}^{3+}(\text{OH})_3$	5.66
Ferropargasite <sup>2,3,5,6</sup>	$\text{NaCa}_2\text{Fe}_4^{2+}\text{Al}_3\text{Si}_6\text{O}_{22}(\text{OH})_2$	80.89
Glauconite <sup>2,5,6,9</sup>	$\text{K}_{0.489}\text{Na}_{0.045}\text{Mg}_{0.281}\text{Al}_{1.387}\text{Fe}_{1.069}^{3+}\text{Fe}_{0.114}^{2+}\text{Si}_{3.327}\text{O}_{10}(\text{OH})_2$	0.73
Goethite <sup>1</sup>	$\text{Fe}^{3+}\text{OOH}$	0.53
Goethite_2 <sup>8</sup>	$\text{Fe}^{3+}\text{OOH}$	-0.02
Hedenbergite <sup>1</sup>	$\text{CaFe}^{2+}(\text{SiO}_3)_2$	19.61
Hematite <sup>1</sup>	$\text{Fe}_2^{3+}\text{O}_3$	0.11
Ilmenite <sup>1</sup>	$\text{Fe}^{2+}\text{TiO}_3$	0.91
Lepidocrocite <sup>8</sup>	$\text{Fe}^{3+}\text{OOH}$	1.39
Pyrite <sup>1</sup>	$\text{Fe}^{2+}\text{S}_2$	-24.66
Schorl <sup>2,5,6,7</sup>	$\text{NaFe}_3^{2+}\text{Al}_6\text{Si}_6\text{O}_{18}(\text{BO}_3)_3(\text{OH})_4$	39.03
Staurolite <sup>2,4,5,6</sup>	$\text{Fe}^{2+}_2\text{Al}_9\text{Si}_4\text{O}_{23}(\text{OH})$	82.97

1. Johnson et al. (2000)

2. Weast et al. (1986)

3. Murphy and Helgeson (1987)

4. Karpov et al. (1971)

5. Oelkers et al. (1995)

6. Shock et al. (1997)

7. Van Hinsberg and Schumacher (2007)

8. Lindsay (1979)

9. Fu (2014)



**Table 5:**  $\Delta G_f^{\circ}$  values for species involved in the dissolution of almandine.

Species	$\Delta G_f^{\circ}$ (kcal/mol)	Source
Almandine	-1187.80	Karpov et al. (1971)
Al <sup>3+</sup>	-115.61	Shock et al. (1997)
Fe <sup>2+</sup>	-21.87	Oelkers et al. (1995)
SiO <sub>2</sub>	-199.19	Oelkers et al. (1995)
H <sub>2</sub> O (l)	-56.69	Weast et al. (1986)

### 3.11.1 Input Data in PHREEQC

In PHREEQC, keywords (in all capital letters) are used to organize keyword data blocks (See input files in Appendix L). Data blocks begin with a keyword and are followed by associated data in subjacent lines. The program uses database files to read keywords and data at the beginning of the simulation to define solution chemistry, mineral and gas phases, as well as various reactions including ion exchange and redox. Simulations in PHREEQC are a set of calculations defined by keyword data blocks and are finalized for the data block using the “END” command (Parkhurst and Appelo, 1999). Input data used for modeling generally includes temperature (temp), pH (the negative log of hydrogen ion activity), species concentrations, one or more mineral phases (EQUILIBRIUM\_PHASES), alkalinity (as  $\text{HCO}_3^-$ ) and pe (the negative log of electron activity), related to field-measured Eh by the following equation:

$$pe = Eh/(2.3RTF-1)$$

where R is the gas constant, T is Temperature, and F is Faraday’s constant. Field Eh values, measured by Sutton and Woods (1995) and Brown (1999), were adjusted to account for the AgCl reference potential by adding 222 mV to the original Eh measurement.

### 3.11.2 Output Data in PHREEQC

The “SELECTED\_OUTPUT” keyword data block is used to facilitate data compilation and analysis for completed simulations by generating a file that is compatible with data management programs such as Microsoft Excel or Sigma Plot (Parkhurst and Appelo, 1999). Output data of interest for this investigation largely include species concentrations, pH, pe, and saturation indices of mineral phases. The saturation index of a mineral is defined as follows:

$$\text{saturation index} = \log (IAP/K_T)$$

where IAP is the ion activity product of the dissolved components in the solution, and  $K_T$  is the solubility product of the solid or gaseous phase at the specified temperature. The saturation index indicates if the solution is undersaturated, oversaturated, or at equilibrium with a particular solid. A negative value denotes that the solution is undersaturated while a saturation index exceeding zero means that the system is oversaturated. Finally, if the saturation index equals zero, the solution is at equilibrium with the solid. Saturation indices can be used to predict whether a mineral is likely to dissolve or precipitate in a particular solution.

### **3.11.3 Model Setup**

Using simplified aquifer compositions (Tables 6 – 7 and Appendix K), a series of preliminary batch simulations and a one-dimensional, transport model were developed to assess the impact of dissolution, precipitation, and cation-exchange on dissolved-Fe concentrations. The models are largely based on geochemical and hydrological data that were acquired during previous investigations of the UCHA and the surficial aquifer. The wells were constructed several kilometers to the east of the Tranters Creek core site (Figure 3) where the UCHA is relatively well confined (Consolvo, 1998). Although the data used to setup the simulations are largely derived from preceding studies, the modeling results provide important insights involving the origin and fate of high-Fe zones in the UCHA. The models are described in detail in the subsections below and a cross-section illustrating the conceptual design for this study is provided in Figure 9.

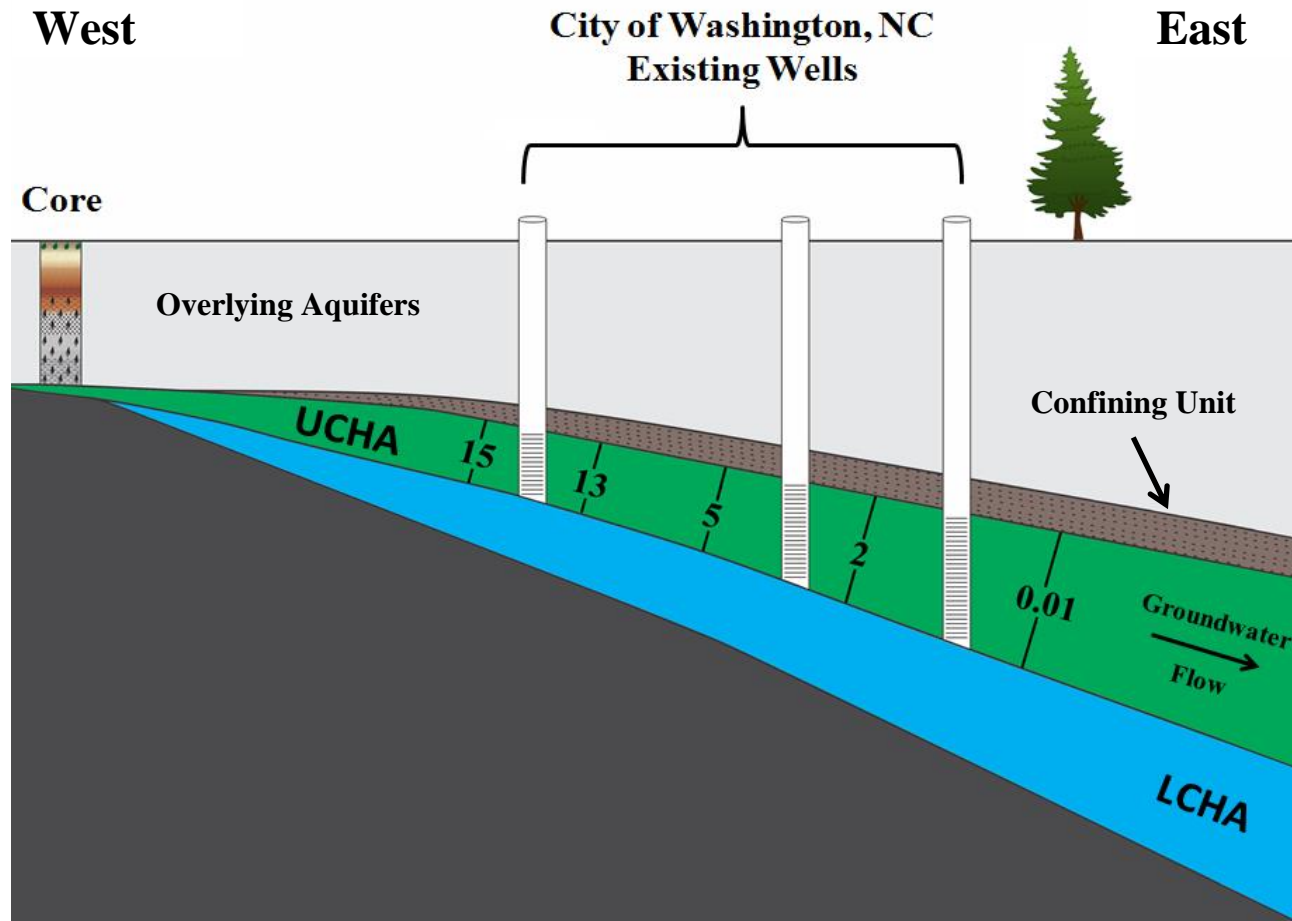


**Figure 9:** Cross-section from near Tranters Creek, NC illustrating conceptual design for this project (not drawn to scale). Two Geoprobe cores were acquired about 8 km west of Washington, NC during this investigation. Preceding investigators measured groundwater chemistry at existing wells near Washington, NC. The existing wells provide data for Fe concentrations in the surficial aquifer (not illustrated) and in the UCHA. The numbers in the green area represent an eastward decline in observed Fe concentrations (mg/L) in the UCHA. The brown layer depicts decreasing confinement of the UCHA from east to west. A map showing the well locations and the core site is presented in Figure 3.

### **3.11.3.1 Simple Dissolution Simulations**

Simple dissolution simulations in this study are batch reactions involving the dissolution of individual Fe-bearing minerals in two different aqueous solutions. The selected solutes represent some common Fe-bearing minerals that may comprise aquifers in NCCP (Table 4). Ten moles of each Fe-bearing mineral (this seemingly large amount ensures that the mineral cannot completely dissolve prior to achieving thermodynamic equilibrium) are added to a hypothetical beaker containing 1 L of either “Pure Water” or “Surficial Groundwater.” These simulations can be used to estimate the maximum Fe concentration that may result via dissolution of the mineral to determine if that mineral is a likely source of high-Fe concentrations observed in the UCHA. To account for possible iron-oxyhydroxide supersaturation, goethite is allowed to precipitate in each simulation. The only elements in “Pure Water” are hydrogen and oxygen (no dissolved O<sub>2</sub> is present) and the default conditions for pressure, temperature, pH, and pe are one standard atmosphere, 25°C, 7, and 4, respectively.

Three separate dissolution simulations were conducted for each mineral using the “Pure Water” solution but at different pH values (5, 7, and 9, respectively) to encompass pH variations in natural groundwater environments. The chemistry of the “Surficial Groundwater” was determined by Whitley (2003) for the surficial aquifer measured at the FE well (Tables 6 – 7 and Figure 3). Total dissolved-Fe concentrations were evaluated to infer the potential of individual Fe-bearing minerals to produce high-Fe concentrations (>0.3 mg/L) in groundwater via simple dissolution reactions.

### **3.11.3.2 Pyrite Oxidation Simulations**

Using PHREEQC, pyrite was titrated with dissolved oxygen O<sub>2</sub> (g) to simulate pyrite oxidation in a near-surface-aquifer environment. The pyrite-oxidation simulations are batch

reactions in which 10 moles of pyrite are equilibrated with 1 L of either the “pure water” or “surficial groundwater” solution. Once the pyrite and groundwater solution reach equilibrium, O<sub>2</sub> (g) was added in one hundred increments (0.08 mg/L each). The dissolved-Fe concentration was recorded after the added O<sub>2</sub> is consumed and equilibrium is established for each increment of the simulation. Groundwater equilibrated with the atmosphere contains approximately 8 mg/L O<sub>2</sub>. Therefore, the maximum dissolved-Fe concentration that may result via pyrite oxidation in a similar surficial groundwater can be estimated at the end of the titration if Fe-bearing minerals do not precipitate from solution.

#### **3.11.3.3 Goethite Reduction in Surficial Groundwater**

Goethite was titrated with CH<sub>2</sub>O to simulate the microbially mediated reduction of iron-oxyhydroxides by dissolved-organic matter (DOC). In this simulation, 10 moles of goethite are equilibrated with 1 L of the “surficial groundwater” solution. According to Spruill et al. (1997), DOC concentrations in shallow NCCP aquifers are commonly less than 5 mg/L. Therefore, a series of titrations adding up to a total of 5 mg/L DOC were conducted to evaluate the potential of iron-oxyhydroxide reduction to produce dissolved-Fe concentrations exceeding 0.3 mg/L.

#### **3.11.3.4 Reactive-Transport Modeling of the UCHA**

Using existing chemical and hydraulic data for the UCHA, a one-dimensional, reactive-transport model was developed to determine the impact of cation-exchange on dissolved-Fe concentrations that may occur along a hypothetical 12 km flow path in the UCHA. In PHREEQC, one-dimensional transport along an aquifer-flow path is represented by a column consisting of a sequence of cells (Figure 10). Each cell represents a mass of aquifer particles in contact with the groundwater. The solution in each cell flows toward the adjacent, cell with a

higher number. The program uses a finite-difference algorithm for calculations involving advective and dispersive transport of solutes (Parkhurst and Appelo, 1999).

The simulated flow path in this investigation consists of 6 individual cells that are each 2 km in length. The reactive-transport model simulates possible geochemical changes that occur as UCHA groundwater flows toward the south and southeast near Washington, NC (Figure 3). The first cell (Cell 0; Solution 0) is dimensionless and represents the recharging solution based on the groundwater chemistry determined by Brown (1999) at well T15 (Tables 6 – 7). The second cell (Cell 1; Solution 1) represents the equilibration of the recharge solution with calcite, which dominates the mineralogy of the UCHA limestone and produces “Solution 1.” Cells 2 – 6 (solutions 2 – 6) contain a low-Fe groundwater (geochemical data from Brown (1999)), which represents the farthest, downgradient water chemistry sampled in the Washington Well field at the Far East well (FE).

Warner (1993) conducted aquifer tests at eight test wells to determine aquifer characteristics of the UCHA near Washington, NC. Using her average value for hydraulic conductivity for these wells (31.8 m/d), 20% porosity (Richard Spruill, pers. comm. 2016), and the hydraulic gradient estimated by Consolvo (1998) for the study area (0.0007 m/m), the resulting groundwater velocity is approximately 0.11 m/day when calculated as follows:

$$V = [K \times (dh/dl)] \div n$$

where V is groundwater velocity, K is hydraulic conductivity (flow rate of water through a cross-sectional area under a unit of hydraulic gradient), n is porosity (ratio of void spaces to the total volume of the aquifer), dh is the difference in head elevation, dl is the length over which dh occurs, dh/dl is the hydraulic gradient. Based on these parameters, the time necessary for the UCHA groundwater to travel 12 km is approximately 300 years.

**Table 6:** Solution data used for geochemical modeling in PHREEQC.

Modeled Groundwater <sup>1</sup>	Well ID <sup>2</sup>	Aquifer	Temperature	pH	pe <sup>3</sup>	O <sub>2</sub>	Alkalinity as HCO <sub>3</sub> <sup>-</sup>	Cl <sup>-</sup>	SO <sub>4</sub> <sup>2-</sup>	Na <sup>+</sup>
Pure Water	NA <sup>3</sup>	NA <sup>3</sup>	25	7.00	4.00	NA <sup>4</sup>	NA <sup>4</sup>	NA <sup>4</sup>	NA <sup>4</sup>	NA <sup>4</sup>
Surficial Water	FE	Surficial	23	5.30	6.44	0.28	24	13.21	17.87	8.96
UCHA Recharge Water	T15	UCHA	17	6.90	3.92	0.00	344	12.30	0.00	14.07
UCHA Downgradient Water	FE	UCHA	18	7.41	2.97	0.00	305	0.73	1.53	8.83

1. The "Pure Water" solution is the default solution used in PHREEQC. The "Surficial Water and the "UCHA Downgradient Water" were measured at the FE well by Whitley (2003) and Brown (1999), respectively. Sutton and Woods (1995) determined the composition of the "UCHA Recharge Water" at T15. Temperatures and concentrations are given in units of °C and mg/L, respectively

2. The locations of modeled wells are shown in Figure 3

3. Except for the "Pure Water" solution, pe values reflect the addition of 0.222 V to their measured Eh values (V) to account for the stable potential of the AgCl reference electrode. The resulting Eh value was then multiplied by 16.9 to calculate redox potential in pe units

4. NA: Not applicable to the "Pure Water" solution



**Table 7:** Solution data used for geochemical modeling in PHREEQC (continued).

Modeled Groundwater	K <sup>+</sup>	Ca <sup>2+</sup>	SiO <sub>2</sub>	F <sup>-</sup>	Mg <sup>2+</sup>	S <sup>2-</sup>	NO <sub>2</sub> <sup>-</sup>	NO <sub>3</sub> <sup>2-</sup>	NH <sub>4</sub> <sup>+</sup>	PO <sub>4</sub> <sup>2-</sup>	Fe <sup>2+</sup>
Pure Water	NA <sup>2</sup>	NA <sup>2</sup>	NA <sup>2</sup>	NA <sup>2</sup>	NA <sup>2</sup>	NA <sup>2</sup>	NA <sup>2</sup>	NA <sup>2</sup>	NA <sup>2</sup>	NA <sup>2</sup>	NA <sup>2</sup>
Surficial Water	3.61	3.15	13.70	0.09	4.31	0.00	0.04	0.97	0.03	0.13	0.07
UCHA Recharge Water	26.35	70.98	34.19	0.22	8.57	0.01	0.002	0.003	0.48	0.63	16.40
UCHA Downgradient Water	5.18	65.80	29.05	0.36	13.21	0.20	0.003	0.002	1.21	0.01	0.01

1. The "Pure Water" solution is the default solution used in PHREEQC. The "Surficial Water and the "UCHA Downgradient Water" were measured at the FE well by Whitley (2003) and Brown (1999), respectively. Sutton and Woods (1995) determined the composition of the "UCHA Recharge Water" at T15 (See Figure 3 for well locations). Concentrations are given in units of mg/L

2. NA: Not applicable to the "Pure Water" solution

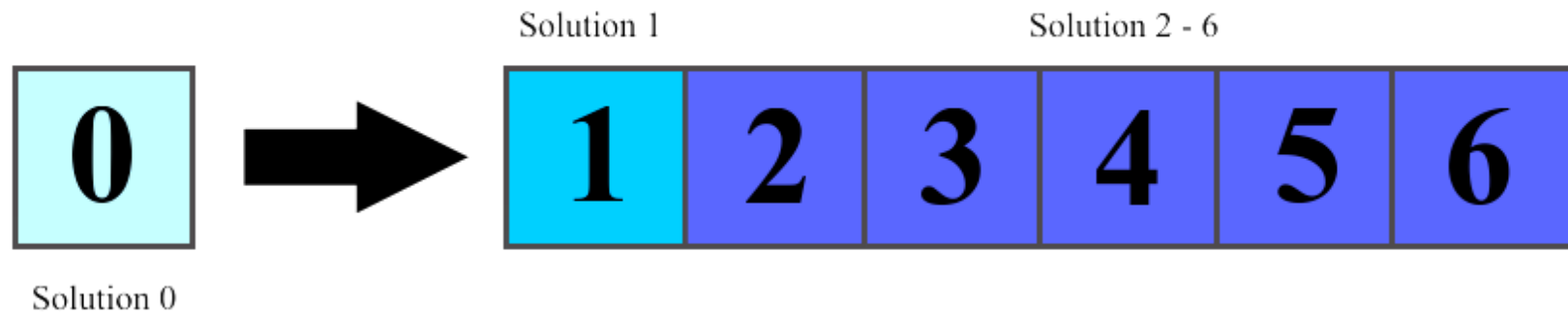


**Figure 10:** Illustration of the one-dimensional flow path in PHREEQC.

#### **3.11.4 Calibration of the Reactive-Transport Model**

Model calibration is the process of changing the values for certain input parameters within a reasonable range to improve the correlation between the modeled output data and the measured geochemical data. Geochemical data acquired by Warner (1993), Sutton and Woods (1995), and Brown (1999) for the seven UCHA wells are presented in Table 8. The distance for each well is referenced to well T15 because it represents the farthest, upgradient well for which geochemical data are available. Because the UCHA is not homogenous and isotropic, local variations in groundwater-flow velocity can result in regional-scale mixing of dissolved constituents. Dispersivity was estimated by trial and error during model calibration to account for the effects of heterogeneous transport of solutes.

Based on point-count data from Mehlhop et al. (2005) and Johnson (1992), glauconite may be an important contributor to CEC in the UCHA. Mehlhop et al. (2005) determined the mineralogy of CHAS samples at six wells located throughout the NCCP. Based on these investigations, peloids, composed of either glauconite or phosphate, comprise between 0.3% and 18% of the CHAS limestone. At the core site, Johnson (1992) found that glauconite comprises approximately 11.2% of the UCHA. Since detailed mineralogical data are lacking for the UCHA near Washington, NC and because the CEC values of glauconite may range from 5 to 39 meq/100g (Thompson and Hower, 1975), the CEC of the UCHA ( $X_{UCHA}$ ) was estimated via trial and error during calibration of the reactive-transport model.

#### **3.11.5 Conservative-Transport Model**

A conservative-transport model was developed to determine the degree to which hydrologic processes may affect groundwater composition along a simulated flow path of the UCHA. Geochemical reactions such as dissolution, precipitation, and cation-exchange reactions

are excluded in the conservative model. Changes in solution chemistry can therefore be solely attributed to progressive mixing of the recharge and downgradient solutions (T15 and FE wells, respectively) that occurs during transport as a result of advection and hydrodynamic dispersion (includes molecular diffusion and mechanical dispersion). Results from the conservative-transport model were compared with the reactive-transport-model results to evaluate the impact of cation exchange on groundwater chemistry.

**Table 8:** Geochemical and transmissivity data for the seven UCHA wells near Washington, NC.

Well ID <sup>1</sup>	Distance <sup>2</sup>	pH	Alkalinity as HCO <sub>3</sub> <sup>-</sup>	Na <sup>+</sup>	K <sup>+</sup>	Mg <sup>2+</sup>	Ca <sup>2+</sup>	Fe <sup>2+</sup>	Transmissivity <sup>3</sup>	Source for Geochemical Data
T15	0	6.9	344	14	26	9	71	16.4	ND <sup>4</sup>	Brown (1999)
CF	5.31	7.6	262	11	ND <sup>4</sup>	4.2	57	7.5	1050	Warner (1993)
W2	6.52	7.34	249	10	1	3	63	2.89	1282	Sutton and Woods (1995)
W4	7.77	7.2	273	9	2.1	4	65	1.13	1366	Sutton and Woods (1995)
W7	8.71	7.1	272	9.6	ND <sup>4</sup>	5.5	78	1.3	1895	Warner (1993)
W3	9.61	7.3	273	7	1	5	62	1.2	1849	Sutton and Woods (1995)
FE	10.69	7.41	305	8.83	5.18	13	66	0.01	2295	Brown (1999)

1. Measured data for wells near Washington, NC (see Figure 3 for well locations). Concentrations are presented in mg/L units

2. Distance from T15 in km

3. Transmissivity values (m<sup>2</sup>/d) from Warner (1993)

4. ND: No Data available

## 4.0 Results

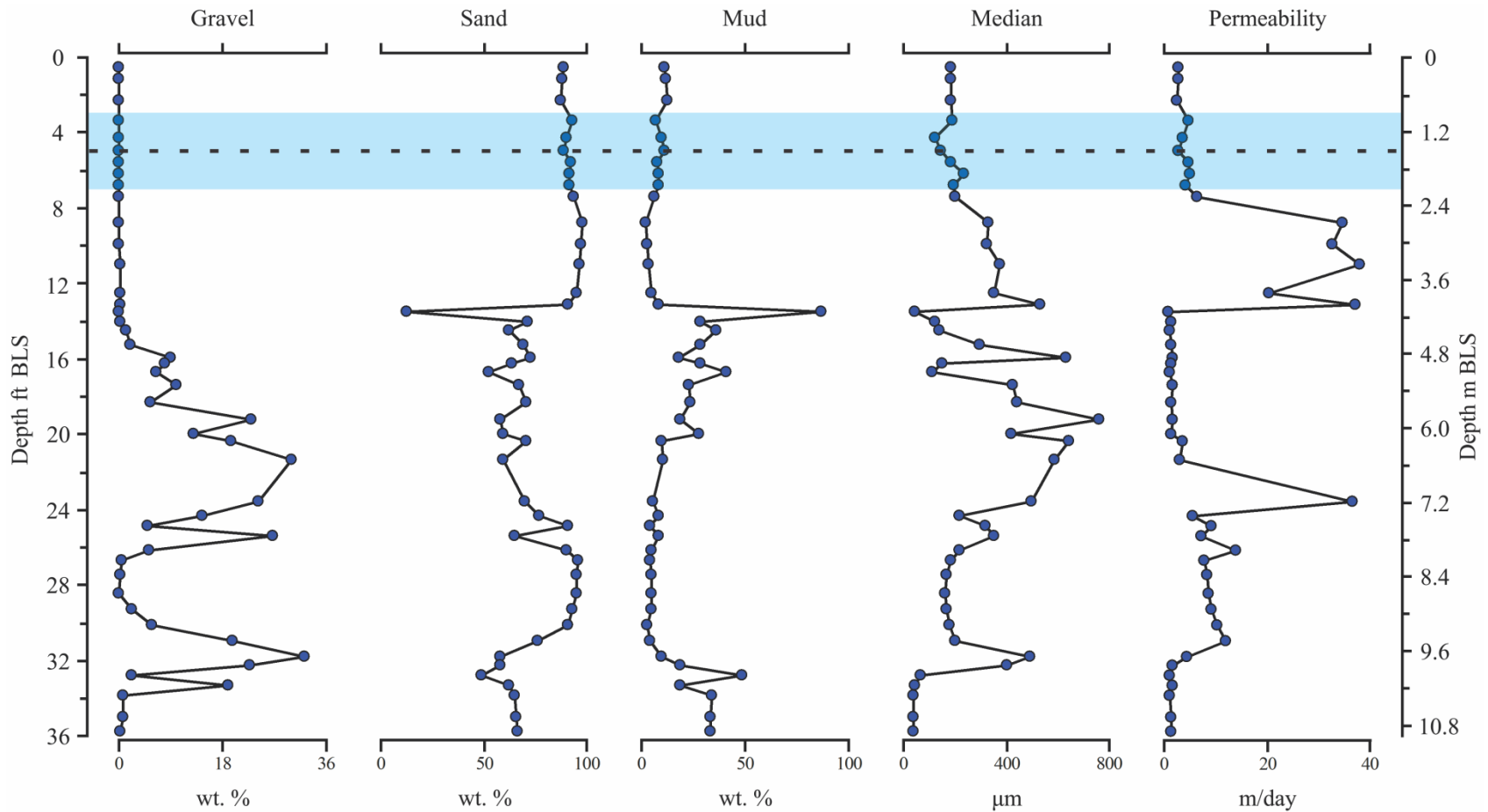
### 4.1 Sediment Descriptions

The 11 m Geoprobe cores are composed of unconsolidated sedimentary material, ranging in grain size from mud to gravel. Depth-related variations in sediment composition are described below and photographs of representative sediments for each 1.2 m interval are displayed with corresponding sediment descriptions in Table 9. The results of grain-size analyses are presented in Figure 11 and Appendix C.

Core samples representing the upper 6 m of the cores are composed of fine -to coarse-grained sands with thin gray, orange, and brown mud layers (<0.3 m thick). The sands consist of moderately well-sorted grains and increase in grain size and permeability to a depth of 4 m BLS. This sequence is underlain by a mud-rich (>18%) and less permeable (grain-size-estimated  $K < 2$  m/d) zone that extends to approximately 6 m BLS. According to Johnson (1992), the surface of the water table at the core site ranges from approximately 0.9 m BLS and 2.2 m BLS but the water table is typically less than 1.5 m BLS (Figure 11).

Sediment samples taken from the upper meter BLS are dark brown and contain abundant organic matter (e.g. bark, grass, roots, leaves, and charcoal). Between one meter and 4 m BLS, the sediments transition from light tan to a strong, orangish-brown color. A distinct zone where the sediment reaches its darkest, orangish-brown color occurs just beneath a mud-rich layer (>85% mud) located at approximately 4.1 m BLS. With increasing depth, the sands then fade from an orangish-brown color to a blueish-gray hue by around 6.4 m BLS. Shell fossils (e.g. gastropods and bivalves) initially become visible by around 4.9 m BLS and generally increase in abundance until 7.3 m BLS; however, their occurrences are highly variable below this depth. A 4.6 m sequence largely consisting of blueish gray, moderately well-sorted to very poorly sorted,










very fine -to coarse sands occurs below 6.4 m BLS. The median grain size generally decreases with depth and below 9.6 m BLS, the proportion of mud-sized grains largely increases with depth.



**Figure 11:** Variations in grain size and grain-size estimated permeability with depth. The blue area denotes typical depth ranges of the water-table surface and the dashed line indicates the mean depth of the water table (Johnson, 1992).



**Table 9:** Photographs of representative sediment intervals and sediment descriptions. Note that these images do not fully account for changes in composition and color.

Depth BLS		Digital Photograph of Representative Sediments	Description
ft	m		
0 - 4	0 - 1.2		Moderately sorted, dark to light brown, fine sand with organic matter
4 - 8	1.2 - 2.4		Moderately sorted, light brown to tan, fine sand
8 - 12	2.4 - 3.7		Moderately well sorted, tan to light tan, medium sand
12 - 16	3.7 - 4.9		Poorly sorted, light tan, medium to coarse, sand transitions to dark brown, sandy mud
16 - 20	4.9 - 6.1		Very poorly sorted, dark brown to orangish brown, fine to coarse, muddy sand with shell fragments
20 - 24	6.1 - 7.3		Poorly sorted, light brownish gray to blueish gray, coarse sand with abundant shell fragments
24 - 28	7.3 - 8.5		Poorly to moderately well sorted, blueish gray, fine to coarse sand with decreasing shell fragments
28 - 32	8.5 - 9.8		Very poorly sorted, gray, fine to coarse sand with abundant shell fragments
32 - 36	9.8 - 11		Poorly sorted, gray, very fine muddy sand with few shell fragments

0 2 cm

## 4.2 Mineralogy

Based on the XRD data, almandine, amphiboles, chlorite, epidote, glauconite, ilmenite, iron-oxyhydroxides, magnetite, pyrite, pyroxenes, siderite, staurolite, and tourmaline are potentially significant, Fe-bearing minerals (Figure 12). Almandine, amphiboles, feldspar, ilmenite, pyroxenes, and quartz were detected in each depth interval that was evaluated. Chlorite peaks were not recognized between 4.3 – 6.7 m BLS or below 8.8 m BLS. Iron-oxyhydroxides and pyrite peaks were only recognized below 3.4 and 4.9 m BLS, respectively. Apatite, calcite, dolomite, and glauconite were detected below approximately 4 m BLS. Epidote, rutile staurolite, and tourmaline were identified in the majority of the 1.2-m-long-core sections. The XRD data suggest that magnetite may not be present in the majority of core samples. Absence on the XRD pattern does not necessarily indicate total absence in the sample due to XRD detection limitations. Generalized formulas and information pertaining to the origins and sources of XRD-detected minerals are shown in Tables 10 – 11.

XRD and microscopy (Figures 12 – 13, Tables 12 – 13) analyses reveal that from the ground surface to approximately 4.1 m BLS, the sediment grains larger than 63  $\mu\text{m}$  are largely composed of quartz (~90%) and feldspar (~10%). In decreasing order of abundance, the dominant trace minerals for this depth interval include ilmenite, amphiboles, pyroxenes, staurolite, and almandine. These five Fe-bearing minerals collectively constitute less than 2% of the total weight of grain-size fractions ranging from sand to gravel. The mud-sized portions for this depth range from around 2% to 13% of the total sample weight and are generally composed of quartz, feldspar, and phyllosilicate minerals (possibly illite, kaolinite, and/or muscovite).

Sand-size samples acquired from 4.1 m to about 6.5 m BLS are predominantly quartz (~30 – 80%), feldspars (~3 – 11%), apatite in the form of phosphate-rich peloids (~6 – 11%), and

shell fragments (~2 - 48%). Iron-bearing minerals collectively comprise about 4% of sand-sized grains. In decreasing order of abundance, the dominant trace minerals for this interval are glauconite, iron-oxyhydroxide, ilmenite, almandine, staurolite, amphiboles, and pyroxenes. The mud-sized fractions range from nearly 10% to almost 90% of the total sample weight and their compositions are predominantly quartz, feldspar, and phyllosilicate minerals.

Common iron-oxyhydroxide morphologies (Table 2) were not observed via microscopy and thus, could not be used for identification. XRD peaks indicate that the bulk of Fe-rich aggregates and grain coatings (Ags/Cs) are most likely comprised of goethite; however, other iron-oxyhydroxides such as ferrihydrite cannot be ruled out because iron-oxyhydroxides are commonly amorphous to poorly crystalline and because they are extremely small (particle size is frequently <20 nm). Reliable identification of iron-oxyhydroxides via XRD analysis is limited to “well crystalline large particles greater than about 30 nm in length” (Cook et al., 1999, p. 60). The formation of lepidocrocite is possible in non-calcareous sediments above approximately 4.9 m BLS but it is less likely to develop below this depth because CO<sub>2</sub> released via carbonate dissolution suppresses lepidocrocite formation (Stucki et al., 2012).

Below 6.5 m BLS, sand-sized sediments are principally quartz (~40 – 80%), shell fossils (~5 – 40% including dolomite), feldspars (~4 – 9%), and apatite peloids (~5 – 9%). In decreasing order of abundance, the dominant trace minerals include ilmenite, glauconite, amphiboles, and pyroxenes. Optical microscopy and SEM/EDX microscopy indicate that calcite-cemented grains and Fe-coated dolomite grains are among the sand-sized constituents but only trace amounts of Fe-rich Ags/Cs were observed below 6.5 m BLS. The mud fractions in this interval range from approximately 3% to nearly 50% of the total sample weight and are generally composed of quartz, calcite, feldspar, pyrite, and phyllosilicate minerals.

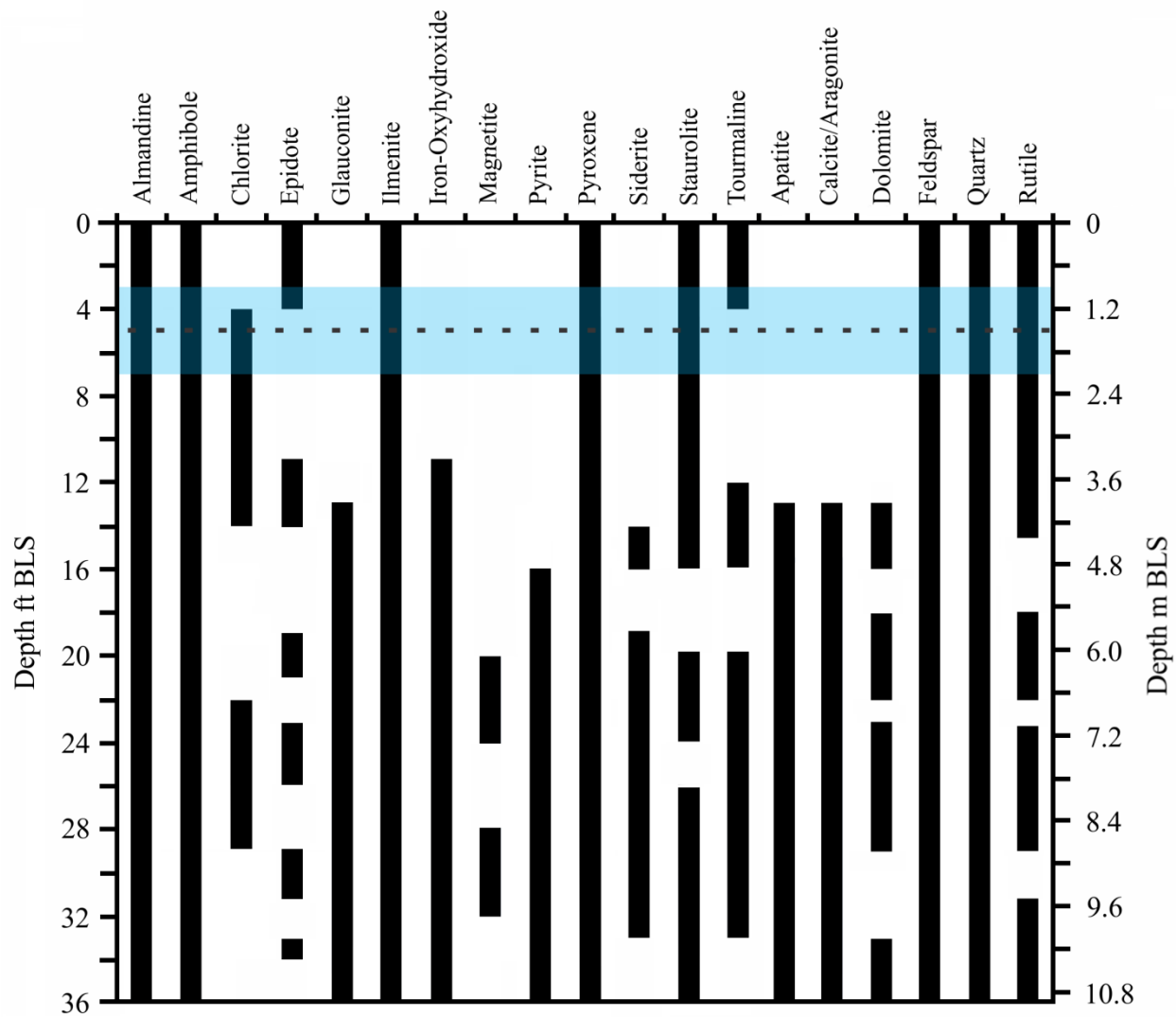


**Figure 12:** XRD-detected minerals by depth. The blue area denotes typical depth ranges of the water-table surface and the dashed line indicates the mean depth of the water table (Johnson, 1992).

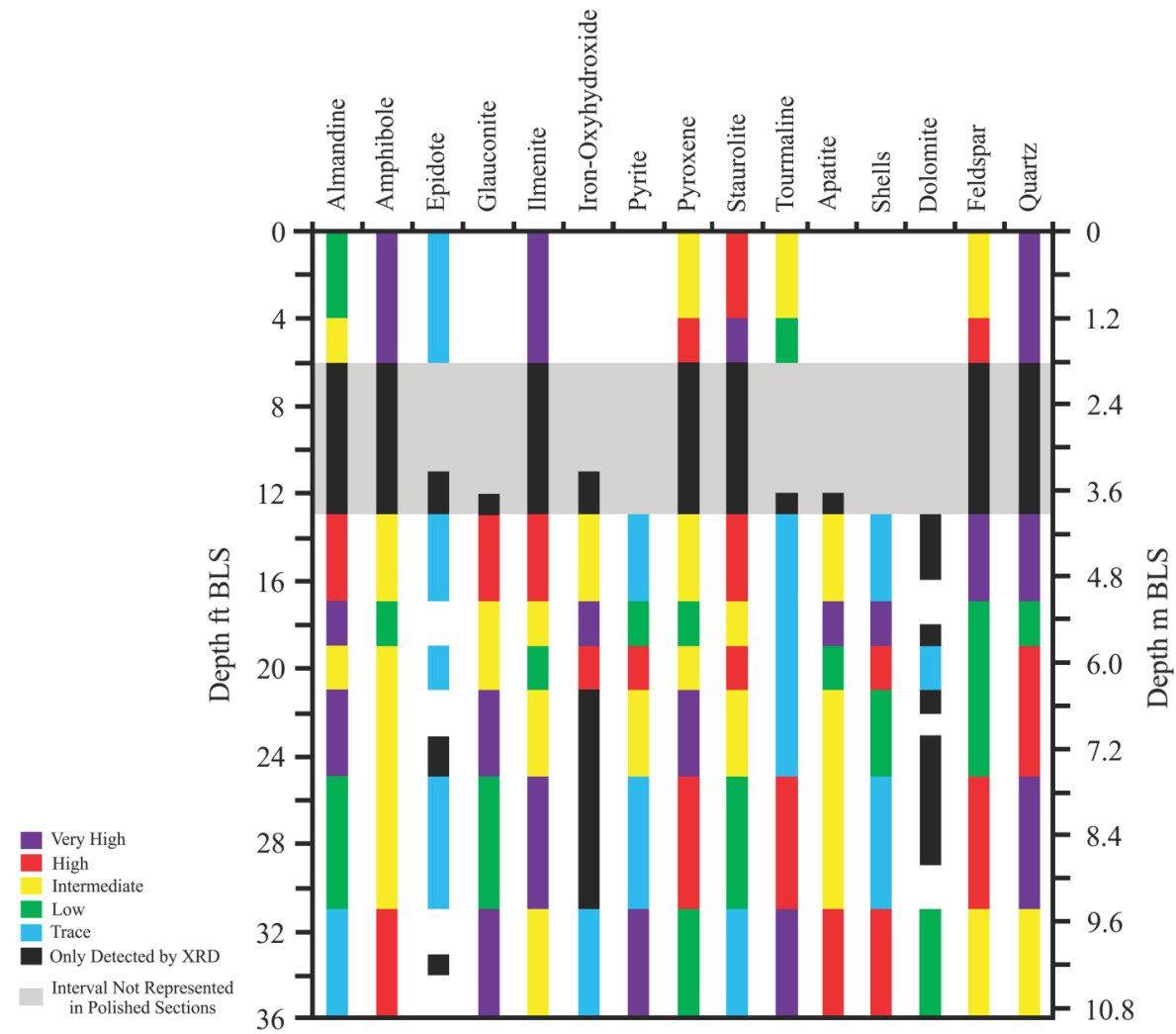


**Figure 13:** Occurrence and relative abundance of minerals that were both detected by XRD and confirmed via microscopy. Note that mineral abundances are relative to each individual mineral. Ranges in the depth of the water table are shown in Figure 12.

**Table 10:** Generalized mineral formulas of XRD-detected minerals.

<b>Mineral</b>	<b>Formula</b>
Almandine	$\text{Fe}^{+2}\text{Al}_2\text{Si}_3\text{O}_{12}$
Amphibole	$(\text{Na},\text{K})_{0-1}(\text{Na},\text{Ca},\text{Mn},\text{Fe}^{2+},\text{Mg})_2(\text{Mg},\text{Fe}^{2+},\text{Mn},\text{Al},\text{Fe}^{3+},\text{Ti})_5(\text{Si},\text{Al},\text{Ti})_8\text{O}_{22}(\text{OH},\text{F},\text{Cl})_2$
Apatite	$\text{Ca}_5(\text{PO}_4,\text{CO}_3)_3(\text{F},\text{Cl},\text{OH})$
Calcite/Aragonite	$\text{CaCO}_3$
Chlorite	$(\text{Mg},\text{Fe}^{2+})_6\text{AlSi}_3\text{O}_{10}(\text{OH})_8$
Dolomite	$\text{CaMg}(\text{CO}_3)_2$
Epidote	$\text{Ca}_2\text{Fe}^{+3}\text{Al}_2\text{Si}_3\text{O}_{12}\text{OH}$
Feldspar	$\text{KAlSi}_3\text{O}_8 - \text{NaAlSi}_3\text{O}_8 - \text{CaAl}_2\text{Si}_2\text{O}_8$
Glauconite	$(\text{K},\text{Na})(\text{Fe}^{3+},\text{Al},\text{Mg})_2(\text{SiAl})_4\text{O}_{10}(\text{OH})_2$
Ilmenite	$\text{Fe}^{+2}\text{TiO}_3$
Iron- Oxyhydroxide	Anhydrous: $\text{FeO}(\text{OH})$ Hydrated: $\text{FeO}(\text{OH})\cdot n\text{H}_2\text{O}$
Magnetite	$\text{Fe}^{2+}\text{Fe}^{3+}_2\text{O}_4$
Pyrite	$\text{Fe}^{+2}\text{S}_2$
Pyroxene	$(\text{Ca},\text{Na},\text{Fe}^{+2},\text{Mg},\text{Mn})(\text{Cr},\text{Al},\text{Fe}^{3+},\text{Mg},\text{Mn},\text{Ti},\text{Fe}^{+2})(\text{Si},\text{Al})_2\text{O}_6$
Quartz	$\text{SiO}_2$
Rutile	$\text{TiO}_2$
Siderite	$\text{Fe}^{2+}\text{CO}_3$
Staurolite	$\text{Fe}^{2+}_2\text{Al}_9\text{Si}_4\text{O}_{23}(\text{OH})$
Tourmaline	$(\text{Na},\text{Ca})(\text{Mg},\text{Li},\text{Al},\text{Fe}^{2+})_3\text{Al}_6(\text{BO}_3)_3\text{Si}_6\text{O}_{18}(\text{OH}_4)$

**Table 11:** Origins, sources, and important characteristics of XRD-detected minerals.

<b>Mineral</b>	<b>Origin/Source/Characteristics</b>	<b>Mineral</b>	<b>Composition/Source/Characteristics</b>
Almandine	Detrital; Piedmont crystalline rocks	Iron-Oxyhydroxide	Authigenic; in situ oxidation of Fe <sup>2+</sup>
Amphibole	Detrital; Piedmont crystalline rocks	Magnetite	Detrital; Piedmont crystalline rocks
Apatite	Non-detrital; fecal pellets from benthic marine organisms; often includes small grains of pyrite	Pyrite	Authigenic; in situ reduction of SO <sub>4</sub> <sup>2-</sup>
Calcite/Aragonite	Non-detrital; shells of marine organisms; often includes small grains of pyrite	Pyroxene	Detrital; Piedmont crystalline rocks
Chlorite	Detrital; Piedmont crystalline rocks	Quartz	Detrital; Piedmont crystalline rocks
Dolomite	Non-detrital; diagenesis in carbonaceous marine sediments	Rutile	Detrital; Piedmont crystalline rocks
Epidote	Detrital; Piedmont crystalline rocks	Siderite	Non-detrital, diagenesis in marine sediments
Feldspar	Detrital; Piedmont crystalline rocks	Staurolite	Detrital; Piedmont crystalline rocks
Glauconite	Non-detrital; diagenesis in marine sediments; often includes small grains of pyrite and other minerals; important for cation exchange capacity	Tourmaline	Detrital; Piedmont crystalline rocks
Ilmenite	Detrital; Piedmont crystalline rocks		

**Table 12:** Abundances of dominant, non-Fe-bearing minerals estimated in polished-thin sections.

Depth Range (m BLS)	Apatite %	Feldspar %	Quartz %	Shells %
0.6 - 1.0		8	91	
1.3 - 1.8		10	88	
4.1 - 5.1	6	11	78	2
5.1 - 5.9	11	3	31	48
5.9 - 6.5	5	3	57	32
6.5 - 7.5	5	4	72	16
8.7 - 9.5	5	9	79	4
8.7 - 10.8	9	7	44	38



**Table 13:** Abundances of dominant, Fe-bearing minerals estimated in polished-thin sections.

Depth Range (m BLS)	Almandine %	Amphibole %	Glaucosite %	Ilmenite %	Iron- Oxyhydro. %	Pyrite %	Pyroxene %	Staurolite %	Tourmaline %
0.6 - 1.0	0.03	0.28		0.58			0.11	0.09	0.05
1.3 - 1.8	0.08	0.35		0.74			0.17	0.17	0.05
4.1 - 5.1	0.22	0.20	0.67	0.63	0.38	0.001	0.18	0.25	0.01
5.1 - 5.9	0.69	0.34	1.51	1.11	1.73	0.02	0.23	0.46	0.03
5.9 - 6.5	0.30	0.44	0.85	0.38	0.90	0.06	0.29	0.40	0.02
6.5 - 7.5	0.44	0.29	0.91	0.44		0.07	0.42	0.23	0.01
8.7 - 9.5	0.11	0.26	0.27	1.61		0.003	0.23	0.12	0.18
8.7 - 10.8	0.02	0.37	0.95	0.37		0.13	0.17	0.04	0.24

### 4.3 Magnetic Separation Results

Using a Frantz Isodynamic Magnetic Separator, samples of sediments from the study area were separated into fractions at settings ranging from 0 amps up through 1.8 amps. Magnetic grains were isolated from less magnetic grains via hand magnet and by changing the current of the Frantz Isodynamic Magnetic Separator. Hereafter, “highly susceptible” and “poorly susceptible” grains refer to grains that were magnetically separated at settings of  $\leq 0.8$  amps (including the grains that were attracted to the hand magnet) and  $\geq 0.8$  amps, respectively. “Magnetically susceptible” grains include both the highly susceptible and poorly susceptible weight fractions while the remaining portion of the sediment sample was not susceptible via the magnetic separation technique (Appendix B). Although this procedure concentrated most Fe-bearing mineral grains for easier identification, it did not completely separate quartz grains with Fe-oxide coatings from those lacking Fe-oxide coatings. Quartz with such coatings was recognized as a potential source of Fe to local groundwater (e.g. Chapelle and Lovley, 1992; Penny et al., 2003; Park et al., 2006).

Samples TC14C: 8 – 12’ #6 and TC14C: 24 – 28’ #21 were not magnetically separated due to time constraints and because sediment-Fe concentrations for comparable TC14 samples (samples from an adjacent core that were acquired at similar depth ranges) are relatively low. Also, after packaging the requisite sample volume for sediment testing via NCAG, the remaining portions of TC14C: 0 – 4’ #1 and TC14C: 20 – 24’ #15 were insufficient for magnetic separation. However, XRF analyses of analogous TC14 samples indicate that the depth range represented by TC14C: 20 – 24’ #15 is likely located in the basal portion of the high-Fe zone (see XRF results). Samples TC14: 20 – 24’ #s 4 – 6 and the remaining portion of XRF sample TC14: 20 – 24’ #7 were amalgamated to constitute sample TC14C: 20 – 24’ #15. Henceforth, the

designation, “TC14C: 20 – 24’ #15”, will collectively refer to the samples TC14: 20 – 24’ #s 4 – 7. The mean of calculated depths (6.2 m BLS) from samples TC14: 20 – 24’ #s 4 – 7 is assigned to TC14C: 20 – 24’ #15 to account for disparities in recovery between TC14 and TC14C core samples.

The weight percentages of magnetically susceptible grains in the sediment samples range from about 0.7 to 14.9% (Figure 14). The recovery of magnetically susceptible grains was <2% for sediment samples acquired from the upper 4 m BLS. The highest concentrations (>6.7%) of magnetically susceptible grains occur at depths ranging from 5.1 to 6.5 m BLS. Intermediate percentages (>2.3 and <6.7%) of magnetically susceptible grains were recovered below 6.5 m BLS. The majority of magnetically susceptible grains were extracted from the 4  $\Phi$  and 3.25  $\Phi$  grain-size fractions; however, this was not quantified because the weights of susceptible grains were collectively determined from three size fractions (screen openings of 2.25  $\Phi$ , 3.25  $\Phi$ , and 4  $\Phi$ ). Magnetic separation data are presented in Appendix D.

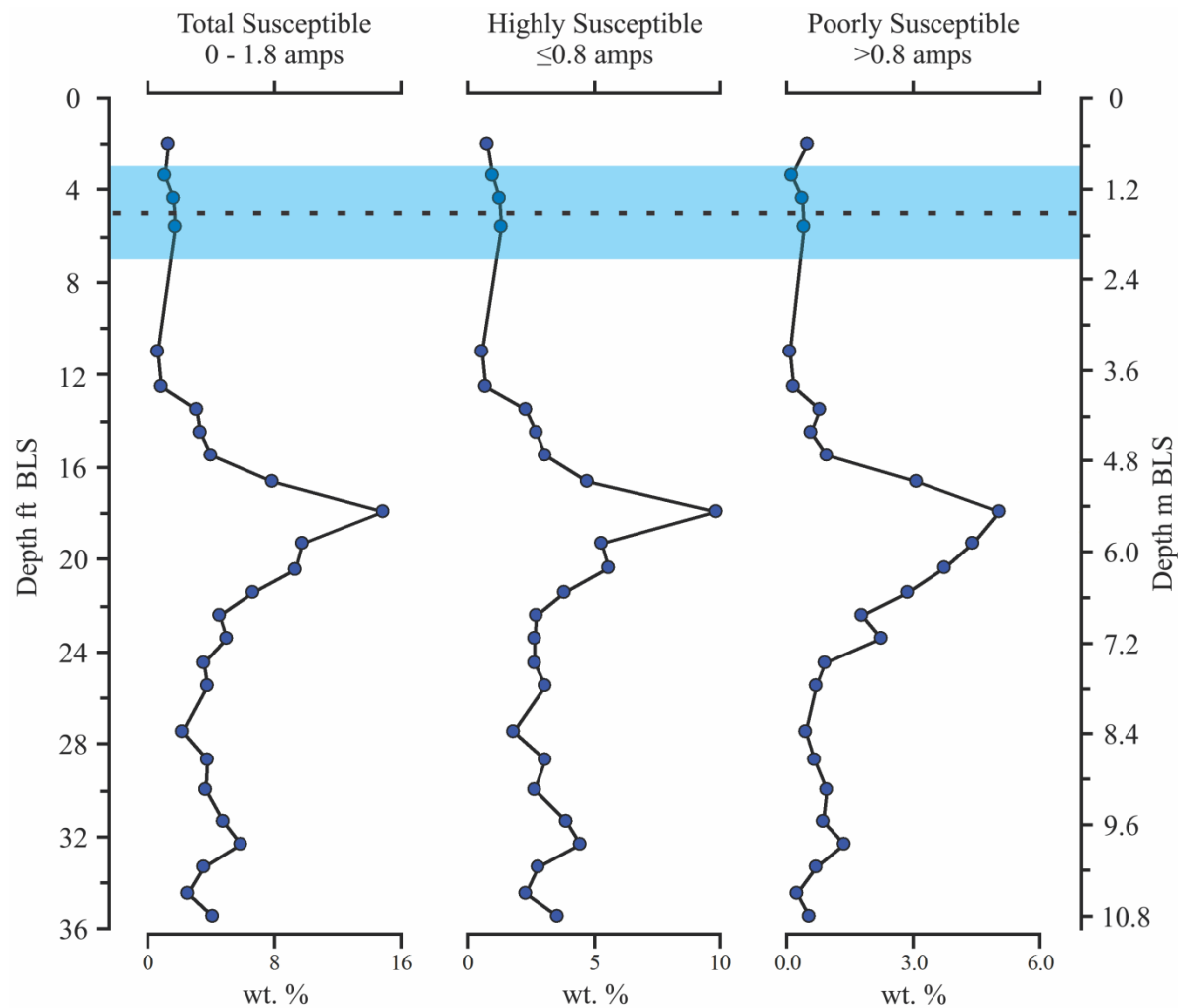


**Figure 14:** Weight percentages of magnetically susceptible grains with depth. The sum of highly susceptible ( $\leq 0.8$  amps) and poorly susceptible ( $> 0.8$  amps) weight fractions collectively comprise the “total susceptible” fraction (0 – 1.8 amps). The blue area denotes typical depth ranges of the water-table surface and the dashed line indicates the mean depth of the water table (Johnson, 1992).

## 4.4 Sediment Geochemistry

### 4.4.1 Statistical Analysis of XRF Results

Two Certified Reference Materials (MRG-1 and NCS DC 71302, Govindaraju, 1994) were subjected to replicate analyses to determine the precision and accuracy of the XRF analyses. Although MRG-1 and NCS DC 71302 were prepared from igneous rocks (gabbro and diorite, respectively), the standards were selected because their collective compositions include accepted values for Al, S, Fe, K, Mg, Mn, Na, P, Si, Ti, Ca, F, Cl, and Sr, which were believed to be sufficient to characterize the general chemical composition of the sediment samples. MRG-1 and NCS DC 71302 were analyzed by XRF 14 and 15 times, respectively and statistical techniques were applied to evaluate the results. The accepted compositions for the reference samples, XRF data, and detailed statistical data are presented in Appendix G.

Statistical analysis of the reference samples reveals that the XRF spectrometer is generally capable of precise measurements but the accuracy was highly variable (Tables 14 – 15). With the exception of F, the coefficients of variation (CV %) for all elements were less than 10 wt. % (typically less than 0.8 wt. %). CV % values for Cl and F were 6.2 wt. % and 10.0 – 43.2 wt. %, respectively. Percent error values were less than  $\pm 21$  wt. % for elements comprising at least 0.7 wt. % of the reference sample. Elements in standards containing less than this amount frequently had large % Errors.

The relatively poor precision and/or accuracy for some elements (Cl, Sr, F, Mn) may be attributed to low concentration. The XRF data indicate that MRG-1 contains approximately 262 ppm Cl; however, the published composition for MRG-1 does not include a value for Cl. The poor quality of the Sr measurements may be due to fact that the flow detector is not well suited for measuring elements heavier than Zn (Aruna et al., 2014). Overall, measurements for NCS DC

71302 were more accurate than MRG-1, however, these discrepancies could not be explained. Based on these data, Fe concentrations may be underestimated by more than 20%.

In 2015, replicate XRF analyses were performed on five pellet samples from TC14 (TC14: 0 – 4' #9, TC14: 12 – 16' #26, TC14: 12 – 16' #35, TC14: 16 – 20' #7, and TC14: 32 – 36' #17) to determine the reproducibility of geochemical data acquired in 2014 (Appendix G). These samples were selected because their compositions are generally representative of the various sediment types from differing depth intervals. The number of additional XRF analyses performed on each pellet sample ranged from 9 to 18 (mean 13) due to pellet breakage by the spectrometer's sample changer.

The results of statistical analyses for the 5 XRF pellet samples confirm that the XRF spectrometer is capable of precise and reproducible measurements of most elemental constituents. With the exceptions of F and Cl, the coefficients of variation for elements comprising the XRF pellet samples was <5.5 wt. %. Overall, the statistical data for the five pellet samples show that the original concentrations are highly reproducible. The average of absolute-percent deviations (AAPD) for 9 out of 14 elements is less than  $\pm 7.1$  wt. % and the AAPD for 50% of the species is less than  $\pm 3.0$  wt. % (Table 16). In addition, Fe values were highly reproducible with an AAPD of 1.8 wt. %. Examination of the plots displaying the 2015 mean concentrations vs the original 2014 concentrations reveals that a very strong linear correlation exists for all of the species ( $R^2$  ranges from 0.92 – 1.0) if the mean Na concentrations are omitted for TC14: 12-16' #26 ( $R^2$  is 0.25 if Na values TC14: 12-16' #26 are included) (Appendix G). Therefore, the statistical data for the pellet samples indicate that Na, Mg, and Cl concentrations may not be reliable. These species appear to have relatively low concentrations in these samples, which, in addition to detection limitations, may explain the inconsistent Na, Mg, and Cl values.

**Table 14:** Statistics for reference standard MRG-1.

Standard <sup>1</sup>	Element <sup>2</sup>	Accepted Value	Mean <sup>3</sup>	Median <sup>3</sup>	Confidence Level <sup>3</sup> (95%)	Standard Deviation <sup>3</sup>	Precision <sup>4</sup> (CV %)	Error <sup>5</sup>	Accuracy <sup>6</sup> (% Error)
MRG-1 (n = 14)	F	0.03	0.06	0.07	0.02	0.03	43.22	0.04	159.43
	Na	0.43	0.38	0.39	0.02	0.03	8.46	-0.05	-11.63
	Mg	8.13	7.56	7.56	0.02	0.03	0.36	-0.57	-7.03
	Al	4.50	3.82	3.86	0.04	0.07	1.94	-0.68	-15.06
	Si	18.38	21.42	21.45	0.05	0.08	0.37	3.04	16.54
	P	0.03	0.03	0.03	1.18E-04	2.05E-04	0.64	0.01	22.86
	S	0.06	0.06	0.06	2.10E-04	3.63E-04	0.59	0.00	1.90
	Cl		261.58	260.96	1.46	2.53	NC <sup>7</sup>	NC <sup>7</sup>	NC <sup>7</sup>
	K	0.15	0.17	0.17	3.10E-04	5.36E-04	0.32	0.02	11.35
	Ca	10.56	11.46	11.45	0.03	0.04	0.39	0.91	8.58
	Ti	2.21	2.14	2.14	3.82E-03	0.01	0.31	-0.08	-3.40
	Mn	0.13	0.11	0.11	5.22E-04	9.04E-04	0.79	-0.02	-13.03
	Fe	12.48	9.93	9.92	0.04	0.06	0.65	-2.56	-20.49
Sr	260	169	169	0.85	1.46	0.86	-90.15	-34.67	

1. The number (n) of replicate XRF analyses performed is indicated below the label of the standard

2. Concentrations are expressed as weight percents except for Cl and Sr, which are in units of ppm (mg/kg)

3. Calculated using Microsoft Excel

4. Precision was determined via the coefficient of variation (CV %).  $CV \% = (\text{standard deviation} \div \text{mean}) \times 100$

5. Error = mean value - accepted value

6. Accuracy was determined via percent error.  $\% \text{ Error} = [(\text{mean} - \text{accepted value}) \div \text{accepted value}] \times 100$

7. NC: Not calculated. An accepted value for this element was not reported by the laboratory

**Table 15:** Statistics for reference standard NCS DC 71302.

Standard <sup>1</sup>	Element <sup>2</sup>	Accepted Value	Mean <sup>3</sup>	Median <sup>3</sup>	Confidence Level <sup>3</sup> (95%)	Standard Deviation <sup>3</sup>	Precision <sup>4</sup> (CV %)	Error <sup>5</sup>	Accuracy <sup>6</sup> (% Error)
NCS DC 71302 (n = 15)	F	0.11	0.08	0.08	4.38E-03	0.01	10.03	-0.03	-29.64
	Na	1.85	1.77	1.78	0.01	0.02	1.13	-0.08	-4.19
	Mg	0.51	0.57	0.57	3.55E-03	0.01	1.13	0.06	12.13
	Al	8.52	8.72	8.66	0.10	0.17	2.00	0.20	2.32
	Si	29.48	28.97	28.96	0.07	0.13	0.44	-0.50	-1.71
	P	0.16	0.14	0.14	3.47E-04	6.27E-04	0.46	-0.02	-13.96
	S	0.02	0.03	0.03	7.25E-04	1.31E-03	5.24	0.002	8.70
	Cl	160.00	217.50	214.32	7.50	13.54	6.23	57.50	35.94
	K	4.29	4.43	4.43	4.09E-03	0.01	0.17	0.14	3.24
	Ca	1.77	1.81	1.81	1.67E-03	3.02E-03	0.17	0.04	2.33
	Ti	0.48	0.47	0.47	1.49E-03	2.70E-03	0.57	-0.01	-1.99
	Mn	0.69	0.07	0.07	3.19E-04	5.76E-04	0.80	-0.62	-89.61
	Fe	3.30	3.09	3.10	0.01	0.02	0.64	-0.21	-6.35
Sr	318	355	355	1.50	2.71	0.76	37.35	11.75	

1. The number (n) of replicate XRF analyses performed is indicated below the label of the standard

2. Concentrations are expressed as weight percents except for Cl and Sr, which are in units of ppm (mg/kg)

3. Calculated using Microsoft Excel

4. Precision was determined via the coefficient of variation (CV %).  $CV \% = (\text{standard deviation} \div \text{mean}) \times 100$

5. Error = mean value - accepted value

6. Accuracy was determined via percent error.  $\% \text{ Error} = [(\text{mean} - \text{accepted value}) \div \text{accepted value}] \times 100$



**Table 16:** Average of absolute-percent deviations of elements comprising the XRF pellet samples.

Element <sup>1</sup>	AAPD <sup>2</sup>
F	18.64
Na	38.81
Mg	33.24
Al	7.07
Si	4.44
P	2.99
S	24.95
Cl <sup>2</sup>	1090.33
K	2.70
Ca	2.85
Ti	1.14
Mn	2.18
Fe	1.78
Sr	0.97

1. The average of absolute-percent deviations (AAPD) was calculated for each element that comprised the XRF pellet samples to determine how well the XRF spectrometer was capable of reproducing the initial 2014 concentrations. Concentrations are expressed as weight percents except for Cl and Sr, which are presented in ppm units
2. Average absolute deviation was calculated as follows: 1. the absolute value of % Deviations was computed for each element shown in Appendix G6. 2. The mean of the resulting absolute-percent deviations for each element was computed for the five XRF pellet samples
3. Only 2 concentrations for Cl were used to calculate AAPD because Cl was not initially detected in 3 XRF pellet samples

#### 4.4.2 XRF Results

Some XRF data were either discarded or the mean concentrations, calculated from more recent (2015) XRF analyses, were used to replace potentially invalid data (Table 17). In the latter case, original (2014) constituent concentrations were replaced to eliminate possible errors resulting from detector overloading or imprecise detection (where the sum of constituent concentrations is  $\leq 80\%$ ). The following subsection presents the XRF results for core TC14. XRF data are presented in Appendix G.

Changes in major and minor elemental concentrations are shown with respect to core depths in Figures 15 and 16, respectively. The XRF data reveal that Si is consistently at its highest concentrations between 0 and 3.6 m BLS. Most of the other constituents reach their lowest values in this depth range. There is a strong negative correlation between Si and Ca below 4.9 m BLS. Ti and Na are relatively high above 2.4 m BLS. Si concentrations generally decrease from the surface to approximately 5.8 m BLS. Fe is consistently at its highest concentrations from 3.7 to 6.1 m BLS. The highest values for Mg, Al, and K occur from 3.7 to 4.9 m BLS where Ti is also relatively high. F, P, and Mn attain their highest concentrations from 4.9 to 6.1 m BLS. A strong positive correlation between Fe and Mn occurs below 4.7 m BLS. From around 5.5 – 7.3 m BLS, Ca and Sr consistently show their highest concentrations. Cl has a major spike at approximately 8.2 m BLS but its concentration remains relatively low (generally below 120 ppm) elsewhere in the core. The highest concentration of Ti occurs at around 8.8 m BLS. S and Na concentrations are highest from 9.8 to 10.1 m BLS.

**Table 17:** A table illustrating potentially problematic XRF data and the corrective action taken. If available, the mean of replicate 2015 XRF analyses (data not used to complete statistics due to an insufficient number of replicate analyses because of pellet breakage) was used to replace some data. If supplementary data were not available for a potentially problematic analysis, the data for that analysis were not reported.

Sample ID	Date Measured	Problem	Action Taken
TC14: 8-12' #8	8/19/14	Detector Overload	Replaced with the mean of 2015 trials
TC14: 8-12' #13	8/19/14	Sum of Concentrations 30.47%	Replaced with the mean of 2015 trials
TC14: 12-16' #3	8/19/14	Sum of Concentrations 43.94%	Discarded
TC14: 12-16' #9	8/19/14	Detector Overload	Discarded
TC14: 12-16' #21	8/19/2014 8/19/2014	Sample Analyzed Twice	Mean of original 2014 trials reported
TC14: 12-16' #35	9/17/15	Sum of Concentrations 72.85%	Discarded
TC14: 16-20' #12	8/19/14	Detector Overload	Discarded
TC14: 20-24' #7	8/19/14	Detector Overload	Replaced with the mean of 2015 trials
TC14: 20-24' #7	9/17/15	Detector Overload	Discarded
TC14: 24-28' #12	8/20/14	Detector Overload	Discarded

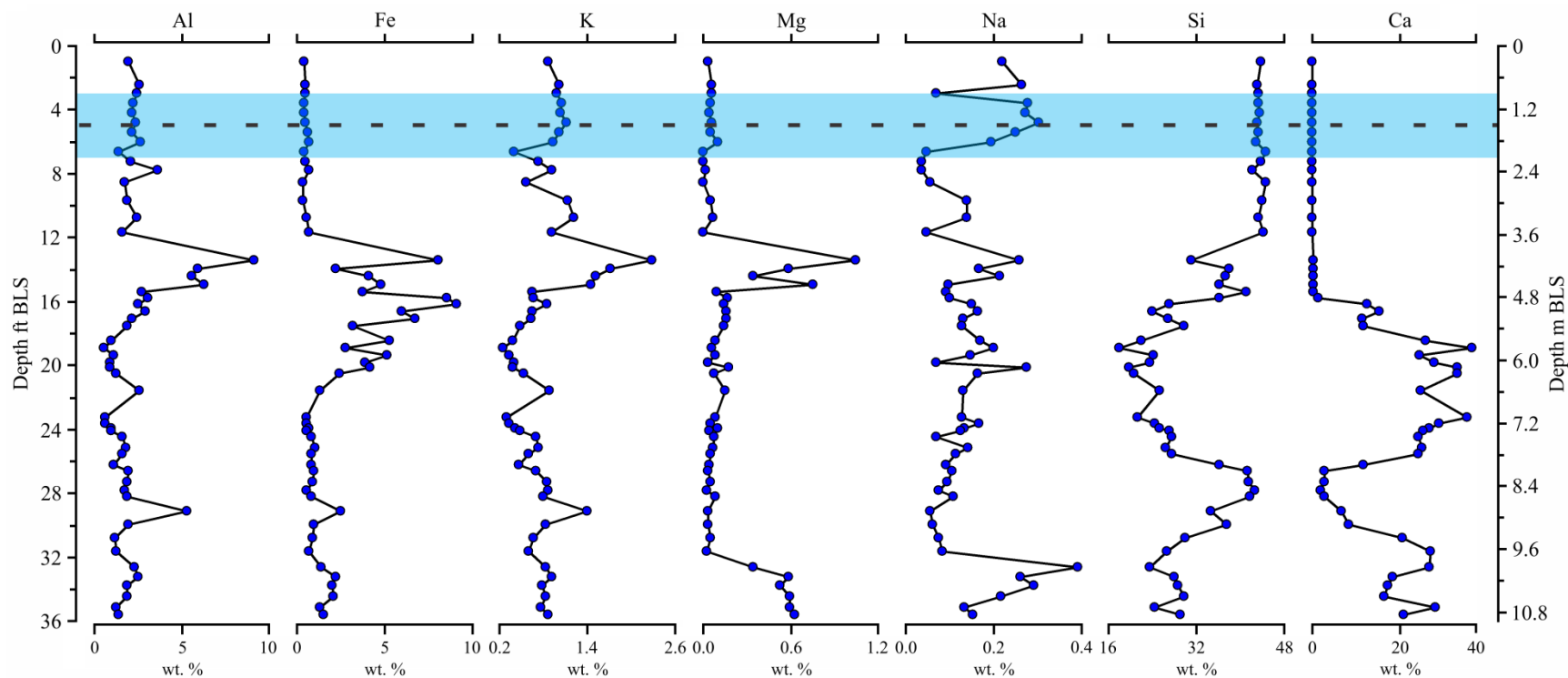


**Figure 15:** XRF-determined changes in major elemental concentrations with depth in TC14. The blue area denotes typical depth ranges of the water-table surface and the dashed line indicates the mean depth of the water table (Johnson, 1992).

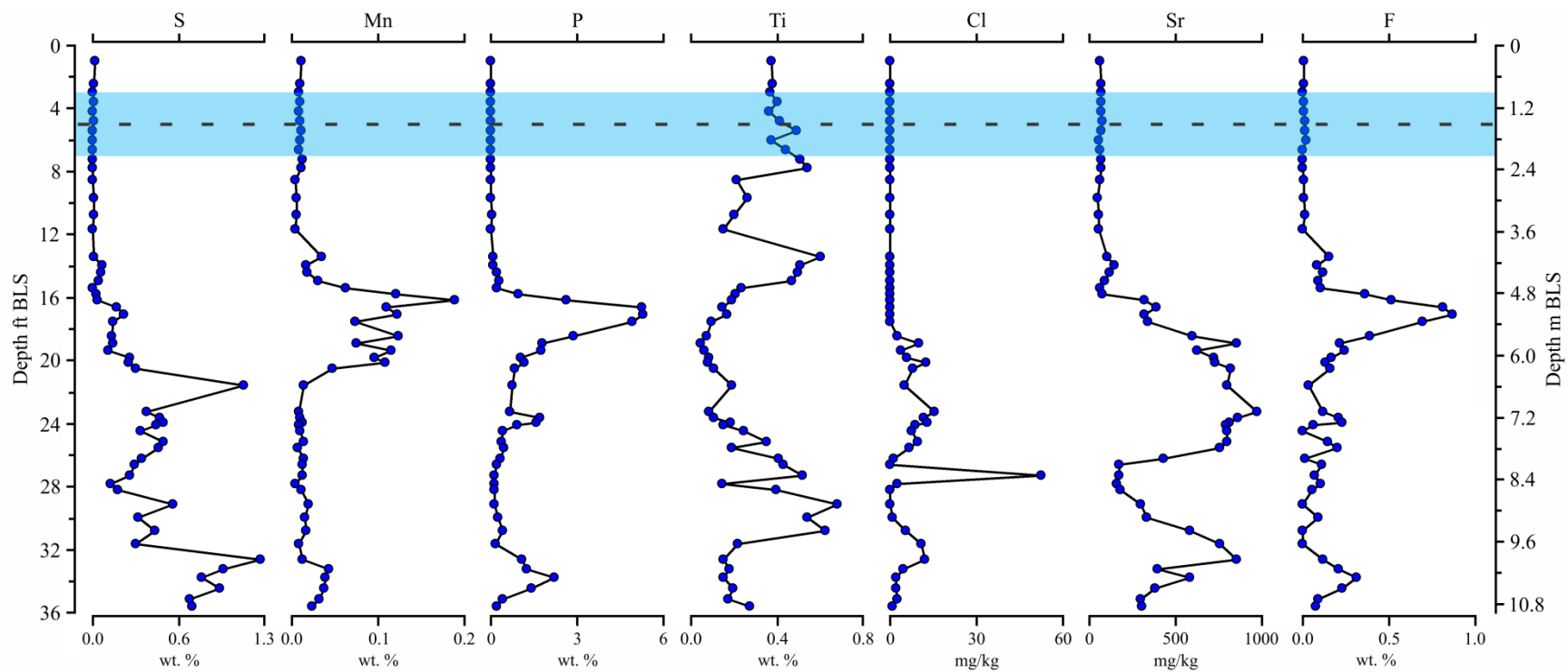


**Figure 16:** XRF-determined changes in minor elemental concentrations with depth in TC14. The blue area denotes typical depth ranges of the water-table surface and the dashed line indicates the mean depth of the water table (Johnson, 1992).

#### **4.4.3 LOI Results**

Nineteen sediment samples from TC14 were subjected to LOI analysis to estimate variations in organic-matter content. Qualitative estimations for % LOI range from 0.0181 to 0.7273 wt. % (Figure 17). LOI values are consistently high from 4.9 to 7.3 m BLS. LOI has a major peak between approximately 9.1 and 10.1 m BLS. LOI data are presented in Appendix H.

#### **4.4.4 NCAG Sediment-Test Results**

The Soil Testing Division of the North Carolina Department of Agriculture determined additional and supplementary geochemical data for 29 TC14C (an adjacent sister core of TC14) sediments samples. This subsection summarizes the results of their analyses. NCAG data are presented in Appendix I.

Humic matter percent by volume (HM %) measures the amount of humic and fulvic acids (chemically active constituents of organic-matter) in a sediment, representing the portion of sediment organic matter that is soluble in a dilute, sodium hydroxide solution (Hardy et al., 2012). HM % generally decreases with increasing depth, ranging from 0.66 to 0.04 vol. % (Figure 17). HM decreases rapidly from 0.66 vol. % near the surface to 0.09 vol. % by 1 m BLS. Subsequently, HM % remains at 0.09 vol. % until around 4.1 m BLS. HM then falls to the lowest measured value of 0.04 vol. % at 4.4 m BLS and, does not change with increasing depth.

Sediment-water pH is a measure of hydrogen-ion activity in the sediment solution (Hardy et al., 2012). pH values range from 4.9 to 8.1 (Figure 17). Sediment samples acquired above 4.9 m BLS are acidic (<5.8) but pH increases sharply to circumneutral/slightly basic (~7.5 – 8.1) by 5.3 m BLS. The largest increase in pH values (4.9 to 8.1) occurs in the depth range of 3.8 to 5.5 m BLS.

Cation exchange capacity (CEC) is a relative measure of the ability of a sediment to hold exchangeable cations (Hardy et al., 2012). CEC, expressed as milliequivalents per 100 cubic centimeters ( $\text{meq}/100 \text{ cm}^3$ ), ranges from 1.1 to 129.1  $\text{meq}/100 \text{ cm}^3$  (Figure 17). The lowest CEC values consistently occur from the surface to approximately 3.8 m BLS. CEC is very high ( $>88 \text{ meq}/100 \text{ cm}^3$ ) from around 4.9 to 7.6 m BLS and below 9.1 m BLS. The largest increase in CEC (from 2.3 to 124.5  $\text{meq}/100\text{cm}^3$ ) occurs between 3.8 to 5.5 m BLS.

Exchangeable acidity (AC) constitutes the portion of CEC that is retained by  $\text{H}^+$  and  $\text{Al}^{3+}$  ions (Hardy et al., 2012). AC ranges from 0 to 2.6  $\text{meq}/100\text{cm}^3$  (Figure 17). AC is relatively constant (0.6 – 1  $\text{meq}/100\text{cm}^3$ ) from the surface to about 4.0 m BLS, peaks at approximately 4.1 m BLS, and rapidly diminishes to 0 by 4.7 m BLS. AC does not increase above 0  $\text{meq}/100\text{cm}^3$  below 4.7 m BLS.

Base saturation (BS %) represents the percentage of CEC that is occupied by basic cations such as  $\text{Ca}^{2+}$ ,  $\text{Mg}^{2+}$ , and  $\text{K}^+$  (Hardy et al., 2012). BS % ranges from 43 to 100% and is variable (mean 64%) above 4.7 m BLS (Figure 17). The values begin increasing steadily at 3.4 m BLS, finally reaching a plateau of 100% at 5.1 m BLS.

Concentration changes for extractable elements are shown with respect to core depths in Figures 18 – 19. The lowest concentrations for most elements occur between 0 and 3.7 m BLS.  $\text{Zn}_e$ ,  $\text{Cu}_e$ , and  $\text{P}_e$  consistently show their highest concentrations between 3.7 and 4.9 m BLS. The highest concentrations of  $\text{Na}_e$  and  $\text{Mn}_e$  occur from 4.9 – 6.1 m BLS, where  $\text{Ca}_e$  is also very high. The largest increase in  $\text{Ca}_e$  (from 1,874 to 23,939  $\text{mg}/\text{dm}^3$ ) and  $\text{Na}_e$  (from 23 to 301  $\text{mg}/\text{dm}^3$ ) occur along a depth range of 4.7 to 5.1 m BLS.  $\text{Mg}_e$ ,  $\text{K}_e$ ,  $\text{Ca}_e$ , and  $\text{S}_e$  are consistently at their highest concentrations between 9.8 – 11.0 m BLS.

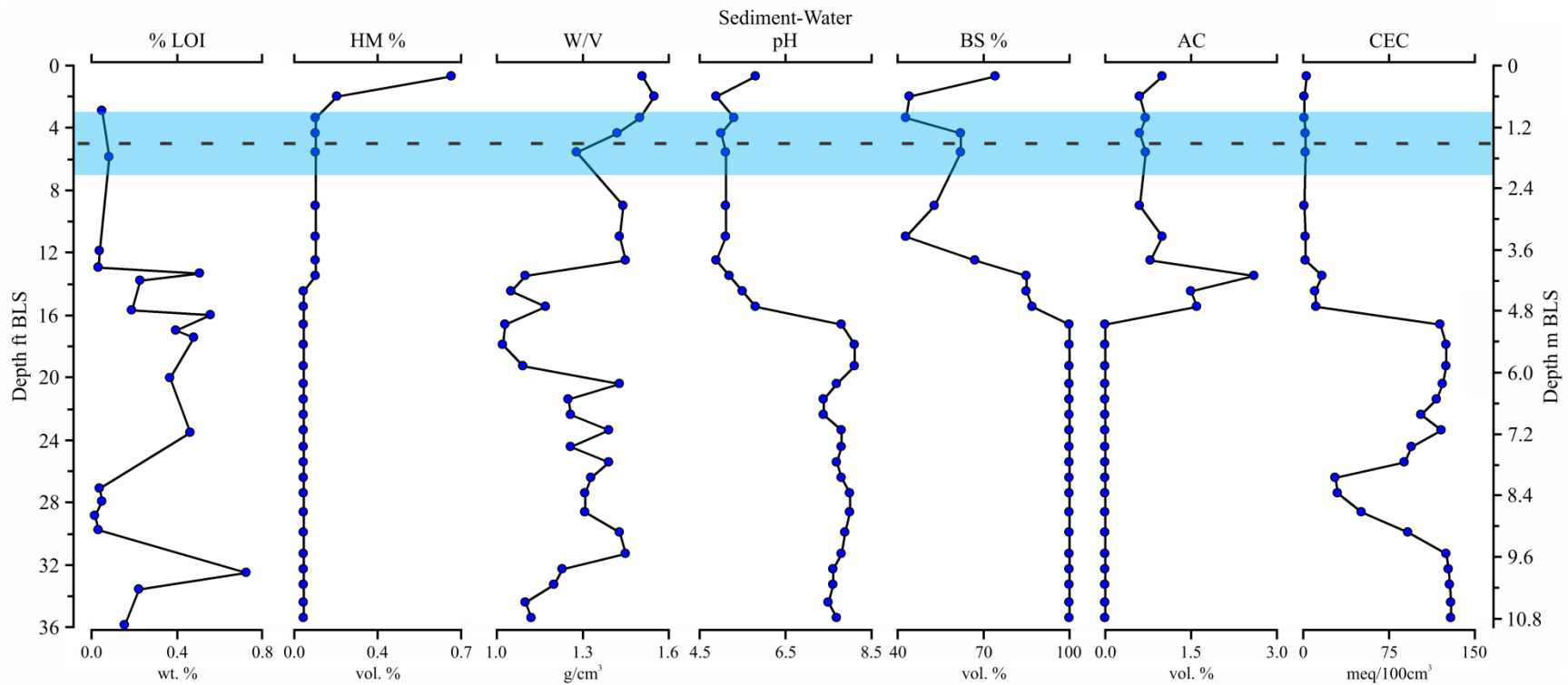


**Figure 17:** Changes in % LOI, HM %, W/V, Sediment-water pH, BS %, AC, and CEC with depth. % LOI and the NCAG-determined parameters are for TC14 and TC14C, respectively. The blue area denotes typical depth ranges of the water-table surface and the dashed line indicates the mean depth of the water table (Johnson, 1992).



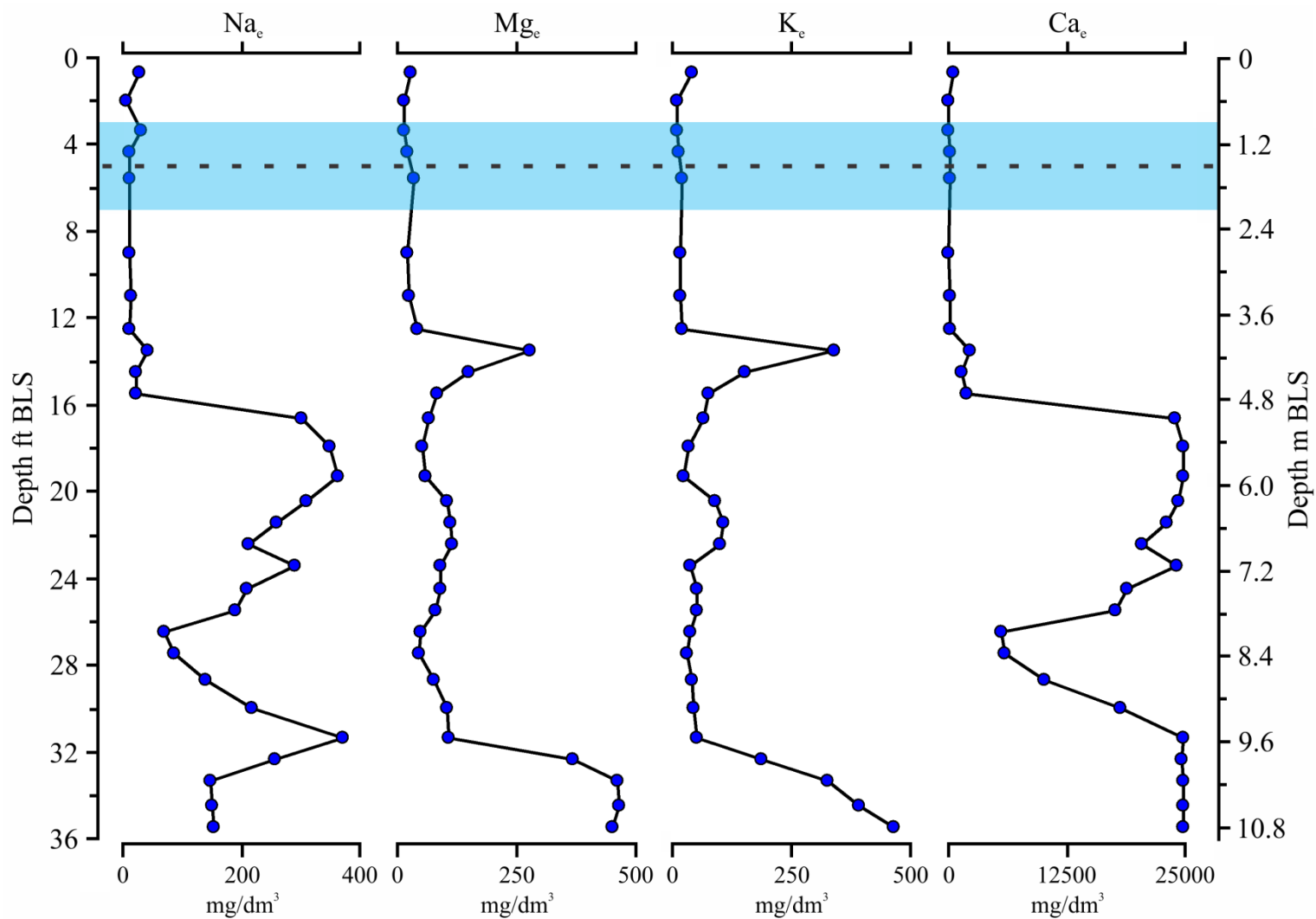


**Figure 18:** NCAG-determined changes in major elemental concentrations with depth in TC14C. The blue area denotes typical depth ranges of the water-table surface and the dashed line indicates the mean depth of the water table (Johnson, 1992).

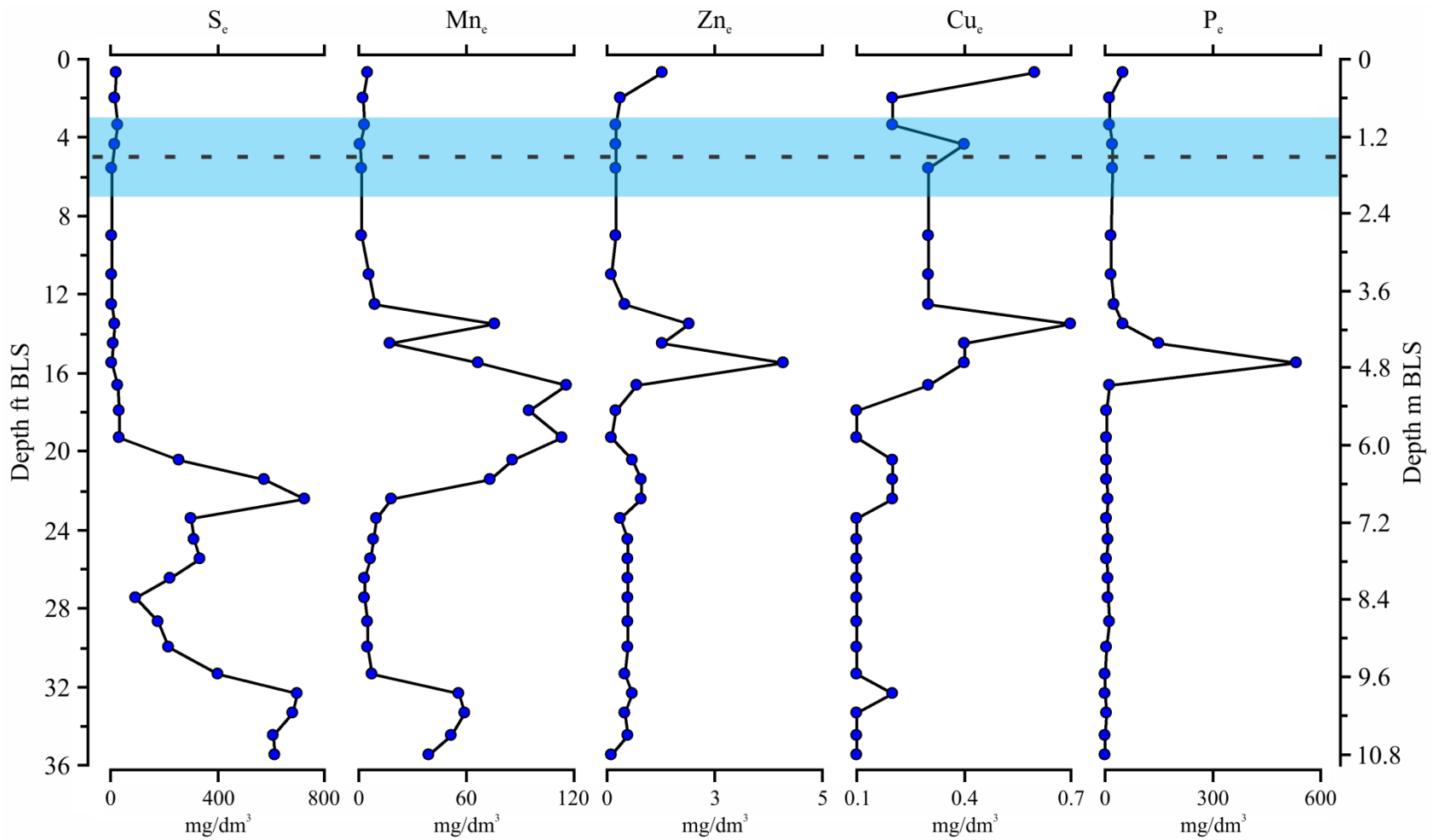


**Figure 19:** NCAG-determined changes in minor elemental concentrations with depth in TC14C. The blue area denotes typical depth ranges of the water-table surface and the dashed line indicates the mean depth of the water table (Johnson, 1992).

#### 4.4.5 Comparison of XRF and NCAG Results

Mean elemental concentrations for nine, 1.2 m depth intervals were calculated to compare the XRF results with the NCAG results via regression analysis and by comparison of concentration profiles. Na, Mg, K, Ca, P, S, and Mn are XRF-determined, total elemental concentrations (i.e. total wt. % concentrations of elements that comprise the TC14 sediment samples). Na<sub>e</sub>, Mg<sub>e</sub>, K<sub>e</sub>, Ca<sub>e</sub>, P<sub>e</sub>, and S<sub>e</sub> are NCAG-determined, extractable-elemental concentrations (i.e. the concentrations (mg/dm<sup>3</sup>) represent how much of the element was liberated from the TC14C sediment samples via the Mehlich-3 extractant). An example comparing the results of comparable XRF and NCAG analyses is presented in Figure 20. The results for the remaining species are presented in Appendix J.

The results of regression analyses reveal a slight correlation for Mg ( $R^2 = 0.68$ ) and strong correlations for Ca, S, and Mn, which had  $R^2$  values of 0.89, 0.96, and 0.93, respectively. Moreover, side by side comparison of concentration profiles for these elements indicates that total concentration of an element is an important control on Mg<sub>e</sub>, Ca<sub>e</sub>, S<sub>e</sub>, and Mn<sub>e</sub> concentrations.

Comparison of XRF and NCAG-determined-concentration profiles and linear regression plots indicate a lack of correlation for Na ( $R^2 = 0.01$ ), K ( $R^2 = 0.02$ ), and P ( $R^2 = 0.04$ ). In addition to detection limitations, discrepancies between the extractable and total-elemental concentrations may be variables controlling element extractability such as the chemistry, crystallinity, and surface area of the minerals containing the elements of interest, as well as, the physical and chemical properties of the other constituents that are present in the sample (Stucki et al., 2012; Wuenscher et al., 2015).

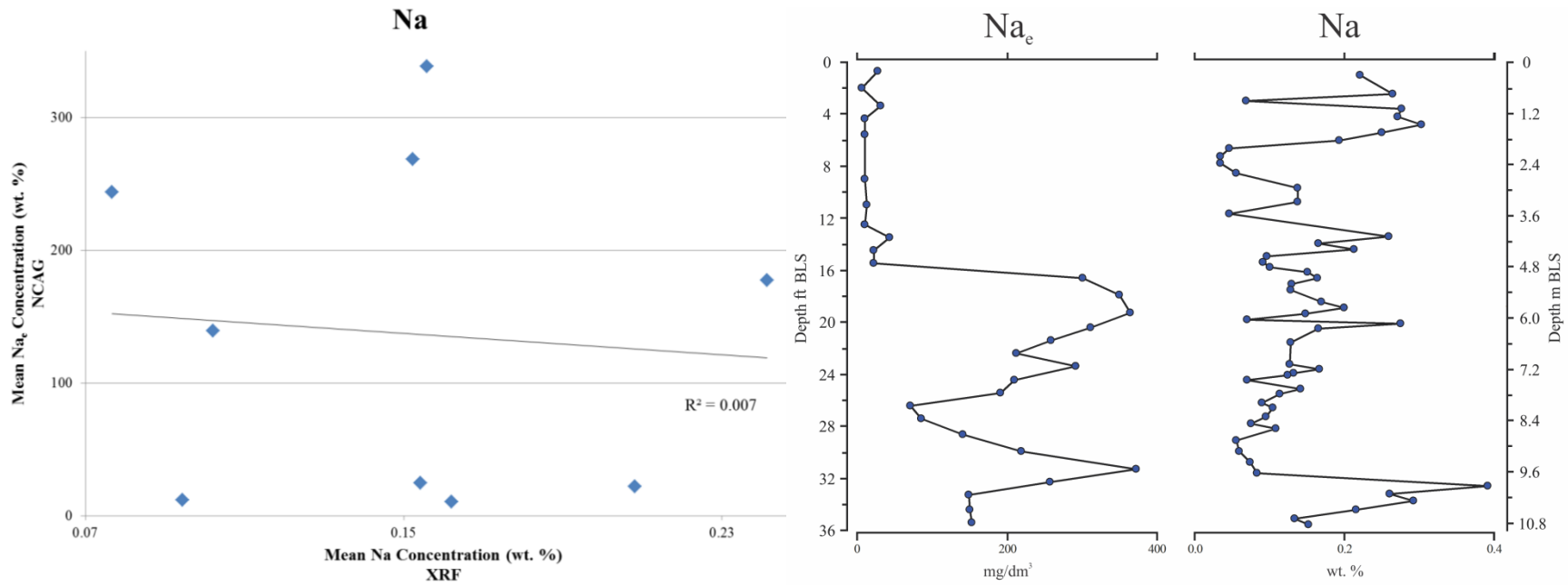


**Figure 20:** Comparison of NCAG and XRF results for sodium. The left plot is a regression analysis of mean Na<sub>e</sub> concentrations (measured by NCAG) and mean Na concentrations (measured by XRF). The graphs on the right are concentration profiles for extractable sodium (Na<sub>e</sub>) and total sodium (Na).

## 4.5 SEM/EDX Results

### 4.5.1 Statistical Analysis of Mineral Standards

An Oxford Instruments INCA X-act EDX system attached to a FEI Quanta 200 Mark 1 Environmental SEM was used to collect SEM and EDX data. The EDX data were processed using the INCA analysis software. Mineral standards analyzed to determine precision and accuracy of the system were albite, almandine, apatite, benitoite, biotite, chlorite, diopside, hematite, kaersutite, magnetite, marcasite, pyrope, rutile, and sanidine (Table 18 and Appendix F). These standards were analyzed an average of about ten times each between 0 – 20 KeV for 30 seconds of live time at a working distance of 11.486 mm.

Analyses of standards indicate that reliable detection of a particular element requires that its concentration in the sample must typically exceed 0.4 wt. %. Because the detector does not analyze for hydrogen and has a limited capacity to measure light elements (atomic number <11), the accepted values for hydrogen, carbon, and fluorine are normalized to 0 wt. % for mineral standards containing these elements to improve comparison of EDX analyses to the accepted values of hydrous mineral standards (e.g. apatite, biotite, chlorite, and kaersutite). Moreover, due to detection-related limitations, O<sub>2</sub> concentrations were estimated for each standard analysis by calculating the difference between 100% and the sum of elemental concentrations (atomic numbers >10). This technique significantly impacts the iron-oxyhydroxide analyses because their water content typically varies from about 5 – 30 wt. % (Harvey and Linton, 1981; Dzombak and Morel, 1990; Jambor and Dutrizac, 1998). For elements that were below detectable limits in more than 25% of evaluated EDX spectra for an individual mineral specimen, ½ of the lowest detected concentration for the element was used for calculations instead of reporting a zero value (Nehls and Akland, 1973).

In silicate minerals, the EDX system tends to overestimate Si by 1 – 9 wt. %, especially in biotite, while in another phyllosilicate, chlorite, it was overestimated by almost 23%. It generally underestimates the other common cations (Al and Ca by 1 – 6 wt. % and Fe by 1 – 8 wt. %), especially Na, which is underestimated by an average of 7 wt. % (particularly in feldspars). Magnesium is underestimated in some silicates and overestimated in others by 1 – 5 wt. %. When present in amounts greater than 1 wt. %, the accuracy of K analyses in feldspars was excellent, but in biotite this element was overestimated by almost 5 wt. %. Analyses of hydrous inosilicates and phyllosilicates tend to be less accurate than those for silicates not containing any hydroxide (OH<sup>-</sup>). Phosphorous and S in non-silicate minerals were overestimated by 5.7 and 3.7 wt. %, respectively. Many elements constituting small proportions (<0.19 wt. %) of standards showed large errors (>50 wt. %).

The Fe-bearing standards (standards comprised of >1 wt. % Fe) include almandine, biotite, chlorite, hematite, kaersutite, magnetite, marcasite, and pyrope. In general, the precision of sheet-silicate analyses for Fe was low (the coefficient of variation (CV) for Fe in chlorite and biotite was about 3.6 wt. % and 5.9 wt. %, respectively) while measurements of Fe in the Fe oxides (hematite and magnetite) were very precise (CV <0.3 wt. %). However, analyses of Fe oxides resulted in the least accurate measurements for Fe (% Error between 7.4 – 10.7 wt. % Fe). Long-term storage of the standards may have resulted in the oxidation of Fe<sup>2+</sup> and subsequent formation of iron-oxyhydroxides on the surfaces of the standards.

**Table 18:** Generalized mineral formulas of EDX reference samples.

<b>Reference Sample</b>	<b>Mineral Formula</b>
Albite	$\text{NaAlSi}_3\text{O}_8$
Almandine	$\text{Fe}^{2+}_3\text{Al}_2\text{Si}_3\text{O}_{12}$
Apatite	$\text{Ca}_5(\text{PO}_4)_3(\text{OH})$
Benitoite	$\text{BaTiSi}_3\text{O}_9$
Biotite	$\text{K}(\text{Mg},\text{Fe}^{2+})_3\text{AlSi}_3\text{O}_{10}(\text{OH})_2$
Chlorite	$\text{Mg}_6\text{AlSi}_3\text{O}_{10}(\text{OH})_8$
Diopside	$\text{CaMgSi}_2\text{O}_6$
Hematite	$\text{Fe}^{3+}_2\text{O}_3$
Kaersutite	$\text{NaCa}_2(\text{Mg},\text{Fe}^{+2})_4\text{TiSi}_6\text{Al}_2\text{O}_{22}(\text{OH})_2$
Magnetite	$\text{Fe}^{2+}\text{Fe}^{3+}_2\text{O}_4$
Marcasite	$\text{Fe}^{2+}\text{S}_2$
Pyrope	$\text{Mg}_3\text{Al}_2\text{Si}_3\text{O}_{12}$
Rutile	$\text{TiO}_2$
Sanidine	$\text{KAlSi}_3\text{O}_8$

#### 4.5.2 Chemistry of Fe-Rich Aggregates and Grain Coatings

The results of microscopy and elemental-mapping of 4 polished-thin sections (PTS:9-12, PTS:13-14, PTS:15-16, PTS: 26-28) indicate the presence of abundant Fe-rich grain aggregates and grain coatings (Ags/Cs). Optical microscopy reveals that the Ags/Cs are dark brown to opaque in plane-polarized light and typically occupy the edges spaces around quartz, feldspar, and dolomite grains and shell fragments (Figure 21A). Most Ags/Cs appear as distinctive bright-white blobs on SEM photomicrographs and contrast well with Fe-deficient minerals (Figure 21C), which are usually darker gray. The areal extent of individual aggregates is highly variable but the thicknesses of grain coatings are more consistent, ranging from about 10 to 30  $\mu\text{m}$  (Figure 22). Collectively, Ags/Cs comprise about 15 – 20% of magnetically susceptible grains (0 – 1.8 amps), found at depths between 4.1 – 6.5 m BLS. The results of XRD analyses reveal that the Ags/Cs are likely composed of one or more iron-oxyhydroxides.

A total of 124 EDX spectra were acquired from magnetically susceptible Ags/Cs to semi-quantitatively determine their elemental compositions. Since Ags/Cs tend to encapsulate a variety of minerals, spectral data for 24 EDX analyses were omitted from statistical evaluation. Data chosen for exclusion were those consisting of >15 wt. % of one or more elemental constituents (excluding Fe and  $\text{O}_2$ ) and those containing <30 wt. % Fe. For elements that were below detectable limits in more than 25% of evaluated EDX spectra,  $\frac{1}{2}$  of the lowest detected concentration for the element was used for calculations instead of reporting a zero value (Nehls and Akland, 1973). Data and statistics for EDX spectra measured from magnetically susceptible Ags/Cs are presented in Appendix F.



Although the compositions of natural iron-oxyhydroxides are highly variable due to their capacity to scavenge a variety of chemical species (e.g. phosphate, arsenate, Si, and Ca), the Fe content of iron-oxyhydroxides is typically >50 wt. % (Harvey and Linton, 1981; Dzombak and Morel, 1990; Jambor and Dutrizac, 1998). Analysis of 100 spectra reveals that the elemental composition of Ags/Cs is dominated by Fe (mean 53 wt. %) and oxygen (mean 30 wt. %) with minor proportions of Na, Mg, Al, Si, P, S, Cl, K, Ca, Ti, and Mn (Table 19 and Appendix F). Iron-oxyhydroxides are likely the most important sources of Fe above 6.4 m BLS because their occurrence appears to correspond with high-Fe concentrations in core samples.

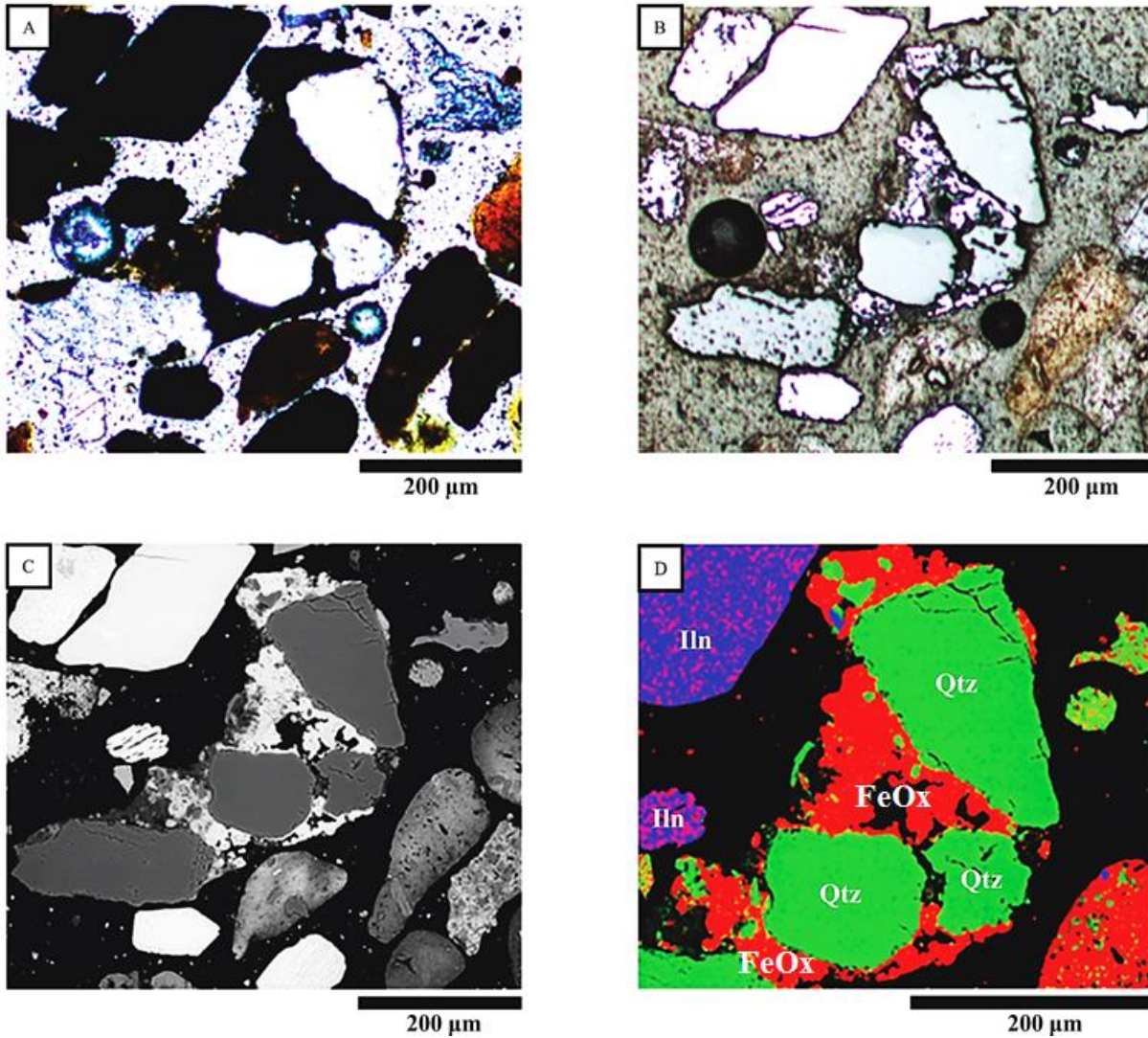
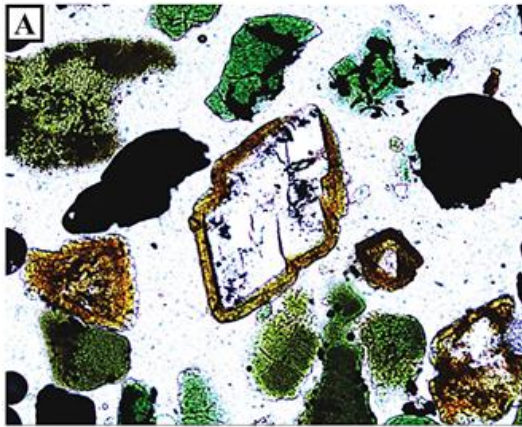
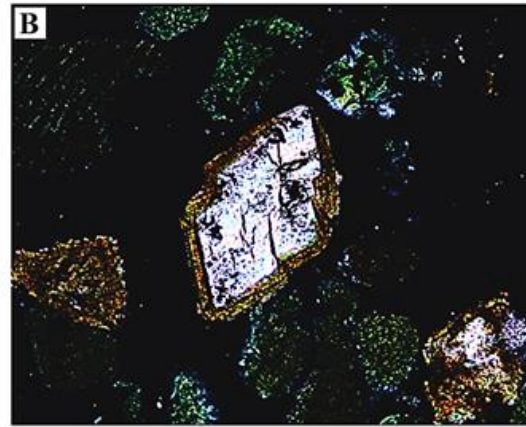


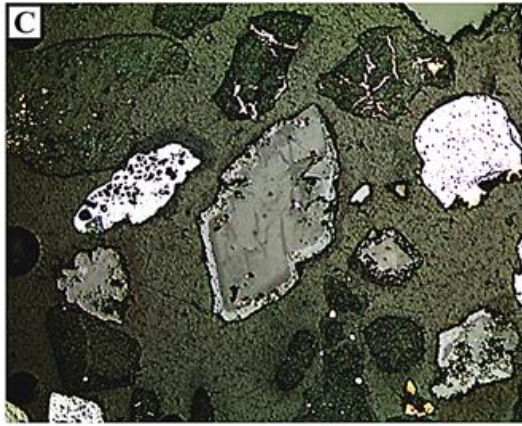
**Figure 21:** Photomicrographs showing ilmenite (Ilm) and iron-oxyhydroxide-aggregates (FeOx) around quartz grains (Qtz). A. Photomicrograph in plane-polarized light. B. Photomicrograph in reflected light. C. SEM image. D. Elemental map overlaying the SEM image in C. Note that blue, green, and red indicate the occurrence of Ti, Si, and Fe, respectively.



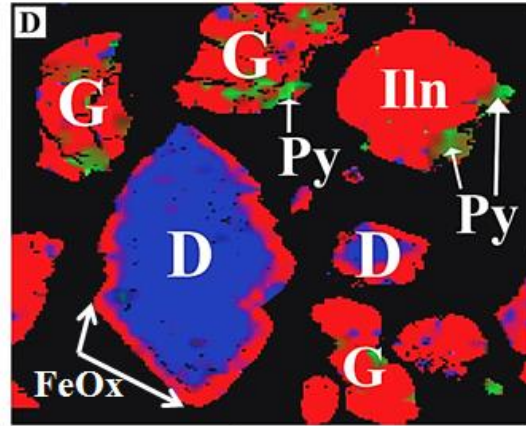
400  $\mu\text{m}$



400  $\mu\text{m}$



400  $\mu\text{m}$



400  $\mu\text{m}$

**Figure 22:** Photomicrographs showing an Fe-rich coating (FeOx) around dolomite (D) and authigenic pyrite (Py) on glauconite (G), ilmenite (Ilm), and dolomite. A. Photomicrograph in plane-polarized-light. B. Photomicrograph in cross-polarized light. C. Photomicrograph in reflected light. D. Elemental map showing areas containing Fe (red), Ca (blue), and S (green).

**Table 19:** EDX statistics of Fe-rich Ags/Cs.

Fe-rich Ags/Cs <sup>1</sup>	Na	Mg	Al	Si	P	S	Cl	K	Ca	Ti	Mn	Fe	O
Mean <sup>2</sup>	0.18	0.35	1.00	8.60	1.66	0.08	0.39	0.24	2.82	0.42	0.78	53.30	30.19
Median	0.17	0.19	0.78	8.89	1.23	0.04	0.35	0.22	2.00	0.20	0.57	53.46	30.14
Standard Deviation <sup>2</sup>	0.11	0.54	0.69	3.04	2.14	0.11	0.20	0.18	2.23	0.67	0.72	5.90	2.42
Sample Variance <sup>2</sup>	0.01	0.29	0.47	9.22	4.58	0.01	0.04	0.03	4.98	0.44	0.52	34.83	5.86
Minimum	0.01	0.01	0.24	2.12	0.30	0.00	0.04	0.01	0.38	0.01	0.00	36.44	25.20
Maximum	0.51	3.85	4.17	20.60	13.46	0.68	1.34	0.99	10.40	3.47	2.93	68.61	37.84
Count <sup>3</sup>	100	100	100	100	100	100	100	100	100	100	100	100	100
Confidence Level (95.0%) <sup>2</sup>	0.02	0.11	0.14	0.60	0.42	0.02	0.04	0.04	0.44	0.13	0.14	1.17	0.48
25th Percentile <sup>2</sup>	0.10	0.13	0.50	7.00	0.90	0.00	0.27	0.09	1.47	0.10	0.31	50.66	28.46
75th Percentile <sup>2</sup>	0.24	0.28	1.38	10.42	1.75	0.09	0.46	0.33	3.22	0.38	0.99	56.78	31.34
1/2 Minimum Value <sup>4</sup>	0.01	0.01	0.12	1.06	0.15	0.00	0.02	0.01	0.19	0.01	0.00	18.22	12.60

1. EDX analysis of 100 Fe-rich Ags/Cs. All concentrations are presented as weight percents

2. Calculated via Microsoft Excel

3. Number of spectra evaluated to compute statistics

4. One half of the minimum-detected value was used to replace concentrations of elements that were not detected in some specimens. Only elements that were detected in at least 25% of specimens were evaluated via statistical analysis

### 4.5.3 Mineral Chemistry

EDX spectra (268) were evaluated from magnetically susceptible fractions (0 – 1.8 amps) to facilitate mineral identification via microscopy. The number of spectra acquired from each polished-thin section (each polished-thin section was comprised of samples representing a specific core interval) for a given mineral specimen was highly variable (ranged from 3 to 62) but the compositions of most minerals were not determined for all depth intervals. In addition, mineral compositions are normalized to zero wt. % of elements that are lighter than O<sub>2</sub> because the EDX system does not reliably measure light elements. These data may provide insight for interpretations relating mineral chemistry and abundance to general trends in sediment chemistry; however, further acquisitions and analyses of EDX spectra are recommended to better substantiate the mineral chemistries that are discussed in the following subsection and shown in Table 20 and Appendix F.

EDX analysis reveals that 18 mineral grains are principally composed of Si (mean 42.0 wt. %) and O (mean 55.4 wt. %), indicating that these grains are quartz (SiO<sub>2</sub>). The EDX system also detected small amounts of Fe, Ti, Al, and Ca in spectra obtained from these grains. Microscopy and XRD data indicate that quartz is the dominant constituent in the majority of core samples and quartz abundance appears to be the major control on Si concentrations.

Based on microscopy and EDX data, six calcite or aragonite (CaCO<sub>3</sub>) grains were largely composed of Ca (mean 33.2 wt. %), Fe (mean 3.5 wt. %), and Si (1.2 wt. %). Other constituents included Cl, Na, Mg, and Al. Calcareous shell fossils are likely the major contributors to sediment-Ca concentrations below 4.9 m BLS. Although Sr was not detected via EDX analysis, shell fossils are probably the most important Sr-containing constituents in the Tranters Creek sediments because Sr commonly substitutes for Ca in marine fossils (Iledgpeth and Ladd, 1957).

Alkali feldspar and plagioclase feldspar were identified from 6 and 4 spectra, respectively. Alkali-feldspar specimens were principally comprised of Si (mean 28.7 wt. %), K (mean 11.7 wt. %), Al (mean 8.9 wt. %), and O (mean 50.5 wt. %) with lesser amounts of Na. Plagioclase-feldspar minerals were composed of Si (mean 26.8 wt. %), Al (mean 12.4 wt. %), Na (mean 5.2 wt. %), and Ca (mean 3.8 wt. %). Optical microscopy indicates that alkali feldspars were generally much more abundant than plagioclase feldspars. Alkali feldspars are likely the most important contributors to high sediment-K concentrations above 4.9 m BLS and plagioclase feldspars may be important sources of Na in the sediments below 4.9 m BLS.

Analysis of 15 EDX spectra suggests that the peloids are apatite. The peloids are principally composed of Ca (mean 34.1 wt. %), P (mean 14.8 wt. %), F (mean 2.7 wt. %), Fe (mean 2.4 wt. %), S (mean 1.5 wt. %), Si (mean 1.3 wt. %) and O (mean 42.4 wt. %) but smaller amounts of Na, Mg, Al, Cl, K, and Ti were also detected. High peloidal abundance corresponds to high concentrations of F in the sediment, which indicates that the peloids are largely carbonate fluorapatite ( $\text{Ca}_5(\text{PO}_4, \text{CO}_3)_3\text{F}$ ).

Twenty-seven mineral specimens had compositions that are consistent with ilmenite ( $\text{FeTiO}_3$ ). These grains were comprised of Ti (mean 31.7 wt. %), Fe (mean 26.8 wt. %), and O (mean 38.6 wt. %). Ilmenite was generally the most abundant Fe-bearing mineral in the cores. Moreover, ilmenite is likely the major source of Ti and may be an important contributor to Mn concentrations in the sediment.

EDX analyses of 27 glauconite  $((\text{K}, \text{Na})(\text{Fe}^{3+}, \text{Al}, \text{Mg})_2(\text{SiAl})_4\text{O}_{10}(\text{OH})_2)$  grains reveal that these grains are composed of Si (mean 22.5 wt. %), Fe (mean 18.2 wt. %), K (mean 4.6 wt. %), Al (mean 3.3 wt. %), Mg (mean 2.2 wt. %), and O (mean 47.1 wt. %). Glauconite was typically

the most abundant Fe-bearing mineral below 4.9 m BLS and may be a significant source of Mg in the sediments.

The principal elements comprising amphiboles (62 spectra) and pyroxenes (24 spectra) were identical. On average, both the amphiboles and pyroxenes were composed of similar amounts of Si (about 19 wt. %), Fe (between 9 and 10 wt. %), Al (between 7 and 8 wt. %), Mg (between 5 and 6 wt. %), and Ti (about 2 wt. %). Mean Ca concentrations were higher in pyroxenes (10.7 wt. %) than in amphiboles (5.8 wt. %). Correlations of sediment chemistry and amphibole and pyroxene abundances were not identified, possibly due to their low abundances in the Tranters Creek sediments.

Forty-six spectra of staurolite ( $\text{Fe}^{2+}_2\text{Al}_9\text{Si}_4\text{O}_{23}(\text{OH})$ ) grains were obtained. The results indicate that the grains were composed of Al (mean 24.0 wt. %), Si (mean 12.6 wt. %), Fe (mean 10.1 wt. %), Ti (mean 1.5 wt. %), Mg (mean 1.0 wt. %), and O (mean 50.9 wt. %). The estimated abundance of staurolite was always less than 0.5 wt. % of total dried sediment weight and as a result, staurolite abundance does not seem to have contributed to any substantial changes in sediment chemistry.

Analysis of 7 tourmaline ( $(\text{Na,Ca})(\text{Mg,Li,Al,Fe}^{2+})_3\text{Al}_6(\text{BO}_3)_3\text{Si}_6\text{O}_{18}(\text{OH}_4)$ ) specimens indicates that tourmaline grains are composed of Si (mean 17.0 wt. %), Al (mean 16.1 wt. %), Fe (7.0 mean wt. %), Mg (mean 3.4 wt. %), Ti (1.6 mean wt. %), Na (mean 1.5 wt. %), and Ca (mean 1.2 wt. %). Tourmaline was the second least-abundant mineral detected in the Tranters Creek sediments and thus, it is not likely to be a significant source of the above-listed elements.

Because pyrite ( $\text{FeS}_2$ ) was easily identifiable via optical microscopy using reflected light, only 3 EDX spectra were evaluated. The pyrite is composed of S (mean 51.3 wt. %), Fe (mean 43.7 wt. %), Si (mean 2.4 wt. %), Ca (mean 2.0 wt. %). Although pyrite was commonly the least

abundant Fe-bearing mineral detected in the sediment cores, pyrite may be the most significant source of S below 6 m BLS.



**Table 20:** Mean chemical compositions of minerals.

Mineral <sup>1</sup>	O	F	Na	Mg	Al	Si	P	S	Cl	K	Ca	Ti	Mn	Fe	n <sup>2</sup>
Quartz	55.4				0.5	42.0					0.2	0.7		1.4	18
Calcite	61.1		0.4	0.3	0.2	1.2			0.4		33.2			3.5	5
Alk. Feldspar	50.5		0.4		8.9	28.7				11.7					6
Plag. Feldspar	52.3		5.2		12.4	26.8					3.8				4
Apatite	42.4	2.7	0.7	0.3	0.4	1.3	14.9	1.5	0.1		34.1	0.5		2.4	15
Ilmenite	38.6			0.4	0.5	1.1			0.1		0.4	31.7	1.0	26.8	27
Glauconite	47.1			2.2	3.3	22.5	0.3		0.2	4.6	0.9	0.9		18.1	27
Amphibole	48.2		1.1	5.7	7.3	18.9				0.8	5.8	2.5		9.9	62
Almandine	43.8			2.0	10.0	17.1					2.2	1.3	3.0	20.8	24
Pyroxene	46.8		0.3	5.3	8.1	19.2					10.7	1.9	0.1	9.0	24
Staurolite	50.9			1.0	24.0	12.6						1.5		10.1	46
Tourmaline	52.5		1.5	3.4	16.1	17.0					1.2	1.6		7.0	7.0
Pyrite				0.2		2.4		51.3		0.4	2.0			43.7	3.0

1. Elemental concentrations presented as weight percents. Mineral compositions are normalized to exclude elements lighter than oxygen

2. The number of EDX spectra that were evaluated to determine mineral composition

## **5.0 Discussion**

Previous studies (Johnson, 1992; Winner and Coble, 1996; Lautier, 2009) and the results of this research indicate that sediments comprising the Geoprobe cores extracted near Washington, NC are part of the Quaternary surficial unit and the Pliocene Yorktown Formation. The surficial unit extends to a depth of approximately 6 m BLS and corresponds with the unconfined, surficial aquifer. The surficial aquifer is largely composed of highly permeable quartz sands but a less permeable layer consisting of muddy sand occurs below 4 m BLS. Although the boundary separating the surficial unit and the Yorktown Formation is transitional, bluish-gray sediments with abundant marine-related constituents (shell fragments, peloids, and glauconite) denote that the depth of the Yorktown Formation ranges from around 6 m BLS to the maximum depth of core penetration (about 11 m BLS). A stratigraphic section illustrating the inferred positions of the unnamed surficial unit and the Yorktown Formation in the cores is presented in Figure 23. Note that the color changes displayed in Figure 23 are relatively sharp; however, the color changes are transitional along each core interval.

### **5.1 Transformation of Iron in Sediments Overlying the UCHA**

Numerous studies (e.g. Chapelle and Lovley, 1992; Amsbaugh, 1996; Brown et al., 1999; Woods et al., 2000; Penny et al., 2003; Park et al., 2006; McMahon and Chapelle, 2008) and evidence from this investigation suggest that the origin of high-dissolved-Fe concentrations in coastal plain aquifers largely involves the reductive dissolution of iron-oxyhydroxide minerals. Distinct hydrogeochemical zones, distinguished by variations in sediment composition, inferred biogeochemical and hydrologic processes, and the degree of atmospheric isolation, are identified in sediments overlying the UCHA in western Beaufort County. These hydrogeochemical zones are discussed in the following subsections and important core data that were used to infer the

proposed zones are presented in Figures 23 – 25 and Table 21. In order of occurrence from the land surface to the maximum depth of core penetration, the zones are as follows:

- Iron Depletion Zone, 0 – 3.8 m BLS
- Iron Pigmentation Zone, 3.8 – 6.4 m BLS
- Iron Sulfide Zone, 6.4 – 11.0 m BLS

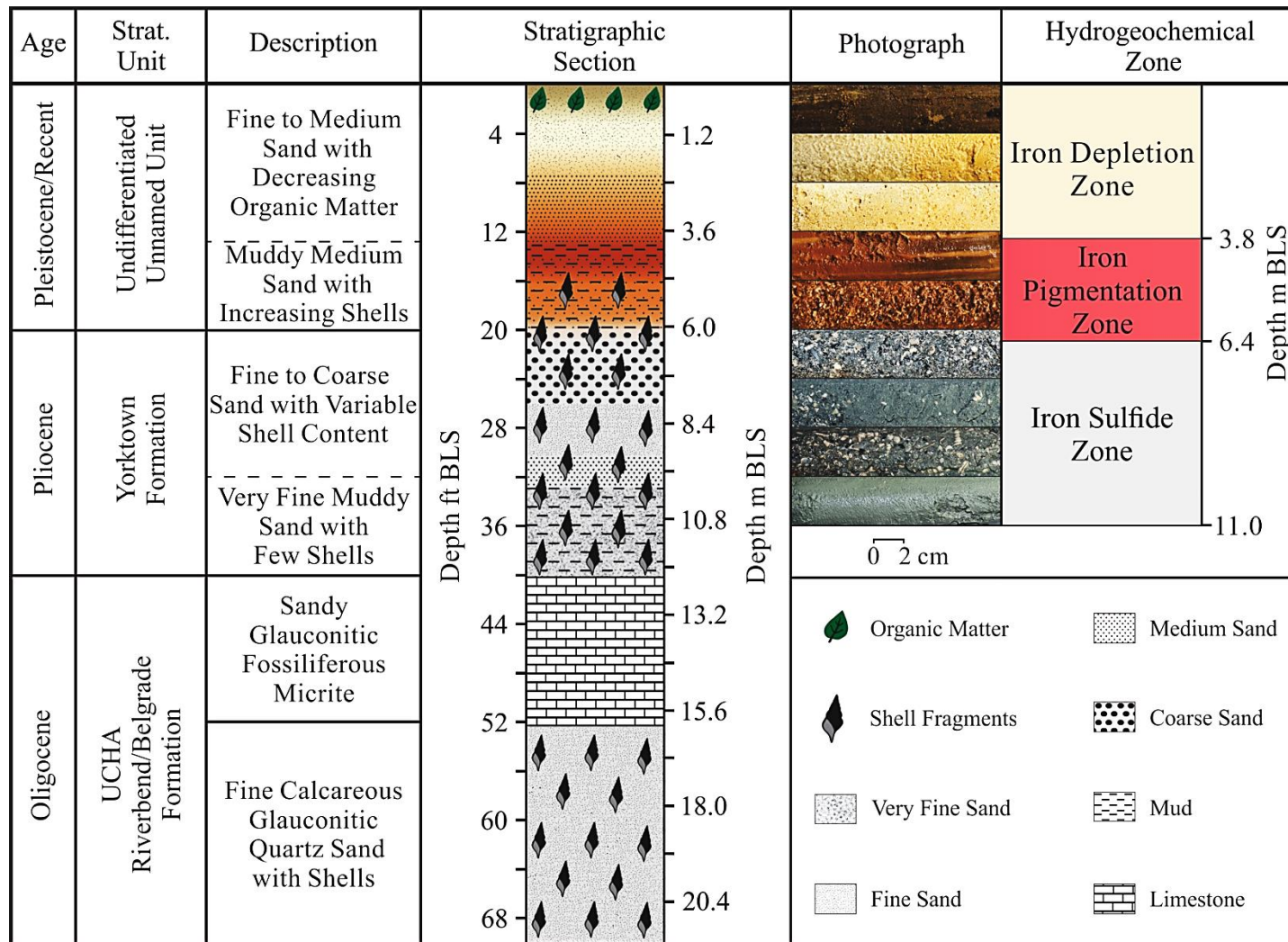


**Figure 23:** Stratigraphic section [modified after Johnson (1992)], sediment photographs and inferred hydrogeochemical zones at the Tranter's Creek core site. Note that the photograph between 3.7 and 4.9 m BLS is located near the bottom of the section, where Fe concentrations are high and the sediment reaches its darkest, orangish brown color.

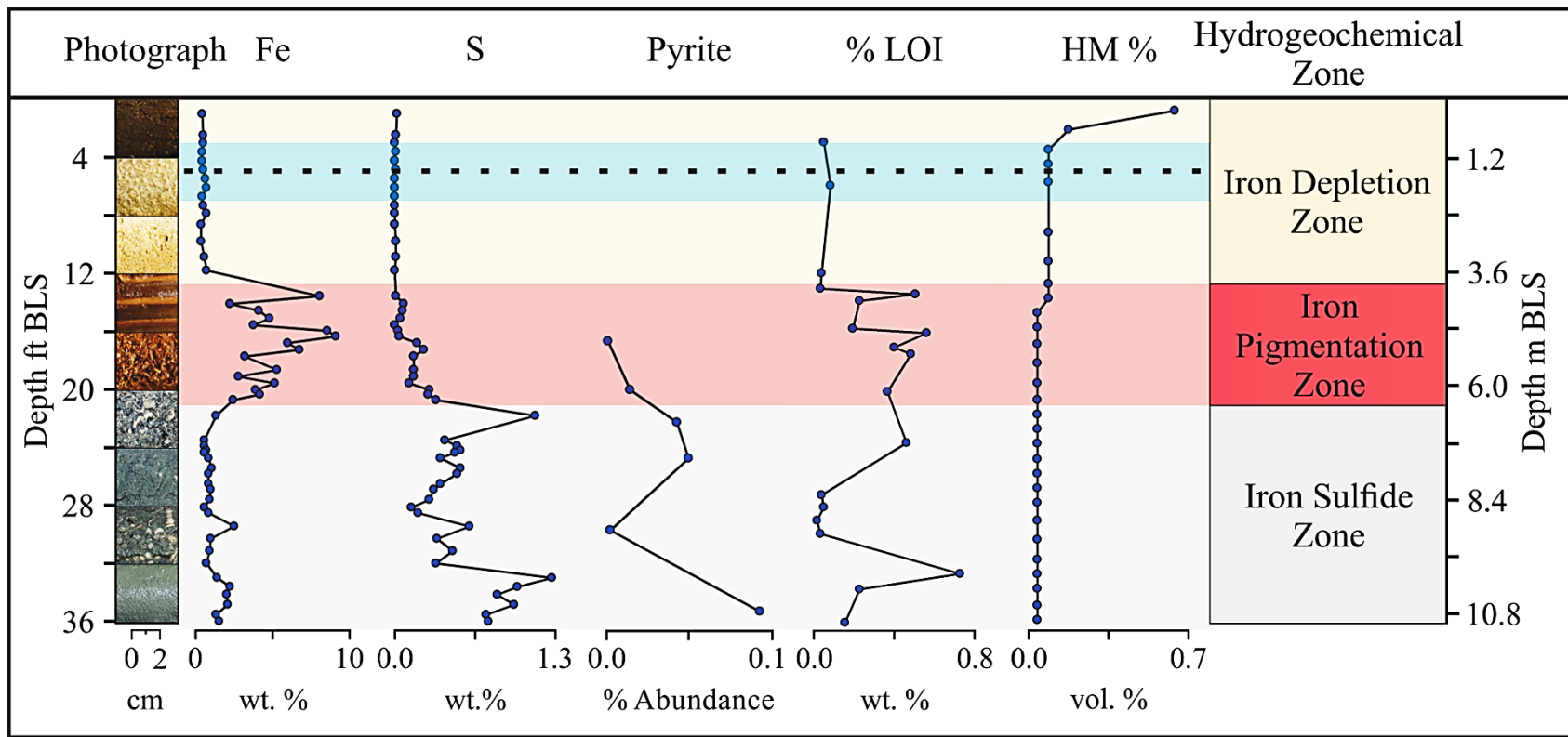


**Figure 24:** Photographs and bivariate plots showing depth-related variations in sediment color and composition (Fe, S, pyrite abundance, % LOI, and HM %). These data, in conjunction with those shown in Figure 25 and Table 21, were used to infer three distinct hydrogeochemical zones. The blue area denotes typical depth ranges of the water-table surface and the dashed line indicates the mean depth of the water table (Johnson, 1992).

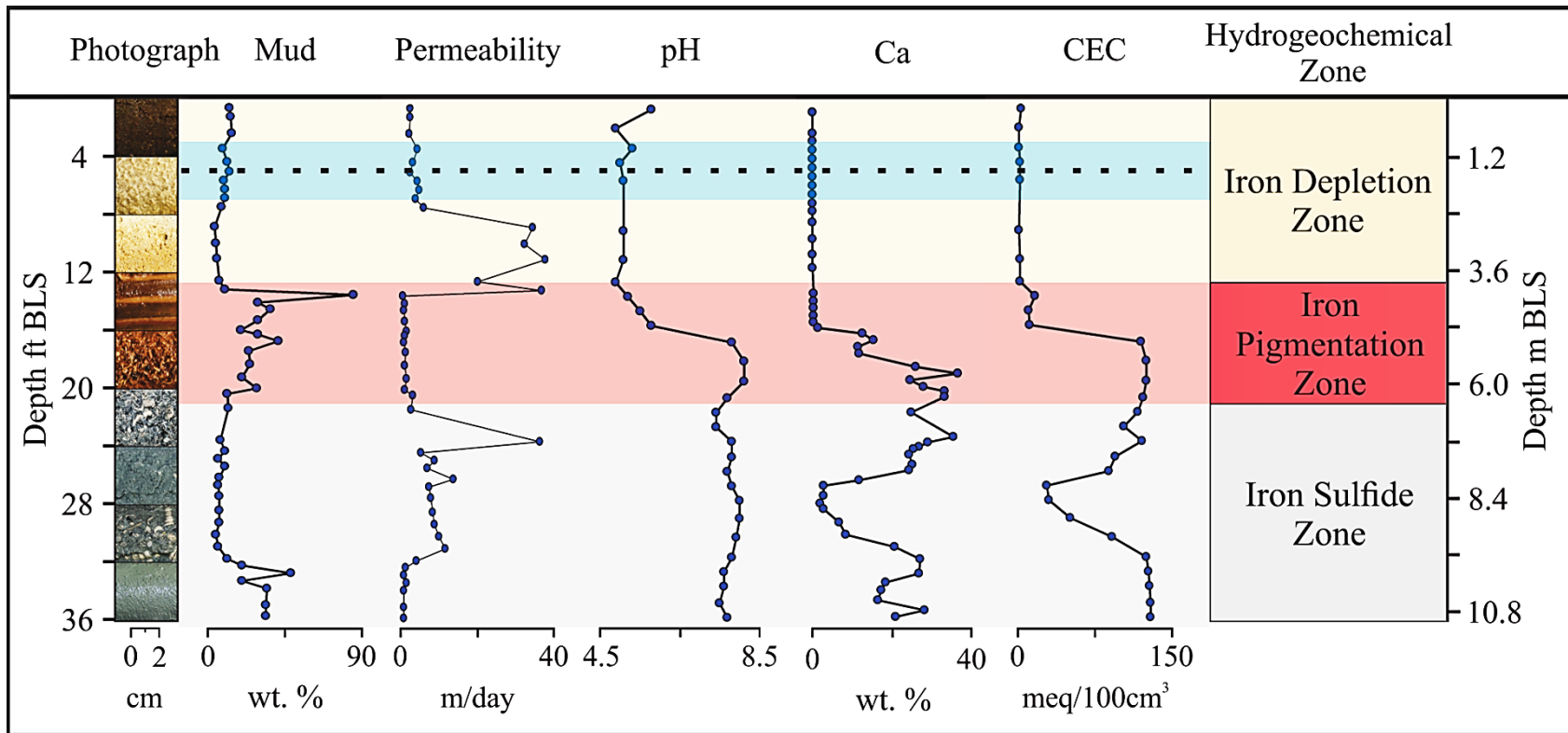


**Figure 25:** Photographs and bivariate plots showing depth-related variations in sediment color and composition (mud content, grain-size-estimated permeability, Ca, and CEC). These data, in conjunction with those shown in Figure 23 and Table 21, were used to infer three distinct hydrogeochemical zones. The blue area denotes typical depth ranges of the water-table surface and the dashed line indicates the mean depth of the water table (Johnson, 1992).

**Table 21:** Mean abundances (estimated from polished-thin sections via optical microscopy) of dominant minerals comprising the Iron Depletion Zone, Iron Pigmentation Zone, and the Iron Sulfide Zone.

Hydrogeochemical Zone		Iron Depletion Zone	Iron Pigmentation Zone	Iron Sulfide Zone
Depth Range (m BLS)		0 - 3.8	3.8 - 6.4	6.4 - 11.0
Non-Fe-Bearing Mineral	Apatite		7	6
	Feldspar	9	6	6
	Quartz	90	55	65
	Shells		27	19
Fe-Bearing Mineral	Almandine	0.1	0.4	0.2
	Amphibole	0.3	0.3	0.3
	Glauconite		1.0	0.7
	Ilmenite	0.7	0.7	0.8
	Iron-Oxyhydroxide		1.0	
	Pyrite		0.02	0.07
	Pyroxene	0.1	0.2	0.3
	Staurolite	0.1	0.4	0.1
Tourmaline	0.05	0.02	0.14	

### 5.1.1 Iron Depletion Zone

The Iron Depletion Zone (IDZ) extends from the ground surface to approximately 3.8 m BLS. This zone is largely comprised of highly permeable quartz (~90 %) and K-rich feldspar (~9%) grains with trace amounts of Fe-bearing minerals (Table 21). Weakly soluble Fe-bearing minerals such as ilmenite, amphiboles, and pyroxenes are typically the principal sources of Fe in near-surface, coastal plain sediments such as the IDZ (e.g. Postma and Brockenhuus-Schack, 1987; Stucki et al., 2012). Microscopic analyses show that ilmenite (~0.7 %) is consistently the most dominant Fe-bearing mineral; however, lesser amounts of amphiboles (~0.3 %), pyroxenes (~0.1 %), staurolite (~0.1 %), almandine (~0.1 %), and tourmaline (~0.05 %) are also present. Fe-bearing minerals constitute less than 1.6 % of the IDZ constituents and as a result, Fe concentrations are consistently low in the sediment (Figure 24). The dominant minerals are resistant to weathering and the sediments are generally mature (i.e. well-sorted and well-rounded grains), suggesting that they were transported over a long distance prior to deposition (e.g. transported from the Piedmont to NCCP) Therefore, mechanical weathering prior to sediment deposition and in-situ chemical weathering over geologic time may explain the low abundance of Fe-bearing constituents in the IDZ.

Sediments comprising the IDZ consistently have low values for sediment-water pH (Figure 25) and low concentrations of  $Ca_e$ ,  $Mg_e$ ,  $Na_e$ , and  $K_e$ . According to data collected approximately 50 km west-northwest of the study area, rainfall is typically acidic (USGS, 2016). Low sediment-water pH values and low concentrations of  $Ca_e$ ,  $Mg_e$ ,  $Na_e$ , and  $K_e$  may be attributed to the percolation of acidic rainfall, which leaches these elements from the IDZ over time and diminishes the capacity of the sediments to buffer infiltrating acidic precipitation (Hardy et al., 2012).



Under oxic and slightly acidic conditions, the transport of weathering-liberated-Fe species is severely inhibited by the low solubility of  $\text{Fe}^{3+}$  and the tendency of  $\text{Fe}^{3+}$  to form iron-oxyhydroxides, which may attach to negatively charged mineral surfaces such as quartz, feldspar, and clay minerals (Ryan and Gschwend, 1992; Penn et al., 2001). However, iron-oxyhydroxides are not observed in the IDZ (Table 21), suggesting that the mobility of dissolved and colloidal Fe compounds likely exceeds the rate of iron-oxyhydroxide accretion. Geochemical conditions in the IDZ are probably favorable for the slow, downgradient migration of Fe species because:

1. groundwater (Figure 25) in the IDZ is acidic and likely oxidizing, resulting in slow and progressive weathering of Fe-bearing minerals,
2. weathering of Fe-bearing minerals results in the formation of mobile species such as Fe complexes and colloidal iron-oxyhydroxides, which tend to remain in suspension in permeable sediments (Ryan and Gschwend, 1992) and,
3. low CEC values (Figure 25) indicate that the sediments have a low capacity to retain Fe cations once they are liberated via the weathering of iron-bearing minerals.

### **5.1.2 Iron Pigmentation Zone**

The Iron Pigmentation Zone (IPZ) extends from the basal portion of the IDZ to approximately 6.4 m BLS. Relative to the IDZ and the subjacent Iron Sulfide Zone, the IPZ sediments are the least permeable (Figure 25) and have the highest mean mud content (27.5 wt. %; Figure 23). The IPZ sediments have a mean CEC of about 76 meq/100  $\text{cm}^3$ , which is an order of magnitude greater than in the IDZ sediments. Approximately 96% of the IPZ sediments are comprised of quartz (~55 %), shell fossils (~27 %), apatite (~7 %), and feldspar (~6 %). Iron-

bearing minerals make up the remaining 4% of IPZ sediments (Table 21). In decreasing order of estimated abundance, the principal Fe-bearing minerals include glauconite (~1.0 %), one or more iron-oxyhydroxides (the principal mineral is probably goethite, ~1.0 %), ilmenite (~0.7 %), almandine (~0.4 %), staurolite (~0.4 %), amphiboles (~0.3 %), pyroxenes (~0.2 %), tourmaline (~0.02 %), and pyrite (~0.02%).

Although crystal morphology can frequently be used to identify well-crystallized iron-oxyhydroxides (Table 2), such morphologies were not observed via SEM, which may suggest that crystallization was recent or inhibited by the presence of interfering compounds in solution such as organic matter, phosphate, and silica (Stucki et al., 2012). XRD patterns indicate that goethite likely comprises the bulk of the crystalline, iron-oxyhydroxides in the IPZ. However, additional iron-oxyhydroxides may be present because poorly ordered varieties such as amorphous ferrihydrite are difficult to identify via XRD analyses (Cook et al., 1999).

Studies of sediment cores reveal that high Fe concentrations in the IPZ correspond with the occurrence of abundant, iron-oxyhydroxides in the form of authigenic Ags/Cs (Figure 24 and Table 21). These Fe-bearing minerals and compounds are mainly concentrated in two, stratigraphically adjacent intervals that are characterized by color changes that occur along a 2.6-m-core interval below the IDZ. Between 4 and 5 m BLS, a relatively high proportion of mud-sized grains (mean 34 wt. %) in the upper IPZ coincides with a general increase in sediment-Fe concentrations (2 to 9 wt. % Fe). With increasing depth, sediment colors along this interval change from light tan to yellowish brown and then, to dark orangish brown. Sediment colors in the lower IPZ progressively change from dark orangish brown near 5 m BLS to a bluish-gray color by approximately 6.4 m BLS. In contrast to the upper IPZ, the lower IPZ, on average, contains less mud (mean 24 wt. %) and Fe (2 to 7 wt. % Fe), which generally decrease with

increasing depth. Qualitatively, yellow, orange, and brown pigmentations correspond to high iron-oxyhydroxide abundances and indicate oxic conditions. The bluish-gray sediments that occur below 6.4 m BLS denote persistent anoxic conditions (Daniels et al., 1961).

#### **5.1.2.1 Iron-Oxyhydroxide Accumulation in the IPZ**

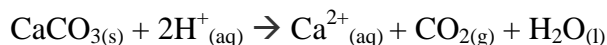
Geochemical profiles showing Fe concentrations and Fe/Al ratios suggest that Fe is associated with clay minerals in the upper meter of the IPZ (Figure 26). It is well established that Al is a good proxy for clay content because Al is a principal element comprising aluminosilicates, it is abundant in most sediments, it behaves conservatively under normal conditions (i.e. Al is largely not affected by diagenetic processes and redox reactions, and anthropogenic inputs of Al are typically insignificant (Din, 1992; Herut and Sandler, 2006; Ho et al., 2012)). Because of these properties, Al is commonly used to normalize for granulometric (grain size) and mineralogical variations (e.g. Bertine and Goldberg, 1977; Herut and Sandler, 2006). Since the Fe exhibits a strong linear relationship with Al in the upper meter of the IPZ (mean Fe/Al ratio = 0.7 and  $R^2 = 0.8$ ), Fe concentrations may denote the presence of one or more Fe-bearing clay minerals (e.g. illite).

Alternatively, electrostatic attraction between the surfaces of clay grains and iron-oxyhydroxides may have enriched the clay fraction with Fe. Increases in organic matter (suggested by increasing % LOI) and mud content likely contributed to higher CEC (Figures 24 – 25). Under acidic conditions, the surfaces of iron-oxyhydroxides are positively charged while the surfaces of quartz, feldspar, organic matter, and clay minerals typically carry a negative charge (Ryan and Gschwend, 1992; Stucki et al., 2012). Previous studies have shown that electrostatic attraction can result in the aggradation of iron-oxyhydroxides in oxic sediments (Ryan and Gschwend, 1992; Stucki et al., 2012). Moreover, high mud content and low

permeability may facilitate electrostatic interactions between the IPZ sediments and suspended iron-oxyhydroxide colloids in groundwater by increasing the reactive-surface area and decreasing the groundwater-flow velocity, respectively. Therefore, as colloidal iron-oxyhydroxides are translocated from the IDZ to mud-rich layers of the IPZ, iron-oxyhydroxides may aggregate in pore spaces or attach to negatively charged mineral surfaces in the IPZ, resulting in higher Fe concentrations.

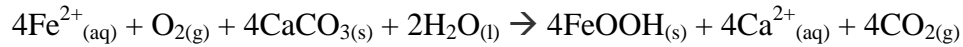
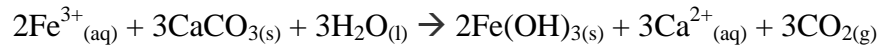
Like Al, studies frequently normalize geochemical results to Fe; however, Fe does not behave conservatively in most aquifers because it is redox sensitive (Herut and Sandler, 2006; Lopez et al., 2006; Ho et al., 2012). The Fe/Al ratios are consistently high (mean 3.5) and variable between approximately 4.7 m BLS and 6.4 m BLS, suggesting that redox reactions involving authigenic iron-oxyhydroxides are the most important factors controlling Fe concentrations in the IPZ.

Important contributors to iron-oxyhydroxide precipitation in the IPZ likely include pH increases and the presence of dissolved O<sub>2</sub>. Data from Johnson (1992) indicate that groundwater pH increases from 5 to 6.3 between approximately 3.2 and 6.1 m BLS (Table 3). Similarly, mean sediment-water pH increases from 5.2 in the IDZ to 6.6 in the IPZ (Figure 25). These pH increases may be attributed to the dissolution of calcareous shell fossils. A reaction representing the dissolution of CaCO<sub>3</sub> can be written as:



In this reaction, calcium carbonate reacts with two hydrogen ions, thereby increasing groundwater pH. An Eh-pH stability diagram for the common Fe species indicates that an increase in groundwater pH increases the likelihood that dissolved Fe will precipitate in the form of iron-oxyhydroxides if changes in redox potential are negligible (Figure 27). In addition,

aquifer carbonates can react with dissolved Fe under oxidizing conditions to precipitate iron-oxyhydroxides (Clarke et al., 1985):



Therefore, the shell fossils and concomitant increases in Fe, Ca, and sediment-water pH (Figures 24 – 25 and Table 21) indicate that carbonate reactions may enhance the formation of iron-oxyhydroxides in the IPZ.

Upward movement of dissolved- $\text{Fe}^{2+}$  from deeper groundwater may contribute to increased iron-oxyhydroxide abundance in the IPZ. Along the oxic-anoxic transition zone in a sediment column, both oxidation and reduction of Fe can result in the formation and dissolution of iron-oxyhydroxides, respectively (Figure 28B). The redox potential of aquifers typically decreases as the groundwater becomes increasingly isolated from the atmosphere due to the depletion of dissolved  $\text{O}_2$  by microbes and redox reactions (Stumm and Morgan, 1996). If increasing depth is assumed to result in decreasing oxygen concentrations, groundwater in the lower IPZ is more reducing and likely contains more dissolved  $\text{Fe}^{2+}$  than the upper IPZ.

Diffusion (the transport of a solute from a zone of higher concentration to an area of lower concentration) and advection (transport of a solute that occurs as a result of groundwater flow) are possible mechanisms by which  $\text{Fe}^{2+}$ -enriched groundwater may travel from deeper depths to shallower depths. According to Johnson (1992), the study area is a discharge zone (an area typified by an increasing vertical-head gradient), which suggests that upward advection is also possible (see Temporal Hydrologic Considerations). In both cases, the upward transport of  $\text{Fe}^{2+}$  can result in the oxidation-induced precipitation of iron-oxyhydroxides.

It is not clear whether the development of iron-oxyhydroxides in the IPZ occurred recently or thousands of years ago, when eustatic sea level and the water table were much lower (see Temporal Hydrologic Considerations). Laboratory experiments indicate that under ideal conditions, reductive dissolution can deplete the majority of ferrihydrite (goethite takes longer) in a sediment over a period ranging from weeks to months; however, the reduction rates for iron-oxyhydroxides can be affected by numerous factors including groundwater chemistry, presence and type of bacteria, and the crystallinity and surface area of the iron-oxyhydroxides (Rabenhorst et al., 2008; Li et al., 2012; Stucki et al., 2012).

#### **5.1.2.2 Iron-Oxyhydroxide Depletion in the IPZ**

Numerous studies (e.g. Chapelle and Lovley, 1992; Amsbaugh, 1996; Brown et al., 1999; Woods et al., 2000; Penny et al., 2003; Park et al., 2006; McMahan and Chapelle, 2008) and evidence from this investigation support the hypothesis that the origin of high-dissolved-Fe concentrations in coastal plain aquifers largely involves reductive dissolution of iron-oxyhydroxide minerals. Microbially catalyzed reduction of iron-oxyhydroxides and concurrent oxidation of organic matter result in the depletion of Fe in sediments and can result in high-dissolved-Fe concentrations in low-O<sub>2</sub> groundwater. Although iron-oxyhydroxides only comprise about 1% of the IPZ sediments, they likely comprise a substantial portion of the sediments' reactive surface area and they are usually much more soluble than detrital-Fe minerals under reducing and circumneutral conditions (Stucki et al., 2012).

Within a groundwater-pH range between 5 and 8, dissolved-Fe concentrations exceeding 0.3 mg/L are usually indicative of microbially catalyzed reduction of iron-oxyhydroxides under suboxic to anoxic conditions (Hem and Cropper, 1960; Chapelle and Lovley, 1992; Chapelle et al., 2001; McMahan and Chapelle, 2008). Existing water-quality data for the lower IPZ indicate

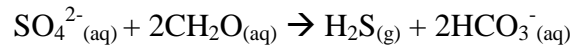
that the groundwater contains little  $\text{SO}_4^{2-}$  and has a dissolved-Fe concentration of 13 mg/L (Johnson, 1992). In addition, relatively high organic matter (inferred by elevated LOI % values) and, depletions in Fe and iron-oxyhydroxide abundances typify the lower IPZ. These data collectively suggest that Fe reduction is a dominant process in the lower IPZ and that the rate of iron-oxyhydroxide reduction consistently exceeds the rate of iron-oxyhydroxide formation and retention. Therefore, the origin of high-dissolved-Fe concentrations in the western portion of the UCHA recharge area likely corresponds to the proximal development of aquifer environments that are similar to the lower IPZ where such environments are hydraulically connected to the UCHA.

### **5.1.3 Iron-Sulfide Zone**

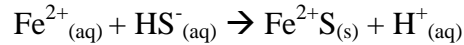
The Iron-Sulfide Zone (ISZ) is recognized below 6.4 m BLS where mean sediment-S concentrations are  $S = 0.5$  wt. % and  $S_e = 427$  mg/dm<sup>3</sup>. In the ISZ, quartz (~65 %), shell fossils (~19 %), apatite (~6 %), and feldspar (~6 %) comprise over 97% of the sediments while iron-bearing minerals make up less than 3% of the minerals (Table 21). In descending order of estimated abundance, the dominant iron-bearing minerals are ilmenite (~0.8 %), glauconite (~0.7 %), amphiboles (~0.3 %), pyroxenes (~0.3%), almandine (~0.2 %), tourmaline (~0.1 %), staurolite (~0.1 %), and pyrite (~0.07 %). Pyrite only occurs in trace amounts and is most abundant below 9 m BLS and its abundance generally corresponds with variations in sediment-sulfur concentrations below 5 m BLS (Figure 24).

Microscopy reveals that pyrite is largely present as framboids or within the pore spaces of shell fragments, glauconite grains, and apatite peloids. Pyrite formation occurs via bacterially mediated reactions that involve the oxidation of organic matter and simultaneous reduction of

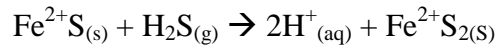
dissolved sulfate under anoxic conditions (in groundwater or localized in a fecal pellet), producing hydrogen sulfide (H<sub>2</sub>S) and bicarbonate (HCO<sub>3</sub><sup>-</sup>):



Following sulfate reduction, dissolved Fe<sup>2+</sup> and H<sub>2</sub>S can react to precipitate a metastable monosulfide-Fe mineral (Fe<sup>2+</sup>S) such as mackinawite:

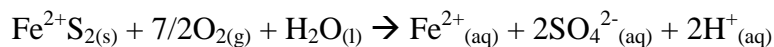


Subsequently, Fe<sup>2+</sup>S may react with H<sub>2</sub>S to form pyrite (Wilkin and Barnes, 1996; Schoonen, 2004; Park et al., 2006):



Although this investigation did not evaluate groundwater geochemistry, dissolved-Fe concentrations in the ISZ may decrease with depth due to the lack of iron-oxyhydroxide reduction, Fe<sup>2+</sup> oxidation and subsequent precipitation via carbonate reactions, and the formation of Fe-sulfide minerals (Berner, 1969; Chapelle and Lovley, 1992). Studies of suboxic, aquatic sediments indicate that sulfate reduction largely occurs after the majority of iron-oxyhydroxides are depleted from sediments (Froelich et al., 1979; Reeburgh, 1983; Chapelle and Lovley, 1992). The lack of iron-oxyhydroxides and occurrence of pyrite suggest that groundwater conditions were probably favorable for sulfate reduction in the ISZ.

The reduction of iron-oxyhydroxides in the overlying IPZ may provide the requisite Fe<sup>2+</sup> to form iron sulfides in the ISZ. Conversely, if groundwater from adjacent layers contains dissolved O<sub>2</sub>, pyrite oxidation can produce dissolved Fe<sup>2+</sup> (Moses and Herman, 1991). Under circumneutral conditions, a reaction illustrating pyrite oxidation by the reduction of dissolved O<sub>2</sub> can be written as follows:





The contribution of pyrite weathering to the formation of high-dissolved-Fe zones in the UCHA recharge area may be negated because  $\text{Fe}^{2+}$  can rapidly oxidize to form iron-oxyhydroxides (e.g. goethite) under oxic conditions:

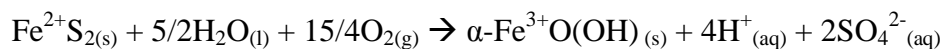
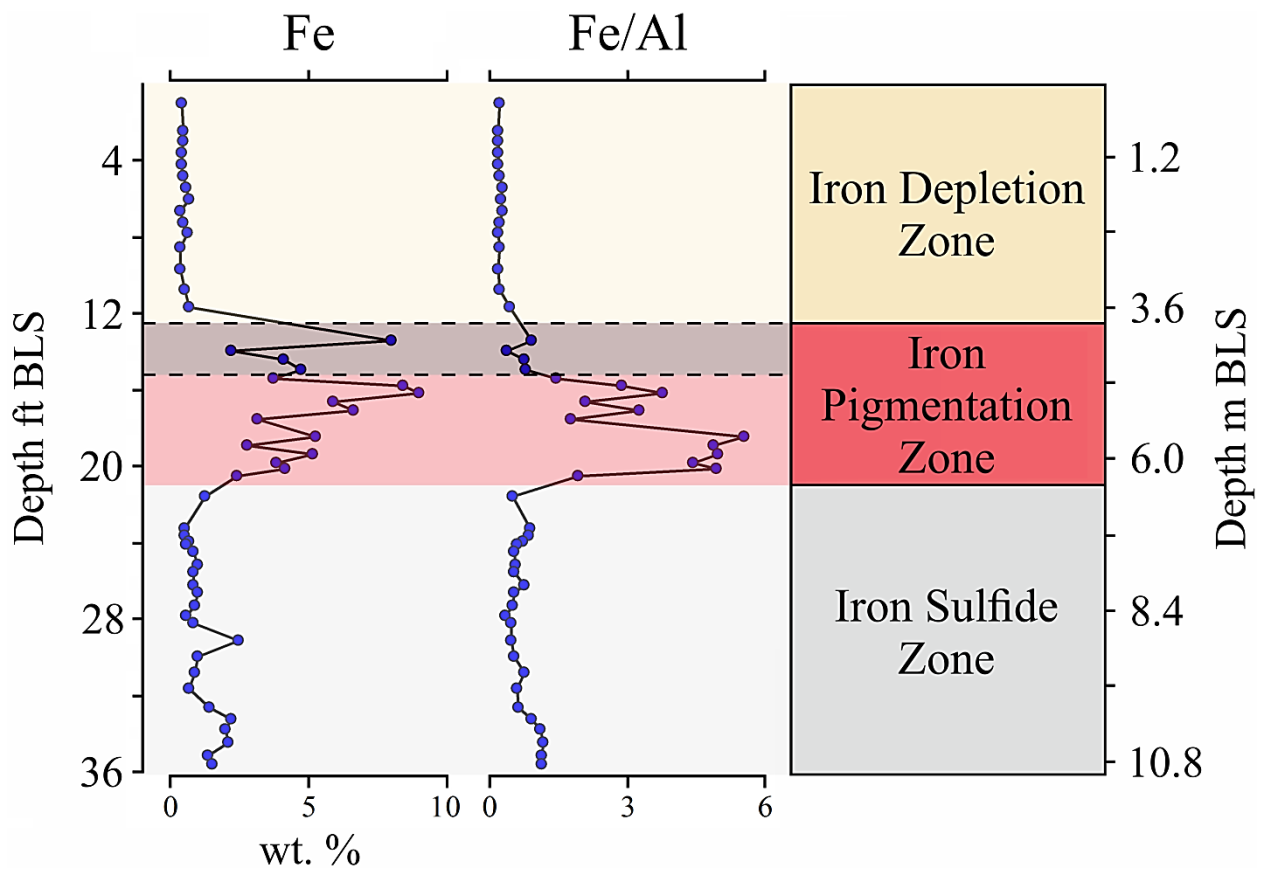


Figure 28 summarizes the inferred migration and evolution of Fe in coastal plain sediments that overlie the UCHA in western Beaufort County. Evaluation of the sediment cores reveals that the mobility and oxidation state of Fe are affected by variations in sediment composition, hydrogeochemical processes, and the degree to which the sediments are isolated from the atmosphere. Weathering of Fe-bearing minerals under acidic and oxic conditions in the IDZ may result in the production of highly mobile Fe species that are likely transferred downgradient to the subjacent IPZ over time (Figure 28A).

As colloidal iron-oxyhydroxides enter the less permeable and mud-rich layer of the IPZ, low-groundwater velocity and electrostatic attraction between positively charged colloids and negatively charged mineral surfaces contribute to the accumulation of iron-oxyhydroxides in the form of Fe-rich Ags/Cs (Figure 28B). As a result of the increasing abundance of iron-oxyhydroxides, IPZ sediments develop yellow, orange, and brown colors and high Fe concentrations. With increasing depth, dissolved  $\text{O}_2$  becomes depleted and conditions become increasingly favorable for the microbially catalyzed reduction of iron-oxyhydroxides via organic matter oxidation. Consequently, iron-oxyhydroxides and Fe concentrations become depleted with increasing distance along the flow path while dissolved  $\text{Fe}^{2+}$  concentrations progressively increase. Dissolved Fe, native to the IPZ or derived from a subjacent zone, may travel upward via diffusion (or advection in a discharge area) to the upper IPZ where dissolved  $\text{O}_2$  is present, resulting in the oxidation of  $\text{Fe}^{2+}$  to  $\text{Fe}^{3+}$  and subsequent precipitation of iron-oxyhydroxides via

hydrolysis or by carbonate reactions with dissolved  $\text{Fe}^{2+}$  and  $\text{Fe}^{3+}$ . Alternatively, dissolved Fe may be transported downgradient by advection from the lower IPZ to the ISZ, where the formation of sulfide minerals may result in decreasing dissolved- $\text{Fe}^{2+}$  concentrations (Figure 28C).

High-dissolved-Fe concentrations in the UCHA likely originate in an environment similar to the lower IPZ where Fe-reducing conditions develop near the upper contact of the UCHA in the western portion of the recharge area. The formation of high-dissolved-Fe concentrations in the UCHA may be dependent on a relatively short flow-path distance between the lower IPZ and the upper contact of the UCHA because processes such as Fe-sulfide precipitation and cation exchange (cation exchange is discussed in the modeling subsections) may result in  $\text{Fe}^{2+}$  depletion below the IPZ.



**Figure 26:** Geochemical profiles illustrating variations in Fe concentrations (wt. %) and Fe/Al ratios with respect to depth and inferred hydrogeochemical zones. The brown area between the dashed lines indicates the Fe is associated with Al (and clay minerals by proxy) in the IPZ.

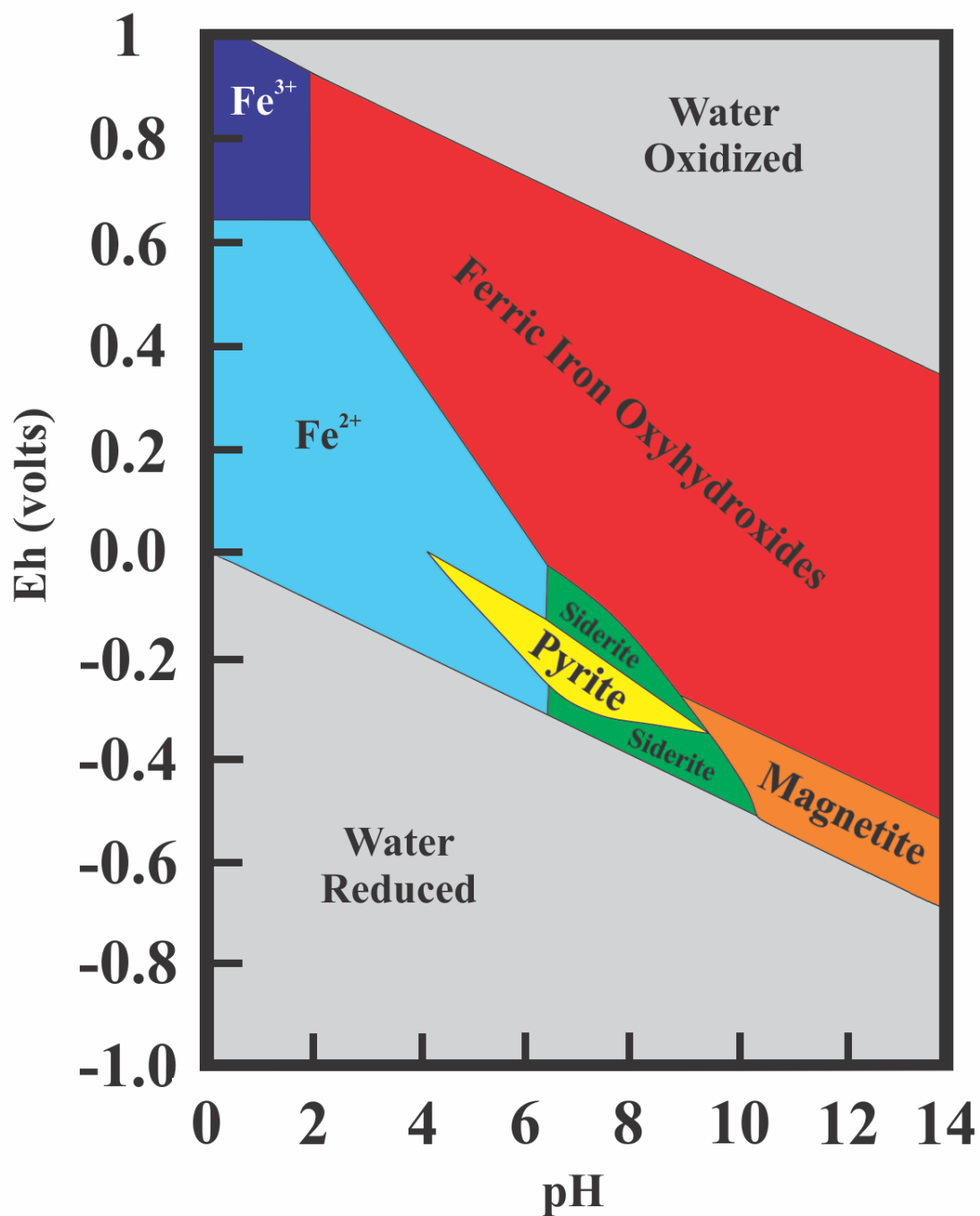


**Figure 27:** Eh-pH stability diagram of aqueous Fe species (shown in shades of blue) and common Fe-bearing minerals (shown in red, green, yellow, and orange) (modified after Garrels and Christ, 1965).

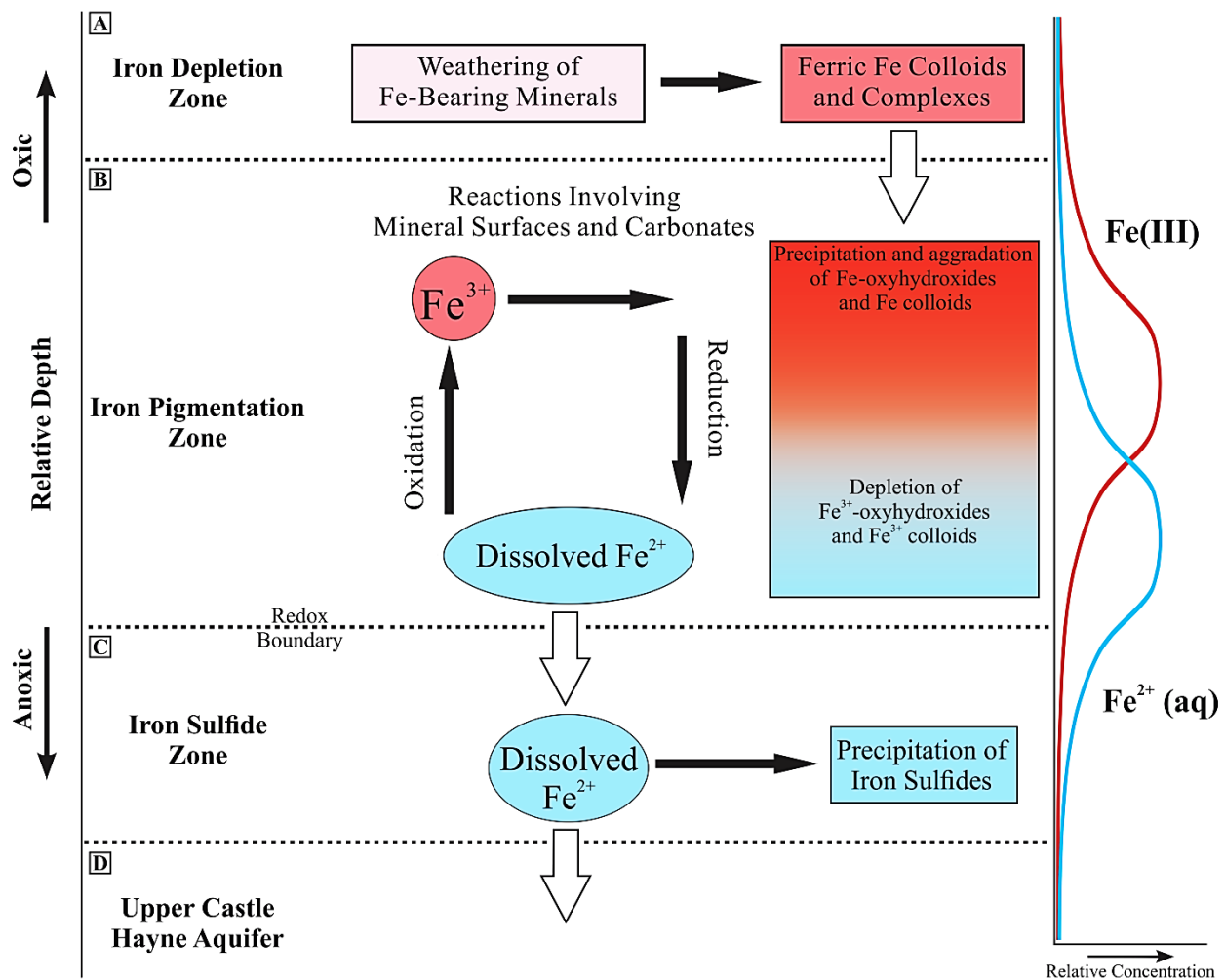


**Figure 28:** A conceptual diagram representing the inferred transformation and transfer of Fe species with increasing relative depth in sediments that overlie the UCHA. Note that the graph on the right side of the figure shows relative changes in solid-phase-ferric iron (in red) and dissolved  $Fe^{2+}$  (in blue) that are expected to occur with increasing depth. The illustrated trend in ferric-Fe concentrations corresponds with sediment-Fe concentrations shown in Figure 24. The trend in dissolved  $Fe^{2+}$  is based on inferred biogeochemical processes (e.g. oxidation and reduction of Fe) that may occur with increasing depth. A. Depicts the formation of mobile-Fe species (colloids and organic complexes) via the weathering of Fe-bearing minerals in the permeable sediments of the IDZ. B. Illustrates the transformation of  $Fe^{3+}$  and  $Fe^{2+}$  along the oxic-anoxic transition zone in the IPZ (modified from Stumm and Morgan, 1996). C. Shows that the formation of sulfide minerals is a possible sink for dissolved  $Fe^{2+}$  in the ISZ. Finally, most of the remaining  $Fe^{2+}$  would likely become incorporated in the UCHA (Figure 28D).

### 5.3 Temporal Hydrologic Considerations

During the height of the Last Glacial Maximum (ca. 26,500 – 19,000 year ago), eustatic sea level was approximately 130 m lower than it is today (Clark et al., 2009). Presumably, the water-table surface was proportionally lower and the vadose zone was likely much thicker at the core site. As a result, O<sub>2</sub>-enriched groundwater reached greater depths because dissolution of atmospheric O<sub>2</sub> in groundwater occurred lower in the sediment column. Moreover, studies indicate that DOC concentrations frequently decrease as the depth of the water table decreases (Pabich, et al., 2007; McMahon and Chapelle, 2008), which would diminish the rate of O<sub>2</sub> reduction, resulting in slower attenuation of dissolved-O<sub>2</sub> concentrations along the flow path. This information suggests that the reduction of iron-oxyhydroxides probably occurred at deeper depths during the Last Glacial Maximum.

More recent variations in the elevation of the water-table surface may also affect the depths at which redox-related processes occur at the core site. Based on existing water-table data, the IDZ sediments are subjected to cyclic wetting and drying above 2.2 m BLS (Figures 24 – 25; Johnson, 1992). Periodic droughts and floods likely result in larger fluctuations in the water table but these data are not available for the study area. When the depth of the water table decreases in a recharge zone (e.g. flooding events), O<sub>2</sub> reduction occurs at shallower depths, possibly resulting in an upward shift in the sequence of electron-accepting processes while the opposite happens when the elevation of the water table is lower.

Johnson (1992) indicates that the underlying aquifers and Tranters Creek are hydraulically connected to each other and that the aquifers usually discharge into Tranters Creek. Although the water chemistry of Tranters Creek was not evaluated, the creek water is probably enriched in dissolved O<sub>2</sub>. Depending on the stage of Tranters Creek and the elevation of the

water table, low-O<sub>2</sub> groundwater from the UCHA and Yorktown aquifer may flow toward the surface and into Tranters Creek or high-O<sub>2</sub> water from Tranters Creek may recharge the underlying aquifers. Based on hydrograph data from Johnson (1992), the latter case does not occur frequently over a one-year period, especially in the UCHA (Figure 29). When the creek stage is periodically higher than the elevation of the water table, surface water from Tranters Creek recharges the surficial aquifer and likely results in a downward shift in the sequence of electron-accepting processes; however, the impact of temporal hydrologic variations on redox conditions cannot be adequately discerned without sufficient water chemistry data.

The groundwater-flow regime proposed by Johnson (1992) for the core site may not fully conform to the sequence of Fe-transformation processes described in the preceding subsections and illustrated in Figure 28 due to the hydrologic complexity that exists at the field site. Groundwater typically flows laterally toward Tranters Creek and vertically toward the surface in the lower aquifers (Johnson, 1992) while groundwater in the surficial aquifer may involve upward flow at deeper depths and downward percolation near the surface. As a result, groundwater at the core site does not contribute to the development of high-Fe zones in the UCHA. Future investigators that wish study potential sources of Fe entering the UCHA should consider choosing a study area where the groundwater consistently recharges the underlying aquifers along relatively simple and stable flow paths to minimize extraneous hydrologic variables.

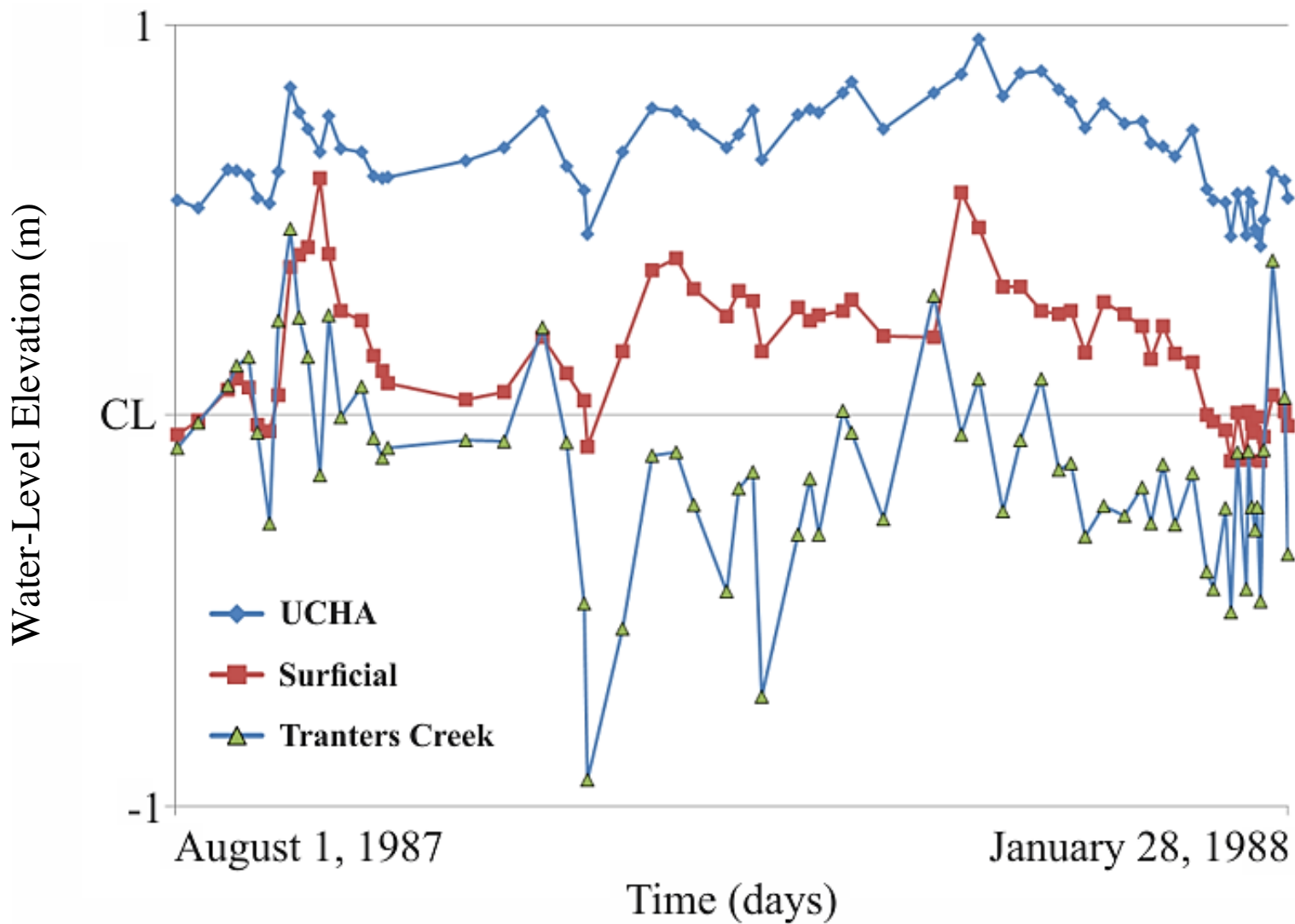


**Figure 29:** Hydrograph showing water-level elevations in the UCHA, surficial aquifer, and Tranters Creek between August 1987 and January 1988 (data from Johnson, 1992). Elevations are referenced to meters above or below mean creek level.



## 5.4 Insights from Modeling

### 5.4.1 Simple Dissolution

The results of the simple-dissolution simulations are presented in Table 22. Simulated dissolution of Fe-bearing minerals in “Pure Water” and “Surficial Water” in PHREEQC shows that minerals containing  $\text{Fe}^{2+}$  release more total-dissolved Fe than those containing only  $\text{Fe}^{3+}$  and dissolved-Fe concentrations generally decrease with increasing pH. Relative to the simulations using “Pure Water,” dissolution of pyrite,  $\text{Fe}^{2+}$ -containing amphiboles, and almandine in the “Surficial Water” solution resulted in very high dissolved-Fe concentrations.

The modeling results indicate that pyrite,  $\text{Fe}^{2+}$ -containing amphiboles, and almandine, may be important contributors to high-dissolved-Fe concentrations entering the UCHA. The simple-dissolution simulations represent a situation in which a single Fe-bearing mineral is in contact with the water solution for a sufficient period of time that permits the establishment of equilibrium. At equilibrium, the largest amount of the mineral that can hypothetically dissolve in 1 liter of the solution at the specified conditions has occurred and the concentration of dissolution-liberated Fe has likely attained its highest value if a portion of the liberated-Fe species did not precipitate from the solution. However, the sediment layers that overlie the UCHA are generally composed of highly permeable sands, suggesting that groundwater residence in these layers is probably short. Weathering of Fe-containing silicate minerals (e.g. garnets and staurolite) can result in the formation of authigenic surface coatings (e.g. gibbsite, iron-oxyhydroxides, and kaolinite) that greatly reduce the rate at which these minerals dissolve under oxidizing conditions (Velbel, 1993). Since the half-lives of most primary Fe-bearing minerals ranges from about 100,000 to over a million years (Holland and Turekian, 2010), the time in

which Fe-bearing minerals are in contact with a specified volume of groundwater may be too brief to permit substantial dissolution of Fe-bearing minerals at the core site.

Except for microbially mediated reduction of iron-oxyhydroxides, which can result in high-Fe groundwater long before equilibrium conditions are established, the dissolution of most Fe-bearing minerals under slightly acidic to circumneutral conditions rarely results in development of high-Fe groundwater because the reaction rates are usually very slow and in the presence of O<sub>2</sub>, dissolution-liberated Fe may result in iron-oxyhydroxide precipitation (Stucki et al., 2012). Therefore, dissolution of detrital Fe-bearing minerals is not likely to result in excessive-Fe concentration (>0.3 mg/L) in the aquifers overlying the UCHA.

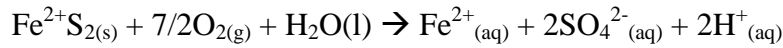
**Table 22:** Results of modeling the dissolution of individual Fe-bearing minerals in “Pure Water” at pH 5, 7, and 9 and the “Surficial Water” at pH 5.3.

Oxidation State	Mineral <sup>1</sup>	"Pure Water"			"Surficial Water"
		pH 5	pH 7	pH 9	pH 5.3
Ferric	Epidote	2.5E-07	2.8E-07	3.1E-07	3.35E-07
	Hematite	1.4E-06	7.4E-08	7.6E-08	9.1E-07
	Ferrihydrite	3.8E-06	2.3E-07	2.3E-07	2.4E-06
	Lepidocrocite	4.4E-06	2.3E-07	2.4E-07	2.4E-06
	Goethite	4.4E-06	2.3E-07	2.4E-07	2.4E-06
	Goethite 2	4.4E-06	2.3E-07	2.4E-07	2.4E-06
Ferric and Ferrous	Glauconite	0.03	0.01	1.09E-02	2.4E-06
Ferrous	Pyrite	0.01	1.5E-03	1.6E-03	1.77
	Hedenbergite	0.03	0.03	0.03	8.8E-03
	Staurolite	0.11	0.03	0.09	1.7E-06
	Schorl	0.20	0.10	0.07	4.6E-06
	Ilmenite	0.24	0.01	1.8E-04	0.03
	Actinolite	0.27	0.14	0.08	11.94
	Ferropargasite	0.33	0.19	0.11	6.12
	Almandine	0.42	0.13	0.06	12.04

1. Ten moles of each Fe-bearing mineral were added to 1 L of solution during the dissolution simulations. Total Fe concentrations are reported in units of mg/L

### 5.4.2 Pyrite Oxidation

The results of the pyrite-oxidation simulations are illustrated in Figures 30 – 33 and Table 23. Pyrite oxidation by O<sub>2</sub> (g) can result in high-Fe concentrations. As O<sub>2</sub> (g) is added to the groundwater solution, pH decreases as dissolved-Fe and dissolved-SO<sub>4</sub><sup>2-</sup> concentrations increase:



The simulations suggest that the secondary drinking water standard (0.3 mg/L Fe) may be exceeded if as little as 0.3 mg/L O<sub>2</sub> (g) reacts with pyrite. If a low-Fe groundwater contains approximately 8 mg/L O<sub>2</sub> (g) under acidic to circumneutral conditions, oxidative dissolution of about 20 mg/L pyrite can release between 8 and 10 mg/L Fe at equilibrium if no other minerals are present.

Mineralogical evaluation of the core samples reveals that pyrite commonly occurs in association with calcareous shell fragments at the base of the IPZ. Therefore, additional PHREEQC simulations incorporating calcite dissolution with pyrite oxidation were conducted to determine how these simultaneous reactions may affect dissolved-Fe concentration in simplified groundwater solutions.

After adding 8 mg/L O<sub>2</sub> (g) to the calcite and pyrite-equilibrated, “Pure Water” solution, about 28 mg/L pyrite dissolved but the highest dissolved-Fe concentration was only 0.01 mg/L. The majority of the Fe that dissolved in the “Pure Water” solution during pyrite oxidation precipitated as goethite. During the initial reaction, pH spikes from 7 to nearly 10 as calcite and pyrite dissolve, resulting in the precipitation of goethite and a lower dissolved-Fe concentration relative to the “Pure Water” simulation that excluded calcite dissolution.

Incorporation of calcite dissolution with pyrite oxidation in the “Surficial Water” solution increased the maximum dissolved-Fe concentration by approximately 20% at the end of the

“Surficial Water” simulation. Calcite dissolution increases the oxidative dissolution of pyrite. Consequently, goethite remained undersaturated throughout the titration, resulting in progressively higher Fe concentrations. Although the pyrite-oxidation simulations suggest that pyrite oxidation can result in high-Fe concentrations, pyrite only occurs in trace amounts at the core site. Further study is needed to determine if pyrite oxidation leads to the development of high-Fe groundwater in UCHA recharge area.

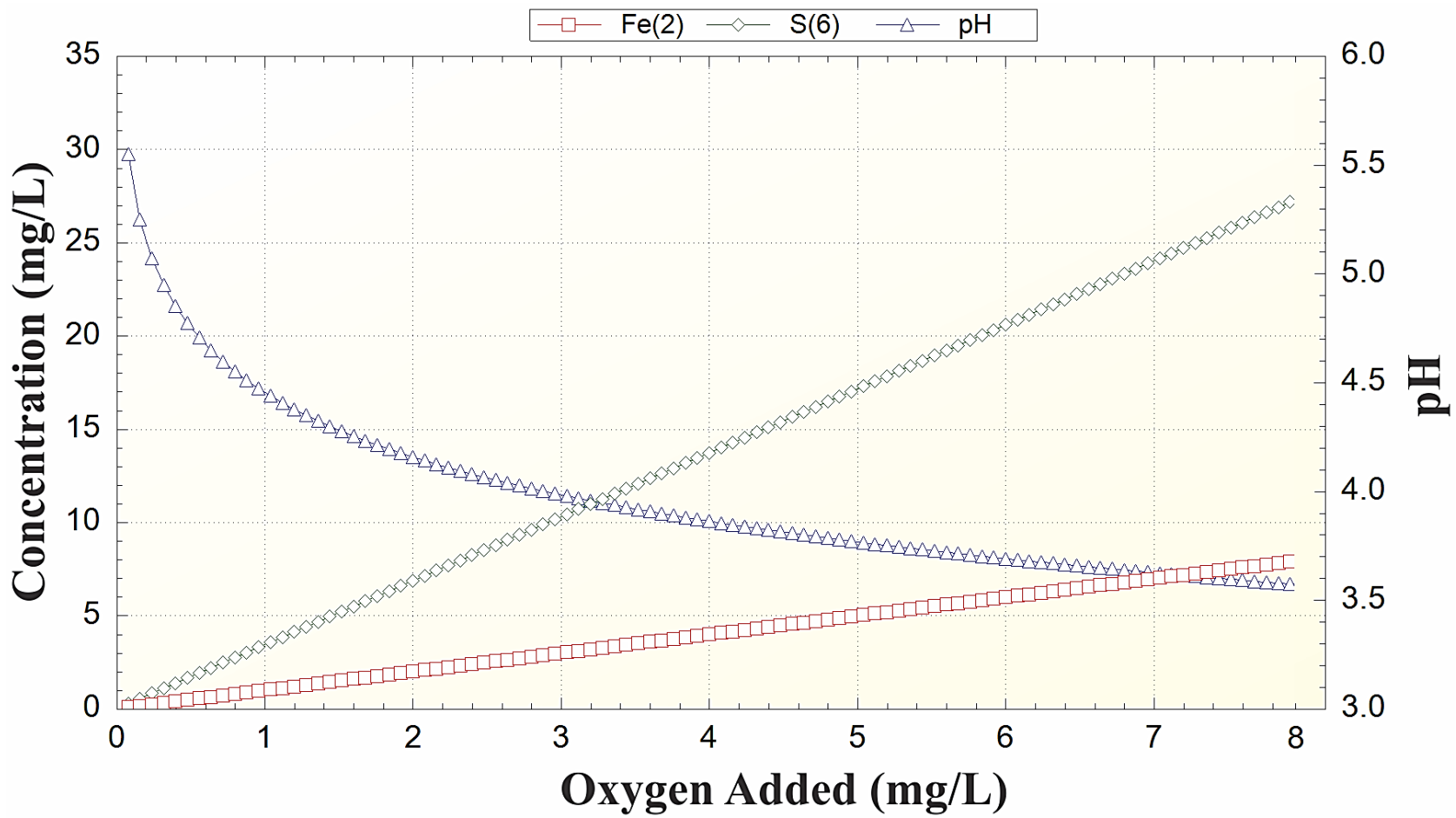


**Figure 30:** Simulation of pyrite titrated with oxygen in the “Pure Water” solution.

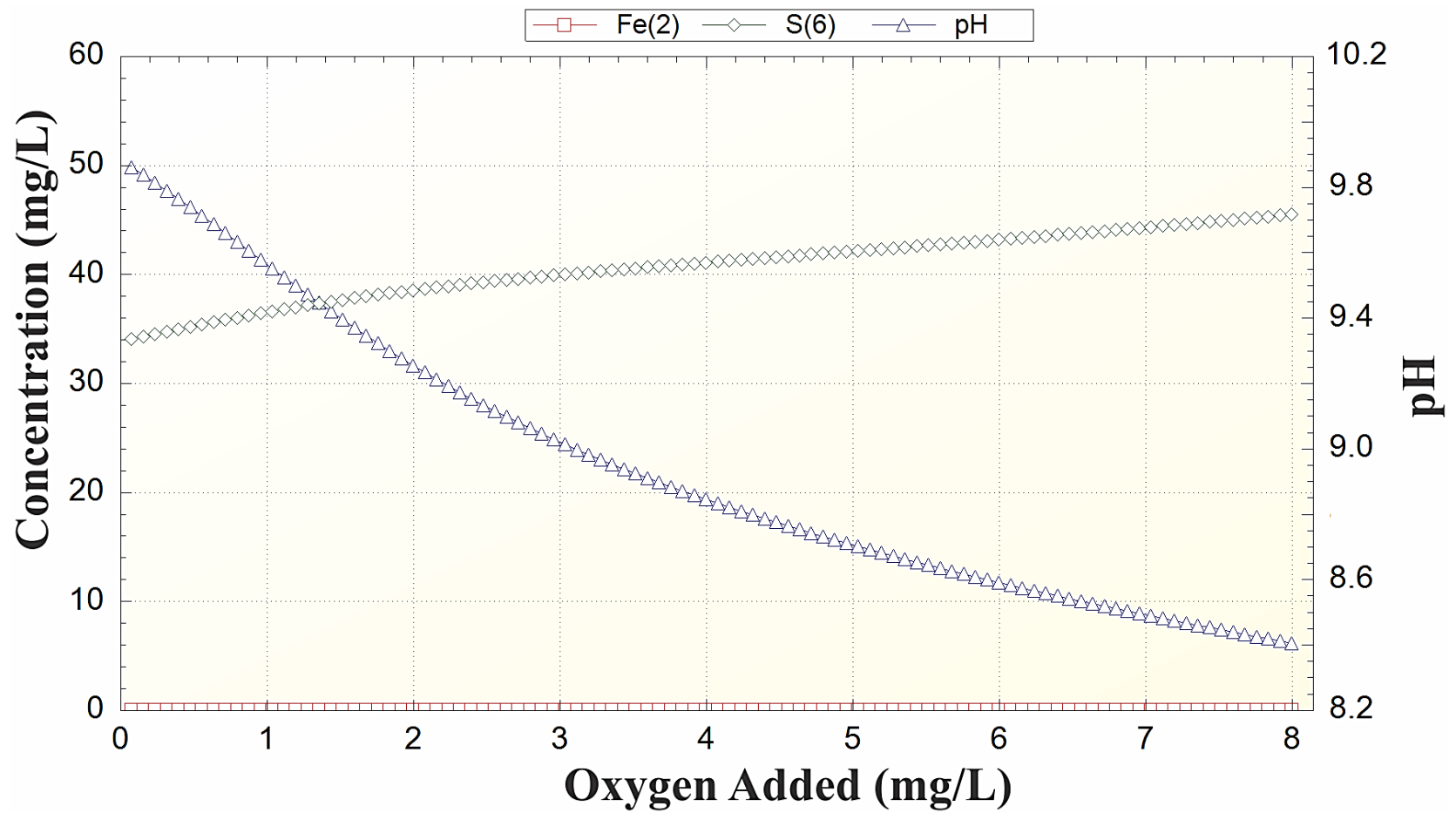


**Figure 31:** Simulation involving pyrite titration with oxygen and simultaneous calcite dissolution in the “Pure Water” solution.

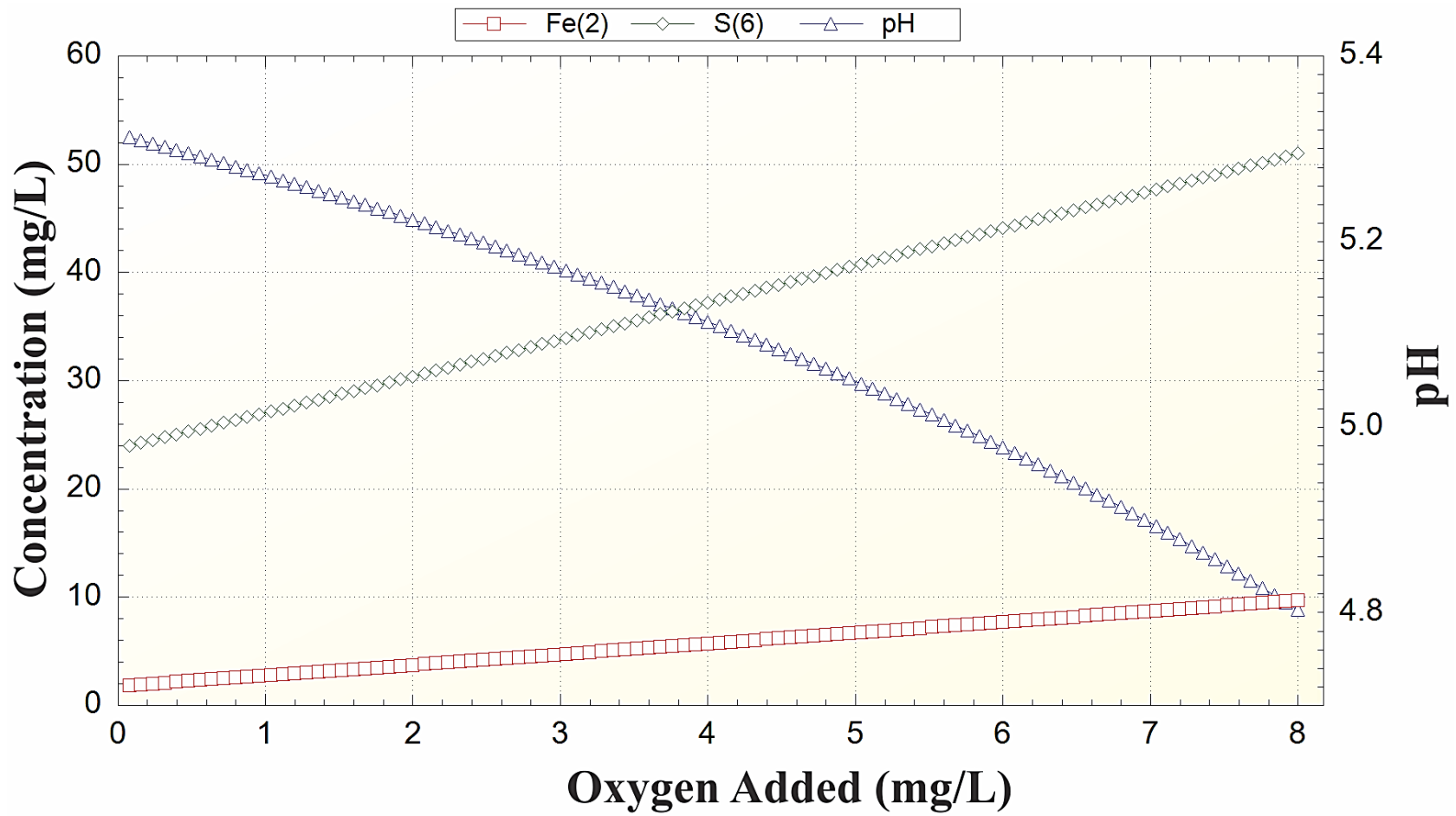


**Figure 32:** Simulation of pyrite titrated with oxygen in the “Surficial” solution.



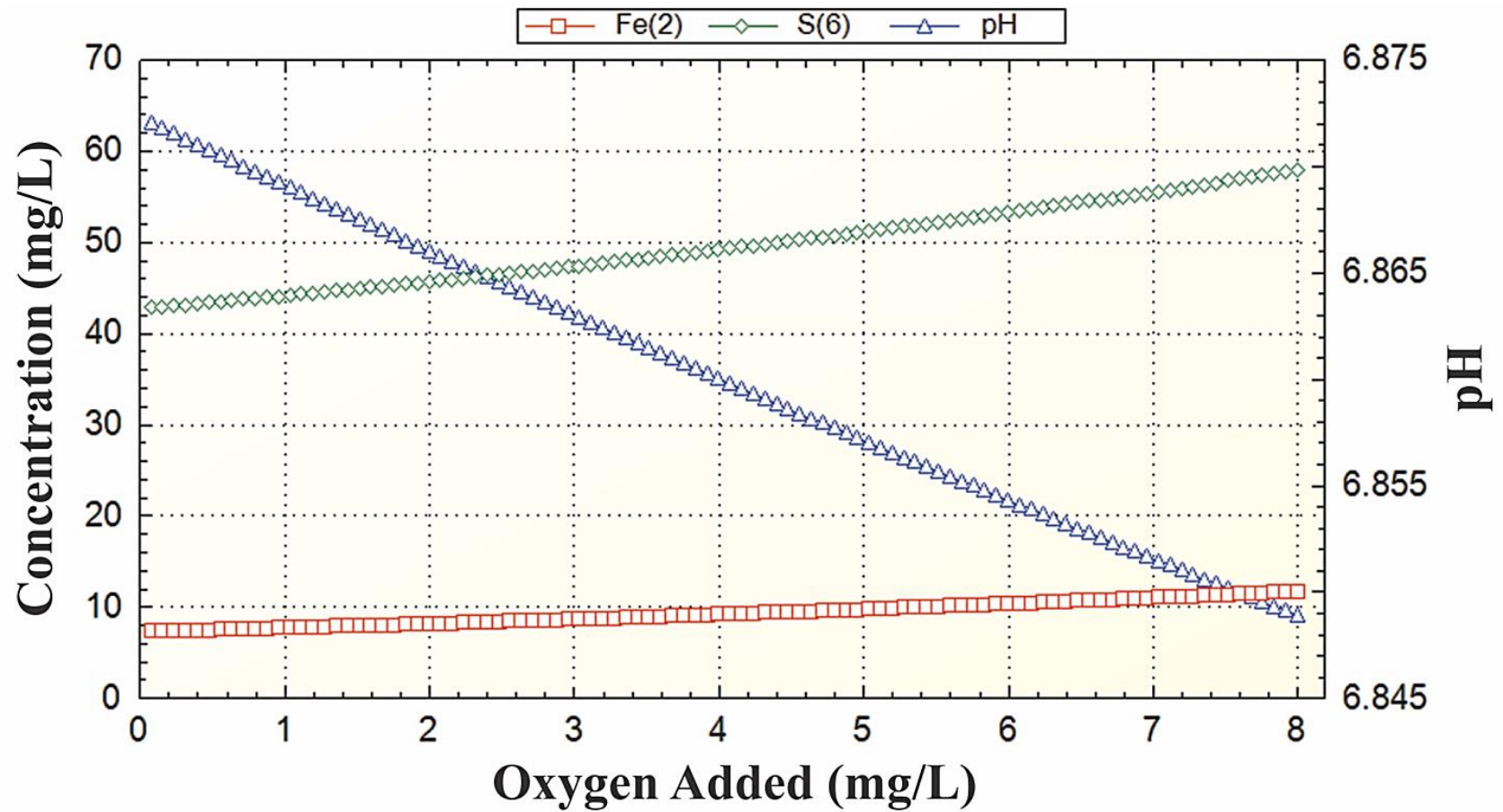


**Figure 33:** Simulation involving pyrite titration with oxygen and simultaneous calcite dissolution in the “Surficial Water” solution.

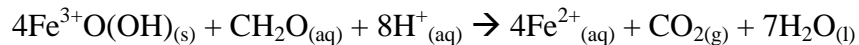
**Table 23:** Results of the pyrite titration with O<sub>2</sub> in the “Pure Water” and “Surficial Water” simulations.

Solution <sup>1</sup>	Initial O <sub>2</sub>	Initial Fe	Final Fe	Pyrite Dissolved	Goethite Precipitated
Pure Water	0	0	7.98	17.14	0
Pure Water with Calcite	0	0	0.01	28.40	21.01
Surficial Water	0.28	0.07	9.68	20.65	0
Surficial Water with Calcite	0.28	0.07	11.68	24.94	0

1. Concentrations are in units of mg/L

### 5.4.3 Goethite Titration with DOC

Simulation of goethite titrated with dissolved organic carbon (DOC) in PHREEQC reveals that goethite reduction can result in elevated Fe concentrations (Figures 34 – 35 and Table 24). After O<sub>2</sub> (g) and NO<sub>3</sub><sup>-</sup> in the “Surficial Water” are depleted by the oxidation of DOC, DOC begins to reduce goethite, resulting in progressively higher dissolved-Fe concentrations as DOC (represented by CH<sub>2</sub>O<sub>(aq)</sub> in the following reaction) is added to the solution:



Sulfate reduction via DOC oxidation occurs simultaneously with goethite reduction to produce very small amounts of S<sup>2-</sup> (in the form of H<sub>2</sub>S); however, Fe reduction remains the primary electron-accepting process until iron-oxyhydroxides are depleted. As a result of incremental production of H<sub>2</sub>S and Fe<sup>2+</sup>, pyrite becomes supersaturated and about 0.4 mg/L pyrite precipitates by the end of the titration. The modeling results suggest that 5 mg/L DOC has the capacity to dissolve just over 100 mg/L goethite in the “Surficial Water,” resulting in a maximum dissolved-Fe concentration of over 65 mg/L, which is more than 20 times greater than the secondary drinking water standard.

Evaluation of the core samples indicates that iron-oxyhydroxides occur in both non-calcareous and calcareous sediments. To account for interactions with aquifer carbonates, an additional titration simulation was conducted to determine how calcite dissolution may impact Fe concentrations during goethite reduction by DOC.

The modeling results demonstrate that calcite dissolution can mitigate reductive dissolution of goethite. The addition of calcite dissolution to the goethite titration model resulted in circumneutral conditions, which reduced the reactivity of goethite. As a result, the

incorporation of calcite dissolution in the goethite-titration simulation reduced the maximum dissolved-Fe concentration from 65.8 to 11.2 mg/L in the “Surficial Water” solution.

For both titration simulations (one that includes calcite dissolution and one that excludes calcite dissolution), the secondary drinking water standard for dissolved Fe is exceeded after 1.2 mg/L DOC reduces around 1.3 mg/L goethite. Future investigations involving the origin of elevated Fe concentrations should include organic matter and DOC to better determine how much DOC may be necessary to produce excessive-Fe concentration in the Fe-reducing zone of an aquifer. These simulations collectively suggest that reductive dissolution of goethite by DOC is most likely to result in excessive-Fe concentration where the groundwater pH is acidic and the abundance of carbonates is low or nonexistent.

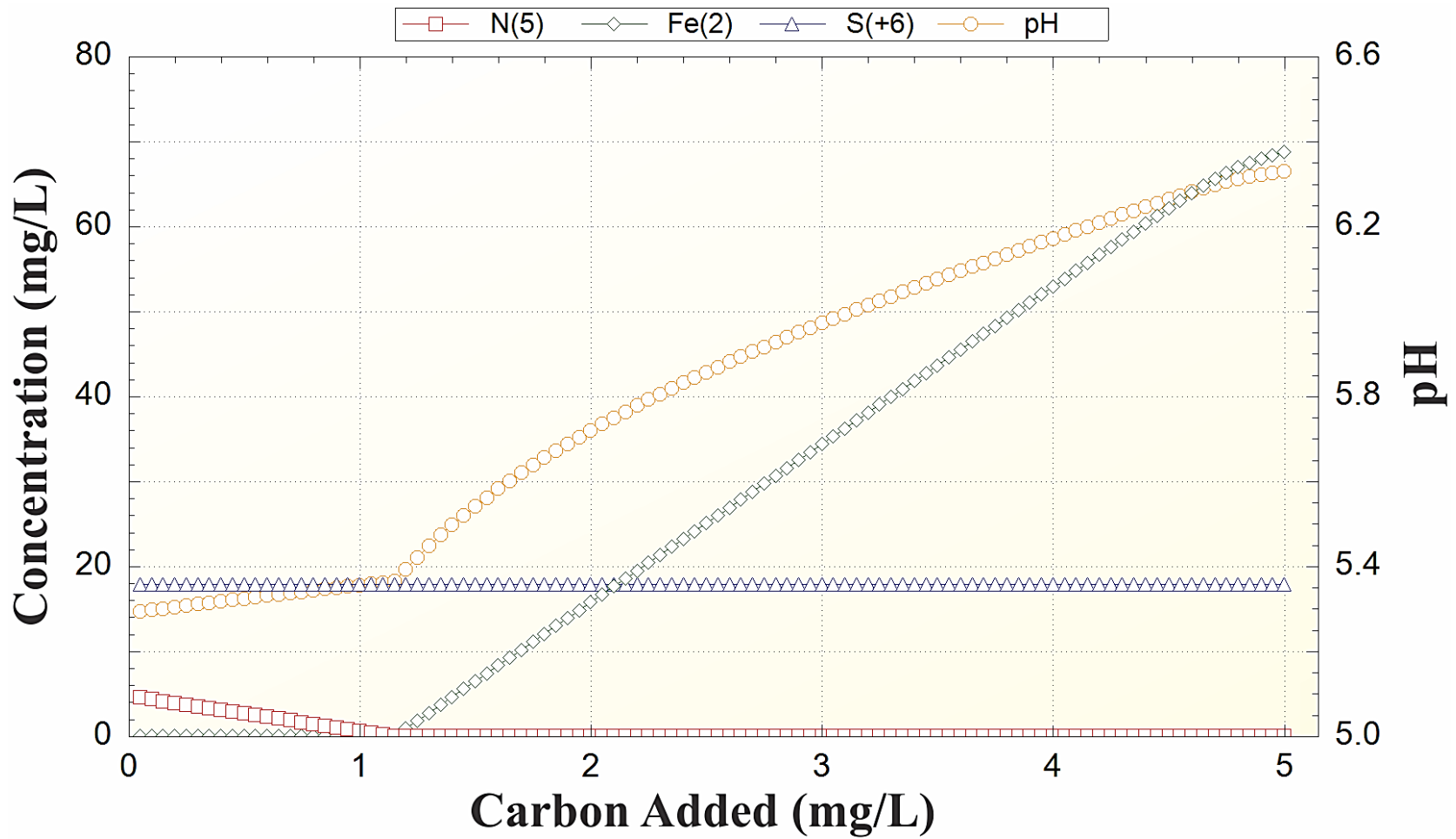


**Figure 34:** Simulations of goethite titrated with DOC in the “Surficial Water” solution.

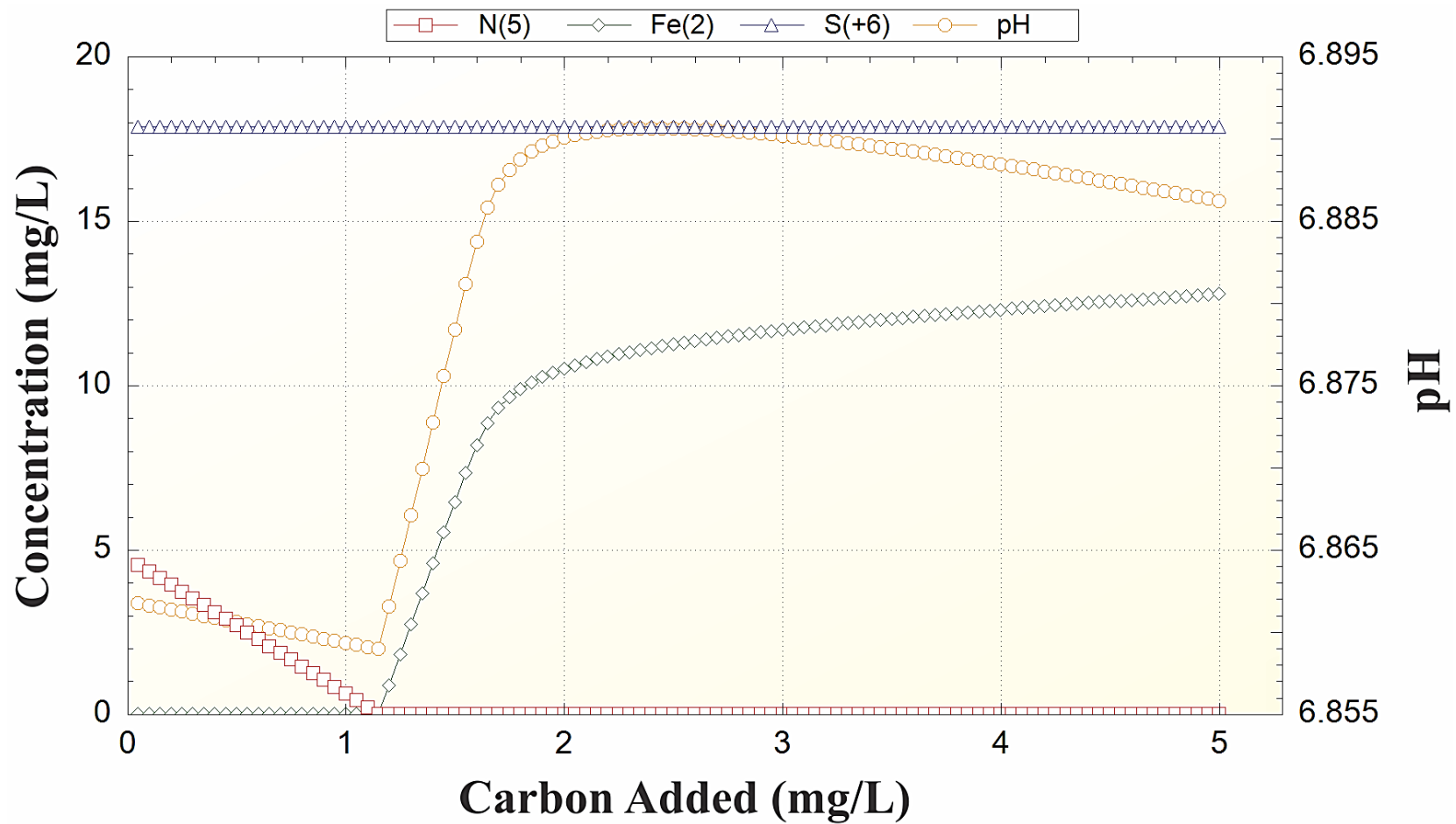


**Figure 35:** Simulations involving goethite titration with DOC and simultaneous calcite dissolution in the “Surficial Water” solution.

**Table 24:** Results of goethite titration with DOC for the “Surficial Water” simulations.

Solution	Initial Fe	Final Fe	Goethite Dissolved	Pyrite Precipitated
Surficial Water	0.07	65.79	104.85	0.36
Surficial Water with Calcite	0.07	11.19	17.70	0.00

1. Concentrations are in units of mg/L

#### 5.4.4 Calibrated Transport Models

Satisfactory reproduction of the observed Fe-concentration trends that occur with increasing distance from T15 was achieved using values of 800 m and 0.115 eq/L for dispersivity and CEC, respectively (Figure 36). According to Appelo and Postma (1993), dispersivity is commonly around 10% of the traveled distance. Based on their approach, a dispersivity of 800 m is about 25% smaller than predicted relative to the distance between T15 and FE (about 10.7 km). Therefore, the composition of the UCHA between T15 and FE may be more homogenous and isotropic than other aquifers, which would result in less mixing during advective transport. However, available hydrologic and geochemical data are not sufficient to reliably predict dispersivity at larger scales.

Using glauconite as the major cation exchanger,  $X_{UCHA}$  (CEC of the UCHA) can be estimated using the following calculation:

$$X_{UCHA} \text{ (eq/L)} = \text{Glauconite Abundance (\%)} \times \text{CEC of Glauconite (meq/g)} \times 1000 \text{ (g/kg)} \\ \times \text{Density of Aquifer Material (kg/L)} \times ([\text{Total Volume} - \text{Porosity}] \div \text{Porosity}) \times 0.001 \text{ eq/meq}$$

Assuming a CEC of 20 meq/100g for glauconite (Kogel et al., 2006), a bulk density of 2.7 kg/L for the UCHA, and a porosity of 20% (Dr. Spruill, pers. comm. 2016), about 5% glauconite is necessary to produce the model-estimated exchange capacity (0.115 eq/L pore water). This estimated abundance for glauconite is within the range reported by Mehlhop et al. (2005). Figure 37 shows that relatively small changes in glauconite abundance can have a substantial impact on dissolved-Fe concentrations via cation-exchange reactions. Further evaluation of the mineralogy may be necessary to evaluate the impact of localized changes in CEC on dissolved-Fe concentrations in the UCHA.



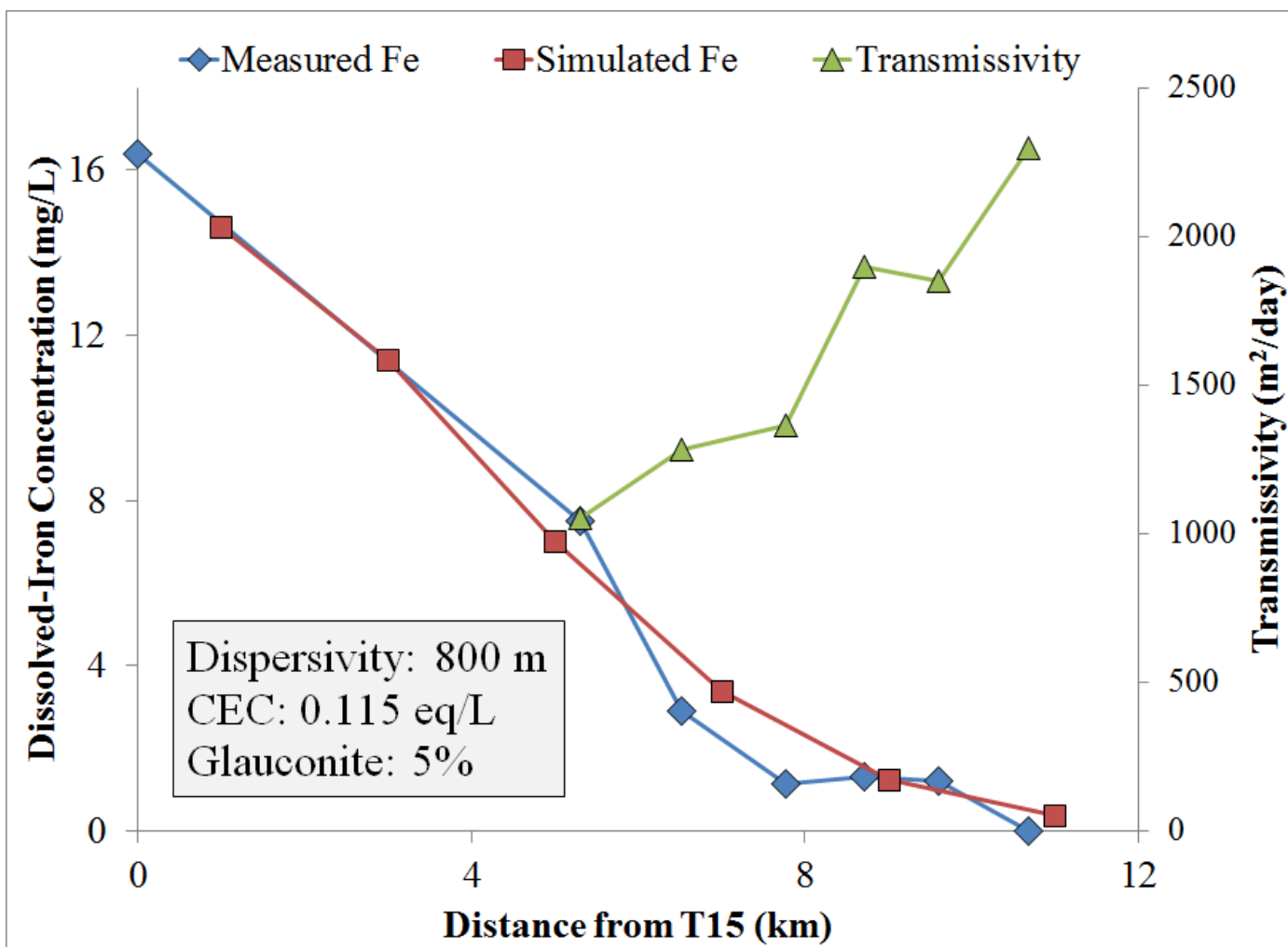


**Figure 36:** Measured and simulated dissolved-Fe concentrations graphed with increasing distance from Well T15 near Washington, NC. Model-estimated values for dispersivity and CEC in the UCHA were 800 m and 0.115 eq/L, respectively. Using the model-estimated CEC value in the UCHA and 20 meq/100g for glauconite, the estimated average abundance of glauconite is about 5% along the flow path. Transmissivity values are from Warner (1993).

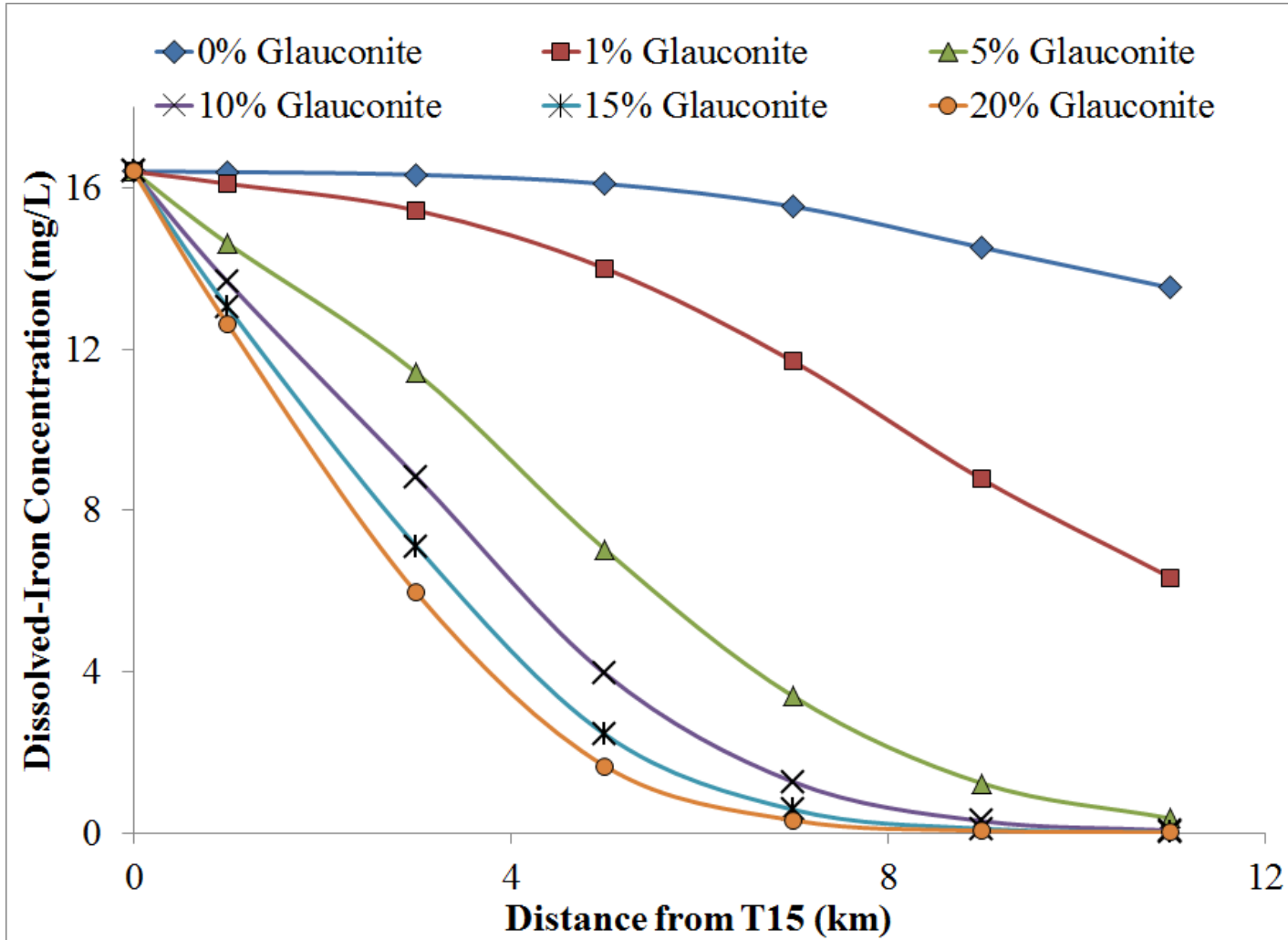


**Figure 37:** Impact of glauconite-abundance variations on dissolved-Fe concentrations along a simulated flow path in the UCHA. Note that these results assume that glauconite is the major cation exchanger and has a CEC of 20 meq/100g.

#### **5.4.4.1 Conservative-Transport Modeling**

The conservative model simulates conservative transport beginning at T15 and ending around 12 km downgradient at the FE well. The results of conservative-transport modeling reveal that transport-related mixing may only account for slight decreases in dissolved-Fe concentrations (<3 mg/L) between the T15 and FE wells (Figure 38). Therefore, physical processes such as advection and dispersion may be relatively insignificant mechanisms by which dissolved-Fe is depleted from groundwater in the UCHA.

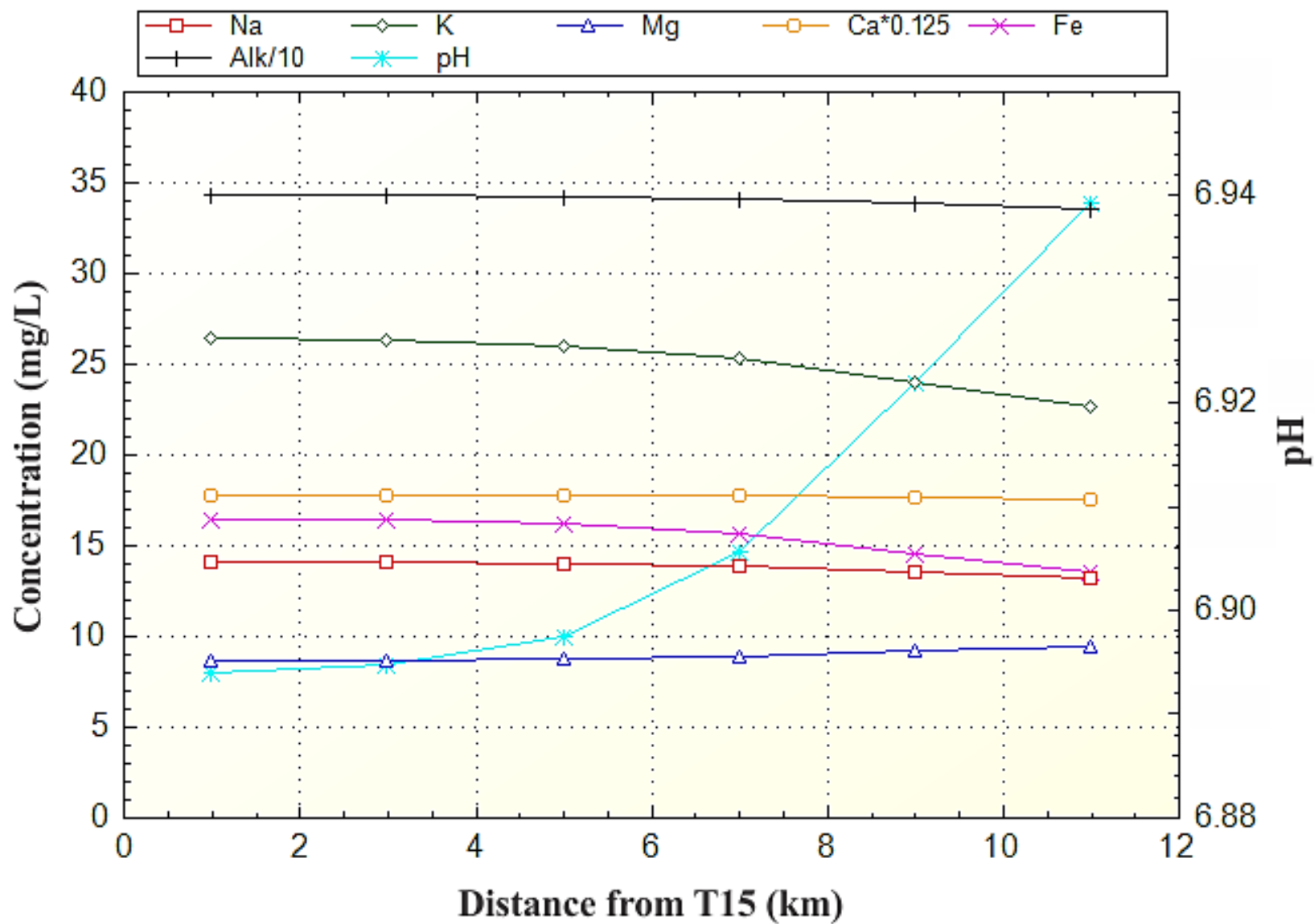


**Figure 38:** Results of the conservative-transport simulation. Note that Ca and alkalinity have been reduced to 1/8 and 1/10, respectively to improve visualization of species that are less concentrated.

#### 5.4.4.2 Reactive-Transport Modeling

Geochemical processes including cation exchange and calcite dissolution are incorporated in the reactive-transport simulation (Figure 39). Mineral precipitation was not included in the reactive-transport model because minerals such as iron-oxyhydroxides, siderite, and pyrite are not significant constituents comprising the UCHA. Moreover, the purpose of the reactive-transport model is to determine if cation exchange is a plausible explanation for the rapid depletion of dissolved-Fe over a relatively short distance in the UCHA.

Comparison of results for the reactive and conservative models reveals that pH and alkalinity are higher in the reactive simulation than the conservative simulation. These increases can largely be explained by calcite dissolution. Figures 38 and 39 also show that cation-exchange reactions may affect  $\text{Na}^+$ ,  $\text{K}^+$ ,  $\text{Mg}^{2+}$ , and  $\text{Fe}^{2+}$  concentrations in the UCHA. These differences can only be explained by cation exchange because the transport models were not setup to include other processes that are capable of affecting the concentrations of these constituents.

Although the reactive-transport simulation demonstrates that cation-exchange reactions can remove substantial amounts of dissolved Fe over a relatively short distance in the UCHA, deviations between simulated and measured Fe concentrations suggest that other factors may affect dissolved-Fe concentrations (Figure 36). For example, transmissivity (defined as the rate of groundwater flow under a unit of hydraulic gradient through a unit width of aquifer thickness) variations may correspond with changes in groundwater-residence time and reservoir size (e.g. hydraulic conductivity may be inversely related to residence time and aquifer thickness is directly related to reservoir size). Aquifer tests conducted by Warner (1993) and Consolvo (1998) reveal that the transmissivity of the UCHA generally increases from west to east near Washington, NC. As a result, eastward increases in transmissivity may augment the

downgradient depletion of dissolved-Fe concentration in the UCHA where the thickening of the UCHA may result in the dilution of the upgradient groundwater by a low-Fe groundwater. In addition to transmissivity variations, relatively small changes in  $X_{UCHA}$  along the UCHA flow path can result in substantial changes in dissolved-Fe concentration (Figure 37). Other variables including leakage into the UCHA from adjacent aquifers and the possibility that the wells are not located precisely along the same flow path of the UCHA may also result in deviations between simulated and measured-Fe concentrations. More robust hydrogeochemical models incorporating detailed investigation of regional differences in hydrology, mineralogy, sediment composition, and groundwater chemistry are needed to determine which processes are most responsible for the rapid depletion of dissolved Fe in the UCHA near Washington, NC.

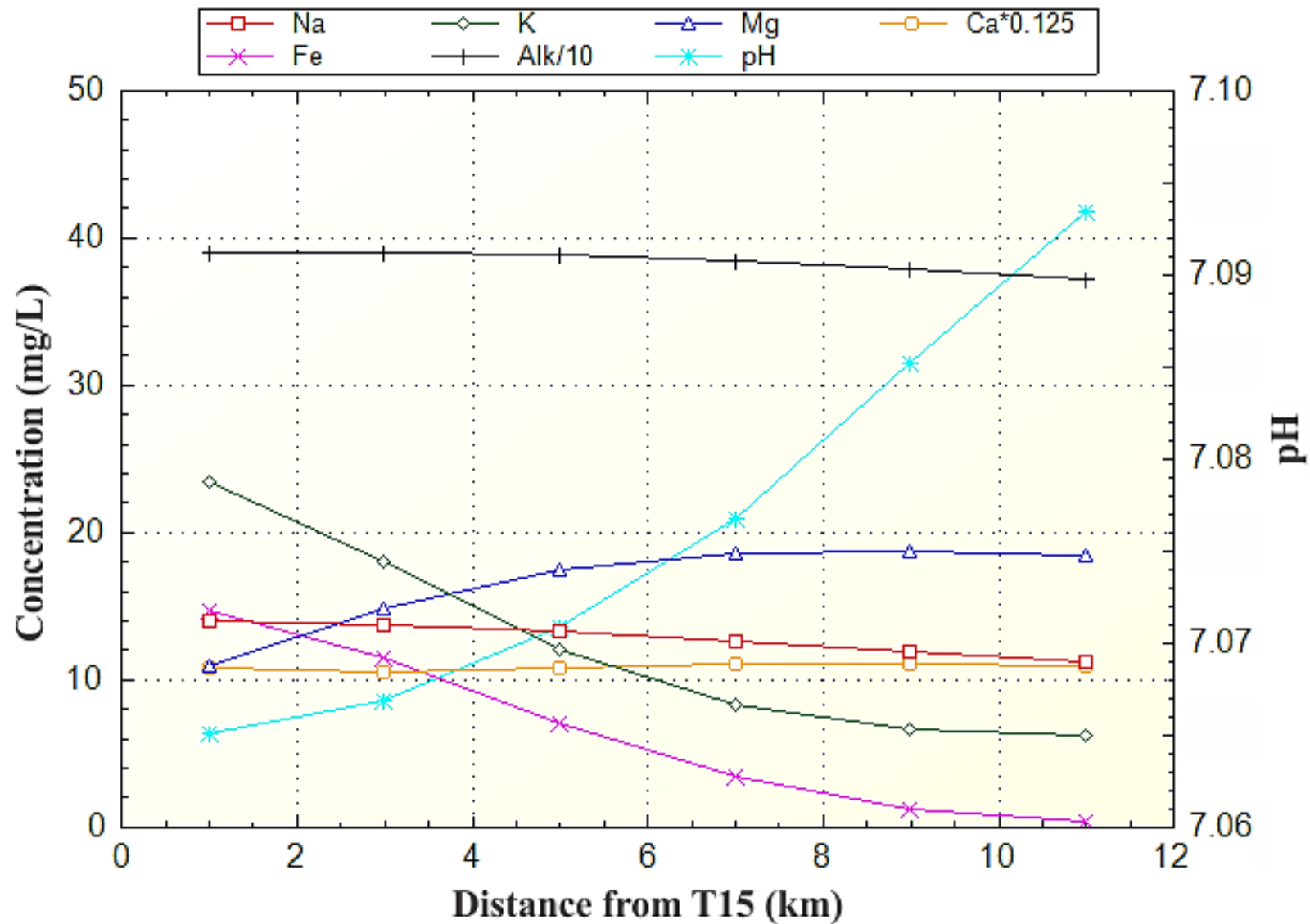


**Figure 39:** Results of the reactive-transport simulation. Note that Ca and alkalinity have been reduced to 1/8 and 1/10, respectively to improve visualization of species that are less concentrated.

## 6.0 Conclusions

This investigation examines the origin and geochemical evolution of high-Fe<sup>2+</sup> zones in the UCHA. It was hypothesized that high-Fe concentrations near the UCHA recharge area are derived from microbially catalyzed reduction of iron-oxyhydroxide compounds in the overlying sediment layers. Subsequently, cation exchange was proposed as a mechanism that could result in the rapid depletion of dissolved Fe over a relatively short distance in the UCHA. The mineralogy, sedimentology, and geochemistry of overlying aquifer materials were studied in detail to identify major Fe-bearing minerals that comprise the overburden near Washington, NC. Preliminary geochemical models were developed to evaluate the potential of common Fe-bearing minerals to yield high dissolved-Fe concentration via dissolution and redox reactions. In addition, the effects of carbonate reactions, permeability, and variations in sediment geochemistry and sedimentological composition on Fe mobility are inferred from batch simulations and core data. Finally, a one-dimensional reactive-transport model was developed to evaluate the potential of cation exchange to deplete high-dissolved-Fe concentrations along a simulated flow path of the UCHA.

Based on core data acquired during this investigation and various geochemical and hydrogeologic data from previous studies (e.g. Johnson, 1992; Warner 1993; Sutton and Woods, 1995; Winner and Coble, 1996; Brown, 1999; Woods et al., 2000; Lautier, 2009), the following conclusions were made:

1. Three hydrogeochemical zones are identified in the 11 m Geoprobe cores to highlight potentially significant attributes and Fe-related processes in the sediments overlying the UCHA. These zones, distinguished by variations in sediment composition, depth, and inferred biogeochemical and hydrologic processes, include the Iron Depletion



Zone (IDZ), Iron Pigmentation Zone (IPZ), and the Iron Sulfide Zone (ISZ). The major processes affecting Fe concentrations in these zones likely include the dissolution and precipitation of Fe-bearing minerals, variations in permeability and CEC, reduction of iron-oxyhydroxides, and carbonate reactions.

2. Fe-bearing minerals comprise less than 2% of the mineralogical constituents in the IDZ. Ilmenite is the dominant Fe-bearing mineral in the IDZ but lesser amounts of amphiboles, pyroxenes, staurolite, almandine, and tourmaline are also present. Relative to the IPZ and ISZ, the IDZ sediments have the highest mean permeability, the lowest mean mud content, the lowest mean CEC, and the lowest mean Fe concentration.
3. Sediments comprising the IDZ have low Ca, Mg, K, and Na concentrations and low CEC values, indicating that the IDZ sediments have a low capacity to buffer infiltrating acidic precipitation and that these sediments are susceptible to leaching by the infiltration of acidic precipitation.
4. Groundwater flowing through the IDZ is acidic and likely oxidizing because the sediments are near the ground surface. Under these conditions, Fe-bearing minerals are only slightly soluble. Fe complexes and colloidal, iron-oxyhydroxides, formed by the weathering of Fe-bearing minerals, tend to remain suspended in groundwater and are required to transport any significant amounts of Fe below the water table. Slow, in-situ chemical weathering may partially explain the low abundances of Fe-bearing minerals in the IDZ.
5. Simulated dissolution of individual Fe-bearing minerals indicates that Fe<sup>2+</sup>-containing minerals are less stable than Fe<sup>3+</sup>-containing minerals under near-surface aquifer

conditions. In general, the initial pH of the groundwater solution is inversely related to total-dissolved-Fe concentrations at equilibrium.

6. The simple-dissolution simulations also indicate that dissolution-liberated Fe may result in iron-oxyhydroxide precipitation. Simple dissolution of Fe<sup>2+</sup>-containing minerals in the overburden would likely result in low-Fe concentrations due to short groundwater-residence times, low abundances of Fe-containing minerals, and possible iron-oxyhydroxide precipitation in the oxic zone (above ~6.4 m BLS).
7. Fe-bearing minerals make up approximately 4% of sediments in the IPZ. In decreasing order of estimated abundance, the principal Fe-bearing minerals include glauconite, one or more iron-oxyhydroxides (the principal mineral is probably goethite), ilmenite, almandine, staurolite, amphiboles, pyroxenes, tourmaline, and pyrite. Relative to the IDZ and ISZ, the IPZ sediments have the lowest mean permeability, the highest mean mud content (27.5 wt. %), and the highest mean Fe concentration (5.0 wt. %). The IPZ sediments have a mean CEC of about 75.8 meq/100 cm<sup>3</sup>, which is an order of magnitude greater than the IDZ sediments.
8. The IPZ consists of two, stratigraphically adjacent intervals that are typified by high sediment-Fe concentrations and transitional color changes that occur along a 2.6 m core interval below the IDZ. Between 3.8 and 5 m BLS, sediment colors in the upper IPZ change from light tan to yellowish brown and then, to dark orangish brown. This interval contains a high proportion of mud-sized grains and coincides with a general increase in sediment-Fe concentrations. Sediment colors in the lower IPZ change from dark orangish brown near 5 m BLS to a bluish gray color by approximately 6.4 m BLS.

The lower IPZ contains less mud than the upper IPZ and sediment-Fe concentrations generally decrease with increasing depth.

9. High Fe concentrations correlate well with yellow, brown, and orange pigmentations and with large increases in pH, CEC, and mud content in the upper IPZ. Qualitatively, yellow, orange, and brown colors correspond with high iron-oxyhydroxide abundances, in the form of Fe-rich Ags/Cs.
10. Sedimentological and geochemical evidence indicates that iron-oxyhydroxides precipitated and became concentrated in the IPZ. As a result of electrostatic attraction, iron-oxyhydroxides tend to form aggregates as they attach to the surfaces of negatively charged grains. The relatively high mud content and low permeability of IPZ sediments may facilitate electrostatic interactions between sediments and suspended iron-oxyhydroxide colloids due to the high surface area of mud-size grains and diminished groundwater-flow velocity. Carbonate reactions likely result in the precipitation of iron-oxyhydroxides in the IPZ and increasing groundwater pH.
11. Evidence suggests that the IPZ transitions from oxidizing conditions to reducing conditions. As a result, both iron-oxyhydroxide precipitation and iron-oxyhydroxide reduction may occur in the upper and lower IPZ, respectively. Dissolved-Fe concentrations may therefore increase with increasing depth in the IPZ. High-dissolved-Fe concentrations in the UCHA are most likely derived from conditions that are similar to the lower IPZ, where microbially catalyzed reduction of abundant iron-oxyhydroxides results in the production of dissolved  $\text{Fe}^{2+}$ .
12. The goethite-titration simulations show that goethite reduction by organic-matter oxidation can result in very high-dissolved-Fe concentrations. After Fe-reducing

conditions are established, iron-oxyhydroxide (represented as goethite in PHREEQC simulations) reduction can rapidly result in progressively higher dissolved-Fe concentration if sufficient DOC is present. The simulations show that the secondary drinking water standard for dissolved Fe is exceeded if 1.2 mg/L DOC reduces around 1.3 mg/L goethite. The goethite-titration simulations also reveal that reductive dissolution of goethite by DOC is most likely to result in excessive-Fe concentration where the abundance of carbonates is low or nonexistent and the groundwater pH is acidic.

13. The ISZ occurs below 6.4 m BLS where the abundance of pyrite and mean sediment-sulfur concentrations ( $S_T = 0.5$  wt. % and  $S_e = 427$  mg/dm<sup>3</sup>) are relatively high. Iron-bearing minerals make up less than 3% of the minerals in the ISZ. In descending order of estimated abundance, the dominant Fe-bearing minerals are ilmenite, glauconite, amphiboles, pyroxenes, almandine, tourmaline, staurolite, and pyrite. Mean permeability and mean mud content are approximately 7.6 m/d and 13.9 wt. %, respectively.
14. The lack of iron-oxyhydroxides and occurrence of pyrite suggest that groundwater conditions were probably favorable for microbially mediated sulfate reduction in the ISZ. The reduction of iron-oxyhydroxides in the IPZ may provide the requisite Fe<sup>2+</sup> to form Fe sulfides in the ISZ; however, the low abundance of pyrite in the ISZ suggests that the formation of Fe-sulfides may be an insignificant sink of dissolved Fe<sup>2+</sup> in the sediments overlying the UCHA.
15. The results of the pyrite-oxidation simulations suggest that reactions involving pyrite and dissolved O<sub>2</sub> can result in high-Fe concentrations. If a low-Fe groundwater is

nearly saturated with  $O_2$  (g) under acidic to circumneutral conditions, dissolution of about 20 mg/L pyrite may result in Fe concentrations ranging from about 8 to 10 mg/L. However, further investigation is needed to determine if pyrite weathering is an important process leading to the formation of high-Fe zones in the UCHA recharge area.

16. The results of reactive-transport modeling show that cation-exchange reactions can substantially deplete dissolved-Fe concentrations along a simulated 12 km flow path in the UCHA. The simulation suggests that about 5% glauconite can successfully reproduce observed Fe concentrations in groundwater near Washington, NC. Transmissivity variations, leakage from adjacent aquifers, differences between the simulated and actual flow paths, and changes in  $X_{UCHA}$  may explain the minor deviations between the simulated and measured Fe concentrations.

## 7.0 References

- Amsbaugh, M.B. 1996. Hydrogeology of the Castle Hayne Aquifer system in Eastern Onslow County, North Carolina: Unpublished Master's Thesis, East Carolina University, Greenville, North Carolina.
- Appelo, C.A.J. and D. Postma. 1993. Groundwater, Geochemistry and Pollution, Second Edition, Balkema, Rotterdam: CRC press.
- Aruna, P., A. Ajitha, and V.U. Rao. 2014. X-Ray fluorescence. *International Journal of Pharmaceutical Research & Analysis* 4 (4): 222 – 228.
- Ball, D.F. 1964. Loss-on-ignition as an estimate of organic matter and organic carbon in non-calcareous soils. *Journal of Soil Science* 15 (1): 84 – 92.
- Bengtsson, L. and M. Enell. 1986. In: Berglund, B.E. eds. *Chemical analysis. Handbook of Holocene Palaeoecology and Palaeohydrology*, Chichester: John Wiley & Sons.
- Berner, R.A. 1969. Migration of iron and sulfur within anaerobic sediments during early diagenesis. *American Journal of Science* 267 (1): 19 – 42.
- Bertine, K.K. and E.D. Goldberg. 1977. History of heavy mineral contamination in shallow coastal sediments around Mitelene, Greece. *International Journal of Environmental Analytical Chemistry* (68): 281 – 293.
- Blott, S.J. and K. Pye. 2001. GRADISTAT: a grain size distribution and statistics package for the analysis of unconsolidated sediments. *Earth Surface Processes and Landforms* 26 (11): 1237 – 1248.
- Breeuwsma, A.J.H.M., J.H.M. Wösten, J.J. Vleeshouwer, A.M. Van Slobbe, and J. Bouma. 1986. Derivation of land qualities to assess environmental problems from soil surveys. *Soil Science Society of America Journal* 50 (1): 186 – 190.
- Brown, C.J., J.D. Coates, and M.A. Schoonen. 1999. Localized sulfate-reducing zones in a coastal plain aquifer. *Ground Water* 37 (4): 505 – 516.
- Brown, R.T. 1999. Groundwater geochemistry of the Castle Hayne Aquifer: Unpublished Master's Thesis, East Carolina University, Greenville, North Carolina.
- Campbell, B.G. and A.L. Coes. 2010. Groundwater availability in the Atlantic Coastal Plain of North and South Carolina. U.S. Geological Survey Professional Paper 1773.
- Chapelle, F.H. and D.R. Lovley. 1992. Competitive exclusion of sulfate reduction by Fe (III)-reducing bacteria: a mechanism for producing discrete zones of high-iron ground water. *Ground Water* 30 (1): 29 – 36.

- Chapelle, F.H. 2001. *Ground-water Microbiology and Geochemistry*, Second Edition, New York: John Wiley & Sons.
- Clark, P.U., A.S. Dyke, J.D. Shakun, A.E. Carlson, J. Clark, B. Wohlfarth, J.X. Mitrovica, S.W. Hostetler, and A.M. McCabe. 2009. The last glacial maximum. *Science* 325 (5941): 710 – 714.
- Clarke, E.T., R.H. Loeppert, and J.M. Ehrman. 1985. Crystallization of iron oxides on calcite surfaces in static systems. *Clays and Clay Minerals* 33 (2): 152 – 158.
- Consolvo, C.A. 1998. Hydrogeologic investigation and wellhead protection planning for the Castle Hayne Aquifer near Washington, North Carolina: Unpublished Master's Thesis, East Carolina University, Greenville, North Carolina.
- Cook, D.C., S.J. Oh, R. Balasubramanian, and M. Yamashita. 1999. The role of goethite in the formation of the protective corrosion layer on steels. *Hyperfine Interactions* 122 (1 – 2): 59 – 70.
- Cornell, R.M. and U. Schwertmann. 2003. *The Iron Oxides: Structure, Properties, Reactions, Occurrences and Uses*, Second Edition, Weinheim: Wiley-VCH.
- Curtis, C.D. 1976. Stability of minerals in surface weathering reactions: a general thermochemical approach. *Earth Surface Processes* 1 (1): 63 – 70.
- Daniels, R.B., G.H. Simonson, and R.L. Handy. 1961. Ferrous iron content and color of sediments. *Soil Science* 91 (6): 378 – 382.
- Dankers, N. and R. Laane. 1983. A comparison of wet oxidation and loss on ignition of organic material in suspended matter. *Environmental Technology* 4 (7): 283 – 290.
- DeWiest, R.J.M. 1969. Hydrologic relationship between the Pamlico River and the Castle Hayne Aquifer in eastern North Carolina. Preprint 830, Annual Meeting on Water Resources Engineering, February 1969. Reston, Virginia: American Society of Civil Engineers.
- Din, Z.B. 1992. Use of aluminum to normalize heavy-metal data from estuarine and coastal sediments of straits of Melaka. *Marine Pollution Bulletin* 24: 484 – 491.
- Dzombak, D.A. and F.M. Morel. 1990. *Surface Complexation Modeling: Hydrous Ferric Oxide*, First Edition, New York: John Wiley & Sons.
- Eggleston, J., and S. Rojstaczer. 2001. The value of grain-size hydraulic conductivity estimates: comparison with high resolution in-situ field hydraulic conductivity. *Geophysical Research Letters* 28 (22): 4255 – 4258.
- Faure, G. 1998. *Principles and Applications of Geochemistry: A Comprehensive Textbook for Geology Students*, Second Edition, Upper Saddle River, New Jersey: Prentice Hall.

- Fine, J.M. and E.L. Kuniandy. 2014. Simulation of groundwater flow and saltwater movement in the Onslow County Area, North Carolina: predevelopment–2010. U.S. Geological Survey Scientific Investigations Report 2013-5236.
- Freeze, R.A. and J.A. Cherry. 1979. Groundwater, First Edition, Upper Saddle River, New Jersey: Prentice Hall.
- Froelich, P.N., G.P. Klinkhammer, M.L. Bender, N.A. Luedtke, G.R. Heath, D. Cullen, P. Dauphin, D. Hammond, B. Hartman, and V. Maynard. 1979. Early oxidation of organic matter in pelagic sediments of the eastern equatorial Atlantic: suboxic diagenesis. *Geochimica et Cosmochimica Acta* 43 (7): 1075 – 1090.
- Fu, Y. 2014. Development and application of numerical modeling for evaluating and predicting hydrogeochemical processes temporally and spatially evolving in petroleum reservoirs: case studies; Miller Oilfield (UK North Sea) and Siri Oilfield (Danish North Sea): Unpublished Ph.D. Dissertation, Clausthal University of Technology, Clausthal-Zellerfeld, Germany.
- Gamus, W.J. 1972. Analysis of factors controlling groundwater flow for prediction of rates of groundwater movement and changing in quality, Atlantic Coastal Plain: Unpublished Ph.D. Thesis, University of Arizona, Tucson, Arizona.
- Garrels, R.M. and C.L. Christ. 1965. Solutions, Minerals, and Equilibria, First Edition, New York: Harper and Row.
- Giese, G.L., J.L. Eimers, and R.W. Coble. 1997. Simulation of ground-water flow in the Coastal Plain aquifer system of North Carolina: U.S. Geological Survey Open-File Report 1404-M.
- Giese, G.L., R.R. Mason, A.G. Strickland, and M.C. Bailey. 1987. North Carolina ground-water quality: U.S. Geological Survey Open-File Report 87-0743.
- Govindaraju, K. 1994. Compilation of working values and sample description for 383 geostandards. *Geostandards Newsletter* 18 (S1): 1 – 158.
- Hardy, D.H., M.R. Tucker, J.K. Messick, and C. Stokes. 2012. Understanding the soil test report. North Carolina Department of Agriculture and Consumer Services.
- Harvey, D.T. and R.W. Linton. 1981. Chemical characterization of hydrous ferric oxides by X-ray photoelectron spectroscopy. *Analytical Chemistry* 53 (11): 1684 – 1688.
- Hazen, A. 1892. Some Physical Properties of Sands and Gravels: with special reference to their use in filtration. Massachusetts State Board of Health, Annual Report, 539 – 556.
- Heath, R.C. 1983. Basic ground-water hydrology. U.S. Geological Survey Water Supply Paper 2220.



- Heiri, O., A.F. Lotter, and G. Lemcke. 2001. Loss on ignition as a method for estimating organic and carbonate content in sediments: reproducibility and comparability of results. *Journal of Paleolimnology* 25 (1): 101 – 110.
- Hem, J.D. and W.H. Cropper. 1960. Chemistry of iron in natural water. U.S. Geological Survey Water Supply Paper 1459.
- Herut, B and A. Sandler. 2006. Normalization methods for pollutants in marine sediments: review and recommendations for the Mediterranean. Israel Oceanographic and Liminological Research and Geological Survey of Israel IOLR Report H18.
- Ho, H.H, R. Swennen, V. Cappuyns, E. Vassilieva, and T. Van Tran. 2012. Necessity of normalization to aluminum to assess the contamination by heavy metals and arsenic in sediments near Haiphong Harbor, Vietnam. *Journal of Asian Earth Sciences* 56: 229 – 239.
- Holland, H.D., and Turekian, K.K. 2010. *Isotope Geochemistry: a derivative of the Treatise on Geochemistry, First Edition*, London: Academic Press, 757 p.
- Holtz, R.D., Kovacs, W.D., and Sheahan, T.C. 2011. *An introduction to geotechnical engineering, Second Edition*, Upper Saddle River, New Jersey: Prentice-Hall.
- Houben, G.J. 2003. Iron oxide incrustations in wells. Part 1: genesis, mineralogy and geochemistry. *Applied Geochemistry* 18 (6): 927 – 939.
- Hounslow, M.W. and B.A. Maher. 1999. Laboratory procedures for quantitative extraction and analysis of magnetic minerals from sediments. *Environmental Magnetism: A Practical Guide*. Quaternary Research Association, Cambridge: 139 – 184.
- Iiedgpeth, J.W. and H.S. Ladd. 1957. *Treatise on Marine Ecology and Paleoecology*. Geological Society of America 67: 1 – 1296
- Ionescu, D., C. Heim, L. Polerecky, V. Thiel, and D. De Beer. 2015. Biotic and abiotic oxidation and reduction of iron at circumneutral pH are inseparable processes under natural conditions. *Geomicrobiology Journal* 32 (3-4): 221 – 230.
- Jambor, J.L. and J.E. Dutrizac. 1998. Occurrence and constitution of natural and synthetic ferrihydrite, a widespread iron oxyhydroxide. *Chemical Reviews* 98 (7): 2549 – 2586.
- Johnson, C., and B. Beard. 2006. Fe isotopes: An emerging technique for understanding modern and ancient biogeochemical cycles. *GSA Today* 16: 4 – 10.
- Johnson, J., G. Anderson, and D. Parkhurst. 2000. Database ‘Thermo. Com. v8. r6. 230’.
- Johnson, J.J. 1992. Evaluation of potential recharge of the Castle Hayne Aquifer system by stream infiltration along Tranters Creek, Beaufort County, North Carolina: Unpublished Master’s Thesis, East Carolina University, Greenville, North Carolina.

- Karpov, I.K., Kiselev, A.I., and Letnikov, F.A. 1971. Chemical thermodynamics in petrology and geochemistry. Irkutsk, Akademia Nauka: 385 p.
- Kogel, J.E., N.C. Trivedi, J.M. Barger, and S.T. Krukowski. 2006. Industrial minerals and rocks: commodities, markets, and uses, Seventh Edition, Littleton, Colorado: Society for Mining, Metallurgy, and Exploration, Inc.
- Lautier, J.C. 2009. Hydrogeologic framework and ground water conditions in the North Carolina East Central Coastal Plain. North Carolina Department of Environment and Natural Resources.
- Li, X., T. Liu, F. Li, W. Zhang, S. Zhou, and Y. Li. 2012. Reduction of Fe (III) in oxyhydroxides by *Shewanella decolorationis* S12 and characterization of the surface properties of iron minerals. *Journal of Soils and Sediments* 12 (2): 217 – 227.
- Lin, C., E.I. Larsen, G.R. Larsen, M.E. Cox, and J.J. Smith. 2012. Bacterially mediated iron cycling and associated biogeochemical processes in a subtropical shallow coastal aquifer: Implications for Groundwater Quality. *Hydrobiologia* 696 (1): 63 – 76.
- Lindsay, W.L. 1979. *Chemical Equilibria in Soils*, First Edition, New York: John Wiley and Sons.
- Lloyd, O.B., Jr., and C.C. Daniel III. 1988. Hydrogeologic setting, water levels, and quality of water from supply wells at the U.S. Marine Corps Air Station, Cherry Point, North Carolina: U.S. Geological Survey Water-Resources Investigations Report 88-4034.
- Lopez, P., E. Navarro, R. Mace, J. Ordonez, L. Caputo, and J. Armengol. 2006. Elemental ratios in sediments as indicators of ecological processes in Spanish reservoirs. *Limnetica* 25(1-2): 499 – 512.
- Lovley, D.R. and S. Goodwin. 1988. Hydrogen concentrations as an indicator of the predominant terminal electron-accepting reactions in aquatic sediments. *Geochimica et Cosmochimica Acta* 52 (12): 2993 – 3003.
- Lyke, W.L. and M.W. Treece. 1988. Hydrogeology and effects of ground-water withdrawals in the Castle Hayne Aquifer in coastal North Carolina, in Lyke, W.L. and T. G. Hoban, eds., *Proceedings of the symposium on coastal water resources*, Wilmington, North Carolina: p. 469 – 478.
- McMahon, P.B. and F.H. Chapelle. 2008. Redox processes and water quality of selected principal aquifer systems. *Ground Water* 46 (2): 259 – 271.
- Mehlhop, D.L.T., T.L. Woods, and D.W. Neal. 2005. Lithology and mineral chemistry of the Castle Hayne Limestone – An important Coastal Plain Aquifer in North Carolina. *Southeastern Geology* 43 (3): 113 – 135.

- Mehlich, A. 1984a. Photometric determination of humic matter in soils, a proposed method. *Communications in Soil Science & Plant Analysis* 15 (12): 1417 – 1422.
- Mehlich, A. 1984b. Mehlich 3 soil test extractant: a modification of Mehlich 2 extractant. *Communications in Soil Science & Plant Analysis* 15 (12): 1409 – 1416.
- Mehlich, A. and S.S. Bowling. 1975. Advances in soil test methods for copper by atomic absorption spectrophotometry. *Communications in Soil Science & Plant Analysis* 6 (2): 113 – 128.
- Melton, E.D., E.D. Swanner, S. Behrens, C. Schmidt, and A. Kappler. 2014. The interplay of microbially mediated and abiotic reactions in the biogeochemical Fe cycle. *Nature Reviews Microbiology* 12 (12): 797 – 808.
- Montes-Hernandez, G., P. Beck, F.C.C.O. Renard, E. Quirico, B. Lanson, R. Chiriac, and N. Findling. 2011. Fast precipitation of acicular goethite from ferric hydroxide gel under moderate temperature (30 and 70 C). *Crystal Growth & Design* 11 (6): 2264 – 2272.
- Moses, C.O. and J.S. Herman. 1991. Pyrite oxidation at circumneutral pH. *Geochimica et Cosmochimica Acta* 55 (2): 471 – 482.
- Murphy, W.M. and H.C. Helgeson. 1987. Thermodynamic and kinetic constraints on reaction rates among minerals and aqueous Solutions. III. Activated complexes and the pH-dependence of the rates of feldspar, pyroxene, wollastonite, and olivine hydrolysis. *Geochimica et Cosmochimica Acta* 51 (12): 3137 – 3153.
- Nealson, K.H. and D. Saffarini. 1994. Iron and manganese in anaerobic respiration: environmental significance, physiology, and regulation. *Annual Reviews in Microbiology* 48 (1): 311 – 343.
- Nehls, G.J. and G.G. Akland. 1973. Procedures for handling aerometric data. *Journal of the Air Pollution Control Association* 23 (3): 180 – 184.
- North Carolina Department of Environment and Natural Resources (NCDENR). 2008. Permit holders in the Central Coastal Plain Capacity Use Area, retrieved 2/16/2015 from [http://www.ncwater.org/Permits\\_and\\_Registration/Capacity\\_Use/Central\\_Coastal\\_Plain/ccpcualist.php](http://www.ncwater.org/Permits_and_Registration/Capacity_Use/Central_Coastal_Plain/ccpcualist.php).
- Oelkers, E.H., Helgeson, H.C., Shock, E.L., Sverjensky, D.A., Johnson, J.W., and Pokrovskii, V. A. 1995. Summary of the apparent standard partial molal Gibbs free energies of formation of aqueous species, minerals, and gases at pressures 1 to 5000 bars and temperatures 25 to 1000 C. *Journal of Physical and Chemical Reference Data* 24 (4): 1401 – 1560.
- Otte, L.J. 1986. Regional perspective on the Castle Hayne Limestone, in D. A. Textoris, ed. *SEPM Field Guide books: Southeastern United States Third Annual Mid-Year Meeting* 1986: 270 – 276.

- Oxford Instruments. 2006. INCA Energy Operator Manual. High Wycombe, United Kingdom: Oxford Instruments Analytical Ltd.
- Pabich, W.J., I. Valiela, and H.F. Hemond. 2001. Relationship between DOC concentration and vadose zone thickness and depth below water table in groundwater of Cape Code, U.S.A. *Biogeochemistry* 55 (3): 247 – 268.
- Park, J., R.A. Sanford, and C.M. Bethke. 2006. Geochemical and microbiological zonation of the Middendorf Aquifer, South Carolina. *Chemical Geology* 230 (1): 88 – 104.
- Parkhurst, D.L. 2015. Personal communication. U.S. Geological Survey, Denver, Colorado.
- Parkhurst, D.L. and C.A.J. Appelo. 1999. User's guide to PHREEQC (Version 2): A computer program for speciation, batch-reaction, one-dimensional transport, and inverse geochemical calculations: U.S. Geological Survey. Water Resources Investigations Report 99-4259.
- Penn, R.L., C. Zhu, H. Xu, and D.R. Veblen. 2001. Iron oxide coatings on sand grains from the Atlantic Coastal Plain: high-resolution transmission electron microscopy characterization. *Geology* 29 (9): 843 – 846.
- Penny, E., M. Lee, and C. Morton. 2003. Groundwater and microbial processes of Alabama coastal plain aquifers. *Water Resources Research* 39 (11): 1320 – 1337.
- Postma, D. and B.S. Brockenhuus-Schack. 1987. Diagenesis of iron in proglacial sand deposits of late-and post-Weichselian Age. *Journal of Sedimentary Research* 57 (6): 1040 – 1053.
- Rabenhorst, M.C., R.R. Bourgault, and B.R. James. 2008. Iron oxyhydroxide reduction in simulated wetland soils: effects of mineralogical composition of IRIS paints. *Soil Science Society of America Journal* 72 (6): 1838-1842.
- Reeburgh, W.S. 1983. Rates of biogeochemical processes in anoxic sediments. *Annual Review of Earth and Planetary Sciences* 11: 269 – 298.
- Reynolds, J.W. and R.K. Spruill. 1995. Ground-water flow simulation for management of a regulated aquifer system: a case study in the North Carolina coastal plain. *Ground Water* 33 (5): 741 – 748.
- Richardson, C.J. 2003. Pocosins: hydrologically isolated or integrated wetlands on the landscape? *Wetlands* 23 (3): 563 – 576.
- Ryan, J.N. and P.M. Gschwend. 1992. Effect of iron diagenesis on the transport of colloidal clay in an unconfined sand aquifer. *Geochimica et Cosmochimica Acta* 56 (4): 1507–1521.
- Santisteban, J.I., R. Mediavilla, E. Lopez-Pamo, C.J. Dabrio, M.B.R. Zapata, M.J.G. García, S. Castano, and P.E. Martínez-Alfaro. 2004. Loss on ignition: a qualitative or quantitative

- method for organic matter and carbonate mineral content in sediments? *Journal of Paleolimnology* 32 (3): 287– 299.
- Schoonen, M.A.A. 2004. Mechanisms of sedimentary pyrite formation. *Geological Society of America Special Paper* 379: 117 – 134.
- Sherwani, J.K. 1980. Public policy for the management of groundwater in the Coastal Plain of North Carolina: University of North Carolina Water Resources Research Institute, Report 129.
- Shock, E.L., D.C. Sassani, M. Willis, and D.A. Sverjensky. 1997. Inorganic species in geologic fluids: correlations among standard molal thermodynamic properties of aqueous ions and hydroxide complexes. *Geochimica et Cosmochimica Acta* 61 (5): 907 –950.
- Spruill, R.K. 2016. Personal communication. East Carolina University, Greenville, North Carolina.
- Spruill, T.B., J.L. Eimers, and A.E. Morey. 1997. Nitrate-nitrogen concentrations in shallow ground water of the coastal plain of the Albemarle-Pamlico Drainage Study Unit, North Carolina and Virginia. US Geological Survey Fact Sheet FS-241-96.
- Stucki, J.W., B.A. Goodman, and U. Schwertmann. 2012. *Iron in Soils and Clay minerals*, First Edition, Dordrecht, Netherlands: Springer Science & Business Media.
- Stumm, W. and J.J. Morgan. 1996. *Aquatic Chemistry: Chemical Equilibria and Rates in Natural Waters*, Third Edition, New York, New York: John Wiley & Sons, 1022 p.
- Sutherland, R.A. 1998. Loss-on-ignition estimates of organic matter and relationships to organic carbon in fluvial bed sediments. *Hydrobiologia* 389 (1 – 3): 153 – 167.
- Sutton, L.C. and T.L. Woods. 1995. Geochemistry of ground water from the Castle Hayne Aquifer in northeastern North Carolina. *Southeastern Geology* 35: 93 – 119.
- Thompson, G.R. and J. Hower. 1975. Mineralogy of glauconite. *Clays and Clay Minerals* 23 (4): 289 – 300.
- Trapp, H., Jr. and M.A. Horn. 1997. *Ground water atlas of the United States, Delaware, Maryland, New Jersey, North Carolina, Pennsylvania, Virginia, West Virginia*: U.S. Geological Survey. Hydrologic Investigations Atlas 730-L.
- U.S. Geological Survey (USGS). 2016. Water quality samples for North Carolina: USGS 0209173196 S1 Weather Station NR Lizzie, NC (MIMS), Greene County, North Carolina. U.S. Department of the Interior, retrieved 9/16/2016 from <http://nwis.waterdata.usgs.gov/nc/nwis/qwdata?>

- US Environmental Protection Agency (USEPA). 2012. 2012 Edition of the drinking water standards and health advisories. EPA Office of Water 822-S-12-001.
- Vance, D.B. 1994. Iron-the environmental impact of a universal element. *National 76 Environmental Journal*. 4 (3): 24 – 25.
- Van Hinsberg, V.J. and J.C. Schumacher. 2007. Using estimated thermodynamic properties to model accessory phases: the case of tourmaline. *Journal of Metamorphic Geology* 25 (7): 769 – 779.
- Van Loon, J.C. and R.R. Barefoot. 2013. *Analytical methods for geochemical exploration*, First Edition, London: Academic Press.
- Velbel, M.A. 1993. Formation of protective surface layers during silicate-mineral weathering under well-leached, oxidizing conditions. *American Mineralogist* 78: 405 – 405.
- Warner, D. 1993. Hydrogeologic study of the Castle Hayne Aquifer system in northern Beaufort County, North Carolina: verification of well field design: Unpublished Master's Thesis, East Carolina University, Greenville, North Carolina.
- Weast, R.C., M.J. Astle, and W.H. Beyer. 1986. *Handbook of Chemistry and Physics*, First Edition, Boca Raton, Florida: CRC Press.
- Whitley, K. 2003. Groundwater geochemistry of the Yorktown and Peedee aquifers in the North Carolina coastal plain: Unpublished Master's Thesis, East Carolina University, Greenville, North Carolina.
- Wiedemeier, T.H. 1999. *Natural attenuation of fuels and chlorinated solvents in the subsurface*, First Edition, New York: John Wiley & Sons.
- Wilder, H.B., T.M. Robison, and K.L. Lindskov. 1978. *Water resources of northeast North Carolina*: U.S. Geological Survey Water-Resources Investigations Report 77-81.
- Wilkin, R.T. and H.L. Barnes. 1996. Pyrite formation by reactions of iron monosulfides with dissolved inorganic and organic sulfur species. *Geochimica et Cosmochimica Acta* 60 (21): 4167 – 4179.
- Winner, M.D., Jr., and R.W. Coble. 1996. *Hydrogeologic framework of the North Carolina Coastal Plain*: U.S. Geological Survey Open-File Report 87-690.
- Woods, T.L., P.D. Fullagar, R.K. Spruill, and L.C. Sutton. 2000. Strontium isotopes and major elements as tracers of ground water evolution: example from the Upper Castle Hayne Aquifer of North Carolina. *Ground Water* 38 (5): 762 – 771.

Wuenschel, R., H. Unterfrauner, R. Peticzka, and F. Zehetner. 2015. A comparison of 14 soil phosphorus extraction methods applied to 50 agricultural soils from central Europe. *Plant Soil Environment* 61 (2): 86 – 96.

Zehnder, A.J.B. and W. Stumm. 1988. *Geochemistry and Biogeochemistry of Anaerobic Habitats*, in *Biology of Anaerobic Microorganisms*, New York: John Wiley & Sons.

## Appendix A: Core Subsample Data

### Appendix A1: TC14 Data

TC14 Core Section	Void Space (m)	Length Recovered (m)	Sample #	Lower Subsample Depth (m)	Upper Subsample Depth (m)	Mean Subsample depth (m)	Adjusted Subsample Depth (m)	Calculated Depth BLS (m)	Analysis Performed or Extra Sample?
TC14: 0-4'	0.45	0.71	1	0.45	0.47	0.46	0.01	0.02	Extra
			2	0.47	0.49	0.48	0.03	0.05	Extra
			3	0.49	0.51	0.50	0.05	0.09	Extra
			4	0.51	0.53	0.52	0.07	0.12	Extra
			5	0.53	0.55	0.54	0.09	0.15	Grain Size
			6	0.55	0.57	0.56	0.11	0.19	Extra
			7	0.57	0.59	0.58	0.13	0.22	Extra
			8	0.59	0.61	0.60	0.15	0.26	Extra
			9	0.61	0.64	0.63	0.18	0.30	XRF
			10	0.64	0.67	0.66	0.21	0.35	Grain Size
			11	0.67	0.70	0.69	0.24	0.40	Extra
			12	0.70	0.73	0.72	0.27	0.46	Extra
			13	0.73	0.76	0.75	0.30	0.51	Extra
			14	0.76	0.79	0.78	0.33	0.56	Extra
			15	0.79	0.81	0.80	0.35	0.60	Grain Size
			16	0.81	0.83	0.82	0.37	0.64	Extra
			17	0.83	0.85	0.84	0.39	0.67	Extra
			18	0.85	0.87	0.86	0.41	0.70	Extra
			19	0.87	0.89	0.88	0.43	0.74	XRF
			20	0.89	0.91	0.90	0.45	0.77	Grain Size



TC14 Core Section	Void Space (m)	Length Recovered (m)	Sample #	Lower Subsample Depth (m)	Upper Subsample Depth (m)	Mean Subsample Depth (m)	Adjusted Subsample Depth (m)	Calculated Depth BLS (m)	Analysis Performed or Extra Sample?
TC14: 0-4'	0.45	0.71	21	0.91	0.93	0.92	0.47	0.81	Extra
			22	0.93	0.95	0.94	0.49	0.84	Extra
			23	0.95	0.97	0.96	0.51	0.88	LOI
			24	0.97	0.99	0.98	0.53	0.91	XRF
			25	0.99	1.01	1.00	0.55	0.94	Grain Size
			26	1.01	1.03	1.02	0.57	0.98	Extra
			27	1.03	1.05	1.04	0.59	1.01	Extra
			28	1.05	1.07	1.06	0.61	1.05	Extra
			29	1.07	1.09	1.08	0.63	1.08	XRF
			30	1.09	1.11	1.10	0.65	1.12	Grain Size
			31	1.11	1.13	1.12	0.67	1.15	Extra
			32	1.13	1.16	1.15	0.70	1.19	Extra
TC14: 4-8'	0.51	0.65	1	0.51	0.53	0.52	0.01	1.24	Extra
			2	0.53	0.55	0.54	0.03	1.28	XRF
			3	0.55	0.57	0.56	0.05	1.31	Grain Size
			4	0.57	0.59	0.58	0.07	1.35	Extra
			5	0.59	0.61	0.60	0.09	1.39	Extra
			6	0.61	0.63	0.62	0.11	1.43	Extra
			7	0.63	0.65	0.64	0.13	1.46	XRF
			8	0.65	0.67	0.66	0.15	1.50	Grain Size
			9	0.67	0.69	0.68	0.17	1.54	Extra
			10	0.69	0.71	0.70	0.19	1.58	Extra
			11	0.71	0.73	0.72	0.21	1.61	Extra
			12	0.73	0.75	0.74	0.23	1.65	XRF

TC14 Core Section	Void Space (m)	Length Recovered (m)	Sample #	Lower Subsample Depth (m)	Upper Subsample Depth (m)	Mean Subsample Depth (m)	Adjusted Subsample Depth (m)	Calculated Depth BLS (m)	Analysis Performed or Extra Sample?
TC14: 4-8'	0.51	0.65	13	0.75	0.77	0.76	0.25	1.69	Grain Size
			14	0.77	0.79	0.78	0.27	1.73	Extra
			15	0.79	0.81	0.80	0.29	1.76	Extra
			16	0.81	0.83	0.82	0.31	1.80	LOI
			17	0.83	0.85	0.84	0.33	1.84	XRF
			18	0.85	0.87	0.86	0.35	1.88	Grain Size
			19	0.87	0.89	0.88	0.37	1.91	Extra
			20	0.89	0.91	0.90	0.39	1.95	Extra
			21	0.91	0.93	0.92	0.41	1.99	Extra
			22	0.93	0.95	0.94	0.43	2.03	Extra
			23	0.95	0.97	0.96	0.45	2.06	Grain Size
			24	0.97	0.99	0.98	0.47	2.10	Extra
			25	0.99	1.01	1.00	0.49	2.14	Extra
			26	1.01	1.03	1.02	0.51	2.18	Extra
			27	1.03	1.05	1.04	0.53	2.21	XRF
			28	1.05	1.07	1.06	0.55	2.25	Grain Size
29	1.07	1.09	1.08	0.57	2.29	Extra			
30	1.09	1.11	1.10	0.59	2.33	Extra			
31	1.11	1.13	1.12	0.61	2.36	XRF			
32	1.13	1.15	1.14	0.63	2.40	Extra			
TC14: 8-12'	0.62	0.54	1	0.62	0.65	0.64	0.02	2.47	Extra
			2	0.65	0.68	0.67	0.05	2.54	Extra
			3	0.68	0.71	0.70	0.08	2.61	XRF

TC14 Core Section	Void Space (m)	Length Recovered (m)	Sample #	Lower Subsample Depth (m)	Upper Subsample Depth (m)	Mean Subsample Depth (m)	Adjusted Subsample Depth (m)	Calculated Depth BLS (m)	Analysis Performed or Extra Sample?			
TC14: 8-12'	0.62	0.54	4	0.71	0.74	0.73	0.11	2.68	Grain Size			
			5	0.74	0.77	0.76	0.14	2.74	Extra			
			6	0.77	0.80	0.79	0.17	2.81	Extra			
			7	0.80	0.83	0.82	0.20	2.88	Extra			
			8	0.83	0.86	0.85	0.23	2.95	XRF			
			9	0.86	0.89	0.88	0.26	3.01	Grain Size			
			10	0.89	0.92	0.91	0.29	3.08	Extra			
			11	0.92	0.95	0.94	0.32	3.15	Extra			
			12	0.95	0.98	0.97	0.35	3.22	Extra			
			13	0.98	1.01	1.00	0.38	3.29	XRF			
			14	1.01	1.04	1.03	0.41	3.35	Grain Size			
			15	1.04	1.07	1.06	0.44	3.42	Extra			
			16	1.07	1.10	1.09	0.47	3.49	Extra			
			17	1.10	1.13	1.12	0.50	3.56	XRF			
			18	1.13	1.16	1.15	0.53	3.62	LOI			
			TC14: 12-16'	0.35	0.81	1	0.35	0.38	0.37	0.02	3.68	Extra
						2	0.38	0.41	0.40	0.05	3.73	Extra
						3	0.41	0.44	0.43	0.08	3.77	Extra
4	0.44	0.47				0.46	0.11	3.82	Grain Size			
5	0.47	0.50				0.49	0.14	3.86	Extra			
6	0.50	0.53				0.52	0.17	3.91	Extra			
7	0.53	0.56				0.55	0.20	3.95	LOI			
8	0.56	0.58				0.57	0.22	3.99	Grain Size			

TC14 Core Section	Void Space (m)	Length Recovered (m)	Sample #	Lower Subsample Depth (m)	Upper Subsample Depth (m)	Mean Subsample Depth (m)	Adjusted Subsample Depth (m)	Calculated Depth BLS (m)	Analysis Performed or Extra Sample?
TC14: 12-16'	0.35	0.81	9	0.58	0.61	0.60	0.25	4.03	XRF
			10	0.61	0.63	0.62	0.27	4.06	LOI
			11	0.63	0.65	0.64	0.29	4.09	XRF
			12	0.65	0.67	0.66	0.31	4.12	Grain Size
			13	0.67	0.69	0.68	0.33	4.15	Extra
			14	0.69	0.71	0.70	0.35	4.18	Extra
			15	0.71	0.73	0.72	0.37	4.21	LOI
			16	0.73	0.75	0.74	0.39	4.24	XRF
			17	0.75	0.77	0.76	0.41	4.27	Grain Size
			18	0.77	0.79	0.78	0.43	4.30	Extra
			19	0.79	0.81	0.80	0.45	4.33	Extra
			20	0.81	0.83	0.82	0.47	4.37	Extra
			21	0.83	0.85	0.84	0.49	4.40	XRF
			22	0.85	0.87	0.86	0.51	4.43	Grain Size
			23	0.87	0.89	0.88	0.53	4.46	Extra
			24	0.89	0.91	0.90	0.55	4.49	Extra
			25	0.91	0.93	0.92	0.57	4.52	Extra
			26	0.93	0.95	0.94	0.59	4.55	XRF
			27	0.95	0.97	0.96	0.61	4.58	Grain Size
			28	0.97	0.99	0.98	0.63	4.61	Extra
			29	0.99	1.01	1.00	0.65	4.64	Extra
			30	1.01	1.03	1.02	0.67	4.67	Extra
			31	1.03	1.05	1.04	0.69	4.70	XRF

TC14 Core Section	Void Space (m)	Length Recovered (m)	Sample #	Lower Subsample Depth (m)	Upper Subsample Depth (m)	Mean Subsample Depth (m)	Adjusted Subsample Depth (m)	Calculated Depth BLS (m)	Analysis Performed or Extra Sample?
TC14: 12-16'	0.35	0.81	32	1.05	1.07	1.06	0.71	4.73	Grain Size
			33	1.07	1.09	1.08	0.73	4.76	Extra
			34	1.09	1.11	1.10	0.75	4.79	LOI
			35	1.11	1.13	1.12	0.77	4.82	XRF
			36	1.13	1.16	1.15	0.80	4.85	Grain Size
TC14: 16-20'	0.3	0.86	1	0.30	0.32	0.31	0.01	4.89	LOI
			2	0.32	0.34	0.33	0.03	4.92	XRF
			3	0.34	0.36	0.35	0.05	4.95	Grain Size
			4	0.36	0.38	0.37	0.07	4.98	Extra
			5	0.38	0.40	0.39	0.09	5.00	Extra
			6	0.40	0.42	0.41	0.11	5.03	Extra
			7	0.42	0.44	0.43	0.13	5.06	XRF
			8	0.44	0.46	0.45	0.15	5.09	Grain Size
			9	0.46	0.48	0.47	0.17	5.12	Extra
			10	0.48	0.50	0.49	0.19	5.15	Extra
			11	0.50	0.52	0.51	0.21	5.17	LOI
			12	0.52	0.54	0.53	0.23	5.20	XRF
			13	0.54	0.56	0.55	0.25	5.23	Grain Size
14	0.56	0.58	0.57	0.27	5.26	Extra			
15	0.58	0.60	0.59	0.29	5.29	Extra			
16	0.60	0.62	0.61	0.31	5.32	LOI			
17	0.62	0.64	0.63	0.33	5.34	XRF			
18	0.64	0.66	0.65	0.35	5.37	Grain Size			

TC14 Core Section	Void Space (m)	Length Recovered (m)	Sample #	Lower Subsample Depth (m)	Upper Subsample Depth (m)	Mean Subsample Depth (m)	Adjusted Subsample Depth (m)	Calculated Depth BLS (m)	Analysis Performed or Extra Sample?
TC14: 16-20'	0.3	0.86	19	0.66	0.68	0.67	0.37	5.40	Extra
			20	0.68	0.70	0.69	0.39	5.43	Extra
			21	0.70	0.72	0.71	0.41	5.46	Extra
			22	0.72	0.74	0.73	0.43	5.49	Extra
			23	0.74	0.76	0.75	0.45	5.51	Grain Size
			24	0.76	0.78	0.77	0.47	5.54	Extra
			25	0.78	0.80	0.79	0.49	5.57	Extra
			26	0.80	0.82	0.81	0.51	5.60	Extra
			27	0.82	0.84	0.83	0.53	5.63	XRF
			28	0.84	0.86	0.85	0.55	5.66	Grain Size
			29	0.86	0.88	0.87	0.57	5.68	Extra
			30	0.88	0.90	0.89	0.59	5.71	Extra
			31	0.90	0.92	0.91	0.61	5.74	Extra
			32	0.92	0.94	0.93	0.63	5.77	XRF
			33	0.94	0.96	0.95	0.65	5.80	Grain Size
			34	0.96	0.98	0.97	0.67	5.83	Extra
			35	0.98	1.00	0.99	0.69	5.85	Extra
			36	1.00	1.02	1.01	0.71	5.88	Extra
			37	1.02	1.04	1.03	0.73	5.91	XRF
			38	1.04	1.06	1.05	0.75	5.94	Grain Size
			39	1.06	1.08	1.07	0.77	5.97	Extra
40	1.08	1.10	1.09	0.79	6.00	Extra			
41	1.10	1.12	1.11	0.81	6.03	Extra			

TC14 Core Section	Void Space (m)	Length Recovered (m)	Sample #	Lower Subsample Depth (m)	Upper Subsample Depth (m)	Mean Subsample Depth (m)	Adjusted Subsample Depth (m)	Calculated Depth BLS (m)	Analysis Performed or Extra Sample?
TC14: 16-20'	0.3	0.86	42	1.12	1.14	1.13	0.83	6.05	XRF
			43	1.14	1.16	1.15	0.85	6.08	Grain Size
TC14: 20-24'	0.13	1.03	1	0.13	0.15	0.14	0.01	6.11	LOI
			2	0.15	0.17	0.16	0.03	6.13	XRF
			3	0.17	0.19	0.18	0.05	6.16	Grain Size
			4	0.19	0.21	0.20	0.07	6.18	TC14C #15
			5	0.21	0.23	0.22	0.09	6.20	TC14C #15
			6	0.23	0.25	0.24	0.11	6.23	TC14C #15
			7	0.25	0.27	0.26	0.13	6.25	XRF and TC14C #15
			8	0.27	0.29	0.28	0.15	6.27	Grain Size
			9	0.29	0.31	0.30	0.17	6.30	Extra
			10	0.31	0.33	0.32	0.19	6.32	Extra
			11	0.33	0.35	0.34	0.21	6.34	Extra
			12	0.35	0.37	0.36	0.23	6.37	Extra
			13	0.37	0.39	0.38	0.25	6.39	Grain Size
			14	0.39	0.41	0.40	0.27	6.42	Extra
			15	0.41	0.43	0.42	0.29	6.44	Extra
			16	0.47	0.51	0.49	0.36	6.52	Extra
			17	0.51	0.55	0.53	0.40	6.57	XRF
			18	0.55	0.59	0.57	0.44	6.62	Grain Size
			19	0.59	0.63	0.61	0.48	6.66	Extra
20	0.63	0.66	0.65	0.52	6.71	Extra			
21	0.66	0.93	0.80	0.67	6.88	Extra			

TC14 Core Section	Void Space (m)	Length Recovered (m)	Sample #	Lower Subsample Depth (m)	Upper Subsample Depth (m)	Mean Subsample Depth (m)	Adjusted Subsample Depth (m)	Calculated Depth BLS (m)	Analysis Performed or Extra Sample?
TC14: 20-24'	0.13	1.03	22	0.93	0.96	0.95	0.82	7.06	Extra
			23	0.96	0.98	0.97	0.84	7.09	XRF
			24	0.98	1.00	0.99	0.86	7.11	Grain Size
			25	4.00	1.02	2.51	2.38	8.91	Extra
			26	1.02	1.04	1.03	0.90	7.16	Extra
			27	1.04	1.06	1.05	0.92	7.18	LOI
			28	1.06	1.08	1.07	0.94	7.21	XRF
			29	1.08	1.10	1.09	0.96	7.23	Grain Size
			30	1.10	1.12	1.11	0.98	7.26	Extra
			31	1.12	1.14	1.13	1.00	7.28	Extra
			32	1.14	1.16	1.15	1.02	7.30	XRF
TC14: 24-28'	0.04	1.12	1	0.04	0.06	0.05	0.01	7.33	Extra
			2	0.06	0.08	0.07	0.03	7.35	XRF
			3	0.08	0.10	0.09	0.05	7.37	Grain Size
			4	0.10	0.12	0.11	0.07	7.39	Extra
			5	0.12	0.14	0.13	0.09	7.41	Extra
			6	0.14	0.16	0.15	0.11	7.43	Extra
			7	0.16	0.18	0.17	0.13	7.46	XRF
			8	0.18	0.20	0.19	0.15	7.48	Grain Size
			9	0.20	0.22	0.21	0.17	7.50	Extra
			10	0.22	0.24	0.23	0.19	7.52	Extra
			11	0.24	0.26	0.25	0.21	7.54	Extra
			12	0.26	0.28	0.27	0.23	7.57	Extra



TC14 Core Section	Void Space (m)	Length Recovered (m)	Sample #	Lower Subsample Depth (m)	Upper Subsample Depth (m)	Mean Subsample Depth (m)	Adjusted Subsample Depth (m)	Calculated Depth BLS (m)	Analysis Performed or Extra Sample?
TC14: 24-28'	0.04	1.12	13	0.28	0.30	0.29	0.25	7.59	Grain Size
			14	0.30	0.32	0.31	0.27	7.61	Extra
			15	0.32	0.34	0.33	0.29	7.63	Extra
			16	0.34	0.36	0.35	0.31	7.65	Extra
			17	0.36	0.38	0.37	0.33	7.67	XRF
			18	0.38	0.40	0.39	0.35	7.70	Grain Size
			19	0.40	0.42	0.41	0.37	7.72	Extra
			20	0.42	0.44	0.43	0.39	7.74	Extra
			21	0.44	0.46	0.45	0.41	7.76	Extra
			22	0.46	0.48	0.47	0.43	7.78	XRF
			23	0.48	0.50	0.49	0.45	7.81	Grain Size
			24	0.50	0.52	0.51	0.47	7.83	Extra
			25	0.52	0.54	0.53	0.49	7.85	Extra
			26	0.54	0.56	0.55	0.51	7.87	Extra
			27	0.56	0.58	0.57	0.53	7.89	Extra
			28	0.58	0.60	0.59	0.55	7.91	Grain Size
			29	0.60	0.62	0.61	0.57	7.94	Extra
			30	0.62	0.64	0.63	0.59	7.96	Extra
			31	0.64	0.66	0.65	0.61	7.98	Extra
			32	0.66	0.68	0.67	0.63	8.00	XRF
			33	0.68	0.70	0.69	0.65	8.02	Grain Size
34	0.70	0.72	0.71	0.67	8.04	Extra			
35	0.72	0.74	0.73	0.69	8.07	Extra			

TC14 Core Section	Void Space (m)	Length Recovered (m)	Sample #	Lower Subsample Depth (m)	Upper Subsample Depth (m)	Mean Subsample Depth (m)	Adjusted Subsample Depth (m)	Calculated Depth BLS (m)	Analysis Performed or Extra Sample?
TC14: 24-28'	0.04	1.12	36	0.74	0.76	0.75	0.71	8.09	Extra
			37	0.76	0.78	0.77	0.73	8.11	XRF
			38	0.78	0.82	0.80	0.76	8.14	Grain Size
			39	0.82	0.86	0.84	0.80	8.19	Extra
			40	0.86	0.90	0.88	0.84	8.23	Extra
			41	0.90	0.94	0.92	0.88	8.27	LOI
			42	0.94	0.98	0.96	0.92	8.32	XRF
			43	0.98	1.02	1.00	0.96	8.36	Grain Size
			44	1.02	1.06	1.04	1.00	8.40	Extra
			45	1.06	1.10	1.08	1.04	8.45	Extra
			46	1.10	1.14	1.12	1.08	8.49	XRF
47	1.14	1.16	1.15	1.11	8.52	LOI			
TC14: 28-32'	0.22	0.94	1	0.22	0.26	0.24	0.02	8.56	Extra
			2	0.26	0.30	0.28	0.06	8.61	XRF
			3	0.30	0.34	0.32	0.10	8.66	Grain Size
			4	0.34	0.38	0.36	0.14	8.72	Extra
			5	0.38	0.42	0.40	0.18	8.77	Extra
			6	0.42	0.46	0.44	0.22	8.82	LOI
			7	0.46	0.50	0.48	0.26	8.87	XRF
			8	0.50	0.54	0.52	0.30	8.92	Grain Size
			9	0.54	0.58	0.56	0.34	8.98	Extra
			10	0.58	0.62	0.60	0.38	9.03	Extra
			11	0.62	0.66	0.64	0.42	9.08	LOI

TC14 Core Section	Void Space (m)	Length Recovered (m)	Sample #	Lower Subsample Depth (m)	Upper Subsample Depth (m)	Mean Subsample Depth (m)	Adjusted Subsample Depth (m)	Calculated Depth BLS (m)	Analysis Performed or Extra Sample?
TC14: 28-32'	0.22	0.94	12	0.66	0.70	0.68	0.46	9.13	XRF
			13	0.70	0.74	0.72	0.50	9.18	Grain Size
			14	0.74	0.78	0.76	0.54	9.23	Extra
			15	0.78	0.82	0.80	0.58	9.29	Extra
			16	0.82	0.86	0.84	0.62	9.34	Extra
			17	0.86	0.90	0.88	0.66	9.39	XRF
			18	0.90	0.94	0.92	0.70	9.44	Grain Size
			19	0.94	0.98	0.96	0.74	9.49	Extra
			20	0.98	1.02	1.00	0.78	9.55	Extra
			21	1.02	1.06	1.04	0.82	9.60	Extra
			22	1.06	1.10	1.08	0.86	9.65	XRF
			23	1.10	1.14	1.12	0.90	9.70	Grain Size
			24	1.14	1.18	1.16	0.94	9.75	Extra
TC14: 32-36'	0.07	1.09	1	0.07	0.10	0.09	0.02	9.77	Extra
			2	0.10	0.13	0.12	0.05	9.80	XRF
			3	0.13	0.16	0.15	0.08	9.84	Grain Size
			4	0.16	0.19	0.18	0.11	9.87	Extra
			5	0.19	0.21	0.20	0.13	9.90	Extra
			6	0.21	0.24	0.23	0.16	9.93	LOI
			7	0.24	0.27	0.26	0.19	9.96	XRF
			8	0.27	0.30	0.29	0.22	9.99	Grain Size
			9	0.30	0.33	0.32	0.25	10.03	Extra
			10	0.33	0.36	0.35	0.28	10.06	Extra

TC14 Core Section	Void Space (m)	Length Recovered (m)	Sample #	Lower Subsample Depth (m)	Upper Subsample Depth (m)	Mean Subsample Depth (m)	Adjusted Subsample Depth (m)	Calculated Depth BLS (m)	Analysis Performed or Extra Sample?
TC14: 32-36'	0.07	1.09	11	0.36	0.39	0.38	0.31	10.09	Extra
			12	0.39	0.42	0.41	0.34	10.13	XRF
			13	0.42	0.45	0.44	0.37	10.16	Grain Size
			14	0.45	0.48	0.47	0.40	10.20	Extra
			15	0.48	0.51	0.50	0.43	10.23	Extra
			16	0.51	0.54	0.53	0.46	10.26	LOI
			17	0.54	0.57	0.56	0.49	10.30	XRF
			18	0.57	0.60	0.59	0.52	10.33	Grain Size
			19	0.60	0.64	0.62	0.55	10.37	Extra
			20	0.64	0.68	0.66	0.59	10.41	Extra
			21	0.68	0.72	0.70	0.63	10.46	Extra
			22	0.72	0.76	0.74	0.67	10.50	Extra
			23	0.76	0.80	0.78	0.71	10.55	Grain Size
			24	0.80	0.84	0.82	0.75	10.59	Extra
			25	0.84	0.88	0.86	0.79	10.64	Extra
			26	0.88	0.92	0.90	0.83	10.68	Extra
			27	0.92	0.96	0.94	0.87	10.73	XRF
			28	0.96	1.00	0.98	0.91	10.77	Grain Size
			29	1.00	1.04	1.02	0.95	10.82	Extra
			30	1.04	1.08	1.06	0.99	10.86	XRF
			31	1.08	1.12	1.10	1.03	10.91	Grain Size
32	1.12	1.16	1.14	1.07	10.95	LOI			

**Appendix A2: TC14C Data**

TC14C Core Section	Void Space (m)	Length Recovered (m)	Sample #	Lower Subsample Depth (m)	Upper Subsample Depth (m)	Mean Subsample Depth (m)	Adjusted Subsample Depth (m)	Calculated Depth BLS (m)	Extra Sample?
TC14C: 0-4'	0.40	0.76	1	0.40	0.66	0.53	0.13	0.20	No
			2	0.66	0.91	0.78	0.38	0.61	Extra
			3	0.91	1.16	1.03	0.63	1.01	Extra
TC14C: 4-8'	0.60	0.56	4	0.70	0.83	0.77	0.06	1.36	Extra
			5	0.83	1.16	0.99	0.29	1.86	Extra
TC14C: 8-12'	0.60	0.56	6	0.60	0.88	0.74	0.14	2.74	Extra
			7	0.88	1.16	1.02	0.42	3.35	Extra
TC14C: 12-16'	0.29	0.87	8	0.29	0.51	0.40	0.11	3.81	Extra
			9	0.51	0.72	0.61	0.32	4.11	Extra
			10	0.72	0.94	0.83	0.54	4.41	Extra
			11	0.94	1.16	1.05	0.76	4.72	Extra
TC14C: 16-20'	0.36	0.81	12	0.36	0.61	0.48	0.13	5.07	Extra
			13	0.61	0.88	0.74	0.39	5.47	Extra
			14	0.88	1.16	1.02	0.67	5.89	Extra
TC14C: 20-24'	0.12	1.05	15	0.12	0.37	0.24	0.13	6.24	No
			16	0.37	0.62	0.49	0.38	6.53	Extra
			17	0.62	0.87	0.74	0.63	6.83	Extra
			18	0.87	1.16	1.01	0.90	7.14	Extra
TC14C: 24-28'	0.17	0.99	19	0.17	0.42	0.29	0.12	7.47	Extra
			20	0.42	0.66	0.54	0.37	7.77	Extra
			21	0.66	0.91	0.78	0.61	8.07	Extra
			22	0.91	1.16	1.03	0.86	8.38	Extra

TC14C Core Section	Void Space (m)	Length Recovered (m)	Sample #	Lower Subsample Depth (m)	Upper Subsample Depth (m)	Mean Subsample Depth (m)	Adjusted Subsample Depth (m)	Calculated Depth BLS (m)	Extra Sample?
TC14C: 28-32'	0.47	0.69	23	0.47	0.70	0.58	0.11	8.74	Extra
			24	0.70	0.93	0.81	0.34	9.14	Extra
			25	0.93	1.16	1.04	0.57	9.55	Extra
TC14C: 32-36'	0.09	1.07	26	0.09	0.26	0.17	0.08	9.85	Extra
			27	0.26	0.62	0.44	0.35	10.15	Extra
			28	0.62	0.89	0.76	0.67	10.51	Extra
			29	0.89	1.16	1.02	0.93	10.82	Extra

## **Appendix B: Descriptions of Analytical Procedures**

### **Appendix B1: Grain-Size Analysis of Sediment Samples**

1. Immediately after subsampling, place wet subsample on pre-weight, plastic weight boat.
2. Weigh the subsample and determine the initial wet weight of the subsample by subtracting the weight of the weigh boat.
3. Record the data and all relevant notes in laboratory notebook.
4. Repeat Steps 1 – 3 for the subsamples for today's batch.
5. Place weighed subsamples in a laboratory oven to dry at 40°C for at least 24 hours.
6. Weigh the subsamples again and record the new weight.
7. Place the subsamples in the laboratory oven to at 40°C for another 12 hours.
8. Weigh the subsamples again and record the new weight.
9. If the new weight is lower than the weight recorded in step 6, repeat steps 7 and 8 until no further weight loss occurs between weighing and drying cycles.
10. Once the subsamples are completely dry and the final dry weights are recorded, calculate the amount of moisture lost by subtracting the initial wet weights by the final dry weights.
11. Soak the sediment samples overnight in a 5% sodium hexametaphosphate (Calgon) solution to deflocculate mud particles.
12. Place a clean, stainless-steel 4  $\Phi$  sieve over a clean glass beaker and wash with ultrapure water to remove the mud portion from each sediment sample.
13. Carefully pour the sand and gravel-sized portion from the sieve into a pre-weighed plastic weigh boat. Using a clean plastic squirt bottle, rinse the sieve with ultrapure water to ensure that all of the sediment is transferred to the weigh boat.
14. Carefully pour the mud portion from the glass beaker into a pre-weighed plastic weigh boat. Using a clean plastic squirt bottle, rinse the glass beaker with ultrapure water to ensure that all of the mud is transferred to the weigh boat.
15. Repeat the drying procedure that is explained in steps 4 – 8.
16. Once the subsamples are completely dry and the final dry weights are recorded, calculate the amount of mud lost by subtracting the final dry weight from the initial dry weight. Seal the mud portion in a plastic bag and store for later use, if needed.
17. Prepare clean sieves for RoTap analysis. Sieves should consist of  $\frac{1}{2}$   $\Phi$  intervals, beginning with -2  $\Phi$  on the top of the stack and 4  $\Phi$  at the bottom of the stack, with a collection pan placed below the 4  $\Phi$  sieve to collect mud-sized grains.
18. Carefully pour the dried mud and sand-sized samples into the -2  $\Phi$  sieve and close the nest of sieves with the lid.
19. Place the nest of sieves into the RoTap machine and run the machine for 15 minutes.
20. Remove the nest of sieves from the RoTap machine, carefully remove each sieve, and transfer the sediment from each sieve to individual, pre-weighed weigh boats.

21. Record the weight for each size fraction and seal in a plastic bag in case it is needed in the future.
22. After all of the grain-size data are recorded, input the grain size data into GRADISTAT 4.0 (Blott and Pye, 2001) to calculate grain-size statistics



## Appendix B2: XRF Pellet Preparation

### I. Sample Disintegration

- A. Wear laboratory gloves to avoid contamination.
- B. Use a ceramic mortar and pestle to grind at least 7 g of dried sediment sample to a fine powder (approximately 63  $\mu\text{m}$ ).
- C. Transfer ground sediment to the stainless steel chamber for the tungsten-carbide-ball mill using stainless steel spatula.
- D. Carefully place two tungsten balls into the chamber using tweezers. Do not allow the balls to drop to avoid spilling the sample.
- E. Place the lid on top of the chamber and hand tighten the lid to seal the chamber.
- F. Place the chamber into the ball mill shaker and tightly secure the chamber to ensure that the chamber does not slip out during agitation.
- G. Close the lid to the ball mill shaker and agitate the sample for ten minutes.
- H. Transfer the ground sample to a labeled sample bag and seal the bag to prevent contamination.
- I. Thoroughly wash all instruments and ball mill components with liquid dish detergent, pipette brushes, and tap water. Then, thoroughly rinse the materials with Ultrapure water.
- J. Make sure that all materials are completely dry before continuing to another sample.

### II. Pellet Preparation Procedure

- A. Wear laboratory gloves to avoid contamination.
- B. Place a clean plastic weigh boat onto a laboratory scale and tare the weight of the weigh boat.
- C. Precisely weigh  $6.0000 \text{ g} \pm 0.0010 \text{ g}$  of ground sediment sample.
- D. Use a stainless steel spatula and small paint brush to transfer the weighed sediment to a plastic mixing chamber. Try to transfer as much of the sample as possible from the weigh boat to the mixing chamber.
- E. Place another clean weigh boat onto a laboratory scale and tare the weight of the weigh boat.
- F. Precisely weigh  $1.2000 \text{ g} \pm 0.0010 \text{ g}$  of binder (PelletBlend Powder – PB100).
- G. Use a stainless steel spatula and small paint brush to transfer the weighed pellet binder to a plastic mixing chamber. Try to transfer as much of the binder as possible from the weigh boat to the mixing chamber.
- H. Carefully place 5 acrylic balls into the chamber using tweezers. Do not allow the balls to drop to avoid spilling the sample.
- I. Seal the lid to the mixing chamber.
- J. Clean the brush using an air compressor to blow air through the bristles.
- K. Place the mixing chamber into the ball mill shaker and tightly secure the chamber to ensure that the chamber does not slip out during agitation. Be careful not to over tighten because the plastic mixing chambers can crack.
- L. Close the lid to the ball mill shaker and agitate the sample for ten minutes to homogenize the samples.
- M. Place a stainless steel pellet into the cylindrical void of a stainless steel dicet.
- N. Use tweezers to center one sheet of pellet film on top of the stainless steel pellet.

- O. Use a clean stainless steel spatula and a small brush paint brush to carefully transfer the homogenized sediment and binder mixture (80% ground sediment and 20% binder) into the cylindrical void of the dicet.
- P. Level the top of the sediment and binder mixture using a stainless steel spatula.
- Q. Use tweezers to center one sheet of pellet film on top of the mixture.
- R. Place another stainless steel pellet on top of the pellet film and use a Kimwipe to remove any powder that may be clinging to the inner cylinder of the dicet.
- S. Slowly insert a stainless steel plunger on top of the stainless steel pellet and transfer the dicet to a hydraulic press.
- T. Form the pellet by pressing the mixture at 40 – 45 psi for at least four minutes using the hydraulic press.
- U. After at least four minutes has elapsed, slowly release the pressure by loosening the pressure release valve.
- V. Carefully, remove the pellet from the dicet and transfer the pellet into a plastic XRF pellet container.
- W. Store the container with the pellet into a desiccator to remove moisture.
- X. Thoroughly wash all instruments and components with liquid dish detergent, pipette brushes, and tap water. Then, thoroughly rinse the materials with Ultrapure water.
- Y. Clean the brush using an air compressor to blow air through the bristles.
- Z. Make sure that all materials are completely dry before continuing to another sample.

### Appendix B3: Loss on Ignition Analysis

(Modified from Bengtsson and Enell, 1986; Heiri et al., 2001)

1. Take a sediment sample and place its contents in a labeled weigh boat.
2. Place the samples, already in the weigh boats, into the drying oven at a temp of about 105°C and leave them there overnight to evaporate all of the water out of the samples.
3. After the samples have been dried, use a mortar and pestle to grind each sample up until there are no sediments clumping together.
4. Homogenize the dry sediment with a glass stir rod and place the samples into a desiccator to remove hygroscopic moisture.
5. Place the crucibles them on an oven pan and into the furnace at a temperature of 550°C for an hour to make sure that it is completely dry and free of contaminants that can interfere with later readings. Use tongs to move and manipulate crucibles both when hot (to prevent burns) and cold (to prevent contamination). Wear protective gloves and remove jewelry to prevent burns.
6. Cool the crucibles to room temperature in a desiccator
7. Weigh the dried, cooled, empty and labeled crucibles and record the weights to an accuracy of +/- 0.1 mg.
8. Transfer approximately 1.2 g of sample to the crucible and immediately record the weight of the sample and crucible. Record the weights as  $W_i$  (initial weight).
9. Place the sample-containing crucibles on an oven pan and place the oven pan. Then, place the oven pan into the furnace at a temperature of 550°C for four hours.
10. After the four hours have elapsed, leave the samples in the furnace to allow them to cool. Once the oven reaches 100°C, remove the samples from the furnace and place them into the desiccator to cool without gaining any moisture.
11. Once the crucibles with ignited samples have cooled to room temperature, weigh the samples and crucibles together. Record the weights as  $W_f$  (final weight).
12. Discard these samples once recording of this final weight is complete.
13. Use the following equation to calculate the percent Loss on Ignition (LOI) and record the data:

$$\% \text{ LOI} = [(W_i - W_f) \div W_i] \times 100\%$$

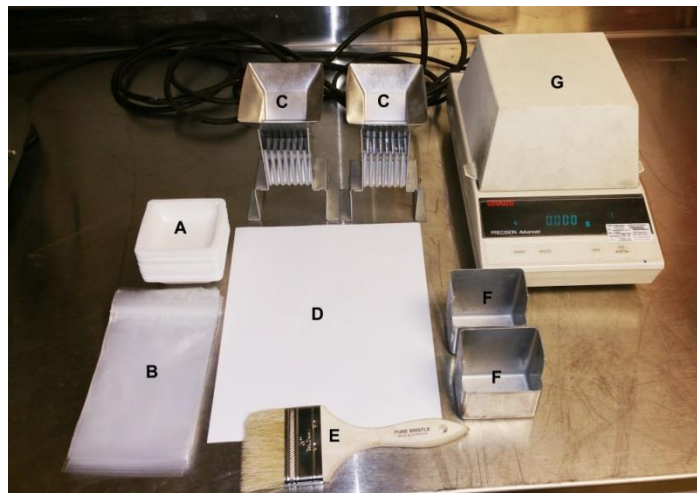
## Appendix B4: Magnetic Separation Procedure

### I. Grain-Size Separation

- A. Prepare clean, stainless-steel sieves for RoTap analysis. Sieves should consist of 1.25  $\Phi$ , 2.25  $\Phi$ , 3.25  $\Phi$ , 4  $\Phi$ , beginning with 1.25  $\Phi$  on the top of the stack and 4  $\Phi$  at the bottom of the stack, with a collection pan placed below the 4  $\Phi$  sieve to collect mud-sized grains.
- B. Carefully pour the sediment samples into the 1.25  $\Phi$  sieve and close the nest of sieves with the lid.
- C. Place the nest of sieves into the RoTap machine and run the machine for 15 minutes.
- D. Remove the nest of sieves from the RoTap machine, carefully remove each sieve, and transfer the sediment from each sieve to individual, pre-weighed weigh boats.
- E. Record the weight for each size fraction and seal in individual plastic bags.

### II. Magnetic Separation using Frantz Isodynamic Magnetic Separator

#### A. Materials Needed



**A** = Weigh Boats **B** = Sample Bags **C** = Sediment Splitters **D** = Printer Paper (or paper plates)  
**E** = Paint Brush **F** = Sample-Collection Pans **G** = Scale **H** Hand Magnet (not shown)

B. Components of the Frantz Isodynamic Separator



**A** = Chutes **B** = Sediment Funnel **C** = Slide Vibrator **D** = Side Slope Angle  
**E** = Side-Slope-Adjuster Wheel **F** = Amp Meter **G** = Slide-Vibrator-Adjustment Knob  
**H** = Slide-Vibrator-Power Switch



**E** = Side-Slope-Adjuster Wheel **I** = Hi/Low Power Switch  
**J** = Magnetic-Coil-Amperage-Adjuster Knob **K** = Power Switch for Magnetic Coil



Forward-Slope-Angle Adjustment Knob  
(Located in the back of the Frantz Magnetic Separator)



**A** = Nonmagnetic Sediment Chute **B** = Magnetic Sediment Chute

### C. Setup and Sample Preparation

1. Carefully pour  $>4 \Phi$  and  $<1.25 \Phi$  size fractions into a pre-weighed weigh boat. Note that mud and  $>1.25\Phi$  will not be magnetically separated to avoid clogging the separator.
2. Measure and record the total weight of each size fraction.

3. Use a hand magnet to remove highly magnetic minerals such as magnetite or pyrrhotite.
4. Place an empty weigh boat on the scale and use the tare function to eliminate the weight of the empty weigh boat. Then, add the hand magnet portion to the weigh boat.
5. Set the Side Slope Angle to  $\sim 20^\circ$  and the forward slope to  $\sim 25^\circ$ .
6. Place a sample-collection pan beneath the nonmagnetic and magnetic, respectively.
7. Arrange printer paper on top of the metal base of the separator as shown below to collect sediment that may spill during separations.



8. Turn on the Power Switch for the Magnetic Coil and make sure that the Hi/Low Power Switch is flipped in the upper position (These switches are located on the right hand side of the Frantz).
9. Rotate the black Magnetic Coil Amperage Adjuster Knob in a clockwise direction to set the separator to 0.2 amps.
10. Turn on the Slide Vibrator by flipping the switch (on the front of the Frantz) to the upper position and by rotating the Slide Vibrator Adjustment Knob in a clockwise direction.
11. Carefully pour the sediment sample into the Sediment Funnel until the funnel is no more than  $\frac{3}{4}$  full to avoid sample spillage.
12. Use the Slide-Vibrator-Adjustment Knob to find the setting that results in the most efficient flow of the material that does not result in obvious sample spillage (A few practice runs could be useful to improve technique).
13. After each grain size fraction has been separated using the 0.2 amp setting, slowly rotate the Magnetic-Coil-Amperage-Adjuster Knob in a counterclockwise direction until the Amperage reading is zero, turn off the Slide-Vibrator-Power Switch, and use the paint brush to clean the chutes.
14. Add sediment collected from the Magnetic Sediment Chute to the weigh boat (containing the portion that was attracted by the hand magnet), record the weight, and place into a labeled sample bag.
15. Repeat Steps 9 – 14 for 0.4 amps, 0.8 amps, 1.2 amps, and the maximum amperage setting to complete the magnetic separations for the sample.

**D. Clean Up between Samples**

1. Set the forward slope to  $90^\circ$  and the side slope to  $0^\circ$
2. Turn on the slide vibrator for ~30 seconds or until sediment stops coming out of the Frantz.
3. Reset the Side Slope Angle to  $\sim 20^\circ$  and the forward slope to  $\sim 25^\circ$  and continue with the separation procedure.



**Appendix B5: XRD Analysis**  
**(Procedure by Dr. Terri Woods, Department of Geological Sciences at East Carolina University)**

**I. Sample Preparation**

**A. Materials needed for preparation of basic powder sample**

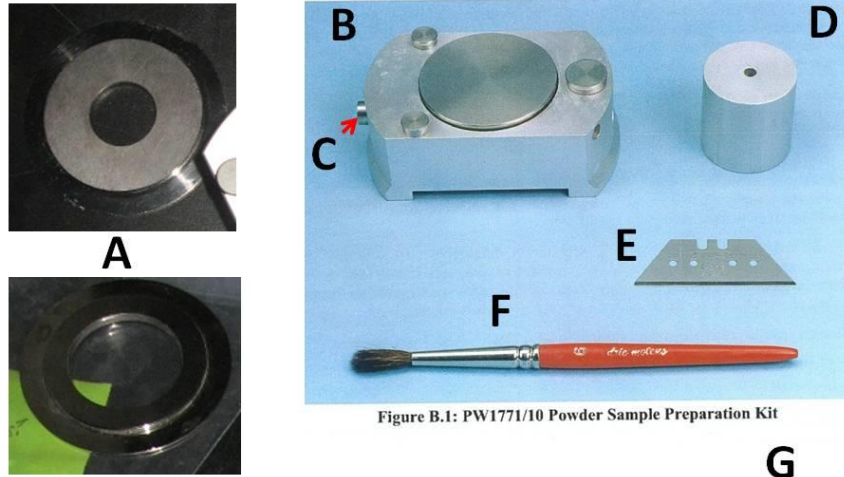
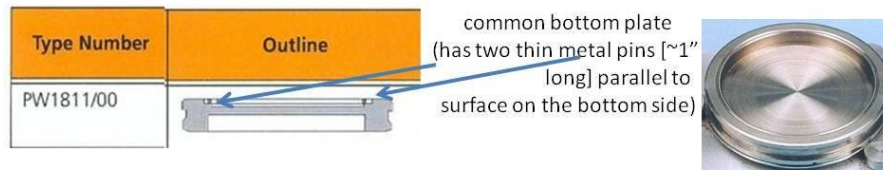


Figure B.1: PW1771/10 Powder Sample Preparation Kit



- B. Use the stainless steel ring that looks like a squashed top hat with a hole in the middle.
- C. Put it in the packing platform/sample prep mount with the “top” of the hat on the top side of the ring.
- D. Push the button on the side of the platform so the ring drops down.
- E. Clean all equipment before powdering your sample, which includes the mortar and pestle. Fill the ring with powdered sample.



Figure B.3: Spreading Powder in Sample Holder Ring

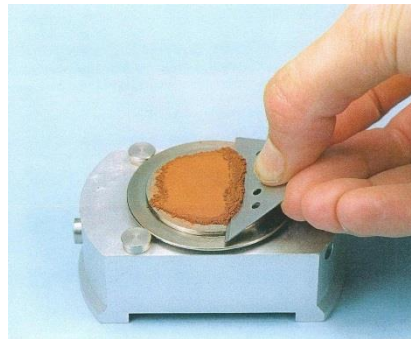
- F. Pack sample down with the stainless steel cylinder alternately turning and pressing.



Figure B.4: Pressing Powder with Powder Press Block

1. Be careful when lifting the table because the central solid ring can fall out and break things on the counter.

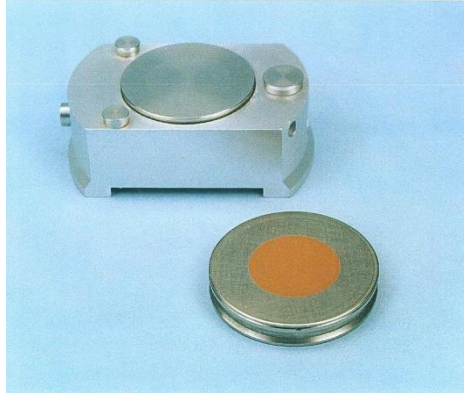
G. Clean and smooth top surface of packed sample with razor blade and clean off “brim” with brush



H. Clamp on the common bottom plate, making sure the pins are parallel to the sample prep table and click gently into place. If you push too sharply the sample will fall out.



I. Pick up the entire “two-ring” assembly and turn it over pressing the release button to free the prepared sample. It may help to tilt the table sideways at about  $45^{\circ}$  to keep sample from falling out of the ring.

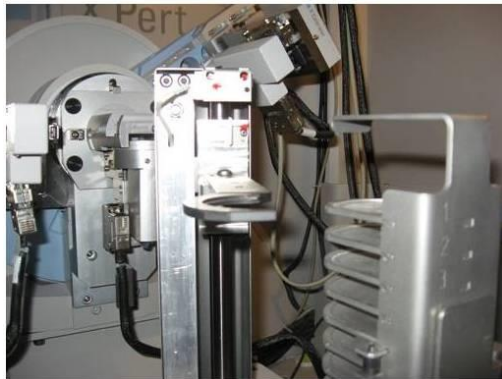


## II. Loading

A. Using both hands very slowly and carefully open instrument doors. Never open the door with the sample in your hand. Be very delicate with the leaded glass doors and move the doors independently and carefully so as to not make any clunking sounds. If the doors will not open, it is because the shutter is open.



B. Place sample holder in top slot of sample rack and close the doors.



## III. Entering computer program and setting machine parameters

**NO THUMB DRIVES ALLOWED UNLESS REFORMATTED!**

A. Wake up the computer by moving the mouse or pressing ENTER. (May take tens of seconds to wake up.)

1. Click on Jim Watson

B. Click on X'pert Data Collector which runs the instrument

C. Log in to computer using your assigned credentials

D. Choose Instrument from the upper toolbar

1. Choose Connect and a dialog box appears

a. Highlight ecu ecu 12/9/2008 15:01 user-1 then Hit OK

- b. Hit OK in the dialogue box that appears
  - c. You'll see the spinning sample changer and the message "Positioning the Instrument"
- 2. DoubleClick Instrument Settings
  - a. DoubleClick to set the current to 25 mA and tension to 40kV
  - b. Make sure Generator and Status are on by clicking to put a "√" in the Generator box
  - c. Hit OK or Apply then OK
- 3. Usually the program will automatically continue, but sometimes you may need to DoubleClick "There is no sample loaded"
  - a. In dialog box select "Load from magazine position 1" 1 is the top position
  - b. Hit OK, watch it move
- 1) You'll see the spinning sample loader icon on the computer screen and the message "Loading Sample"
- E. Machine may automatically load sample or you should
  - 1. DoubleClick "Movement not moving"
    - a. Under Movement choose spinning
    - b. Under Revolution time choose 16
    - c. Hit OK

#### IV. Running sample

- A. Choose Measure from the upper toolbar
  - 1. DoubleClick Program
  - 2. In the "Open Program" dialog box that appears, select Mauger's method "3-73 2 scans" and click OK.
    - a. Every  $10^\circ$  of  $2\theta$  take about 1 minute
    - b. If you want to change to another method to do slow scans of specific  $2\theta$  regions, go to File and New Program.
  - 3. Put in sample name & ID, and Prepared by info
    - a. MAKE SURE TO WRITE DOWN THE SCAN # AND MAKE IT PART OF THE SAMPLE ID
  - 4. Hit OK
- B. Machine will now run pattern and you'll hear a click when the X-rays come on and the doors lock.
- C. To expand to double screens, click the Restore button at the very top right corner then extend the right side of the program screen to fill the monitor so you get a good view of the evolving pattern.

#### V. Instrument Shutdown

- A. Close window showing finished pattern
  - 1. Program automatically saves your finished pattern
- B. Return to X'Pert Data Collector and set Current back to 15 mA and Tension back down to 30K. Hit OK
- C. Exit X'pert Data Collector by choosing File and Exit.
- D. In "Close Data Collector" dialogue box, choose (highlight) "Close control window and shut down the data collector" and hit OK.

## VI. Pattern Treatment

### A. DoubleClick X'Pert Highscore Plus

1. Choose File and select the "Mauger single scans".
2. Choose Open
3. DoubleClick on file name of sample just run
4. The completed pattern will appear on the screen, 2<sup>nd</sup> scan will be in a different color

### B. Choose Treatment from top toolbar

1. Choose Merge Scans
  - a. Choose Simple Sum (Avg)
2. In box hit Sum, then Replace. (Print the pattern if you want using the printer icon)
3. Go back to Treatment, Choose Determine Background
  - a. Hit Subtract in box, then Replace
  - b. Print the merged pattern if you want
4. Go back to Treatment, Choose Search Peaks
  - a. Choose Search peaks
  - b. Choose Accept
  - c. Vertical Dashed lines indicate peaks
  - d.  $K\alpha_{II}$  may mask a real peak & has lower energy than  $\alpha_{I}$ .  $K\alpha_{II}$  peaks kick in at  $35^\circ 2\theta$ . ( $\alpha_{I} / \alpha_{II} = 0.5$ ). As  $2\theta$  increases, the separation between  $\alpha_{I}$  and  $\alpha_{II}$  increases.  $K\beta$  is knocked out by Nickel filter. If there's a shoulder to the left of a peak, that's another peak, not a  $K\alpha$

### C. The sample pattern on the screen will now be modified by the addition of small "v" symbols and vertical dashes above each peak. On the right, facing page click on the Peak List to get the information on all these peaks.

1. Different color lines will appear on the pattern
  - a. Red equals the actual pattern you just ran
  - b. Blue equals the simulated  $K\alpha_{I}$  pattern for the identified mineral

### D. The dashes with "v" symbols indicate peaks which have not been associated with a mineral

### E. Clean up the pattern by removing anomalous peaks (ones that are just a slight high in the background) and adding lines for peaks not indicated by vertical lines.

1. Click on the pattern itself to stretch a box around peaks you wish to magnify and study.
  - a. Small, unknown peaks at high  $2\theta$  values may just be peaks from an already-identified mineral. Such high  $2\theta$  peaks may not have been on the XRD data card from which reference peaks for each mineral were loaded into the computer.
2. Make sure Peak List is on the screen to your right by clicking on Peak List on the right
3. To add peaks go to Treatment; then Insert Peak. Align the green line where you want to add the peak and click. Doubleclick outside the pattern to exit or go back to Treatment and re-click Insert Peak.
4. To delete a peak just put the mouse on the "v" symbol over the desired peak making sure it is the one highlighted in the Peak List.

a. Then hit the delete key.

5. After pulling up Peak List to delete peaks hit Pattern List to return to search results.

## VII. Pattern Analysis

A. Choose Analysis, then Search & Match, then Execute Search & Match

1. Hit Search in the dialog box

2. Hit OK

B. Dashes with “v” symbols indicate peaks which have not been associated with a mineral. On the right screen (facing page) scroll down the mineral list looking for likely minerals that could account for the unidentified peaks.

1. If you want details of one of these potential minerals in the bottom list just doubleclick on the mineral name. If it is a mineral you will be dealing with frequently, record the number of its Reference Pattern so you can find it easily the next time.

2. Drag potential minerals from the list up into the Peak List of identified minerals.

3. If the reference pattern stops early at say  $50^\circ 2\Theta$ , then it won't accept peaks above the limit of the reference pattern.

4. Bragg's Equation:  $n\lambda = 2d\sin\Theta$

a. increasing  $2\Theta =$  low d-spacing

C. You can also retrieve Reference Patterns to compare with your unknown.

1. Click Reference Pattern on top toolbar, choose Retrieve a pattern, and then choose Text Search

a. Type in the name of the mineral of interest and hit Load. These minerals will be added to your Peak List.

b. You can also choose Reference Code if you know the number for the mineral.

c. After retrieving patterns by reference code you can get a new view on the upper half of the left monitor by hitting “Analyze” under spectrum to see the pattern again.

D. Hit Analyze again and you'll see which peaks are now accounted for

E. If you want to see a list of  $2\theta$  and I for a mineral doubleclick on the mineral name in your Peak List.

F. You can usually delete minerals from the Peak List if they have “UNK” in the column.

G. Write down the Reference Codes for any minerals that may show up in your samples and delete most of the listings for a mineral just keeping a single representative one for reference.

## VII. Saving data and analysis

A. Choose File, then Save As and name the analysis file for the sample you just ran (keep the scan # the machine gave your sample

1. Hit Save

B. Generate a Printable Report of the data and analysis by choosing Create Word Report under the “Reports” tab at top.

1. Choose Fancy or Default depending on how much detail you want.

2. The first page of the report will appear on the screen. It may be hidden by another window so reduce other windows until you see your report.

- C. Print report in Word if desired. Hit OK
- D. Computer saves all raw data and analysis files
- E. Make sure you shut down the instrument in X'Pert Data Collector
- F. Data Viewer shows both scans and graph without the background. Use for quick and dirty look at the data.

## Appendix C: Results of Grain-Size Analyses

### Appendix C1: Grain-Size Data

Sample ID <sup>1</sup>	Wet Wt.	Dry Wt.	-2 $\Phi$	-1.5 $\Phi$	-1 $\Phi$	-0.5 $\Phi$	0 $\Phi$	0.5 $\Phi$
0-4' #5	37.43	35.29	0.00	0.00	0.00	0.05	0.03	0.14
0-4' #10	58.48	53.31	0.00	0.00	0.01	0.04	0.02	0.13
0-4' #15 & 20	89.58	80.62	0.00	0.00	0.00	0.01	0.03	0.16
0-4' #25 & 30	103.39	83.70	0.00	0.00	0.00	0.04	0.04	0.18
4-8' #3	35.32	28.72	0.00	0.00	0.00	0.00	0.00	0.01
4-8' #8	57.35	47.32	0.00	0.00	0.00	0.00	0.02	0.02
4-8' #13	44.82	36.44	0.00	0.00	0.00	0.00	0.02	0.03
4-8' #18	47.16	39.50	0.00	0.00	0.00	0.00	0.01	0.06
4-8' #23	56.35	47.47	0.00	0.00	0.00	0.00	0.01	0.03
4-8' #28	38.17	32.25	0.00	0.00	0.00	0.00	0.00	0.02
8-12' #4	83.99	69.49	0.00	0.00	0.00	0.09	0.14	1.36
8-12' #9	81.10	67.73	0.00	0.00	0.02	0.13	0.14	1.63
8-12' #14	71.65	60.19	0.00	0.00	0.16	1.66	1.34	5.58
12-16' #4	74.86	63.14	0.00	0.00	0.12	0.56	5.90	3.25
12-16' #8	72.34	60.82	0.00	0.04	0.14	3.06	2.87	11.64
12-16' #12	38.16	20.58	0.00	0.00	0.00	0.03	0.03	0.20
12-16' #17	54.80	40.48	0.00	0.00	0.07	0.44	0.14	0.52
12-16' #22	40.23	27.68	0.12	0.08	0.14	0.34	0.16	0.53
12-16' #27 & 32	104.23	76.69	0.13	0.22	1.26	0.81	3.99	7.03
12-16' #36	42.90	32.08	1.30	0.68	0.87	3.23	2.11	6.44
16-20' #3	16.50	11.45	0.72	0.10	0.13	0.16	0.32	0.45
16-20' #8	26.17	16.51	0.53	0.10	0.44	0.26	0.32	0.69
16-20' #13 & 18	80.71	60.64	2.24	1.21	2.61	5.45	1.98	6.11

1. Retained weights (g) for grain-size analyses of TC14 sediment samples



Sample ID <sup>1</sup>	1 $\Phi$	1.5 $\Phi$	2 $\Phi$	2.5 $\Phi$	3 $\Phi$	3.5 $\Phi$	4 $\Phi$	Pan
0-4' #5	0.31	1.45	6.27	10.41	6.62	4.12	1.94	0.18
0-4' #10	0.41	2.02	8.96	15.46	9.78	6.54	3.34	0.19
0-4' #15 & 20	0.56	2.99	14.34	25.06	13.73	8.79	4.65	0.24
0-4' #25 & 30	0.42	2.53	15.01	28.50	15.18	10.16	5.74	0.44
4-8' #3	0.04	0.34	3.19	8.59	0.88	10.93	1.87	0.05
4-8' #8	0.07	0.47	3.09	12.38	12.92	8.91	4.02	0.22
4-8' #13	0.16	1.08	5.54	12.78	8.23	4.04	1.76	0.06
4-8' #18	0.55	4.75	13.44	10.47	4.33	2.38	1.15	0.05
4-8' #23	0.18	1.42	10.12	16.01	7.45	5.32	2.79	0.14
4-8' #28	0.11	1.08	6.60	12.03	5.81	3.24	1.35	0.04
8-12' #4	5.96	20.98	28.14	8.69	1.72	0.55	0.19	0.02
8-12' #9	6.26	17.96	27.57	9.29	1.78	0.69	0.28	0.03
8-12' #14	8.38	15.52	18.35	5.91	0.86	0.30	0.13	0.00
12-16' #4	9.77	11.46	12.47	11.18	4.54	0.58	0.13	0.01
12-16' #8	15.24	14.77	6.51	1.04	0.17	0.17	0.14	0.00
12-16' #12	0.22	0.27	0.16	0.08	0.13	0.63	0.93	0.06
12-16' #17	0.84	2.44	6.10	5.06	3.97	5.75	3.38	0.23
12-16' #22	0.97	2.33	4.37	3.37	1.85	1.99	1.32	0.05
12-16' #27 & 32	8.89	12.67	12.11	6.78	3.00	1.52	0.35	0.27
12-16' #36	4.35	1.57	1.04	1.56	1.80	0.92	0.35	0.05
16-20' #3	0.53	0.48	1.04	1.52	1.02	1.64	0.44	0.02
16-20' #8	0.96	1.65	1.34	0.99	0.60	1.51	0.39	0.02
16-20' #13 & 18	7.14	7.85	4.20	2.82	2.59	1.85	0.81	0.05

1. Retained weights (g) for grain-size analyses of TC14 sediment samples

Sample ID <sup>1</sup>	Wet Wt.	Dry Wt.	-2 $\Phi$	-1.5 $\Phi$	-1 $\Phi$	-0.5 $\Phi$	0 $\Phi$	0.5 $\Phi$
16-20' #23 & 28	74.37	55.61	0.71	0.69	1.59	2.11	3.19	7.13
16-20' #33 & 38	95.65	73.86	7.83	3.45	4.08	8.08	2.39	9.52
16-20' #43	67.67	49.27	3.31	1.65	1.48	1.67	1.60	3.25
20-24' #3 & 8	ND <sup>2</sup>	103.85	7.38	5.80	6.88	13.47	4.52	10.49
20-24' #13 & 18	ND <sup>2</sup>	164.02	34.41	7.34	7.27	11.53	3.46	10.12
20-24' #24 & 29	ND <sup>2</sup>	91.12	15.60	3.76	2.87	5.14	1.58	5.63
24-28' #3 & 8	117.55	100.86	4.40	4.73	5.53	6.25	4.24	5.33
24-28' #13	79.87	69.37	0.61	0.67	2.12	4.59	1.65	5.33
24-28' #18 & 23	119.10	102.28	4.93	17.37	4.92	4.34	3.64	4.58
24-28' #28 & 33	122.97	104.19	2.79	1.11	1.48	2.70	0.71	1.79
24-28' #38	118.61	98.41	0.00	0.21	0.16	0.15	0.22	0.29
24-28' #43	100.22	85.32	0.05	0.17	0.06	0.16	0.09	0.23
28-32' #3	93.95	86.51	0.00	0.02	0.06	0.25	0.15	0.62
28-32' #8	89.71	77.95	1.46	0.10	0.16	0.41	0.21	0.78
28-32' #13	98.42	81.04	2.04	1.03	1.65	3.15	0.79	2.00
28-32' #18	121.67	99.58	15.43	2.55	1.67	2.11	0.52	1.51
28-32' #23	92.15	78.92	19.82	2.61	3.11	5.41	1.33	3.47
32-36' #3	86.22	73.24	8.65	3.77	3.62	4.68	1.41	3.78
32-36' #8	85.90	66.05	0.24	0.55	0.60	0.62	0.61	1.08
32-36' #13	68.41	57.42	6.56	1.82	2.03	2.63	0.84	2.35
32-36' #18	80.73	64.72	0.14	0.16	0.25	0.24	0.37	0.54
32-36' #23 & 28	223.25	182.55	0.79	0.28	0.45	0.87	0.23	0.86
32-36' #31	98.24	82.50	0.13	0.00	0.10	0.23	0.29	0.44

1. Retained weights (g) for grain-size analyses of TC14 sediment samples

2. ND: No data

Sample ID <sup>1</sup>	1 $\Phi$	1.5 $\Phi$	2 $\Phi$	2.5 $\Phi$	3 $\Phi$	3.5 $\Phi$	4 $\Phi$	Pan
16-20' #23 & 28	9.10	8.99	4.02	1.69	0.32	2.21	0.59	0.02
16-20' #33 & 38	9.48	3.57	2.06	2.00	1.27	0.56	0.01	0.08
16-20' #43	6.85	9.49	2.92	1.01	0.32	1.60	0.51	0.08
20-24' #3 & 8	11.03	13.20	9.50	4.55	3.11	2.12	1.21	0.26
20-24' #13 & 18	13.87	22.18	16.15	6.73	5.56	4.90	2.67	0.30
20-24' #24 & 29	10.98	21.81	12.84	3.43	1.19	1.02	0.56	0.05
24-28' #3 & 8	4.49	5.31	5.61	10.88	22.07	11.08	2.57	0.11
24-28' #13	7.87	9.86	5.95	8.21	12.03	5.89	1.55	0.03
24-28' #18 & 23	4.88	6.30	7.25	14.31	11.16	8.72	1.03	0.17
24-28' #28 & 33	2.03	3.42	16.84	45.30	16.10	3.71	0.82	0.05
24-28' #38	0.38	0.67	4.29	48.20	10.75	27.93	1.11	0.04
24-28' #43	0.30	0.47	2.19	32.65	33.25	9.49	2.20	0.03
28-32' #3	1.02	1.66	2.40	26.87	39.20	8.39	1.56	0.05
28-32' #8	1.17	1.71	2.09	24.13	33.64	7.16	1.18	0.03
28-32' #13	1.87	2.12	2.11	22.14	31.26	7.15	1.31	0.06
28-32' #18	1.88	2.42	3.20	26.77	30.37	5.72	1.35	0.11
28-32' #23	3.50	3.62	3.95	11.79	8.11	3.50	1.19	0.09
32-36' #3	4.97	7.04	5.77	5.65	3.04	2.15	2.78	0.09
32-36' #8	1.00	3.41	4.53	5.77	0.90	8.07	4.75	0.27
32-36' #13	3.51	5.21	4.96	6.93	5.18	1.55	1.15	0.05
32-36' #18	2.63	11.71	2.48	2.61	17.91	2.52	0.11	0.11
32-36' #23 & 28	2.10	4.02	7.90	41.57	37.86	13.39	7.18	0.45
32-36' #31	2.45	3.10	4.37	13.68	9.48	15.04	3.53	0.25

1. Retained weights (g) for grain-size analyses of TC14 sediment samples

## Appendix C2: Grain-Size Percentages and Error

Sample ID <sup>1</sup>	Very Coarse Sand <sup>2</sup>	Coarse Sand <sup>2</sup>	Medium Sand <sup>2</sup>	Fine Sand <sup>2</sup>	Very Fine Sand <sup>2</sup>	Gravel <sup>2</sup>	Sand <sup>2</sup>	Mud <sup>2</sup>	Error <sup>3</sup>	Median Grain Size <sup>4</sup>	Depth <sup>5</sup>
0-4' #5	0.21	1.29	21.83	48.17	17.14	0.00	88.64	11.36	0.17	185.70	0.15
0-4' #10	0.11	1.02	20.71	47.63	18.65	0.01	88.12	11.87	-0.62	182.10	0.35
0-4' #15 & 20	0.06	0.90	21.55	48.22	16.71	0.00	87.44	12.56	-0.22	187.10	0.69
0-4' #25 & 30	0.09	0.72	20.97	52.20	19.00	0.00	92.98	7.02	-0.02	190.40	1.03
4-8' #3	0.00	0.19	12.31	33.03	44.68	0.00	90.21	9.79	-0.22	120.30	1.31
4-8' #8	0.04	0.18	7.54	53.57	27.37	0.00	88.70	11.30	-0.20	145.40	1.50
4-8' #13	0.04	0.51	18.16	57.63	15.90	0.00	92.24	7.76	0.07	186.50	1.69
4-8' #18	0.03	1.52	44.85	36.51	8.69	0.00	91.59	8.41	2.67	234.80	1.88
4-8' #23	0.03	0.44	24.39	49.60	17.14	0.00	91.60	8.40	-0.38	195.90	2.06
4-8' #28	0.00	0.38	23.75	55.23	14.21	0.00	93.57	6.43	0.18	199.00	2.25
8-12' #4	0.34	10.54	70.71	14.98	1.07	0.00	97.64	2.36	-0.05	328.60	2.68
8-12' #9	0.39	11.68	67.41	16.40	1.43	0.02	97.31	2.67	-0.30	322.10	3.01
8-12' #14	4.97	23.21	56.31	11.25	0.72	0.26	96.47	3.27	-0.07	375.60	3.35
12-16' #4	10.26	20.67	37.99	24.95	1.13	0.19	95.00	4.81	-0.21	350.70	3.82
12-16' #8	9.72	44.10	34.92	1.99	0.50	0.30	91.22	8.49	0.20	529.70	3.99
12-16' #12	0.25	2.00	2.06	1.02	7.54	0.00	12.86	87.14	0.47	46.57	4.12
12-16' #17	1.44	3.38	21.21	22.44	22.67	0.17	71.13	28.70	-0.52	121.10	4.27
12-16' #22	1.80	5.45	24.34	18.96	12.02	1.24	62.56	36.19	-0.57	137.70	4.43

1. Grain-size percentages, sieve error, and median grain size for TC14 grain-size samples

2. Grain-size percentages are expressed as weight percents

3. Weight percent sieve error

$$\text{Sieve error} = [(\text{initial dry weight (g)} - \text{total weight retained (g)}) \div \text{initial dry weight (g)}] \times 100$$

4. Median grain size in microns

5. Depth in meters below the land surface

Sample ID <sup>1</sup>	Very Coarse Sand <sup>2</sup>	Coarse Sand <sup>2</sup>	Medium Sand <sup>2</sup>	Fine Sand <sup>2</sup>	Very Fine Sand <sup>2</sup>	Gravel <sup>2</sup>	Sand <sup>2</sup>	Mud <sup>2</sup>	Error <sup>3</sup>	Median Grain Size <sup>4</sup>	Depth <sup>5</sup>
12-16' #27 & 32	5.83	19.36	30.13	11.89	2.27	1.95	69.49	28.56	7.24	297.30	4.65
12-16' #36	16.66	33.66	8.15	10.48	3.96	8.88	72.91	18.20	-0.08	634.20	4.85
16-20' #3	3.96	8.23	12.63	21.22	17.34	7.99	63.38	28.63	4.66	148.60	4.95
16-20' #8	3.48	9.93	17.99	9.58	11.43	6.43	52.41	41.16	0.62	113.80	5.09
16-20' #23 & 28	9.54	29.19	23.40	3.60	5.04	5.38	70.78	23.84	-0.05	441.40	5.59
16-20' #33 & 38	15.68	28.46	8.43	4.90	0.86	23.01	58.32	18.67	-9.63	761.90	5.87
16-20' #43	6.65	20.53	25.23	2.71	4.28	13.11	59.40	27.48	-0.17	420.90	6.08
20-24' #3 & 8	17.37	20.79	21.92	7.40	3.22	19.38	70.70	9.92	-0.31	640.80	6.21
20-24' #13 & 18	9.16	14.67	23.44	7.51	4.63	29.97	59.41	10.62	-0.29	585.10	6.50
20-24' #24 & 29	7.35	18.18	37.93	5.06	1.73	24.34	70.25	5.42	0.23	499.00	7.17
24-28' #3 & 8	10.40	9.74	10.83	32.68	13.54	14.54	77.19	8.27	-0.03	218.10	7.42
24-28' #13	9.01	19.04	22.81	29.19	10.73	4.89	90.77	4.33	-0.07	316.20	7.59
24-28' #18 & 23	7.82	9.28	13.27	24.96	9.55	26.67	64.88	8.45	-0.22	353.90	7.75
24-28' #28 & 33	3.29	3.68	19.54	59.22	4.37	5.19	90.11	4.71	-0.49	217.90	7.97
24-28' #38	0.37	0.68	5.04	59.99	29.55	0.38	95.63	3.99	-0.15	186.80	8.14
24-28' #43	0.29	0.62	3.13	77.35	13.72	0.33	95.10	4.57	-0.14	168.10	8.36
28-32' #3	0.46	1.89	4.70	76.49	11.51	0.09	95.06	4.85	-0.15	163.80	8.66
28-32' #8	0.80	2.50	4.88	74.11	10.69	2.20	92.98	4.83	0.00	167.30	8.92
28-32' #13	4.86	4.77	5.23	65.90	10.43	5.81	91.19	3.00	0.00	176.60	9.18
28-32' #18	2.64	3.41	5.65	57.44	7.11	19.75	76.25	4.00	-0.11	199.30	9.44

1. Grain-size percentages, sieve error, and median grain size for TC14 grain-size samples

2. Grain-size percentages are expressed as weight percents

3. Weight percent sieve error

$$\text{Sieve error} = [(\text{initial dry weight (g)} - \text{total weight retained (g)}) \div \text{initial dry weight (g)}] \times 100$$

4. Median grain size in microns

5. Depth in meters below the land surface

Sample ID <sup>1</sup>	Very Coarse Sand <sup>2</sup>	Coarse Sand <sup>2</sup>	Medium Sand <sup>2</sup>	Fine Sand <sup>2</sup>	Very Fine Sand <sup>2</sup>	Gravel <sup>2</sup>	Sand <sup>2</sup>	Mud <sup>2</sup>	Error <sup>3</sup>	Median Grain Size <sup>4</sup>	Depth <sup>5</sup>
28-32' #23	8.55	8.84	9.59	25.22	5.94	32.37	58.14	9.49	-0.05	491.00	9.70
32-36' #3	8.61	12.36	18.08	12.27	6.96	22.65	58.28	19.07	-3.31	401.30	9.84
32-36' #8	1.97	3.33	12.72	10.70	20.55	2.22	49.26	48.51	-5.56	67.54	9.99
32-36' #13	6.34	10.67	18.54	22.08	4.93	18.96	62.57	18.47	-4.47	45.51	10.16
32-36' #18	0.97	5.01	22.43	32.41	4.15	0.87	64.97	34.16	-2.21	38.15	10.33
32-36' #23 & 28	0.62	1.67	6.75	44.99	11.65	0.86	65.69	33.45	-3.29	38.32	10.66
32-36' #31	0.66	3.64	9.39	29.12	23.35	0.29	66.16	33.55	-3.62	38.30	10.91

1. Grain-size percentages, sieve error, and median grain size for TC14 grain-size samples

2. Grain-size percentages are expressed as weight percents

3. Weight percent sieve error.

$$\text{Sieve error} = [(\text{initial dry weight (g)} - \text{total weight retained (g)}) \div \text{initial dry weight (g)}] \times 100$$

4. Median grain size in microns

5. Depth in meters below the land surface

### Appendix C3: Grain-Size Statistics and Hydraulic Conductivity

Sample ID <sup>1</sup>	Textural Group	Mean Type	Modal Distribution	Skewness	Sorting <sup>2</sup>	D <sub>10</sub> <sup>3</sup>	K <sup>4</sup>	Depth <sup>5</sup>
0-4' #5	Muddy Sand	Fine Sand	Bimodal	Very Fine Skewed	0.92	0.06	2.89	0.15
0-4' #10	Slightly Gravelly Muddy Sand	Fine Sand	Unimodal	Very Fine Skewed	0.92	0.06	2.74	0.35
0-4' #15&20	Muddy Sand	Fine Sand	Bimodal	Very Fine Skewed	0.94	0.05	2.57	0.69
0-4' #25&30	Sand	Fine Sand	Unimodal	Very Fine Skewed	0.81	0.07	4.67	1.03
4-8' #3	Sand	Fine Sand	Bimodal	Coarse Skewed	0.79	0.06	3.51	1.31
4-8' #8	Muddy Sand	Fine Sand	Unimodal	Fine Skewed	0.81	0.06	2.91	1.50
4-8' #13	Sand	Fine Sand	Unimodal	Very Fine Skewed	0.78	0.07	4.77	1.69
4-8' #18	Sand	Fine Sand	Unimodal	Very Fine Skewed	0.88	0.08	5.12	1.88
4-8' #23	Sand	Fine Sand	Unimodal	Very Fine Skewed	0.84	0.07	4.16	2.06
4-8' #28	Sand	Fine Sand	Unimodal	Very Fine Skewed	0.76	0.09	6.30	2.25
8-12' #4	Sand	Medium Sand	Unimodal	Symmetrical	0.56	0.20	34.73	2.68
8-12' #9	Slightly Gravelly Sand	Medium Sand	Unimodal	Coarse Skewed	0.61	0.19	32.72	3.01
8-12' #14	Slightly Gravelly Sand	Medium Sand	Unimodal	Symmetrical	0.77	0.21	38.03	3.35
12-16' #4	Slightly Gravelly Sand	Medium Sand	Bimodal	Fine Skewed	1.05	0.15	20.36	3.82
12-16' #8	Slightly Gravelly Sand	Coarse Sand	Trimodal	Coarse Skewed	1.15	0.21	37.24	3.99
12-16' #12	Sandy Mud	Mud	Unimodal	Symmetrical	0.54	0.03	0.98	4.12

1. Grain-size statistics and hydraulic conductivity for TC14 grain-size samples

2. D<sub>10</sub>: Sorting in Φ units

3. The grain size (mm) that is 10% finer by weigh; also called the effective grain size

4. K: Grain-size-estimated values of hydraulic conductivity in meters per day:  $K \text{ (m/day)} = 864 \times (D_{10})^2$

5. Depth in meters below the land surface

Sample ID <sup>1</sup>	Textural Group	Mean Type	Modal Distribution	Skewness	Sorting <sup>2</sup>	D <sub>10</sub> <sup>3</sup>	K <sup>4</sup>	Depth <sup>5</sup>
12-16' #17	Slightly Gravelly Muddy Sand	Very Fine Sand	Trimodal	Symmetrical	1.28	0.04	1.36	4.27
12-16' #22	Slightly Gravelly Muddy Sand	Fine Sand	Trimodal	Fine Skewed	1.44	0.04	1.23	4.43
12-16' #27&32	Slightly Gravelly Muddy Sand	Fine Sand	Bimodal	Fine Skewed	1.77	0.04	1.36	4.65
12-16' #36	Gravelly Muddy Sand	Medium Sand	Polymodal	Very Fine Skewed	2.17	0.05	1.81	4.85
16-20' #3	Gravelly Muddy Sand	Fine Sand	Polymodal	Coarse Skewed	2.03	0.04	1.36	4.95
16-20' #8	Gravelly Muddy Sand	Fine Sand	Polymodal	Very Coarse Skewed	1.92	0.04	1.17	5.09
16-20' #13&18	Gravelly Muddy Sand	Medium Sand	Polymodal	Fine Skewed	2.21	0.04	1.55	5.30
16-20' #23&28	Gravelly Muddy Sand	Medium Sand	Trimodal	Very Fine Skewed	1.96	0.04	1.51	5.59
16-20' #33&38	Gravelly Muddy Sand	Coarse Sand	Polymodal	Fine Skewed	2.49	0.05	1.77	5.87
16-20' #43	Gravelly Muddy Sand	Medium Sand	Polymodal	Fine Skewed	2.30	0.04	1.39	6.08
20-24' #3&8	Gravelly Muddy Sand	Coarse Sand	Polymodal	Symmetrical	1.94	0.06	3.60	6.21
20-24' #13&18	Gravelly Muddy Sand	Coarse Sand	Polymodal	Symmetrical	2.30	0.06	3.16	6.50
20-24' #24&29	Gravelly Sand	Coarse Sand	Trimodal	Very Coarse Skewed	1.95	0.21	36.74	7.17
24-28' #3&8	Gravelly Sand	Medium Sand	Polymodal	Very Coarse Skewed	1.99	0.08	5.57	7.42
24-28' #13	Slightly Gravelly Sand	Medium Sand	Trimodal	Symmetrical	1.44	0.10	9.13	7.59

1. Grain-size statistics and hydraulic conductivity for TC14 grain-size samples

2. D<sub>10</sub>: Sorting in Φ units

3. The grain size (mm) that is 10% finer by weigh; also called the effective grain size

4. K: Grain-size-estimated values of hydraulic conductivity in meters per day:  $K \text{ (m/day)} = 864 \times (D_{10})^2$

5. Depth in meters below the land surface



Sample ID <sup>1</sup>	Textural Group	Mean Type	Modal Distribution	Skewness	Sorting <sup>2</sup>	D <sub>10</sub> <sup>3</sup>	K <sup>4</sup>	Depth <sup>5</sup>
24-28' #18&23	Gravelly Muddy Sand	Coarse Sand	Trimodal	Coarse Skewed	2.16	0.09	7.29	7.75
24-28' #28&33	Gravelly Sand	Fine Sand	Unimodal	Coarse Skewed	1.05	0.13	14.09	7.97
24-28' #38	Slightly Gravelly Sand	Fine Sand	Bimodal	Very Fine Skewed	0.56	0.10	7.83	8.14
24-28' #43	Slightly Gravelly Sand	Fine Sand	Unimodal	Fine Skewed	0.53	0.10	8.28	8.36
28-32' #3	Slightly Gravelly Sand	Fine Sand	Unimodal	Symmetrical	0.58	0.10	8.78	8.66
28-32' #13	Gravelly Sand	Fine Sand	Unimodal	Very Coarse Skewed	1.17	0.11	10.45	9.18
28-32' #18	Gravelly Sand	Medium Sand	Bimodal	Very Coarse Skewed	2.10	0.12	11.91	9.44
28-32' #23	Muddy Sandy Gravel	Coarse Sand	Polymodal	Coarse Skewed	2.33	0.07	4.36	9.70
32-36' #3	Gravelly Muddy Sand	Medium Sand	Polymodal	Symmetrical	2.51	0.04	1.75	9.84
32-36' #8	Slightly Gravelly Muddy Sand	Very Fine Sand	Trimodal	Very Coarse Skewed	1.45	0.04	1.11	9.99
32-36' #13	Gravelly Muddy Sand	Medium Sand	Polymodal	Coarse Skewed	2.44	0.05	1.79	10.16
32-36' #18	Slightly Gravelly Muddy Sand	Fine Sand	Trimodal	Symmetrical	1.44	0.04	1.26	10.33
32-36' #23&28	Slightly Gravelly Muddy Sand	Very Fine Sand	Bimodal	Fine Skewed	1.12	0.04	1.27	10.66
32-36' #31	Slightly Gravelly Muddy Sand	Very Fine Sand	Trimodal	Symmetrical	1.19	0.04	1.27	10.91

1. Grain-size statistics and hydraulic conductivity for TC14 grain-size samples

2. D<sub>10</sub>: Sorting in  $\Phi$  units

3. The grain size (in mm) that is 10% finer by weigh; also called the effective grain size

4. K: Grain-size-estimated values of hydraulic conductivity in meters per day:  $K \text{ (m/day)} = 864 \times (D_{10})^2$

5. Depth in meters below the land surface

## Appendix D: Results of Magnetic Separations

### Appendix D1: Grain-Size Data Used in Magnetic Separations

Sample ID <sup>1</sup>	Dry Weight	1.25 $\Phi$	2.25 $\Phi$	3.25 $\Phi$	4 $\Phi$	Pan	Depth <sup>2</sup>
0-4' #1	ND <sup>3</sup>	ND <sup>3</sup>	ND <sup>3</sup>	ND <sup>3</sup>	ND <sup>3</sup>	ND <sup>3</sup>	ND <sup>3</sup>
0-4' #2	118.73	2.17	45.02	47.02	13.55	10.43	0.61
0-4' #3	268.25	2.71	99.16	93.55	28.69	37.05	1.01
4-8' #4	244.9	2.16	75.46	118.49	30.09	17.92	1.36
4-8' #5	291.37	6.42	143.93	104.03	21.28	14.40	1.86
8-12' #6	286.51	62.94	185.24	28.19	2.22	6.17	2.74
8-12' #7	299.86	95.99	181.05	11.68	0.87	8.84	3.35
12-16' #8	224.14	122.32	83.40	5.85	1.02	10.15	3.81
12-16' #9	78.30	3.78	0.00	0.00	12.55	59.13	4.11
12-16' #10	100.6	11.50	27.35	16.39	4.21	40.90	4.41
12-16' #11	199.10	99.68	28.18	23.56	4.58	39.28	4.72
16-20' #12	167.98	65.20	24.67	14.69	2.01	44.90	5.07
16-20' #13	216.38	98.00	20.72	11.00	2.04	82.69	5.47
16-20' #14	234.07	166.64	23.73	4.47	0.90	20.19	5.89
20-24' #15 <sup>4</sup>	127.52	93.91	23.58	7.61	1.87	0.52	6.24
20-24' #16	255.67	159.24	30.83	17.25	6.53	22.15	6.53
20-24' #17	252.69	125.23	39.78	25.90	6.14	31.48	6.83
20-24' #18	333.26	202.61	78.73	15.30	3.04	10.51	7.14
24-28' #19	275.66	57.78	51.63	106.01	10.06	20.62	7.47
24-28' #20	234.99	75.24	0.00	0.00	130.32	10.09	7.77
24-28' #21	187.83	14.24	54.93	100.99	5.61	11.05	8.07
24-28' #22	240.99	12.68	64.03	147.17	8.17	7.92	8.38
28-32' #23	155.08	8.02	0.00	0.00	119.69	7.02	8.74
28-32' #24	127.24	45.84	0.00	0.00	63.39	8.67	9.14
28-32' #25	32.01	18.01	0.00	0.00	9.50	1.06	9.55
32-36' #26	60.27	13.11	0.00	0.00	27.57	14.18	9.85
32-36' #27	429.28	123.78	48.72	109.73	14.05	82.97	10.15
32-36' #28	220.46	25.80	27.27	83.33	6.05	59.10	10.51
32-36' #29	151.14	4.17	0.00	0.00	103.76	33.63	10.82

1. Total dry sample weights (g) and retained weights (g) for TC14C fractions

2. Depth in meters below the land surface

3. ND: No data

4. Samples TC14:20-24 #'s 4-7 were combined to approximate the composition of TC14C:20-24 #15 due to insufficient amount of leftover sample

## Appendix D2: Magnetic Separation Data

Sample ID <sup>1</sup>	Non-Sus. <sup>2</sup>	Highly Sus. <sup>2</sup>	Poorly Sus. <sup>2</sup>	Total Magnetics <sup>2</sup>	Depth <sup>3</sup>
0-4' #1	ND <sup>4</sup>	ND <sup>4</sup>	ND <sup>4</sup>	ND <sup>4</sup>	ND <sup>4</sup>
0-4' #2	98.71	0.80	0.49	1.29	0.61
0-4' #3	98.85	1.01	0.13	1.15	1.01
4-8' #4	98.35	1.28	0.37	1.65	1.36
4-8' #5	98.23	1.34	0.43	1.77	1.86
8-12' #6	ND <sup>4</sup>	ND <sup>4</sup>	ND <sup>4</sup>	ND <sup>4</sup>	2.74
8-12' #7	99.33	0.57	0.10	0.67	3.35
12-16' #8	99.11	0.72	0.17	0.89	3.81
12-16' #9	96.90	2.30	0.80	3.10	4.11
12-16' #10	96.68	2.73	0.58	3.32	4.41
12-16' #11	96.00	3.05	0.95	4.00	4.72
16-20' #12	92.14	4.76	3.09	7.86	5.07
16-20' #13	85.12	9.85	5.03	14.88	5.47
16-20' #14	90.24	5.33	4.43	9.76	5.89
20-24' #15 <sup>3</sup>	90.69	5.56	3.75	9.31	6.24
20-24' #16	93.28	3.83	2.89	6.72	6.53
20-24' #17	95.49	2.71	1.80	4.51	6.83
20-24' #18	95.04	2.69	2.27	4.96	7.14
24-28' #19	96.40	2.66	0.93	3.60	7.47
24-28' #20	96.22	3.07	0.71	3.78	7.77
24-28' #21	ND <sup>4</sup>	ND <sup>4</sup>	ND <sup>4</sup>	ND <sup>4</sup>	8.07
24-28' #22	97.74	1.81	0.45	2.26	8.38
28-32' #23	96.23	3.11	0.66	3.77	8.74
28-32' #24	96.39	2.68	0.94	3.61	9.14
28-32' #25	95.20	3.93	0.87	4.80	9.55
32-36' #26	94.16	4.48	1.36	5.84	9.85
32-36' #27	96.47	2.82	0.70	3.53	10.15
32-36' #28	97.46	2.29	0.25	2.54	10.51
32-36' #29	95.91	3.55	0.54	4.09	10.82

1. Magnetic separation data for TC14C subsamples. All values are expressed as weight percents

2. Non-susceptible (Non-Sus.), highly susceptible (Highly Sus.)(isolated at  $\leq 0.8$ amps), poorly susceptible (Poorly Sus.)(isolated at  $> 0.8$ amps), and total magnetic fractions. Total magnetics equals the sum of highly and poorly susceptible grains

3. Depth in meters below the land surface

4. ND: No Data

### Appendix E: Polished-Thin-Section Data

Polished-Thin Section ID <sup>1</sup>	Grain-Size Range	Magnetic Susceptibility	Sample ID <sup>2</sup>	Sample Weight <sup>3</sup>	Quadrant <sup>4</sup>	Mean Sample Depth <sup>5</sup>
PTS: 2-5	Sand	NS <sup>6</sup>	0 - 4' #2	1.28	A	1.2
	(>4Φ - <1.25 Φ)	NS <sup>6</sup>	0 - 4' #3	1.08	A	
	Sand	NS <sup>6</sup>	4 - 8' #4	2.72	B	
	(>4Φ - <1.25 Φ)	NS <sup>6</sup>	4 - 8' #5	2.37	B	
	Sand	S <sup>7</sup>	0 - 4' #2	1.02	C	
	(>4Φ - <1.25 Φ)	S <sup>7</sup>	0 - 4' #3	1.53	C	
	Sand	S <sup>7</sup>	4 - 8' #4	1.96	D	
	(>4Φ - <1.25 Φ)	S <sup>7</sup>	4 - 8' #5	1.75	D	

1. Each polished-thin section was prepared using multiple samples from TC14C
2. Samples are from TC14C
3. Weight of fractions (g) from TC14 sediment samples that were combined for each quadrant of the polished-thin section
4. Each polished-thin section includes 4 quadrants (A, B, C, and D) that are comprised of magnetically separated fractions
5. Mean depth (m BLS) of all TC14 sediment samples that comprise each polished-thin section
6. NS: Non-susceptible using hand magnet or Frantz Isodynamic Magnetic Separator
7. S: Susceptible using hand magnet or Frantz Isodynamic Separator

Polished- Thin Section ID <sup>1</sup>	Grain-Size Range	Magnetic Susceptibility	Sample ID <sup>2</sup>	Sample Weight <sup>3</sup>	Quadrant <sup>4</sup>	Mean Sample Depth <sup>5</sup>
PTS: 9-12	Mud ( $<4\Phi$ )	NP <sup>6</sup>	12 - 16' #9	1.98	A	4.6
		NP <sup>6</sup>	12 - 16' #10	2.08	A	
		NP <sup>6</sup>	12 - 16' #11	2.09	A	
	Sand ( $>4\Phi - <1.25\Phi$ )	NP <sup>6</sup>	16 - 20' #12	2.03	A	
		NS <sup>7</sup>	12 - 16' #9	1.66	B	
		NS <sup>7</sup>	12 - 16' #10	1.66	B	
		NS <sup>7</sup>	12 - 16' #11	1.68	B	
		NS <sup>7</sup>	16 - 20' #12	1.67	B	
		HS <sup>8</sup>	12 - 16' #9	0.19	C	
	Sand ( $>4\Phi - <1.25\Phi$ )	HS <sup>8</sup>	12 - 16' #10	0.89	C	
		HS <sup>8</sup>	12 - 16' #11	0.93	C	
		HS <sup>8</sup>	16 - 20' #12	1.01	C	
	Sand ( $>4\Phi - <1.25\Phi$ )	PS <sup>9</sup>	12 - 16' #9	0.06	D	
		PS <sup>9</sup>	12 - 16' #10	0.15	D	
PS <sup>9</sup>		12 - 16' #11	0.32	D		
PS <sup>9</sup>		16 - 20' #12	1.10	D		

1. Each polished-thin section was prepared using multiple samples from TC14C
2. Samples are from TC14C
3. Weight of fractions (g) from TC14 sediment samples that were combined for each quadrant of the polished-thin section
4. Each polished-thin section includes 4 quadrants (A, B, C, and D) that are comprised of magnetically separated fractions
5. Mean depth (m BLS) of all TC14 sediment samples that comprise each polished-thin section
6. NP: Not processed to prevent clogging of the instrument
7. NS: Non-susceptible using hand magnet or Frantz Isodynamic Magnetic Separator.
8. HS: Highly susceptible; magnetically susceptible by hand magnet or by setting the magnetic separator to  $\leq 0.8$  amps
9. PS: Poorly susceptible; magnetically susceptible only by setting the magnetic separator to  $>0.8$  amps

Polished-Thin Section ID <sup>1</sup>	Grain-Size Range	Magnetic Susceptibility	Sample ID <sup>2</sup>	Sample Weight <sup>3</sup>	Quadrant <sup>4</sup>	Mean Sample Depth <sup>5</sup>
PTS: 13-14	Mud	NP <sup>6</sup>	16 - 20' #13	4.06	A	5.5
	(<4 Φ)	NP <sup>6</sup>	16 - 20' #14	4.11	A	
	Sand	NP <sup>6</sup>	16 - 20' #13	3.11	B	
	(>4Φ - <1.25 Φ)	NS <sup>7</sup>	16 - 20' #14	3.05	B	
	Sand	HS <sup>8</sup>	16 - 20' #13	0.97	C	
	(>4Φ - <1.25 Φ)	HS <sup>8</sup>	16 - 20' #14	0.77	C	
	Sand	PS <sup>9</sup>	16 - 20' #13	1.32	D	
	(>4Φ - <1.25 Φ)	PS <sup>9</sup>	16 - 20' #14	0.92	D	

1. Each polished-thin section was prepared using multiple samples from TC14C
2. Samples are from TC14C
3. Weight of fractions (g) from TC14 sediment samples that were combined for each quadrant of the polished-thin section
4. Each polished-thin section includes 4 quadrants (A, B, C, and D) that are comprised of magnetically separated fractions
5. Mean depth (m BLS) of all TC14 sediment samples that comprise each polished-thin section
6. NP: Not processed to prevent clogging of the instrument
7. NS: Non-susceptible using hand magnet or Frantz Isodynamic Magnetic Separator.
8. HS: Highly susceptible; magnetically susceptible by hand magnet or by setting the magnetic separator to  $\leq 0.8$  amps
9. PS: Poorly susceptible; magnetically susceptible only by setting the magnetic separator to  $>0.8$  amps

Polished-Thin Section ID <sup>1</sup>	Grain-Size Range	Magnetic Susceptibility	Sample ID <sup>2</sup>	Sample Weight <sup>3</sup>	Quadrant <sup>4</sup>	Mean Sample Depth <sup>5</sup>
PTS: 15-16	Mud	NP <sup>6</sup>	20 - 24' #15	5.00	A	6.2
	(<4 Φ)	NP <sup>6</sup>	20 - 24' #16	4.95	A	
	Sand	NS <sup>7</sup>	20 - 24' #15	4.35	B	
	(>4Φ - <1.25 Φ)	NS <sup>7</sup>	20 - 24' #16	4.30	B	
	Sand	HS <sup>8</sup>	20 - 24' #15	1.91	C	
	(>4Φ - <1.25 Φ)	HS <sup>8</sup>	20 - 24' #16	1.49	C	
	Sand	PS <sup>9</sup>	20 - 24' #15	1.71	D	
	(>4Φ - <1.25 Φ)	PS <sup>9</sup>	20 - 24' #16	1.04	D	

1. Each polished-thin section was prepared using multiple samples from TC14C
2. Samples are from TC14C
3. Weight of fractions (g) from TC14 sediment samples that were combined for each quadrant of the polished-thin section
4. Each polished-thin section includes 4 quadrants (A, B, C, and D) that are comprised of magnetically separated fractions
5. Mean depth (m BLS) of all TC14 sediment samples that comprise each polished-thin section
6. NP: Not processed to prevent clogging of the instrument
7. NS: Non-susceptible using hand magnet or Frantz Isodynamic Magnetic Separator.
8. HS: Highly susceptible; magnetically susceptible by hand magnet or by setting the magnetic separator to  $\leq 0.8$  amps
9. PS: Poorly susceptible; magnetically susceptible only by setting the magnetic separator to  $>0.8$  amps

Polished-Thin Section ID <sup>1</sup>	Grain-Size Range	Magnetic Susceptibility	Sample ID <sup>2</sup>	Sample Weight <sup>3</sup>	Quadrant <sup>4</sup>	Mean Sample Depth <sup>5</sup>
PTS: 17-19	Mud ( $<4\Phi$ )	NP <sup>6</sup>	20 - 24' #17	2.02	A	7.0
		NP <sup>6</sup>	20 - 24' #18	2.06	A	
		NP <sup>6</sup>	24 - 28' #19	2.08	A	
	Sand ( $>4\Phi - <1.25\Phi$ )	NS <sup>7</sup>	20 - 24' #17	3.16	B	
		NS <sup>7</sup>	20 - 24' #18	3.12	B	
		NS <sup>7</sup>	24 - 28' #19	3.10	B	
	Sand ( $>4\Phi - <1.25\Phi$ )	HS <sup>8</sup>	20 - 24' #17	1.17	C	
		HS <sup>8</sup>	20 - 24' #18	1.24	C	
		HS <sup>8</sup>	24 - 28' #19	1.29	C	
	Sand ( $>4\Phi - <1.25\Phi$ )	PS <sup>9</sup>	20 - 24' #17	0.99	D	
		PS <sup>9</sup>	20 - 24' #18	1.70	D	
		PS <sup>9</sup>	24 - 28' #19	0.67	D	

1. Each polished-thin section was prepared using multiple samples from TC14C
2. Samples are from TC14C
3. Weight of fractions (g) from TC14 sediment samples that were combined for each quadrant of the polished-thin section
4. Each polished-thin section includes 4 quadrants (A, B, C, and D) that are comprised of magnetically separated fractions
5. Mean depth (m BLS) of all TC14 sediment samples that comprise each polished-thin section
6. NP: Not processed to prevent clogging of the instrument
7. NS: Non-susceptible using hand magnet or Frantz Isodynamic Magnetic Separator.
8. HS: Highly susceptible; magnetically susceptible by hand magnet or by setting the magnetic separator to  $\leq 0.8$  amps
9. PS: Poorly susceptible; magnetically susceptible only by setting the magnetic separator to  $>0.8$  amps



Polished-Thin Section ID <sup>1</sup>	Grain-Size Range	Magnetic Susceptibility	Sample ID <sup>2</sup>	Sample Weight <sup>3</sup>	Quadrant <sup>4</sup>	Mean Sample Depth <sup>5</sup>
PTS: 23-25	Mud ( $<4\Phi$ )	NP <sup>6</sup>	28 - 32' #23	1.00	A	9.1
		NP <sup>6</sup>	28 - 32' #24	1.01	A	
		NP <sup>6</sup>	28 - 32' #25	0.96	A	
	Sand ( $>4\Phi - <1.25\Phi$ )	NS <sup>7</sup>	28 - 32' #23	3.76	B	
		NS <sup>7</sup>	28 - 32' #24	3.77	B	
		NS <sup>7</sup>	28 - 32' #25	3.77	B	
	Sand ( $>4\Phi - <1.25\Phi$ )	HS <sup>8</sup>	28 - 32' #23	2.00	C	
		HS <sup>8</sup>	28 - 32' #24	1.70	C	
		HS <sup>8</sup>	28 - 32' #25	0.17	C	
	Sand ( $>4\Phi - <1.25\Phi$ )	PS <sup>9</sup>	28 - 32' #23	0.26	D	
		PS <sup>9</sup>	28 - 32' #24	0.59	D	
PS <sup>9</sup>		28 - 32' #25	0.89	D		

1. Each polished-thin section was prepared using multiple samples from TC14C
2. Samples are from TC14C
3. Weight of fractions (g) from TC14 sediment samples that were combined for each quadrant of the polished-thin section
4. Each polished-thin section includes 4 quadrants (A, B, C, and D) that are comprised of magnetically separated fractions
5. Mean depth (m BLS) of all TC14 sediment samples that comprise each polished-thin section
6. NP: Not processed to prevent clogging of the instrument
7. NS: Non-susceptible using hand magnet or Frantz Isodynamic Magnetic Separator.
8. HS: Highly susceptible; magnetically susceptible by hand magnet or by setting the magnetic separator to  $\leq 0.8$  amps
9. PS: Poorly susceptible; magnetically susceptible only by setting the magnetic separator to  $>0.8$  amps

Polished-Thin Section ID <sup>1</sup>	Grain-Size Range	Magnetic Susceptibility	Sample ID <sup>2</sup>	Sample Weight <sup>3</sup>	Quadrant <sup>4</sup>	Mean Sample Depth <sup>5</sup>
PTS: 26-28	Mud ( $<4\Phi$ )	NP <sup>6</sup>	32 - 36' #26	2.01	A	9.8
		NP <sup>6</sup>	32 - 36' #27	2.03	A	
		NP <sup>6</sup>	32 - 36' #28	2.04	A	
	Sand ( $>4\Phi$ - $<1.25\Phi$ )	NS <sup>7</sup>	32 - 36' #26	6.24	B	
		NS <sup>7</sup>	32 - 36' #27	6.20	B	
		NS <sup>7</sup>	32 - 36' #28	6.24	B	
	Sand ( $>4\Phi$ - $<1.25\Phi$ )	HS <sup>8</sup>	32 - 36' #26	0.90	C	
		HS <sup>8</sup>	32 - 36' #27	1.45	C	
		HS <sup>8</sup>	32 - 36' #28	0.91	C	
	Sand ( $>4\Phi$ - $<1.25\Phi$ )	PS <sup>9</sup>	32 - 36' #26	0.21	D	
		PS <sup>9</sup>	32 - 36' #27	0.64	D	
		PS <sup>9</sup>	32 - 36' #28	0.40	D	

1. Each polished-thin section was prepared using multiple samples from TC14C
2. Samples are from TC14C
3. Weight of fractions (g) from TC14 sediment samples that were combined for each quadrant of the polished-thin section
4. Each polished-thin section includes 4 quadrants (A, B, C, and D) that are comprised of magnetically separated fractions
5. Mean depth (m BLS) of all TC14 sediment samples that comprise each polished-thin section
6. NP: Not processed to prevent clogging of the instrument
7. NS: Non-susceptible using hand magnet or Frantz Isodynamic Magnetic Separator.
8. HS: Highly susceptible; magnetically susceptible by hand magnet or by setting the magnetic separator to  $\leq 0.8$  amps
9. PS: Poorly susceptible; magnetically susceptible only by setting the magnetic separator to  $>0.8$  amps

## Appendix F: EDX Data

### Appendix F1: Composition and Statistics of Mineral Standards

Reference Mineral	Element	Accepted Value <sup>1</sup>	Value Normalized w/o H, C, and F <sup>2</sup>	Mean <sup>3</sup>	Confidence Level (95%)	Standard Deviation <sup>4</sup>	CV % <sup>5</sup>	% Error <sup>6</sup>	Normalized Error <sup>7</sup>
Albite (n = 9)	Na	8.60		7.75	0.05	0.07	0.90	-9.88	
	Al	10.34		9.74	0.07	0.09	0.92	-5.80	
	Si	32.03		33.20	0.07	0.09	0.27	3.65	
	K	0.18		0.07	0.04	0.05	71.43	-61.11	
	Ca	0.09		0.03	0.02	0.02	66.67	-66.67	
	O	48.76		49.21	0.03	0.03	0.06	0.92	
Almandine (n = 11)	Mg	6.45		5.93	0.09	0.13	2.19	-8.06	
	Al	11.67		11.24	0.10	0.14	1.25	-3.68	
	Si	18.32		19.26	0.08	0.11	0.57	5.13	
	Ca	3.00		2.95	0.01	0.02	0.68	-1.67	
	Mn	0.46		0.44	0.04	0.06	13.64	-4.35	
	Fe	18.09		17.90	0.16	0.23	1.28	-1.05	
	O	42.01		42.28	0.06	0.09	0.21	0.64	

1. Values given in weight percent element

2. Accepted values are normalized to dry weight by recalculating total weight % excluding H, C, and F

3. Mean of n analyses of each standard

4. Standard deviation of n standard analyses

5. CV %: Coefficient of Variation = (standard deviation ÷ mean) × 100

6. % Error: Percent Error = [(mean - accepted value) ÷ accepted value] × 100

7. Normalized Error for apatite, biotite, chlorite, and kaersutite calculated using the normalized accepted value

Reference Mineral	Element	Accepted Value <sup>1</sup>	Value Normalized w/o H, C, and F <sup>2</sup>	Mean <sup>3</sup>	Confidence Level (95%)	Standard Deviation <sup>4</sup>	CV % <sup>5</sup>	% Error <sup>6</sup>	Normalized Error <sup>7</sup>
	H	0.20	NA <sup>8</sup>	NA <sup>8</sup>	NA <sup>8</sup>	NA <sup>8</sup>	NA <sup>8</sup>	NA <sup>8</sup>	NA <sup>8</sup>
Apatite (n = 10)	P	18.50	18.54	19.59	0.10	0.14	0.71	5.89	5.68
	Ca	39.89	39.97	39.38	0.16	0.23	0.58	-1.28	-1.48
	O	41.41	41.49	41.03	0.06	0.09	0.22	-0.92	-1.12
	Si	20.38		20.70	0.07	0.10	0.48	1.57	
Benitoite (n = 11)	Ti	11.58		11.26	0.27	0.40	3.55	-2.76	
	Ba	33.21		33.08	0.42	0.62	1.87	-0.39	
	O	34.82		34.96	0.14	0.21	0.60	0.40	

1. Values given in weight percent element

2. Accepted values are normalized to dry weight by recalculating total weight % excluding H, C, and F

3. Mean of n analyses of each standard

4. Standard deviation of n standard analyses

5. CV %: Coefficient of Variation = (standard deviation ÷ mean) × 100

6. % Error: Percent Error = [(mean - accepted value) ÷ accepted value] x 100

7. Normalized Error for apatite, biotite, chlorite, and kaersutite calculated using the normalized accepted value

8. NA: Not analyzed

Reference Mineral	Element	Accepted Value <sup>1</sup>	Value Normalized w/o H, C, and F <sup>2</sup>	Mean <sup>3</sup>	Confidence Level (95%)	Standard Deviation <sup>4</sup>	CV % <sup>5</sup>	% Error <sup>6</sup>	Normalized Error <sup>7</sup>
	H	0.46	NA <sup>8</sup>	NA <sup>8</sup>	NA <sup>8</sup>	NA <sup>8</sup>	NA <sup>8</sup>	NA <sup>8</sup>	NA <sup>8</sup>
	Mg	11.77	11.82	11.97	0.24	0.34	2.84	1.70	1.24
	Al	8.01	8.05	7.97	0.08	0.12	1.51	-0.50	-0.95
	Si	18.10	18.18	19.75	0.14	0.20	1.01	9.12	8.62
Biotite (n = 10)	K	8.23	8.27	8.66	0.29	0.41	4.73	5.22	4.75
	Ca	0.07	0.07	0.28	0.10	0.14	50.00	300.00	298.20
	Ti	1.06	1.06	0.98	0.04	0.06	6.12	-7.55	-7.96
	Mn	0.03	0.03	0.06	0.04	0.05	83.33	100.00	99.10
	Fe	8.33	8.37	8.01	0.33	0.47	5.87	-3.84	-4.27
	O	43.95	44.15	42.31	0.18	0.25	0.59	-3.73	-4.16

1. Values given in weight percent element

2. Accepted values are normalized to dry weight by recalculating total weight % excluding H, C, and F

3. Mean of n analyses of each standard

4. Standard deviation of n standard analyses

5. CV %: Coefficient of Variation = (standard deviation ÷ mean) × 100

6. % Error: Percent Error = [(mean - accepted value) ÷ accepted value] x 100

7. Normalized Error for apatite, biotite, chlorite, and kaersutite calculated using the normalized accepted value

8. NA: Not analyzed

Reference Mineral	Element	Accepted Value <sup>1</sup>	Value Normalized w/o H, C, and F <sup>2</sup>	Mean <sup>3</sup>	Confidence Level (95%)	Standard Deviation <sup>4</sup>	CV % <sup>5</sup>	% Error <sup>6</sup>	Normalized Error <sup>7</sup>
Chlorite (n = 11)	H	1.54	NA <sup>8</sup>	NA <sup>8</sup>	NA <sup>8</sup>	NA <sup>8</sup>	NA <sup>8</sup>	NA <sup>8</sup>	NA <sup>8</sup>
	C	0.02	NA <sup>8</sup>	NA <sup>8</sup>	NA <sup>8</sup>	NA <sup>8</sup>	NA <sup>8</sup>	NA <sup>8</sup>	NA <sup>8</sup>
	F	0.02	NA <sup>8</sup>	NA <sup>8</sup>	NA <sup>8</sup>	NA <sup>8</sup>	NA <sup>8</sup>	NA <sup>8</sup>	NA <sup>8</sup>
	Mg	20.21	20.45	21.42	0.18	0.27	1.26	5.99	4.73
	Al	9.57	9.69	11.18	0.08	0.12	1.07	16.82	15.43
	Si	14.04	14.21	17.45	0.13	0.20	1.15	24.29	22.81
	Ca	0.02	0.02	NC <sup>10</sup>	NC <sup>10</sup>	NC <sup>10</sup>	NC <sup>10</sup>	NC <sup>10</sup>	NC <sup>10</sup>
	Cr	0.67	0.68	1.29	0.07	0.10	7.75	92.54	90.25
	Fe	2.57	2.60	2.81	0.07	0.10	3.56	9.34	8.04
	Ni	0.19	0.19	0.24	0.08	0.12	50.00	26.32	24.81
O	51.54	52.16	45.61	0.30	0.44	0.96	-11.51	-12.56	

1. Values given in weight percent element

2. Accepted values are normalized to dry weight by recalculating total weight % excluding H, C, and F

3. Mean of n analyses of each standard

4. Standard deviation of n standard analyses

5. CV %: Coefficient of Variation = (standard deviation ÷ mean) × 100

6. % Error: Percent Error = [(mean - accepted value) ÷ accepted value] × 100

7. Normalized Error for apatite, biotite, chlorite, and kaersutite calculated using the normalized accepted value

8. NA: Not analyzed

9. NC: Not calculated because the element was not detected in more than 25% of analyses.

Reference Mineral	Element	Accepted Value <sup>1</sup>	Value Normalized w/o H, C, and F <sup>2</sup>	Mean <sup>3</sup>	Confidence Level (95%)	Standard Deviation <sup>4</sup>	CV % <sup>5</sup>	% Error <sup>6</sup>	Normalized Error <sup>7</sup>
Diopside (n = 11)	Mg	11.23		10.71	0.12	0.19	1.77	-4.63	
	Al	0.05		0.05	0.03	0.05	100.00	0.00	
	Si	25.88		26.53	0.07	0.11	0.41	2.51	
	Ca	18.39		18.00	0.12	0.18	1.00	-2.12	
	Ti	0.05		0.06	0.03	0.05	83.33	20.00	
	Mn	0.04		0.04	0.02	0.02	50.00	0.00	
	Fe	0.04		0.05	0.03	0.05	100.00	25.00	
	O	44.30		44.56	0.03	0.04	0.09	0.59	
Hematite (n = 6)	Mg	0.03		0.13	0.08	0.08	61.54	333.33	
	Al	0.10		0.11	0.07	0.07	63.64	10.00	
	V	0.04		0.05	0.07	0.06	120.00	25.00	
	Fe	69.86		77.35	0.18	0.17	0.22	10.72	
	O	30.06		23.37	0.06	0.06	0.26	-22.26	

1. Values given in weight percent element

2. Accepted values are normalized to dry weight by recalculating total weight % excluding H, C, and F

3. Mean of n analyses of each standard

4. Standard deviation of n standard analyses.

5. CV: Coefficient of Variation = (standard deviation ÷ mean) × 100

6. % Error: Percent error = [(mean - accepted value) ÷ accepted value] × 100

7. Normalized error for apatite, biotite, chlorite, and kaersutite calculated using the normalized accepted value

Reference Mineral	Element	Accepted Value <sup>1</sup>	Value Normalized w/o H, C, and F <sup>2</sup>	Mean <sup>3</sup>	Confidence Level (95%)	Standard Deviation <sup>4</sup>	CV % <sup>5</sup>	% Error <sup>6</sup>	Normalized Error <sup>7</sup>
Kaersutite (n = 11)	H	0.22	NA <sup>8</sup>	NA <sup>8</sup>	NA <sup>8</sup>	NA <sup>8</sup>	NA <sup>8</sup>	NA <sup>8</sup>	NA <sup>8</sup>
	Na	1.81	1.82	1.77	0.04	0.05	2.82	-2.21	-2.81
	Mg	7.57	7.62	7.57	0.11	0.17	2.25	0.00	-0.61
	Al	6.54	6.58	6.65	0.09	0.14	2.11	1.68	1.06
	Si	18.74	18.86	20.05	0.08	0.12	0.60	6.99	6.34
	K	0.97	0.98	0.89	0.02	0.04	4.49	-8.25	-8.81
	Ca	8.26	8.31	8.24	0.09	0.13	1.58	-0.24	-0.85
	Ti	3.02	3.04	3.27	0.08	0.12	3.67	8.28	7.62
	Mn	0.14	0.14	0.10	0.04	0.06	60.00	-28.57	-29.01
	Fe	9.51	9.57	8.87	0.13	0.20	2.25	-6.73	-7.30
O	42.83	43.09	42.58	0.04	0.07	0.16	-0.58	-1.19	

1. Values given in weight percent element

2. Accepted values are normalized to dry weight by recalculating total weight % excluding H, C, and F

3. Mean of n analyses of each standard

4. Standard deviation of n standard analyses.

5. CV: Coefficient of Variation = (standard deviation ÷ mean) × 100

6. % Error: Percent error = [(mean - accepted value) ÷ accepted value] x 100

7. Normalized error for apatite, biotite, chlorite, and kaersutite calculated using the normalized accepted value

8. NA: Not analyzed



Reference Mineral	Element	Accepted Value <sup>1</sup>	Value Normalized w/o H, C, and F <sup>2</sup>	Mean <sup>3</sup>	Confidence Level (95%)	Standard Deviation <sup>4</sup>	CV % <sup>5</sup>	% Error <sup>6</sup>	Normalized Error <sup>7</sup>
Magnetite (n = 8)	Cr	0.14		0.20	0.02	0.03	15.00	42.86	
	Fe	72.19		77.52	0.05	0.06	0.08	7.38	
	O	26.67		22.28	0.05	0.06	0.27	-16.46	
Marcasite (n = 11)	S	53.46		55.11	0.79	1.18	2.14	3.09	
	Fe	46.54		44.89	0.79	1.18	2.63	-3.55	
Pyrope (n = 11)	Mg	11.52		11.85	0.06	0.09	0.76	2.86	
	Al	11.65		11.05	0.10	0.16	1.45	-5.15	
	Si	20.15		20.48	0.09	0.13	0.63	1.64	
	Ca	3.62		3.39	0.04	0.06	1.77	-6.35	
	Cr	1.52		1.77	0.05	0.08	4.52	16.45	
	Mn	0.25		0.29	0.04	0.05	17.24	16.00	
	Fe	6.35		6.19	0.08	0.12	1.94	-2.52	
	O	44.94		44.99	0.04	0.06	0.13	0.11	

1. Values given in weight percent element

2. Accepted values are normalized to dry weight by recalculating total weight % excluding H, C, and F

3. Mean of n analyses of each standard

4. Standard deviation of n standard analyses.

5. CV: Coefficient of Variation = (standard deviation ÷ mean) × 100

6. % Error: Percent error = [(mean - accepted value) ÷ accepted value] × 100

7. Normalized error for apatite, biotite, chlorite, and kaersutite calculated using the normalized accepted value

Reference Mineral	Element	Accepted Value <sup>1</sup>	Value Normalized w/o H, C, and F <sup>2</sup>	Mean <sup>3</sup>	Confidence Level (95%)	Standard Deviation <sup>4</sup>	CV % <sup>5</sup>	% Error <sup>6</sup>	Normalized Error <sup>7</sup>
Rutile (n = 11)	Ti	59.10		59.29	0.16	0.24	0.40	0.32	
	V	0.38		0.24	0.16	0.24	100.00	-36.84	
	Fe	0.66		0.53	0.09	0.13	24.53	-19.70	
	O	39.86		39.94	0.03	0.04	0.10	0.20	
Sanidine (n = 11)	Na	2.23		2.03	0.07	0.11	5.42	-8.97	
	Al	9.93		9.31	0.07	0.10	1.07	-6.24	
	Si	30.23		30.93	0.08	0.12	0.39	2.32	
	K	10.05		10.08	0.09	0.13	1.29	0.30	
	Fe	0.14		0.21	0.03	0.04	19.05	50.00	
	O	46.28		46.46	0.04	0.05	0.11	0.39	

1. Values given in weight percent element

2. Accepted values are normalized to dry weight by recalculating total weight % excluding H, C, and F

3. Mean of n analyses of each standard

4. Standard deviation of n standard analyses.

5. CV: Coefficient of Variation = (standard deviation ÷ mean) × 100

6. % Error: Percent error = [(mean - accepted value) ÷ accepted value] × 100

7. Normalized error for apatite, biotite, chlorite, and kaersutite calculated using the normalized accepted value

## Appendix F2: Replicate-EDX-Analysis Data of Reference Standards

Albite <sup>1</sup>	Na	Al	Si	K	Ca	O
Trial 1	7.86	9.79	33.06	0.11	0.04	49.14
Trial 2	7.67	9.58	33.37	0.12	0.04	49.23
Trial 3	7.68	9.84	33.09	0.15	0.07	49.18
Trial 4	7.71	9.74	33.24	0.07	0.00	49.23
Trial 5	7.84	9.64	33.23	0.03	0.06	49.20
Trial 6	7.69	9.77	33.20	0.07	0.05	49.22
Trial 7	7.75	9.84	33.16	0.00	0.01	49.24
Trial 8	7.73	9.68	33.28	0.08	0.01	49.23
Trial 9	7.78	9.75	33.18	0.04	0.03	49.21

1. Replicate EDX analyses of albite. All concentrations are presented as weight percents

Almandine <sup>1</sup>	Mg	Al	Si	Ca	Mn	Fe	O
Trial 1	6.04	11.02	19.29	2.94	0.51	17.96	42.22
Trial 2	5.70	10.95	19.36	2.95	0.56	18.32	42.15
Trial 3	6.19	11.19	18.96	2.97	0.42	18.14	42.13
Trial 4	5.99	11.40	19.29	2.94	0.36	17.63	42.39
Trial 5	5.86	11.22	19.22	2.95	0.42	18.12	42.22
Trial 6	5.99	11.34	19.30	2.93	0.43	17.63	42.37
Trial 7	5.83	11.22	19.31	2.99	0.40	17.99	42.27
Trial 8	5.90	11.34	19.23	2.96	0.37	17.90	42.30
Trial 9	5.90	11.28	19.41	2.95	0.46	17.62	42.39
Trial 10	5.84	11.36	19.26	2.92	0.43	17.88	42.31
Trial 11	5.95	11.29	19.24	2.98	0.50	17.75	42.29

1. Replicate EDX analyses of almandine. All concentrations are presented as weight percents

Apatite <sup>1</sup>	P	Ca	O
Trial 1	19.84	38.99	41.18
Trial 2	19.33	39.82	40.85
Trial 3	19.74	39.15	41.12
Trial 4	19.64	39.31	41.05
Trial 5	19.66	39.28	41.06
Trial 6	19.60	39.37	41.03
Trial 7	19.54	39.48	40.99
Trial 8	19.48	39.57	40.95
Trial 9	19.56	39.44	41.00
Trial 10	19.54	39.44	41.02

1. Replicate EDX analyses of apatite. All concentrations are presented as weight percents

Benitoite <sup>1</sup>	Si	Ti	Ba	O
Trial 1	20.69	10.98	33.52	34.81
Trial 2	20.43	11.28	33.57	34.72
Trial 3	20.68	11.35	32.98	34.99
Trial 4	20.70	11.30	33.01	34.98
Trial 5	20.71	11.39	32.87	35.03
Trial 6	20.80	10.97	33.32	34.91
Trial 7	20.66	11.00	33.55	34.79
Trial 8	20.73	10.97	33.46	34.84
Trial 9	20.77	10.74	33.71	34.77
Trial 10	20.74	11.91	32.05	35.31
Trial 11	20.76	11.99	31.88	35.37

1. Replicate EDX analyses of benitoite. All concentrations are presented as weight percents

Biotite <sup>1</sup>	Mg	Al	Si	K	Ca	Ti	Mn	Fe	O
Trial 1	12.02	7.85	19.69	8.65	0.29	1.00	0.00	8.26	42.24
Trial 2	11.67	8.15	19.71	8.89	0.29	0.94	0.05	8.05	42.25
Trial 3	11.91	7.96	19.81	8.88	0.12	1.05	0.09	7.85	42.33
Trial 4	11.96	7.92	19.78	8.80	0.20	1.01	0.10	7.91	42.31
Trial 5	12.13	7.95	19.95	8.22	0.45	1.00	0.16	7.62	42.54
Trial 6	12.24	8.07	19.82	8.08	0.45	0.93	0.01	7.85	42.53
Trial 7	12.33	8.06	19.87	8.18	0.43	0.87	0.07	7.62	42.56
Trial 8	11.17	8.10	19.24	9.38	0.06	1.07	0.07	9.23	41.70
Trial 9	12.17	7.86	19.74	8.53	0.37	1.02	0.02	7.95	42.34
Trial 10	12.10	7.80	19.88	8.97	0.16	0.95	0.02	7.80	42.33

1. Replicate EDX analyses of biotite. All concentrations are presented as weight percents

Chlorite <sup>1</sup>	Mg	Al	Si	Ca	Cr	Fe	Ni	O
Trial 1	21.07	11.21	17.63	0.02	1.36	2.70	0.52	45.49
Trial 2	21.58	10.99	17.71	0.10	1.25	2.92	0.36	45.09
Trial 3	20.87	11.27	16.99	ND <sup>2</sup>	1.49	2.61	0.29	46.49
Trial 4	21.37	10.96	17.39	ND <sup>2</sup>	1.28	2.70	0.20	46.09
Trial 5	21.53	11.16	17.40	ND <sup>2</sup>	1.18	2.83	0.21	45.70
Trial 6	21.56	11.24	17.56	0.04	1.31	2.91	0.11	45.27
Trial 7	21.59	11.21	17.45	0.07	1.27	2.92	0.21	45.28
Trial 8	21.56	11.07	17.40	ND <sup>2</sup>	1.33	2.85	0.10	45.68
Trial 9	21.81	11.32	17.48	0.01	1.34	2.81	0.24	44.99
Trial 10	21.23	11.24	17.33	ND <sup>2</sup>	1.09	2.82	0.26	46.03
Trial 11	21.47	11.29	17.66	0.06	1.26	2.82	0.11	45.32

1. Replicate EDX analyses of chlorite. All concentrations are presented as weight percents

2. ND: Not detected

Diopside <sup>1</sup>	Mg	Al	Si	Ca	Ti	Mn	Fe	O
Trial 1	10.64	0.01	26.46	18.27	0.01	0.07	0.08	44.47
Trial 2	10.60	0.16	26.54	17.85	0.13	0.05	0.08	44.60
Trial 3	10.39	0.04	26.49	18.37	0.13	0.08	0.00	44.50
Trial 4	10.65	0.06	26.64	18.01	0.02	0.02	0.05	44.57
Trial 5	10.75	0.04	26.60	17.90	0.05	0.05	0.00	44.61
Trial 6	10.71	0.06	26.56	17.95	0.06	0.06	0.00	44.59
Trial 7	10.71	0.03	26.60	18.01	0.03	0.01	0.03	44.59
Trial 8	10.63	0.08	26.52	17.97	0.09	0.05	0.10	44.56
Trial 9	11.16	0.07	26.25	17.72	0.10	0.03	0.15	44.51
Trial 10	10.78	0.01	26.54	18.02	0.02	0.01	0.07	44.55
Trial 11	10.77	0.01	26.63	17.87	0.01	0.05	0.05	44.60

1. Replicate EDX analyses of diopside. All concentrations are presented as weight percents

Hematite <sup>1</sup>	Mg	Al	V	Fe	O
Trial 1	0.13	0.07	0.02	77.44	22.35
Trial 2	0.27	0.23	0.00	77.05	22.45
Trial 3	0.08	0.11	0.15	77.26	22.40
Trial 4	0.05	0.09	0.10	77.40	22.36
Trial 5	0.10	0.13	0.01	77.40	22.36
Trial 6	0.14	0.03	0.01	77.54	22.28

1. Replicate EDX analyses of hematite. All concentrations are presented as weight percents

Kaersutite <sup>1</sup>	Na	Mg	Al	Si	K	Ca	Ti	Mn	Fe	O
Trial 1	1.74	7.69	6.61	20.08	0.89	8.45	3.17	0.02	8.78	42.58
Trial 2	1.75	7.72	6.61	19.95	0.87	8.19	3.24	0.11	9.02	42.54
Trial 3	1.90	7.40	6.55	20.05	0.95	8.40	3.50	0.04	8.64	42.57
Trial 4	1.76	7.31	6.93	20.22	0.84	8.12	3.29	0.17	8.61	42.75
Trial 5	1.74	7.32	6.82	20.12	0.94	8.00	3.33	0.19	8.90	42.63
Trial 6	1.73	7.71	6.76	19.96	0.87	8.25	3.25	0.05	8.82	42.61
Trial 7	1.72	7.74	6.64	19.95	0.91	8.27	3.34	0.06	8.80	42.58
Trial 8	1.83	7.66	6.64	19.89	0.87	8.26	3.32	0.10	8.93	42.52
Trial 9	1.74	7.66	6.62	20.01	0.85	8.31	3.31	0.11	8.80	42.59
Trial 10	1.79	7.45	6.40	20.28	0.90	8.11	3.04	0.20	9.33	42.51
Trial 11	1.73	7.65	6.59	20.08	0.90	8.29	3.20	0.07	8.95	42.56

1. Replicate EDX analyses of Kaersutite. All concentrations are presented as weight percents

Magnetite <sup>1</sup>	Cr	Fe	O
Trial 1	0.23	77.47	22.30
Trial 2	0.22	77.48	22.30
Trial 3	0.24	77.46	22.30
Trial 4	0.16	77.55	22.29
Trial 5	0.18	77.53	22.29
Trial 6	0.18	77.53	22.29
Trial 7	0.19	77.52	22.29
Trial 8	0.20	77.66	22.14

1. Replicate EDX analyses of magnetite. All concentrations are presented as weight percents

Marcasite <sup>1</sup>	S	Fe
Trial 1	54.43	45.57
Trial 2	53.97	46.03
Trial 3	54.42	45.58
Trial 4	56.87	43.13
Trial 5	56.71	43.29
Trial 6	55.60	44.40
Trial 7	54.88	45.12
Trial 8	54.73	45.27
Trial 9	55.49	44.51
Trial 10	52.99	47.01
Trial 11	56.06	43.94

1. Replicate EDX analyses of marcasite. All concentrations are presented as weight percents

Pyrope <sup>1</sup>	Mg	Al	Si	Ca	Cr	Mn	Fe	O
Trial 1	11.84	10.70	20.64	3.52	1.80	0.16	6.39	44.94
Trial 2	11.77	11.15	20.30	3.38	1.91	0.30	6.27	44.91
Trial 3	11.99	11.02	20.35	3.31	1.87	0.31	6.20	44.94
Trial 4	11.92	11.12	20.45	3.34	1.73	0.27	6.18	45.01
Trial 5	11.90	10.91	20.58	3.40	1.80	0.33	6.06	45.01
Trial 6	11.76	11.10	20.61	3.35	1.75	0.29	6.06	45.07
Trial 7	11.86	11.03	20.52	3.38	1.69	0.32	6.20	44.99
Trial 8	11.94	10.97	20.42	3.37	1.83	0.27	6.24	44.95
Trial 9	11.84	11.23	20.28	3.44	1.74	0.34	6.18	44.94
Trial 10	11.65	11.26	20.62	3.41	1.71	0.25	5.98	45.12
Trial 11	11.87	11.03	20.46	3.39	1.65	0.34	6.30	44.96

1. Replicate EDX analyses of pyrope. All concentrations are presented as weight percents



Rutile <sup>1</sup>	Ti	V	Fe	O
Trial 1	59.16	0.11	0.88	39.86
Trial 2	59.50	0.07	0.50	39.94
Trial 3	59.59	0.03	0.47	39.91
Trial 4	59.38	0.15	0.54	39.94
Trial 5	59.23	0.29	0.53	39.95
Trial 6	59.32	0.27	0.44	39.97
Trial 7	59.40	0.10	0.57	39.93
Trial 8	59.47	0.11	0.48	39.95
Trial 9	59.41	0.10	0.57	39.93
Trial 10	58.91	0.73	0.33	40.02
Trial 11	58.85	0.64	0.53	39.98

1. Replicate EDX analyses of rutile.

All concentrations are presented as weight percents

Sanidine	Na	Al	Si	K	Fe	Ba	O
Trial 1	2.05	9.21	31.08	10.31	0.14	0.68	46.53
Trial 2	2.11	9.09	31.16	10.10	0.27	0.71	46.55
Trial 3	1.78	9.28	30.95	10.26	0.23	1.05	46.44
Trial 4	2.02	9.36	30.85	9.98	0.24	1.14	46.42
Trial 5	2.03	9.45	30.86	9.90	0.16	1.12	46.48
Trial 6	2.13	9.36	30.89	9.95	0.17	1.03	46.47
Trial 7	2.07	9.24	30.95	10.07	0.16	1.07	46.44
Trial 8	2.12	9.40	30.81	10.01	0.26	0.95	46.44
Trial 9	2.11	9.36	30.76	10.13	0.21	1.07	46.36
Trial 10	1.91	9.39	30.94	10.16	0.24	0.84	46.51
Trial 11	1.95	9.26	30.99	9.97	0.21	1.16	46.46

1. Replicate EDX analyses of sanidine. All concentrations are presented as weight percents

**Appendix F3: Eliminated EDX Spectra from Statistical Evaluation of Iron-oxyhydroxide  
Aggregates and Coatings**

Polished- Thin Section Id <sup>1</sup>	Spectrum	Na	Mg	Al	Si	P	S
PTS:9-12	1	0.22	0.22	1.03	5.85	15.01	0.02
PTS:9-12	2	0.10	0.12	0.72	6.43	15.06	0.02
PTS:9-12	3	0.19	0.21	0.71	5.25	15.44	0.16
PTS:9-12	4	0.19	0.20	0.49	5.97	14.99	0.19
PTS:9-12	5	0.06	0.14	1.40	5.23	14.53	0.08
PTS:9-12	6	0.02	0.25	1.23	5.94	14.81	ND <sup>2</sup>
PTS:9-12	7	0.01	0.50	2.64	9.59	12.14	0.10
PTS:9-12	8	0.09	0.21	2.01	6.71	10.68	0.03
PTS:9-12	9	ND <sup>2</sup>	0.13	0.63	5.65	9.49	0.14
PTS:9-12	10	0.39	0.18	2.66	9.12	2.82	11.14
PTS:9-12	11	0.43	0.12	3.57	7.10	3.14	10.95
PTS:9-12	12	0.01	0.15	0.80	20.60	1.35	0.02

1. Elemental concentrations (weight percent) of iron-oxyhydroxide aggregates and coatings for eliminated spectra. These spectra were eliminated from statistical evaluation because they consist of >15 wt. % of one or more elemental constituents (excluding iron and oxygen) and/or these spectra contain <30 wt. % Fe

2. ND: Not detected

Polished- Thin Section Id <sup>1</sup>	Spectrum	Cl	K	Ca	Ti	Mn	Fe	O
PTS:9-12	1	0.87	0.16	33.32	0.20	0.09	1.81	41.21
PTS:9-12	2	0.25	0.03	33.35	0.29	0.09	1.91	41.64
PTS:9-12	3	0.17	0.03	34.07	0.10	0.28	2.06	41.33
PTS:9-12	4	0.19	0.10	33.08	0.26	0.28	2.75	41.33
PTS:9-12	5	0.49	0.41	32.64	1.06	0.12	2.94	40.90
PTS:9-12	6	0.34	0.35	32.07	0.07	0.13	3.66	41.15
PTS:9-12	7	0.63	0.62	26.05	1.52	0.07	4.01	42.13
PTS:9-12	8	0.39	0.61	22.12	0.12	0.24	18.84	37.95
PTS:9-12	9	0.38	0.10	25.99	ND <sup>2</sup>	0.58	20.84	36.08
PTS:9-12	10	0.32	4.49	1.42	0.51	ND <sup>2</sup>	24.73	42.23
PTS:9-12	11	0.39	4.85	1.84	0.56	ND <sup>2</sup>	25.68	41.39
PTS:9-12	12	0.25	0.18	1.93	0.35	0.31	36.44	37.62

1. Elemental concentrations (weight percent) of iron-oxyhydroxide aggregates and coatings for eliminated spectra. These spectra were eliminated from statistical evaluation because they consist of >15 wt. % of one or more elemental constituents (excluding iron and oxygen) and/or these spectra contain <30 wt. % Fe

2. ND: Not detected

Polished- Thin Section Id <sup>1</sup>	Spectrum	Na	Mg	Al	Si	P	S
PTS:9-12	13	0.02	0.20	0.38	18.23	0.88	0.05
PTS:13-14	14	0.52	0.19	0.78	4.86	15.43	0.26
PTS:13-14	15	0.38	0.28	0.93	5.54	13.08	0.22
PTS:13-14	16	0.15	0.70	4.40	14.63	0.45	ND <sup>2</sup>
PTS:13-14	17	0.04	0.56	4.73	15.31	0.40	ND <sup>2</sup>
PTS:13-14	18	0.17	0.64	4.86	20.41	0.49	0.08
PTS:13-14	19	0.18	0.42	1.75	9.58	8.90	0.07
PTS:13-14	20	0.15	1.02	8.02	21.38	0.53	0.11
PTS:15-16	21	0.05	0.38	0.57	2.99	0.21	0.06
PTS:15-16	22	ND <sup>2</sup>	0.74	5.11	17.74	1.02	0.02
PTS:15-16	23	0.25	0.42	6.18	15.58	0.77	0.07
PTS:26-28	24	ND <sup>2</sup>	11.69	0.44	2.45	0.03	0.37

1. Elemental concentrations (weight percent) of iron-oxyhydroxide aggregates and coatings for eliminated spectra. These spectra were eliminated from statistical evaluation because they consist of >15 wt. % of one or more elemental constituents (excluding iron and oxygen) and/or these spectra contain <30 wt. % Fe

2. ND: Not detected

Polished- Thin Section Id <sup>1</sup>	Spectrum	Cl	K	Ca	Ti	Mn	Fe	O
PTS:9-12	13	0.28	0.05	0.93	0.29	0.38	42.91	35.42
PTS:13-14	14	0.23	0.09	33.76	0.03	0.30	2.42	41.14
PTS:13-14	15	0.35	0.12	28.47	ND <sup>2</sup>	0.30	11.01	39.31
PTS:13-14	16	0.56	1.03	2.99	1.04	27.56	11.41	35.07
PTS:13-14	17	0.48	1.19	2.72	0.87	25.94	12.24	35.52
PTS:13-14	18	0.75	1.24	2.33	0.79	15.72	13.56	38.98
PTS:13-14	19	0.88	0.41	17.61	0.38	0.22	21.56	38.03
PTS:13-14	20	0.64	2.17	1.69	0.65	0.25	22.31	41.08
PTS:15-16	21	0.14	0.23	0.43	29.67	0.61	31.03	33.64
PTS:15-16	22	0.39	0.53	2.39	0.23	0.42	33.77	37.62
PTS:15-16	23	0.39	2.55	1.21	0.26	0.99	35.08	36.23
PTS:26-28	24	0.30	0.42	23.75	1.95	0.87	27.31	30.42

1. Elemental concentrations (weight percent) of iron-oxyhydroxide aggregates and coatings for eliminated spectra. These spectra were eliminated from statistical evaluation because they consist of >15 wt. % of one or more elemental constituents (excluding iron and oxygen) and/or these spectra contain <30 wt. % Fe

2. ND: Not detected

**Appendix F4: Elemental Concentrations Measured from Iron-oxyhydroxide Aggregates and Coatings**

Polished-Thin Section Id <sup>1</sup>	Spectrum	Na	Mg	Al	Si	P	S
PTS:9-12	1	0.10	0.42	1.45	9.03	5.10	ND <sup>2</sup>
PTS:9-12	2	0.35	0.11	1.87	7.06	12.67	ND <sup>2</sup>
PTS:9-12	3	0.42	0.09	1.38	6.70	13.26	0.02
PTS:9-12	4	0.34	0.18	0.75	5.08	13.46	ND <sup>2</sup>
PTS:9-12	5	0.31	0.28	2.09	11.96	1.82	0.16
PTS:9-12	6	0.14	0.27	4.17	11.20	2.21	0.16
PTS:9-12	7	0.40	0.54	3.85	12.67	0.55	0.04
PTS:9-12	8	0.30	0.33	1.59	11.42	1.80	ND <sup>2</sup>
PTS:9-12	9	0.09	0.15	0.60	11.61	2.10	0.05
PTS:9-12	10	0.20	0.38	1.93	10.59	1.61	0.11
PTS:9-12	11	0.09	0.08	1.19	8.44	2.21	ND <sup>2</sup>
PTS:9-12	12	0.21	0.09	0.92	9.14	2.58	0.10
PTS:9-12	13	0.15	0.14	0.63	11.13	1.66	ND <sup>2</sup>
PTS:9-12	14	0.12	0.10	0.49	11.57	0.95	ND <sup>2</sup>
PTS:9-12	15	0.06	0.19	0.87	10.42	0.99	0.04
PTS:9-12	16	0.19	0.10	0.47	10.54	0.85	0.08
PTS:9-12	17	ND <sup>2</sup>	0.12	0.50	10.49	0.79	0.00
PTS:9-12	18	ND <sup>2</sup>	ND <sup>2</sup>	0.51	7.64	2.12	0.03
PTS:9-12	19	0.24	0.20	1.75	6.00	1.93	0.03
PTS:9-12	20	0.07	0.25	1.09	6.75	0.96	0.05

1. Elemental concentrations (weight percent) of iron-oxyhydroxide aggregates and coatings for evaluated spectra

2. ND: Not detected

Polished- Thin Section Id <sup>1</sup>	Spectrum	Cl	K	Ca	Ti	Mn	Fe	O
PTS:9-12	1	0.67	0.29	10.40	0.46	0.31	37.86	33.92
PTS:9-12	2	0.17	0.48	0.86	0.21	0.12	38.28	37.84
PTS:9-12	3	0.37	0.36	0.96	0.18	ND <sup>2</sup>	38.46	37.81
PTS:9-12	4	0.50	0.26	1.07	0.29	0.00	41.43	36.62
PTS:9-12	5	0.54	0.48	3.06	0.29	0.98	44.99	33.04
PTS:9-12	6	0.47	0.41	1.67	0.19	ND <sup>2</sup>	45.42	33.68
PTS:9-12	7	0.26	0.79	1.12	0.18	0.24	46.22	33.15
PTS:9-12	8	1.18	0.54	2.83	0.24	0.18	47.48	32.12
PTS:9-12	9	0.36	0.18	3.60	0.09	0.65	48.29	32.23
PTS:9-12	10	0.34	0.38	2.17	0.22	0.53	49.74	31.83
PTS:9-12	11	1.34	0.20	3.89	0.42	0.90	50.91	30.33
PTS:9-12	12	0.28	0.16	3.88	0.14	0.01	51.30	31.20
PTS:9-12	13	0.30	0.06	2.09	0.38	0.30	51.64	31.52
PTS:9-12	14	0.27	0.09	0.89	0.41	0.59	53.43	31.08
PTS:9-12	15	0.33	0.19	1.49	0.16	0.67	54.07	30.54
PTS:9-12	16	0.14	0.05	1.11	0.35	0.40	55.31	30.42
PTS:9-12	17	0.29	ND <sup>2</sup>	1.26	0.33	0.44	55.52	30.26
PTS:9-12	18	0.11	0.04	2.73	0.04	0.21	57.08	29.48
PTS:9-12	19	0.63	0.17	1.07	0.17	ND <sup>2</sup>	59.16	28.66
PTS:9-12	20	0.44	0.25	1.74	0.26	0.47	59.42	28.24

1. Elemental concentrations (weight percent) of iron-oxyhydroxide aggregates and coatings for evaluated spectra

2. ND: Not detected.

Polished- Thin Section Id <sup>1</sup>	Spectrum	Na	Mg	Al	Si	P	S
PTS:9-12	21	0.05	0.23	0.89	6.51	1.50	0.01
PTS:9-12	22	0.11	0.13	0.65	6.45	1.58	ND <sup>2</sup>
PTS:9-12	23	0.15	ND <sup>2</sup>	0.50	7.56	0.35	0.05
PTS:9-12	24	0.15	0.07	0.81	3.49	2.84	0.03
PTS:13-14	25	0.20	0.34	1.89	10.40	2.90	ND <sup>2</sup>
PTS:13-14	26	0.15	0.21	1.29	13.71	1.93	ND <sup>2</sup>
PTS:13-14	27	0.27	0.19	1.24	11.10	2.72	0.06
PTS:13-14	28	0.28	0.26	1.21	8.37	2.21	0.05
PTS:13-14	29	0.08	0.01	0.31	11.55	1.79	0.05
PTS:13-14	30	0.05	0.32	2.51	8.10	2.03	0.04
PTS:13-14	31	0.03	0.13	0.40	10.22	0.82	ND <sup>2</sup>
PTS:13-14	32	0.51	0.01	0.75	10.17	1.29	ND <sup>2</sup>
PTS:13-14	33	0.33	0.16	1.63	9.21	1.29	ND <sup>2</sup>
PTS:13-14	34	ND <sup>2</sup>	0.24	0.70	10.15	1.47	ND <sup>2</sup>
PTS:13-14	35	0.35	0.16	0.85	9.34	1.12	0.02
PTS:13-14	36	0.04	0.09	0.71	7.30	1.80	ND <sup>2</sup>
PTS:13-14	37	0.20	0.09	0.49	8.49	1.90	0.01
PTS:13-14	38	0.17	0.04	0.55	8.93	1.17	0.03
PTS:13-14	39	0.14	0.11	0.78	8.77	1.18	ND <sup>2</sup>
PTS:13-14	40	0.08	0.10	0.56	5.58	1.07	0.07

1. Elemental concentrations (weight percent) of iron-oxyhydroxide aggregates and coatings for evaluated spectra.

2. ND: Not detected



Polished- Thin Section Id <sup>1</sup>	Spectrum	Cl	K	Ca	Ti	Mn	Fe	O
PTS:9-12	21	0.30	0.25	1.93	0.09	0.16	59.74	28.36
PTS:9-12	22	0.20	0.20	2.00	0.08	0.17	60.16	28.27
PTS:9-12	23	0.32	0.16	0.38	0.17	0.26	62.28	27.84
PTS:9-12	24	0.21	0.22	1.72	0.12	0.12	62.87	27.37
PTS:13-14	25	0.41	0.49	5.21	0.09	0.70	44.59	32.78
PTS:13-14	26	0.50	0.22	2.87	0.10	0.04	45.30	33.69
PTS:13-14	27	0.29	0.32	4.88	0.03	0.37	45.74	32.80
PTS:13-14	28	0.48	0.25	4.04	1.21	1.78	49.02	30.84
PTS:13-14	29	0.28	0.11	3.08	ND <sup>2</sup>	0.28	50.73	31.72
PTS:13-14	30	0.25	0.63	3.41	0.14	0.11	51.66	30.77
PTS:13-14	31	0.23	0.04	1.54	2.90	0.44	52.40	30.85
PTS:13-14	32	0.35	ND <sup>2</sup>	2.06	0.21	0.68	53.41	30.56
PTS:13-14	33	0.34	0.53	1.99	0.31	0.37	53.48	30.37
PTS:13-14	34	0.87	0.13	1.93	0.09	0.25	53.65	30.53
PTS:13-14	35	0.54	0.21	1.72	0.46	0.50	54.74	29.97
PTS:13-14	36	0.82	0.13	3.27	0.29	1.24	55.27	29.06
PTS:13-14	37	0.28	0.08	2.85	0.05	0.17	55.53	29.85
PTS:13-14	38	0.37	0.02	1.93	0.19	1.42	55.62	29.56
PTS:13-14	39	0.31	0.05	1.85	0.06	1.29	55.93	29.52
PTS:13-14	40	0.43	ND <sup>2</sup>	3.50	0.13	2.88	58.17	27.43

1. Elemental concentrations (weight percent) of iron-oxyhydroxide aggregates and coatings for evaluated spectra

2. ND: Not detected.

Polished- Thin Section Id <sup>1</sup>	Spectrum	Na	Mg	Al	Si	P	S
PTS:13-14	41	0.05	0.18	0.45	7.94	0.91	ND <sup>2</sup>
PTS:13-14	42	0.17	0.14	0.36	6.74	1.06	0.06
PTS:13-14	43	0.26	0.26	0.35	7.03	1.46	0.05
PTS:13-14	44	ND <sup>2</sup>	0.04	0.26	7.38	1.04	0.19
PTS:13-14	45	0.15	0.11	0.73	6.59	0.96	ND <sup>2</sup>
PTS:13-14	46	0.29	0.05	0.34	3.22	0.37	0.28
PTS:15-16	47	0.14	0.66	2.62	9.39	0.42	0.11
PTS:15-16	48	0.23	1.29	2.65	10.42	0.30	0.09
PTS:15-16	49	0.14	0.27	1.49	10.07	1.96	0.06
PTS:15-16	50	0.19	0.16	0.44	8.01	1.82	0.04
PTS:15-16	51	0.08	0.28	1.52	12.24	1.35	0.02
PTS:15-16	52	0.12	0.03	0.38	12.85	1.29	0.04
PTS:15-16	53	0.19	0.34	1.98	10.73	1.30	0.04
PTS:15-16	54	0.42	0.31	1.42	10.62	1.40	ND <sup>2</sup>
PTS:15-16	55	0.10	0.25	1.57	11.08	1.21	0.08
PTS:15-16	56	0.05	0.25	1.61	11.03	1.13	ND <sup>2</sup>
PTS:15-16	57	0.40	0.10	0.26	7.45	1.88	0.05
PTS:15-16	58	0.14	0.12	0.60	10.32	1.85	0.07
PTS:15-16	59	0.12	0.22	0.42	11.61	1.51	ND <sup>2</sup>
PTS:15-16	60	0.25	0.25	1.14	10.25	1.21	0.03

1. Elemental concentrations (weight percent) of iron-oxyhydroxide aggregates and coatings for evaluated spectra.

2. ND: Not detected

Polished- Thin Section Id <sup>1</sup>	Spectrum	Cl	K	Ca	Ti	Mn	Fe	O
PTS:13-14	41	0.26	0.03	1.19	0.68	1.14	58.42	28.76
PTS:13-14	42	0.46	0.07	2.01	0.02	2.33	58.64	27.93
PTS:13-14	43	0.31	ND <sup>2</sup>	1.81	0.32	0.74	58.86	28.56
PTS:13-14	44	0.28	ND <sup>2</sup>	1.56	0.17	0.10	60.57	28.41
PTS:13-14	45	0.25	0.04	1.80	0.14	0.36	60.96	27.91
PTS:13-14	46	0.23	0.10	0.86	0.12	0.32	68.61	25.20
PTS:15-16	47	0.26	0.61	0.96	11.21	0.30	39.66	33.66
PTS:15-16	48	0.47	0.51	5.56	0.13	1.17	45.67	31.51
PTS:15-16	49	0.66	0.37	3.19	0.03	2.93	47.38	31.44
PTS:15-16	50	0.47	0.15	9.73	0.05	1.03	47.85	30.05
PTS:15-16	51	0.58	0.49	2.11	0.09	0.36	48.59	32.30
PTS:15-16	52	0.42	ND <sup>2</sup>	1.76	0.22	0.87	49.88	32.15
PTS:15-16	53	0.45	0.47	1.99	0.38	0.29	50.23	31.62
PTS:15-16	54	0.44	0.58	2.26	0.19	0.79	50.26	31.30
PTS:15-16	55	0.34	0.22	1.91	0.24	0.86	50.55	31.60
PTS:15-16	56	0.29	0.46	2.14	0.27	0.63	50.70	31.46
PTS:15-16	57	0.60	0.04	7.12	0.03	1.72	50.97	29.39
PTS:15-16	58	0.35	0.23	3.21	0.32	0.41	51.13	31.23
PTS:15-16	59	0.35	0.11	2.24	ND <sup>2</sup>	0.42	51.48	31.52
PTS:15-16	60	0.25	0.07	2.43	0.23	1.34	51.67	30.88

1. Elemental concentrations (weight percent) of iron-oxyhydroxide aggregates and coatings for evaluated spectra

2. ND: Not detected.

Polished- Thin Section Id <sup>1</sup>	Spectrum	Na	Mg	Al	Si	P	S
PTS:15-16	61	0.21	0.21	1.38	10.46	1.15	0.05
PTS:15-16	62	0.28	0.31	0.77	9.46	1.73	0.08
PTS:15-16	63	0.19	0.21	1.01	10.10	1.52	0.01
PTS:15-16	64	0.20	0.15	0.44	9.95	1.66	0.12
PTS:15-16	65	0.24	0.18	0.93	10.00	1.52	ND <sup>2</sup>
PTS:15-16	66	0.02	0.19	1.43	10.42	0.88	0.08
PTS:15-16	67	0.30	0.33	0.91	9.47	1.24	0.06
PTS:15-16	68	0.14	0.36	1.74	9.80	1.14	0.16
PTS:15-16	69	0.34	0.18	0.81	9.61	1.37	0.01
PTS:15-16	70	0.17	0.18	0.88	9.50	1.18	0.05
PTS:15-16	71	0.26	0.17	0.48	9.21	1.58	ND <sup>2</sup>
PTS:15-16	72	0.06	0.18	0.79	8.93	1.28	ND <sup>2</sup>
PTS:15-16	73	0.04	0.23	1.16	9.41	0.98	0.10
PTS:15-16	74	0.22	0.20	1.41	8.84	0.97	0.01
PTS:15-16	75	0.17	0.02	0.39	8.69	1.42	0.01
PTS:15-16	76	0.12	0.23	0.75	7.80	1.18	0.04
PTS:15-16	77	0.22	0.31	1.02	8.20	1.03	0.05
PTS:15-16	78	0.13	0.23	0.56	8.22	1.45	ND <sup>2</sup>
PTS:15-16	79	0.17	0.17	1.07	8.61	0.74	0.04
PTS:15-16	80	0.27	0.18	1.25	7.39	0.80	0.03

1. Elemental concentrations (weight percent) of iron-oxyhydroxide aggregates and coatings for evaluated spectra.

2. ND: Not detected

Polished- Thin Section Id <sup>1</sup>	Spectrum	Cl	K	Ca	Ti	Mn	Fe	O
PTS:15-16	61	0.32	0.11	1.71	0.11	1.24	52.08	30.97
PTS:15-16	62	0.66	0.31	2.41	0.18	1.13	52.14	30.53
PTS:15-16	63	0.45	0.25	2.01	0.09	1.02	52.33	30.80
PTS:15-16	64	0.33	0.07	3.26	ND <sup>2</sup>	0.66	52.42	30.74
PTS:15-16	65	0.67	0.23	2.18	0.29	0.48	52.60	30.70
PTS:15-16	66	0.28	0.23	1.67	0.25	0.61	53.13	30.81
PTS:15-16	67	0.79	0.44	1.66	0.38	0.90	53.33	30.17
PTS:15-16	68	0.37	0.40	1.23	0.15	0.34	53.41	30.77
PTS:15-16	69	0.47	0.06	1.50	0.23	0.75	54.40	30.26
PTS:15-16	70	0.46	0.25	1.78	0.18	0.65	54.62	30.10
PTS:15-16	71	0.38	0.06	2.47	ND <sup>2</sup>	0.62	54.73	30.03
PTS:15-16	72	0.45	0.22	2.18	0.15	1.21	54.83	29.73
PTS:15-16	73	0.26	0.37	1.12	0.74	0.42	54.97	30.21
PTS:15-16	74	0.42	0.21	1.59	0.82	0.41	54.98	29.90
PTS:15-16	75	0.59	0.12	1.77	0.42	0.73	56.19	29.48
PTS:15-16	76	0.27	0.06	2.70	0.42	0.80	56.51	29.13
PTS:15-16	77	0.42	0.24	2.01	0.08	0.59	56.59	29.23
PTS:15-16	78	0.28	0.20	2.09	0.34	0.42	56.68	29.40
PTS:15-16	79	0.36	0.25	1.37	0.13	0.20	57.66	29.22
PTS:15-16	80	0.18	0.27	0.93	0.15	0.46	59.57	28.53

1. Elemental concentrations (weight percent) of iron-oxyhydroxide aggregates and coatings for evaluated spectra

2. ND: Not detected.

Polished- Thin Section Id <sup>1</sup>	Spectrum	Na	Mg	Al	Si	P	S
PTS:15-16	81	0.29	0.07	0.58	7.59	0.92	0.17
PTS:15-16	82	0.23	0.13	0.55	7.55	0.74	ND <sup>2</sup>
PTS:15-16	83	0.15	0.22	0.82	7.09	0.95	ND <sup>2</sup>
PTS:15-16	84	0.11	0.23	0.78	6.92	0.85	0.01
PTS:15-16	85	0.16	0.46	0.49	4.23	0.77	0.20
PTS:15-16	86	0.33	0.18	0.40	4.70	0.75	0.26
PTS:15-16	87	ND <sup>2</sup>	0.16	0.47	5.75	0.78	0.16
PTS:26-28	88	0.23	3.85	0.66	3.01	0.38	0.29
PTS:26-28	89	0.20	0.84	2.00	6.31	0.34	0.29
PTS:26-28	90	0.12	1.66	0.93	3.76	1.27	0.20
PTS:26-28	91	0.46	1.32	0.71	3.07	0.36	0.50
PTS:26-28	92	0.03	1.38	1.72	3.70	0.43	0.32
PTS:26-28	93	0.13	1.88	0.60	2.22	0.43	0.22
PTS:26-28	94	0.32	0.93	0.24	9.38	1.35	0.68
PTS:26-28	95	0.24	1.68	0.43	2.14	0.30	0.29
PTS:26-28	96	0.15	1.77	0.61	2.12	0.45	0.28
PTS:26-28	97	0.19	1.63	1.51	2.85	0.49	0.22
PTS:26-28	98	0.26	0.27	0.67	9.83	0.73	0.05
PTS:26-28	99	ND <sup>2</sup>	0.23	0.60	7.17	0.96	0.09
PTS:26-28	100	0.24	0.16	0.48	6.66	0.91	0.19

1. Elemental concentrations (weight percent) of iron-oxyhydroxide aggregates and coatings for evaluated spectra.

2. ND: Not detected

Polished- Thin Section Id <sup>1</sup>	Spectrum	Cl	K	Ca	Ti	Mn	Fe	O
PTS:15-16	81	0.04	0.07	1.37	0.08	0.57	59.64	28.62
PTS:15-16	82	0.24	0.09	1.37	0.21	0.47	60.14	28.28
PTS:15-16	83	0.12	0.16	0.96	0.04	0.62	60.63	28.23
PTS:15-16	84	0.24	0.27	0.86	0.13	0.57	61.02	28.01
PTS:15-16	85	0.25	0.13	4.23	ND <sup>2</sup>	0.71	61.84	26.54
PTS:15-16	86	0.27	0.13	3.68	ND <sup>2</sup>	0.66	61.92	26.73
PTS:15-16	87	0.22	0.06	0.99	0.06	0.41	63.75	27.17
PTS:26-28	88	0.40	0.54	10.17	1.22	2.40	49.44	27.41
PTS:26-28	89	0.49	0.99	5.78	0.90	2.13	50.95	28.79
PTS:26-28	90	0.39	0.41	7.90	1.52	2.18	51.75	27.91
PTS:26-28	91	0.37	0.38	7.01	3.47	2.68	52.33	27.34
PTS:26-28	92	0.49	0.50	7.22	1.57	2.49	52.61	27.53
PTS:26-28	93	0.30	0.22	8.40	2.96	2.34	53.63	26.66
PTS:26-28	94	0.48	0.30	1.06	0.79	ND <sup>2</sup>	53.70	30.77
PTS:26-28	95	0.36	0.34	7.76	3.15	2.32	54.57	26.42
PTS:26-28	96	0.47	0.21	8.11	2.45	1.90	55.06	26.42
PTS:26-28	97	0.37	0.27	7.54	0.55	2.57	55.15	26.67
PTS:26-28	98	0.21	0.28	1.26	0.65	0.28	55.46	30.05
PTS:26-28	99	0.22	0.31	1.40	0.71	0.65	59.18	28.47
PTS:26-28	100	0.16	0.31	1.19	0.48	0.47	60.71	28.05

1. Elemental concentrations (weight percent) of iron-oxyhydroxide aggregates and coatings for evaluated spectra

2. ND: Not detected.

### Appendix F5: Mineral Chemistry Data

Polished-Thin Section ID <sup>1</sup>	Mineral	O	Na	Al	Si	K
PTS:2-5	Alkali Feldspar	50.38	ND <sup>2</sup>	8.89	28.88	11.85
PTS:2-5	Alkali Feldspar	48.65	ND <sup>2</sup>	9.12	29.63	12.60
PTS:2-5	Alkali Feldspar	50.33	ND <sup>2</sup>	8.95	28.71	12.01
PTS:2-5	Alkali Feldspar	50.33	0.67	8.78	28.96	11.25
PTS:15-16	Alkali Feldspar	55.21	0.36	8.04	25.95	10.44
PTS:26-28	Alkali Feldspar	48.08	0.57	9.42	30.06	11.87

1. Concentrations (weight percent) of elements comprising alkali feldspar

2. ND: Not detected



Polished-Thin Section ID <sup>1</sup>	Mineral	O	Mg	Al	Si	Ca	Ti	Mn	Fe
PTS:9-12	Almandine	44.47	2.07	9.98	17.53	1.01	ND <sup>2</sup>	2.12	22.82
PTS:9-12	Almandine	44.55	1.52	10.22	16.83	0.71	ND <sup>2</sup>	6.00	20.17
PTS:9-12	Almandine	45.03	0.77	9.46	16.92	4.54	ND <sup>2</sup>	8.59	14.69
PTS:9-12	Almandine	44.68	1.21	9.91	17.34	0.87	ND <sup>2</sup>	2.48	23.51
PTS:13-14	Almandine	45.07	1.16	9.37	17.08	3.87	ND <sup>2</sup>	0.83	22.63
PTS:13-14	Almandine	44.80	1.48	9.82	16.81	0.00	ND <sup>2</sup>	3.40	23.68
PTS:13-14	Almandine	44.61	0.66	9.42	16.98	1.23	ND <sup>2</sup>	11.96	15.13
PTS:17-19	Almandine	40.46	1.50	10.78	18.34	2.05	1.08	4.60	21.20
PTS:17-19	Almandine	40.50	2.32	10.96	18.03	0.90	1.24	3.08	22.96
PTS:17-19	Almandine	40.61	2.37	10.76	18.30	1.64	0.96	2.59	22.77
PTS:17-19	Almandine	41.68	4.31	10.94	19.22	2.19	0.33	0.94	20.40
PTS:17-19	Almandine	41.18	3.90	10.91	18.53	0.87	1.06	0.78	22.78
PTS:17-19	Almandine	40.27	1.01	10.33	17.98	4.35	1.90	1.55	22.61
PTS:17-19	Almandine	40.83	2.23	10.54	18.50	4.58	1.04	1.04	21.24
PTS:23-25	Almandine	44.75	1.14	9.42	16.03	4.30	2.19	0.72	21.46
PTS:23-25	Almandine	44.93	0.58	9.60	16.02	2.69	1.87	7.23	17.08
PTS:23-25	Almandine	45.05	1.46	9.43	15.91	0.58	1.78	1.86	23.94
PTS:23-25	Almandine	45.74	4.13	9.71	16.22	3.41	2.71	0.54	17.53
PTS:23-25	Almandine	47.83	5.45	9.51	15.84	0.86	2.51	ND <sup>2</sup>	18.01
PTS:23-25	Almandine	46.13	4.20	9.74	16.47	1.17	2.42	1.07	18.79
PTS:23-25	Almandine	44.94	1.65	9.40	16.29	4.22	2.60	0.56	20.35
PTS:23-25	Almandine	44.72	0.76	9.44	16.45	3.98	1.77	0.74	22.14
PTS:23-25	Almandine	44.45	0.73	9.89	15.76	0.82	1.81	4.13	22.40
PTS:23-25	Almandine	44.82	1.60	9.40	16.05	1.04	2.01	4.45	20.62

1. Concentrations (weight percent) of elements comprising almandine

2. ND: Not detected

Polished-Thin Section ID <sup>1</sup>	Mineral	O	Na	Mg	Al	Si	Cl	K	Ca	Ti	Fe
PTS:2-5	Amphibole	51.37	ND <sup>2</sup>	1.67	5.95	19.60	ND <sup>2</sup>	3.65	ND <sup>2</sup>	2.76	15.00
PTS:2-5	Amphibole	52.46	ND <sup>2</sup>	1.47	7.81	20.38	ND <sup>2</sup>	2.65	ND <sup>2</sup>	1.91	13.32
PTS:2-5	Amphibole	49.00	0.80	6.86	4.47	19.90	ND <sup>2</sup>	0.72	6.83	2.26	9.16
PTS:2-5	Amphibole	47.46	0.75	5.14	5.48	18.50	ND <sup>2</sup>	0.70	6.78	2.76	12.42
PTS:2-5	Amphibole	48.81	1.28	7.15	6.49	18.64	ND <sup>2</sup>	0.53	6.53	2.53	8.03
PTS:2-5	Amphibole	49.69	ND <sup>2</sup>	9.92	1.12	22.92	ND <sup>2</sup>	ND <sup>2</sup>	7.08	3.38	5.90
PTS:2-5	Amphibole	49.47	0.68	9.29	3.38	22.77	ND <sup>2</sup>	ND <sup>2</sup>	7.22	1.63	5.56
PTS:2-5	Amphibole	49.18	0.91	9.69	2.56	23.85	ND <sup>2</sup>	ND <sup>2</sup>	6.92	1.17	5.73
PTS:2-5	Amphibole	54.72	1.26	3.65	15.81	17.26	ND <sup>2</sup>	ND <sup>2</sup>	0.52	1.71	5.07
PTS:2-5	Amphibole	49.23	0.54	9.79	2.51	22.23	ND <sup>2</sup>	ND <sup>2</sup>	6.96	2.77	5.97
PTS:9-12	Amphibole	48.38	0.91	6.37	5.63	19.68	ND <sup>2</sup>	0.88	7.19	0.55	10.41
PTS:9-12	Amphibole	48.00	0.94	5.79	5.22	18.62	ND <sup>2</sup>	1.14	6.94	1.54	11.80
PTS:17-19	Amphibole	42.97	1.37	7.01	7.00	21.34	0.19	0.28	7.72	1.45	10.67
PTS:23-25	Amphibole	47.96	1.12	5.30	5.45	17.68	ND <sup>2</sup>	1.23	6.35	2.81	12.09
PTS:23-25	Amphibole	47.39	1.03	5.49	5.60	17.84	ND <sup>2</sup>	1.19	6.64	3.13	11.69
PTS:23-25	Amphibole	46.03	1.13	5.40	4.41	18.37	0.91	1.17	6.74	3.55	12.29
PTS:23-25	Amphibole	48.55	1.03	5.76	5.23	17.37	ND <sup>2</sup>	1.09	6.42	3.49	11.05

1. Concentrations (weight percent) of elements comprising amphiboles

2. ND: Not detected

Polished-Thin Section ID <sup>1</sup>	Mineral	O	Na	Mg	Al	Si	Cl	K	Ca	Ti	Fe
PTS:23-25	Amphibole	47.92	1.04	5.46	5.08	17.90	ND <sup>2</sup>	1.08	6.46	2.93	12.14
PTS:23-25	Amphibole	45.30	1.09	5.42	4.45	17.53	ND <sup>2</sup>	1.08	6.70	4.38	14.05
PTS:23-25	Amphibole	46.40	1.02	3.40	5.27	17.57	ND <sup>2</sup>	1.07	6.66	2.44	16.16
PTS:23-25	Amphibole	47.50	1.26	5.53	5.86	17.87	ND <sup>2</sup>	1.05	6.78	2.53	11.61
PTS:23-25	Amphibole	47.80	1.30	5.91	4.48	17.75	ND <sup>2</sup>	0.96	6.12	3.31	12.37
PTS:23-25	Amphibole	47.51	1.06	5.85	5.04	17.84	ND <sup>2</sup>	0.95	6.60	3.12	12.03
PTS:23-25	Amphibole	47.63	0.89	5.31	5.52	18.29	ND <sup>2</sup>	0.90	6.82	2.46	12.17
PTS:23-25	Amphibole	47.81	0.98	5.90	4.61	18.13	ND <sup>2</sup>	0.80	6.77	3.07	11.94
PTS:23-25	Amphibole	47.90	0.91	5.63	4.78	18.22	ND <sup>2</sup>	0.80	6.76	2.74	12.27
PTS:23-25	Amphibole	46.81	1.15	5.90	3.92	18.10	0.55	0.77	6.40	3.69	12.71
PTS:23-25	Amphibole	47.51	1.38	6.26	6.01	17.35	ND <sup>2</sup>	0.76	6.48	4.10	10.15
PTS:23-25	Amphibole	48.07	1.32	6.72	5.46	18.20	ND <sup>2</sup>	0.76	6.76	2.64	10.07
PTS:23-25	Amphibole	47.65	0.99	4.57	5.79	17.51	ND <sup>2</sup>	0.76	6.73	2.72	13.29
PTS:23-25	Amphibole	48.35	1.18	6.57	5.60	18.06	ND <sup>2</sup>	0.72	6.34	3.46	9.71
PTS:23-25	Amphibole	47.67	0.92	4.60	5.65	17.56	ND <sup>2</sup>	0.68	6.70	2.57	13.64
PTS:23-25	Amphibole	47.15	1.48	5.21	6.23	17.67	0.88	0.67	6.11	2.46	12.14
PTS:23-25	Amphibole	47.61	1.77	5.46	5.87	16.58	0.51	0.66	6.11	3.90	11.52
PTS:23-25	Amphibole	47.32	1.23	3.55	6.61	17.29	ND <sup>2</sup>	0.59	6.55	2.67	14.18

1. Concentrations (weight percent) of elements comprising amphiboles

2. ND: Not detected

Polished-Thin Section ID <sup>1</sup>	Mineral	O	Na	Mg	Al	Si	Cl	K	Ca	Ti	Fe
PTS:23-25	Amphibole	47.79	1.10	4.18	6.02	16.91	ND <sup>2</sup>	0.50	6.49	3.32	13.69
PTS:23-25	Amphibole	46.28	0.79	5.59	15.95	19.87	0.22	0.16	5.29	1.60	4.25
PTS:23-25	Amphibole	47.00	ND <sup>2</sup>	0.25	10.73	16.33	0.14	ND <sup>2</sup>	13.38	2.41	9.75
PTS:23-25	Amphibole	48.05	1.13	5.43	6.51	18.29	ND <sup>2</sup>	ND <sup>2</sup>	6.59	2.51	11.49
PTS:23-25	Amphibole	48.49	1.15	7.22	6.39	18.56	ND <sup>2</sup>	ND <sup>2</sup>	6.38	2.60	9.22
PTS:23-25	Amphibole	48.21	0.64	7.99	4.23	20.42	ND <sup>2</sup>	ND <sup>2</sup>	7.29	2.22	9.00
PTS:23-25	Amphibole	47.75	0.93	6.47	5.02	19.17	ND <sup>2</sup>	ND <sup>2</sup>	6.53	2.60	11.52
PTS:23-25	Amphibole	47.21	0.71	6.43	5.11	19.84	ND <sup>2</sup>	ND <sup>2</sup>	7.12	2.98	10.60
PTS:23-25	Amphibole	47.87	1.67	6.40	5.72	18.64	ND <sup>2</sup>	ND <sup>2</sup>	5.82	2.51	11.36
PTS:23-25	Amphibole	45.71	0.97	6.46	4.56	20.22	ND <sup>2</sup>	ND <sup>2</sup>	7.33	3.54	11.21
PTS:23-25	Amphibole	48.50	0.97	5.86	6.45	17.88	ND <sup>2</sup>	ND <sup>2</sup>	6.58	2.97	10.80
PTS:23-25	Amphibole	49.12	1.22	8.80	3.83	20.48	ND <sup>2</sup>	ND <sup>2</sup>	6.29	2.23	8.04
PTS:23-25	Amphibole	49.71	1.15	6.42	4.94	18.61	ND <sup>2</sup>	ND <sup>2</sup>	6.39	2.27	10.51
PTS:23-25	Amphibole	48.86	1.24	5.82	6.14	18.62	ND <sup>2</sup>	ND <sup>2</sup>	6.72	2.23	10.38
PTS:23-25	Amphibole	48.61	0.73	8.10	3.20	20.85	ND <sup>2</sup>	ND <sup>2</sup>	6.87	2.45	9.20
PTS:23-25	Amphibole	48.15	1.08	5.96	5.57	19.10	ND <sup>2</sup>	ND <sup>2</sup>	6.56	2.29	11.28
PTS:23-25	Amphibole	49.09	1.32	8.25	4.79	19.65	ND <sup>2</sup>	ND <sup>2</sup>	6.16	2.69	8.05
PTS:23-25	Amphibole	47.59	1.17	6.24	5.45	18.82	ND <sup>2</sup>	ND <sup>2</sup>	6.50	3.03	11.21

1. Concentrations (weight percent) of elements comprising amphiboles

2. ND: Not detected

Polished-Thin Section ID <sup>1</sup>	Mineral	O	Na	Mg	Al	Si	Cl	K	Ca	Ti	Fe
PTS:23-25	Amphibole	54.95	1.62	2.76	13.90	15.19	ND <sup>2</sup>	ND <sup>2</sup>	ND <sup>2</sup>	2.90	8.69
PTS:26-28	Amphibole	47.24	1.27	8.16	15.45	19.86	0.20	0.16	5.28	0.43	1.95
PTS:26-28	Amphibole	46.88	1.69	4.33	19.34	19.62	0.34	0.14	2.58	0.57	4.50
PTS:26-28	Amphibole	47.16	1.46	5.28	18.84	19.34	0.36	ND <sup>2</sup>	3.56	0.99	3.03
PTS:26-28	Amphibole	46.59	1.87	4.20	18.21	19.40	0.21	ND <sup>2</sup>	3.25	0.97	5.28
PTS:26-28	Amphibole	46.10	2.04	4.48	17.23	20.08	0.36	ND <sup>2</sup>	1.63	1.39	6.68
PTS:26-28	Amphibole	47.38	1.55	5.41	18.99	20.05	0.29	ND <sup>2</sup>	2.75	0.60	2.98

1. Concentrations (weight percent) of elements comprising amphiboles

2. ND: Not detected.

Polished-Thin Section ID <sup>1</sup>	Spectrum	O	F	Na	Mg	Al	Si	P	S	Cl	Ca	Ti	Fe
PTS:9-12	Apatite	45.76	3.59	0.54	ND <sup>2</sup>	ND <sup>2</sup>	0.60	14.21	0.91	ND <sup>2</sup>	32.58	ND <sup>2</sup>	1.81
PTS:13-14	Apatite	45.69	ND <sup>2</sup>	0.57	ND <sup>2</sup>	ND <sup>2</sup>	0.82	14.67	2.66	ND <sup>2</sup>	31.91	ND <sup>2</sup>	3.69
PTS:13-14	Apatite	48.13	ND <sup>2</sup>	0.75	ND <sup>2</sup>	ND <sup>2</sup>	ND <sup>2</sup>	14.72	0.93	ND <sup>2</sup>	33.34	ND <sup>2</sup>	2.14
PTS:13-14	Apatite	48.89	ND <sup>2</sup>	0.68	ND <sup>2</sup>	ND <sup>2</sup>	2.72	13.56	0.89	ND <sup>2</sup>	30.67	ND <sup>2</sup>	2.60
PTS:17-19	Apatite	40.73	ND <sup>2</sup>	0.74	ND <sup>2</sup>	0.87	2.22	14.88	1.28	0.21	33.91	1.87	3.29
PTS:17-19	Apatite	40.83	ND <sup>2</sup>	0.53	0.31	0.81	1.25	16.23	0.85	ND <sup>2</sup>	36.15	0.83	2.23
PTS:23-25	Apatite	46.30	ND <sup>2</sup>	0.71	ND <sup>2</sup>	ND <sup>2</sup>	0.75	13.70	1.89	ND <sup>2</sup>	30.59	2.38	3.68
PTS:23-25	Apatite	40.99	ND <sup>2</sup>	0.78	0.45	0.93	2.07	15.40	1.09	0.16	36.51	0.25	1.36
PTS:23-25	Apatite	41.19	ND <sup>2</sup>	0.76	0.49	1.00	2.19	15.25	1.33	0.17	34.43	0.91	2.27
PTS:23-25	Apatite	42.10	ND <sup>2</sup>	0.62	0.43	0.68	0.71	14.34	4.15	ND <sup>2</sup>	31.21	ND <sup>2</sup>	5.76
PTS:23-25	Apatite	38.82	4.75	0.72	0.29	0.19	0.84	15.63	1.12	0.16	36.14	0.15	1.19
PTS:23-25	Apatite	39.04	4.15	0.72	0.29	0.25	0.98	14.98	1.73	0.17	36.03	ND <sup>2</sup>	1.67
PTS:26-28	Apatite	39.38	3.73	0.54	0.50	0.27	1.27	15.33	1.22	0.18	36.09	ND <sup>2</sup>	1.49
PTS:26-28	Apatite	38.96	4.39	0.69	0.36	0.28	0.60	15.43	1.28	0.18	36.82	0.16	0.84
PTS:26-28	Apatite	39.68	3.94	0.66	0.36	0.57	1.82	14.64	1.73	0.21	34.91	0.16	1.32

1. Concentrations (weight percent) of elements comprising apatite

2. ND: Not detected

Polished-Thin Section ID <sup>1</sup>	Mineral	O	Na	Mg	Al	Si	Cl	Ca	Fe
PTS:9-12	Calcite	60.11	0.33	ND <sup>2</sup>	0.37	1.26	0.52	33.65	3.77
PTS:13-14	Calcite	58.53	0.40	0.42	ND <sup>2</sup>	0.98	ND <sup>2</sup>	34.81	4.86
PTS:13-14	Calcite	57.42	0.45	ND <sup>2</sup>	0.26	1.43	0.42	35.48	4.54
PTS:13-14	Calcite	61.74	0.47	ND <sup>2</sup>	ND <sup>2</sup>	1.28	0.62	32.19	3.70
PTS:26-28	Calcite	67.76	ND <sup>2</sup>	0.48	0.19	0.93	0.18	29.98	0.46

1. Concentrations (weight percent) of elements comprising calcite

2. ND: Not detected

Polished-Thin Section ID <sup>1</sup>	Mineral	O	Mg	Al	Si	P	Cl	K	Ca	Ti	Fe
PTS:9-12	Glauconite	50.64	2.41	5.43	20.97	ND <sup>2</sup>	ND <sup>2</sup>	4.70	ND <sup>2</sup>	2.76	13.09
PTS:9-12	Glauconite	49.65	2.22	3.48	21.96	ND <sup>2</sup>	ND <sup>2</sup>	4.81	0.58	ND <sup>2</sup>	17.30
PTS:9-12	Glauconite	51.54	1.94	4.34	21.81	ND <sup>2</sup>	ND <sup>2</sup>	3.31	0.70	0.67	15.69
PTS:9-12	Glauconite	48.75	2.78	2.83	22.42	1.24	ND <sup>2</sup>	6.26	2.24	ND <sup>2</sup>	13.47
PTS:9-12	Glauconite	46.96	2.08	2.50	21.95	ND <sup>2</sup>	ND <sup>2</sup>	5.03	0.47	ND <sup>2</sup>	21.01
PTS:9-12	Glauconite	51.74	1.76	5.36	20.13	0.98	ND <sup>2</sup>	2.04	1.12	0.74	16.13
PTS:9-12	Glauconite	49.65	2.61	3.40	22.61	ND <sup>2</sup>	ND <sup>2</sup>	6.29	0.83	ND <sup>2</sup>	14.61
PTS:9-12	Glauconite	49.66	2.11	2.13	22.10	ND <sup>2</sup>	ND <sup>2</sup>	5.07	0.46	ND <sup>2</sup>	18.47
PTS:9-12	Glauconite	50.31	1.93	4.39	20.88	1.43	ND <sup>2</sup>	2.79	0.68	ND <sup>2</sup>	17.59
PTS:9-12	Glauconite	50.14	1.91	4.02	22.08	0.75	ND <sup>2</sup>	3.36	0.76	ND <sup>2</sup>	16.98
PTS:9-12	Glauconite	48.11	1.86	2.85	18.83	0.72	ND <sup>2</sup>	4.01	ND <sup>2</sup>	ND <sup>2</sup>	23.63
PTS:13-14	Glauconite	50.05	2.10	4.08	23.41	ND <sup>2</sup>	ND <sup>2</sup>	3.31	1.10	ND <sup>2</sup>	15.95
PTS:13-14	Glauconite	48.66	2.77	1.53	23.28	ND <sup>2</sup>	ND <sup>2</sup>	6.47	ND <sup>2</sup>	ND <sup>2</sup>	17.29
PTS:13-14	Glauconite	48.06	1.59	2.71	22.06	ND <sup>2</sup>	ND <sup>2</sup>	3.66	1.15	ND <sup>2</sup>	20.77
PTS:13-14	Glauconite	47.78	2.00	1.79	22.15	ND <sup>2</sup>	ND <sup>2</sup>	5.06	0.77	ND <sup>2</sup>	20.44
PTS:17-19	Glauconite	41.12	2.65	3.19	24.34	ND <sup>2</sup>	0.40	5.59	0.68	1.37	20.65
PTS:17-19	Glauconite	41.60	2.57	2.95	24.24	ND <sup>2</sup>	0.34	5.31	0.75	1.15	21.09
PTS:17-19	Glauconite	42.66	2.15	3.44	25.47	0.63	0.39	3.78	1.98	1.70	17.79
PTS:17-19	Glauconite	41.05	2.14	2.13	22.58	0.25	0.24	5.57	0.92	2.09	23.02

1. Concentrations (weight percent) of elements comprising glauconite

2. ND: Not detected



Polished-Thin Section ID <sup>1</sup>	Mineral	O	Mg	Al	Si	P	Cl	K	Ca	Ti	Fe
PTS:17-19	Glauconite	45.83	1.71	1.85	18.99	0.18	0.26	4.34	1.04	1.53	24.28
PTS:17-19	Glauconite	42.58	2.28	4.85	26.11	ND <sup>2</sup>	0.72	3.89	1.22	1.28	17.08
PTS:17-19	Glauconite	40.54	2.48	2.84	24.29	ND <sup>2</sup>	0.30	6.15	0.57	1.75	21.07
PTS:17-19	Glauconite	42.80	2.35	5.24	25.61	0.37	0.78	3.61	1.52	1.35	16.38
PTS:23-25	Glauconite	49.64	2.04	2.42	20.66	ND <sup>2</sup>	ND <sup>2</sup>	3.86	0.73	2.09	18.55
PTS:23-25	Glauconite	49.85	1.94	3.52	21.17	ND <sup>2</sup>	ND <sup>2</sup>	5.42	0.51	2.11	15.48
PTS:23-25	Glauconite	50.33	2.19	3.22	21.19	ND <sup>2</sup>	ND <sup>2</sup>	5.06	0.51	1.30	16.20
PTS:26-28	Glauconite	41.96	3.58	2.83	25.03	0.61	0.34	6.52	2.87	0.25	16.00

1. Concentrations (weight percent) of elements comprising glauconite

2. ND: Not detected

Polished-Thin Section ID <sup>1</sup>	Mineral	O	Mg	Al	Si	Cl	Ca	Ti	Mn	Fe
PTS:2-5	Ilmenite	38.37	0.38	ND <sup>2</sup>	ND <sup>2</sup>	ND <sup>2</sup>	ND <sup>2</sup>	29.97	1.34	29.94
PTS:2-5	Ilmenite	42.47	ND <sup>2</sup>	ND <sup>2</sup>	ND <sup>2</sup>	ND <sup>2</sup>	ND <sup>2</sup>	29.96	2.21	25.36
PTS:2-5	Ilmenite	39.44	0.54	ND <sup>2</sup>	ND <sup>2</sup>	ND <sup>2</sup>	ND <sup>2</sup>	30.37	0.22	29.43
PTS:2-5	Ilmenite	37.68	0.33	ND <sup>2</sup>	ND <sup>2</sup>	ND <sup>2</sup>	ND <sup>2</sup>	29.19	0.68	32.12
PTS:2-5	Ilmenite	41.91	ND <sup>2</sup>	ND <sup>2</sup>	ND <sup>2</sup>	ND <sup>2</sup>	ND <sup>2</sup>	33.78	0.38	23.92
PTS:2-5	Ilmenite	38.54	ND <sup>2</sup>	ND <sup>2</sup>	ND <sup>2</sup>	ND <sup>2</sup>	ND <sup>2</sup>	30.16	3.27	28.02
PTS:2-5	Ilmenite	42.12	0.69	ND <sup>2</sup>	ND <sup>2</sup>	ND <sup>2</sup>	ND <sup>2</sup>	28.24	0.76	28.20
PTS:2-5	Ilmenite	43.57	ND <sup>2</sup>	ND <sup>2</sup>	ND <sup>2</sup>	ND <sup>2</sup>	ND <sup>2</sup>	31.98	0.70	23.74
PTS:2-5	Ilmenite	46.08	0.60	ND <sup>2</sup>	ND <sup>2</sup>	ND <sup>2</sup>	ND <sup>2</sup>	34.33	2.69	16.30
PTS:9-12	Ilmenite	40.26	ND <sup>2</sup>	ND <sup>2</sup>	ND <sup>2</sup>	ND <sup>2</sup>	ND <sup>2</sup>	26.75	0.63	32.36
PTS:13-14	Ilmenite	39.24	ND <sup>2</sup>	ND <sup>2</sup>	ND <sup>2</sup>	ND <sup>2</sup>	ND <sup>2</sup>	27.54	1.09	32.13
PTS:17-19	Ilmenite	33.87	1.20	1.51	2.78	0.13	0.32	29.29	0.78	30.11
PTS:17-19	Ilmenite	33.48	0.38	1.13	2.53	0.21	0.33	29.98	0.42	31.53
PTS:17-19	Ilmenite	35.92	0.34	0.90	1.85	0.25	0.48	39.58	0.35	20.33
PTS:17-19	Ilmenite	36.29	0.22	1.21	1.43	ND <sup>2</sup>	0.41	41.09	1.04	18.30
PTS:17-19	Ilmenite	32.85	0.23	1.56	1.49	0.12	0.21	29.65	0.56	33.34
PTS:17-19	Ilmenite	33.25	0.22	0.58	1.45	0.14	0.46	31.86	2.24	29.79
PTS:17-19	Ilmenite	32.76	0.67	1.35	2.37	ND <sup>2</sup>	0.50	27.05	2.07	33.22
PTS:17-19	Ilmenite	34.71	0.22	0.74	1.30	0.17	0.33	37.67	1.22	23.65
PTS:23-25	Ilmenite	47.19	0.36	ND <sup>2</sup>	ND <sup>2</sup>	ND <sup>2</sup>	ND <sup>2</sup>	37.19	0.31	14.94
PTS:23-25	Ilmenite	40.20	0.30	ND <sup>2</sup>	ND <sup>2</sup>	ND <sup>2</sup>	ND <sup>2</sup>	33.44	1.05	25.01
PTS:23-25	Ilmenite	37.25	1.05	ND <sup>2</sup>	ND <sup>2</sup>	ND <sup>2</sup>	ND <sup>2</sup>	28.89	0.52	32.30
PTS:23-25	Ilmenite	39.47	0.65	ND <sup>2</sup>	ND <sup>2</sup>	ND <sup>2</sup>	ND <sup>2</sup>	27.65	ND <sup>2</sup>	32.23
PTS:23-25	Ilmenite	42.73	0.33	ND <sup>2</sup>	ND <sup>2</sup>	ND <sup>2</sup>	ND <sup>2</sup>	25.17	0.97	30.80
PTS:23-25	Ilmenite	41.67	0.29	ND <sup>2</sup>	ND <sup>2</sup>	ND <sup>2</sup>	ND <sup>2</sup>	32.60	0.65	24.78
PTS:26-28	Ilmenite	35.67	0.23	0.30	1.67	0.19	2.54	38.34	0.97	20.08
PTS:26-28	Ilmenite	35.59	0.41	0.48	2.53	0.16	2.89	34.26	0.32	23.34

1. Concentrations (weight percent) of elements comprising ilmenite

2. ND: Not detected

Polished-Thin Section ID <sup>1</sup>	Mineral	O	Na	Al	Si	Ca
PTS:23-25	Plagioclase Feldspar	51.68	5.73	13.15	29.43	ND <sup>2</sup>
PTS:23-25	Plagioclase Feldspar	52.36	4.87	12.51	25.48	4.79
PTS:23-25	Plagioclase Feldspar	52.66	5.14	11.89	26.19	4.13
PTS:23-25	Plagioclase Feldspar	52.42	5.24	11.92	26.22	4.21

1. Concentrations (weight percent) of elements comprising plagioclase feldspar

2. ND: Not detected

Polished- Thin Section ID <sup>1</sup>	Mineral	Mg	Si	S	K	Ca	Fe
--	---------	----	----	---	---	----	----

PTS:26-28	Pyrite	0.25	3.05	49.30	0.50	1.77	45.13
PTS:26-28	Pyrite	0.26	1.57	53.21	0.30	1.97	42.70
PTS:26-28	Pyrite	0.25	2.56	51.44	0.45	2.14	43.16

1. Concentrations (weight percent) of elements comprising pyrite

Polished-Thin Section ID <sup>1</sup>	Mineral	O	Na	Mg	Al	Si	Ca	Ti	Mn	Fe
PTS:2-5	Pyroxene	50.10	ND <sup>2</sup>	11.36	1.34	24.16	6.77	1.70	ND <sup>2</sup>	4.57
PTS:2-5	Pyroxene	48.09	ND <sup>2</sup>	ND <sup>2</sup>	11.11	16.27	13.45	2.40	ND <sup>2</sup>	8.67
PTS:2-5	Pyroxene	48.98	ND <sup>2</sup>	10.43	0.85	24.61	7.65	1.93	ND <sup>2</sup>	5.55
PTS:17-19	Pyroxene	46.57	ND <sup>2</sup>	14.92	1.83	23.75	0.77	0.21	ND <sup>2</sup>	11.95
PTS:17-19	Pyroxene	42.46	ND <sup>2</sup>	ND <sup>2</sup>	12.51	19.00	15.39	1.29	0.30	9.05
PTS:17-19	Pyroxene	43.91	ND <sup>2</sup>	13.33	0.97	24.38	0.82	1.27	0.13	15.19
PTS:17-19	Pyroxene	42.25	1.12	5.49	6.88	19.70	8.04	2.02	0.29	14.21
PTS:17-19	Pyroxene	43.45	0.74	8.63	3.71	23.61	8.04	1.61	0.30	9.91
PTS:17-19	Pyroxene	42.01	ND <sup>2</sup>	ND <sup>2</sup>	12.07	18.43	15.32	1.80	0.20	10.16
PTS:17-19	Pyroxene	44.17	0.80	8.77	1.72	23.12	14.92	1.93	0.08	4.49
PTS:17-19	Pyroxene	42.50	ND <sup>2</sup>	ND <sup>2</sup>	12.00	19.17	14.90	1.18	ND <sup>2</sup>	10.26
PTS:23-25	Pyroxene	44.14	0.97	8.92	1.39	24.51	14.33	0.29	0.14	5.31
PTS:23-25	Pyroxene	47.67	ND <sup>2</sup>	ND <sup>2</sup>	8.79	15.82	13.25	1.90	ND <sup>2</sup>	12.56
PTS:23-25	Pyroxene	48.42	ND <sup>2</sup>	ND <sup>2</sup>	13.08	16.61	13.74	2.26	ND <sup>2</sup>	5.89
PTS:23-25	Pyroxene	47.96	ND <sup>2</sup>	ND <sup>2</sup>	11.02	15.93	13.51	2.36	ND <sup>2</sup>	9.21
PTS:23-25	Pyroxene	48.29	ND <sup>2</sup>	ND <sup>2</sup>	11.33	16.09	13.25	2.46	ND <sup>2</sup>	8.58
PTS:23-25	Pyroxene	48.07	ND <sup>2</sup>	ND <sup>2</sup>	11.13	15.87	13.37	2.51	ND <sup>2</sup>	9.06
PTS:23-25	Pyroxene	48.04	ND <sup>2</sup>	ND <sup>2</sup>	9.53	15.99	13.21	2.09	ND <sup>2</sup>	11.14
PTS:23-25	Pyroxene	48.06	ND <sup>2</sup>	ND <sup>2</sup>	11.10	16.22	13.47	2.21	ND <sup>2</sup>	8.94
PTS:23-25	Pyroxene	48.10	ND <sup>2</sup>	ND <sup>2</sup>	11.39	16.61	13.54	1.95	ND <sup>2</sup>	8.40
PTS:23-25	Pyroxene	47.55	ND <sup>2</sup>	ND <sup>2</sup>	12.92	16.23	13.67	2.86	ND <sup>2</sup>	6.78
PTS:23-25	Pyroxene	49.35	0.23	ND <sup>2</sup>	12.00	16.40	13.24	1.78	ND <sup>2</sup>	6.99
PTS:23-25	Pyroxene	48.80	ND <sup>2</sup>	11.49	0.85	23.51	2.17	1.99	ND <sup>2</sup>	11.19

1. Concentrations (weight percent) of elements comprising pyroxenes

2. ND: Not detected

Polished- Thin Section ID <sup>1</sup>	Mineral	O	Mg	Al	Si	Ti	Fe
PTS:2-5	Staurolite	50.79	0.91	23.68	11.77	2.59	10.26
PTS:2-5	Staurolite	50.75	0.91	23.07	13.31	1.68	10.28
PTS:2-5	Staurolite	51.78	1.16	24.28	12.86	1.34	8.58
PTS:2-5	Staurolite	50.85	0.75	23.54	12.13	2.86	9.87
PTS:2-5	Staurolite	50.73	0.83	22.89	12.23	2.65	10.67
PTS:2-5	Staurolite	51.59	1.25	22.93	11.72	3.30	9.21
PTS:2-5	Staurolite	51.29	1.03	23.41	11.87	2.65	9.75
PTS:2-5	Staurolite	50.82	1.13	24.26	13.11	1.14	9.54
PTS:2-5	Staurolite	51.30	0.86	24.07	13.27	1.24	9.26
PTS:2-5	Staurolite	51.11	1.18	22.42	14.12	1.88	9.30
PTS:2-5	Staurolite	54.97	ND <sup>2</sup>	15.88	14.98	3.54	10.63
PTS:2-5	Staurolite	51.00	0.99	22.27	14.27	2.54	8.92
PTS:9-12	Staurolite	50.16	0.98	24.24	12.64	0.76	11.22
PTS:9-12	Staurolite	50.31	0.95	24.76	13.19	0.45	10.34
PTS:9-12	Staurolite	50.56	1.35	24.67	13.46	ND <sup>2</sup>	9.97
PTS:9-12	Staurolite	50.04	1.09	25.56	13.01	ND <sup>2</sup>	10.30
PTS:9-12	Staurolite	50.35	1.07	24.41	12.79	0.51	10.87
PTS:9-12	Staurolite	50.78	0.91	25.02	12.84	ND <sup>2</sup>	10.44
PTS:9-12	Staurolite	50.16	0.66	25.21	12.32	0.63	11.02
PTS:9-12	Staurolite	50.71	0.81	25.05	12.86	0.48	10.09
PTS:9-12	Staurolite	50.79	0.86	24.40	12.89	0.84	10.22
PTS:13-14	Staurolite	50.62	0.97	24.22	12.37	ND <sup>2</sup>	11.82
PTS:13-14	Staurolite	50.60	1.29	24.34	13.98	ND <sup>2</sup>	9.79
PTS:13-14	Staurolite	50.75	1.31	24.97	13.09	ND <sup>2</sup>	9.88
PTS:15-16	Staurolite	50.42	0.98	24.51	13.01	ND <sup>2</sup>	11.08
PTS:15-16	Staurolite	50.90	1.03	25.66	13.15	ND <sup>2</sup>	9.27
PTS:23-25	Staurolite	50.69	0.99	23.91	12.79	1.89	9.73
PTS:23-25	Staurolite	50.78	0.91	24.95	12.76	0.59	10.01
PTS:23-25	Staurolite	50.44	0.89	25.51	12.36	ND <sup>2</sup>	10.80
PTS:23-25	Staurolite	49.89	0.70	25.28	12.41	0.60	11.11
PTS:23-25	Staurolite	50.51	0.88	25.28	12.62	ND <sup>2</sup>	10.71

1. Concentrations (weight percent) of elements comprising staurolite

2. ND: Not detected

Polished- Thin Section ID <sup>1</sup>	Mineral	O	Mg	Al	Si	Ti	Fe
PTS:23-25	Staurolite	51.53	0.55	24.66	12.48	1.80	8.98
PTS:23-25	Staurolite	51.56	0.62	25.15	12.46	1.42	8.79
PTS:23-25	Staurolite	51.22	1.11	23.47	12.64	1.87	9.69
PTS:23-25	Staurolite	51.30	1.00	24.34	12.73	1.71	8.92
PTS:23-25	Staurolite	50.36	1.43	23.15	11.93	2.41	10.72
PTS:23-25	Staurolite	51.47	1.11	23.40	11.30	2.73	9.99
PTS:23-25	Staurolite	51.42	1.14	24.00	12.07	2.28	9.09
PTS:23-25	Staurolite	51.09	0.80	23.71	11.69	2.45	10.25
PTS:23-25	Staurolite	51.64	0.64	23.67	11.64	2.79	9.62
PTS:23-25	Staurolite	50.82	1.23	23.25	11.86	2.37	10.47
PTS:23-25	Staurolite	50.17	0.94	23.30	11.39	2.93	11.28
PTS:23-25	Staurolite	50.90	1.00	23.50	11.27	2.72	10.61
PTS:23-25	Staurolite	50.54	0.88	24.17	12.65	1.24	10.52
PTS:23-25	Staurolite	51.89	0.55	25.17	12.39	1.67	8.33
PTS:23-25	Staurolite	50.26	1.15	23.64	11.14	3.49	10.33

1. Concentrations (weight percent) of elements comprising staurolite

Polished-Thin Section ID <sup>1</sup>	Mineral	O	Na	Mg	Al	Si	Ca	Ti	Fe
PTS:2-5	Tourmaline	52.77	1.72	ND <sup>2</sup>	14.39	15.74	ND <sup>2</sup>	2.31	13.07
PTS:2-5	Tourmaline	54.93	1.33	3.57	16.34	17.03	0.76	ND <sup>2</sup>	6.04
PTS:23-25	Tourmaline	54.67	1.33	3.66	14.73	15.54	0.85	2.01	7.21
PTS:23-25	Tourmaline	54.68	1.41	3.31	14.34	15.44	1.13	2.46	7.23
PTS:23-25	Tourmaline	55.43	1.46	3.10	15.02	15.05	0.52	2.69	6.73
PTS:26-28	Tourmaline	47.39	1.74	4.38	19.01	19.90	2.46	0.65	4.47
PTS:26-28	Tourmaline	47.29	1.74	4.39	19.03	20.01	2.50	0.58	4.45

1. Concentrations (weight percent) of elements comprising tourmaline

2. ND: Not detected.



**Appendix F6: Statistics of Evaluated Minerals**

Alkali Feldspar <sup>1</sup>	O	Na	Al	Si	K
Mean <sup>2</sup>	50.49	0.36	8.87	28.70	11.67
Median <sup>2</sup>	50.33	0.27	8.92	28.92	11.86
Standard Deviation <sup>2</sup>	2.51	0.22	0.46	1.44	0.74
Sample Variance <sup>2</sup>	6.31	0.05	0.21	2.08	0.55
Minimum	48.08	0.18	8.04	25.95	10.44
Maximum	55.21	0.67	9.42	30.06	12.60
Count <sup>3</sup>	6	6	6	6	6
Confidence Level (95.0%) <sup>2</sup>	2.64	0.23	0.48	1.51	0.78
1/2 Minimum Value <sup>4</sup>	24.04	0.18	0.09	12.97	5.22

1. EDX analysis of 6 alkali feldspar grains. All concentrations are presented as weight percents.

2. Calculated via Microsoft Excel

3. Number of spectra evaluated to compute statistics

4. One half of the minimum-detected value was used to replace concentrations of elements that were not detected in some specimens. Only elements that were detected in at least 25% of specimens were evaluated for statistics

Almandine <sup>1</sup>	O	Mg	Al	Si	Ca	Ti	Mn	Fe
Mean <sup>2</sup>	43.84	2.01	9.96	17.06	2.16	1.27	2.98	20.79
Median <sup>2</sup>	44.70	1.51	9.78	16.88	1.44	1.16	1.99	21.35
Standard Deviation <sup>2</sup>	2.13	1.37	0.57	1.02	1.55	0.92	2.95	2.64
Sample Variance <sup>2</sup>	4.53	1.88	0.33	1.04	2.42	0.84	8.71	6.97
Minimum	40.27	0.58	9.37	15.76	0.00	0.33	0.54	14.69
Maximum	47.83	5.45	10.96	19.22	4.58	2.71	11.96	23.94
Count <sup>3</sup>	24	24	24	24	24	24	24	24
Confidence Level (95.0%) <sup>2</sup> 1/2	0.90	0.58	0.24	0.43	0.66	0.39	1.25	1.12
Minimum Value <sup>4</sup>	20.14	0.29	4.68	7.88	0.00	0.17	0.27	7.35

1. EDX analysis of 24 almandine grains. All concentrations are presented as weight percents

2. Calculated via Microsoft Excel

3. Number of spectra evaluated to compute statistics

4. One half of the minimum-detected value was used to replace concentrations of elements that were not detected in some specimens  
Only elements that were detected in at least 25% of specimens were evaluated for statistics

Amphiboles <sup>1</sup>	O	Na	Mg	Al	Si	K	Ca	Ti	Fe
Mean <sup>2</sup>	48.17	1.06	5.65	7.28	18.94	0.77	5.80	2.47	9.86
Median <sup>2</sup>	47.84	1.09	5.78	5.60	18.61	0.52	6.54	2.55	10.73
Standard Deviation <sup>2</sup>	1.89	0.39	2.08	4.61	1.64	1.35	2.32	0.88	3.29
Sample Variance <sup>2</sup>	3.57	0.16	4.31	21.26	2.69	1.82	5.40	0.77	10.85
Minimum	42.97	0.54	0.25	1.12	15.19	0.14	0.52	0.43	1.95
Maximum	54.95	2.04	9.92	19.34	23.85	7.59	13.38	4.38	16.16
Count <sup>3</sup>	62	62	62	62	62	62	62	62	62
Confidence Level (95.0%) <sup>2</sup>	0.48	0.10	0.53	1.17	0.42	0.34	0.59	0.22	0.84
1/2 Minimum Value <sup>4</sup>	21.49	0.27	0.13	0.28	7.59	0.07	0.26	0.21	0.97

1. EDX analysis of 62 amphibole grains. All concentrations are presented as weight percents

2. Calculated via Microsoft Excel

3. Number of spectra evaluated to compute statistics

4. One half of the minimum-detected value was used to replace concentrations of elements that were not detected in some specimens. Only elements that were detected in at least 25% of specimens were evaluated for statistics

Apatite <sup>1</sup>	O	F	Na	Mg	Al	Si	P	S	Cl	Ca	Ti	Fe
Mean <sup>2</sup>	42.43	2.71	0.67	0.29	0.42	1.28	14.86	1.54	0.13	34.08	0.48	2.35
Median <sup>2</sup>	40.99	1.80	0.69	0.29	0.27	0.98	14.88	1.28	0.16	34.43	0.15	2.14
Standard Deviation <sup>2</sup>	3.52	1.19	0.09	0.14	0.35	0.74	0.72	0.87	0.05	2.24	0.73	1.29
Sample Variance <sup>2</sup>	12.38	1.42	0.01	0.02	0.12	0.55	0.52	0.76	0.00	5.01	0.53	1.67
Minimum	38.82	1.80	0.53	0.30	0.10	0.30	13.56	0.85	0.16	30.59	0.16	0.84
Maximum	48.89	4.75	0.78	0.50	1.00	2.72	16.23	4.15	0.21	36.82	2.38	5.76
Count <sup>3</sup>	15	15	15	15	15	15	15	15	15	15	15	15
Confidence Level (95.0%) <sup>2</sup> 1/2	1.95	0.66	0.05	0.08	0.19	0.41	0.40	0.48	0.03	1.24	0.40	0.72
Minimum Value <sup>4</sup>	19.41	1.80	0.27	0.15	0.05	0.15	6.78	0.42	0.08	15.30	0.08	0.42

1. EDX analysis of 15 apatite grains. All concentrations are presented as weight percents

2. Calculated via Microsoft Excel

3. Number of spectra evaluated to compute statistics

4. One half of the minimum-detected value was used to replace concentrations of elements that were not detected in some specimens. Only elements that were detected in at least 25% of specimens were evaluated for statistics

Calcite <sup>1</sup>	O	Na	Mg	Al	Si	Cl	Ca	Fe
Mean <sup>2</sup>	61.11	0.36	0.31	0.20	1.18	0.37	33.22	3.47
Median <sup>2</sup>	60.11	0.40	0.21	0.19	1.26	0.42	33.65	3.77
Standard Deviation <sup>2</sup>	4.06	0.12	0.13	0.12	0.21	0.22	2.20	1.75
Sample Variance <sup>2</sup>	16.48	0.01	0.02	0.01	0.04	0.05	4.84	3.07
Minimum	57.42	0.33	0.42	0.19	0.93	0.18	29.98	0.46
Maximum	67.76	0.47	0.48	0.37	1.43	0.62	35.48	4.86
Count <sup>3</sup>	5	5	5	5	5	5	5	5
Confidence Level (95.0%) <sup>2</sup>	5.04	0.15	0.17	0.14	0.26	0.28	2.73	2.18
1/2 Minimum Value <sup>4</sup>	28.71	0.17	0.21	0.10	0.47	0.09	14.99	0.23

1. EDX analysis of 5 calcite grains. All concentrations are presented as weight percents
2. Calculated via Microsoft Excel
3. Number of spectra evaluated to compute statistics
4. One half of the minimum-detected value was used to replace concentrations of elements that were not detected in some specimens. Only elements that were detected in at least 25% of specimens were evaluated for statistics

Glauconite <sup>1</sup>	O	Mg	Al	Si	P	Cl	K	Ca	Ti	Fe
Mean <sup>2</sup>	47.10	2.23	3.31	22.46	0.32	0.22	4.64	0.92	0.88	18.15
Median <sup>2</sup>	48.66	2.14	3.19	22.10	0.09	0.12	4.81	0.75	0.67	17.30
Standard Deviation <sup>2</sup>	3.75	0.42	1.10	1.90	0.39	0.18	1.21	0.62	0.83	3.00
Sample Variance <sup>2</sup>	14.08	0.17	1.21	3.61	0.15	0.03	1.46	0.38	0.69	8.98
Minimum	40.54	1.59	1.53	18.83	0.18	0.24	2.04	0.46	0.25	13.09
Maximum	51.74	3.58	5.43	26.11	1.43	0.78	6.52	2.87	2.76	24.28
Count <sup>3</sup>	27	27	27	27	27	27	27	27	27	27
Confidence Level (95.0%) <sup>2</sup>	1.48	0.17	0.44	0.75	0.15	0.07	0.48	0.24	0.33	1.19
1/2 Minimum Value <sup>4</sup>	20.27	0.80	0.77	9.41	0.09	0.12	1.02	0.23	0.13	6.55

1. EDX analysis of 27 glauconite grains. All concentrations are presented as weight percents

2. Calculated via Microsoft Excel

3. Number of spectra evaluated to compute statistics

4. One half of the minimum-detected value was used to replace concentrations of elements that were not detected in some specimens. Only elements that were detected in at least 25% of specimens were evaluated for statistics

Ilmenite <sup>1</sup>	O	Mg	Al	Si	Cl	Ca	Ti	Mn	Fe
Mean <sup>2</sup>	38.58	0.38	0.46	1.13	0.09	0.38	31.67	1.02	26.84
Median <sup>2</sup>	38.54	0.33	0.15	0.65	0.06	0.11	30.16	0.76	28.20
Standard Deviation <sup>2</sup>	4.04	0.28	0.48	0.71	0.06	0.68	4.14	0.80	5.45
Sample Variance <sup>2</sup>	16.36	0.08	0.23	0.51	0.00	0.47	17.15	0.65	29.69
Minimum	32.72	0.19	0.30	1.30	0.12	0.21	25.17	0.22	14.94
Maximum	47.19	1.20	1.56	2.78	0.25	2.86	40.96	3.27	33.33
Count <sup>3</sup>	27	27	27	27	27	27	27	27	27
Confidence Level (95.0%) <sup>2</sup>	1.60	0.11	0.19	0.28	0.02	0.27	1.64	0.32	2.16
1/2 Minimum Value <sup>4</sup>	16.36	0.10	0.15	0.65	0.06	0.11	12.585	0.11	7.47

1. EDX analysis of 27 ilmenite grains. All concentrations are presented as weight percents

2. Calculated via Microsoft Excel

3. Number of spectra evaluated to compute statistics

4. One half of the minimum-detected value was used to replace concentrations of elements that were not detected in some specimens. Only elements that were detected in at least 25% of specimens were evaluated for statistics

Plagioclase Feldspar <sup>1</sup>	O	Na	Al	Si	Ca
Mean <sup>2</sup>	52.28	5.24	12.37	26.83	3.80
Median <sup>2</sup>	52.39	5.19	12.21	26.20	4.17
Standard Deviation <sup>2</sup>	0.42	0.36	0.60	1.77	1.19
Sample Variance <sup>2</sup>	0.17	0.13	0.36	3.13	1.42
Minimum	51.68	4.87	11.89	25.48	4.14
Maximum	52.66	5.73	13.15	29.43	4.79
Count <sup>3</sup>	4.00	4.00	4.00	4.00	4.00
Confidence Level (95.0%) <sup>2</sup>	0.66	0.57	0.95	2.82	1.89
1/2 Minimum Value <sup>4</sup>	25.84	2.43	5.94	12.74	2.07

1. EDX analysis of 4 plagioclase feldspar grains. All concentrations are presented as weight percents

2. Calculated via Microsoft Excel

3. Number of spectra evaluated to compute statistics

4. One half of the minimum-detected value was used to replace concentrations of elements that were not detected in some specimens. Only elements that were detected in at least 25% of specimens were evaluated for statistics



Pyrite <sup>1</sup>	Mg	Si	S	K	Ca	Fe
Mean <sup>2</sup>	0.25	2.40	51.31	0.41	1.96	43.66
Median <sup>2</sup>	0.25	2.56	51.44	0.45	1.97	43.16
Standard Deviation <sup>2</sup>	0.00	0.75	1.96	0.11	0.18	1.29
Sample Variance <sup>2</sup>	0.00	0.57	3.83	0.01	0.03	1.66
Minimum	0.25	1.57	49.30	0.30	1.77	42.70
Maximum	0.26	3.05	53.21	0.50	2.14	45.13
Count <sup>3</sup>	3	3	3	3	3	3
Confidence Level (95.0%) <sup>2</sup>	0.01	1.87	4.86	0.26	0.46	3.20
1/2 Minimum Value <sup>4</sup>	0.12	0.79	24.65	0.15	0.88	21.35

1. EDX analysis of 3 pyrite grains. All concentrations are presented as weight percents

2. Calculated via Microsoft Excel

3. Number of spectra evaluated to compute statistics

4. One half of the minimum-detected value was used to replace concentrations of elements that were not detected in some specimens. Only elements that were detected in at least 25% of specimens were evaluated for statistics

Pyroxenes <sup>1</sup>	O	Na	Mg	Al	Si	Ca	Ti	Mn	Fe
Mean <sup>2</sup>	46.82	0.30	5.26	8.08	19.21	10.73	1.86	0.09	8.97
Median <sup>2</sup>	48.00	0.12	2.05	11.06	17.52	13.31	1.94	0.04	8.99
Standard Deviation <sup>2</sup>	3.07	0.38	4.39	4.94	3.62	5.03	0.65	0.09	2.86
Sample Variance <sup>2</sup>	9.45	0.15	19.30	24.36	13.11	25.29	0.42	0.01	8.18
Minimum	42.01	0.23	4.10	0.85	15.08	0.72	0.21	0.08	4.49
Maximum	54.62	1.39	14.92	14.40	24.61	15.39	2.86	0.30	15.19
Count <sup>3</sup>	24	24	24	24	24	24	24	24	24
Confidence Level (95.0%) <sup>2</sup>	1.30	0.16	1.86	2.08	1.53	2.12	0.27	0.04	1.21
1/2 Minimum Value <sup>4</sup>	21.01	0.12	2.05	0.43	7.54	0.36	0.11	0.04	2.25

1. EDX analysis of 24 pyroxene grains. All concentrations are presented as weight percents

2. Calculated via Microsoft Excel

3. Number of spectra evaluated to compute statistics

4. One half of the minimum-detected value was used to replace concentrations of elements that were not detected in some specimens. Only elements that were detected in at least 25% of specimens were evaluated for statistic

Staurolite <sup>1</sup>	O	Mg	Al	Si	Ti	Fe
Mean <sup>2</sup>	50.93	0.96	23.98	12.60	1.53	10.06
Median <sup>2</sup>	50.79	0.98	24.23	12.64	1.55	10.15
Standard Deviation <sup>2</sup>	0.78	0.23	1.49	0.80	1.07	0.79
Sample Variance <sup>2</sup>	0.61	0.05	2.22	0.64	1.15	0.62
Minimum	49.89	0.55	15.88	11.14	0.45	8.33
Maximum	54.97	1.43	25.66	14.98	3.54	11.82
Count <sup>3</sup>	46	46	46	46	46	46
Confidence Level (95.0%) <sup>2</sup>	0.23	0.07	0.44	0.24	0.32	0.23
1/2 Minimum Value <sup>4</sup>	24.95	0.28	7.94	5.57	0.23	4.17

1. EDX analysis of 46 staurolite grains. All concentrations are presented as weight percents

2. Calculated via Microsoft Excel

3. Number of spectra evaluated to compute statistics

4. One half of the minimum-detected value was used to replace concentrations of elements that were not detected in some specimens. Only elements that were detected in at least 25% of specimens were evaluated for statistics

Tourmaline <sup>1</sup>	O	Na	Mg	Al	Si	Ca	Ti	Fe
Mean <sup>2</sup>	52.45	1.53	3.42	16.12	16.96	1.21	1.57	7.03
Median <sup>2</sup>	54.67	1.46	3.57	15.02	15.74	0.85	2.01	6.73
Standard Deviation <sup>2</sup>	3.59	0.19	0.96	2.09	2.14	0.91	1.02	2.91
Sample Variance <sup>2</sup>	12.88	0.04	0.92	4.37	4.57	0.83	1.04	8.48
Minimum	47.29	1.33	3.10	14.34	15.05	0.52	0.58	4.45
Maximum	55.43	1.74	4.39	19.03	20.01	2.50	2.69	13.07
Count <sup>3</sup>	7	7	7	7	7	7	7	7
Confidence Level (95.0%) <sup>2</sup>	3.32	0.18	0.89	1.93	1.98	0.84	0.94	2.69
1/2 Minimum Value <sup>4</sup>	23.65	0.66	1.55	7.17	7.53	0.26	0.29	2.22

1. EDX analysis of 7 tourmaline grains. All concentrations are presented as weight percents

2. Calculated via Microsoft Excel

3. Number of spectra evaluated to compute statistics

4. One half of the minimum-detected value was used to replace concentrations of elements that were not detected in some specimens. Only elements that were detected in at least 25% of specimens were evaluated for statistics

## Appendix G: XRF Data

### Appendix G1: Pellet Data and Descriptions of Reference Samples

Standard Id <sup>1</sup>	Standard Description	Sediment Weight <sup>2</sup>	Binder Weight <sup>2</sup>	Source/Distributor
02BR73	Andesite	12	15	Dr. Eric Horsman, ECU
1646a	Estuarine sediment	6.001	6.602	NIST <sup>3</sup>
2586	Soil with lead from paint	6.001	6.902	NIST <sup>3</sup>
2702	Inorganics in marine sediment	6.001	6.601	NIST <sup>3</sup>
2704	River sediment	6.001	6.601	NIST <sup>3</sup>
98a NBS	Plastic clay	6.001	6.6	NIST <sup>3</sup>
AGV-2	Andesite	12	15	USGS <sup>3</sup>
GSP-2	Granodiorite	12	15	USGS <sup>3</sup>
MAG-1	Marine sediment	6	6.6	USGS <sup>3</sup>
MRG-1	Gabbro	9.396	11.388	CCRMP <sup>3</sup>
NCS DC 71302	Diorite	12	15	BSCI
NIM-D	NIM-D	11.561	14.287	MINTEK <sup>3</sup>
NIM-L	Lujavrite	12.421	14.979	MINTEK <sup>3</sup>
NIM-N	Norite	12.653	14.993	MINTEK <sup>3</sup>
NIM-P	Pyroxenite	13.151	16.03	MINTEK <sup>3</sup>
NIM-S	Syenite	8.812	10.571	MINTEK <sup>3</sup>
NIM_G	Granite	9.068	10.917	MINTEK <sup>3</sup>
SCo-1	Cody Shale	6.005	7.201	USGS <sup>3</sup>
Skd-1	Quartz Diorite	12	15	Russia Standard (6103-9)
SY-2	Syenite	12.845	15.193	CCRMP <sup>3</sup>
SY-3	Syenite	11.802	14.56	CCRMP <sup>3</sup>

1. Reference XRF pellets were selected from the Department of Geological Sciences' repository at East Carolina University

2. Weight in grams

3. Govindaraju (1994)

**Appendix G2: Accepted Values of XRF Reference Samples**

Standard Id <sup>1</sup>	Al	S	Fe	K	Mg	Mn	Na	P	Si	Ti	Ca	F	Cl	Sr
02BR73	8.92	0.04	3.02	1.75	0.78	0.10	2.82	0.07	29.48	0.25	2.90			1181
1646a	2.30	0.35	2.01	0.86	0.34	0.02	0.60	0.03	40.00	0.46	0.52			68
2586	6.65		5.16	0.98	1.71	0.10	0.38	0.10	29.15	0.61	2.22			84
2702	8.41	1.50	7.91	2.05	0.99	0.18	0.55	0.16	30.26	0.88	0.34			120
2704	6.11	0.40	4.11	2.00	1.20	0.06	0.45	0.10	29.08	0.46	2.60			130
98a NBS	17.56			0.86	0.25		0.05	0.05	22.85	0.97	0.22			330
AGV-2	8.95		4.68	2.39	1.08	0.06	2.53	0.21	27.72	0.63	3.72	0.04		658
GSP-2	7.89		3.43	4.47	0.58	0.02	1.68	0.13	31.13	0.40	1.50	0.30		240
MAG-1	8.68	0.39	4.82	2.95	1.81	0.08	2.31	0.07	23.54	0.45	0.98	0.08	31000	150
MRG-1	4.50	0.06	12.48	0.15	8.13	0.13	0.43	0.03	18.38	2.21	10.56	0.03		260
NCS DC 71302	8.52	0.02	3.30	4.29	0.51	0.69	1.85	0.16	29.48	0.48	1.77	0.11	160	318
NIM-D	0.16		11.87	0.01	26.24	0.17	0.02	0.00	18.21	0.01	0.20	0.42	400	3
NIM-L	7.22	0.07	7.02	4.57	0.17	0.60	5.05	0.03	24.49	0.29	2.30	0.44		4600
NIM-N	8.73		6.37	0.21	4.52	0.14	1.48	0.01	24.61	0.12	8.22			260
NIM-P	2.21		8.84	0.07	15.27	0.17	0.22	0.01	23.89	0.12	1.90			32
NIM-S	9.18		1.01	12.74	0.28	0.01	0.26	0.05	29.74	0.03	0.49	0.01		62
NIM_G	6.39		1.43	4.14	0.04	0.02	2.03	0.00	35.39	0.05	0.56	0.42		10
SCo-1	7.25	0.06	3.59	2.30	1.64	0.04	0.54	0.09	29.36	0.38	1.87	0.08	51	170
Skd-1	8.76		2.95	2.47	1.84	0.07	2.15	0.07	28.26	0.52	3.46	0.07	110	410
SY-2	6.41	0.01	4.41	3.72	1.63	0.25	2.62	0.19	28.09	0.08	5.70	0.51		285
SY-3	6.25	0.05	4.49	3.49	1.61	0.25	2.50	0.24	27.90	0.09	5.90	0.66		306

1. Elemental concentrations are presented as weight percents except for Cl and Sr, which are in ppm

**Appendix G3: Sediment and Binder Weights of TC14 Pellet Samples**

Sample ID	Sediment Weight <sup>1</sup>	Binder Weight <sup>1</sup>	Final Weight <sup>1</sup>	Depth <sup>2</sup>
0-4' #9	6.0005	1.2001	7.2006	0.3
0-4' #19	6.0006	1.2007	7.2013	0.7
0-4' #24	6.0007	1.2005	7.2012	0.9
0-4' #29	6.0001	1.2007	7.2008	1.1
4-8' #2	6.0007	1.2007	7.2014	1.3
4-8' #7	6.0007	1.2003	7.2010	1.5
4-8' #12	6.0003	1.2003	7.2006	1.7
4-8' #17	6.0008	1.2004	7.2012	1.8
4-8' #22	6.0004	1.2008	7.2012	2.0
4-8' #27	6.0002	1.2002	7.2004	2.2
4-8' #31	6.0004	1.2002	7.2006	2.4
8-12' #3	6.0004	1.2004	7.2008	2.6
8-12' #8	6.0002	1.2001	7.2003	2.9
8-12' #13	6.0003	1.2008	7.2011	3.3
8-12' #17	6.0007	1.2007	7.2014	3.6
12-16' #11	6.0006	1.2005	7.2011	4.1
12-16' #16	6.0007	1.2005	7.2012	4.2
12-16' #21	6.0004	1.2003	7.2007	4.4
12-16' #26	6.0008	1.2004	7.2012	4.5
12-16' #31	6.0002	1.2007	7.2009	4.7
12-16' #35	6.0004	1.2007	7.2011	4.8
16-20' #2	6.0002	1.2003	7.2005	4.9
16-20' #7	6.0007	1.2004	7.2011	5.1
16-20' #17	6.0008	1.2002	7.2010	5.2
16-20' #27	6.0005	1.2003	7.2008	5.3
16-20' #32	6.0006	1.2001	7.2007	5.6
16-20' #37	6.0005	1.2003	7.2008	5.8
16-20' #42	6.0005	1.2000	7.2005	5.9
20-24' #2	6.0008	1.2008	7.2016	6.1
20-24' #7	6.0007	1.2008	7.2015	6.1
20-24' #12	6.0008	1.2007	7.2015	6.2
20-24' #17	6.0006	1.2001	7.2007	6.6
20-24' #23	6.0008	1.2007	7.2015	7.1

1. Weights are presented in grams

2. Depth is expressed in meters below the land surface

Sample ID	Sediment Weight <sup>1</sup>	Binder Weight <sup>1</sup>	Final Weight <sup>1</sup>	Depth <sup>2</sup>
20-24' #28	6.0009	1.2001	7.2010	7.2
20-24' #32	6.0007	1.2003	7.2010	7.3
24-28' #7	6.0006	1.2004	7.2010	7.5
24-28' #17	6.0002	1.2006	7.2008	7.7
24-28' #22	6.0008	1.2009	7.2017	7.8
24-28' #32	6.0007	1.2001	7.2008	8.0
24-28' #37	6.0003	1.2006	7.2009	8.1
24-28' #42	6.0003	1.2000	7.2003	8.3
24-28' #46	6.0004	1.2001	7.2005	8.5
28-32' #2	6.0003	1.2001	7.2004	8.6
28-32' #7	6.0007	1.2001	7.2008	8.9
28-32' #12	6.0008	1.2003	7.2011	9.1
28-32' #17	6.0006	1.2005	7.2011	9.4
28-32' #22	6.0006	1.2007	7.2013	9.6
32-36' #2	6.0006	1.2000	7.2006	10.0
32-36' #7	6.0004	1.2004	7.2008	10.1
32-36' #12	6.0008	1.2004	7.2012	10.3
32-36' #17	6.0008	1.2005	7.2013	10.5
32-36' #27	6.0004	1.2003	7.2007	10.7
32-36' #30	6.0007	1.2006	7.2013	10.9

1. Weights are presented in grams

2. Depth is expressed in meters below the land surface



#### Appendix G4: Total Elemental Concentrations of TC14 Pellet Samples

Sample ID <sup>1</sup>	Sum of Concentrations	Al	S	Fe	K	Mg	Mn	Depth <sup>2</sup>
0-4' #9	100.93	1.91	0.02	0.42	0.87	0.04	0.01	0.3
0-4' #19	100.71	2.53	0.01	0.48	1.02	0.06	0.01	0.7
0-4' #24	101.42	2.40	0.00	0.47	1.00	0.06	0.01	0.9
0-4' #29	101.00	2.20	0.01	0.43	1.05	0.05	0.01	1.1
4-8' #2	102.41	2.11	0.00	0.42	1.06	0.05	0.01	1.3
4-8' #7	101.99	2.29	0.01	0.48	1.13	0.06	0.01	1.5
4-8' #12	101.38	2.14	0.00	0.60	1.02	0.05	0.01	1.7
4-8' #17	99.73	2.54	0.00	0.68	0.94	0.10	0.01	1.8
4-8' #22	80.05	1.08	ND <sup>3</sup>	0.31	0.33	ND <sup>3</sup>	0.01	2.0
4-8' #27	101.71	2.05	ND <sup>3</sup>	0.47	0.74	ND <sup>3</sup>	0.01	2.2
4-8' #31	91.28	3.18	0.00	0.60	0.84	0.02	0.01	2.4
8-12' #3	82.78	1.36	ND <sup>3</sup>	0.29	0.46	ND <sup>3</sup>	0.00	2.6
8-12' #8	83.47	1.53	0.01	0.31	0.95	0.04	0.00	2.9
8-12' #13	82.15	1.92	0.00	0.45	0.99	0.05	0.00	3.3
8-12' #17	80.30	1.25	0.00	0.55	0.74	ND <sup>3</sup>	0.00	3.6
12-16' #11	96.22	8.46	0.01	7.73	2.19	1.01	0.03	4.1
12-16' #16	99.62	5.66	0.07	2.22	1.71	0.59	0.02	4.2
12-16' #21	97.11	5.22	0.06	3.99	1.46	0.33	0.02	4.4
12-16' #26	95.91	5.76	0.04	4.57	1.38	0.73	0.03	4.5
12-16' #31	92.34	2.39	0.00	3.48	0.59	0.08	0.06	4.7
12-16' #35	90.44	2.66	0.02	7.68	0.60	0.15	0.11	4.8
16-20' #2	91.39	2.18	0.03	8.25	0.77	0.13	0.17	4.9
16-20' #7	90.04	2.67	0.16	5.62	0.61	0.15	0.10	5.1
16-20' #17	95.56	1.94	0.21	6.37	0.60	0.15	0.12	5.2
16-20' #27	97.15	1.73	0.14	3.08	0.46	0.14	0.07	5.3
16-20' #32	92.70	0.88	0.13	4.90	0.35	0.08	0.11	5.6
16-20' #37	95.23	0.54	0.14	2.65	0.23	0.06	0.07	5.8
16-20' #42	90.79	0.94	0.10	4.68	0.30	0.08	0.10	5.9

1. Initial 2014 XRF elemental concentrations (wt. %)

2. Depth is expressed in meters below the land surface

3. ND: Not Detected

Sample ID <sup>1</sup>	Na	P	Si	Ti	Ca	F	Cl	Sr
0-4' #9	0.18	0.01	44.20	0.38	0.07	0.01	ND <sup>2</sup>	64
0-4' #19	0.22	0.01	43.39	0.38	0.07	0.01	ND <sup>2</sup>	68
0-4' #24	0.06	0.01	44.00	0.37	0.07	0.00	ND <sup>2</sup>	68
0-4' #29	0.23	0.01	43.80	0.41	0.08	0.01	ND <sup>2</sup>	72
4-8' #2	0.23	0.01	44.59	0.37	0.07	0.01	ND <sup>2</sup>	69
4-8' #7	0.25	0.01	44.08	0.42	0.08	0.01	ND <sup>2</sup>	78
4-8' #12	0.21	0.01	43.89	0.50	0.07	0.01	ND <sup>2</sup>	69
4-8' #17	0.16	0.02	42.88	0.37	0.05	0.02	ND <sup>2</sup>	58
4-8' #22	0.03	ND <sup>2</sup>	35.80	0.35	ND <sup>2</sup>	0.00	ND <sup>2</sup>	51
4-8' #27	0.03	0.01	44.59	0.52	0.02	0.00	ND <sup>2</sup>	68
4-8' #31	0.03	0.01	38.56	0.49	0.03	0.00	ND <sup>2</sup>	62
8-12' #3	0.04	0.00	36.89	0.17	ND <sup>2</sup>	0.01	ND <sup>2</sup>	52
8-12' #8	0.09	0.02	36.70	0.22	0.02	0.01	ND <sup>2</sup>	43
8-12' #13	0.09	0.02	35.59	0.17	0.01	0.01	ND <sup>2</sup>	45
8-12' #17	0.03	0.00	35.58	0.12	0.00	ND <sup>2</sup>	ND <sup>2</sup>	47
12-16' #11	0.20	0.08	29.80	0.58	0.40	0.15	ND <sup>2</sup>	101
12-16' #16	0.13	0.08	37.89	0.51	0.40	0.08	ND <sup>2</sup>	148
12-16' #21	0.17	0.20	36.27	0.48	0.33	0.11	ND <sup>2</sup>	112
12-16' #26	0.08	0.27	34.64	0.45	0.35	0.09	ND <sup>2</sup>	84
12-16' #31	0.07	0.20	37.92	0.22	0.18	0.10	ND <sup>2</sup>	56
12-16' #35	0.07	0.88	32.60	0.19	1.35	0.32	ND <sup>2</sup>	70
16-20' #2	0.11	2.39	24.67	0.18	11.46	0.47	ND <sup>2</sup>	293
16-20' #7	0.12	4.92	22.58	0.14	14.46	0.76	1	363
16-20' #17	0.10	5.00	25.38	0.16	10.96	0.82	ND <sup>2</sup>	302
16-20' #27	0.10	4.73	28.65	0.09	11.26	0.67	ND <sup>2</sup>	328
16-20' #32	0.13	2.65	20.23	0.07	24.15	0.36	21	549
16-20' #37	0.15	1.72	17.17	0.04	34.94	0.21	95	809
16-20' #42	0.11	1.59	21.93	0.06	22.26	0.22	34	565

1. Initial 2014 XRF elemental concentrations presented as weight percents except for Cl and Sr, which are in ppm

2. ND: Not Detected

Sample ID <sup>1</sup>	Sum of Concentrations	Al	S	Fe	K	Mg	Mn	Depth <sup>2</sup>
20-24' #2	91.51	0.80	0.24	3.55	0.36	0.03	0.09	6.1
20-24' #7	90.04	0.76	0.24	3.77	0.35	0.16	0.10	6.1
20-24' #12	89.98	1.11	0.29	2.17	0.47	0.07	0.04	6.2
20-24' #17	90.77	2.28	1.00	1.17	0.80	0.14	0.01	6.6
20-24' #28	91.53	0.58	0.45	0.49	0.30	0.04	0.01	7.2
20-24' #32	91.94	0.85	0.47	0.62	0.38	0.09	0.01	7.3
24-28' #2	88.42	0.82	0.41	0.50	0.43	0.04	0.01	7.3
24-28' #7	90.13	1.41	0.32	0.78	0.64	0.07	0.01	7.5
24-28' #17	92.90	1.64	0.48	0.95	0.69	0.06	0.01	7.7
24-28' #22	92.31	1.43	0.45	0.76	0.56	0.04	0.01	7.8
24-28' #32	91.85	1.00	0.33	0.77	0.43	0.04	0.01	8.0
24-28' #37	94.09	1.75	0.29	0.94	0.65	0.03	0.01	8.1
24-28' #42	80.24	1.45	0.22	0.72	0.69	0.04	0.01	8.3
24-28' #46	90.68	1.53	0.12	0.52	0.78	0.02	0.00	8.5
28-32' #2	91.85	1.68	0.17	0.78	0.74	0.08	0.01	8.6
28-32' #7	92.57	4.71	0.54	2.29	1.29	0.03	0.02	8.9
28-32' #12	87.16	1.61	0.29	0.86	0.72	0.03	0.01	9.1
28-32' #17	84.61	0.99	0.39	0.75	0.56	0.04	0.01	9.4
28-32' #22	85.82	1.03	0.27	0.61	0.52	0.02	0.01	9.6
32-36' #2	94.38	2.06	1.15	1.33	0.78	0.32	0.01	10.0
32-36' #7	96.14	2.29	0.92	2.13	0.88	0.56	0.04	10.1
32-36' #12	97.36	1.78	0.77	1.97	0.76	0.51	0.04	10.3
32-36' #17	96.17	1.74	0.89	2.02	0.80	0.57	0.04	10.5
32-36' #27	93.55	1.10	0.67	1.27	0.72	0.56	0.03	10.7
32-36' #30	93.38	1.25	0.68	1.44	0.81	0.58	0.02	10.9

1. Initial 2014 XRF elemental concentrations (wt. %)

2. Depth is expressed in meters below the land surface

Sample ID <sup>1</sup>	Na	P	Si	Ti	Ca	F	Cl	Sr
20-24' #2	0.05	0.94	21.56	0.07	25.65	0.15	53	660
20-24' #7	0.20	1.06	17.71	0.07	29.82	0.12	111	654
20-24' #12	0.12	0.74	18.60	0.10	30.02	0.14	72	739
20-24' #17	0.10	0.68	22.94	0.17	22.55	0.03	46	726
20-24' #28	0.12	1.57	22.25	0.10	26.50	0.19	107	785
20-24' #32	0.10	1.45	23.27	0.17	24.74	0.21	120	745
24-28' #2	0.09	0.82	24.00	0.13	22.50	0.06	77	698
24-28' #7	0.05	0.37	24.85	0.22	21.97	ND <sup>2</sup>	67	722
24-28' #17	0.11	0.36	24.62	0.33	23.38	0.13	89	739
24-28' #22	0.09	0.43	25.47	0.18	22.35	0.19	63	699
24-28' #32	0.07	0.30	33.36	0.38	10.87	0.01	13	397
24-28' #37	0.08	0.19	38.91	0.40	2.72	0.11	ND <sup>2</sup>	166
24-28' #42	0.06	0.11	33.28	0.42	2.21	0.05	422	137
24-28' #46	0.06	0.13	38.70	0.13	1.79	0.10	21	147
28-32' #2	0.08	0.13	38.28	0.37	2.48	0.05	ND <sup>2</sup>	163
28-32' #7	0.04	0.12	32.00	0.63	6.20	ND <sup>2</sup>	ND <sup>2</sup>	277
28-32' #12	0.04	0.20	32.74	0.47	7.37	0.08	6	293
28-32' #17	0.05	0.34	25.44	0.53	17.55	ND <sup>2</sup>	46	494
28-32' #22	0.06	0.16	22.86	0.19	23.21	ND <sup>2</sup>	94	652
32-36' #2	0.30	1.03	22.10	0.14	25.40	0.11	115	803
32-36' #7	0.20	1.21	26.93	0.17	17.77	0.20	42	377
32-36' #12	0.23	2.15	27.76	0.14	16.83	0.30	20	563
32-36' #17	0.17	1.37	28.61	0.19	15.89	0.22	21	368
32-36' #27	0.10	0.40	22.88	0.16	26.39	0.08	25	278
32-36' #30	0.12	0.19	27.07	0.26	19.62	0.07	9	284

1. Initial 2014 XRF elemental concentrations presented as weight percents except for Cl and Sr, which are in ppm

2. ND: Not Detected

**Appendix G5: Results of Replicate XRF Analyses**

MRG-1 <sup>1</sup>	Al	S	Fe	K	Mg	Mn	Na	P	Si	Ti	Ca	F	Cl	Sr
Accepted Value	4.50	0.06	12.48	0.15	8.13	0.13	0.43	0.03	18.38	2.21	10.56	0.03		260
Trial 1	3.71	0.06	9.98	0.17	7.56	0.12	0.39	0.03	21.30	2.14	11.43	0.07	261	172
Trial 2	3.71	0.06	9.99	0.17	7.56	0.12	0.39	0.03	21.29	2.14	11.43	0.07	265	171
Trial 3	3.72	0.06	9.99	0.17	7.57	0.12	0.39	0.03	21.31	2.14	11.45	0.08	259	171
Trial 4	3.88	0.06	9.98	0.17	7.56	0.12	0.39	0.03	21.47	2.14	11.46	0.07	260	169
Trial 5	3.87	0.06	10.00	0.17	7.56	0.12	0.38	0.03	21.46	2.14	11.46	0.07	259	172
Trial 6	3.87	0.06	10.00	0.17	7.55	0.12	0.38	0.03	21.48	2.14	11.47	0.07	263	171
Trial 7	3.84	0.06	9.84	0.17	7.54	0.11	0.29	0.03	21.43	2.13	11.42	0.05	260	169
Trial 8	3.83	0.06	9.84	0.17	7.53	0.11	0.42	0.03	21.42	2.13	11.43	0.03	264	169
Trial 9	3.84	0.06	9.86	0.17	7.55	0.11	0.34	0.03	21.44	2.13	11.43	0.03	262	166
Trial 10	3.72	0.06	9.82	0.17	7.53	0.11	0.39	0.03	21.32	2.13	11.41	0.04	261	168
Trial 11	3.88	0.06	9.92	0.17	7.62	0.11	0.39	0.03	21.49	2.14	11.52	0.05	258	170
Trial 12	3.88	0.06	9.91	0.17	7.62	0.11	0.35	0.03	21.50	2.15	11.51	0.14	266	169
Trial 13	3.89	0.06	9.92	0.17	7.58	0.11	0.39	0.03	21.48	2.14	11.54	0.08	260	170
Trial 14	3.89	0.06	9.89	0.17	7.57	0.11	0.39	0.03	21.50	2.14	11.53	0.07	262	170

1.2015 replicate analyses of reference sample MRG-1 (gabbro). Elemental concentrations are presented as weight percents except for Cl and Sr, which are in ppm

NCS DC 71302 <sup>1</sup>	Al	S	Fe	K	Mg	Mn	Na	P	Si	Ti	Ca	F	Cl	Sr
Accepted Value	8.52	0.02	3.30	4.29	0.51	0.69	1.85	0.16	29.48	0.48	1.77	0.11	160	318
Trial 1	8.59	0.02	3.11	4.42	0.57	0.07	1.79	0.13	28.90	0.47	1.80	0.08	212	358
Trial 2	8.58	0.02	3.10	4.42	0.57	0.07	1.78	0.13	28.88	0.47	1.80	0.08	219	355
Trial 3	8.56	0.03	3.10	4.42	0.57	0.07	1.78	0.14	28.84	0.47	1.80	0.07	219	357
Trial 4	8.70	0.03	3.11	4.44	0.57	0.07	1.79	0.14	28.99	0.47	1.81	0.08	212	357
Trial 5	8.70	0.02	3.12	4.43	0.57	0.07	1.78	0.14	28.97	0.47	1.81	0.07	217	361
Trial 6	8.70	0.02	3.11	4.43	0.57	0.07	1.78	0.14	28.96	0.47	1.81	0.08	214	356
Trial 7	8.66	0.03	3.10	4.44	0.57	0.07	1.78	0.14	28.98	0.47	1.81	0.08	211	358
Trial 8	8.65	0.03	3.10	4.43	0.57	0.07	1.78	0.14	28.97	0.47	1.81	0.07	217	357
Trial 9	8.65	0.03	3.10	4.43	0.57	0.07	1.77	0.13	28.92	0.47	1.81	0.08	219	355
Trial 10	8.56	0.03	3.06	4.43	0.56	0.07	1.74	0.13	28.85	0.47	1.80	0.09	211	353
Trial 11	8.67	0.03	3.06	4.44	0.55	0.07	1.75	0.14	28.92	0.47	1.81	0.09	202	351
Trial 12	8.63	0.02	3.06	4.43	0.56	0.07	1.75	0.13	28.87	0.47	1.81	0.08	209	353
Trial 13	8.98	0.02	3.06	4.43	0.56	0.07	1.73	0.13	29.05	0.47	1.80	0.10	205	352
Trial 14	9.08	0.03	3.10	4.44	0.57	0.07	1.76	0.14	29.28	0.48	1.81	0.07	246	355
Trial 15	9.05	0.03	3.10	4.44	0.57	0.07	1.75	0.14	29.22	0.48	1.81	0.08	251	352

1.2015 replicate analyses of reference sample NCS DC 71302. Elemental concentrations are presented as weight percents except for Cl and Sr, which are in ppm

TC14 0-4' #9 <sup>1</sup>	Al	S	Fe	K	Mg	Mn	Na	P	Si	Ti	Ca	F	Cl	Sr
Original Value	1.91	0.02	0.42	0.87	0.04	0.01	0.18	0.01	44.20	0.38	0.07	0.01	ND <sup>2</sup>	64
Trial 1	1.79	0.01	0.42	0.86	0.04	0.01	0.18	0.02	41.55	0.37	0.07	0.01	21	65
Trial 2	1.79	0.01	0.42	0.86	0.04	0.01	0.18	0.02	41.51	0.37	0.07	0.01	28	64
Trial 3	1.79	0.01	0.42	0.86	0.04	0.01	0.18	0.02	41.44	0.37	0.07	0.01	27	63
Trial 4	1.83	0.01	0.42	0.86	0.04	0.01	0.18	0.02	41.86	0.37	0.07	0.00	18	63
Trial 5	1.84	0.01	0.42	0.86	0.04	0.01	0.18	0.02	41.78	0.37	0.07	0.01	23	63
Trial 6	1.83	0.01	0.42	0.86	0.04	0.01	0.18	0.02	41.80	0.37	0.07	0.01	25	63
Trial 7	1.82	0.01	0.42	0.87	0.04	0.01	0.18	0.02	41.68	0.37	0.07	0.01	21	64
Trial 8	1.82	0.01	0.42	0.87	0.04	0.01	0.18	0.02	41.73	0.37	0.07	0.01	23	65
Trial 9	1.82	0.01	0.42	0.86	0.04	0.01	0.18	0.02	41.66	0.37	0.07	0.01	21	64
Trial 10	1.79	0.01	0.42	0.87	0.04	0.01	0.19	0.02	41.52	0.37	0.07	0.01	25	65
Trial 11	1.83	0.01	0.42	0.87	0.04	0.01	0.18	0.02	41.72	0.37	0.07	0.01	20	63
Trial 12	1.82	0.01	0.42	0.87	0.04	0.01	0.18	0.02	41.73	0.37	0.07	0.01	17	63
Trial 13	1.89	0.02	0.42	0.87	0.04	0.01	0.15	0.02	42.00	0.37	0.07	0.05	14	65
Trial 14	1.90	0.02	0.42	0.87	0.04	0.01	0.17	0.02	42.15	0.37	0.07	0.01	7	65

1. 2015 replicate analyses of pellet sample TC14: 0-4' #9. Elemental concentrations are presented as weight percents except for Cl and Sr, which are in ppm

2. ND: Not detected

TC14 12-16' #26 <sup>1</sup>	Al	S	Fe	K	Mg	Mn	Na	P	Si	Ti	Ca	F	Cl	Sr
Original Value	5.76	0.04	4.57	1.38	0.73	0.03	0.08	0.27	34.64	0.45	0.35	0.09	ND <sup>2</sup>	84
Trial 1	5.13	0.01	4.46	1.33	0.74	0.03	0.16	0.27	32.86	0.45	0.34	0.10	ND <sup>2</sup>	85
Trial 2	5.13	0.01	4.45	1.32	0.74	0.03	0.17	0.27	32.82	0.45	0.34	0.10	ND <sup>2</sup>	84
Trial 3	5.12	0.01	4.44	1.32	0.74	0.03	0.17	0.27	32.76	0.45	0.34	0.10	ND <sup>2</sup>	83
Trial 4	5.24	0.01	4.47	1.33	0.74	0.03	0.17	0.27	32.99	0.45	0.35	0.10	ND <sup>2</sup>	82
Trial 5	5.23	0.01	4.46	1.33	0.74	0.03	0.17	0.27	32.92	0.45	0.34	0.10	ND <sup>2</sup>	84
Trial 6	5.23	0.01	4.45	1.33	0.73	0.03	0.17	0.27	32.82	0.45	0.34	0.10	ND <sup>2</sup>	85
Trial 7	5.45	0.01	4.40	1.33	0.74	0.03	0.18	0.27	33.11	0.45	0.35	0.11	ND <sup>2</sup>	84
Trial 8	5.40	0.01	4.39	1.33	0.71	0.03	0.18	0.27	32.99	0.45	0.34	0.10	ND <sup>2</sup>	83
Trial 9	5.32	0.01	4.38	1.33	0.73	0.03	0.17	0.27	32.80	0.44	0.34	0.10	ND <sup>2</sup>	81

1. 2015 replicate analyses of pellet sample TC14: 0-4' #9. Elemental concentrations are presented as weight percents except for Cl and Sr, which are in ppm

2. Not detected



TC14 12-16' #35 <sup>1</sup>	Al	S	Fe	K	Mg	Mn	Na	P	Si	Ti	Ca	F	Cl	Sr
Original Value	2.66	0.02	7.68	0.60	0.15	0.11	0.07	0.88	32.60	0.19	1.35	0.32	ND <sup>2</sup>	70
Trial 1	2.34	0.03	7.61	0.57	0.24	0.11	0.10	0.84	31.06	0.19	1.31	0.25	21	69
Trial 2	2.34	0.03	7.61	0.58	0.24	0.11	0.10	0.84	31.01	0.19	1.31	0.25	24	70
Trial 3	2.33	0.03	7.60	0.57	0.24	0.11	0.10	0.84	30.99	0.19	1.31	0.24	17	70
Trial 4	2.43	0.03	7.64	0.58	0.24	0.11	0.10	0.84	31.27	0.19	1.31	0.24	26	71
Trial 5	2.44	0.03	7.63	0.57	0.24	0.11	0.10	0.84	31.27	0.19	1.31	0.25	18	72
Trial 6	2.44	0.03	7.64	0.58	0.24	0.11	0.10	0.84	31.21	0.19	1.31	0.24	17	71
Trial 7	2.39	0.03	7.63	0.58	0.24	0.11	0.10	0.84	31.19	0.19	1.32	0.25	14	70
Trial 8	2.40	0.03	7.64	0.58	0.24	0.11	0.10	0.84	31.12	0.19	1.32	0.24	14	70
Trial 9	2.40	0.03	7.65	0.58	0.24	0.11	0.10	0.84	31.02	0.19	1.32	0.24	13	71
Trial 10	2.33	0.03	7.52	0.58	0.24	0.11	0.11	0.84	30.86	0.19	1.32	0.24	2	69
Trial 11	2.40	0.03	7.54	0.58	0.24	0.11	0.10	0.84	30.97	0.19	1.32	0.24	ND <sup>2</sup>	70
Trial 12	2.40	0.03	7.53	0.58	0.24	0.11	0.10	0.84	30.87	0.19	1.31	0.24	ND <sup>2</sup>	71
Trial 13	2.55	0.02	7.56	0.58	0.24	0.11	0.11	0.86	31.28	0.19	1.32	0.26	ND <sup>2</sup>	69
Trial 14	2.53	0.02	7.59	0.59	0.24	0.11	0.10	0.86	31.21	0.19	1.32	0.24	ND <sup>2</sup>	71

1.2015 replicate analyses of pellet sample TC14: 12-16' #35. Elemental concentrations are presented as weight percents except for Cl and Sr, which are in ppm

TC14														
16-20' #7	Al	S	Fe	K	Mg	Mn	Na	P	Si	Ti	Ca	F	Cl	Sr
Original Value	2.67	0.16	5.62	0.61	0.15	0.10	0.12	4.92	22.58	0.14	14.46	0.76	1	363
Trial 1	2.38	0.18	5.54	0.59	0.28	0.10	0.14	4.82	21.77	0.14	14.05	0.70	25	368
Trial 2	2.37	0.18	5.53	0.59	0.28	0.10	0.14	4.83	21.76	0.14	14.04	0.71	24	365
Trial 3	2.37	0.18	5.52	0.59	0.28	0.10	0.14	4.80	21.72	0.14	14.04	0.70	29	365
Trial 4	2.53	0.18	5.56	0.59	0.28	0.10	0.14	4.84	21.95	0.14	14.12	0.71	25	368
Trial 5	2.54	0.18	5.55	0.59	0.28	0.10	0.14	4.84	21.94	0.14	14.10	0.70	25	367
Trial 6	2.54	0.18	5.54	0.59	0.28	0.10	0.14	4.82	21.90	0.14	14.09	0.68	22	367
Trial 7	2.49	0.18	5.55	0.60	0.28	0.10	0.14	4.86	21.87	0.14	14.16	0.70	18	367
Trial 8	2.48	0.18	5.54	0.59	0.28	0.10	0.14	4.84	21.81	0.14	14.14	0.71	16	366
Trial 9	2.47	0.18	5.54	0.59	0.27	0.10	0.14	4.82	21.73	0.14	14.11	0.71	15	369

1.2015 replicate analyses of pellet sample TC14: 16-20' #7. Elemental concentrations are presented as weight percents except for Cl and Sr, which are in ppm

TC14 32-36' #17	Al	S	Fe	K	Mg	Mn	Na	P	Si	Ti	Ca	F	Cl	Sr
Original Value	1.74	0.89	2.02	0.80	0.57	0.04	0.17	1.37	28.61	0.19	15.89	0.22	21	368
Trial 1	1.58	0.87	1.98	0.78	0.58	0.04	0.15	1.33	27.41	0.19	15.58	0.19	67	365
Trial 2	1.59	0.87	1.98	0.78	0.58	0.04	0.15	1.33	27.38	0.19	15.57	0.20	63	364
Trial 3	1.58	0.87	1.97	0.78	0.58	0.04	0.15	1.33	27.37	0.19	15.53	0.20	61	363
Trial 4	1.69	0.87	1.98	0.79	0.58	0.04	0.15	1.33	27.72	0.19	15.58	0.20	64	364
Trial 5	1.69	0.87	1.98	0.78	0.58	0.04	0.15	1.33	27.70	0.19	15.57	0.20	61	363
Trial 6	1.69	0.87	1.97	0.78	0.58	0.04	0.15	1.33	27.66	0.19	15.57	0.20	68	365
Trial 7	1.66	0.87	1.97	0.79	0.58	0.04	0.16	1.33	27.65	0.19	15.60	0.20	68	360
Trial 8	1.67	0.87	1.96	0.78	0.58	0.04	0.15	1.34	27.65	0.19	15.59	0.20	60	362
Trial 9	1.67	0.87	1.95	0.78	0.57	0.03	0.15	1.34	27.64	0.19	15.58	0.21	62	359
Trial 10	1.59	0.87	1.95	0.79	0.57	0.03	0.16	1.33	27.40	0.19	15.60	0.21	66	361
Trial 11	1.68	0.87	1.96	0.79	0.57	0.04	0.16	1.34	27.69	0.19	15.65	0.21	61	360
Trial 12	1.68	0.87	1.96	0.79	0.57	0.04	0.14	1.34	27.66	0.19	15.64	0.20	60	360
Trial 13	1.70	0.87	1.95	0.79	0.58	0.04	0.15	1.34	27.68	0.19	15.62	0.17	53	361
Trial 14	1.65	0.87	1.95	0.79	0.58	0.04	0.15	1.34	27.56	0.19	15.62	0.20	51	360
Trial 15	1.69	0.87	1.95	0.79	0.57	0.04	0.15	1.34	27.63	0.19	15.67	0.20	42	360
Trial 16	1.65	0.88	1.97	0.79	0.57	0.04	0.15	1.33	27.52	0.19	15.66	0.19	41	361
Trial 17	1.69	0.88	1.95	0.79	0.57	0.03	0.15	1.35	27.55	0.19	15.62	0.19	37	360
Trial 18	1.70	0.89	1.95	0.79	0.58	0.03	0.15	1.35	27.64	0.19	15.75	0.19	23	363

1.2015 replicate analyses of pellet sample TC14: 32-36' #17. Elemental concentrations are presented as weight percents except for Cl and Sr, which are in ppm

### Appendix G6: Statistics of XRF Pellet Samples

Sample <sup>1</sup>	Element <sup>2</sup>	Initial Value <sup>3</sup>	Mean <sup>4</sup>	Median	Confidence Level (95%)	Standard Deviation	Precision <sup>5</sup> (CV %)	Deviation <sup>6</sup>	% Deviation <sup>7</sup>	
TC14: 0-4' #9 (n = 14)	F	0.01	0.01	0.01	5.85E-03	1.01E-02	96.53	0.00	31.25	
	Na	0.18	0.18	0.18	4.95E-03	8.57E-03	4.86	0.00	-2.45	
	Mg	0.04	0.04	0.04	8.59E-04	1.49E-03	3.45	0.01	21.43	
	Al	1.91	1.83	1.82	0.02	0.03	1.83	-0.09	-4.67	
	Si	44.20	41.72	41.72	0.11	0.20	0.47	-2.48	-5.61	
	P	0.01	0.02	0.02	1.46E-04	2.53E-04	1.62	0.00	5.25	
	S	0.02	0.01	0.01	2.74E-04	4.75E-04	3.37	0.00	-17.23	
	Cl	NC <sup>8</sup>	NC <sup>8</sup>	NC <sup>8</sup>	NC <sup>8</sup>	NC <sup>8</sup>	NC <sup>8</sup>	NC <sup>8</sup>	NC <sup>8</sup>	NC <sup>8</sup>
	K	0.87	0.86	0.86	1.04E-03	1.80E-03	0.21	0.00	-0.51	
	Ca	0.07	0.07	0.07	5.23E-04	9.05E-04	1.25	0.00	4.42	
	Ti	0.38	0.37	0.37	4.44E-04	7.70E-04	0.21	-0.01	-2.31	
	Mn	0.01	0.01	0.01	1.90E-04	3.30E-04	2.88	0.00	5.61	
	Fe	0.42	0.42	0.42	1.97E-03	3.42E-03	0.81	0.00	0.73	
Sr	64.39	64.01	64.01	0.49	0.84	1.31	-0.38	-0.59		

1. Pellet samples evaluated once in 2014 and multiple times in 2015. The number (n) of replicate XRF analyses

2. Concentrations are expressed as weight percents except for Cl and Sr, which are in ppm

3. The initial concentration measured in 2014

4. Mean concentration for replicate analyses conducted in 2015

5. Precision of the 2015 analyses was determined via CV %.  $CV \% = (\text{standard deviation} \div \text{mean}) \times 100$

6. Deviation = mean value - initial value

7. Reproducibility of 2014 values was determined via % Deviation.  $\% \text{ Deviation} = [(\text{mean} - \text{initial value}) \div \text{initial value}] \times 100$

8. NC: Not calculated. This element was not detected in 2014

Sample <sup>1</sup>	Element <sup>2</sup>	Initial Value <sup>3</sup>	Mean <sup>4</sup>	Median	Confidence Level (95%)	Standard Deviation	Precision <sup>5</sup> (CV %)	Deviation <sup>6</sup>	% Deviation <sup>7</sup>
TC14:12-16' #26 (n = 9)	F	0.09	0.10	0.10	2.89E-03	3.76E-03	3.72	0.02	18.69
	Na	0.08	0.17	0.17	4.98E-03	6.47E-03	3.81	0.09	125.42
	Mg	0.73	0.73	0.74	7.84E-03	0.01	1.39	0.01	0.93
	Al	5.76	5.25	5.23	0.09	0.12	2.29	-0.51	-8.86
	Si	34.64	32.90	32.86	0.09	0.11	0.35	-1.74	-5.03
	P	0.27	0.27	0.27	1.05E-03	1.36E-03	0.51	-0.01	-1.99
	S	0.04	0.01	0.01	3.39E-04	4.41E-04	4.31	-0.03	-76.77
	Cl	NC <sup>8</sup>	NC <sup>8</sup>	NC <sup>8</sup>	NC <sup>8</sup>	NC <sup>8</sup>	NC <sup>8</sup>	NC <sup>8</sup>	NC <sup>8</sup>
	K	1.38	1.33	1.33	3.08E-03	4.01E-03	0.30	-0.05	-3.90
	Ca	0.35	0.34	0.34	7.49E-04	9.75E-04	0.28	-0.01	-3.00
	Ti	0.45	0.45	0.45	5.38E-04	6.99E-04	0.16	0.00	-0.81
	Mn	0.03	0.03	0.03	2.98E-04	3.87E-04	1.33	0.00	-0.88
Fe	4.57	4.43	4.45	0.03	0.03	0.78	-0.14	-3.04	
Sr	84.09	83.42	83.85	0.89	1.15	1.38	-0.67	-0.80	

1. Pellet samples evaluated once in 2014 and multiple times in 2015. The number (n) of replicate XRF analyses

2. Concentrations are expressed as weight percents except for Cl and Sr, which are in ppm

3. The initial concentration measured in 2014

4. Mean concentration for replicate analyses conducted in 2015

5. Precision of the 2015 analyses was determined via CV %.  $CV \% = (\text{standard deviation} \div \text{mean}) \times 100$

6. Deviation = mean value - initial value

7. Reproducibility of 2014 values was determined via % Deviation.  $\% \text{ Deviation} = [(\text{mean} - \text{initial value}) \div \text{initial value}] \times 100$

8. NC: Not calculated. This element was not detected in 2014

Sample <sup>1</sup>	Element <sup>2</sup>	Initial Value <sup>3</sup>	Mean <sup>4</sup>	Median	Confidence Level (95%)	Standard Deviation	Precision <sup>5</sup> (CV %)	Deviation <sup>6</sup>	% Deviation <sup>7</sup>
TC14: 12-16' #35 (n = 14)	F	0.32	0.24	0.24	3.96E-05	6.30E-03	2.59	-0.08	-24.66
	Na	0.07	0.10	0.10	3.77E-06	1.51E-03	1.45	0.03	42.44
	Mg	0.15	0.24	0.24	2.10E-06	1.12E-03	0.46	0.09	57.67
	Al	2.66	2.41	2.40	8.47E-03	0.07	2.78	-0.25	-9.45
	Si	32.60	31.10	31.09	0.05	0.15	0.47	-1.51	-4.63
	P	0.88	0.84	0.84	1.48E-04	8.04E-03	0.95	-0.03	-3.74
	S	0.02	0.03	0.03	2.15E-06	1.47E-03	5.44	0.00	17.39
	Cl	NC <sup>8</sup>	NC <sup>8</sup>	NC <sup>8</sup>	NC <sup>8</sup>	NC <sup>8</sup>	NC <sup>8</sup>	NC <sup>8</sup>	NC <sup>8</sup>
	K	0.60	0.58	0.58	1.26E-05	3.24E-03	0.56	-0.02	-3.76
	Ca	1.35	1.32	1.31	3.27E-05	4.83E-03	0.37	-0.03	-2.54
	Ti	0.19	0.19	0.19	1.07E-06	8.01E-04	0.43	0.00	0.21
	Mn	0.11	0.11	0.11	5.32E-07	6.42E-04	0.60	0.00	-1.37
Fe	7.68	7.60	7.61	2.55E-03	0.04	0.59	-0.08	-1.01	
Sr	70	70	70.41	0.79	0.89	1.26	0.53	0.76	

1. Pellet samples evaluated once in 2014 and multiple times in 2015. The number (n) of replicate XRF analyses

2. Concentrations are expressed as weight percents except for Cl and Sr, which are in ppm

3. The initial concentration measured in 2014

4. Mean concentration for replicate analyses conducted in 2015

5. Precision of the 2015 analyses was determined via CV %.  $CV \% = (\text{standard deviation} \div \text{mean}) \times 100$

6. Deviation = mean value - initial value

7. Reproducibility of 2014 values was determined via % Deviation.  $\% \text{ Deviation} = [(\text{mean} - \text{initial value}) \div \text{initial value}] \times 100$

8. NC: Not calculated. This element was not detected in 2014

Sample <sup>1</sup>	Element <sup>2</sup>	Initial Value <sup>3</sup>	Mean <sup>4</sup>	Median	Confidence Level (95%)	Standard Deviation	Precision <sup>5</sup> (CV %)	Deviation <sup>6</sup>	% Deviation <sup>7</sup>
TC14: 16-20' #7 (n = 9)	F	0.76	0.70	0.70	6.43E-03	8.37E-03	1.19	-0.06	-7.63
	Na	0.12	0.14	0.14	1.78E-03	2.32E-03	1.65	0.02	12.83
	Mg	0.15	0.28	0.28	1.03E-03	1.34E-03	0.48	0.13	85.17
	Al	2.67	2.46	2.48	0.06	0.07	2.93	-0.20	-7.67
	Si	22.58	21.83	21.81	0.07	0.09	0.41	-0.76	-3.36
	P	4.92	4.83	4.83	0.01	0.02	0.39	-0.09	-1.76
	S	0.16	0.18	0.18	6.66E-04	8.66E-04	0.48	0.02	11.25
	Cl	1.05	22.05	24.11	3.80	4.94	22.43	21.00	2009.74
	K	0.61	0.59	0.59	1.57E-03	2.04E-03	0.34	-0.02	-3.05
	Ca	14.46	14.10	14.10	0.03	0.04	0.32	-0.36	-2.51
	Ti	0.14	0.14	0.14	3.26E-04	4.24E-04	0.30	0.00	0.58
Mn	0.10	0.10	0.10	3.14E-04	4.08E-04	0.39	0.00	0.42	
Fe	5.62	5.54	5.54	8.19E-03	0.01	0.19	-0.07	-1.33	
Sr	363.21	366.86	367.02	0.99	1.28	0.35	3.66	1.01	

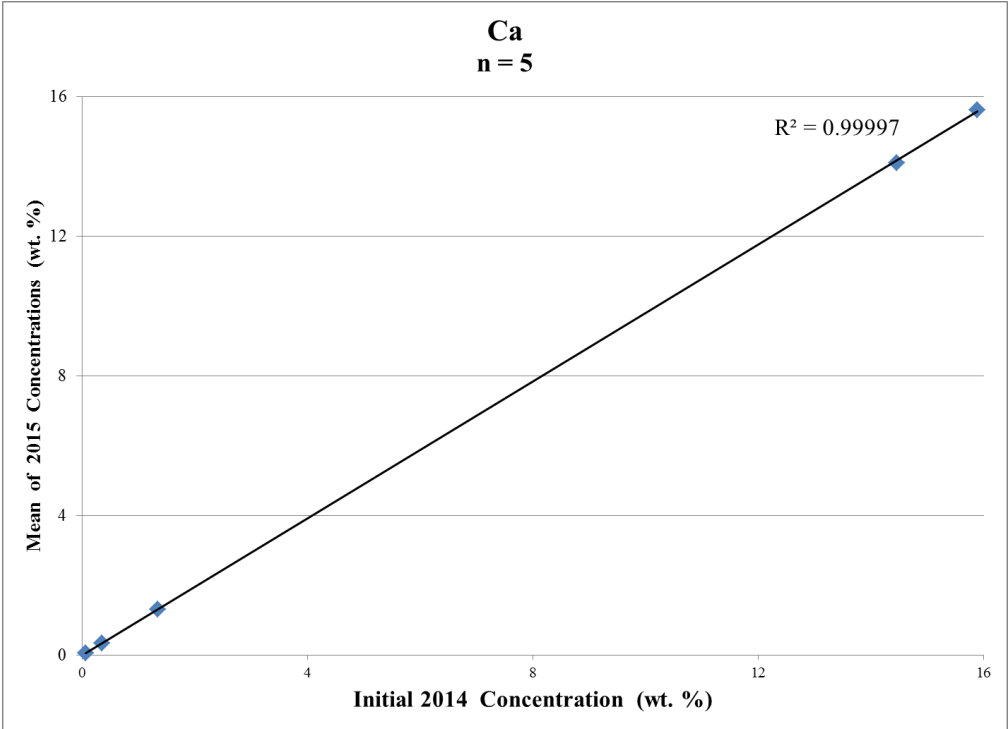
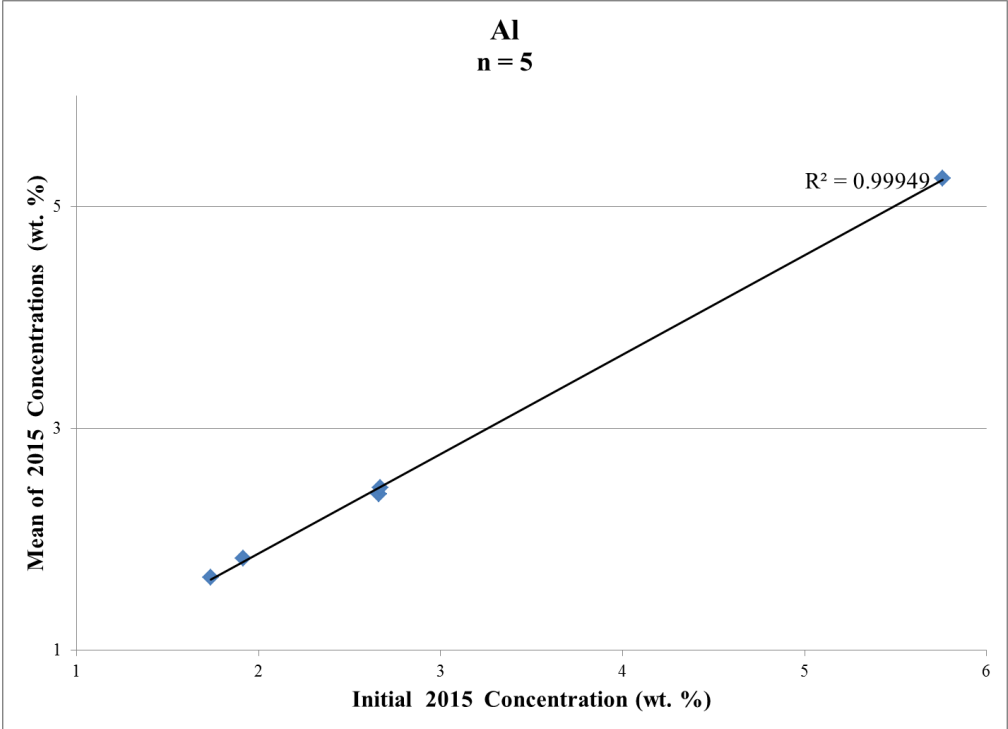
1. Pellet samples evaluated once in 2014 and multiple times in 2015. The number (n) of replicate XRF analyses
2. Concentrations are expressed as weight percents except for Cl and Sr, which are in ppm
3. The initial concentration measured in 2014
4. Mean concentration for replicate analyses conducted in 2015
5. Precision of the 2015 analyses was determined via CV %.  $CV \% = (\text{standard deviation} \div \text{mean}) \times 100$
6. Deviation = mean value - initial value
7. Reproducibility of 2014 values was determined via % Deviation.  $\% \text{ Deviation} = [(\text{mean} - \text{initial value}) \div \text{initial value}] \times 100$
8. NC: Not calculated. This element was not detected in 2014

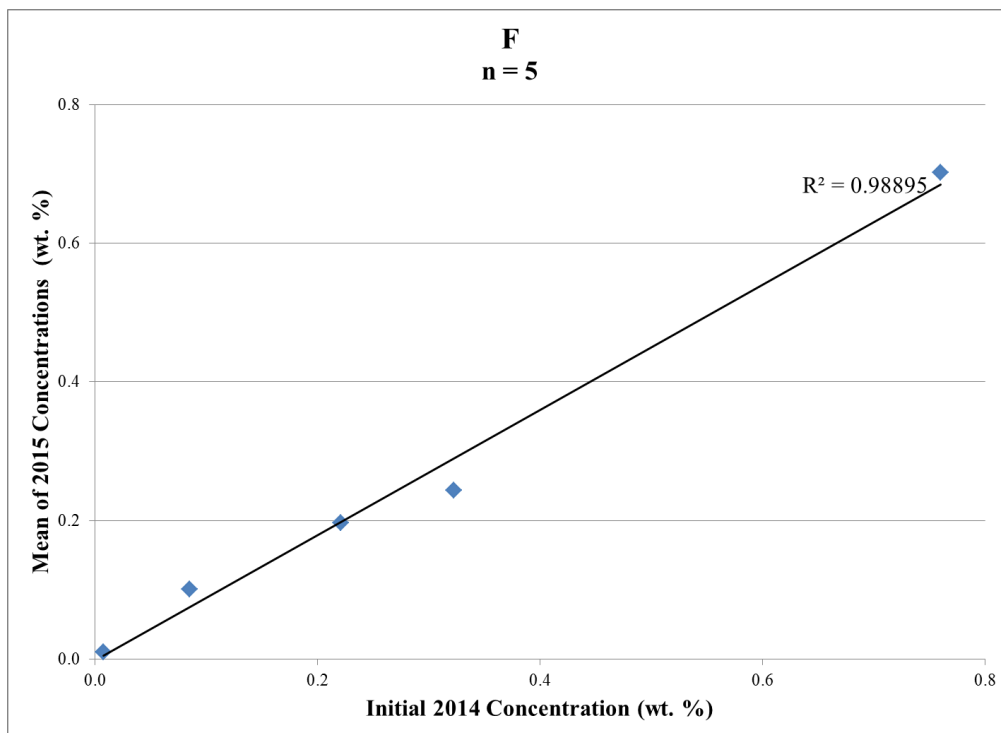
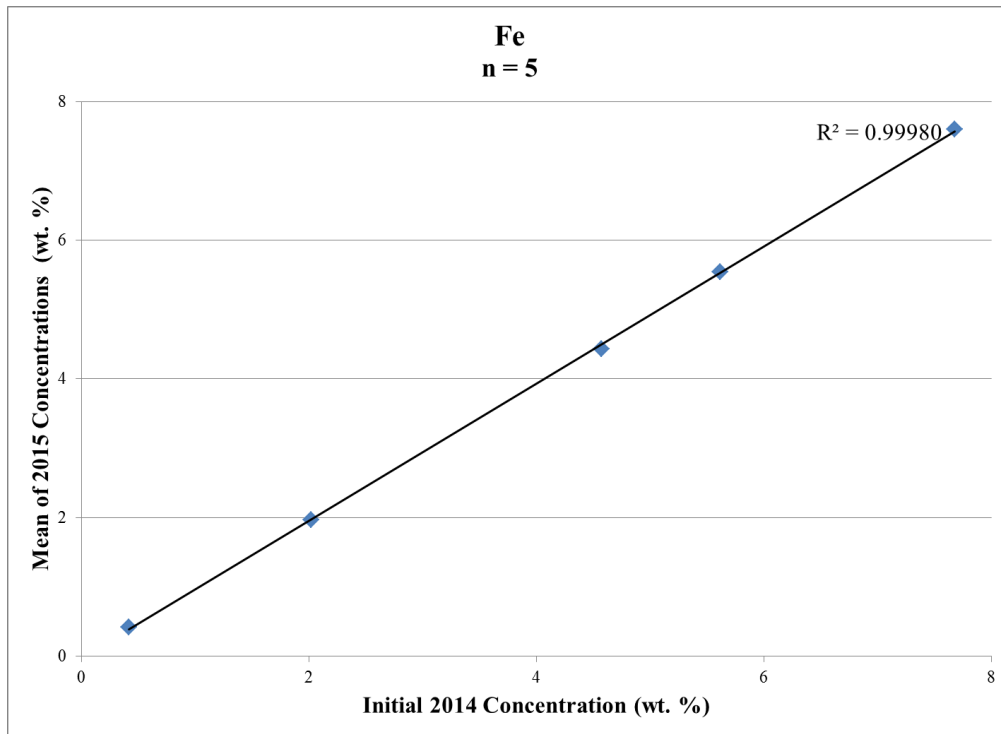
Sample <sup>1</sup>	Element <sup>2</sup>	Initial Value <sup>3</sup>	Mean <sup>4</sup>	Median	Confidence Level (95%)	Standard Deviation	Precision <sup>5</sup> (CV %)	Deviation <sup>6</sup>	% Deviation <sup>7</sup>
TC14: 32-36' #17 (n = 18)	F	0.22	0.20	0.20	4.43E-03	8.91E-03	4.53	-0.02	-10.96
	Na	0.17	0.15	0.15	2.43E-03	4.89E-03	3.25	-0.02	-10.91
	Mg	0.57	0.58	0.58	1.92E-03	3.86E-03	0.67	0.01	0.98
	Al	1.74	1.66	1.67	0.02	0.04	2.64	-0.08	-4.69
	Si	28.61	27.58	27.64	0.06	0.12	0.43	-1.03	-3.60
	P	1.37	1.34	1.33	2.37E-03	4.77E-03	0.36	-0.03	-2.19
	S	0.89	0.87	0.87	2.71E-03	5.45E-03	0.63	-0.02	-2.13
	Cl	20.66	55.98	60.93	6.28	12.63	22.57	35.31	170.92
	K	0.80	0.79	0.79	1.25E-03	2.51E-03	0.32	-0.02	-2.28
	Ca	15.89	15.61	15.60	0.02	0.05	0.32	-0.28	-1.76
	Ti	0.19	0.19	0.19	1.99E-04	4.01E-04	0.21	0.00	1.81
	Mn	0.04	0.04	0.04	1.65E-04	3.31E-04	0.93	0.00	-2.60
Fe	2.02	1.96	1.96	5.59E-03	0.01	0.57	-0.06	-2.80	
Sr	367.98	361.69	360.66	0.99	1.99	0.55	-6.30	-1.71	

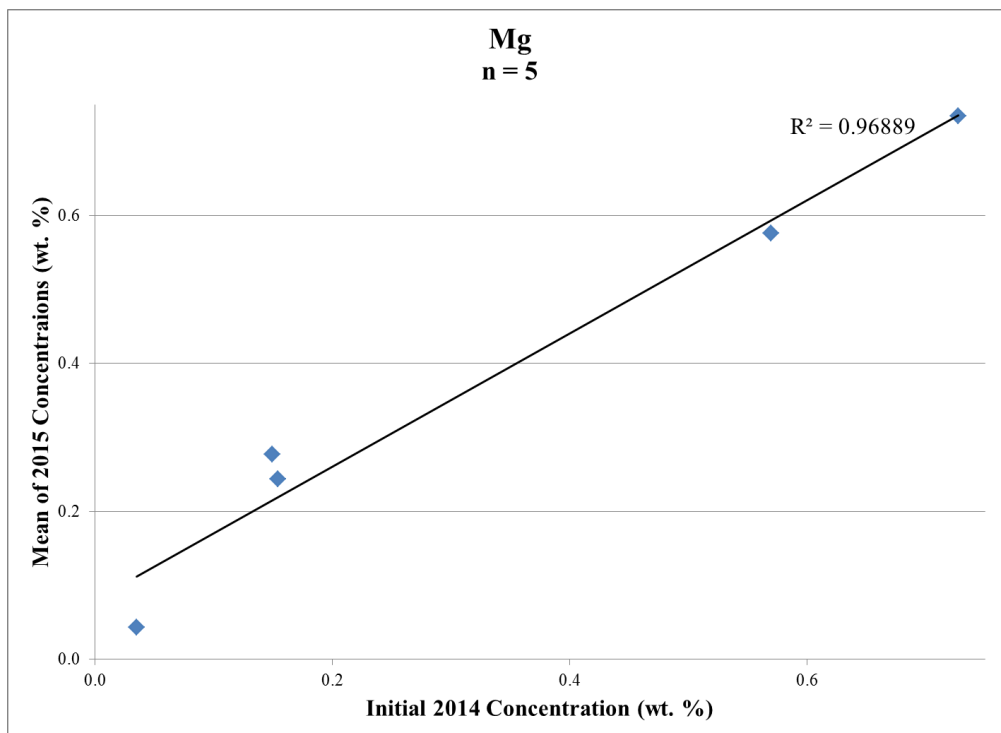
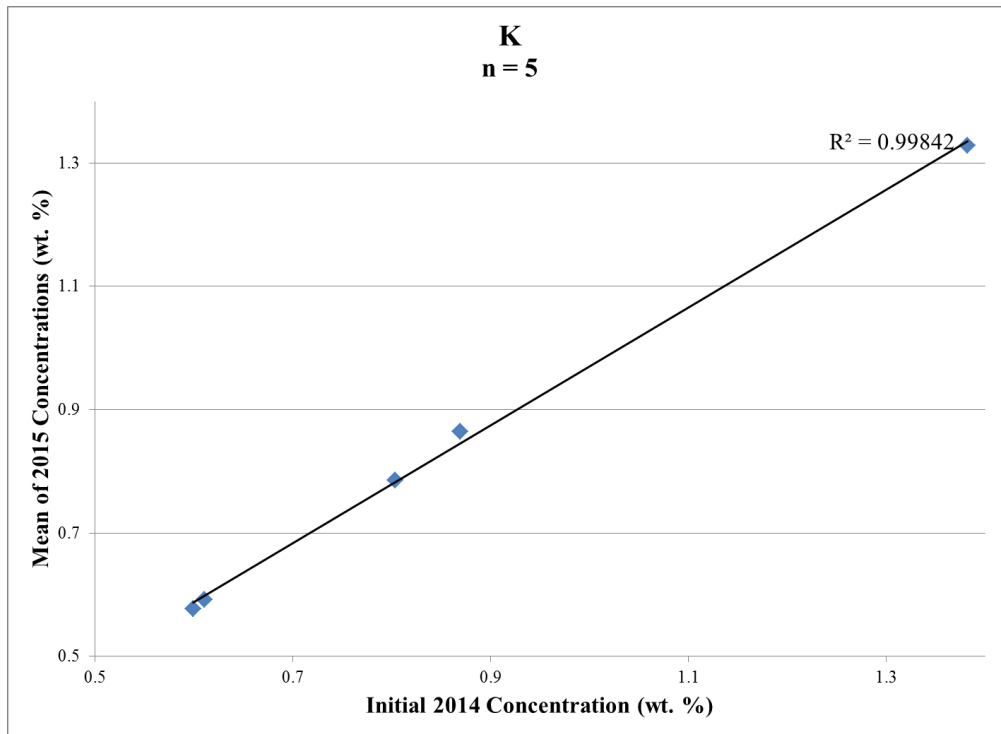
1. Pellet samples evaluated once in 2014 and multiple times in 2015. The number (n) of replicate XRF analyses
2. Concentrations are expressed as weight percents except for Cl and Sr, which are in ppm
3. The initial concentration measured in 2014
4. Mean concentration for replicate analyses conducted in 2015
5. Precision of the 2015 analyses was determined via CV %.  $CV \% = (\text{standard deviation} \div \text{mean}) \times 100$
6. Deviation = mean value - initial value
7. Reproducibility of 2014 values was determined via % Deviation.  $\% \text{ Deviation} = [(\text{mean} - \text{initial value}) \div \text{initial value}] \times 100$
8. NC: Not calculated. This element was not detected in 2014

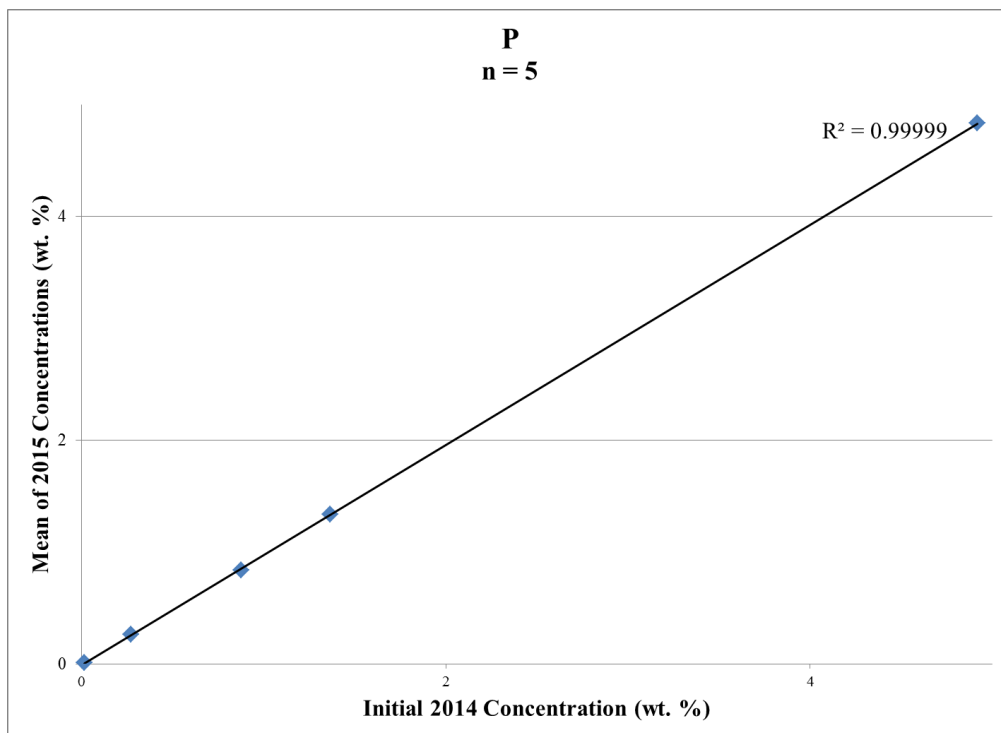
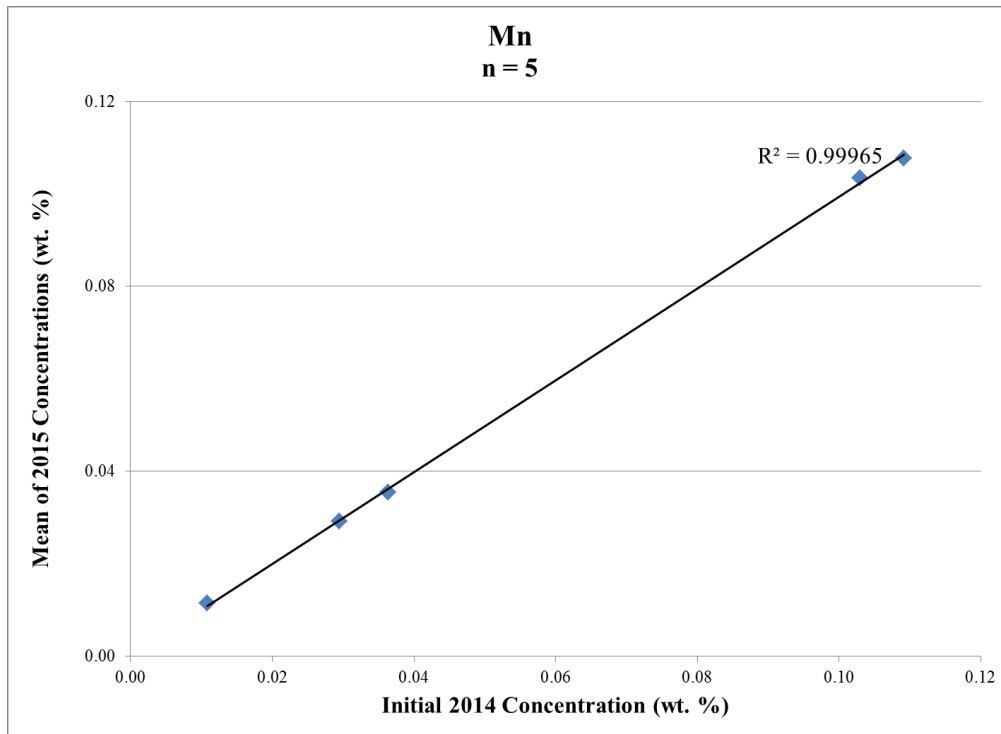


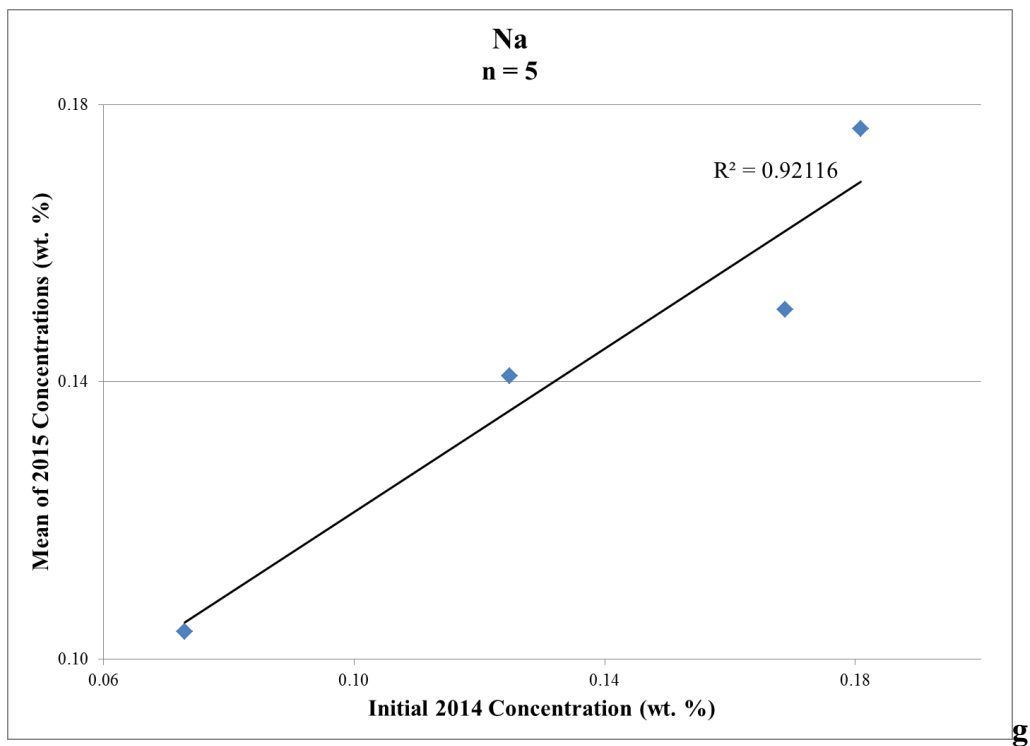
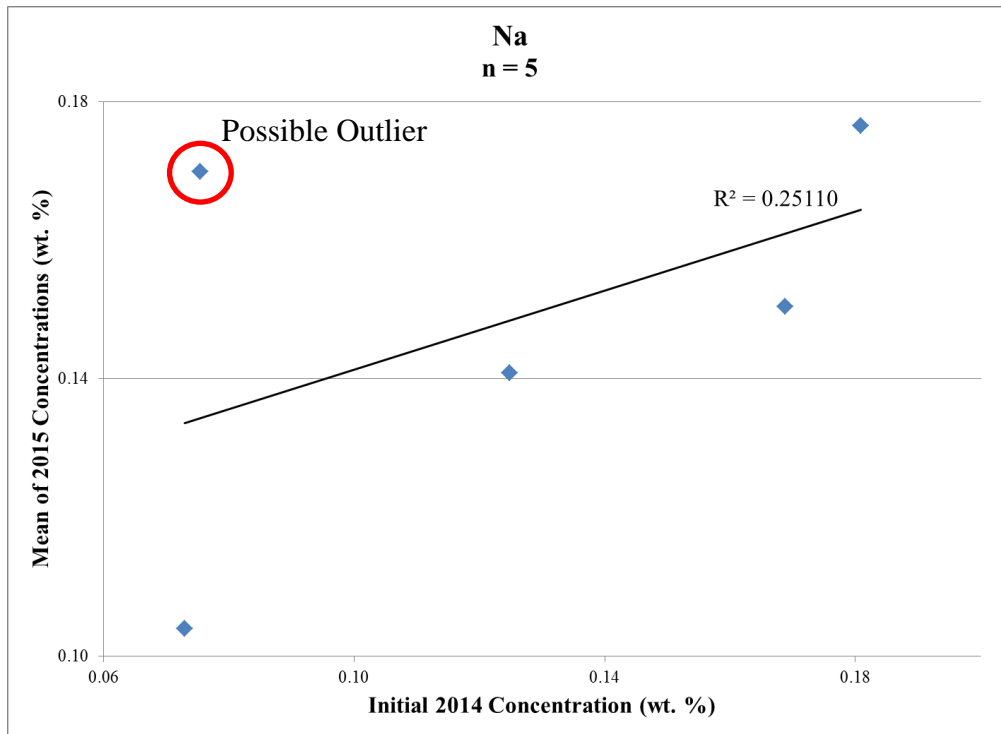
**Appendix G7: Linear Regression Plots comparing the Initial 2014 Concentration with the Mean concentration of 2015 Analyses for TC14 Pellet Samples**

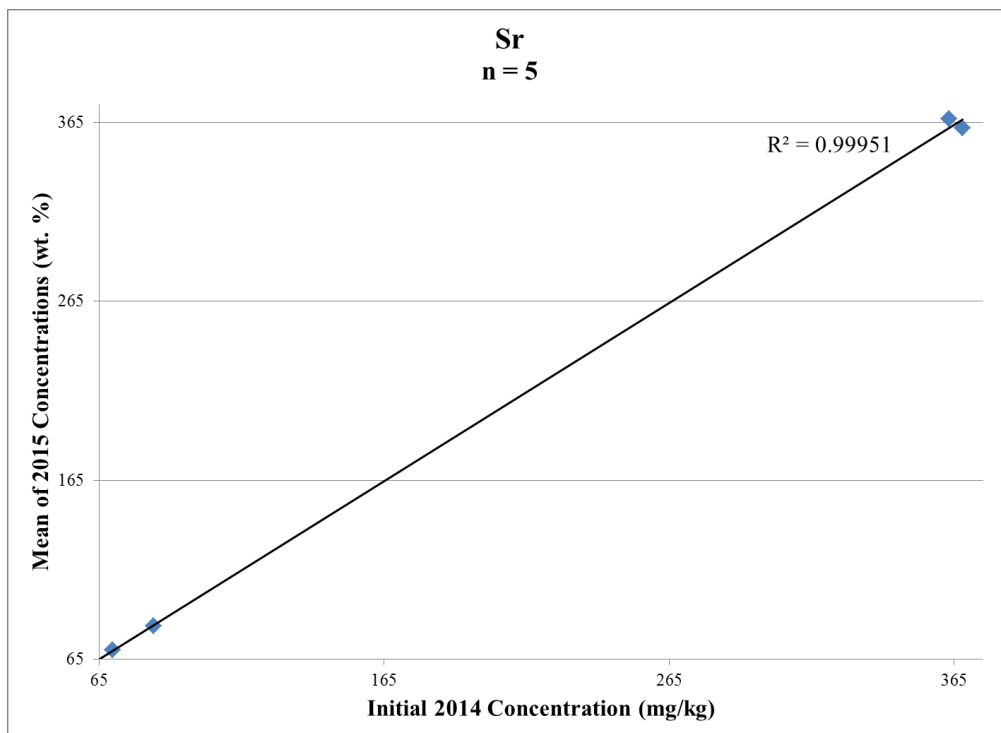
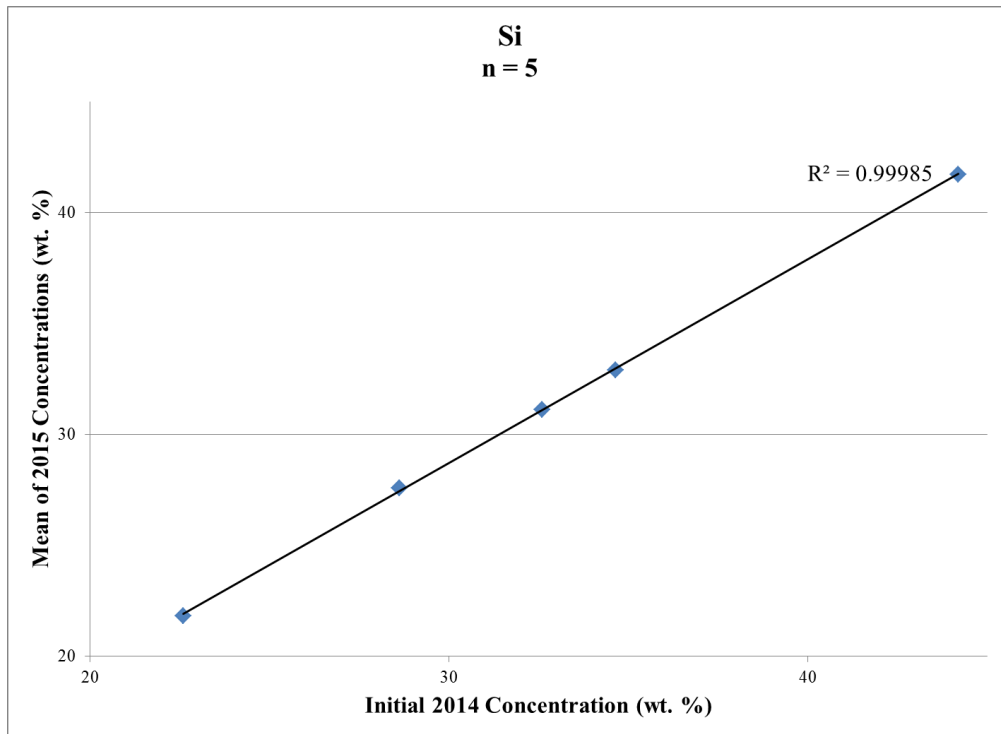


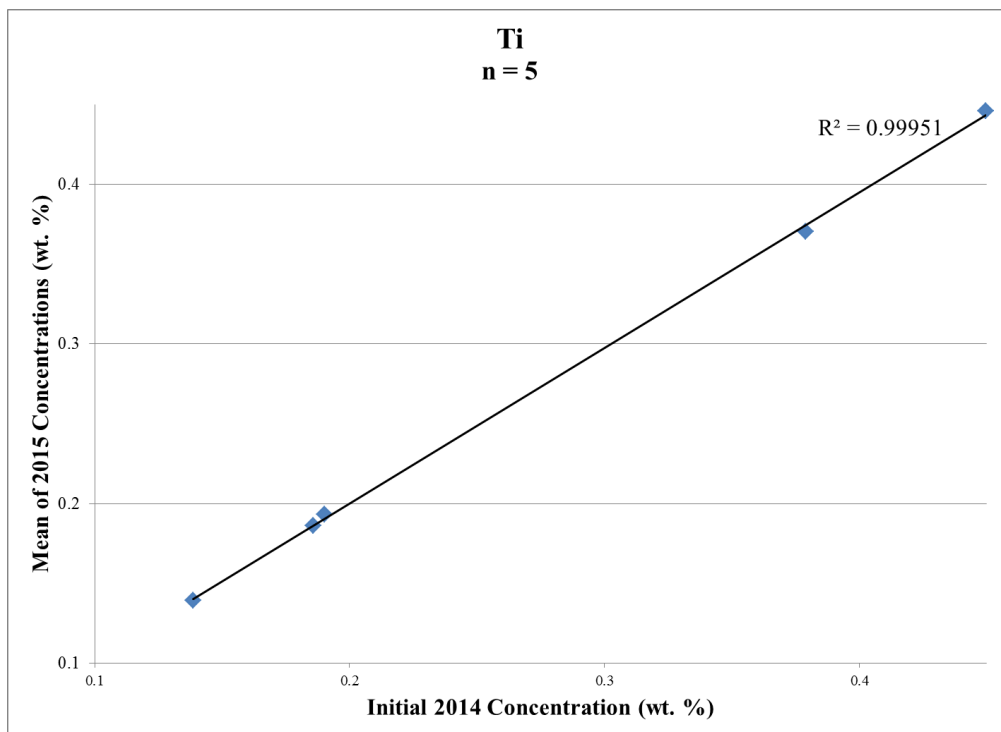
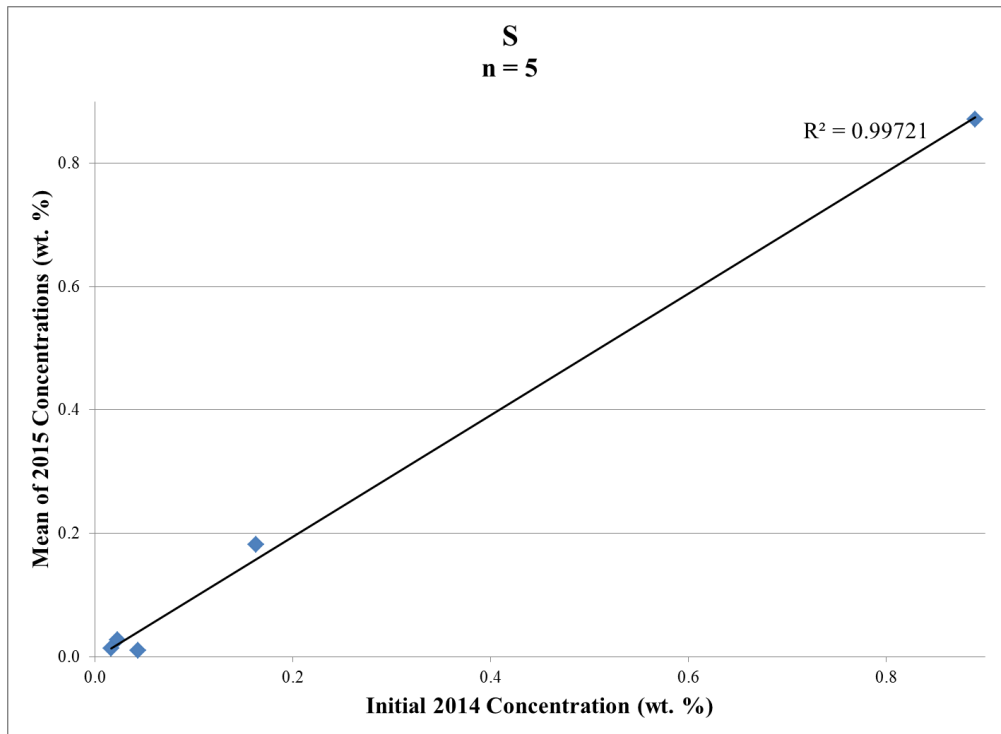












### Appendix H: LOI Data

Sample ID <sup>1</sup>	Dry Sample Weight	Crucible Weight	Initial Weight	Final Weight	% LOI <sup>2</sup>	Depth
0-4' #23	1.1993	8.6618	9.8611	9.8559	0.0527	0.9
4-8' #16	1.1986	8.6643	9.8629	9.8548	0.0821	1.8
8-12' #18	1.2007	7.4502	8.6509	8.6477	0.0370	3.6
12-16' #7	1.1986	9.5847	10.7833	10.7797	0.0334	4.0
12-16' #10	1.1937	8.2483	9.4420	9.3941	0.5073	4.1
12-16' #15	1.1974	5.2154	6.4128	6.3981	0.2292	4.2
12-16' #34	1.1977	8.8596	10.0573	10.0380	0.1919	4.8
16-20' #1	1.1952	8.3071	9.5023	9.4491	0.5599	4.9
16-20' #11	1.1974	8.0904	9.2878	9.2507	0.3994	5.2
16-20' #16	1.1991	8.2271	9.4262	9.3806	0.4838	5.3
20-24' #1	1.2002	8.5834	9.7836	9.7475	0.3690	6.1
20-24' #27	1.1993	8.6361	9.8354	9.7898	0.4636	7.2
24-28' #41	1.2004	5.2933	6.4937	6.4910	0.0416	8.3
24-28' #47	1.2007	8.7128	9.9135	9.9084	0.0514	8.5
28-32' #6	1.1978	8.7318	9.9296	9.9278	0.0181	8.8
28-32' #11	1.1995	7.1889	8.3884	8.3857	0.0322	9.1
32-36' #6	1.1984	9.0171	10.2155	10.1412	0.7273	9.9
32-36' #16	1.1991	9.6509	10.8500	10.8255	0.2258	10.3
32-36' #32	1.2003	6.9860	8.1863	8.1737	0.1539	11.0

1. TC14 sediment samples selected for LOI analysis. weights are in grams, % LOI values are expressed as weight percents, and depths in meters below the land surface

2. % LOI = [(Initial Weight – Final Weight) ÷ Initial Weight] × 100



## Appendix I: NCAG DATA

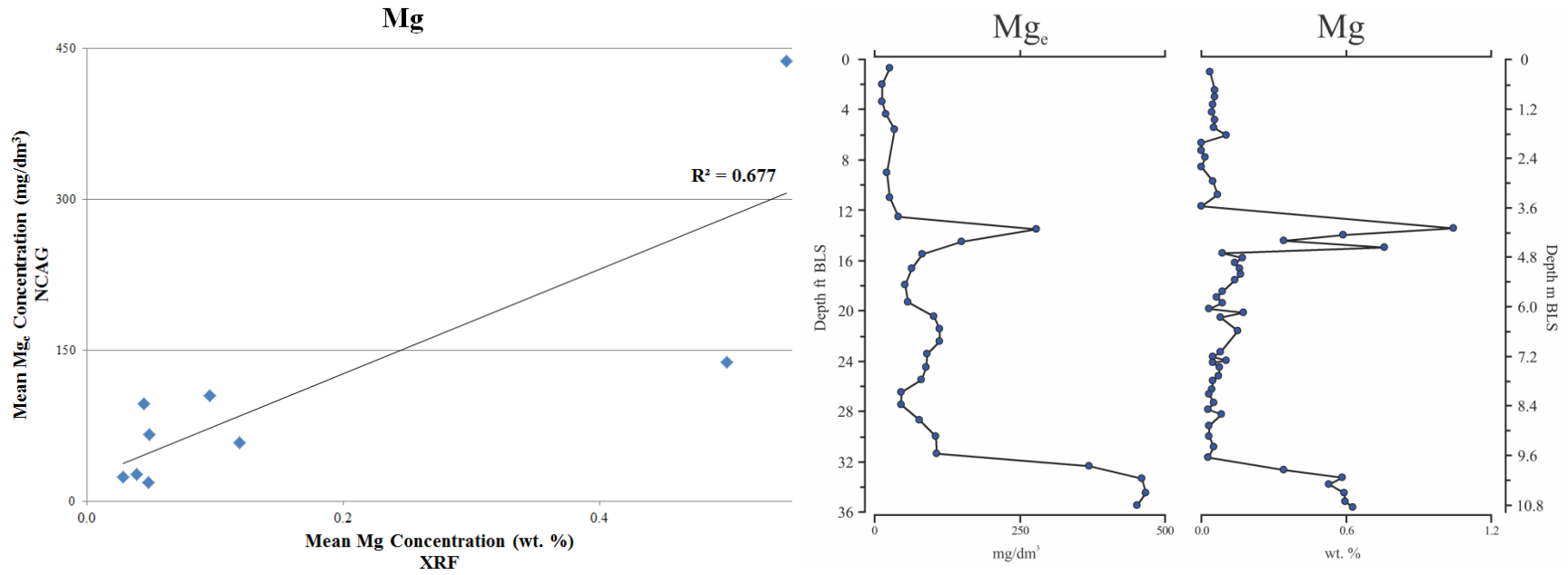
Sample ID <sup>1</sup>	HM % <sup>2</sup>	W/V <sup>3</sup>	CEC <sup>4</sup>	BS % <sup>2</sup>	Ac <sup>4</sup>	Sediment-Water pH	P <sub>e</sub> <sup>5</sup>	K <sub>e</sub> <sup>5</sup>	Ca <sub>e</sub> <sup>5</sup>	Mg <sub>e</sub> <sup>5</sup>
0-4' #1	0.66	1.47	3.6	74	1	5.8	50	41	472	27
0-4' #2	0.18	1.51	1.1	44	0.6	4.9	12	10	74	14
0-4' #3	0.09	1.46	1.3	43	0.7	5.3	12	11	79	14
4-8' #4	0.09	1.38	1.7	62	0.6	5	20	13	172	20
4-8' #5	0.09	1.24	1.8	62	0.7	5.1	19	20	158	34
8-12' #6	0.09	1.4	1.2	53	0.6	5.1	16	17	82	22
8-12' #7	0.09	1.39	1.7	43	1	5.1	15	18	93	26
12-16' #8	0.09	1.41	2.3	67	0.8	4.9	25	21	226	42
12-16' #9	0.09	1.06	17.1	85	2.6	5.2	52	341	2272	279
12-16' #10	0.04	1.01	10.3	85	1.5	5.5	150	152	1439	150
12-16' #11	0.04	1.13	11.8	87	1.6	5.8	534	75	1874	83
16-20' #12	0.04	0.99	120.2	100	0	7.8	14	67	23939	65
16-20' #13	0.04	0.98	124.5	100	0	8.1	6	35	24851	52
16-20' #14	0.04	1.05	124.6	100	0	8.1	3	24	24866	58
20-24' #15	0.04	1.39	122.3	100	0	7.7	3	92	24298	103
20-24' #16	0.04	1.21	116.8	100	0	7.4	5	107	23159	112
20-24' #17	0.04	1.22	103.1	100	0	7.4	8	99	20432	113
20-24' #18	0.04	1.35	120.9	100	0	7.8	6	38	24065	91
24-28' #19	0.04	1.22	95.1	100	0	7.8	7	53	18884	89
24-28' #20	0.04	1.35	88.5	100	0	7.7	5	52	17578	81
24-28' #21	0.04	1.29	28.2	100	0	7.8	7	39	5549	47
24-28' #22	0.04	1.27	29.8	100	0	8	7	31	5873	46
28-32' #23	0.04	1.27	51.2	100	0	8	14	40	10108	78
28-32' #24	0.04	1.39	91.9	100	0	7.9	4	46	18226	105
28-32' #25	0.04	1.41	124.5	100	0	7.8	2	51	24747	108
32-36' #26	0.04	1.19	126.7	100	0	7.6	2	186	24693	369
32-36' #27	0.04	1.16	128.4	100	0	7.6	4	325	24811	461
32-36' #28	0.04	1.06	129.1	100	0	7.5	2	393	24904	467
32-36' #29	0.04	1.08	128.9	100	0	7.7	1	467	24837	452

1. TC14C samples sent to the NCAG's Soil Testing Division for geochemical analysis
2. Units for percent humic matter and base saturation are expressed as volume percents
3. Weight per volume (g/cm<sup>3</sup>)
4. Cation exchange Capacity and exchangeable acidity are presented in units of meq/100cm<sup>3</sup>
5. Extractable concentrations of phosphorus, potassium, calcium, and magnesium (mg/dm<sup>3</sup>)
6. Depth is presented as meters below the land surface

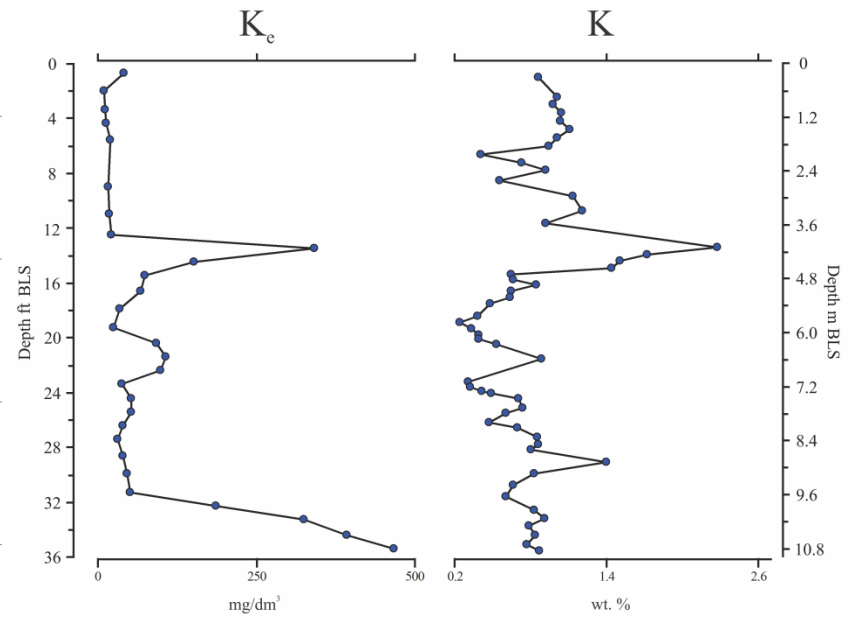
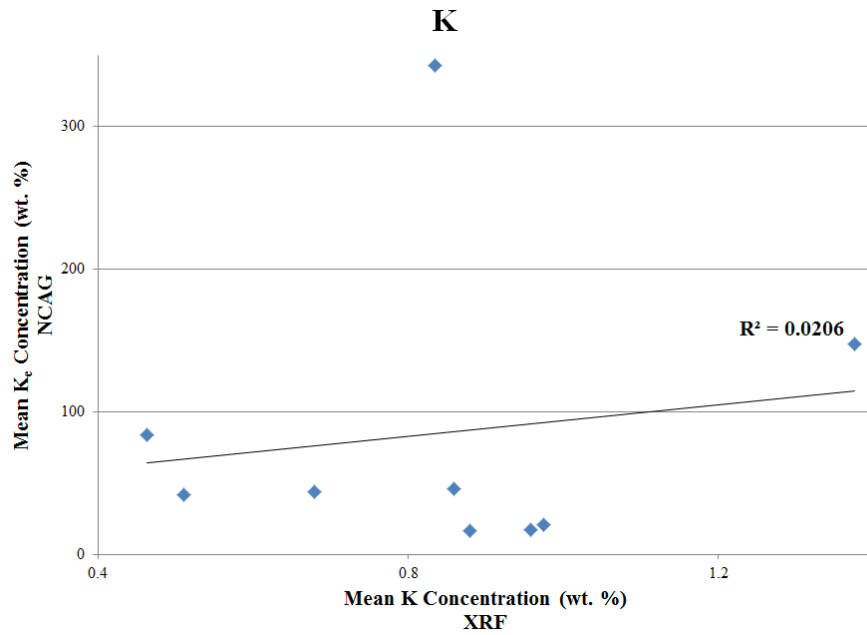
Sample ID <sup>1</sup>	S <sub>e</sub> <sup>5</sup>	Mn <sub>e</sub> <sup>5</sup>	Zn <sub>e</sub> <sup>5</sup>	Cu <sub>e</sub> <sup>5</sup>	Na <sub>e</sub> <sup>5</sup>	K <sub>e</sub> <sup>5</sup>	Ca <sub>e</sub> <sup>5</sup>	Mg <sub>e</sub> <sup>5</sup>	Depth <sup>6</sup>
0-4' #1	21	5	1.3	0.6	0.1	0.1	2.36	0.22	0.2
0-4' #2	14	2.4	0.3	0.2	0	0.03	0.37	0.12	0.6
0-4' #3	28	3	0.2	0.2	0.1	0.03	0.4	0.12	1.0
4-8' #4	14	1.2	0.2	0.4	0	0.03	0.86	0.16	1.4
4-8' #5	8	1.4	0.2	0.3	0	0.05	0.79	0.28	1.9
8-12' #6	5	1.7	0.2	0.3	0	0.04	0.41	0.18	2.7
8-12' #7	7	6.1	0.1	0.3	0.1	0.05	0.47	0.21	3.3
12-16' #8	6	9.4	0.4	0.3	0	0.05	1.13	0.35	3.8
12-16' #9	16	76	1.9	0.7	0.2	0.87	11.36	2.29	4.1
12-16' #10	9	17.4	1.3	0.4	0.1	0.39	7.2	1.23	4.4
12-16' #11	8	66.5	4.1	0.4	0.1	0.19	9.37	0.68	4.7
16-20' #12	29	115.7	0.7	0.3	1.3	0.17	119.7	0.53	5.1
16-20' #13	32	95.1	0.2	0.1	1.5	0.09	124.26	0.43	5.5
16-20' #14	35	113.1	0.1	0.1	1.6	0.06	124.33	0.48	5.9
20-24' #15	260	86	0.6	0.2	1.4	0.24	121.49	0.85	6.2
20-24' #16	576	73.7	0.8	0.2	1.1	0.27	115.8	0.92	6.5
20-24' #17	726	18.5	0.8	0.2	0.9	0.25	102.16	0.93	6.8
20-24' #18	301	9.6	0.3	0.1	1.3	0.1	120.33	0.75	7.1
24-28' #19	316	8.7	0.5	0.1	0.9	0.14	94.42	0.73	7.5
24-28' #20	336	6.3	0.5	0.1	0.8	0.13	87.89	0.67	7.8
24-28' #21	222	3.3	0.5	0.1	0.3	0.1	27.75	0.39	8.1
24-28' #22	93	3.3	0.5	0.1	0.4	0.08	29.37	0.38	8.4
28-32' #23	180	4.7	0.5	0.1	0.6	0.1	50.54	0.64	8.7
28-32' #24	216	5	0.5	0.1	1	0.12	91.13	0.86	9.1
28-32' #25	400	7.9	0.4	0.1	1.6	0.13	123.74	0.89	9.5
32-36' #26	699	55.7	0.6	0.2	1.1	0.48	123.47	3.03	9.8
32-36' #27	684	58.9	0.4	0.1	0.6	0.83	124.06	3.79	10.2
32-36' #28	609	51.5	0.5	0.1	0.7	1.01	124.52	3.84	10.5
32-36' #29	618	39.5	0.5	0.1	0.7	1.19	124.19	3.72	10.8

1. TC14C samples sent to the NCAG's Soil Testing Division for geochemical analysis
2. Units for percent humic matter and base saturation are expressed as volume percents
3. Weight per volume (g/cm<sup>3</sup>)
4. Cation exchange Capacity and exchangeable acidity are presented in units of meq/100cm<sup>3</sup>
5. Extractable concentrations of phosphorus, potassium, calcium, and magnesium (mg/dm<sup>3</sup>)
6. Depth is presented as meters below the land surface

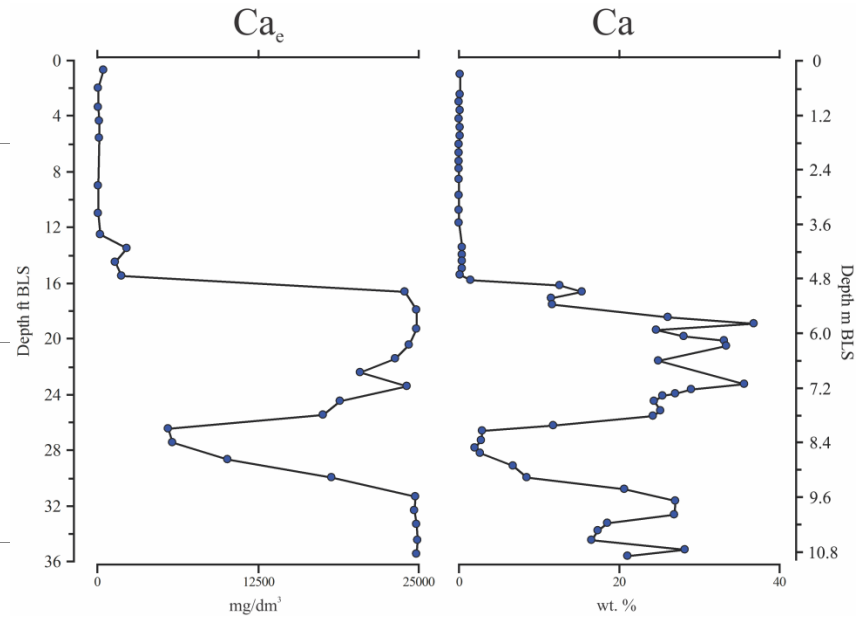
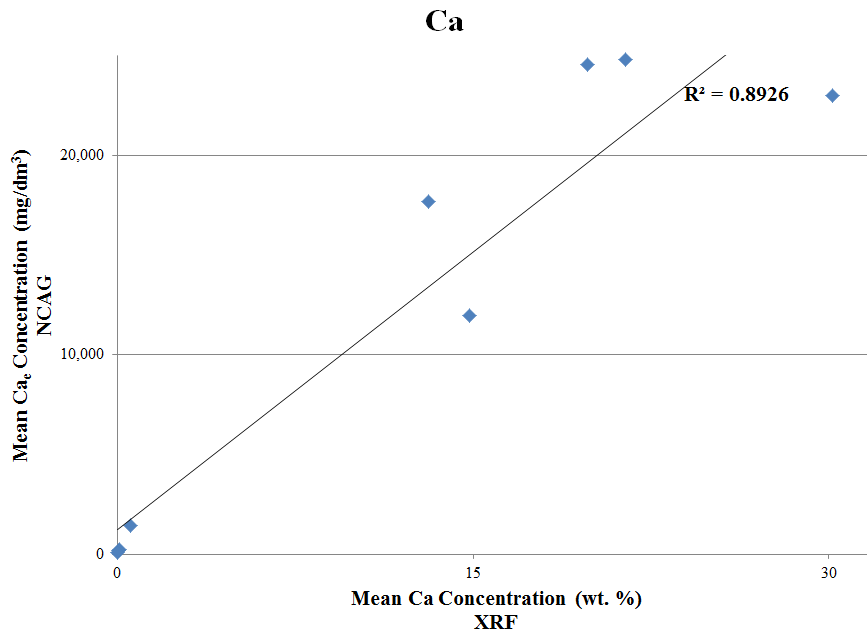
## Appendix J: Comparison of XRF and NCAG Results



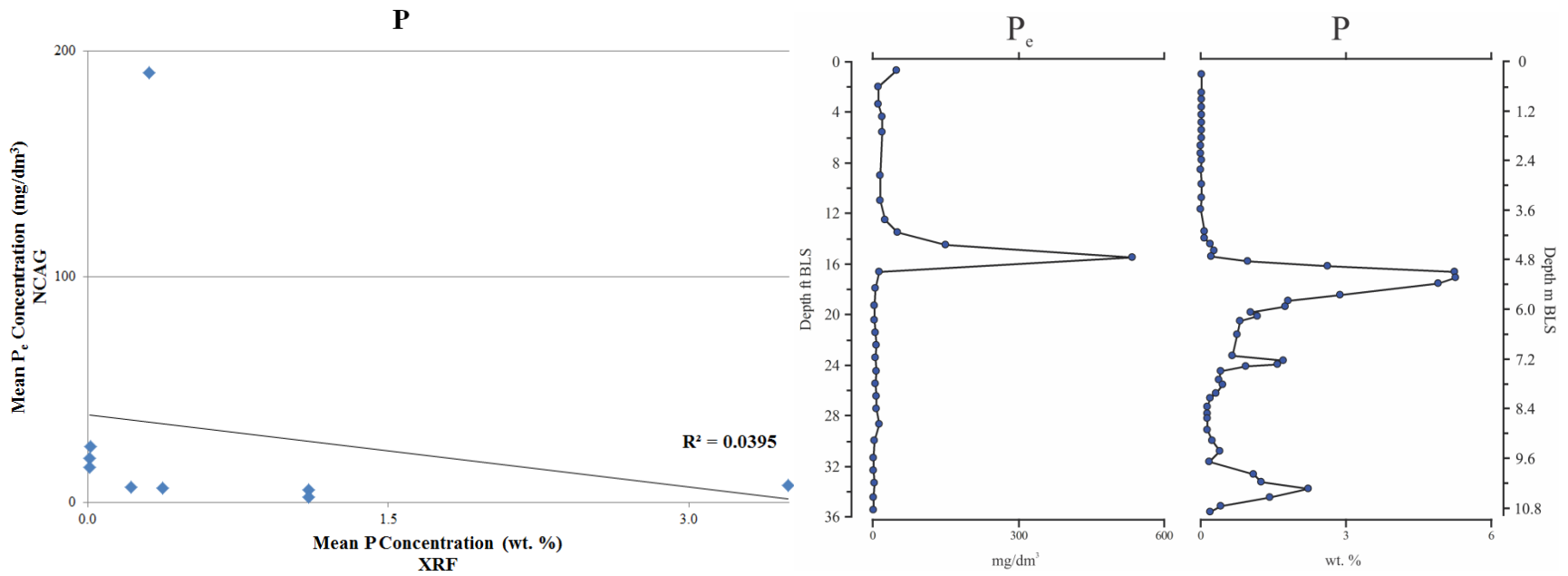
Comparison of NCAG and XRF results for magnesium. The left graph is a regression analysis of mean Mg<sub>e</sub> concentrations (measured by NCAG) and mean Mg concentrations (measured by XRF). The right graph shows concentration profiles for extractable magnesium and total magnesium



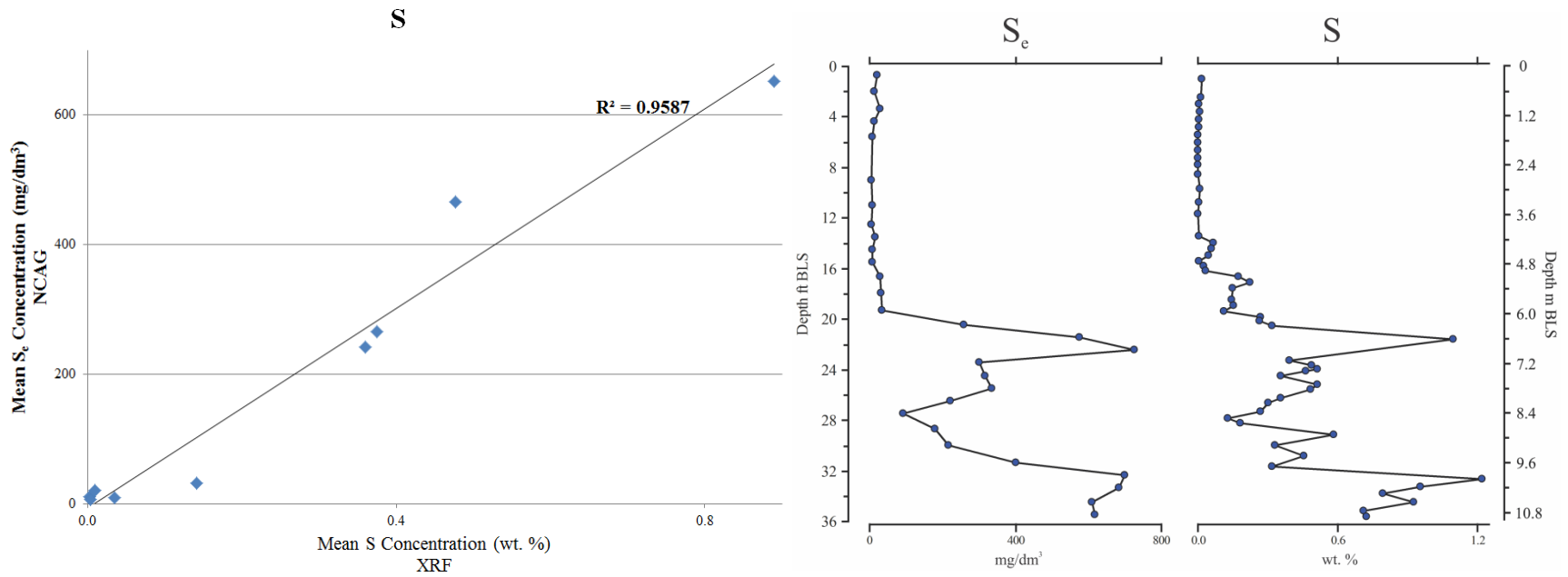
Comparison of NCAG and XRF results for potassium. The left plot is a regression analysis of mean K<sub>c</sub> concentrations (measured by NCAG) and mean K concentrations (measured by XRF). The graph on the right shows concentration profiles for extractable potassium and total potassium



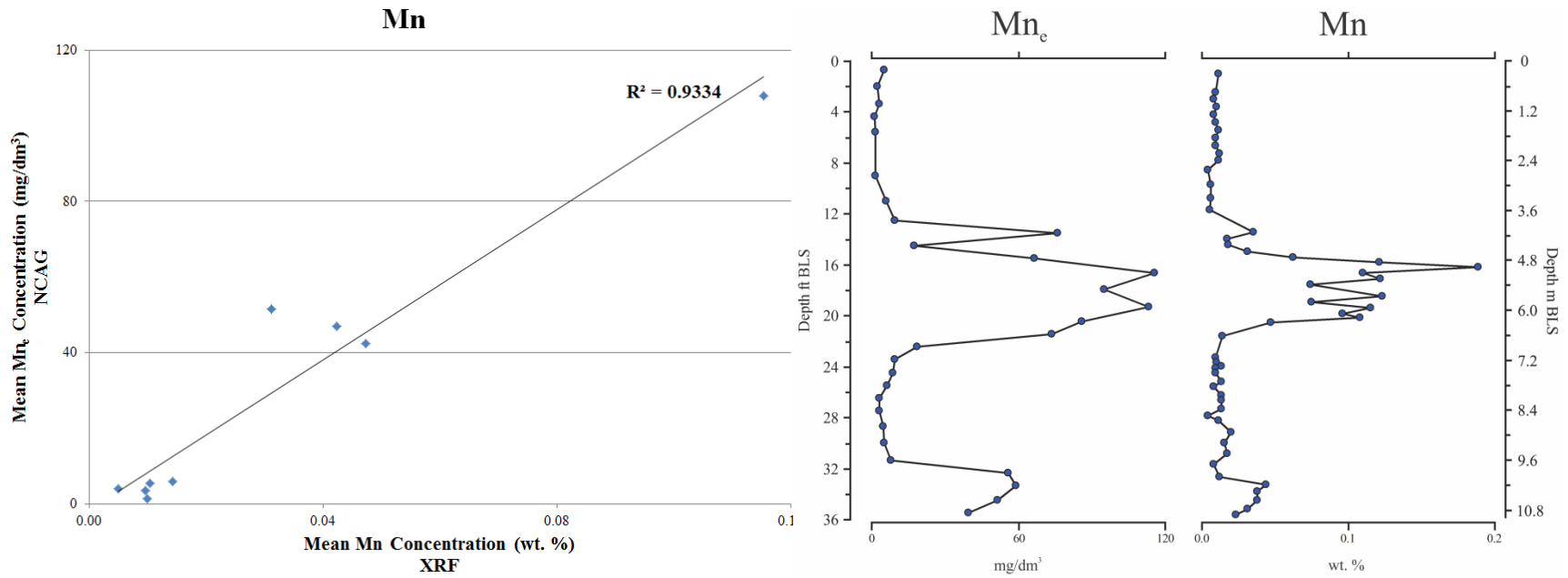
Comparison of NCAG and XRF results for calcium. The left plot is a regression analysis of mean  $Ca_e$  concentrations (measured by NCAG) and mean Ca concentrations (measured by XRF). The graph on the right shows concentration profiles for extractable calcium and total calcium



Comparison of NCAG and XRF results for phosphorous. The left plot is a regression analysis of mean P<sub>e</sub> concentrations (measured by NCAG) and mean P concentrations (measured by XRF). The graph on the right shows concentration profiles for extractable phosphorous and total phosphorous



Comparison of NCAG and XRF results for sulfur. The left plot is a regression analysis of mean  $S_e$  concentrations (measured by NCAG) and mean S concentrations (measured by XRF). The graph on the right shows concentration profiles for extractable sulfur and total sulfur



Comparison of NCAG and XRF results for manganese. The left plot is a regression analysis of mean Mn<sub>e</sub> concentrations (measured by NCAG) and mean Mn concentrations (measured by XRF). The graph on the right shows concentration profiles for extractable manganese and total manganese



## Appendix K: Results of Geochemical Modeling and PHREEQC Input Files

### Appendix K1: Simple Dissolution in Pure Water at pH 5

Solution <sup>1</sup>	pH	pe	Alkalinity as HCO <sub>3</sub> <sup>-</sup>	Dissolved Fe	S.I. <sup>2</sup> Hematite	S.I. <sup>2</sup> Goethite	S.I. <sup>2</sup> Lepidocrocite	S.I. <sup>2</sup> Fe(OH) <sub>3</sub>	S.I. <sup>2</sup> Pyrite
Epidote	9.08	2.03	7.53	2.50E-07	1	0	-1	-5	-1000
Hematite	5.00	12.86	-0.61	1.41E-06	0	0	-1	-6	-1000
Fe(OH) <sub>3</sub>	5.07	12.52	-0.52	3.75E-06	1	0	-1	-5	-1000
Lepidocrocite	5.00	12.73	-0.61	4.41E-06	1	0	-1	-5	-1000
Goethite	5.00	12.69	-0.61	4.37E-06	1	0	-1	-5	-1000
Goethite_2	5.00	12.64	-0.61	4.37E-06	1	0	-1	-5	-1000
Glauconite	5.84	2.40	0.70	0.03	1	0	-1	-5	-1000
Pyrite	5.01	-1.28	-0.59	0.01	-12	-7	-7	-12	0
Hedenbergite	9.73	-8.98	5.62	0.03	1	0	-1	-5	-1000
Staurolite	5.89	-0.68	1.21	0.11	-4	-2	-3	-7	-1000
Schorl	6.45	-1.60	1.22	0.20	-2	-1	-2	-6	-1000
Ilmenite	5.83	-0.72	-0.09	0.24	-3	-2	-3	-7	-1000
Actinolite	8.94	-7.84	0.71	0.27	1	0	-1	-5	-1000
Ferropargasite	8.98	-8.01	5.42	0.33	1	0	-1	-5	-1000
Almandine	7.49	-3.79	1.21	0.42	1	0	-1	-5	-1000

1. Chemistry of the “Pure Water” solution at equilibrium with 10 moles of individual Fe-bearing minerals.

Concentrations are presented in units of mg/L

2. S.I: Saturation indices of selected iron-oxyhydroxides and pyrite. Saturation index (S.I.) =  $\log(\text{IAP})/K_T$  where IAP is the ion activity product of the dissolved components in solution, and  $K_T$  is the solubility of the solid or gaseous phase at the specified temperature

### Appendix K2: Simple Dissolution in Pure Water at pH 7

Solution <sup>1</sup>	pH	pe	Alkalinity as HCO <sub>3</sub> <sup>-</sup>	Dissolved Fe	S.I. <sup>2</sup> Hematite	S.I. <sup>2</sup> Goethite	S.I. <sup>2</sup> Lepidocrocite	S.I. <sup>2</sup> Fe(OH) <sub>3</sub>	S.I. <sup>2</sup> Pyrite
Pure Water	7.00	4.00	-2.23E-04	0.00	-1000	-1000	-1000	-1000	-1000
Epidote	9.27	0.61	7.42	2.81E-07	1	0	-1	-5	-1000
Hematite	7.00	10.90	0.00	7.41E-08	0	0	-1	-6	-1000
Fe(OH) <sub>3</sub>	7.00	6.75	0.00	2.33E-07	1	0	-1	-5	-1000
Lepidocrocite	7.00	6.51	0.00	2.33E-07	1	0	-1	-5	-1000
Goethite	7.00	6.58	0.00	2.31E-07	1	0	-1	-5	-1000
Goethite_2	7.00	6.67	0.00	2.31E-07	1	0	-1	-5	-1000
Glauconite	7.35	-1.78	0.58	0.01	1	0	-1	-5	-1000
Pyrite	7.04	-3.77	0.00	0.00	-7	-4	-5	-9	0
Hedenbergite	9.78	-9.02	6.01	0.03	1	0	-1	-5	-1000
Staurolite	6.67	-1.66	0.47	0.03	-2	-2	-2	-7	-1000
Schorl	7.83	-4.17	0.93	0.10	1	0	-1	-5	-1000
Ilmenite	7.42	-2.65	0.01	0.01	-1	-1	-2	-6	-1000
Actinolite	9.10	-8.01	0.95	0.14	1	0	-1	-5	-1000
Ferropargasite	9.12	-8.18	5.47	0.19	1	0	-1	-5	-1000
Almandine	8.48	-6.22	0.59	0.13	1	0	-1	-5	-1000

1. Chemistry of the “Pure Water” solution at equilibrium with 10 moles of individual Fe-bearing minerals.

Concentrations are presented in units of mg/L

2. S.I.: Saturation indices of selected iron-oxyhydroxides and pyrite. Saturation index (S.I.) =  $\log(\text{IAP})/K_T$  where IAP is the ion activity product of the dissolved components in solution, and  $K_T$  is the solubility of the solid or gaseous phase at the specified temperature

### Appendix K3: Simple Dissolution in Pure Water at pH 9

Solution <sup>1</sup>	pH	pe	Alkalinity as HCO <sub>3</sub> <sup>-</sup>	Dissolved Fe	S.I. <sup>2</sup> Hematite	S.I. <sup>2</sup> Goethite	S.I. <sup>2</sup> Lepidocrocite	S.I. <sup>2</sup> Fe(OH) <sub>3</sub>	S.I. <sup>2</sup> Pyrite
Pure Water	9.00	4.00	0.59	0.00	-1000	-1000	-1000	-1000	-1000
Epidote	9.40	5.48	7.55	3.15E-07	1	0	-1	-5	-1000
Hematite	9.00	8.91	0.59	7.64E-08	0	0	-1	-6	-1000
Fe(OH) <sub>3</sub>	8.93	1.19	0.50	2.33E-07	1	0	-1	-5	-1000
Lepidocrocite	9.00	0.63	0.59	2.40E-07	1	0	-1	-5	-1000
Goethite	9.00	0.80	0.59	2.38E-07	1	0	-1	-5	-1000
Goethite_2	9.00	0.92	0.59	2.38E-07	1	0	-1	-5	-1000
Glauconite	8.96	-6.51	1.22	0.01	1	0	-1	-5	-1000
Pyrite	9.00	-6.01	0.59	0.00	1	0	-1	-5	0
Hedenbergite	9.82	-9.05	6.41	0.03	1	0	-1	-5	-1000
Staurolite	8.68	-6.64	2.23	0.09	1	0	-1	-5	-1000
Schorl	8.92	-7.20	1.47	0.07	1	0	-1	-5	-1000
Ilmenite	9.00	-4.84	0.59	0.00	1	0	-1	-5	-1000
Actinolite	9.27	-8.18	1.33	0.08	1	0	-1	-5	-1000
Ferropargasite	9.27	-8.33	5.71	0.11	1	0	-1	-5	-1000
Almandine	9.02	-7.37	0.93	0.06	1	0	-1	-5	-1000

1. Chemistry of the “Pure Water” solution at equilibrium with 10 moles of individual Fe-bearing minerals. Concentrations are presented in units of mg/L

2. S.I.: Saturation indices of selected iron-oxyhydroxides and pyrite. Saturation index (S.I.) =  $\log(\text{IAP})/K_T$  where IAP is the ion activity product of the dissolved components in solution, and  $K_T$  is the solubility of the solid or gaseous phase at the specified temperature

### Appendix K4: Simple Dissolution in Surficial Water

Solution <sup>1</sup>	pH	pe	Alkalinity as HCO <sub>3</sub> <sup>-</sup>	Dissolved Fe	S.I. <sup>2</sup> Hematite	S.I. <sup>2</sup> Goethite	S.I. <sup>2</sup> Lepidocrocite	S.I. <sup>2</sup> Fe(OH) <sub>3</sub>	S.I. <sup>2</sup> Pyrite
Pure Water	5.30	6.44	24.01	0.07	-1000	-1000	-1000	-1000	-1000
Epidote	6.49	13.81	326.43	3.35E-07	1	0	-1	-5	-241
Hematite	5.29	15.01	23.68	9.14E-07	0	0	-1	-6	-236
Fe(OH) <sub>3</sub>	5.30	14.99	20.06	2.38E-06	1	0	-1	-5	-236
Lepidocrocite	5.29	15.01	23.68	2.41E-06	1	0	-1	-5	-236
Goethite	5.29	15.01	23.68	2.41E-06	1	0	-1	-5	-236
Goethite_2	5.29	15.01	23.68	2.41E-06	1	0	-1	-5	-236
Glauconite	5.30	15.01	23.79	2.39E-06	1	0	-1	-5	-236
Pyrite	5.32	-0.94	25.09	1.77	-6	-3	-4	-8	0
Hedenbergite	8.72	-4.84	325.70	0.01	1	0	-1	-5	-3
Staurolite	5.94	6.83	344.30	1.71E-06	1	0	-1	-5	-125
Schorl	5.76	6.75	176.46	4.57E-06	1	0	-1	-5	-121
Ilmenite	5.38	3.89	28.21	0.03	1	0	-1	-5	-70
Actinolite	6.81	-2.67	210.07	11.94	1	0	-1	-5	0
Ferropargasite	6.97	-2.84	454.33	6.12	1	0	-1	-5	0
Almandine	5.79	0.14	127.60	12.04	1	0	-1	-5	-22

1. Chemistry of the "Surficial Water" solution at equilibrium with 10 moles of individual Fe-bearing minerals.

Concentrations are presented in units of mg/L

2. S.I.: Saturation indices of selected iron-oxyhydroxides and pyrite. Saturation index (S.I.) =  $\log(\text{IAP})/K_T$  where IAP is the ion activity product of the dissolved components in solution, and  $K_T$  is the solubility of the solid or gaseous phase at the specified temperature

### Appendix K5: Pyrite Titration with Oxygen in Pure Water

Oxygen Added <sup>1</sup>	pH	pe	Alkalinity as HCO <sub>3</sub> <sup>-</sup>	Dissolved Fe	SO <sub>4</sub> <sup>2-</sup>	S <sup>2-</sup>	S.I. <sup>2</sup> Hematite	S.I. <sup>2</sup> Goethite	S.I. <sup>2</sup> Lepidocrocite	S.I. <sup>2</sup> Fe(OH) <sub>3</sub>
0.00	7.00	4.00	0.00	0.00	0.00	0.00	-1000	-1000	-1000	-1000
0.08	5.55	-1.57	-0.17	0.08	0.27	1.25E-03	-8	-4	-5	-9
0.16	5.25	-1.17	-0.35	0.16	0.55	1.37E-03	-8	-5	-5	-10
0.24	5.07	-0.93	-0.52	0.24	0.82	1.45E-03	-8	-5	-6	-10
0.32	4.95	-0.76	-0.70	0.32	1.10	1.51E-03	-8	-5	-6	-10
0.40	4.85	-0.63	-0.87	0.40	1.37	1.56E-03	-9	-5	-6	-10
0.48	4.77	-0.52	-1.04	0.48	1.65	1.60E-03	-9	-5	-6	-10
0.56	4.70	-0.43	-1.22	0.56	1.92	1.64E-03	-9	-5	-6	-10
0.64	4.65	-0.35	-1.39	0.64	2.20	1.67E-03	-9	-5	-6	-10
0.72	4.60	-0.28	-1.57	0.72	2.47	1.70E-03	-9	-5	-6	-10
0.80	4.55	-0.22	-1.74	0.80	2.75	1.73E-03	-9	-5	-6	-10
0.88	4.51	-0.17	-1.92	0.88	3.02	1.75E-03	-9	-5	-6	-10
0.96	4.47	-0.12	-2.09	0.96	3.29	1.77E-03	-9	-5	-6	-10
1.04	4.44	-0.07	-2.26	1.04	3.57	1.80E-03	-9	-5	-6	-10
1.12	4.41	-0.03	-2.44	1.12	3.84	1.82E-03	-9	-5	-6	-10
1.20	4.38	0.01	-2.61	1.20	4.12	1.84E-03	-9	-5	-6	-10
1.28	4.35	0.05	-2.79	1.28	4.39	1.86E-03	-9	-5	-6	-10
1.36	4.32	0.09	-2.96	1.36	4.67	1.87E-03	-9	-5	-6	-10
1.44	4.30	0.12	-3.14	1.44	4.94	1.89E-03	-9	-5	-6	-10

1. Composition of the "Pure Water" solution as a total of 8 mg/L oxygen is added to 10 moles of pyrite. Concentrations are presented in units of mg/L

2. S.I.: Saturation indices of selected iron-oxyhydroxides. Saturation index (S.I.) =  $\log(\text{IAP})/K_T$  where IAP is the ion activity product of the dissolved components in solution, and  $K_T$  is the solubility of the solid or gaseous phase at the specified temperature

Oxygen Added <sup>1</sup>	pH	pe	Alkalinity as HCO <sub>3</sub> <sup>-</sup>	Dissolved Fe	SO <sub>4</sub> <sup>2-</sup>	S <sup>2-</sup>	S.I. <sup>2</sup> Hematite	S.I. <sup>2</sup> Goethite	S.I. <sup>2</sup> Lepidocrocite	S.I. <sup>2</sup> Fe(OH) <sub>3</sub>
1.52	4.27	0.15	-3.31	1.52	5.22	1.91E-03	-9	-5	-6	-10
1.60	4.25	0.18	-3.48	1.60	5.49	1.92E-03	-9	-5	-6	-10
1.68	4.23	0.21	-3.66	1.68	5.76	1.94E-03	-9	-5	-6	-10
1.76	4.21	0.24	-3.83	1.76	6.04	1.95E-03	-9	-5	-6	-10
1.84	4.19	0.26	-4.01	1.84	6.31	1.97E-03	-9	-5	-6	-10
1.92	4.17	0.29	-4.18	1.92	6.59	1.98E-03	-9	-5	-6	-10
2.00	4.16	0.31	-4.36	2.00	6.86	1.99E-03	-10	-5	-6	-10
2.08	4.14	0.33	-4.53	2.08	7.14	2.00E-03	-10	-5	-6	-10
2.16	4.12	0.35	-4.70	2.16	7.41	2.02E-03	-10	-5	-6	-10
2.24	4.11	0.37	-4.88	2.23	7.69	2.03E-03	-10	-5	-6	-10
2.32	4.09	0.40	-5.05	2.31	7.96	2.04E-03	-10	-5	-6	-10
2.40	4.08	0.41	-5.23	2.39	8.23	2.05E-03	-10	-5	-6	-10
2.48	4.06	0.43	-5.40	2.47	8.51	2.06E-03	-10	-5	-6	-10
2.56	4.05	0.45	-5.58	2.55	8.78	2.07E-03	-10	-5	-6	-10
2.64	4.04	0.47	-5.75	2.63	9.06	2.08E-03	-10	-5	-6	-10
2.72	4.03	0.49	-5.93	2.71	9.33	2.09E-03	-10	-5	-6	-10
2.80	4.01	0.50	-6.10	2.79	9.61	2.10E-03	-10	-5	-6	-10
2.88	4.00	0.52	-6.27	2.87	9.88	2.11E-03	-10	-5	-6	-10
2.96	3.99	0.54	-6.45	2.95	10.16	2.12E-03	-10	-5	-6	-10
3.04	3.98	0.55	-6.62	3.03	10.43	2.13E-03	-10	-5	-6	-10
3.12	3.97	0.57	-6.80	3.11	10.70	2.14E-03	-10	-5	-6	-10

1. Composition of the "Pure Water" solution as a total of 8 mg/L oxygen is added to 10 moles of pyrite. Concentrations are presented in units of mg/L

2. S.I.: Saturation indices of selected iron-oxyhydroxides. Saturation index (S.I.) =  $\log(\text{IAP})/K_T$  where IAP is the ion activity product of the dissolved components in solution, and  $K_T$  is the solubility of the solid or gaseous phase at the specified temperature

Oxygen Added <sup>1</sup>	pH	pe	Alkalinity as HCO <sub>3</sub> <sup>-</sup>	Dissolved Fe	SO <sub>4</sub> <sup>2-</sup>	S <sup>2-</sup>	S.I. <sup>2</sup> Hematite	S.I. <sup>2</sup> Goethite	S.I. <sup>2</sup> Lepidocrocite	S.I. <sup>2</sup> Fe(OH) <sub>3</sub>
3.20	3.96	0.58	-6.97	3.19	10.98	2.15E-03	-10	-5	-6	-10
3.28	3.95	0.59	-7.15	3.27	11.25	2.16E-03	-10	-5	-6	-11
3.36	3.94	0.61	-7.32	3.35	11.53	2.17E-03	-10	-5	-6	-11
3.44	3.93	0.62	-7.49	3.43	11.80	2.18E-03	-10	-5	-6	-11
3.52	3.92	0.63	-7.67	3.51	12.08	2.19E-03	-10	-5	-6	-11
3.60	3.91	0.65	-7.84	3.59	12.35	2.19E-03	-10	-5	-6	-11
3.68	3.90	0.66	-8.02	3.67	12.63	2.20E-03	-10	-5	-6	-11
3.76	3.89	0.67	-8.19	3.75	12.90	2.21E-03	-10	-5	-6	-11
3.84	3.88	0.68	-8.37	3.83	13.18	2.22E-03	-10	-5	-6	-11
3.92	3.87	0.70	-8.54	3.91	13.45	2.22E-03	-10	-5	-6	-11
4.00	3.86	0.71	-8.71	3.99	13.72	2.23E-03	-10	-5	-6	-11
4.08	3.85	0.72	-8.89	4.07	14.00	2.24E-03	-10	-5	-6	-11
4.16	3.84	0.73	-9.06	4.15	14.27	2.25E-03	-10	-5	-6	-11
4.24	3.84	0.74	-9.24	4.23	14.55	2.25E-03	-10	-5	-6	-11
4.32	3.83	0.75	-9.41	4.31	14.82	2.26E-03	-10	-5	-6	-11
4.40	3.82	0.76	-9.59	4.39	15.10	2.27E-03	-10	-5	-6	-11
4.48	3.81	0.77	-9.76	4.47	15.37	2.28E-03	-10	-5	-6	-11
4.56	3.81	0.78	-9.93	4.55	15.65	2.28E-03	-10	-5	-6	-11
4.64	3.80	0.79	-10.11	4.63	15.92	2.29E-03	-10	-6	-6	-11
4.72	3.79	0.80	-10.28	4.71	16.19	2.30E-03	-10	-6	-6	-11
4.80	3.78	0.81	-10.46	4.79	16.47	2.30E-03	-10	-6	-6	-11

1. Composition of the "Pure Water" solution as a total of 8 mg/L oxygen is added to 10 moles of pyrite. Concentrations are presented in units of mg/L

2. S.I.: Saturation indices of selected iron-oxyhydroxides. Saturation index (S.I.) =  $\log(\text{IAP})/K_T$  where IAP is the ion activity product of the dissolved components in solution, and  $K_T$  is the solubility of the solid or gaseous phase at the specified temperature

Oxygen Added <sup>1</sup>	pH	pe	Alkalinity as HCO <sub>3</sub> <sup>-</sup>	Dissolved Fe	SO <sub>4</sub> <sup>2-</sup>	S <sup>2-</sup>	S.I. <sup>2</sup> Hematite	S.I. <sup>2</sup> Goethite	S.I. <sup>2</sup> Lepidocrocite	S.I. <sup>2</sup> Fe(OH) <sub>3</sub>
4.88	3.78	0.82	-10.63	4.87	16.74	2.31E-03	-10	-6	-6	-11
4.96	3.77	0.83	-10.81	4.95	17.02	2.32E-03	-10	-6	-6	-11
5.04	3.76	0.84	-10.98	5.03	17.29	2.32E-03	-10	-6	-6	-11
5.12	3.76	0.85	-11.15	5.11	17.57	2.33E-03	-10	-6	-6	-11
5.20	3.75	0.86	-11.33	5.19	17.84	2.33E-03	-10	-6	-6	-11
5.28	3.74	0.87	-11.50	5.27	18.12	2.34E-03	-10	-6	-6	-11
5.36	3.74	0.87	-11.68	5.35	18.39	2.35E-03	-10	-6	-6	-11
5.44	3.73	0.88	-11.85	5.43	18.66	2.35E-03	-10	-6	-6	-11
5.52	3.72	0.89	-12.03	5.51	18.94	2.36E-03	-10	-6	-6	-11
5.60	3.72	0.90	-12.20	5.59	19.21	2.36E-03	-10	-6	-6	-11
5.68	3.71	0.91	-12.37	5.67	19.49	2.37E-03	-10	-6	-6	-11
5.76	3.71	0.92	-12.55	5.75	19.76	2.38E-03	-10	-6	-6	-11
5.84	3.70	0.92	-12.72	5.83	20.04	2.38E-03	-10	-6	-6	-11
5.92	3.70	0.93	-12.90	5.91	20.31	2.39E-03	-10	-6	-6	-11
6.00	3.69	0.94	-13.07	5.98	20.59	2.39E-03	-10	-6	-6	-11
6.08	3.68	0.95	-13.25	6.06	20.86	2.40E-03	-10	-6	-6	-11
6.16	3.68	0.95	-13.42	6.14	21.14	2.40E-03	-10	-6	-6	-11
6.24	3.67	0.96	-13.59	6.22	21.41	2.41E-03	-10	-6	-6	-11
6.32	3.67	0.97	-13.77	6.30	21.68	2.41E-03	-10	-6	-6	-11
6.40	3.66	0.98	-13.94	6.38	21.96	2.42E-03	-10	-6	-6	-11
6.48	3.66	0.98	-14.12	6.46	22.23	2.42E-03	-10	-6	-6	-11

1. Composition of the "Pure Water" solution as a total of 8 mg/L oxygen is added to 10 moles of pyrite. Concentrations are presented in units of mg/L

2. S.I.: Saturation indices of selected iron-oxyhydroxides. Saturation index (S.I.) =  $\log(\text{IAP})/K_T$  where IAP is the ion activity product of the dissolved components in solution, and  $K_T$  is the solubility of the solid or gaseous phase at the specified temperature



Oxygen Added <sup>1</sup>	pH	pe	Alkalinity as HCO <sub>3</sub> <sup>-</sup>	Dissolved Fe	SO <sub>4</sub> <sup>2-</sup>	S <sup>2-</sup>	S.I. <sup>2</sup> Hematite	S.I. <sup>2</sup> Goethite	S.I. <sup>2</sup> Lepidocrocite	S.I. <sup>2</sup> Fe(OH) <sub>3</sub>
6.56	3.65	0.99	-14.29	6.54	22.51	2.43E-03	-10	-6	-6	-11
6.64	3.65	1.00	-14.47	6.62	22.78	2.44E-03	-10	-6	-6	-11
6.72	3.64	1.00	-14.64	6.70	23.06	2.44E-03	-10	-6	-6	-11
6.80	3.64	1.01	-14.81	6.78	23.33	2.45E-03	-10	-6	-6	-11
6.88	3.63	1.02	-14.99	6.86	23.61	2.45E-03	-10	-6	-6	-11
6.96	3.63	1.02	-15.16	6.94	23.88	2.46E-03	-10	-6	-6	-11
7.04	3.62	1.03	-15.34	7.02	24.15	2.46E-03	-10	-6	-6	-11
7.12	3.62	1.04	-15.51	7.10	24.43	2.47E-03	-10	-6	-6	-11
7.20	3.61	1.04	-15.69	7.18	24.70	2.47E-03	-10	-6	-6	-11
7.28	3.61	1.05	-15.86	7.26	24.98	2.47E-03	-10	-6	-6	-11
7.36	3.60	1.05	-16.03	7.34	25.25	2.48E-03	-10	-6	-6	-11
7.44	3.60	1.06	-16.21	7.42	25.53	2.48E-03	-10	-6	-6	-11
7.52	3.59	1.07	-16.38	7.50	25.80	2.49E-03	-10	-6	-7	-11
7.60	3.59	1.07	-16.56	7.58	26.08	2.49E-03	-10	-6	-7	-11
7.68	3.59	1.08	-16.73	7.66	26.35	2.50E-03	-10	-6	-7	-11
7.76	3.58	1.08	-16.91	7.74	26.62	2.50E-03	-10	-6	-7	-11
7.84	3.58	1.09	-17.08	7.82	26.90	2.51E-03	-10	-6	-7	-11
7.92	3.57	1.10	-17.26	7.90	27.17	2.51E-03	-10	-6	-7	-11
8.00	3.57	1.10	-17.43	7.98	27.45	2.52E-03	-10	-6	-7	-11

1. Composition of the "Pure Water" solution as a total of 8 mg/L oxygen is added to 10 moles of pyrite. Concentrations are presented in units of mg/L

2. S.I.: Saturation indices of selected iron-oxyhydroxides. Saturation index (S.I.) =  $\log(\text{IAP})/K_T$  where IAP is the ion activity product of the dissolved components in solution, and  $K_T$  is the solubility of the solid or gaseous phase at the specified temperature

### Appendix K6: Pyrite Titration with Oxygen and Simultaneous Calcite Dissolution in Pure Water

Oxygen Added <sup>1</sup>	pH	pe	Alkalinity as HCO <sub>3</sub> <sup>-</sup>	Dissolved Fe	SO <sub>4</sub> <sup>2-</sup>	S <sup>2-</sup>	S.I. <sup>2</sup> Hematite	S.I. <sup>2</sup> Goethite	S.I. <sup>2</sup> Lepidocrocite	S.I. <sup>2</sup> Fe(OH) <sub>3</sub>
0.00	7.00	4.00	0.00	0.00	0.00	0.00	-1000	-1000	-1000	-1000
0.08	9.86	-6.48	8.34	6.87E-05	34.08	0.01	1	0	-1	-5
0.16	9.84	-6.45	8.20	7.28E-05	34.30	0.01	1	0	-1	-5
0.24	9.81	-6.42	8.07	7.73E-05	34.51	0.01	1	0	-1	-5
0.32	9.79	-6.39	7.95	8.23E-05	34.73	0.01	1	0	-1	-5
0.40	9.76	-6.36	7.85	8.79E-05	34.95	0.01	1	0	-1	-5
0.48	9.74	-6.32	7.77	9.41E-05	35.16	0.01	1	0	-1	-5
0.56	9.71	-6.29	7.70	1.01E-04	35.37	0.01	1	0	-1	-5
0.64	9.69	-6.26	7.65	1.08E-04	35.58	0.01	1	0	-1	-5
0.72	9.66	-6.22	7.62	1.17E-04	35.79	0.01	1	0	-1	-5
0.80	9.63	-6.19	7.61	1.26E-04	36.00	0.01	1	0	-1	-5
0.88	9.60	-6.15	7.61	1.36E-04	36.20	0.01	1	0	-1	-5
0.96	9.58	-6.12	7.64	1.47E-04	36.40	0.01	1	0	-1	-5
1.04	9.55	-6.08	7.68	1.60E-04	36.59	0.01	1	0	-1	-5
1.12	9.52	-6.05	7.74	1.73E-04	36.78	0.01	1	0	-1	-5
1.20	9.50	-6.02	7.82	1.88E-04	36.96	4.70E-03	1	0	-1	-5
1.28	9.47	-5.98	7.92	2.04E-04	37.14	4.39E-03	1	0	-1	-5
1.36	9.45	-5.95	8.03	2.21E-04	37.31	4.11E-03	1	0	-1	-5
1.44	9.42	-5.92	8.16	2.39E-04	37.48	3.84E-03	1	0	-1	-5

1. Composition of the "Pure Water" solution as a total of 8 mg/L oxygen is added to 10 moles of pyrite and 10 moles of calcite. Concentrations are presented in units of mg/L

2. S.I.: Saturation indices of selected iron-oxyhydroxides. Saturation index (S.I.) =  $\log(\text{IAP})/K_T$  where IAP is the ion activity product of the dissolved components in solution, and  $K_T$  is the solubility of the solid or gaseous phase at the specified temperature

Oxygen Added <sup>1</sup>	pH	pe	Alkalinity as HCO <sub>3</sub> <sup>-</sup>	Dissolved Fe	SO <sub>4</sub> <sup>2-</sup>	S <sup>2-</sup>	S.I. <sup>2</sup> Hematite	S.I. <sup>2</sup> Goethite	S.I. <sup>2</sup> Lepidocrocite	S.I. <sup>2</sup> Fe(OH) <sub>3</sub>
1.52	9.39	-5.88	8.31	2.59E-04	37.64	3.60E-03	1	0	-1	-5
1.60	9.37	-5.85	8.46	2.81E-04	37.80	3.37E-03	1	0	-1	-5
1.68	9.35	-5.82	8.63	3.04E-04	37.96	3.17E-03	1	0	-1	-5
1.76	9.32	-5.79	8.82	3.28E-04	38.10	2.98E-03	1	0	-1	-5
1.84	9.30	-5.76	9.01	3.54E-04	38.25	2.80E-03	1	0	-1	-5
1.92	9.28	-5.73	9.21	3.82E-04	38.39	2.64E-03	1	0	-1	-5
2.00	9.25	-5.71	9.42	4.12E-04	38.52	2.50E-03	1	0	-1	-5
2.08	9.23	-5.68	9.65	4.43E-04	38.65	2.36E-03	1	0	-1	-5
2.16	9.21	-5.65	9.88	4.76E-04	38.78	2.24E-03	1	0	-1	-5
2.24	9.19	-5.63	10.11	5.11E-04	38.90	2.12E-03	1	0	-1	-5
2.32	9.17	-5.60	10.36	5.47E-04	39.02	2.01E-03	1	0	-1	-5
2.40	9.15	-5.58	10.60	5.85E-04	39.14	1.91E-03	1	0	-1	-5
2.48	9.13	-5.55	10.86	6.26E-04	39.25	1.82E-03	1	0	-1	-5
2.56	9.11	-5.53	11.12	6.68E-04	39.36	1.74E-03	1	0	-1	-5
2.64	9.10	-5.50	11.38	7.12E-04	39.47	1.66E-03	1	0	-1	-5
2.72	9.08	-5.48	11.65	7.58E-04	39.58	1.58E-03	1	0	-1	-5
2.80	9.06	-5.46	11.93	8.06E-04	39.68	1.51E-03	1	0	-1	-5
2.88	9.04	-5.44	12.20	8.56E-04	39.78	1.45E-03	1	0	-1	-5
2.96	9.03	-5.42	12.48	9.08E-04	39.88	1.39E-03	1	0	-1	-5
3.04	9.01	-5.40	12.77	9.62E-04	39.98	1.33E-03	1	0	-1	-5
3.12	9.00	-5.38	13.05	1.02E-03	40.07	1.28E-03	1	0	-1	-5

1. Composition of the "Pure Water" solution as a total of 8 mg/L oxygen is added to 10 moles of pyrite and 10 moles of calcite. Concentrations are presented in units of mg/L

2. S.I.: Saturation indices of selected iron-oxyhydroxides. Saturation index (S.I.) =  $\log(\text{IAP})/K_T$  where IAP is the ion activity product of the dissolved components in solution, and  $K_T$  is the solubility of the solid or gaseous phase at the specified temperature

Oxygen Added <sup>1</sup>	pH	pe	Alkalinity as HCO <sub>3</sub> <sup>-</sup>	Dissolved Fe	SO <sub>4</sub> <sup>2-</sup>	S <sup>2-</sup>	S.I. <sup>2</sup> Hematite	S.I. <sup>2</sup> Goethite	S.I. <sup>2</sup> Lepidocrocite	S.I. <sup>2</sup> Fe(OH) <sub>3</sub>
3.20	8.98	-5.36	13.34	1.08E-03	40.17	1.23E-03	1	0	-1	-5
3.28	8.97	-5.34	13.63	1.14E-03	40.26	1.18E-03	1	0	-1	-5
3.36	8.95	-5.32	13.92	1.20E-03	40.35	1.14E-03	1	0	-1	-5
3.44	8.94	-5.30	14.22	1.27E-03	40.45	1.10E-03	1	0	-1	-5
3.52	8.92	-5.28	14.52	1.33E-03	40.54	1.06E-03	1	0	-1	-5
3.60	8.91	-5.27	14.82	1.40E-03	40.62	1.02E-03	1	0	-1	-5
3.68	8.90	-5.25	15.12	1.47E-03	40.71	9.87E-04	1	0	-1	-5
3.76	8.88	-5.23	15.42	1.55E-03	40.80	9.54E-04	1	0	-1	-5
3.84	8.87	-5.22	15.72	1.63E-03	40.89	9.23E-04	1	0	-1	-5
3.92	8.86	-5.20	16.03	1.71E-03	40.97	8.93E-04	1	0	-1	-5
4.00	8.84	-5.18	16.33	1.79E-03	41.06	8.64E-04	1	0	-1	-5
4.08	8.83	-5.17	16.64	1.87E-03	41.14	8.38E-04	1	0	-1	-5
4.16	8.82	-5.15	16.95	1.96E-03	41.23	8.12E-04	1	0	-1	-5
4.24	8.81	-5.14	17.26	2.05E-03	41.31	7.88E-04	1	0	-1	-5
4.32	8.80	-5.12	17.57	2.14E-03	41.39	7.65E-04	1	0	-1	-5
4.40	8.79	-5.11	17.88	2.24E-03	41.48	7.42E-04	1	0	-1	-5
4.48	8.77	-5.09	18.19	2.33E-03	41.56	7.21E-04	1	0	-1	-5
4.56	8.76	-5.08	18.50	2.43E-03	41.64	7.01E-04	1	0	-1	-5
4.64	8.75	-5.07	18.81	2.54E-03	41.73	6.82E-04	1	0	-1	-5
4.72	8.74	-5.05	19.13	2.64E-03	41.81	6.63E-04	1	0	-1	-5
4.80	8.73	-5.04	19.44	2.75E-03	41.89	6.46E-04	1	0	-1	-5

1. Composition of the "Pure Water" solution as a total of 8 mg/L oxygen is added to 10 moles of pyrite and 10 moles of calcite. Concentrations are presented in units of mg/L

2. S.I.: Saturation indices of selected iron-oxyhydroxides. Saturation index (S.I.) =  $\log(\text{IAP})/K_T$  where IAP is the ion activity product of the dissolved components in solution, and  $K_T$  is the solubility of the solid or gaseous phase at the specified temperature

Oxygen Added <sup>1</sup>	pH	pe	Alkalinity as HCO <sub>3</sub> <sup>-</sup>	Dissolved Fe	SO <sub>4</sub> <sup>2-</sup>	S <sup>2-</sup>	S.I. <sup>2</sup> Hematite	S.I. <sup>2</sup> Goethite	S.I. <sup>2</sup> Lepidocrocite	S.I. <sup>2</sup> Fe(OH) <sub>3</sub>
4.88	8.72	-5.03	19.75	2.86E-03	41.97	6.29E-04	1	0	-1	-5
4.96	8.71	-5.01	20.07	2.98E-03	42.06	6.12E-04	1	0	-1	-5
5.04	8.70	-5.00	20.38	3.09E-03	42.14	5.97E-04	1	0	-1	-5
5.12	8.69	-4.99	20.70	3.21E-03	42.22	5.82E-04	1	0	-1	-5
5.20	8.68	-4.98	21.02	3.34E-03	42.31	5.68E-04	1	0	-1	-5
5.28	8.67	-4.96	21.33	3.47E-03	42.39	5.54E-04	1	0	-1	-5
5.36	8.66	-4.95	21.65	3.60E-03	42.47	5.40E-04	1	0	-1	-5
5.44	8.65	-4.94	21.97	3.73E-03	42.56	5.28E-04	1	0	-1	-5
5.52	8.64	-4.93	22.28	3.86E-03	42.64	5.15E-04	1	0	-1	-5
5.60	8.63	-4.92	22.60	4.00E-03	42.73	5.04E-04	1	0	-1	-5
5.68	8.63	-4.90	22.92	4.15E-03	42.81	4.92E-04	1	0	-1	-5
5.76	8.62	-4.89	23.24	4.29E-03	42.90	4.81E-04	1	0	-1	-5
5.84	8.61	-4.88	23.56	4.44E-03	42.98	4.70E-04	1	0	-1	-5
5.92	8.60	-4.87	23.87	4.60E-03	43.07	4.60E-04	1	0	-1	-5
6.00	8.59	-4.86	24.19	4.75E-03	43.15	4.50E-04	1	0	-1	-5
6.08	8.58	-4.85	24.51	4.91E-03	43.24	4.41E-04	1	0	-1	-5
6.16	8.57	-4.84	24.83	0.01	43.33	4.31E-04	1	0	-1	-5
6.24	8.57	-4.83	25.15	0.01	43.41	4.22E-04	1	0	-1	-5
6.32	8.56	-4.82	25.47	0.01	43.50	4.14E-04	1	0	-1	-5
6.40	8.55	-4.81	25.79	0.01	43.59	4.05E-04	1	0	-1	-5
6.48	8.54	-4.80	26.11	0.01	43.68	3.97E-04	1	0	-1	-5

1. Composition of the "Pure Water" solution as a total of 8 mg/L oxygen is added to 10 moles of pyrite and 10 moles of calcite. Concentrations are presented in units of mg/L

2. S.I.: Saturation indices of selected iron-oxyhydroxides. Saturation index (S.I.) =  $\log(\text{IAP})/K_T$  where IAP is the ion activity product of the dissolved components in solution, and  $K_T$  is the solubility of the solid or gaseous phase at the specified temperature

Oxygen Added <sup>1</sup>	pH	pe	Alkalinity as HCO <sub>3</sub> <sup>-</sup>	Dissolved Fe	SO <sub>4</sub> <sup>2-</sup>	S <sup>2-</sup>	S.I. <sup>2</sup> Hematite	S.I. <sup>2</sup> Goethite	S.I. <sup>2</sup> Lepidocrocite	S.I. <sup>2</sup> Fe(OH) <sub>3</sub>
6.56	8.53	-4.79	26.43	0.01	43.77	3.89E-04	1	0	-1	-5
6.64	8.53	-4.78	26.74	0.01	43.86	3.82E-04	1	0	-1	-5
6.72	8.52	-4.77	27.06	0.01	43.95	3.74E-04	1	0	-1	-5
6.80	8.51	-4.76	27.38	0.01	44.04	3.67E-04	1	0	-1	-5
6.88	8.50	-4.75	27.70	0.01	44.13	3.60E-04	1	0	-1	-5
6.96	8.50	-4.74	28.02	0.01	44.22	3.54E-04	1	0	-1	-5
7.04	8.49	-4.73	28.34	0.01	44.32	3.47E-04	1	0	-1	-5
7.12	8.48	-4.72	28.66	0.01	44.41	3.41E-04	1	0	-1	-5
7.20	8.47	-4.71	28.98	0.01	44.50	3.35E-04	1	0	-1	-5
7.28	8.47	-4.70	29.30	0.01	44.60	3.29E-04	1	0	-1	-5
7.36	8.46	-4.69	29.61	0.01	44.69	3.23E-04	1	0	-1	-5
7.44	8.45	-4.68	29.93	0.01	44.79	3.17E-04	1	0	-1	-5
7.52	8.45	-4.68	30.25	0.01	44.89	3.12E-04	1	0	-1	-5
7.60	8.44	-4.67	30.57	0.01	44.98	3.06E-04	1	0	-1	-5
7.68	8.43	-4.66	30.89	0.01	45.08	3.01E-04	1	0	-1	-5
7.76	8.42	-4.65	31.21	0.01	45.18	2.96E-04	1	0	-1	-5
7.84	8.42	-4.64	31.52	0.01	45.28	2.91E-04	1	0	-1	-5
7.92	8.41	-4.63	31.84	0.01	45.38	2.86E-04	1	0	-1	-5
8.00	8.41	-4.62	32.16	0.01	45.48	2.81E-04	1	0	-1	-5

1. Composition of the "Pure Water" solution as a total of 8 mg/L oxygen is added to 10 moles of pyrite and 10 moles of calcite. Concentrations are presented in units of mg/L

2. S.I.: Saturation indices of selected iron-oxyhydroxides. Saturation index (S.I.) =  $\log(\text{IAP})/K_T$  where IAP is the ion activity product of the dissolved components in solution, and  $K_T$  is the solubility of the solid or gaseous phase at the specified temperature

### Appendix K7: Pyrite Titration with Oxygen in Surficial Water

Oxygen Added <sup>1</sup>	pH	pe	Alkalinity as HCO <sub>3</sub> <sup>-</sup>	Dissolved Fe	SO <sub>4</sub> <sup>2-</sup>	S <sup>2-</sup>	S.I. <sup>2</sup> Hematite	S.I. <sup>2</sup> Goethite	S.I. <sup>2</sup> Lepidocrocite	S.I. <sup>2</sup> Fe(OH) <sub>3</sub>
0.00	5.30	6.44	24.01	0.07	17.88	0.00	-1000	-1000	-1000	-1000
0.08	5.31	-0.93	24.92	1.84	23.97	1.96E-04	-6	-3	-4	-8
0.16	5.31	-0.92	24.76	1.92	24.23	1.92E-04	-6	-3	-4	-8
0.24	5.31	-0.92	24.59	1.99	24.49	1.89E-04	-6	-3	-4	-8
0.32	5.30	-0.91	24.42	2.07	24.75	1.86E-04	-6	-3	-4	-8
0.40	5.30	-0.91	24.25	2.14	25.01	1.83E-04	-5	-3	-4	-8
0.48	5.29	-0.90	24.08	2.22	25.27	1.80E-04	-5	-3	-4	-8
0.56	5.29	-0.90	23.91	2.30	25.53	1.78E-04	-5	-3	-4	-8
0.64	5.29	-0.89	23.74	2.37	25.80	1.75E-04	-5	-3	-4	-8
0.72	5.28	-0.88	23.57	2.45	26.06	1.73E-04	-5	-3	-4	-8
0.80	5.28	-0.88	23.40	2.53	26.33	1.71E-04	-5	-3	-4	-8
0.88	5.28	-0.87	23.23	2.60	26.59	1.69E-04	-5	-3	-4	-8
0.96	5.27	-0.87	23.05	2.68	26.86	1.67E-04	-5	-3	-4	-8
1.04	5.27	-0.86	22.88	2.76	27.13	1.65E-04	-5	-3	-4	-8
1.12	5.27	-0.86	22.71	2.84	27.39	1.63E-04	-5	-3	-4	-8
1.20	5.26	-0.85	22.54	2.91	27.66	1.62E-04	-5	-3	-4	-8
1.28	5.26	-0.84	22.37	2.99	27.93	1.60E-04	-5	-3	-4	-8
1.36	5.25	-0.84	22.19	3.07	28.20	1.59E-04	-5	-3	-4	-8
1.44	5.25	-0.83	22.02	3.15	28.47	1.57E-04	-5	-3	-4	-8

1. Composition of the "Surficial Water" solution as a total of 8 mg/L oxygen is added to 10 moles of pyrite. Concentrations are presented in units of mg/L

2. S.I.: Saturation indices of selected iron-oxyhydroxides. Saturation index (S.I.) =  $\log(\text{IAP})/K_T$  where IAP is the ion activity product of the dissolved components in solution, and  $K_T$  is the solubility of the solid or gaseous phase at the specified temperature

Oxygen Added <sup>1</sup>	pH	pe	Alkalinity as HCO <sub>3</sub> <sup>-</sup>	Dissolved Fe	SO <sub>4</sub> <sup>2-</sup>	S <sup>2-</sup>	S.I. <sup>2</sup> Hematite	S.I. <sup>2</sup> Goethite	S.I. <sup>2</sup> Lepidocrocite	S.I. <sup>2</sup> Fe(OH) <sub>3</sub>
1.52	5.25	-0.83	21.85	3.23	28.74	1.56E-04	-5	-3	-4	-8
1.60	5.24	-0.82	21.67	3.31	29.01	1.55E-04	-5	-3	-4	-8
1.68	5.24	-0.82	21.50	3.38	29.28	1.54E-04	-5	-3	-4	-8
1.76	5.24	-0.81	21.33	3.46	29.55	1.53E-04	-5	-3	-4	-8
1.84	5.23	-0.80	21.15	3.54	29.82	1.52E-04	-5	-3	-4	-8
1.92	5.23	-0.80	20.98	3.62	30.09	1.51E-04	-5	-3	-4	-8
2.00	5.22	-0.79	20.81	3.70	30.36	1.50E-04	-5	-3	-4	-8
2.08	5.22	-0.79	20.63	3.78	30.63	1.49E-04	-5	-3	-4	-8
2.16	5.22	-0.78	20.46	3.86	30.90	1.48E-04	-5	-3	-4	-8
2.24	5.21	-0.77	20.29	3.94	31.18	1.47E-04	-5	-3	-4	-8
2.32	5.21	-0.77	20.11	4.01	31.45	1.47E-04	-5	-3	-4	-8
2.40	5.20	-0.76	19.94	4.09	31.72	1.46E-04	-5	-3	-4	-8
2.48	5.20	-0.76	19.77	4.17	31.99	1.45E-04	-5	-3	-4	-8
2.56	5.19	-0.75	19.59	4.25	32.26	1.45E-04	-5	-3	-4	-8
2.64	5.19	-0.75	19.42	4.33	32.54	1.44E-04	-5	-3	-4	-8
2.72	5.19	-0.74	19.24	4.41	32.81	1.44E-04	-5	-3	-4	-8
2.80	5.18	-0.73	19.07	4.49	33.08	1.43E-04	-5	-3	-4	-8
2.88	5.18	-0.73	18.90	4.57	33.35	1.43E-04	-5	-3	-4	-8
2.96	5.17	-0.72	18.72	4.65	33.63	1.42E-04	-5	-3	-4	-8
3.04	5.17	-0.72	18.55	4.73	33.90	1.42E-04	-5	-3	-4	-8
3.12	5.16	-0.71	18.38	4.81	34.17	1.42E-04	-5	-3	-4	-8

1. Composition of the "Surficial Water" solution as a total of 8 mg/L oxygen is added to 10 moles of pyrite. Concentrations are presented in units of mg/L

2. S.I.: Saturation indices of selected iron-oxyhydroxides. Saturation index (S.I.) =  $\log(\text{IAP})/K_T$  where IAP is the ion activity product of the dissolved components in solution, and  $K_T$  is the solubility of the solid or gaseous phase at the specified temperature



Oxygen Added <sup>1</sup>	pH	pe	Alkalinity as HCO <sub>3</sub> <sup>-</sup>	Dissolved Fe	SO <sub>4</sub> <sup>2-</sup>	S <sup>2-</sup>	S.I. <sup>2</sup> Hematite	S.I. <sup>2</sup> Goethite	S.I. <sup>2</sup> Lepidocrocite	S.I. <sup>2</sup> Fe(OH) <sub>3</sub>
3.20	5.16	-0.70	18.20	4.89	34.45	1.41E-04	-5	-3	-4	-8
3.28	5.16	-0.70	18.03	4.97	34.72	1.41E-04	-5	-3	-4	-8
3.36	5.15	-0.69	17.85	5.05	34.99	1.41E-04	-5	-3	-4	-8
3.44	5.15	-0.68	17.68	5.12	35.27	1.41E-04	-5	-3	-4	-8
3.52	5.14	-0.68	17.51	5.20	35.54	1.40E-04	-5	-3	-4	-8
3.60	5.14	-0.67	17.33	5.28	35.81	1.40E-04	-5	-3	-4	-8
3.68	5.13	-0.67	17.16	5.36	36.09	1.40E-04	-5	-3	-4	-8
3.76	5.13	-0.66	16.98	5.44	36.36	1.40E-04	-5	-3	-4	-8
3.84	5.12	-0.65	16.81	5.52	36.63	1.40E-04	-5	-3	-4	-8
3.92	5.12	-0.65	16.64	5.60	36.91	1.40E-04	-5	-3	-4	-8
4.00	5.11	-0.64	16.46	5.68	37.18	1.40E-04	-5	-3	-4	-8
4.08	5.11	-0.63	16.29	5.76	37.46	1.40E-04	-5	-3	-4	-8
4.16	5.10	-0.63	16.11	5.84	37.73	1.40E-04	-5	-3	-4	-8
4.24	5.10	-0.62	15.94	5.92	38.00	1.40E-04	-5	-3	-4	-8
4.32	5.09	-0.61	15.77	6.00	38.28	1.40E-04	-5	-3	-4	-8
4.40	5.09	-0.61	15.59	6.08	38.55	1.40E-04	-5	-3	-4	-8
4.48	5.08	-0.60	15.42	6.16	38.83	1.41E-04	-5	-3	-4	-8
4.56	5.08	-0.59	15.25	6.24	39.10	1.41E-04	-5	-3	-4	-8
4.64	5.07	-0.59	15.07	6.32	39.38	1.41E-04	-5	-3	-4	-8
4.72	5.07	-0.58	14.90	6.40	39.65	1.41E-04	-5	-3	-4	-8
4.80	5.06	-0.57	14.72	6.48	39.93	1.42E-04	-5	-3	-4	-8

1. Composition of the "Surficial Water" solution as a total of 8 mg/L oxygen is added to 10 moles of pyrite. Concentrations are presented in units of mg/L

2. S.I.: Saturation indices of selected iron-oxyhydroxides. Saturation index (S.I.) =  $\log(\text{IAP})/K_T$  where IAP is the ion activity product of the dissolved components in solution, and  $K_T$  is the solubility of the solid or gaseous phase at the specified temperature

Oxygen Added <sup>1</sup>	pH	pe	Alkalinity as HCO <sub>3</sub> <sup>-</sup>	Dissolved Fe	SO <sub>4</sub> <sup>2-</sup>	S <sup>2-</sup>	S.I. <sup>2</sup> Hematite	S.I. <sup>2</sup> Goethite	S.I. <sup>2</sup> Lepidocrocite	S.I. <sup>2</sup> Fe(OH) <sub>3</sub>
4.88	5.06	-0.57	14.55	6.56	40.20	1.42E-04	-5	-3	-4	-8
4.96	5.05	-0.56	14.38	6.64	40.47	1.42E-04	-5	-3	-4	-8
5.04	5.05	-0.55	14.20	6.72	40.75	1.43E-04	-5	-3	-4	-8
5.12	5.04	-0.55	14.03	6.80	41.02	1.43E-04	-5	-3	-4	-8
5.20	5.04	-0.54	13.86	6.88	41.30	1.43E-04	-5	-3	-4	-8
5.28	5.03	-0.53	13.68	6.96	41.57	1.44E-04	-5	-3	-4	-8
5.36	5.02	-0.53	13.51	7.04	41.85	1.44E-04	-5	-3	-4	-8
5.44	5.02	-0.52	13.34	7.12	42.12	1.45E-04	-5	-3	-4	-8
5.52	5.01	-0.51	13.16	7.20	42.40	1.45E-04	-5	-3	-4	-8
5.60	5.01	-0.50	12.99	7.28	42.67	1.46E-04	-5	-3	-4	-8
5.68	5.00	-0.50	12.81	7.36	42.95	1.46E-04	-5	-3	-4	-8
5.76	5.00	-0.49	12.64	7.44	43.22	1.47E-04	-5	-3	-4	-8
5.84	4.99	-0.48	12.47	7.52	43.50	1.48E-04	-5	-3	-4	-8
5.92	4.98	-0.47	12.29	7.60	43.77	1.48E-04	-5	-3	-4	-8
6.00	4.98	-0.47	12.12	7.68	44.05	1.49E-04	-5	-3	-4	-8
6.08	4.97	-0.46	11.95	7.76	44.32	1.50E-04	-5	-3	-4	-8
6.16	4.97	-0.45	11.77	7.84	44.60	1.50E-04	-5	-3	-4	-8
6.24	4.96	-0.44	11.60	7.92	44.87	1.51E-04	-5	-3	-4	-8
6.32	4.95	-0.44	11.43	8.00	45.15	1.52E-04	-5	-3	-4	-8
6.40	4.95	-0.43	11.25	8.08	45.42	1.53E-04	-5	-3	-4	-8
6.48	4.94	-0.42	11.08	8.16	45.70	1.54E-04	-5	-3	-4	-8

1. Composition of the "Surficial Water" solution as a total of 8 mg/L oxygen is added to 10 moles of pyrite. Concentrations are presented in units of mg/L

2. S.I.: Saturation indices of selected iron-oxyhydroxides. Saturation index (S.I.) = log(IAP)/K<sub>T</sub> where IAP is the ion activity product of the dissolved components in solution, and K<sub>T</sub> is the solubility of the solid or gaseous phase at the specified temperature

Oxygen Added <sup>1</sup>	pH	pe	Alkalinity as HCO <sub>3</sub> <sup>-</sup>	Dissolved Fe	SO <sub>4</sub> <sup>2-</sup>	S <sup>2-</sup>	S.I. <sup>2</sup> Hematite	S.I. <sup>2</sup> Goethite	S.I. <sup>2</sup> Lepidocrocite	S.I. <sup>2</sup> Fe(OH) <sub>3</sub>
6.56	4.93	-0.41	10.91	8.24	45.98	1.55E-04	-5	-3	-4	-8
6.64	4.93	-0.40	10.73	8.32	46.25	1.56E-04	-5	-3	-4	-8
6.72	4.92	-0.39	10.56	8.40	46.53	1.57E-04	-6	-3	-4	-8
6.80	4.91	-0.39	10.39	8.48	46.80	1.58E-04	-6	-3	-4	-8
6.88	4.91	-0.38	10.21	8.56	47.08	1.59E-04	-6	-3	-4	-8
6.96	4.90	-0.37	10.04	8.64	47.35	1.60E-04	-6	-3	-4	-8
7.04	4.89	-0.36	9.87	8.72	47.63	1.61E-04	-6	-3	-4	-8
7.12	4.89	-0.35	9.70	8.80	47.91	1.62E-04	-6	-3	-4	-8
7.20	4.88	-0.34	9.52	8.88	48.18	1.64E-04	-6	-3	-4	-8
7.28	4.87	-0.33	9.35	8.96	48.46	1.65E-04	-6	-3	-4	-8
7.36	4.86	-0.33	9.18	9.04	48.73	1.66E-04	-6	-3	-4	-8
7.44	4.86	-0.32	9.00	9.12	49.01	1.68E-04	-6	-3	-4	-8
7.52	4.85	-0.31	8.83	9.20	49.29	1.69E-04	-6	-3	-4	-8
7.60	4.84	-0.30	8.66	9.28	49.56	1.71E-04	-6	-3	-4	-8
7.68	4.83	-0.29	8.49	9.36	49.84	1.72E-04	-6	-3	-4	-8
7.76	4.83	-0.28	8.31	9.44	50.11	1.74E-04	-6	-3	-4	-8
7.84	4.82	-0.27	8.14	9.52	50.39	1.75E-04	-6	-3	-4	-9
7.92	4.81	-0.26	7.97	9.60	50.67	1.77E-04	-6	-3	-4	-9
8.00	4.80	-0.25	7.80	9.68	50.94	1.79E-04	-6	-3	-4	-9

1. Composition of the "Surficial Water" solution as a total of 8 mg/L oxygen is added to 10 moles of pyrite. Concentrations are presented in units of mg/L

2. S.I.: Saturation indices of selected iron-oxyhydroxides. Saturation index (S.I.) =  $\log(\text{IAP})/K_T$  where IAP is the ion activity product of the dissolved components in solution, and  $K_T$  is the solubility of the solid or gaseous phase at the specified temperature

### Appendix K8: Pyrite Titration with Oxygen and Simultaneous Calcite Dissolution in Surficial Water

Oxygen Added <sup>1</sup>	pH	pe	Alkalinity as HCO <sub>3</sub> <sup>-</sup>	Dissolved Fe	SO <sub>4</sub> <sup>2-</sup>	S <sup>2-</sup>	S.I. <sup>2</sup> Hematite	S.I. <sup>2</sup> Goethite	S.I. <sup>2</sup> Lepidocrocite	S.I. <sup>2</sup> Fe(OH) <sub>3</sub>
0.00	5.30	6.44	24.01	0.07	17.88	0.00	-1000	-1000	-1000	-1000
0.08	6.87	-2.69	364.31	7.30	42.76	1.34E-05	0	0	-1	-5
0.16	6.87	-2.69	364.43	7.34	42.87	1.33E-05	0	0	-1	-5
0.24	6.87	-2.69	364.54	7.37	42.98	1.33E-05	0	0	-1	-5
0.32	6.87	-2.69	364.66	7.40	43.10	1.33E-05	0	0	-1	-5
0.40	6.87	-2.69	364.78	7.43	43.21	1.33E-05	0	0	-1	-5
0.48	6.87	-2.69	364.89	7.47	43.32	1.32E-05	0	0	-1	-5
0.56	6.87	-2.69	365.01	7.50	43.44	1.32E-05	0	0	-1	-5
0.64	6.87	-2.69	365.12	7.53	43.55	1.32E-05	0	0	-1	-5
0.72	6.87	-2.69	365.24	7.57	43.66	1.31E-05	0	0	-1	-5
0.80	6.87	-2.69	365.35	7.60	43.78	1.31E-05	0	0	-1	-5
0.88	6.87	-2.69	365.47	7.63	43.90	1.31E-05	0	0	-1	-5
0.96	6.87	-2.69	365.58	7.67	44.02	1.30E-05	0	0	-1	-5
1.04	6.87	-2.69	365.69	7.70	44.13	1.30E-05	0	0	-1	-5
1.12	6.87	-2.69	365.81	7.74	44.25	1.30E-05	0	0	-1	-5
1.20	6.87	-2.69	365.92	7.77	44.37	1.29E-05	0	0	-1	-5
1.28	6.87	-2.69	366.04	7.81	44.49	1.29E-05	0	0	-1	-5
1.36	6.87	-2.68	366.15	7.84	44.62	1.29E-05	0	0	-1	-5
1.44	6.87	-2.68	366.26	7.88	44.74	1.28E-05	0	0	-1	-5

1. Composition of the "Surficial Water" solution as a total of 8 mg/L oxygen is added to 10 moles of pyrite and 10 moles of calcite. Concentrations are presented in units of mg/L

2. S.I.: Saturation indices of selected iron-oxyhydroxides. Saturation index (S.I.) =  $\log(\text{IAP})/K_T$  where IAP is the ion activity product of the dissolved components in solution, and  $K_T$  is the solubility of the solid or gaseous phase at the specified temperature

Oxygen Added <sup>1</sup>	pH	pe	Alkalinity as HCO <sub>3</sub> <sup>-</sup>	Dissolved Fe	SO <sub>4</sub> <sup>2-</sup>	S <sup>2-</sup>	S.I. <sup>2</sup> Hematite	S.I. <sup>2</sup> Goethite	S.I. <sup>2</sup> Lepidocrocite	S.I. <sup>2</sup> Fe(OH) <sub>3</sub>
1.52	6.87	-2.68	366.38	7.91	44.86	1.28E-05	0	0	-1	-5
1.60	6.87	-2.68	366.49	7.95	44.99	1.28E-05	0	0	-1	-5
1.68	6.87	-2.68	366.60	7.99	45.11	1.27E-05	0	0	-1	-5
1.76	6.87	-2.68	366.71	8.02	45.24	1.27E-05	0	0	-1	-5
1.84	6.87	-2.68	366.83	8.06	45.36	1.27E-05	1	0	-1	-5
1.92	6.87	-2.68	366.94	8.10	45.49	1.26E-05	1	0	-1	-5
2.00	6.87	-2.68	367.05	8.13	45.62	1.26E-05	1	0	-1	-5
2.08	6.87	-2.68	367.16	8.17	45.75	1.26E-05	1	0	-1	-5
2.16	6.87	-2.68	367.28	8.21	45.88	1.25E-05	1	0	-1	-5
2.24	6.87	-2.68	367.39	8.25	46.01	1.25E-05	1	0	-1	-5
2.32	6.87	-2.68	367.50	8.29	46.14	1.25E-05	1	0	-1	-5
2.40	6.86	-2.68	367.61	8.32	46.28	1.24E-05	1	0	-1	-5
2.48	6.86	-2.68	367.72	8.36	46.41	1.24E-05	1	0	-1	-5
2.56	6.86	-2.68	367.83	8.40	46.54	1.24E-05	1	0	-1	-5
2.64	6.86	-2.68	367.94	8.44	46.68	1.23E-05	1	0	-1	-5
2.72	6.86	-2.67	368.05	8.48	46.82	1.23E-05	1	0	-1	-5
2.80	6.86	-2.67	368.16	8.52	46.95	1.23E-05	1	0	-1	-5
2.88	6.86	-2.67	368.27	8.56	47.09	1.22E-05	1	0	-1	-5
2.96	6.86	-2.67	368.38	8.60	47.23	1.22E-05	1	0	-1	-5
3.04	6.86	-2.67	368.49	8.64	47.37	1.22E-05	1	0	-1	-5
3.12	6.86	-2.67	368.60	8.68	47.51	1.21E-05	1	0	-1	-5

1. Composition of the "Surficial Water" solution as a total of 8 mg/L Oxygen is added to 10 moles of pyrite and 10 moles of calcite. Concentrations are presented in units of mg/L

2. S.I.: Saturation indices of selected iron-oxyhydroxides. Saturation index (S.I.) =  $\log(\text{IAP})/K_T$  where IAP is the ion activity product of the dissolved components in solution, and  $K_T$  is the solubility of the solid or gaseous phase at the specified temperature

Oxygen Added <sup>1</sup>	pH	pe	Alkalinity as HCO <sub>3</sub> <sup>-</sup>	Dissolved Fe	SO <sub>4</sub> <sup>2-</sup>	S <sup>2-</sup>	S.I. <sup>2</sup> Hematite	S.I. <sup>2</sup> Goethite	S.I. <sup>2</sup> Lepidocrocite	S.I. <sup>2</sup> Fe(OH) <sub>3</sub>
3.20	6.86	-2.67	368.71	8.72	47.65	1.21E-05	1	0	-1	-5
3.28	6.86	-2.67	368.82	8.77	47.79	1.21E-05	1	0	-1	-5
3.36	6.86	-2.67	368.93	8.81	47.94	1.20E-05	1	0	-1	-5
3.44	6.86	-2.67	369.04	8.85	48.08	1.20E-05	1	0	-1	-5
3.52	6.86	-2.67	369.14	8.89	48.23	1.20E-05	1	0	-1	-5
3.60	6.86	-2.67	369.25	8.93	48.37	1.19E-05	1	0	-1	-5
3.68	6.86	-2.67	369.36	8.98	48.52	1.19E-05	1	0	-1	-5
3.76	6.86	-2.67	369.47	9.02	48.67	1.19E-05	1	0	-1	-5
3.84	6.86	-2.67	369.58	9.06	48.82	1.18E-05	1	0	-1	-5
3.92	6.86	-2.67	369.68	9.11	48.97	1.18E-05	1	0	-1	-5
4.00	6.86	-2.67	369.79	9.15	49.12	1.18E-05	1	0	-1	-5
4.08	6.86	-2.66	369.90	9.19	49.27	1.17E-05	1	0	-1	-5
4.16	6.86	-2.66	370.00	9.24	49.42	1.17E-05	1	0	-1	-5
4.24	6.86	-2.66	370.11	9.28	49.57	1.17E-05	1	0	-1	-5
4.32	6.86	-2.66	370.22	9.33	49.73	1.16E-05	1	0	-1	-5
4.40	6.86	-2.66	370.32	9.37	49.89	1.16E-05	1	0	-1	-5
4.48	6.86	-2.66	370.43	9.42	50.04	1.16E-05	1	0	-1	-5
4.56	6.86	-2.66	370.54	9.46	50.20	1.15E-05	1	0	-1	-5
4.64	6.86	-2.66	370.64	9.51	50.36	1.15E-05	1	0	-1	-5
4.72	6.86	-2.66	370.75	9.56	50.52	1.15E-05	1	0	-1	-5
4.80	6.86	-2.66	370.85	9.60	50.67	1.14E-05	1	0	-1	-5

1. Composition of the "Surficial Water" solution as a total of 8 mg/L Oxygen is added to 10 moles of pyrite and 10 moles of calcite. Concentrations are presented in units of mg/L

2. S.I.: Saturation indices of selected iron-oxyhydroxides. Saturation index (S.I.) =  $\log(\text{IAP})/K_T$  where IAP is the ion activity product of the dissolved components in solution, and  $K_T$  is the solubility of the solid or gaseous phase at the specified temperature

Oxygen Added <sup>1</sup>	pH	pe	Alkalinity as HCO <sub>3</sub> <sup>-</sup>	Dissolved Fe	SO <sub>4</sub> <sup>2-</sup>	S <sup>2-</sup>	S.I. <sup>2</sup> Hematite	S.I. <sup>2</sup> Goethite	S.I. <sup>2</sup> Lepidocrocite	S.I. <sup>2</sup> Fe(OH) <sub>3</sub>
4.88	6.86	-2.66	370.96	9.65	50.84	1.14E-05	1	0	-1	-5
4.96	6.86	-2.66	371.06	9.70	51.00	1.14E-05	1	0	-1	-5
5.04	6.86	-2.66	371.17	9.74	51.16	1.13E-05	1	0	-1	-5
5.12	6.86	-2.66	371.27	9.79	51.32	1.13E-05	1	0	-1	-5
5.20	6.86	-2.66	371.38	9.84	51.49	1.13E-05	1	0	-1	-5
5.28	6.86	-2.66	371.48	9.89	51.65	1.12E-05	1	0	-1	-5
5.36	6.86	-2.66	371.58	9.94	51.82	1.12E-05	1	0	-1	-5
5.44	6.86	-2.65	371.69	9.98	51.99	1.12E-05	1	0	-1	-5
5.52	6.86	-2.65	371.79	10.03	52.16	1.11E-05	1	0	-1	-5
5.60	6.86	-2.65	371.89	10.08	52.33	1.11E-05	1	0	-1	-5
5.68	6.86	-2.65	372.00	10.13	52.50	1.11E-05	1	0	-1	-5
5.76	6.85	-2.65	372.10	10.18	52.67	1.10E-05	1	0	-1	-5
5.84	6.85	-2.65	372.20	10.23	52.84	1.10E-05	1	0	-1	-5
5.92	6.85	-2.65	372.31	10.28	53.01	1.10E-05	1	0	-1	-5
6.00	6.85	-2.65	372.41	10.33	53.19	1.09E-05	1	0	-1	-5
6.08	6.85	-2.65	372.51	10.38	53.36	1.09E-05	1	0	-1	-5
6.16	6.85	-2.65	372.61	10.43	53.53	1.09E-05	1	0	-1	-5
6.24	6.85	-2.65	372.71	10.49	53.71	1.08E-05	1	0	-1	-5
6.32	6.85	-2.65	372.82	10.54	53.89	1.08E-05	1	0	-1	-5
6.40	6.85	-2.65	372.92	10.59	54.07	1.08E-05	1	0	-1	-5
6.48	6.85	-2.65	373.02	10.64	54.25	1.08E-05	1	0	-1	-5

1. Composition of the "Surficial Water" solution as a total of 8 mg/L Oxygen is added to 10 moles of pyrite and 10 moles of calcite. Concentrations are presented in units of mg/L

2. S.I.: Saturation indices of selected iron-oxyhydroxides. Saturation index (S.I.) =  $\log(\text{IAP})/K_T$  where IAP is the ion activity product of the dissolved components in solution, and  $K_T$  is the solubility of the solid or gaseous phase at the specified temperature

### Appendix K9: Goethite Titration in Surficial Water

DOC Added <sup>1</sup>	pH	pe	Alkalinity as HCO <sub>3</sub> <sup>-</sup>	Dissolved Fe	Dissolved Oxygen	SO <sub>4</sub> <sup>2-</sup>	S <sup>2-</sup>	NO <sub>3</sub> <sup>-</sup>
0.00	5.30	6.44	24.01	0.07	0.28	17.88	0.00	4.30
0.05	5.29	14.68	23.68	2.41E-06	0.01	17.88	0.00	4.54
0.10	5.30	14.25	23.87	2.39E-06	1.37E-04	17.88	0.00	4.35
0.15	5.30	14.21	24.07	2.37E-06	9.82E-05	17.88	0.00	4.14
0.20	5.30	14.19	24.28	2.35E-06	7.94E-05	17.88	0.00	3.93
0.25	5.31	14.16	24.48	2.34E-06	6.72E-05	17.88	0.00	3.73
0.30	5.31	14.15	24.68	2.32E-06	5.83E-05	17.88	0.00	3.52
0.35	5.31	14.13	24.89	2.30E-06	5.13E-05	17.88	0.00	3.31
0.40	5.32	14.11	25.09	2.29E-06	4.55E-05	17.88	0.00	3.11
0.45	5.32	14.10	25.29	2.27E-06	4.06E-05	17.88	0.00	2.90
0.50	5.32	14.08	25.49	2.25E-06	3.62E-05	17.88	0.00	2.70
0.55	5.33	14.07	25.70	2.24E-06	3.24E-05	17.88	0.00	2.49
0.60	5.33	14.05	25.90	2.22E-06	2.89E-05	17.88	0.00	2.28
0.65	5.33	14.03	26.10	2.21E-06	2.57E-05	17.88	0.00	2.08
0.70	5.34	14.02	26.31	2.19E-06	2.28E-05	17.88	0.00	1.87
0.75	5.34	14.00	26.51	2.18E-06	2.00E-05	17.88	0.00	1.66
0.80	5.34	13.98	26.71	2.16E-06	1.74E-05	17.88	0.00	1.46
0.85	5.35	13.96	26.92	2.15E-06	1.49E-05	17.88	0.00	1.25
0.90	5.35	13.94	27.12	2.13E-06	1.25E-05	17.88	0.00	1.04
0.95	5.35	13.91	27.32	2.12E-06	1.02E-05	17.88	0.00	0.84
1.00	5.36	13.88	27.53	2.11E-06	7.92E-06	17.88	0.00	0.63
1.05	5.36	13.84	27.73	2.09E-06	5.61E-06	17.88	0.00	0.42
1.10	5.36	13.78	27.93	2.08E-06	3.21E-06	17.88	0.00	0.22
1.15	5.37	13.51	28.14	2.07E-06	2.79E-07	17.88	0.00	0.01
1.20	5.39	2.37	30.07	0.88	0.00	17.88	9.22E-32	0.00
1.25	5.42	1.98	32.11	1.81	0.00	17.88	6.53E-29	0.00
1.30	5.45	1.72	34.14	2.74	0.00	17.88	3.82E-27	0.00
1.35	5.47	1.53	36.17	3.67	0.00	17.88	8.06E-26	0.00
1.40	5.50	1.36	38.20	4.60	0.00	17.88	9.63E-25	0.00
1.45	5.52	1.22	40.23	5.53	0.00	17.88	7.97E-24	0.00
1.50	5.54	1.09	42.26	6.46	0.00	17.88	5.09E-23	0.00
1.55	5.56	0.97	44.30	7.39	0.00	17.88	2.67E-22	0.00
1.60	5.58	0.87	46.33	8.32	0.00	17.88	1.21E-21	0.00
1.65	5.60	0.77	48.36	9.25	0.00	17.88	4.81E-21	0.00

1. Composition of the "Surficial Water" solution as a total of 5 mg/L DOC is added to 10 moles of goethite. Concentrations are presented in units of mg/L



DOC Added <sup>1</sup>	pH	pe	Alkalinity as HCO <sub>3</sub> <sup>-</sup>	Dissolved Fe	Dissolved Oxygen	SO <sub>4</sub> <sup>2-</sup>	S <sup>2-</sup>	NO <sub>3</sub> <sup>-</sup>
1.70	5.62	0.68	50.39	10.18	0.00	17.88	1.74E-20	0.00
1.75	5.64	0.59	52.42	11.11	0.00	17.88	5.74E-20	0.00
1.80	5.66	0.50	54.46	12.04	0.00	17.88	1.77E-19	0.00
1.85	5.67	0.43	56.49	12.97	0.00	17.88	5.09E-19	0.00
1.90	5.69	0.35	58.52	13.90	0.00	17.88	1.39E-18	0.00
1.95	5.70	0.28	60.55	14.83	0.00	17.88	3.61E-18	0.00
2.00	5.72	0.21	62.58	15.76	0.00	17.88	8.98E-18	0.00
2.05	5.74	0.14	64.61	16.69	0.00	17.88	2.15E-17	0.00
2.10	5.75	0.08	66.65	17.62	0.00	17.88	4.95E-17	0.00
2.15	5.76	0.02	68.68	18.55	0.00	17.88	1.11E-16	0.00
2.20	5.78	-0.04	70.71	19.48	0.00	17.88	2.40E-16	0.00
2.25	5.79	-0.10	72.74	20.41	0.00	17.88	5.07E-16	0.00
2.30	5.81	-0.15	74.77	21.34	0.00	17.88	1.04E-15	0.00
2.35	5.82	-0.21	76.80	22.27	0.00	17.88	2.10E-15	0.00
2.40	5.83	-0.26	78.84	23.20	0.00	17.88	4.15E-15	0.00
2.45	5.84	-0.31	80.87	24.13	0.00	17.88	8.02E-15	0.00
2.50	5.86	-0.36	82.90	25.06	0.00	17.88	1.52E-14	0.00
2.55	5.87	-0.41	84.93	25.99	0.00	17.88	2.85E-14	0.00
2.60	5.88	-0.46	86.96	26.92	0.00	17.88	5.23E-14	0.00
2.65	5.89	-0.51	89.00	27.85	0.00	17.88	9.48E-14	0.00
2.70	5.91	-0.56	91.03	28.78	0.00	17.88	1.69E-13	0.00
2.75	5.92	-0.60	93.06	29.71	0.00	17.88	2.99E-13	0.00
2.80	5.93	-0.65	95.09	30.64	0.00	17.88	5.21E-13	0.00
2.85	5.94	-0.69	97.12	31.57	0.00	17.88	8.97E-13	0.00
2.90	5.95	-0.73	99.15	32.50	0.00	17.88	1.53E-12	0.00
2.95	5.96	-0.77	101.18	33.43	0.00	17.88	2.58E-12	0.00
3.00	5.97	-0.82	103.22	34.36	0.00	17.88	4.32E-12	0.00
3.05	5.98	-0.86	105.25	35.29	0.00	17.88	7.15E-12	0.00
3.10	5.99	-0.90	107.28	36.22	0.00	17.88	1.17E-11	0.00
3.15	6.00	-0.94	109.31	37.15	0.00	17.88	1.91E-11	0.00
3.20	6.01	-0.97	111.34	38.08	0.00	17.88	3.09E-11	0.00
3.25	6.03	-1.01	113.37	39.00	0.00	17.88	4.96E-11	0.00
3.30	6.04	-1.05	115.40	39.93	0.00	17.88	7.91E-11	0.00
3.35	6.05	-1.09	117.43	40.86	0.00	17.88	1.25E-10	0.00
3.40	6.06	-1.13	119.46	41.79	0.00	17.88	1.97E-10	0.00
3.45	6.07	-1.16	121.49	42.72	0.00	17.88	3.09E-10	0.00

1. Composition of the "Surficial Water" solution as a total of 5 mg/L DOC is added to 10 moles of goethite. Concentrations are presented in units of mg/L

DOC Added <sup>1</sup>	pH	pe	Alkalinity as HCO <sub>3</sub> <sup>-</sup>	Dissolved Fe	Dissolved Oxygen	SO <sub>4</sub> <sup>2-</sup>	S <sup>2-</sup>	NO <sub>3</sub> <sup>-</sup>
3.50	6.08	-1.20	123.52	43.65	0.00	17.88	4.80E-10	0.00
3.55	6.09	-1.24	125.55	44.58	0.00	17.88	7.43E-10	0.00
3.60	6.10	-1.27	127.58	45.51	0.00	17.88	1.14E-09	0.00
3.65	6.11	-1.31	129.61	46.43	0.00	17.88	1.75E-09	0.00
3.70	6.11	-1.34	131.63	47.36	0.00	17.88	2.67E-09	0.00
3.75	6.12	-1.38	133.66	48.29	0.00	17.88	4.06E-09	0.00
3.80	6.13	-1.41	135.69	49.22	0.00	17.88	6.14E-09	0.00
3.85	6.14	-1.44	137.71	50.14	0.00	17.88	9.26E-09	0.00
3.90	6.15	-1.48	139.74	51.07	0.00	17.88	1.39E-08	0.00
3.95	6.16	-1.51	141.76	51.99	0.00	17.88	2.08E-08	0.00
4.00	6.17	-1.55	143.79	52.92	0.00	17.88	3.09E-08	0.00
4.05	6.18	-1.58	145.81	53.84	0.00	17.88	4.60E-08	0.00
4.10	6.19	-1.61	147.83	54.77	0.00	17.88	6.80E-08	0.00
4.15	6.20	-1.64	149.84	55.69	0.00	17.88	1.00E-07	0.00
4.20	6.21	-1.68	151.86	56.61	0.00	17.88	1.48E-07	0.00
4.25	6.22	-1.71	153.86	57.53	0.00	17.88	2.16E-07	0.00
4.30	6.23	-1.74	155.87	58.44	0.00	17.88	3.16E-07	0.00
4.35	6.24	-1.77	157.85	59.35	0.00	17.88	4.59E-07	0.00
4.40	6.25	-1.80	159.81	60.24	0.00	17.88	6.63E-07	0.00
4.45	6.25	-1.83	161.73	61.12	0.00	17.88	9.47E-07	0.00
4.50	6.26	-1.86	163.57	61.95	0.00	17.88	1.33E-06	0.00
4.55	6.27	-1.89	165.29	62.74	0.00	17.88	1.83E-06	0.00
4.60	6.28	-1.91	166.86	63.46	0.00	17.88	2.43E-06	0.00
4.65	6.28	-1.93	168.23	64.08	0.00	17.88	3.12E-06	0.00
4.70	6.29	-1.95	169.41	64.62	0.00	17.88	3.86E-06	0.00
4.75	6.29	-1.97	170.42	65.08	0.00	17.88	4.62E-06	0.00
4.80	6.30	-1.98	171.28	65.47	0.00	17.88	5.37E-06	0.00
4.85	6.30	-1.99	172.01	65.80	0.00	17.88	6.11E-06	0.00
4.90	6.30	-1.99	172.28	65.82	0.00	17.69	6.18E-06	0.00
4.95	6.30	-1.99	172.50	65.80	0.00	17.50	6.19E-06	0.00
5.00	6.30	-2.00	172.72	65.79	0.00	17.30	6.20E-06	0.00

1. Composition of the "Surficial Water" solution as a total of 5 mg/L DOC is added to 10 moles of goethite. Concentrations are presented in units of mg/L

DOC Added	S.I. <sup>1</sup> Hematite	S.I. <sup>1</sup> Goethite	S.I. <sup>1</sup> Lepidocrocite	S.I. <sup>1</sup> Fe(OH) <sub>3</sub>	S.I. <sup>1</sup> Pyrite
0.00	-1000	-1000	-1000	-1000	-1000
0.05	1	0	-1	-5	-231
0.10	1	0	-1	-5	-224
0.15	1	0	-1	-5	-224
0.20	1	0	-1	-5	-224
0.25	1	0	-1	-5	-223
0.30	1	0	-1	-5	-223
0.35	1	0	-1	-5	-223
0.40	1	0	-1	-5	-223
0.45	1	0	-1	-5	-223
0.50	1	0	-1	-5	-222
0.55	1	0	-1	-5	-222
0.60	1	0	-1	-5	-222
0.65	1	0	-1	-5	-222
0.70	1	0	-1	-5	-222
0.75	1	0	-1	-5	-222
0.80	1	0	-1	-5	-221
0.85	1	0	-1	-5	-221
0.90	1	0	-1	-5	-221
0.95	1	0	-1	-5	-220
1.00	1	0	-1	-5	-220
1.05	1	0	-1	-5	-220
1.10	1	0	-1	-5	-219
1.15	1	0	-1	-5	-215
1.20	1	0	-1	-5	-48
1.25	1	0	-1	-5	-43
1.30	1	0	-1	-5	-39
1.35	1	0	-1	-5	-37
1.40	1	0	-1	-5	-35
1.45	1	0	-1	-5	-33
1.50	1	0	-1	-5	-32
1.55	1	0	-1	-5	-30
1.60	1	0	-1	-5	-29

1. S.I.: Saturation indices of selected iron-oxyhydroxides and pyrite. Saturation index (S.I.) =  $\log(\text{IAP})/K_T$  where IAP is the ion activity product of the dissolved components in solution, and  $K_T$  is the solubility of the solid or gaseous phase at the specified temperature

DOC Added	S.I. <sup>1</sup> Hematite	S.I. <sup>1</sup> Goethite	S.I. <sup>1</sup> Lepidocrocite	S.I. <sup>1</sup> Fe(OH) <sub>3</sub>	S.I. <sup>1</sup> Pyrite
1.65	1	0	-1	-5	-28
1.70	1	0	-1	-5	-27
1.75	1	0	-1	-5	-26
1.80	1	0	-1	-5	-25
1.85	1	0	-1	-5	-24
1.90	1	0	-1	-5	-23
1.95	1	0	-1	-5	-23
2.00	1	0	-1	-5	-22
2.05	1	0	-1	-5	-21
2.10	1	0	-1	-5	-21
2.15	1	0	-1	-5	-20
2.20	1	0	-1	-5	-19
2.25	1	0	-1	-5	-19
2.30	1	0	-1	-5	-18
2.35	1	0	-1	-5	-18
2.40	1	0	-1	-5	-17
2.45	1	0	-1	-5	-16
2.50	1	0	-1	-5	-16
2.55	1	0	-1	-5	-15
2.60	1	0	-1	-5	-15
2.65	1	0	-1	-5	-14
2.70	1	0	-1	-5	-14
2.75	1	0	-1	-5	-14
2.80	1	0	-1	-5	-13
2.85	1	0	-1	-5	-13
2.90	1	0	-1	-5	-12
2.95	1	0	-1	-5	-12
3.00	1	0	-1	-5	-11
3.05	1	0	-1	-5	-11
3.10	1	0	-1	-5	-11
3.15	1	0	-1	-5	-10
3.20	1	0	-1	-5	-10
3.25	1	0	-1	-5	-9

1. S.I.: Saturation indices of selected iron-oxyhydroxides and pyrite. Saturation index (S.I.) =  $\log(\text{IAP})/K_T$  where IAP is the ion activity product of the dissolved components in solution, and  $K_T$  is the solubility of the solid or gaseous phase at the specified temperature

DOC Added	S.I. <sup>1</sup> Hematite	S.I. <sup>1</sup> Goethite	S.I. <sup>1</sup> Lepidocrocite	S.I. <sup>1</sup> Fe(OH) <sub>3</sub>	S.I. <sup>1</sup> Pyrite
3.30	1	0	-1	-5	-9
3.35	1	0	-1	-5	-9
3.40	1	0	-1	-5	-8
3.45	1	0	-1	-5	-8
3.50	1	0	-1	-5	-8
3.55	1	0	-1	-5	-7
3.60	1	0	-1	-5	-7
3.65	1	0	-1	-5	-7
3.70	1	0	-1	-5	-6
3.75	1	0	-1	-5	-6
3.80	1	0	-1	-5	-6
3.85	1	0	-1	-5	-5
3.90	1	0	-1	-5	-5
3.95	1	0	-1	-5	-5
4.00	1	0	-1	-5	-4
4.05	1	0	-1	-5	-4
4.10	1	0	-1	-5	-4
4.15	1	0	-1	-5	-3
4.20	1	0	-1	-5	-3
4.25	1	0	-1	-5	-3
4.30	1	0	-1	-5	-2
4.35	1	0	-1	-5	-2
4.40	1	0	-1	-5	-2
4.45	1	0	-1	-5	-2
4.50	1	0	-1	-5	-1
4.55	1	0	-1	-5	-1
4.60	1	0	-1	-5	-1
4.65	1	0	-1	-5	-1
4.70	1	0	-1	-5	0
4.75	1	0	-1	-5	0
4.80	1	0	-1	-5	0
4.85	1	0	-1	-5	0
4.90	1	0	-1	-5	0

1. Saturation indices of selected iron-oxhydroxides and pyrite. Saturation index (S.I.) =  $\log(\text{IAP})/K_T$  where IAP is the ion activity product of the dissolved components in solution, and  $K_T$  is the solubility of the solid or gaseous phase at the specified temperature

DOC Added	S.I. <sup>1</sup> Hematite	S.I. <sup>1</sup> Goethite	S.I. <sup>1</sup> Lepidocrocite	S.I. <sup>1</sup> Fe(OH) <sub>3</sub>	S.I. <sup>1</sup> Pyrite
4.95	1	0	-1	-5	0
5.00	1	0	-1	-5	0

1. Saturation indices of selected iron-oxyhydroxides and pyrite.  
Saturation index (S.I.) =  $\log(\text{IAP})/K_T$  where IAP is the ion activity product of the dissolved components in solution, and  $K_T$  is the solubility of the solid or gaseous phase at the specified temperature

**Appendix K10: Goethite Titration with DOC and Simultaneous Calcite Dissolution in Surficial Water**

DOC Added <sup>1</sup>	pH	pe	Alkalinity as HCO <sub>3</sub> <sup>-</sup>	Dissolved Fe	Dissolved Oxygen	SO <sub>4</sub> <sup>2-</sup>	S <sup>2-</sup>	NO <sub>3</sub> <sup>-</sup>
0.00	5.30	6.44	24.01	0.07	0.28	17.88	0.00	4.30
0.05	6.86	13.11	367.51	2.54E-07	6.65E-03	17.88	0.00	4.54
0.10	6.86	12.37	367.66	2.54E-07	7.25E-06	17.88	0.00	4.35
0.15	6.86	12.33	367.81	2.54E-07	5.23E-06	17.88	0.00	4.14
0.20	6.86	12.31	367.97	2.54E-07	4.26E-06	17.88	0.00	3.93
0.25	6.86	12.29	368.12	2.54E-07	3.63E-06	17.88	0.00	3.73
0.30	6.86	12.28	368.27	2.54E-07	3.17E-06	17.88	0.00	3.52
0.35	6.86	12.27	368.42	2.54E-07	2.80E-06	17.88	0.00	3.31
0.40	6.86	12.25	368.58	2.54E-07	2.50E-06	17.88	0.00	3.11
0.45	6.86	12.24	368.73	2.54E-07	2.25E-06	17.88	0.00	2.90
0.50	6.86	12.23	368.88	2.54E-07	2.02E-06	17.88	0.00	2.70
0.55	6.86	12.22	369.04	2.54E-07	1.82E-06	17.88	0.00	2.49
0.60	6.86	12.21	369.19	2.54E-07	1.63E-06	17.88	0.00	2.28
0.65	6.86	12.20	369.34	2.54E-07	1.46E-06	17.88	0.00	2.08
0.70	6.86	12.18	369.49	2.54E-07	1.30E-06	17.88	0.00	1.87
0.75	6.86	12.17	369.65	2.54E-07	1.15E-06	17.88	0.00	1.66
0.80	6.86	12.16	369.80	2.54E-07	1.01E-06	17.88	0.00	1.46
0.85	6.86	12.14	369.95	2.54E-07	8.68E-07	17.88	0.00	1.25
0.90	6.86	12.12	370.10	2.54E-07	7.34E-07	17.88	0.00	1.04
0.95	6.86	12.10	370.26	2.54E-07	6.01E-07	17.88	0.00	0.84
1.00	6.86	12.07	370.41	2.54E-07	4.69E-07	17.88	0.00	0.63
1.05	6.86	12.04	370.56	2.54E-07	3.34E-07	17.88	0.00	0.42
1.10	6.86	11.98	370.71	2.54E-07	1.92E-07	17.88	0.00	0.22
1.15	6.86	11.71	370.87	2.54E-07	1.68E-08	17.88	0.00	0.01
1.20	6.86	-1.53	371.02	0.88	0.00	17.88	3.62E-15	0.00
1.25	6.86	-1.85	371.18	1.81	0.00	17.88	1.27E-12	0.00
1.30	6.87	-2.04	371.34	2.74	0.00	17.88	3.83E-11	0.00
1.35	6.87	-2.18	371.49	3.67	0.00	17.88	4.36E-10	0.00
1.40	6.87	-2.28	371.64	4.59	0.00	17.88	2.92E-09	0.00
1.45	6.88	-2.37	371.79	5.51	0.00	17.88	1.39E-08	0.00
1.50	6.88	-2.45	371.93	6.41	0.00	17.88	5.15E-08	0.00
1.55	6.88	-2.50	372.07	7.21	0.00	17.88	1.45E-07	0.00
1.60	6.88	-2.54	372.20	7.81	0.00	17.88	2.90E-07	0.00

1. Composition of the "Surficial Water" solution as a total of 5 mg/L DOC is added to 10 moles of goethite and 10 moles of calcite. Concentrations are presented in units of mg/L

DOC Added <sup>1</sup>	pH	pe	Alkalinity as HCO <sub>3</sub> <sup>-</sup>	Dissolved Fe	Dissolved Oxygen	SO <sub>4</sub> <sup>2-</sup>	S <sup>2-</sup>	NO <sub>3</sub> <sup>-</sup>
1.65	6.88	-2.57	372.31	8.20	0.00	17.88	4.48E-07	0.00
1.70	6.88	-2.59	372.41	8.48	0.00	17.88	5.98E-07	0.00
1.75	6.88	-2.60	372.51	8.68	0.00	17.88	7.36E-07	0.00
1.80	6.89	-2.61	372.60	8.84	0.00	17.88	8.64E-07	0.00
1.85	6.89	-2.61	372.70	8.98	0.00	17.88	9.84E-07	0.00
1.90	6.89	-2.62	372.79	9.09	0.00	17.88	1.10E-06	0.00
1.95	6.89	-2.63	372.88	9.19	0.00	17.88	1.20E-06	0.00
2.00	6.89	-2.63	372.97	9.28	0.00	17.88	1.30E-06	0.00
2.05	6.89	-2.63	373.07	9.36	0.00	17.88	1.40E-06	0.00
2.10	6.89	-2.64	373.16	9.43	0.00	17.88	1.49E-06	0.00
2.15	6.89	-2.64	373.25	9.50	0.00	17.88	1.58E-06	0.00
2.20	6.89	-2.64	373.34	9.56	0.00	17.88	1.66E-06	0.00
2.25	6.89	-2.65	373.43	9.62	0.00	17.88	1.75E-06	0.00
2.30	6.89	-2.65	373.51	9.68	0.00	17.88	1.82E-06	0.00
2.35	6.89	-2.65	373.60	9.73	0.00	17.88	1.90E-06	0.00
2.40	6.89	-2.65	373.69	9.78	0.00	17.88	1.98E-06	0.00
2.45	6.89	-2.66	373.78	9.83	0.00	17.88	2.05E-06	0.00
2.50	6.89	-2.66	373.87	9.87	0.00	17.88	2.12E-06	0.00
2.55	6.89	-2.66	373.96	9.91	0.00	17.88	2.19E-06	0.00
2.60	6.89	-2.66	374.05	9.96	0.00	17.88	2.26E-06	0.00
2.65	6.89	-2.66	374.14	10.00	0.00	17.88	2.33E-06	0.00
2.70	6.89	-2.66	374.22	10.03	0.00	17.88	2.39E-06	0.00
2.75	6.89	-2.66	374.31	10.07	0.00	17.88	2.46E-06	0.00
2.80	6.89	-2.67	374.40	10.11	0.00	17.88	2.52E-06	0.00
2.85	6.89	-2.67	374.49	10.14	0.00	17.88	2.58E-06	0.00
2.90	6.89	-2.67	374.58	10.18	0.00	17.88	2.65E-06	0.00
2.95	6.89	-2.67	374.67	10.21	0.00	17.88	2.71E-06	0.00
3.00	6.89	-2.67	374.75	10.24	0.00	17.88	2.76E-06	0.00
3.05	6.89	-2.67	374.84	10.27	0.00	17.88	2.82E-06	0.00
3.10	6.89	-2.67	374.93	10.31	0.00	17.88	2.88E-06	0.00
3.15	6.89	-2.67	375.02	10.34	0.00	17.88	2.94E-06	0.00
3.20	6.89	-2.67	375.10	10.37	0.00	17.88	2.99E-06	0.00
3.25	6.88	-2.68	375.19	10.39	0.00	17.88	3.05E-06	0.00

1. Composition of the "Surficial Water" solution as a total of 5 mg/L DOC is added to 10 moles of goethite and 10 moles of calcite. Concentrations are presented in units of mg/L



DOC Added <sup>1</sup>	pH	pe	Alkalinity as HCO <sub>3</sub> <sup>-</sup>	Dissolved Fe	Dissolved Oxygen	SO <sub>4</sub> <sup>2-</sup>	S <sup>2-</sup>	NO <sub>3</sub> <sup>-</sup>
3.30	6.88	-2.68	375.28	10.42	0.00	17.88	3.10E-06	0.00
3.35	6.88	-2.68	375.37	10.45	0.00	17.88	3.16E-06	0.00
3.40	6.88	-2.68	375.46	10.48	0.00	17.88	3.21E-06	0.00
3.45	6.88	-2.68	375.54	10.50	0.00	17.88	3.26E-06	0.00
3.50	6.88	-2.68	375.63	10.53	0.00	17.88	3.31E-06	0.00
3.55	6.88	-2.68	375.72	10.56	0.00	17.88	3.36E-06	0.00
3.60	6.88	-2.68	375.81	10.58	0.00	17.88	3.41E-06	0.00
3.65	6.88	-2.68	375.89	10.61	0.00	17.88	3.46E-06	0.00
3.70	6.88	-2.68	375.98	10.63	0.00	17.88	3.51E-06	0.00
3.75	6.88	-2.68	376.07	10.66	0.00	17.88	3.56E-06	0.00
3.80	6.88	-2.68	376.15	10.68	0.00	17.88	3.61E-06	0.00
3.85	6.88	-2.68	376.24	10.71	0.00	17.88	3.66E-06	0.00
3.90	6.88	-2.68	376.33	10.73	0.00	17.88	3.71E-06	0.00
3.95	6.88	-2.68	376.42	10.75	0.00	17.88	3.75E-06	0.00
4.00	6.88	-2.69	376.50	10.78	0.00	17.88	3.80E-06	0.00
4.05	6.88	-2.69	376.59	10.80	0.00	17.88	3.85E-06	0.00
4.10	6.88	-2.69	376.68	10.82	0.00	17.88	3.89E-06	0.00
4.15	6.88	-2.69	376.76	10.84	0.00	17.88	3.94E-06	0.00
4.20	6.88	-2.69	376.85	10.87	0.00	17.88	3.98E-06	0.00
4.25	6.88	-2.69	376.94	10.89	0.00	17.88	4.03E-06	0.00
4.30	6.88	-2.69	377.03	10.91	0.00	17.88	4.07E-06	0.00
4.35	6.88	-2.69	377.11	10.93	0.00	17.88	4.11E-06	0.00
4.40	6.88	-2.69	377.20	10.95	0.00	17.88	4.16E-06	0.00
4.45	6.88	-2.69	377.29	10.97	0.00	17.88	4.20E-06	0.00
4.50	6.88	-2.69	377.37	10.99	0.00	17.88	4.24E-06	0.00
4.55	6.88	-2.69	377.46	11.01	0.00	17.88	4.29E-06	0.00
4.60	6.88	-2.69	377.55	11.03	0.00	17.88	4.33E-06	0.00
4.65	6.88	-2.69	377.63	11.05	0.00	17.88	4.37E-06	0.00
4.70	6.88	-2.69	377.72	11.07	0.00	17.88	4.41E-06	0.00
4.75	6.88	-2.69	377.81	11.09	0.00	17.88	4.45E-06	0.00
4.80	6.88	-2.69	377.90	11.11	0.00	17.88	4.49E-06	0.00
4.85	6.88	-2.69	377.98	11.13	0.00	17.88	4.53E-06	0.00
4.90	6.88	-2.69	378.07	11.15	0.00	17.88	4.57E-06	0.00

1. Composition of the "Surficial Water" solution as a total of 5 mg/L DOC is added to 10 moles of goethite and 10 moles of calcite. Concentrations are presented in units of mg/L

DOC Added <sup>1</sup>	pH	pe	Alkalinity as HCO <sub>3</sub> <sup>-</sup>	Dissolved Fe	Dissolved Oxygen	SO <sub>4</sub> <sup>2-</sup>	S <sup>2-</sup>	NO <sub>3</sub> <sup>-</sup>
4.95	6.88	-2.69	378.16	11.17	0.00	17.88	4.61E-06	0.00
5.00	6.88	-2.69	378.24	11.19	0.00	17.88	4.65E-06	0.00

1. Composition of the "Surficial Water" solution as a total of 5 mg/L DOC is added to 10 moles of goethite and 10 moles of calcite. Concentrations are presented in units of mg/L

DOC Added	S.I. <sup>1</sup> Hematite	S.I. <sup>1</sup> Goethite	S.I. <sup>1</sup> Lepidocrocite	S.I. <sup>1</sup> Fe(OH) <sub>3</sub>	S.I. <sup>1</sup> Pyrite
0.00	-1000	-1000	-1000	-1000	-1000
0.05	1	0	-1	-5	-237
0.10	1	0	-1	-5	-226
0.15	1	0	-1	-5	-226
0.20	1	0	-1	-5	-225
0.25	1	0	-1	-5	-225
0.30	1	0	-1	-5	-225
0.35	1	0	-1	-5	-225
0.40	1	0	-1	-5	-225
0.45	1	0	-1	-5	-224
0.50	1	0	-1	-5	-224
0.55	1	0	-1	-5	-224
0.60	1	0	-1	-5	-224
0.65	1	0	-1	-5	-224
0.70	1	0	-1	-5	-223
0.75	1	0	-1	-5	-223
0.80	1	0	-1	-5	-223
0.85	1	0	-1	-5	-223
0.90	1	0	-1	-5	-223
0.95	1	0	-1	-5	-222
1.00	1	0	-1	-5	-222
1.05	1	0	-1	-5	-221
1.10	1	0	-1	-5	-220
1.15	1	0	-1	-5	-216
1.20	1	0	-1	-5	-18
1.25	1	0	-1	-5	-13
1.30	1	0	-1	-5	-10
1.35	1	0	-1	-5	-8
1.40	1	0	-1	-5	-7
1.45	1	0	-1	-5	-5
1.50	1	0	-1	-5	-4
1.55	1	0	-1	-5	-4
1.60	1	0	-1	-5	-3

1. Saturation indices of selected iron-oxyhydroxides and pyrite. Saturation index (S.I.) =  $\log(\text{IAP})/K_T$  where IAP is the ion activity product of the dissolved components in solution, and  $K_T$  is the solubility of the solid or gaseous phase at the specified temperature

DOC Added	S.I. <sup>1</sup> Hematite	S.I. <sup>1</sup> Goethite	S.I. <sup>1</sup> Lepidocrocite	S.I. <sup>1</sup> Fe(OH) <sub>3</sub>	S.I. <sup>1</sup> Pyrite
1.65	1	0	-1	-5	-3
1.70	1	0	-1	-5	-2
1.75	1	0	-1	-5	-2
1.80	1	0	-1	-5	-2
1.85	1	0	-1	-5	-2
1.90	1	0	-1	-5	-2
1.95	1	0	-1	-5	-2
2.00	1	0	-1	-5	-2
2.05	1	0	-1	-5	-2
2.10	1	0	-1	-5	-2
2.15	1	0	-1	-5	-2
2.20	1	0	-1	-5	-2
2.25	1	0	-1	-5	-2
2.30	1	0	-1	-5	-1
2.35	1	0	-1	-5	-1
2.40	1	0	-1	-5	-1
2.45	1	0	-1	-5	-1
2.50	1	0	-1	-5	-1
2.55	1	0	-1	-5	-1
2.60	1	0	-1	-5	-1
2.65	1	0	-1	-5	-1
2.70	1	0	-1	-5	-1
2.75	1	0	-1	-5	-1
2.80	1	0	-1	-5	-1
2.85	1	0	-1	-5	-1
2.90	1	0	-1	-5	-1
2.95	1	0	-1	-5	-1
3.00	1	0	-1	-5	-1
3.05	1	0	-1	-5	-1
3.10	1	0	-1	-5	-1
3.15	1	0	-1	-5	-1
3.20	1	0	-1	-5	-1
3.25	1	0	-1	-5	-1

1. Saturation indices of selected iron-oxyhydroxides and pyrite. Saturation index (S.I.) =  $\log(\text{IAP})/K_T$  where IAP is the ion activity product of the dissolved components in solution, and  $K_T$  is the solubility of the solid or gaseous phase at the specified temperature

DOC Added	S.I. <sup>1</sup> Hematite	S.I. <sup>1</sup> Goethite	S.I. <sup>1</sup> Lepidocrocite	S.I. <sup>1</sup> Fe(OH) <sub>3</sub>	S.I. <sup>1</sup> Pyrite
3.30	1	0	-1	-5	-1
3.35	1	0	-1	-5	-1
3.40	1	0	-1	-5	-1
3.45	1	0	-1	-5	-1
3.50	1	0	-1	-5	-1
3.55	1	0	-1	-5	-1
3.60	1	0	-1	-5	-1
3.65	1	0	-1	-5	-1
3.70	1	0	-1	-5	-1
3.75	1	0	-1	-5	-1
3.80	1	0	-1	-5	-1
3.85	1	0	-1	-5	-1
3.90	1	0	-1	-5	-1
3.95	1	0	-1	-5	-1
4.00	1	0	-1	-5	-1
4.05	1	0	-1	-5	-1
4.10	1	0	-1	-5	-1
4.15	1	0	-1	-5	-1
4.20	1	0	-1	-5	-1
4.25	1	0	-1	-5	-1
4.30	1	0	-1	-5	-1
4.35	1	0	-1	-5	-1
4.40	1	0	-1	-5	-1
4.45	1	0	-1	-5	-1
4.50	1	0	-1	-5	-1
4.55	1	0	-1	-5	-1
4.60	1	0	-1	-5	-1
4.65	1	0	-1	-5	-1
4.70	1	0	-1	-5	-1
4.75	1	0	-1	-5	-1
4.80	1	0	-1	-5	-1
4.85	1	0	-1	-5	-1
4.90	1	0	-1	-5	-1

1. Saturation indices of selected iron-oxyhydroxides and pyrite. Saturation index (S.I.) =  $\log(\text{IAP})/K_T$  where IAP is the ion activity product of the dissolved components in solution, and  $K_T$  is the solubility of the solid or gaseous phase at the specified temperature

DOC Added	S.I. <sup>1</sup> Hematite	S.I. <sup>1</sup> Goethite	S.I. <sup>1</sup> Lepidocrocite	S.I. <sup>1</sup> Fe(OH) <sub>3</sub>	S.I. <sup>1</sup> Pyrite
4.95	1	0	-1	-5	-1
5.00	1	0	-1	-5	-1

1. Saturation indices of selected iron-oxyhydroxides and pyrite.  
Saturation index (S.I.) =  $\log(\text{IAP}/K_T)$  where IAP is the ion activity product of the dissolved components in solution, and  $K_T$  is the solubility of the solid or gaseous phase at the specified temperature

### Appendix K11: Percent Glauconite and Simulated Dissolved-Fe Concentrations

Distance <sup>1</sup>	0%	1%	5%	10%	15%	20%
0	16.4	16.4	16.4	16.4	16.4	16.4
1	16.4	16.1	14.6	13.7	13.0	12.6
3	16.3	15.4	11.4	8.8	7.1	6.0
5	16.1	14.0	7.0	3.9	2.4	1.7
7	15.5	11.7	3.4	1.3	0.6	0.3
9	14.5	8.8	1.2	0.3	0.1	0.1
11	13.5	6.3	0.4	0.1	0.0	0.0

1. Percent glauconite and simulated dissolved-Fe concentrations (mg/L) with increasing distance (km) along a simulated flow path in the UCHA. The values for cation exchange capacity and dispersivity used in the reactive transport model are 0.115 eq/L and 800 m, respectively. Glauconite is assumed to have an average CEC of 20 meq/100g and the density and porosity of the UCHA are assumed to be 2.7 kg/L and 20%, respectively

### Appendix K12: Conservative Model Results

Distance <sup>1</sup>	pH	pe	Alkalinity as HCO <sub>3</sub> <sup>-</sup>	Na <sup>+</sup>	K <sup>+</sup>	Mg <sup>2+</sup>	Ca <sup>2+</sup>	Fe <sup>2+</sup>	S.I. <sup>2</sup> Hematite	S.I. <sup>2</sup> Goethite	S.I. <sup>2</sup> Lepidocrocite	S.I. <sup>2</sup> Fe(OH) <sub>3</sub>	S.I. <sup>2</sup> Pyrite	S.I. <sup>2</sup> Siderite
1	7	-3	343	14	26	9	71	16	1	0	-1	-5	-7	0
3	7	-3	342	14	26	9	71	16	1	0	-1	-5	-7	0
5	7	-3	342	14	26	9	71	16	1	0	-1	-5	-6	0
7	7	-3	340	14	25	9	71	16	1	0	-1	-5	-6	0
9	7	-3	338	13	24	9	70	15	1	0	-1	-5	-5	0
11	7	-3	335	13	23	9	70	14	1	0	-1	-5	-5	0

1. Conservative transport model results. Elemental concentrations (mg/L) are shown with respect to increasing distance (km) along a simulated flow path in the UCHA. Dispersivity used in the conservative transport model is 800 m

2. S.I.: Saturation indices of common authigenic iron-minerals. Saturation index (S.I.) =  $\log(\text{IAP})/K_T$  where IAP is the ion activity product of the dissolved components in solution, and  $K_T$  is the solubility of the solid or gaseous phase at the specified temperature



### Appendix K13: Reactive Transport Model Results

Distance <sup>1</sup>	pH	pe	Alkalinity as HCO <sub>3</sub> <sup>-</sup>	Na <sup>+</sup>	K <sup>+</sup>	Mg <sup>2+</sup>	Ca <sup>2+</sup>	Fe <sup>2+</sup>	S.I. <sup>2</sup> Hematite	S.I. <sup>2</sup> Goethite	S.I. <sup>2</sup> Lepidocrocite	S.I. <sup>2</sup> Fe(OH) <sub>3</sub>	S.I. <sup>2</sup> Pyrite	S.I. <sup>2</sup> Siderite
1	7	-3	390	14	23	11	86	15	1	1	0	-5	-7	1
3	7	-3	389	14	18	15	84	11	1	0	0	-5	-7	0
5	7	-3	388	13	12	17	86	7	1	0	-1	-5	-7	0
7	7	-3	384	13	8	18	88	3	0	0	-1	-6	-7	0
9	7	-3	378	12	7	19	88	1	-1	-1	-1	-6	-6	0
11	7	-3	371	11	6	18	87	0	-2	-1	-2	-7	-7	-1

1. Reactive transport model results. Elemental concentrations (mg/L) are shown with respect to increasing distance (km) along a simulated flow path in the UCHA. The values for cation exchange capacity and dispersivity used in the reactive transport model are 0.115 eq/L and 800 m, respectively

2. S.I.: Saturation indices of common authigenic iron-minerals. Saturation index (S.I.) =  $\log(\text{IAP})/K_T$  where IAP is the ion activity product of the dissolved components in solution, and  $K_T$  is the solubility of the solid or gaseous phase at the specified temperature

## Appendix L: PHREEQC Input Files

### Appendix L1: Dissolving Individual Fe-Bearing Minerals in Pure Water at pH 5

#### SOLUTION 1

temp 25  
pH 5  
pe 4  
redox pe  
units mmol/kgw  
density 1  
-water 1 # kg

#### EQUILIBRIUM\_PHASES 1

Epidote 0 10  
Goethite\_2 0 0

#### SELECTED\_OUTPUT 1

-file C:\Users\Mark Akland\Desktop\modeling.xls  
-reset false  
-solution true  
-step true  
-pH true  
-Alkalinity true  
-pe true  
-reaction true  
-totals Fe Fe(2) Fe(3)  
-saturation\_indices Hematite Goethite Lepidocrocite Fe(OH)3 Pyrite

END

#### SOLUTION 2

temp 25  
pH 5  
pe 4  
redox pe  
units mmol/kgw  
density 1  
-water 1 # kg

#### EQUILIBRIUM\_PHASES 2

Hematite 0 10  
Goethite\_2 0 0

End

SOLUTION 3

temp 25  
pH 5  
pe 4  
redox pe  
units mmol/kgw  
density 1  
-water 1 # kg

EQUILIBRIUM\_PHASES 3

Fe(OH)<sub>3</sub> 0 10  
Goethite\_2 0 0

End

SOLUTION 4

temp 25  
pH 5  
pe 4  
redox pe  
units mmol/kgw  
density 1  
-water 1 # kg

EQUILIBRIUM\_PHASES 4

Lepidocrocite 0 10  
Goethite\_2 0 0

End

SOLUTION 5

temp 25  
pH 5  
pe 4  
redox pe  
units mmol/kgw  
density 1  
-water 1 # kg

EQUILIBRIUM\_PHASES 5

Goethite 0 10 # Lyndsay  
Goethite\_2 0 0

End

SOLUTION 6

temp 25

pH 5  
pe 4  
redox pe  
units mmol/kgw  
density 1  
-water 1 # kg

EQUILIBRIUM\_PHASES 6

Goethite\_2 0 10  
Goethite 0 0

End

SOLUTION 7

temp 25  
pH 5  
pe 4  
redox pe  
units mmol/kgw  
density 1  
-water 1 # kg

EQUILIBRIUM\_PHASES 7

Glaucosite 0 10  
Goethite\_2 0 0

End

SOLUTION 8

temp 25  
pH 5  
pe 4  
redox pe  
units mmol/kgw  
density 1  
-water 1 # kg

EQUILIBRIUM\_PHASES 8

Pyrite 0 10  
Goethite\_2 0 0

End

SOLUTION 9

temp 25  
pH 5

pe 4  
redox pe  
units mmol/kgw  
density 1  
-water 1 # kg

EQUILIBRIUM\_PHASES 9

Hedenbergite 0 10  
Goethite\_2 0 0

End

SOLUTION 10

temp 25  
pH 5  
pe 4  
redox pe  
units mmol/kgw  
density 1  
-water 1 # kg

EQUILIBRIUM\_PHASES 10

Staurolite 0 10  
Goethite\_2 0 0

End

SOLUTION 11

temp 25  
pH 5  
pe 4  
redox pe  
units mmol/kgw  
density 1  
-water 1 # kg

EQUILIBRIUM\_PHASES 11

Schorl 0 10  
Goethite\_2 0 0

End

SOLUTION 12

temp 25  
pH 5  
pe 4

redox pe  
units mmol/kgw  
density 1  
-water 1 # kg

EQUILIBRIUM\_PHASES 12

Ilmenite 0 10  
Goethite\_2 0 0

End

SOLUTION 13

temp 25  
pH 5  
pe 4  
redox pe  
units mmol/kgw  
density 1  
-water 1 # kg

EQUILIBRIUM\_PHASES 13

Actinolite 0 10  
Goethite\_2 0 0

End

SOLUTION 14

temp 25  
pH 5  
pe 4  
redox pe  
units mmol/kgw  
density 1  
-water 1 # kg

EQUILIBRIUM\_PHASES 14

Ferropargasite 0 10  
Goethite\_2 0 0

End

SOLUTION 15

temp 25  
pH 5  
pe 4  
redox pe

units mmol/kgw  
density 1  
-water 1 # kg

EQUILIBRIUM\_PHASES 16

Almandine 0 10

Goethite\_2 0 0

End

## Appendix L2: Dissolving Individual Fe-Bearing Minerals in Pure Water at pH 7

### SOLUTION 1

temp 25  
pH 7  
pe 4  
redox pe  
units mmol/kgw  
density 1  
-water 1 # kg

### EQUILIBRIUM\_PHASES 1

Epidote 0 10  
Goethite\_2 0 0

### SELECTED\_OUTPUT 1

-file C:\Users\Mark Akland\Desktop\modeling.xls  
-reset false  
-solution true  
-step true  
-pH true  
-Alkalinity true  
-pe true  
-reaction true  
-totals Fe Fe(2) Fe(3)  
-saturation\_indices Hematite Goethite Lepidocrocite Fe(OH)3 Pyrite

END

### SOLUTION 2

temp 25  
pH 7  
pe 4  
redox pe  
units mmol/kgw  
density 1  
-water 1 # kg

### EQUILIBRIUM\_PHASES 2

Hematite 0 10  
Goethite\_2 0 0

End



SOLUTION 3

temp 25  
pH 7  
pe 4  
redox pe  
units mmol/kgw  
density 1  
-water 1 # kg

EQUILIBRIUM\_PHASES 3

Fe(OH)<sub>3</sub> 0 10  
Goethite\_2 0 0

End

SOLUTION 4

temp 25  
pH 7  
pe 4  
redox pe  
units mmol/kgw  
density 1  
-water 1 # kg

EQUILIBRIUM\_PHASES 4

Lepidocrocite 0 10  
Goethite\_2 0 0

End

SOLUTION 5

temp 25  
pH 7  
pe 4  
redox pe  
units mmol/kgw  
density 1  
-water 1 # kg

EQUILIBRIUM\_PHASES 5

Goethite 0 10 # Lyndsay  
Goethite\_2 0 0

End

SOLUTION 6

temp 25  
pH 7  
pe 4  
redox pe  
units mmol/kgw  
density 1  
-water 1 # kg

EQUILIBRIUM\_PHASES 6

Goethite\_2 0 10  
Goethite 0 0

End

SOLUTION 7

temp 25  
pH 7  
pe 4  
redox pe  
units mmol/kgw  
density 1  
-water 1 # kg

EQUILIBRIUM\_PHASES 7

Glauconite 0 10  
Goethite\_2 0 0

End

SOLUTION 8

temp 25  
pH 7  
pe 4  
redox pe  
units mmol/kgw  
density 1  
-water 1 # kg

EQUILIBRIUM\_PHASES 8

Pyrite 0 10  
Goethite\_2 0 0

End

SOLUTION 9

temp 25  
pH 7  
pe 4  
redox pe  
units mmol/kgw  
density 1  
-water 1 # kg

EQUILIBRIUM\_PHASES 9

Hedenbergite 0 10  
Goethite\_2 0 0

End

SOLUTION 10

temp 25  
pH 7  
pe 4  
redox pe  
units mmol/kgw  
density 1  
-water 1 # kg

EQUILIBRIUM\_PHASES 10

Staurolite 0 10  
Goethite\_2 0 0

End

SOLUTION 11

temp 25  
pH 7  
pe 4  
redox pe  
units mmol/kgw  
density 1  
-water 1 # kg

EQUILIBRIUM\_PHASES 11

Schorl 0 10  
Goethite\_2 0 0

End

SOLUTION 12

temp 25  
pH 7  
pe 4  
redox pe  
units mmol/kgw  
density 1  
-water 1 # kg

EQUILIBRIUM\_PHASES 12

Ilmenite 0 10  
Goethite\_2 0 0

End

SOLUTION 13

temp 25  
pH 7  
pe 4  
redox pe  
units mmol/kgw  
density 1  
-water 1 # kg

EQUILIBRIUM\_PHASES 13

Actinolite 0 10  
Goethite\_2 0 0

End

SOLUTION 14

temp 25  
pH 7  
pe 4  
redox pe  
units mmol/kgw  
density 1  
-water 1 # kg

EQUILIBRIUM\_PHASES 14

Ferropargasite 0 10  
Goethite\_2 0 0

End

SOLUTION 15

temp 25  
pH 7  
pe 4  
redox pe  
units mmol/kgw  
density 1  
-water 1 # kg

EQUILIBRIUM\_PHASES 15

Almandine 0 10  
Goethite\_2 0 0

End

### Appendix L3: Dissolving Individual Fe-Bearing Minerals in Pure Water at pH 9

#### SOLUTION 1

temp 25  
pH 9  
pe 4  
redox pe  
units mmol/kgw  
density 1  
-water 1 # kg

#### EQUILIBRIUM\_PHASES 1

Epidote 0 10  
Goethite\_2 0 0

#### SELECTED\_OUTPUT 1

-file C:\Users\Mark Akland\Desktop\modeling.xls  
-reset false  
-solution true  
-step true  
-pH true  
-Alkalinity true  
-pe true  
-reaction true  
-totals Fe Fe(2) Fe(3)  
-saturation\_indices Hematite Goethite Lepidocrocite Fe(OH)3 Pyrite

END

#### SOLUTION 2

temp 25  
pH 9  
pe 4  
redox pe  
units mmol/kgw  
density 1  
-water 1 # kg

#### EQUILIBRIUM\_PHASES 2

Hematite 0 10  
Goethite\_2 0 0

End

SOLUTION 3

temp 25  
pH 9  
pe 4  
redox pe  
units mmol/kgw  
density 1  
-water 1 # kg

EQUILIBRIUM\_PHASES 3

Fe(OH)<sub>3</sub> 0 10  
Goethite\_2 0 0

End

SOLUTION 4

temp 25  
pH 9  
pe 4  
redox pe  
units mmol/kgw  
density 1  
-water 1 # kg

EQUILIBRIUM\_PHASES 4

Lepidocrocite 0 10  
Goethite\_2 0 0

End

SOLUTION 5

temp 25  
pH 9  
pe 4  
redox pe  
units mmol/kgw  
density 1  
-water 1 # kg

EQUILIBRIUM\_PHASES 5

Goethite 0 10 # Lyndsay  
Goethite\_2 0 0

End

SOLUTION 6

temp 25  
pH 9  
pe 4  
redox pe  
units mmol/kgw  
density 1  
-water 1 # kg

EQUILIBRIUM\_PHASES 6

Goethite\_2 0 10  
Goethite 0 0

End

SOLUTION 7

temp 25  
pH 9  
pe 4  
redox pe  
units mmol/kgw  
density 1  
-water 1 # kg

EQUILIBRIUM\_PHASES 7

Glaucosite 0 10  
Goethite\_2 0 0

End

SOLUTION 8

temp 25  
pH 9  
pe 4  
redox pe  
units mmol/kgw  
density 1  
-water 1 # kg

EQUILIBRIUM\_PHASES 8

Pyrite 0 10  
Goethite\_2 0 0

End



SOLUTION 9

temp 25  
pH 9  
pe 4  
redox pe  
units mmol/kgw  
density 1  
-water 1 # kg

EQUILIBRIUM\_PHASES 9

Hedenbergite 0 10  
Goethite\_2 0 0

End

SOLUTION 10

temp 25  
pH 9  
pe 4  
redox pe  
units mmol/kgw  
density 1  
-water 1 # kg

EQUILIBRIUM\_PHASES 10

Staurolite 0 10  
Goethite\_2 0 0

End

SOLUTION 11

temp 25  
pH 9  
pe 4  
redox pe  
units mmol/kgw  
density 1  
-water 1 # kg

EQUILIBRIUM\_PHASES 11

Schorl 0 10  
Goethite\_2 0 0

End

SOLUTION 12

temp 25  
pH 9  
pe 4  
redox pe  
units mmol/kgw  
density 1  
-water 1 # kg

EQUILIBRIUM\_PHASES 12

Ilmenite 0 10  
Goethite\_2 0 0

End

SOLUTION 13

temp 25  
pH 9  
pe 4  
redox pe  
units mmol/kgw  
density 1  
-water 1 # kg

EQUILIBRIUM\_PHASES 13

Actinolite 0 10  
Goethite\_2 0 0

End

SOLUTION 14

temp 25  
pH 9  
pe 4  
redox pe  
units mmol/kgw  
density 1  
-water 1 # kg

EQUILIBRIUM\_PHASES 14

Ferropargasite 0 10  
Goethite\_2 0 0

End

SOLUTION 15

temp 25  
pH 9  
pe 4  
redox pe  
units mmol/kgw  
density 1  
-water 1 # kg

EQUILIBRIUM\_PHASES 15

Almandine 0 10  
Goethite\_2 0 0

End

**Appendix L4: Dissolving Individual Fe-Bearing Minerals in Surficial Water [water chemistry from Woods et al. (2000)]**

SOLUTION 1

temp 23  
pH 5.3  
pe 6.439 # Adjusted for platinum electrode potential  
redox pe  
units mg/l  
density 1  
O(0) 0.282  
Alkalinity 24 as HCO3  
Cl(-1) 13.21  
S(+6) 17.87  
Na 8.96  
K 3.61  
Ca 3.15  
Si 13.7  
F 0.089  
Mg 4.31  
N(+5) 0.971  
N(+3) 0.035  
N(-3) 0.026 as NH4  
P 0.129 as PO4  
Fe(+2) 0.07  
-water 1 # kg

EQUILIBRIUM\_PHASES 1

Epidote 0 10  
Goethite\_2 0 0

SELECTED\_OUTPUT 1

-file C:\Users\Mark Akland\Desktop\modeling.xls  
-reset false  
-solution true  
-step true  
-pH true  
-Alkalinity true  
-pe true  
-reaction true  
-totals Fe Fe(2) Fe(3)  
-saturation\_indices Hematite Goethite Lepidocrocite Fe(OH)3 Pyrite

END

## SOLUTION 2

temp	23
pH	5.3
pe	6.439 # Adjusted for platinum electrode potential
redox	pe
units	mg/l
density	1
O(0)	0.282
Alkalinity	24 as HCO <sub>3</sub>
Cl(-1)	13.21
S(+6)	17.87
Na	8.96
K	3.61
Ca	3.15
Si	13.7
F	0.089
Mg	4.31
N(+5)	0.971
N(+3)	0.035
N(-3)	0.026 as NH <sub>4</sub>
P	0.129 as PO <sub>4</sub>
Fe(+2)	0.07
-water	1 # kg

## EQUILIBRIUM\_PHASES 2

Hematite	0 10
Goethite_2	0 0

End

## SOLUTION 3

temp	23
pH	5.3
pe	6.439 # Adjusted for platinum electrode potential
redox	pe
units	mg/l
density	1
O(0)	0.282
Alkalinity	24 as HCO <sub>3</sub>
Cl(-1)	13.21
S(+6)	17.87
Na	8.96
K	3.61
Ca	3.15
Si	13.7
F	0.089

Mg 4.31  
N(+5) 0.971  
N(+3) 0.035  
N(-3) 0.026 as NH4  
P 0.129 as PO4  
Fe(+2) 0.07  
-water 1 # kg

EQUILIBRIUM\_PHASES 3

Fe(OH)3 0 10  
Goethite\_2 0 0

End

SOLUTION 4

temp 23  
pH 5.3  
pe 6.439 # Adjusted for platinum electrode potential  
redox pe  
units mg/l  
density 1  
O(0) 0.282  
Alkalinity 24 as HCO3  
Cl(-1) 13.21  
S(+6) 17.87  
Na 8.96  
K 3.61  
Ca 3.15  
Si 13.7  
F 0.089  
Mg 4.31  
N(+5) 0.971  
N(+3) 0.035  
N(-3) 0.026 as NH4  
P 0.129 as PO4  
Fe(+2) 0.07  
-water 1 # kg

EQUILIBRIUM\_PHASES 4

Lepidocrocite 0 10  
Goethite\_2 0 0

End

SOLUTION 5

temp	23
pH	5.3
pe	6.439 # Adjusted for platinum electrode potential
redox	pe
units	mg/l
density	1
O(0)	0.282
Alkalinity	24 as HCO3
Cl(-1)	13.21
S(+6)	17.87
Na	8.96
K	3.61
Ca	3.15
Si	13.7
F	0.089
Mg	4.31
N(+5)	0.971
N(+3)	0.035
N(-3)	0.026 as NH4
P	0.129 as PO4
Fe(+2)	0.07
-water	1 # kg

EQUILIBRIUM\_PHASES 5

Goethite	0 10 # Lyndsay
Goethite_2	0 0

End

SOLUTION 6

temp	23
pH	5.3
pe	6.439 # Adjusted for platinum electrode potential
redox	pe
units	mg/l
density	1
O(0)	0.282
Alkalinity	24 as HCO3
Cl(-1)	13.21
S(+6)	17.87
Na	8.96
K	3.61
Ca	3.15
Si	13.7
F	0.089

Mg 4.31  
N(+5) 0.971  
N(+3) 0.035  
N(-3) 0.026 as NH4  
P 0.129 as PO4  
Fe(+2) 0.07  
-water 1 # kg

EQUILIBRIUM\_PHASES 6

Goethite\_2 0 10  
Goethite 0 0

End

SOLUTION 7

temp 23  
pH 5.3  
pe 6.439 # Adjusted for platinum electrode potential  
redox pe  
units mg/l  
density 1  
O(0) 0.282  
Alkalinity 24 as HCO3  
Cl(-1) 13.21  
S(+6) 17.87  
Na 8.96  
K 3.61  
Ca 3.15  
Si 13.7  
F 0.089  
Mg 4.31  
N(+5) 0.971  
N(+3) 0.035  
N(-3) 0.026 as NH4  
P 0.129 as PO4  
Fe(+2) 0.07  
-water 1 # kg

EQUILIBRIUM\_PHASES 7

Glaucosite 0 10  
Goethite\_2 0 0

End



SOLUTION 8

temp	23
pH	5.3
pe	6.439 # Adjusted for platinum electrode potential
redox	pe
units	mg/l
density	1
O(0)	0.282
Alkalinity	24 as HCO3
Cl(-1)	13.21
S(+6)	17.87
Na	8.96
K	3.61
Ca	3.15
Si	13.7
F	0.089
Mg	4.31
N(+5)	0.971
N(+3)	0.035
N(-3)	0.026 as NH4
P	0.129 as PO4
Fe(+2)	0.07
-water	1 # kg

EQUILIBRIUM\_PHASES 8

Pyrite	0 10
Goethite_2	0 0

End

SOLUTION 9

temp	23
pH	5.3
pe	6.439 # Adjusted for platinum electrode potential
redox	pe
units	mg/l
density	1
O(0)	0.282
Alkalinity	24 as HCO3
Cl(-1)	13.21
S(+6)	17.87
Na	8.96
K	3.61
Ca	3.15
Si	13.7
F	0.089

Mg 4.31  
N(+5) 0.971  
N(+3) 0.035  
N(-3) 0.026 as NH4  
P 0.129 as PO4  
Fe(+2) 0.07  
-water 1 # kg

EQUILIBRIUM\_PHASES 9

Hedenbergite 0 10  
Goethite\_2 0 0

End

SOLUTION 10

temp 23  
pH 5.3  
pe 6.439 # Adjusted for platinum electrode potential  
redox pe  
units mg/l  
density 1  
O(0) 0.282  
Alkalinity 24 as HCO3  
Cl(-1) 13.21  
S(+6) 17.87  
Na 8.96  
K 3.61  
Ca 3.15  
Si 13.7  
F 0.089  
Mg 4.31  
N(+5) 0.971  
N(+3) 0.035  
N(-3) 0.026 as NH4  
P 0.129 as PO4  
Fe(+2) 0.07  
-water 1 # kg

EQUILIBRIUM\_PHASES 10

Staurolite 0 10  
Goethite\_2 0 0

End

SOLUTION 11

temp	23
pH	5.3
pe	6.439 # Adjusted for platinum electrode potential
redox	pe
units	mg/l
density	1
O(0)	0.282
Alkalinity	24 as HCO <sub>3</sub>
Cl(-1)	13.21
S(+6)	17.87
Na	8.96
K	3.61
Ca	3.15
Si	13.7
F	0.089
Mg	4.31
N(+5)	0.971
N(+3)	0.035
N(-3)	0.026 as NH <sub>4</sub>
P	0.129 as PO <sub>4</sub>
Fe(+2)	0.07
-water	1 # kg

EQUILIBRIUM\_PHASES 11

Schorl 0 10  
Goethite\_2 0 0

End

SOLUTION 12

temp	23
pH	5.3
pe	6.439 # Adjusted for platinum electrode potential
redox	pe
units	mg/l
density	1
O(0)	0.282
Alkalinity	24 as HCO <sub>3</sub>
Cl(-1)	13.21
S(+6)	17.87
Na	8.96
K	3.61
Ca	3.15
Si	13.7
F	0.089

Mg	4.31
N(+5)	0.971
N(+3)	0.035
N(-3)	0.026 as NH4
P	0.129 as PO4
Fe(+2)	0.07
-water	1 # kg

EQUILIBRIUM\_PHASES 12

Ilmenite	0 10
Goethite_2	0 0

End

SOLUTION 13

temp	23
pH	5.3
pe	6.439 # Adjusted for platinum electrode potential
redox	pe
units	mg/l
density	1
O(0)	0.282
Alkalinity	24 as HCO3
Cl(-1)	13.21
S(+6)	17.87
Na	8.96
K	3.61
Ca	3.15
Si	13.7
F	0.089
Mg	4.31
N(+5)	0.971
N(+3)	0.035
N(-3)	0.026 as NH4
P	0.129 as PO4
Fe(+2)	0.07
-water	1 # kg

EQUILIBRIUM\_PHASES 13

Actinolite	0 10
Goethite_2	0 0

End

SOLUTION 14

temp	23
pH	5.3
pe	6.439 # Adjusted for platinum electrode potential
redox	pe
units	mg/l
density	1
O(0)	0.282
Alkalinity	24 as HCO3
Cl(-1)	13.21
S(+6)	17.87
Na	8.96
K	3.61
Ca	3.15
Si	13.7
F	0.089
Mg	4.31
N(+5)	0.971
N(+3)	0.035
N(-3)	0.026 as NH4
P	0.129 as PO4
Fe(+2)	0.07
-water	1 # kg

EQUILIBRIUM\_PHASES 14

Ferropargasite	0	10
Goethite_2	0	0

End

SOLUTION 15

temp	23
pH	5.3
pe	6.439 # Adjusted for platinum electrode potential
redox	pe
units	mg/l
density	1
O(0)	0.282
Alkalinity	24 as HCO3
Cl(-1)	13.21
S(+6)	17.87
Na	8.96
K	3.61
Ca	3.15
Si	13.7
F	0.089

Mg	4.31
N(+5)	0.971
N(+3)	0.035
N(-3)	0.026 as NH4
P	0.129 as PO4
Fe(+2)	0.07
-water	1 # kg

EQUILIBRIUM\_PHASES 15

Almandine 0 10

Goethite\_2 0 0

End

## Appendix L5: Titrating 10 moles of Pyrite with 8 mg/L Oxygen in Pure Water

### SOLUTION 1

temp 25  
pH 7  
pe 4  
redox pe  
units mmol/kgw  
density 1  
-water 1 # kg

### EQUILIBRIUM\_PHASES 1

Pyrite 0 10  
Goethite\_2 0 0

### REACTION 1

O2(g) 1  
5e-4 in 100 steps

### SELECTED\_OUTPUT 1

-file C:\Users\Mark Akland\Desktop\modeling.xls  
-reset false  
-solution true  
-step true  
-pH true  
-Alkalinity true  
-pe true  
-reaction true  
-totals Fe Fe(2) Fe(3) S(+6) S(-2)  
-saturation\_indices Hematite Goethite Lepidocrocite Fe(OH)3

### USER\_GRAPH

heading O(0) Fe(2) S(6) Ca pH

-chart\_title "Titrating Pyrite w/ 8 mg/L Oxygen in Pure water with 10 moles of calcite"

-axis\_titles "Oxygen added, mg/L" "Concentration, mg/L"

-start

10 graph\_x step\_no \* 8/100

20 graph\_y tot("Fe(2)")\*55845, tot("S(6)")\*96066, tot("Ca")\*40078

50 graph\_sy -la("H+")

END

**Appendix L6: Titrating 10 moles of Pyrite with 8 mg/L Oxygen in Pure Water and 10 moles of Calcite**

SOLUTION 1

temp 25  
pH 7  
pe 4  
redox pe  
units mmol/kgw  
density 1  
-water 1 # kg

EQUILIBRIUM\_PHASES 1

Pyrite 0 10  
Calcite 0 10  
Goethite\_2 0 0

REACTION 1

O2(g) 1  
5e-4 in 100 steps

SELECTED\_OUTPUT 1

-file C:\Users\Mark Akland\Desktop\modeling.xls  
-reset false  
-solution true  
-step true  
-pH true  
-Alkalinity true  
-pe true  
-reaction true  
-totals Fe Fe(2) Fe(3) S(+6) S(-2)  
-saturation\_indices Hematite Goethite Lepidocrocite Fe(OH)3

USER\_GRAPH

heading O(0) Fe(2) S(6) Ca pH

-chart\_title "Titrating Pyrite w/ 8 mg/L Oxygen in Pure water with 10 moles of calcite"  
-axis\_titles "Oxygen added, mg/L" "Concentration, mg/L"  
-start  
10 graph\_x step\_no \* 8/100  
20 graph\_y tot("Fe(2)")\*55845, tot("S(6)")\*96066, tot("Ca")\*40078  
50 graph\_sy -la("H+")

END



**Appendix L7: Titrating 10 moles of Pyrite with 8 mg/L Oxygen in Surficial Water [(water chemistry from Whitley (2003)]**

SOLUTION 1

temp 23  
pH 5.3  
pe 6.439 # Adjusted for platinum electrode potential  
redox pe  
units mg/l  
density 1  
O(0) 0.282  
Alkalinity 24 as HCO3  
Cl(-1) 13.21  
S(+6) 17.87  
Na 8.96  
K 3.61  
Ca 3.15  
Si 13.7  
F 0.089  
Mg 4.31  
N(+5) 0.971  
N(+3) 0.035  
N(-3) 0.026 as NH4  
P 0.129 as PO4  
Fe(+2) 0.07  
-water 1 # kg

EQUILIBRIUM\_PHASES 1

Pyrite 0 10  
Goethite\_2 0 0

REACTION 1

O2(g) 1  
5e-4 in 100 steps

SELECTED\_OUTPUT 1

-file C:\Users\Mark Akland\Desktop\modeling.xls  
-reset false  
-solution true  
-step true  
-pH true  
-Alkalinity true  
-pe true  
-reaction true  
-totals Fe Fe(2) Fe(3) S(+6) S(-2)  
-saturation\_indices Hematite Goethite Lepidocrocite Fe(OH)3

```
USER_GRAPH
heading O(0) Fe(2) S(6) pH
-chart_title "Titrating Pyrite w/ 8 mg/L Oxygen in Surficial Water"
-axis_titles "Oxygen added, mg/L" "Concentration, mg/L"
-start
10 graph_x step_no * 8/100
20 graph_y tot("Fe(2)")*55845, tot("S(6)")*96066
50 graph_sy -la("H+")

END
```

**Appendix L8: Titrating 10 moles of Pyrite and 10 moles of Calcite with 8 mg/L Oxygen in Surficial Water [(water chemistry from Whitley (2003)]**

SOLUTION 1

temp 23  
pH 5.3  
pe 6.439 # Adjusted for platinum electrode potential  
redox pe  
units mg/l  
density 1  
O(0) 0.282  
Alkalinity 24 as HCO<sub>3</sub>  
Cl(-1) 13.21  
S(+6) 17.87  
Na 8.96  
K 3.61  
Ca 3.15  
Si 13.7  
F 0.089  
Mg 4.31  
N(+5) 0.971  
N(+3) 0.035  
N(-3) 0.026 as NH<sub>4</sub>  
P 0.129 as PO<sub>4</sub>  
Fe(+2) 0.07  
-water 1 # kg

EQUILIBRIUM\_PHASES 1

Pyrite 0 10  
Calcite 0 10  
Goethite\_2 0 0

REACTION 1

O<sub>2</sub>(g) 1  
5e-4 in 100 steps

SELECTED\_OUTPUT 1

-file C:\Users\Mark Akland\Desktop\modeling.xls  
-reset false  
-solution true  
-step true  
-pH true  
-Alkalinity true  
-pe true  
-reaction true  
-totals Fe Fe(2) Fe(3) S(+6) S(-2)

```
-saturation_indices Hematite Goethite Lepidocrocite Fe(OH)3
USER_GRAPH
heading O(0) Fe(2) S(6) pH
-chart_title "Titrating Pyrite w/ 8 mg/L Oxygen in Surficial Water"
-axis_titles "Oxygen added, mg/L" "Concentration, mg/L"
-start
10 graph_x step_no * 8/100
20 graph_y tot("Fe(2)")*55845, tot("S(6)")*96066
50 graph_sy -la("H+")

END
```

**Appendix L9: Titrating 10 moles Goethite with 5 mg/L DOC in Surficial Water [(water chemistry from Whitley (2003)]**

SOLUTION 1

temp 23  
pH 5.3  
pe 6.439 # Adjusted for platinum electrode potential  
redox pe  
units mg/l  
density 1  
O(0) 0.282  
Alkalinity 24 as HCO3  
Cl(-1) 13.21  
S(+6) 17.87  
Na 8.96  
K 3.61  
Ca 3.15  
Si 13.7  
F 0.089  
Mg 4.31  
N(+5) 0.971  
N(+3) 0.035  
N(-3) 0.026 as NH4  
P 0.129 as PO4  
Fe(+2) 0.07  
-water 1 # kg

EQUILIBRIUM\_PHASES 1

Goethite\_2 0 10  
Pyrite 0 0

SOLUTION\_MASTER\_SPECIES

C(0) CH2O 0 30.03

SOLUTION\_SPECIES

$\text{CO}_2 + 4\text{H}^+ + 4\text{e}^- = \text{CH}_2\text{O} + \text{H}_2\text{O}$   
log\_k -4.8

REACTION 1

CH2O 1  
4.1628507201732e-4 in 100 steps

SELECTED\_OUTPUT 1

-file C:\Users\Mark Akland\Desktop\modeling.xls  
-reset false  
-solution true

-step true  
-pH true  
-Alkalinity true  
-pe true  
-reaction true  
-totals Fe Fe(2) Fe(3) O(0) S(+6) S(-2) N(+5)  
-saturation\_indices Hematite Goethite Lepidocrocite Fe(OH)3 Pyrite

USER\_GRAPH

heading C(0) N(5) Fe(2) S(+6) pH

-axis\_titles "Carbon added, mg/L" "Concentration, mg/L"

-start

10 graph\_x step\_no \* 5/100

20 graph\_y tot("N(5)")\*62007, tot("Fe(2)")\*55845, tot("S(6)")\*96000

50 graph\_sy -la("H+")

END

**Appendix L10: Titrating 10 moles Goethite and 10 moles Calcite with 5 mg/L DOC in Surficial Water [(water chemistry from Whitley (2003)]**

SOLUTION 1

temp 23  
pH 5.3  
pe 6.439 # Adjusted for platinum electrode potential  
redox pe  
units mg/l  
density 1  
O(0) 0.282  
Alkalinity 24 as HCO3  
Cl(-1) 13.21  
S(+6) 17.87  
Na 8.96  
K 3.61  
Ca 3.15  
Si 13.7  
F 0.089  
Mg 4.31  
N(+5) 0.971  
N(+3) 0.035  
N(-3) 0.026 as NH4  
P 0.129 as PO4  
Fe(+2) 0.07  
-water 1 # kg

EQUILIBRIUM\_PHASES 1

Goethite\_2 0 10  
Calcite 0 10  
Pyrite 0 0

SOLUTION\_MASTER\_SPECIES

C(0) CH2O 0 30.03

SOLUTION\_SPECIES

CO2 + 4H+ + 4e- = CH2O + H2O  
log\_k -4.8

REACTION 1

CH2O 1  
4.1628507201732e-4 in 100 steps

SELECTED\_OUTPUT 1

-file C:\Users\Mark Akland\Desktop\modeling.xls  
-reset false

-solution true  
-step true  
-pH true  
-Alkalinity true  
-pe true  
-reaction true  
-totals Fe Fe(2) Fe(3) O(0) S(+6) S(-2) N(+5)  
-saturation\_indices Hematite Goethite Lepidocrocite Fe(OH)3 Pyrite

USER\_GRAPH

heading C(0) N(5) Fe(2) S(+6) pH

-axis\_titles "Carbon added, mg/L" "Concentration, mg/L"

-start

10 graph\_x step\_no \* 5/100

20 graph\_y tot("N(5)")\*62007, tot("Fe(2)")\*55845, tot("S(6)")\*96000

50 graph\_sy -la("H+")

END



## Appendix L11: Conservative-Transport Model

SOLUTION 0 # T15 speciated. Data from Brown (1999)

temp	17.0
pH	6.90
pe	3.921
redox	pe
units	mg/l
density	1
Alkalinity	344 as HCO <sub>3</sub>
Cl(-1)	12.3
Na	14.07
K	26.35
Ca	70.98
Si	34.19
F	0.22
Mg	8.57
S(-2)	0.0145
N(+5)	0.0026
N(+3)	0.0021
N(-3)	0.48 as NH <sub>4</sub>
P	0.626 as PO <sub>4</sub>
Fe(+2)	16.4
-water	1 # kg

END

SOLUTION 0 # T15 speciated. Data from Brown (1999)

temp	17.0
pH	6.90
pe	3.921
redox	pe
units	mg/l
density	1
Alkalinity	344 as HCO <sub>3</sub>
Cl(-1)	12.3
Na	14.07
K	26.35
Ca	70.98
Si	34.19
F	0.22
Mg	8.57
S(-2)	0.0145
N(+5)	0.0026
N(+3)	0.0021
N(-3)	0.48 as NH <sub>4</sub>

P 0.626 as PO4  
Fe(+2) 16.4  
-water 1 # kg

END

SOLUTION 1 # T15 water equilibrated with calcite. Data from Brown (1999)

temp 17.0  
pH 6.90  
pe 3.921  
redox pe  
units mg/l  
density 1  
Alkalinity 344 as HCO3  
Cl(-1) 12.3  
Na 14.07  
K 26.35  
Ca 70.98  
Si 34.19  
F 0.22  
Mg 8.57  
S(-2) 0.0145  
N(+5) 0.0026  
N(+3) 0.0021  
N(-3) 0.48 as NH4  
P 0.626 as PO4  
Fe(+2) 16.4  
-water 1 # kg

SAVE solution 1

END

SOLUTION 2-6 # Low Fe UCH water Far East. Data from Brown(1999)

temp 18.0  
pH 7.41  
pe 2.974  
redox pe  
units mg/l  
density 1  
Alkalinity 305 as HCO3  
Cl(-1) 0.726  
S(+6) 1.53  
Na 8.83  
K 5.18  
Ca 65.80

Si 29.05  
F 0.36  
Mg 13.21  
S(-2) 0.2  
N(+5) 0.0015  
N(+3) 0.0032  
N(-3) 1.21 as NH4  
P 0.013 as PO4  
Fe(+2) 0.01  
-water 1 # kg

SAVE solution 2-6

END

TRANSPORT # Assuming a UCH flow velocity of 0.365 ft/day = 40.6 m/yr = 1.55e9 secs to traverse one cell

-cells 6; -lengths 2000 # m  
-time\_step 1.55315e9 # v = 40.6 m/yr (25.23 miles/ka)  
-flow\_direction forward; -shifts 6  
-dispersivities 800; -punch\_frequency 100

END

TRANSPORT

-cells 6;  
-time\_step 0 # v = 40.6 m/yr (25.23 miles/ka)  
-flow\_direction forward; -shifts 1  
-dispersivities 0;

SELECTED\_OUTPUT 1

-file C:\Users\Mark Akland\Desktop\modeling.xls  
-reset false  
-solution true  
-step false  
-pH true  
-Alkalinity true  
-pe true  
-reaction false  
-distance true  
-time true  
-totals Fe Fe(2) Fe(3) Ca K Na Mg S(-2)  
-saturation\_indices Hematite Goethite\_2 Lepidocrocite Fe(OH)3 Pyrite Siderite

USER\_PUNCH

-head cell time/yr dist/kilometers Na K Mg Ca Fe S(-2) Alk pH

```
10 punch cell_no, total_time / (3600 * 24 * 365)
20 n = 0
30 punch (cell_no - n) * 2.0 - 1.0
40 punch tot("Na")*22990, tot("K")*39098, tot("Mg")*24305, tot("Ca")*40078,
tot("Fe")*55845, tot("S(-2)")*32066, Alk*61018, -la("H+")
```

#### USER\_GRAPH

```
-heading dist Na K Mg Ca*0.125 Fe Alk/10 pH
-chart_title "Conservative Transport Model"
-initial_solutions true
-plot_concentration_vs x
-axis_titles "Distance / m" "mg/L"
-axis_scale x_axis 0 12000 2000
-start
10 graph_x dist
20 graph_y tot("Na")*22990, tot("K")*39098, tot("Mg")*24305, tot("Ca")*5009.75,
tot("Fe")*55845, Alk*6101.8
50 graph_sy -la("H+")
END
```

## Appendix L12: Reactive-Transport Model

SOLUTION 0 # T15 speciated. Data from Brown (1999)

temp	17.0
pH	6.90
pe	3.921
redox	pe
units	mg/l
density	1
Alkalinity	344 as HCO <sub>3</sub>
Cl(-1)	12.3
Na	14.07
K	26.35
Ca	70.98
Si	34.19
F	0.22
Mg	8.57
S(-2)	0.0145
N(+5)	0.0026
N(+3)	0.0021
N(-3)	0.48 as NH <sub>4</sub>
P	0.626 as PO <sub>4</sub>
Fe(+2)	16.4
-water	1 # kg

END

SOLUTION 0 # T15 speciated. Data from Brown (1999)

temp	17.0
pH	6.90
pe	3.921
redox	pe
units	mg/l
density	1
Alkalinity	344 as HCO <sub>3</sub>
Cl(-1)	12.3
Na	14.07
K	26.35
Ca	70.98
Si	34.19
F	0.22
Mg	8.57
S(-2)	0.0145
N(+5)	0.0026
N(+3)	0.0021
N(-3)	0.48 as NH <sub>4</sub>

P 0.626 as PO4  
Fe(+2) 16.4  
-water 1 # kg

END

SOLUTION 1 # T15 water equilibrated with calcite Brown (1999)

temp 17.0  
pH 6.90  
pe 3.921  
redox pe  
units mg/l  
density 1  
Alkalinity 344 as HCO3  
Cl(-1) 12.3  
Na 14.07  
K 26.35  
Ca 70.98  
Si 34.19  
F 0.22  
Mg 8.57  
S(-2) 0.0145  
N(+5) 0.0026  
N(+3) 0.0021  
N(-3) 0.48 as NH4  
P 0.626 as PO4  
Fe(+2) 16.4  
-water 1 # kg

EQUILIBRIUM\_PHASES 1

Calcite 0 10

SAVE solution 1

END

SOLUTION 2-6 # Low Fe UCH water Far East. Data from Brown (1999)

temp 18.0  
pH 7.41  
pe 2.974  
redox pe  
units mg/l  
density 1  
Alkalinity 305 as HCO3  
Cl(-1) 0.726  
S(+6) 1.53

Na 8.83  
K 5.18  
Ca 65.80  
Si 29.05  
F 0.36  
Mg 13.21  
S(-2) 0.2  
N(+5) 0.0015  
N(+3) 0.0032  
N(-3) 1.21 as NH4  
P 0.013 as PO4  
Fe(+2) 0.01  
-water 1 # kg

EQUILIBRIUM\_PHASES 1

Calcite 0 10

SAVE solution 2-6

END

EXCHANGE 2-6

X 0.115; -equil 2 # Assume 5% glauconite, 20 meq/100g, aquifer density of 2.7 kg/L, and 20% porosity

END

TRANSPORT # Assuming a UCH flow velocity of 0.365 ft/day = 40.6 m/yr = 1.55e9 secs to traverse one cell

-cells 6; -lengths 2000 # m  
-time\_step 1.55315e9 # v = 40.6 m/yr (25.23 miles/ka)  
-flow\_direction forward; -shifts 6  
-dispersivities 800; -punch\_frequency 100

END

TRANSPORT

-cells 6;  
-time\_step 0 # v = 40.6 m/yr (25.23 miles/ka)  
-flow\_direction forward; -shifts 1  
-dispersivities 0;

SELECTED\_OUTPUT 1

-file C:\Users\Mark Akland\Desktop\modeling.xls  
-reset false  
-solution true

```

-step          false
-pH            true
-Alkalinity    true
-pe            true
-reaction      false
-distance      true
-time          true
-totals        Fe Fe(2) Fe(3) Ca Si K P Na Mg S(-2)
-saturation_indices Hematite Goethite_2 Lepidocrocite Fe(OH)3 Pyrite Siderite

```

#### USER\_PUNCH

```

-head cell time/yr dist/kilometers Na K Mg Ca Fe S(-2) Alk pH
10 punch cell_no, total_time / (3600 * 24 * 365)
20 n = 0
30 punch (cell_no - n) * 2.0 - 1.0
40 punch tot("Na")*22990, tot("K")*39098, tot("Mg")*24305, tot("Ca")*40078,
tot("Fe")*55845, tot("S(-2)")*32066, Alk*61018, -la("H+")

```

#### USER\_GRAPH

```

-heading dist Na K Mg Ca*0.125 Fe Alk/10 pH
-chart_title "Reactive Transport Model"
-initial_solutions true
-plot_concentration_vs x
-axis_titles "Distance / m" "mg/L"
-axis_scale x_axis 0 12000 2000
-start
10 graph_x dist
20 graph_y tot("Na")*22990, tot("K")*39098, tot("Mg")*24305, tot("Ca")*5009.75,
tot("Fe")*55845, Alk*6101.8
50 graph_sy -la("H+")
END

```



